Design, Synthesis, and Evaluation of Pyrazinoic Acid-Derived Antituberculars for Drug-Resistant *Mycobacterium tuberculosis*

A DISSERTATION
SUBMITTED TO THE FACULTY OF THE
UNIVERSITY OF MINNESOTA
BY

Malcolm Spencer Cole

IN PARTIAL FULFILLMENT OF THE REQUIREMENTS
FOR THE DEGREE OF
DOCTOR OF PHILOSOPHY

ADVISOR: Dr. Courtney C. Aldrich

CO-ADVISOR: Dr. Anthony D. Baughn

January 2022

Acknowledgements

First and foremost, I'd like to thank my advisor Dr. Courtney Aldrich for his support and guidance throughout my graduate school career. Courtney provided the space and environment to expand my skills as a scientist, and demonstrated incalculable patience in giving me the time I needed to stumble through my research and writing. He has always given his students a great degree of freedom to make scientific mistakes and learn from these experiences, and I am grateful to have been a member of his lab for six long years. I'd also like to thank my co-advisor, Dr. Anthony (Tony) Baughn, who accepted me into his lab as a microbiology neophyte and allowed me to broaden my horizons as a medicinal chemist. I'm confident I've made countless mistakes when setting up microbiology experiments or presenting on TB metabolism, but Tony always provided invaluable feedback without making me feel ignorant or unskilled. His patience and warmth made me feel like a welcome addition to his lab and TB(+B) lab meetings. Also, he came up with the original idea for the cephalosporin-POA conjugate- who knows where my PhD would've gone without him. I would also thank my other committee members, Dr. Gunda Georg and Dr. Daniel Harki, for reviewing my thesis and providing valuable feedback on my research.

Next, I need to thank all the fellow scientists I've worked with over the years, who did the hard work of teaching me how to be a (semi-)successful medicinal chemist. I'd like to thank Dr. Joe Buonomo for providing the bulk of my training, as well as steady friendship and professional guidance over the years. I feel that I didn't appreciate how much Joe's knowledge and perspectives had shaped my own research until after he graduated and I had to rough it on my own. I also need to thank Dr. John Schultz, my lab "twin," for joining Courtney's lab with me and taking some of the heat off from the boss; and Scott Brody, for joining the year after and serving a similar role. John and Scott helped me grow both professionally and personally, and were always willing to lend

an ear as I vented about some new trial or tribulation going on in my work. Thanks for all your friendship and support over the years (and thanks Scott for being [mostly] a good sport every time Ohio State beat Michigan in football). I would also like to thank former Aldrich lab members Dr. Evan Alexander, Dr. Matthew Bockman, Dr. Carter Eiden, Dr. Neeraj Mishra and Dr. Surendra Dawadi for your mentorship early in my research career, and current members Pooja Hegde, Tian Lan, Dr. Marzena Brinkmann and Dr. Kaja Berg as well for your help in furthering my research. I thank Eric Hess, my former mentee, for allowing me to teach you chemistry and gain research experience- I hope you'll find your experiences helpful in your medical career. I'd also like to thank the other members of my Med Chem class, particularly Dmitri Konorev, for your support and camaraderie as we struggled through classes and research problems together.

I'd also like to thank my many research collaborators, beginning with Michael Howe, Dr. Elise Lamont and Dr. Yusuke Minato in the Baughn lab- Michael in particular has been the single most important outside collaborator in helping me further my research and grow as a scientist. I thank collaborators Dr. Thomas Dick and Dr. Gerhard Gruber for your support and guidance with the POA analogues project, as well as Dr. Wassihun Wedajo Aragaw (Dick lab) and Drs. Priya Ragunathan, Chitra Latka, and Malathy Sony Subramanian (Gruber lab). Additionally, I'd like to thank Dr. Alon Herschhorn for your guidance and patience as a collaborator developing probes for HIV envelope glycoprotein, and Drs. Anna Tischler and Tyler Bold for your valuable feedback at TB+B lab meetings.

Finally, I'd like to thank my friends and family for providing encouragement, distraction, and moral support throughout the course of my education. Nick, Matt, Alex, Clay, Kyle, Dan, Teja: thank you for pushing me to succeed and cheering me up when I failed. Kelly: thank you for your unwavering support as a partner and a friend. You've never stopped believing in me and you

brighten my darkest grad student days with your warmth and positivity. The last two years with you have been pretty great, which is saying a lot- I mean, there's a pandemic going on and I'm a seventh year grad student…. Jackie, Collin, and Mom: thank you for all you've done for me over the years. You've always remained patient with my sluggishness and grad school was no exception. The last few years have been difficult but your support and encouragement allowed me to believe in myself and push through to the end. I love you all dearly.

Dedication

To my parents, who gave so much of themselves for their children

To my Uncle Steve, who stimulated my intellectual curiosity and inspired me

To my twin, Jackie, who believed in me and made me want to believe in myself, too.

Abstract

Tuberculosis (TB), an infectious disease caused by the pathogen *Mycobacterium tuberculosis* (*Mtb*), is a major cause of suffering worldwide. The impact of this disease has been exacerbated by the ongoing coronavirus pandemic, reversing much recent progress that had increased diagnosis and treatment rates in the preceding decade. In addition to ongoing issues related to public health shortcomings and lack of access to treatment, the emergence and spread of resistant strains is an increasing cause for concern. While the antitubercular pipeline has produced a few new antibiotics in the 21st century, more novel treatments are urgently needed to keep abreast of resistant strains. This dissertation describes efforts to create new therapeutic options for resistant TB, centered around pyrazinoic acid (POA), the active form of pyrazinamide (PZA), an important first-line TB drug.

Recently, a growing number of reports have highlighted the promise of β-lactam conjugates in selectively targeting resistant organisms. β-lactams are a widely-employed class of antibiotics that target cell wall biosynthesis. Bacteria can evade this activity through expression of β-lactamases, powerful enzymes that destroy the electrophilic β-lactam warhead. However, researchers have learned to take advantage of this resistance mechanism, designing β-lactam conjugates that release a molecular payload following β-lactamase cleavage. This strategy, referred to here as β-lactamase-mediated fragmentation, is explored in great detail in **Chapter 1**, including descriptions of its discovery and applications in a variety of fields, including diagnostics, cellular imaging, and antibiotic design. **Chapter 2** describes our own work in this space, designing β-lactam conjugates bearing POA as a *Mtb*-selective warhead. This strategy circumvents the most common resistance mechanism against PZA, imparting activity in an *Mtb* macrophage infection model (where conventional β-lactams are typically ineffective). We also

provide preliminary mechanistic evidence that our conjugates act as codrugs, achieving antibacterial activity through action of the β-lactam scaffold as well as the POA warhead. In **Chapter 3**, we remove the β-lactam scaffold on focus on POA itself, reporting a series of new analogues featuring substitutions on the pyrazine ring. We identify several analogues with improved activity over POA, and use biochemical techniques to demonstrate they are inhibitors of PanD, a putative target of POA. We use the structure of our most active lead and recent structural insights into PanD to design additional inhibitors with comparable antimycobacterial activity, providing proof-of-concept for future structure-based design of new PanD inhibitors.

Table of Contents

List of Tables

List of Figures

List of Abbreviations

ACQ	Aggregation-caused quenching
AIE	Aggregation-induced emission
ATc	Anhydrotetracycline
ATP	Adenosine triphosphate
AMP	Adenosine monophosphate
BAPA	N-benzoyl-L-Arg-*p*-nitroaniline
BL	β-lactam
BLase	β-lactamase
BLI	β-lactamase inhibitor
CALB	Lipase B from *Candida antarctica*
CE	Collision energy
CF	Cystic fibrosis
CFUs	Colony forming units
CM	Cephamycin
CoA	Coenzyme A
CS	Cephalosporin
CXP	Exit potential
DABCYL	4-(dimethylaminoazo)benzene-4-carboxylic acid
DBO	Diazabicyclooctane
DCM	Dichloromethane
DHFR	Dihydrofolate reductase
DMSO	Dimethylsulfoxide
DNB	Dinitrobenzamide
DP	Declustering potential
DPA	Dipicolinic acid
EMB	Ethambutol
ESBL	Extended-spectrum β-lactamase
ESI	Electrospray ionization
FA	Formic acid
FAS	Fatty acid synthase
fLuc	Firefly luciferase
FMT	Fluorescence-mediated molecular tomography
FoR	Frequency of resistance
FRET	Fluorescence resonance energy transfer
GFP	Green fluorescent protein
GMP	Guanosine monophosphate
HBSS	Hank's Buffered Saline
HPLC	High performance liquid chromatography

HRMS	High resolution mass spectrometry
Hz	Hertz
IC	Inhibitory concentration
INH	Isoniazid
I.S.	Internal standard
ITC	Isothermal titration calorimetry
LOD	Limit of detection
MBL	Metallo-β-lactamase
MDR-TB	Multidrug-resistant tuberculosis
MOI	Multiplicity of infection
MS	Mass spectrometry
MIC	Minimum inhibitory concentration
Mtb	*Mycobacterium tuberculosis*
Mtx	Methotrexate
NAD^+	Nicotinamide adenine dinucleotide
NAMN	Nicotinamide mononucleotide
NDM	New Delhi metallo β-lactamase
NF-AT	Nuclear factor of activated T-cells
NIH	National Institutes of Health
NIR	Near infrared
NMR	Nuclear magnetic resonance
NO	Nitric oxide
NTHI	Nontypeable *Haemophilus influenzae*
OADC	Oleate-albumin-dextrose-catalase
OD	Optical density
PADAC	Pyridine-2-azo-*p*-dimethylaniline cephalosporin
PBP	Penicillin binding protein
PDB	Protein data bank
PET	Photoinduced electron transfer
PK	Pharmacokinetic
PMF	Proton motive force
POA	Pyrazinoic acid
Pyr	Pyrithione
PZA	Pyrazinamide
RFP	Red fluorescent protein
RIF	Rifampicin
rt	Room temperature
SAR	Structure-activity relationship
SEC	Size exclusion chromatography
SGF	Simulated gastric fluid
TB	Tuberculosis
TCA	Trichloroacetic acid

TFA	Trifluoroacetic acid
THF	Tetrahydrofuran
TNB	Thionitrobenzoic acid
TLC	Thin layer chromatography
TPE	Tetraphenylethylene
Tre	Trehalose
TQ	Thioquinoline
UTI	Urinary tract infection
UV-vis	Ultraviolet-visual light
WHO	World Health Organization
WT	Wild type
XDR-TB	Extensively drug-resistant tuberculosis

Chapter 1. β-Lactamase-Mediated Fragmentation: Historical Perspectives and Recent Advances in Diagnostics, Imaging, and Antibacterial Design

Malcolm S. Cole, Courtney C. Aldrich

MSC conceived of the topic, performed the literature search, and wrote and edited the chapter.

CCA provided feedback and edited the chapter.

Chapter 1. β-Lactamase-Mediated Fragmentation: Historical Perspectives and Recent Advances in Diagnostics, Imaging, and Antibacterial Design

The emergence of β-lactam (BL) antibiotics in the early 20th century represented a remarkable advancement in human medicine, allowing for the widespread treatment of infectious diseases that had plagued humanity throughout history. Yet, this triumph was followed closely by the emergence of a bacterial weapon to destroy BLs: the β-lactamase (BLase). BLase production is a primary mechanism of resistance to BL antibiotics, and the spread of new isoforms with expanded hydrolytic activity represents a pressing threat to global health. Nonetheless, researchers have developed strategies that take advantage of this defense mechanism, exploiting BLase activity in the creation of probes, diagnostic tools, and even novel antibiotics selective for resistant organisms. Early discoveries in the 1960s and '70s demonstrating that certain BLs expel a leaving group upon BLase cleavage have spawned an entire field dedicated to employing this selective release mechanism, termed BLase-mediated fragmentation. Chemical probes have been developed for imaging and studying BLase-expressing organisms in the laboratory, and diagnosing BL-resistant infections in the clinic. Perhaps most promising, new antibiotics have been developed that use BLase-mediated fragmentation to selectively release cytotoxic chemical "warheads" at the site of infection, reducing off-target effects and allowing for the repurposing of putative antibiotics against resistant organisms. This review will provide some historical background to the emergence of this field, and highlight some exciting recent reports that demonstrate the promise of this unique release mechanism.

1.1 Introduction to β-Lactams and β-Lactamases

1.1.1 β-Lactam Antibiotics: Historical Perspective

Following the discovery of penicillin in 1929 by Alexander Fleming, β-lactam (BL) antibiotics have enjoyed unprecedented success as a therapeutic class. Widespread use of penicillin G in the 1940s and '50s preceded the discovery of methods to isolate a synthetic precursor, 6-aminopenicillanic acid (6-APA), which allowed semisynthetic access to a wide variety of new penicillin analogues featuring modifications at the N6 side chain.[1] Analogous discovery of cephalosporin C, in 1953 by G.G.F. Newton and E.P. Abraham, and in 1960 of its modular precursor 7-aminocephalosporanic acid (7-ACA) stimulated generation of a similar library of cephalosporin-based antibiotics.[1] These early discoveries paved the way for additional BL classes, such as cephamycins (1971), monobactams (1976), carbapenems (1976), and the fully synthetic penems (1978).[2] Additional chemical iterations have since produced new generations within each class, and new β-lactams are still being discovered and approved for clinical use.[3-6] Changes incorporated in subsequent generations confer desirable properties such as oral bioavailability, increased spectrum of activity, and perhaps most importantly, endurance against resistance mechanisms. Like any conventional antibiotic, resistance to the β-lactams developed rapidly following their widespread adoption (observed as early as 1940)[1, 7] and has remained a constant adversary in their clinical application.

1.1.2 Resistance to β-Lactams: β-Lactamases

β-lactams inhibit growth of bacteria by inhibiting penicillin-binding proteins (PBPs), enzymes responsible for forming strengthening crosslinks in peptidoglycan, a structural component of the cell wall. Mimicking the endogenous peptide substrate of PBPs (frequently a terminal D-Ala D-Ala dipeptide), β-lactams form stable acyl-enzyme intermediates with an active site nucleophilic

residue; typically Ser is labelled in PBPs, although some classes can also label other peptidoglycan-modifying enzymes, such as L,D-transpeptidases, containing a nucleophilic Cys residue.[8] A wide variety of resistance mechanisms allow bacteria to evade this covalent inactivation. Expression of alternative PBPs with reduced binding affinity for β-lactams, such as PBP2a in MRSA, or upregulation of PBP expression are important resistant mechanisms in Gram-positive organisms.[9] Gram-negative bacteria have several additional methods for evading β-lactam treatment due to their distinctive outer membrane, such as reduced expression of transport proteins and production of xenobiotic efflux pumps.[9] However, the earliest identified form of resistance, and the one with arguably the greatest clinical significance today, is expression of β-lactam-hydrolyzing enzymes called β-lactamases (BLases).

Enzymes capable of destroying BLs were first identified by Abraham *et al* in extracts from *E. coli* in 1940, preceding their widespread clinical use.[7] This "penicillinase," later identified as an AmpC cephalosporinase, inactivated the antibiotic, abolishing activity against normally BL-susceptible *S. aureus*.[7, 9] Mirroring this initial finding, the development of novel BL classes has been followed closely by the discovery of BLases catalyzing their hydrolysis. BLases can be found in both Gram-positive and -negative organisms; enzymes are typically secreted by Gram-positive organisms and bound within the periplasmic space for Gram-negatives.[10] Expression can be constitutive or induced, either through direct sensing of the BL warhead (via acylation) or indirect sensing of cell wall damage (via muropeptides and other peptidoglycan fragments).[11] Genes encoding these resistance enzymes can either be chromosomally encoded or transferred between organisms through mobile genetic elements, such as plasmids and transposons, which significantly contribute to the spread and overall success of BLase-mediated resistance.[9-10] BLase expression is the most significant resistance mechanism for Gram-negative infections, and BLase-mediated

resistance continues to accelerate globally: rates of *blaZ* expression in *Staphylocci* have increased from less than 20% in the 1940s to greater than 85% today;[12] TEM-1, a plasmid-encoded Ambler class A BLase, is found in 70% of *Enterobacteriaceae* infections;[12] and extended-spectrum BLases (ESBLs) such as CTX-M, which hydrolyze most penicillins and later-generation (oxyimino) cephalosporins and are resistant to conventional BLase inhibitors (BLIs), are found in nearly 40% of Gram-negative infections.[13-14] This alarming rise in BLase expression underscores the need for novel approaches capable of identifying, studying, and selectively targeting these resistant organisms.

1.1.3 β-Lactamase Applications: Exploiting Resistance

Despite their role in disrupting antibiotic therapy, β-lactamases have also more recently been adapted for a growing number of applications in chemical biology and drug design. The substrate selectivity and robust kinetics of β-lactamase activity, and their lack of endogenous expression in eukaryotic cells, make these enzymes attractive reporters when combined with specially designed β-lactam probes. These molecules undergo fragmentation following BLase cleavage, releasing a reporter molecule such as a chromophore or fluorophore that can be subsequently detected with analytical methods (**Figure 1**). Through this approach, β-lactamase activity can be identified and even visualized, allowing for diagnosis of BL-resistant infections, imaging and sorting of BLase-expressing cells, and more. Additionally, the absence of BLase expression in eukaryotic cells also presents an opportunity for selective therapeutic intervention via β-lactam prodrugs, which fragment upon BLase cleavage to liberate a bioactive species. This approach allows for selective delivery of a molecular "payload" at the site of BLase activity, achieving specific targeting of resistant organisms. Through these methods, the BLase resistance mechanism evolved by prokaryotes to overcome BL treatment can be exploited for the

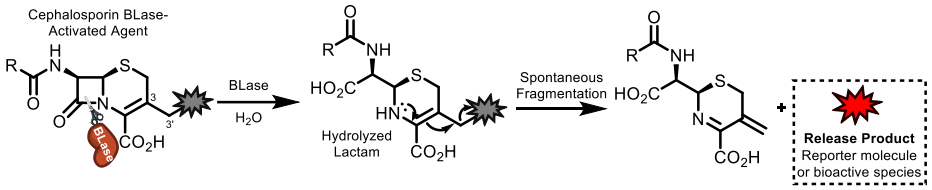

Figure 1. Activation mechanism of BLase-activated cephalosporins.

advancement of medical science and human health. This chapter will provide an overview of progress in the development of fragmentation-based BL-probes, and their applications in detecting and targeting BLase expression. Historical findings and landmark approaches will be discussed, and recent advances in the field will be highlighted.

1.1.4 Early Discoveries: BLase-Mediated Fragmentation in Cephalosporins

In the early 1960s, discovery and isolation of the cephalosporin precursor 7-ACA enabled access to a new class of semi-synthetic BLs. This opportunity led to significant interest towards a greater understanding of the chemistry of this molecular class. In pursuit of this knowledge, Eggers *et al.* began studies examining the stability of cephalosporins to nucleophilic attack.[15] Previous mechanistic studies with penicillins had demonstrated inactivation by alcohols proceeded via metal-catalyzed nucleophilic addition into the BL ring, yielding penicilloic esters.[16] In performing analogous studies with cephalosporins, treatment with benzylic alcohol in base yielded an unexpected product: cleavage of the BL ring resulted in deacylation, suggesting a fragmentation

process (**Figure 2**).[15] Eggers and coworkers proposed a concerted prototrophic rearrangement, noting it "unusual" that a reaction with a primary leaving group would proceed so readily.

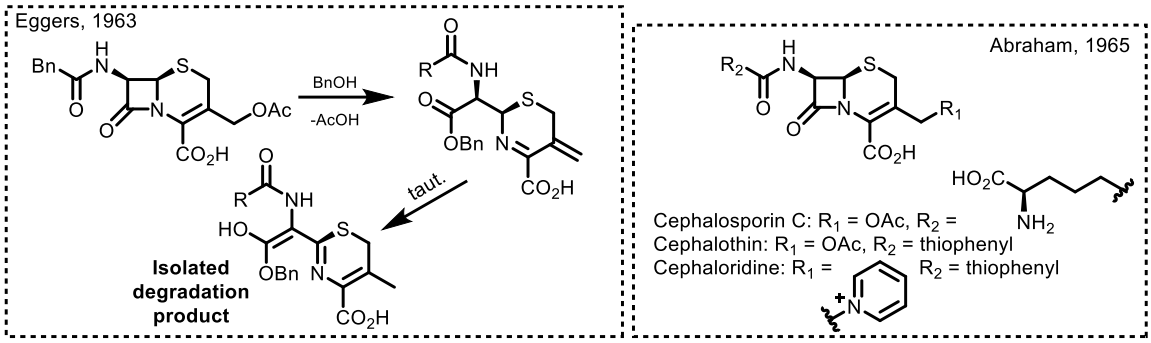

Figure 2. Early Evidence of BLase-Mediated Fragmentation.

The proposed product was synthesized and confirmed, employing recently developed 7-ACA chemistry. To our knowledge, this study presents the first evidence of this C-3′ elimination process following cleavage of the BL ring.[15] Arguably more foundational in launching the field was a study performed two years later, in the lab of Sir Edward Abraham. Following his landmark discovery of penicillinase in 1940, Abraham's lab pioneered research exploring this emerging threat to public health.[7] In the mid 1960s, studies were underway investigating previous reports of β-lactamase activity in the supernatant of *Pseudomonas pyocyanea* cultures.[17] While assessing the susceptibility of recently-discovered cephalosporins to this hydrolysis, Abraham and colleagues discovered that certain cephalosporins released an additional equivalent of acid upon exposure. Notably, a common feature in these molecules was the presence of a potentially acidic leaving group at the C-3′ position: an acetyl group for cephalosporin C and cephalothin, and a pyridinium species for cephaloridine (**Figure 2**). Notably, analogous tests with a deacylated version of cephalosporin C removed this extra equivalent of produced acid. This observation led Abraham *et al* to the same conclusion as Eggers two years earlier: cleavage of the β-lactam ring, and subsequent liberation of the N-5 lone pair, leads to fragmentation and elimination of a suitable leaving group at the C-3′

position.[18] Critically, the researchers were able to demonstrate that this process occurs irrespective of the mechanism of ring cleavage; enzymatic as well as base-catalyzed cleavage produced the same result. Subsequent reports by Abraham and others characterizing the elimination reaction,[19-24] including detailed modeling studies,[25-27] paved the way for an entire field of β-lactam fragmentation tools, including novel antibiotics, diagnostics, cellular imaging, anticancer approaches employing antibody-enzyme conjugates, and many more. This chapter will explore these approaches and highlight recent novel examples, with a specific emphasis on developments following Rao's excellent 2008 review of the field.[28]

1.2 Diagnostics: Lactam Fragmentation for β-Lactamase Reporters

The earliest applications of β-lactam fragmentation involved the use of chromogenic reporters for diagnosis of infection with BLase-expressing organisms. BLase expression is the most clinically relevant resistance mechanism in Gram-negative bacteria.[9, 12] Treatment success, as well as preventing further spread of resistant organisms, is dependent upon early identification of BLase activity in infected patients. Therefore, approaches allowing for rapid, cost-effective identification of BLase expression are critical for antibacterial therapy and public health.

1.2.1 Early methods for detection

Prior to the 1970s, several methods existed for BLase diagnosis (**Figure 3**). The earliest and most straightforward of these was bioassay determination, in which bacteria were sampled directly from a patient, cultured and challenged with BL antibiotics *in vitro*. Although a straightforward and useful approach, this protocol requires significant time as well as access to specialized knowledge and equipment for culturing infectious organisms.[29] To circumvent this

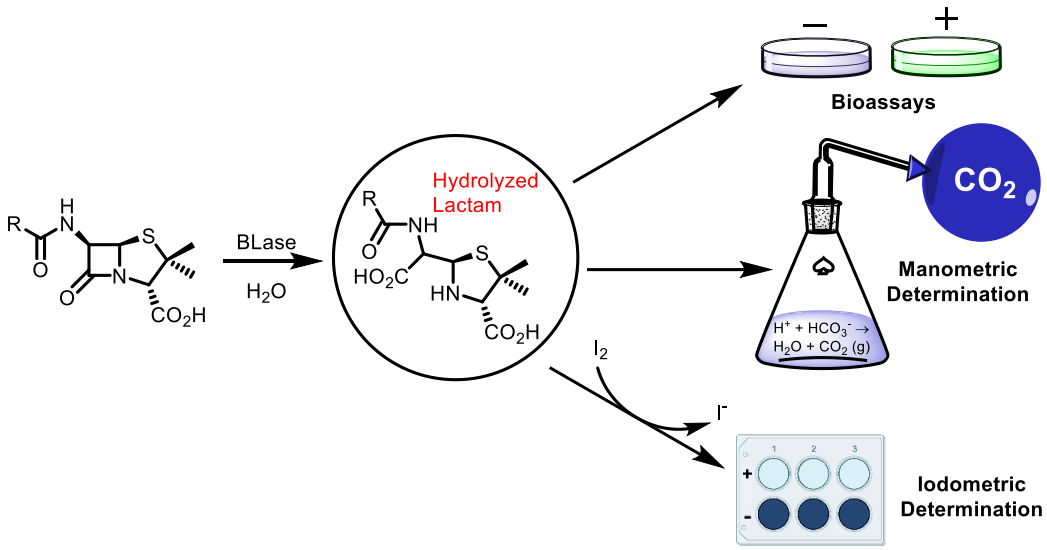

Figure 3. Early Methods of BLase Detection. Created with BioRender.com.

limitation, reporter assays exploiting the chemistry of hydrolyzed BLs were developed in the decade following BLase discovery. Manometric determination, developed for BLase detection in 1947, involves measuring CO_2 produced following neutralization of bicarbonate and thus, indirectly, acid production; hydrolysis of the BL ring yields a carboxylic acid and can be quantified through this approach.[30-31] This protocol is more specific for detecting BL cleavage, providing a quantitative approach to measuring BLase activity. Manometry would also theoretically circumvent the need for culturing bacteria; however, in practice the low sensitivity of this approach and susceptibility to interferences limited its clinical utility as a diagnostic.[30] Around the same time, an iodometric detection method was developed to quantify BLase activity.[32] Iodine, in complex with starch, forms a deep purple complex; the product of penicillin hydrolysis, penicilloic acid (but not intact penicillin) converts the complexed iodine to charged iodide, which is unable to complex with starch. In this manner, BLase activity can be quantified by the degree of decolorization observed in a given sample. Following these initial reports, modifications allowing for increased sensitivity and robustness, direct application in clinical cultures, and even advanced

diagnostic materials such as paper-based test strips were developed and employed successfully both in academic and clinical settings.[33-36] However, limitations to these approaches persisted, including marginal sensitivity and incompatibility with reductants or iodine-absorbing interferences such as proteins. The approach also proved more useful for penicillins than for later generations of BLs, such as cephalosporins, due to decreased rates of iodine consumption.[34-35]

1.2.2 BL-Based Diagnostics: Nitrocefin

In the early 1970s, researchers at Glaxo Research Limited searching for novel β-lactam antibiotics discovered a cephalosporin with interesting spectroscopic properties.[37] When cultured with organisms expressing BLases, the culture medium turned a vibrant red color. Interestingly, BL-susceptible cultures did not undergo this change, suggesting a BLase-specific mechanism for the observation. Based on the molecular structure, O'Callaghan and colleagues postulated the cephalosporin was undergoing a chemical change following BLase cleavage, similar to the fragmentation reaction previously observed for cephaloridine.[19] A dramatic shift in absorbance maximum (to 482 nm, compared to ~260 nm for conventional cephalosporins) was attributed to conjugation between the liberated lone pair of the thiazine nitrogen and the dinitrophenyl group; while this example doesn't involve elimination of a C-3′ leaving group, it relies upon the same principle of electron flux between the liberated lone pair of the BL nitrogen and a C-3′ electron acceptor. Subsequent isolation of the cleavage product confirmed its identity as the chromogenic species. This newly discovered cephalosporin, nitrocefin, would go on to enjoy widespread use both as a tool compound to study BLase kinetics and as a selective reporter of BLase expression.[38-40] Critical to its success as a diagnostic was its excellent spectrum of susceptibility against a range of BLases, including penicillinases, which are typically unable to hydrolyze cephalosporins. O'Callaghan and coworkers speculated the electron-withdrawing dinitrophenyl group activates the

BL ring, allowing for this expanded susceptibility.[37] These initial studies with nitrocefin (along with cephacetrile, a non-C-3′-based probe developed around the same time) served as proof of concept for the experimental and clinical utility of a BL-based BLase reporter, and despite limitations related to its stability and synthetic accessibility, nitrocefin is still used in diagnostic applications today.[41]

1.2.3 BL-Based Diagnostics: Pyridine-2-Azo-*p*-Dimethylaniline Cephalosporin (PADAC) and CENTA

In the early 1980s, chemists at Hoechst AG in Germany identified two new cephalosporin-based probes, PADAC and CENTA, that more fully exploited the fragmentation mechanism reported by Eggers and colleagues two decades prior. PADAC, inspired by the pyridinium leaving group of cephaloridine, releases a chromogenic azopyridine species upon BL cleavage, with concomitant color change from purple to yellow (570 nm to 465 nm).[42] CENTA similarly releases a chromophore, thionitrobenzoic acid (TNB), upon fragmentation, inducing a less vibrant shift in absorbance (345 nm to 410 nm).[43] These novel reporters proved advantageous over nitrocefin in several ways. Firstly, both probes were significantly easier to synthesize than nitrocefin, through previously developed C-3′ substitution chemistry from 7-ACA. This ease of access also arose due to their relative stability compared to nitrocefin, which also presented advantages in biological assays, where the lability of nitrocefin had proved limiting. Subsequent studies with both reporters rendered more apparent their comparative strengths and weaknesses. PADAC's dramatic color change is easily visible to the naked eye, suggesting greater utility in field diagnostics. Unfortunately, the increased stability of PADAC limits its applications in these studies, where it demonstrates reduced sensitivity for BLase activity compared to nitrocefin and increased susceptibility to interferences.[43] CENTA has an improved spectrum of BLase susceptibility

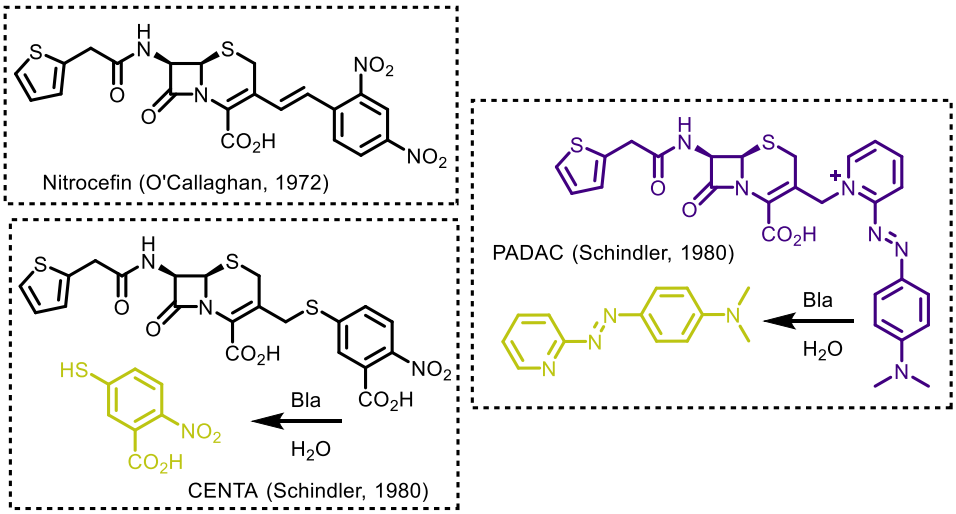

Figure 4. Early BL-Based BLase Diagnostics.

compared to PADAC, and is also cheaper to synthesize from the widely available Ellman's reagent (DTNB). However, the more modest color change is difficult to observe unaided, necessitating the use of specialized equipment, such as UV-vis spectrometers, that may be less practical for rapid, point-of-care diagnostics.[43] Thus, while these novel probes represented a significant step forward from the original proof of concept, nitrocefin, and CENTA is still widely used today, limitations remained regarding their utility for detection and diagnosis of resistant organisms in the clinic.[44-46]

1.2.4 Fluorescence-based reporters: Next-generation BLase diagnostics

Recent developments in the chemistry of BLase-activated diagnostics have replaced the simpler chromophores of PADAC and CENTA with more robust fluorescent dyes, such as coumarin and Tokyo green. Fluorophores require fluorescence excitement to produce signal and are bulkier than simpler chromophores but possess several key advantages, including increased sensitivity and decreased background in colored media.[47] Inspired by pioneering advances in chemical biology using these fluorescent reporters for other systems, Tsien and colleagues

developed the first fluorescence-based BLase probe in 1998 for imaging studies, which will be discussed in more detail in the Imaging Applications section.[48] This approach has also produced promising results in BLase diagnostics; many early applications have been reviewed previously.[28] A key distinction in fluorescence-based reporter studies is the type of system employed: either a lone fluorophore as the leaving group, or a FRET-type donor-acceptor fluorophore pair, such as the one used in Tsien's pioneering report.[48] FRET-based reporters typically employ a donor fluorophore attached to the unreleased amido side chain (N7 for cephalosporins) and have the advantage of increased sensitivity due to a greater difference in the coupled (uncleaved) and uncoupled (cleaved) states, which fluoresce at different wavelengths and can be directly compared to minimize assay variability.[49] Conversely, simpler non-FRET probes demonstrate greater background fluorescence but also generally display improved cleavage kinetics, as the addition of a second bulky fluorophore can significantly inhibit recognition by BLases. Given the relative strengths of each approach, it is not surprising that both strategies remain widely used in the field today. One older example of a FRET-based reporter is a study by Zhang *et al* using a N-7 fluorescein donor and C-3′ rhodamine acceptor (**Figure 5**).[49] Excitation of the fluorescein at 440 nm leads to FRET and emission from the rhodamine at 590 nm for the intact probe; BLase cleavage induces release of the acceptor, shifting the new fluorescence maximum to 520 nm. After demonstrating their N7-amino probe (C-1) was cleaved by TEM-1, the authors introduced an N7-oxyimino sidechain (C-2) and were able to inhibit cleavage by TEM-1 while retaining susceptibility to broader-spectrum BLases such as NDM-1.[49] Currently, FRET-based reporters are more commonly used for imaging applications; in comparison, a number of diagnostic applications of non-FRET probes have been reported in the last decade. One recent report by Mao and coworkers describes a probe (CFCC-2, Figure 3) featuring an activatable difluoromethyl coumarin reporter,

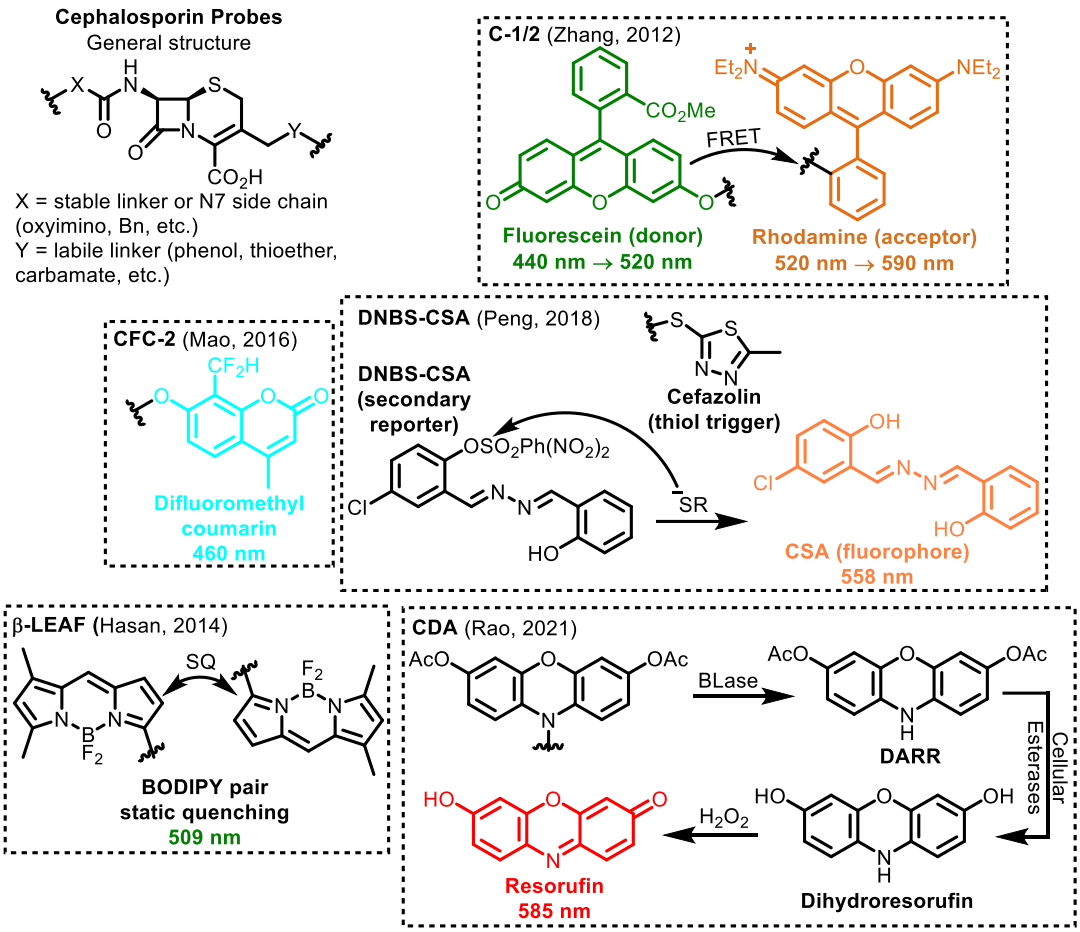

Figure 5. Cephalosporin-Based Diagnostics Probes for BLase Detection.

which reveals a powerful quinone methide electrophile that covalently labels nucleophilic residues following BLase-mediated release.[50] Covalent labeling turns on fluorescence of the coumarin and also prevents diffusion from the cleavage site, presenting utility in cell labeling experiments as well as diagnostics.[50] Another recent report describes an indirect detection assay that exploits BLase-mediated fragmentation in a known antibiotic, cefazolin, which releases a thiol-containing thiadiazole species.[51] The researchers designed a masked salicylaldehyde azine, DNBS-CSA, which is converted to the unmasked, "on" fluorophore in the presence of thiol (**Figure 5**). This probe avoids synthetically challenging modification of the BL scaffold and also presents a fluorophore impervious to aggregation caused quenching (ACQ), a phenomenon observed for other commonly-used fluorophores such as indolium and fluorescein that provides an upper limit to possible probe concentrations in diagnostics assays (thus, limiting their sensitivity).[51-52] This approach also translated well to paper test strips, highlighting its practicality as a diagnostic tool with broad clinical utility.[51] Another diagnostic tool recently described employs dual BODIPY fluorophores at the N-7 and C-3′ positions, taking advantage of a phenomenon known as "static quenching", which prevents excitation of neighboring fluorophores due to changes in their electronic ground state.[53] Unlike FRET, which results in fluorescence at different maxima depending on the proximity of the donor and acceptor, static quenching results in fluorescence "turn off" when the fluorophores are in close proximity, and "turns on" when fragmentation occurs. The authors termed their probe β-lactamase enzyme-activated fluorophore (β-LEAF, **Figure 5**), and it was derived from a prior molecule (β-lactamase enzyme-activated photosensitizer, β-LEAP) which employed a light-activated phenothiazine reporter but had limited utility as a diagnostic.[54] Optimization of fluorophores and linkers identified a dual-BODIPY probe with significantly higher fluorescence release upon BLase cleavage; subsequent studies with BLase-expressing *S. aureus*

confirmed the viability of the probe as a rapid BLase diagnostic. Further analysis provided a putative diagnostic workflow to determine the susceptibility of a given BL to turnover, potentially allowing for continued use of more stable BLs against BLase-expressing organisms in the clinic.[53] Finally, a very recent report has described a probe (CDA, **Figure 5**) with a longer wavelength resorufin reporter, reducing background and increasing assay sensitivity.[55] This strategy takes additional advantage from a "dual-caged" strategy, wherein oxidation and subsequent esterification of the fluorophore essentially abolishes fluorescence of the uncleaved probe, further decreasing background.[55] BLase cleavage and release of the fluorophore triggers an activation cascade in which the pro-fluorophore (DARR, **Figure 5**), following diffusion across the cellular membrane, is first de-esterified by intracellular esterases to yield a reduced form of the fluorophore (dihydroresorufin). Following sample treatment with hydrogen peroxide, this is oxidized to the active fluorophore, turning on fluorescence. These multiple steps required to initiate fluorescent signal substantially reduce background signal from the uncleaved reporter. Colony-forming units (CFUs) of BLase-expressing organisms as low as 10^3 were detected in processed urine samples, demonstrating this excellent sensitivity.[55]

1.2.5 Fluorescence-based reporters: BLase-selective approaches

The approaches described thus far have created general, broad-specificity BLase reporters. However, there is also significant interest in developing probe molecules with selectivity for individual BLase enzymes or classes, such as ESBLs and carbapenemases. More precise identification of BLase activity can guide medical professionals in prescribing BLase-stable, later-generation BL antibiotics, and can even assist in rapidly diagnosing the organisms present in an infection.[53, 56-57] Many advances in this field have been developed by Rao and colleagues, following their initial studies on imaging reporters in collaboration with Tsien.[47, 58-59] In 2012, Rao *et al*

reported a new application of their probe technology for diagnostic applications in *Mycobacterium tuberculosis* (*Mtb*). *Mtb* is resistant to most BLs, due to expression of a chromosomally-encoded Ambler class A BLase, encoded by *blaC*. *Mtb* is also resistant to many other conventional antibiotics and requires application of a specific regimen of first-line agents over the course of several months; as a result, early diagnosis of *Mtb* infection is critical to treatment success. Rao and colleagues had the idea to use BLase-sensitive reporters for rapid *Mtb* diagnosis; unfortunately, contemporary BL-based probes were also hydrolyzed by BLases expressed from more common infections, such as TEM-1 and BlaZ. In order to generate BlaC-specific probes, Rao *et al* synthesized cephamycin-based reporters, distinguished by an α-methoxy substitution at C7, which exploit the increased flexibility of BlaC's substrate specificity (omega) loop compared to other commonly observed BLases.[56] The researchers synthesized an umbelliferone-based probe, CDC-OMe (**Figure 6**), which displayed preferential susceptibility to BlaC over TEM-1, demonstrated by a nearly 9,000-fold difference in turnover rate (k_{cat}). A cephalosporin probe lacking the C7-methoxy, CDC-1, was hydrolyzed more rapidly by TEM-1, demonstrating its role in the observed selectivity. A Tokyo Green-based probe (CDG-OMe, Figure 4) displayed greater utility in cell-based assays due to the longer excitation and emission wavelengths of the dye, which proved less susceptible to interference from the cellular background. *In vitro* studies with CDG-OMe against BLase-expresing *E. coli* demonstrated high sensitivity to BlaC (detecting as little as 1 fmol of enzyme) and robust selectivity (>3,000-fold) for BlaC over TEM-1.[56] Encouragingly, CDG-OMe was also able to selectively identify *Mtb* in unprocessed sputum samples from cystic fibrosis patients, with a limit of detection (LoD) as low as 10 CFUs. The CDC and CDG probes were further elaborated upon in a 2014 study, where Rao *et al* showed that modification at the C2 position conferred additional benefits, with the cyclopropyl-modified probe

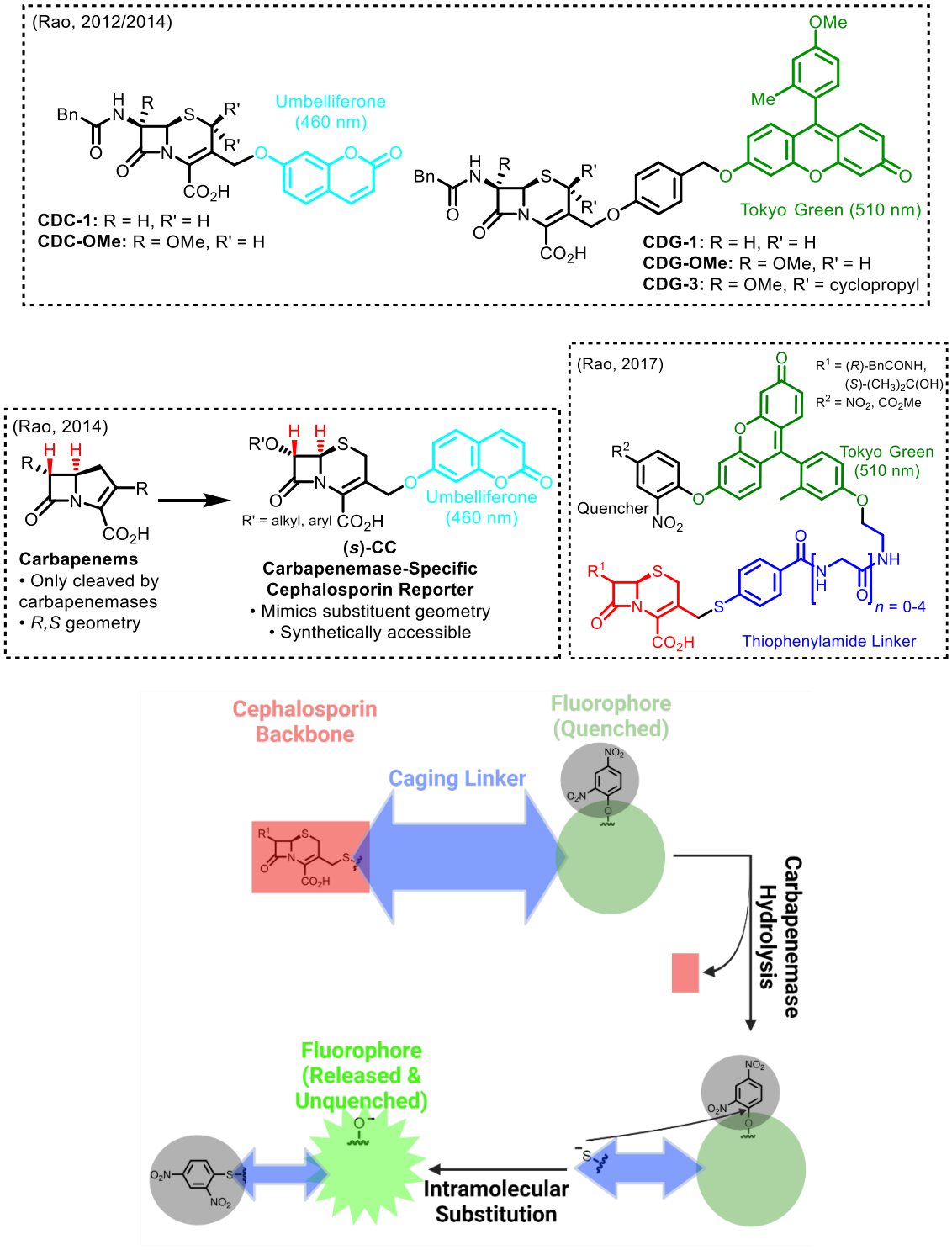

Figure 6. BLase-Specific Fluorogenic Probes. Created with BioRender.com.

CDG-3 displaying improved sensitivity and >100,000-fold selectivity for BlaC over TEM-1.[60] Screening of additional BLases from Ambler classes A, B (metallo-β-lactamases, MBLs) and C confirmed exquisite selectivity for the mycobacterial enzyme. Additional studies demonstrated similar sensitivity to CDG-OMe in detecting mycobacteria in unprocessed sputum; when clinical sputum samples were assessed, CDG-3 displayed a high sensitivity (90%) but only moderate selectivity (73%) with several false positives. In addition to these promising early studies, these fluorescent probes have also been employed in microfluidics-based *Mtb* diagnostics and for the identification of illegal BLase use to destroy residual BL antibiotics in milk.[61-62]

Another target of the selective probe technology developed by Rao *et al* has been carbapenemases, a class of BLases including KPC (Ambler class A), NDM (class B), and OXA-48 (class D). Carbapenemases are capable of hydrolyzing carbapenems, the BL class with the greatest spectrum of activity, and contribute to an increasing trend of carbapenem resistance observed in common human pathogens such as *Enterobacteriaceae* and *Pseudomonas aeruginosa*.[57, 60] Initially, the researchers developed an umbelliferone-based cephalosporin reporter featuring unconventional *S* geometry at the C7 position. By matching the trans stereochemistry of carbapenems at the analogous C5-C6 positions, Rao *et al* were able to achieve selective susceptibility to carbapenemases, with moderate sensitivity towards resistant strains (capable of detecting between 10^4-10^5 CFUs). Additional discrimination between serine-based BLases and MBLs was conferred through modification of the C-7 R' group.[60] The group further elaborated upon their *R,S*-cephalosphorin probe design in a subsequent publication, again employing Tokyo Green as a favorable, longer-wavelength reporter (**Figure 6**).[63] A novel caged linker strategy was employed, featuring a physiologically stable thiophenyl ether linker and a separate, labile dinitrophenyl quencher coupled to the fluorescent reporter. BLase cleavage induces release of the

thiophenyl linker, which uncages the fluorophore via intramolecular attack on the dinitrophenyl quencher (**Figure 6**).[63] This caging linker strategy significantly improves substrate turnover, as bulky fluorophores directly coupled at the C-3′ position can interfere with BLase binding.[63] Other recent applications developing reporters specific for individual BLases include a ceftazidime-derived N7-oxyimino cephalosporin, which selectively releases a BODIPY fluorophore in the presence of extended-spectrum BLases (ESBLs);[64] and carbapenem-based reporters that selectively detect carbapenemases (conjugated BODIPY fluorophore;[65] coumarin probes)[66] and MBLs (umbelliferone fluorophore)[67] (**Figure 7**).

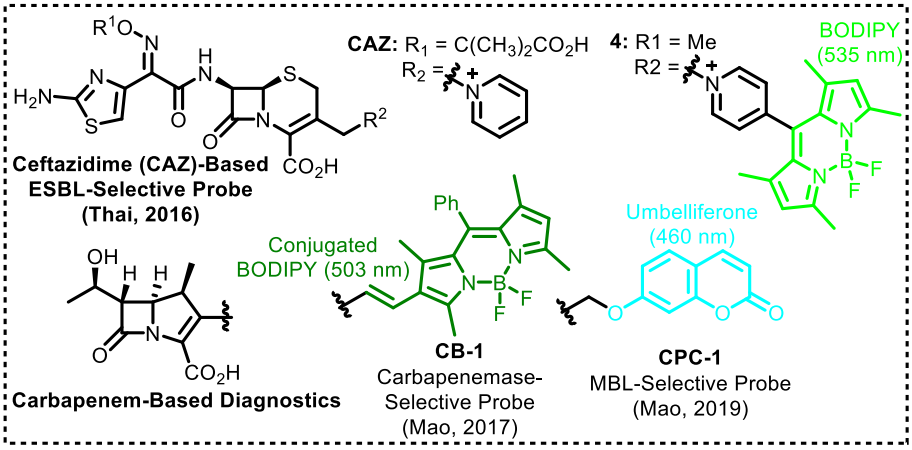

Figure 7. Other Recent Approaches to BLase-Selective Diagnostics.

1.2.6 Non-Fluorogenic BLase Diagnostics

Although fluorogenic reporters have seen widespread use in diagnostics applications, alternative reporters have also been explored. Non-fluorogenic reporters have a number of advantages over their counterparts: eliminating bulky fluorophores removes the need for specialized instrumentation and can also improve hydrolysis kinetics. Many of these strategies employ chromophores or polymerizing agents that are more easily monitored with the naked eye, providing greater applicability to field diagnostics or low resource healthcare settings. One

interesting strategy employs a hydrogelator peptide reporter, which spontaneously forms nanofibrils in aqueous media upon release from the cleaved cephalosporin (**Figure 8**).[68] Hydrogel formation begins quickly (~20 mins after BLase exposure) and is easily visible to the naked eye through changes to sample opacity and viscosity. The reporter was able to successfully identify BLase-expressing cultures with greater accuracy than the diagnostic standard, nitrocefin.[68] A recent report combines a more conventional chromophore reporter with an N-7 polymerizing agent to create BLase-sensitive biomaterials (**Figure 8**).[69] Alkekhia and coworkers created cephalosporin probes featuring a chromogenic 4-nitrobenzenethiol reporter and a maleimide-activated N-7 side chain. Mild click chemistry was employed to functionalize a 4-arm-PEG-SH polymer with this probe and to form cross-links between polymer chains, creating a diagnostic biomaterial capable of forming BLase-sensitive hydrogels (**Figure 8**). This technology demonstrated similar diagnostic ability to both CENTA and nitrocefin, and the authors have proposed using this strategy with other polymers to create more robust biomaterials that could be incorporated into surfaces or medical devices for point-of-contact identification of BLase-expressing organisms.[69]

Another recently explored approach with a non-fluorogenic reporter, termed DETECT, employs a dual enzyme assay to achieve signal amplification and enhanced sensitivity.[70-71] BLase cleavage of a cephalosporin probe releases thiophenol, which acts not as reporter but a trigger for a secondary enzyme, papain, an amidase caged through a disulfide bond on its active site Cys. The thiophenol trigger cleaves the disulfide cage, allowing the activated papain to turn over a second substrate, N-benzoyl-$_{L}$-Arg-*p*-nitroaniline (BAPA), releasing a *p*-nitroaniline chromophore that can be monitored visually with UV-vis spectrophotometry.[70] The use of a secondary enzyme and reporter allows for signal amplification because one thiophenol trigger can activate thousands of papain enzymes, enhancing the colorimetric output of the BLase activity by several orders of

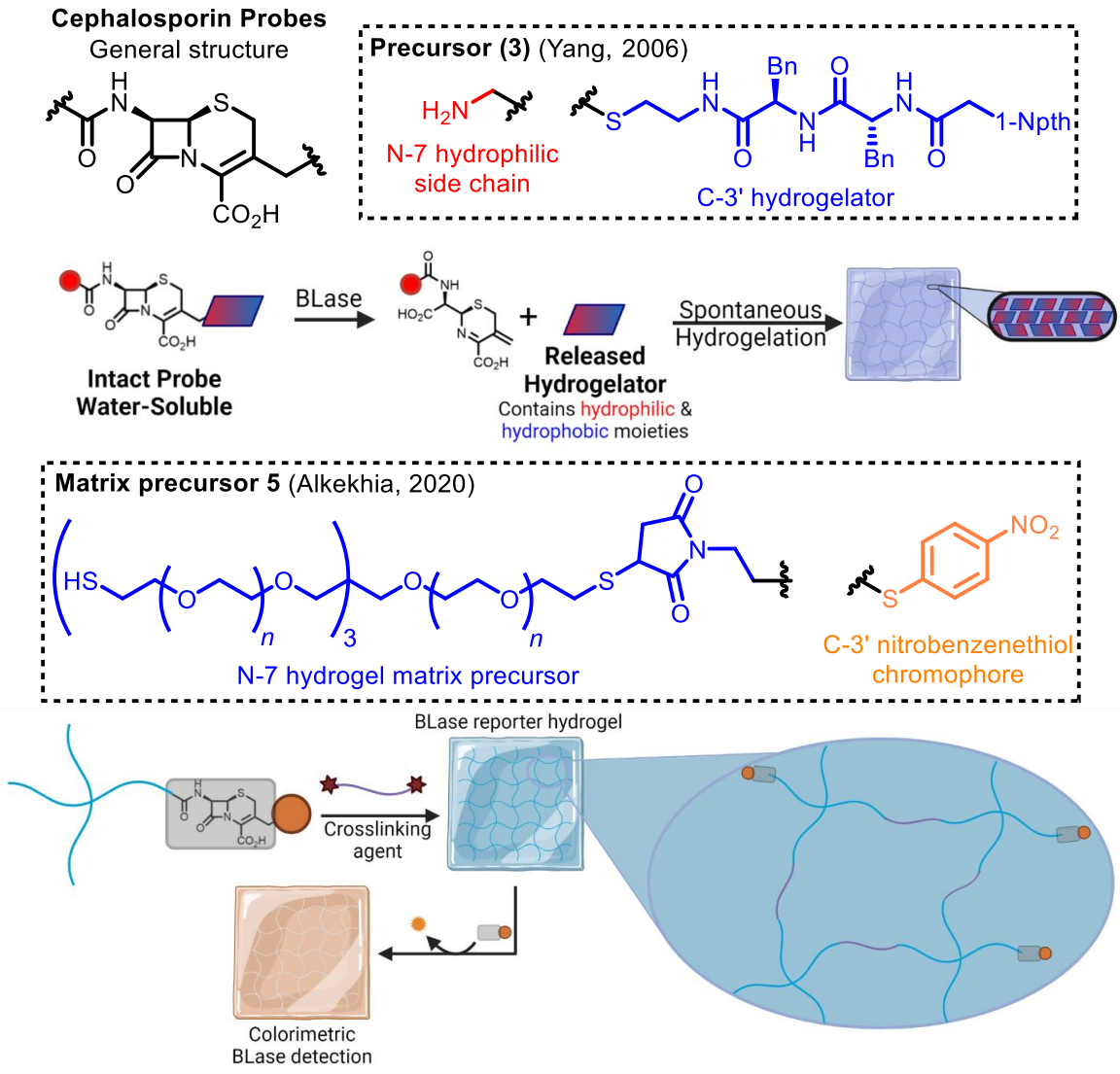

Figure 8. Hydrogels as BLase Diagnostics. Created with BioRender.com.

magnitude compared to conventional BL-chromophore probes (LOD for TEM-1 = 100 fM, compared to 4 nM for nitrocefin).[70] This increased signal allows for detection of as few as 10^4 CFUs of BLase-expressing organisms, which corresponds to the lower-range for urine samples from urinary tract infection (UTI) patients; indeed, the DETECT system proved highly accurate (88% accuracy, n=34) at detecting BLase activity in unprocessed urine samples from suspected UTI patients, demonstrating the clinical utility of this approach.[70]

A final recent diagnostic application of this technology describes the use of a chemiluminescent dioxetane reporter, which spontaneously degrades following release to emit light without the need for fluorescence excitation.[72] Unlike fluorophore-based approaches, which are susceptible to interference via fluorescence of analytes present in the sample (autofluorescence), chemiluminescence has virtually no background, allowing for improved sensitivity with excellent signal-to-noise ratios.[73-75] Following the example of chemiluminescent dioxetane reporters for other enzymes,[73, 76-77] the authors developed a reporter (CCP, **Figure 9**) featuring a thiophenol linker, which decreases the high pH normally required for spontaneous degradation of phenol dioxetanes.[72] Enzymatic assays demonstrated broad susceptibility to a variety of BLases with excellent sensitivity, improving on the commercially available fluorogenic reporter fluorocillin by 25,000-fold. Subsequent assays proved successful in identifying BLase activity from 10^6 CFUs of bacteria

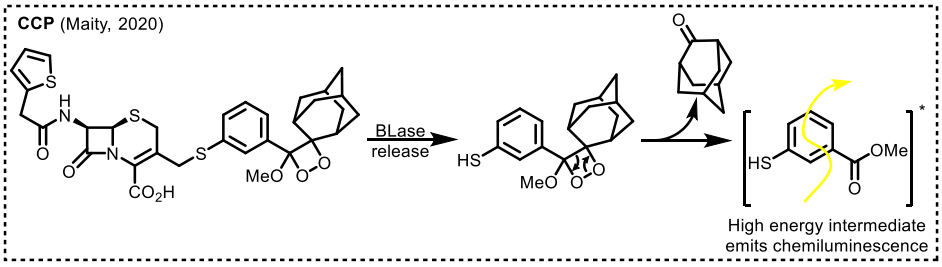

Figure 9. Chemiluminescent BLase Detection via a Dioxetane Reporter.

cultured from UTI patient urine samples, highlighting the utility of this strategy as a diagnostic approach.[72] A similar approach has also been explored using disulfide-caged dioxetanes, which indirectly detect BLase activity through uncaging by H_2S, a byproduct of cephem and penem hydrolysis.[78]

1.3 Imaging: Lactam-Based Probes and Their Applications

As demonstrated in the previous section, BL probes have shown great promise for the diagnosis of BL-resistant infections. However, this modality has several other potential applications as well. One particularly important use of this strategy has originated in the field of chemical biology, where BLase-sensitive probes are used to achieve reporting and imaging of cellular processes, such as gene expression. BLase enzymes possess a number of properties desirable in chemical biology applications: high substrate specificity, rapid turnover, robust stability in a variety of conditions (temperature, pH, buffers), small molecular weight, and low cytotoxicity.[28, 48, 79] In order to realize the potential of BLases for chemical biology approaches, a variety of BLase-sensitive tool compounds have been created. Many of these probes take advantage of BLase-mediated fragmentation in order to release a reporter at the site of β-lactamase activity, resulting in selective labelling or signaling for visualizing gene expression, disease progression, and more.

1.3.1 Imaging Applications: Early Developments

The first study to employ BLase as a reporter was described by Moore and coworkers in 1997.[80] Prior to this report, several other hydrolyzing enzymes had been used for monitoring gene expression through release or turnover of fluorescent dyes, including luciferase, β-galactosidase, and green fluorescent protein (GFP).[81-83] Moore *et al* envisioned using BLase as a robust and

versatile enzymatic reporter, in combination with the previously developed chromogenic probes nitrocefin and PADAC.[80] A549 human lung adenocarcinoma cells were transfected with plasmids encoding TEM-1 BLase from *E. coli*. The wild type enzyme contains a signal peptide which achieves localization in the periplasm; in order to visualize localization within different cellular regions, additional plasmids replacing this signal peptide with a methionine and a membrane-spanning domain were created. Following transfection, turnover of the chromogenic substrates was observed; additionally, localization of TEM-1 was achieved depending on the isoform, with >90% of activity detected extracellularly, intracellularly, and membrane-bound for the wild type, methionine, and membrane-spanning forms respectively.[80] This technology proved compatible with a wide variety of cell types and was also capable of reporting BLase activity *in vivo*, through tissue transfection of the plasmid or implantation of pre-transfected cells.[80]

Shortly following this initial study, a seminal report by Zlokarnik and colleagues was described with improved applicability for chemical biology approaches.[48] The authors sought to resolve the limitations of Moore's reporter assay, including low sensitivity, poor signal-to-noise, and high interference from variations in cell size and probe concentration. A novel fluorescent cephalosporin probe (CCF2/AM, **Figure 10**) was designed to overcome the limitations of the simpler chromogenic reporters previously explored.[48] This new reporter exploited the BLase fragmentation reaction through a FRET donor-acceptor pair, which allowed for more specific monitoring of probe turnover. BLase cleavage results in elimination of the FRET acceptor, disrupting FRET and shifting emission to a shorter wavelength; by monitoring the ratio of intensities at the longer (paired) and shorter (unpaired) wavelengths, BLase activity can be quantified independently of probe concentration and other potential interferences.[48] The use of

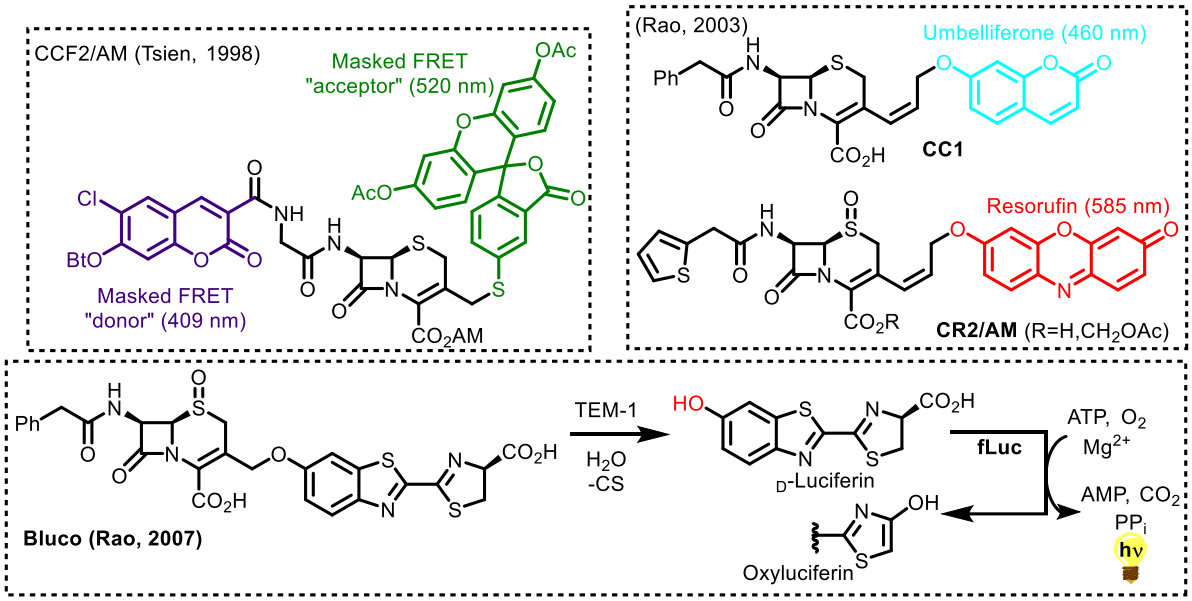

Figure 10. Early Fluorogenic and Bioluminogenic BLase Probes for Imaging Applications.

fluorogenic probes improves sensitivity and decreases signal background, as described previously in this review. Additionally, the use of a thioether linkage minimizes fluorescence of the cleaved thiol acceptor, further decreasing background. This ingenious probe design demonstrated high sensitivity (capable of detecting as little as 5 fM enzyme *in vitro*) and was also employed to visualize differential gene expression *in vivo*. The authors transfected cells with the TEM-1 gene regulated by a promoter, such as nuclear factor of activated T-cells (NF-AT) or glucocorticoid response elements; addition of the corresponding activator, such as dexamethasone, induced BLase expression, which could be observed on the level of individual cells and used to measure gene expression kinetics. Flow cytometry was used to sort cells by gene expression based upon color, which the authors proposed as a potential alternative selection mechanism to conventional antibiotic resistance-based selection.[48] This highly innovative probe design was used to monitor a number of other biological processes in the subsequent years, including signal transduction and HIV fusion in T cells and protein-protein interactions in a variety of systems.[84-89]

A subsequent innovation in BL probe design was reported by Rao *et al* in 2003. Inspired by the success of CCF2, the authors sought to create a similar fluorescent probe (CC1, **Figure 10**) with improved cellular permeability and aqueous solubility. By replacing the FRET donor-acceptor pair with a single fluorescent umbelliferone leaving group, the probe size was reduced and permeability was improved.[47] A resorufin-based probe (CR2, **Figure 10**) was also developed, allowing for excitation and emission at longer wavelengths and thus reducing interference associated with autofluorescence. Oxidation of the thiazine sulfur prevented undesirable $\Delta 2$ isomerization; membrane penetration was further improved through masking of the cephalosporin carboxylate, allowing for imaging of transfected Jurkat cells expressing TEM-1 at concentrations as low as 500 fM.[47] A subsequent study in 2007 developed a bioluminogenic BLase substrate,

Bluco, for imaging of BLase expression in cells co-transfected with firefly luciferase (fLuc) (**Figure 10**).[59] Bioluminescence is superior to fluorescent probes *in vivo*, due to enhanced tissue penetration and no requirement for fluorescence excitation. This new strategy was successfully applied to image TEM-1/fLuc-transfected COS7 cells in a live mouse model following intravenous Bluco administration.[59] Similar, simple fluorophore-releasing probes have been employed for a number of applications, including monitoring of *S. aureus* with a near-infrared hemicyanine fluorophore, as well as fluorogenic substrates of metallo-BLases and TEM-1.[90-92]

1.3.2 Imaging Applications: Visualizing Mycobacteria *In Vivo*

Initially, BLase-based imaging approaches were used for observing gene expression in transfected cells, as described in the previous section and in early reviews on the field.[28, 48, 84, 89] However, more recent approaches have applied this technology to study bacteria with inherent BLase expression, such as *Mtb*. As described previously, the mycobacterial BLase BlaC is chromosomally encoded and can be exploited for specific diagnosis of the disease; this expression has also been exploited for *in vivo* imaging, both to study the organism itself and to observe infections in real time within patients. The first probes designed with this purpose were near-infrared (NIR) FRET-based reporters developed by Rao *et al*.[93] In an earlier expansion on their initial studies with fluorogenic probes,[47] the authors had reported a FRET-based reporter (CNIR1/2, **Figure 11**) suitable for NIR imaging (λ_{max} = 660 nm) in live cells.[58] NIR and IR reporters employ longer-wavelength light than fluorogenic counterparts, allowing for improved tissue penetration, reduced background due to autofluorescence, and lower cytotoxicity compared to shorter, more energetic wavelengths.[58] Using this probe, the authors had successfully visualized TEM-1-expressing transfected C6 glioma cells; unfortunately, the bulky FRET fluorophore-quencher groups inhibited cell penetration, necessitating high probe concentrations and functionalization

with $_D$-glucosamine.[58] In a subsequent study, the authors successfully applied this technology to achieve the first reported small molecule probe for *in vivo* imaging of an infectious disease.[93] Probes with minor modifications to the CNIR fluorophore and quencher were synthesized (CNIR5-10, **Figure 11**), and successfully achieved fluorescent labelling of *Mtb in vitro* with high sensitivity (LoD = 6 ± 2 x 10^2 CFUs). The most sensitive probe, CNIR5, also successfully labelled bacteria engulfed in activated macrophages; this model more accurately simulates an *in vivo* TB infection, in which bacteria are engulfed in macrophages within complex granulomas, necessitating probes capable of penetrating eukaryotic cell membranes.[94-95] The CNIR probes were subsequently evaluated in a murine TB model, and pulmonary infections were observed 24 and 48 h after IV probe administration via 3D-fluorescence-mediated molecular tomography (FMT). As few as 10^4 CFUs were successfully imaged in the lungs of infected mice; treatment of infected mice with first-line antituberculars isonizaid and rifampicin resulted in infection reduction that was observable by FMT, demonstrating the utility of this technology in monitoring a therapeutic response *in vivo*.[93, 96] Several years later, the authors reported an improved probe, CNIR800, featuring a longer wavelength IRDye 800CW fluorophore, further increasing signal-to-noise and sensitivity.[63] CNIR800 reduces the LoD to approximately 100 CFUs *in vitro* and less than 1000 CFUs in an *in vivo* murine pulmonary infection model, achieves maximum fluorescence within 6h after administration, and also achieves detection of non-pulmonary infections within deep tissue.[63] A follow-up study employing intravital fiber-optic excitation, which provides better tissue penetration than conventional FMT, further decreased the *in vivo* LoD to 100 CFUs, providing the most substantive evidence yet for the promise of NIR probes for rapid detection and monitoring of *Mtb* infections.[97]

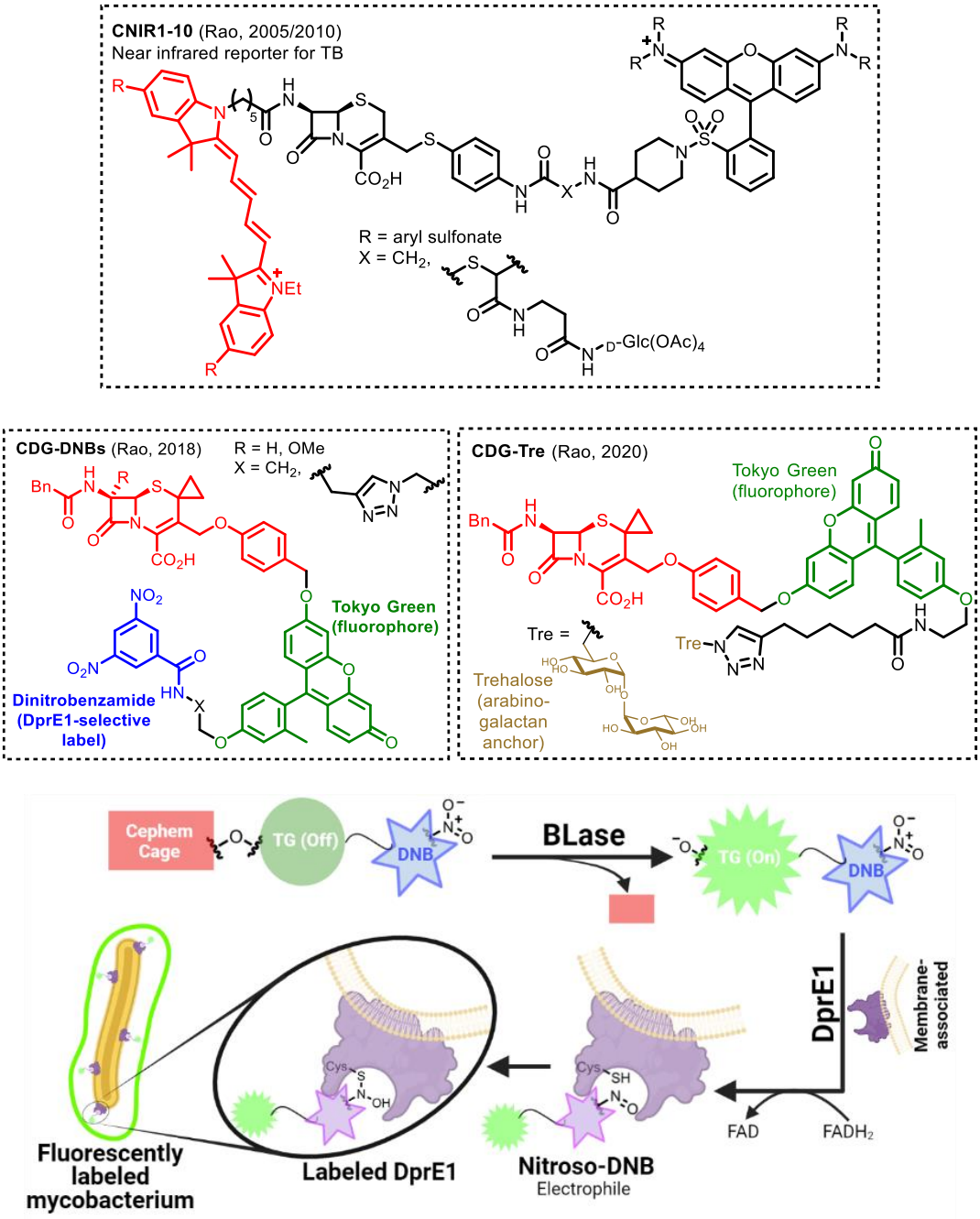

Figure 11. Fluorescent Probes for *In Vivo* Labeling and Imaging of *Mtb*. Created with BioRender.com.

In another elaboration of their previous work, Rao and coworkers have also recently developed fluorogenic probes with Tokyo Green dyes that achieve single-cell labelling of mycobacteria.[56, 62-63, 98] These probes contain both a BLase-sensitive cephem trigger and an anchoring moiety capable of selective, irreversible labelling of a mycobacterial protein (CDG-DNBs, **Figure 11**). This warhead is derived from dinitrobenzamides (DNBs), one of two classes of aryl nitro-containing antimycobacterials currently in clinical trials.[99-103] These molecules are suicide inhibitors of DprE1, a flavin-dependent oxidoreductase essential for synthesis of arabinans, structural components of the complex mycobacterial cell wall. DprE1 binds and reduces the inhibitor, forming an electrophilic nitroso group, which reacts with a cysteine electrophile present near the enzyme active site.[101] This mechanism achieves irreversible inhibition of DprE1, but the authors envisioned that this binding could also be employed as a selection mechanism in the design of mycobacterial reporters. The probes created by Rao *et al* are initially activated via BLase activity, like previous approaches explored in this review, as the Tokyo Green fluorophore lacks fluorescence without a free phenol; however, the addition of a mycobacteria-specific anchoring moiety attaches the fluorescent probe to the cell membrane, conferring an additional layer of selectivity over other BLase-expressing bacteria, which do not retain fluorescence following washing (**Figure 11**).[98] Addition of a 7-α methoxy substituent, as developed previously for TB diagnostics, conferred selective labelling of *Mtb* over other mycobacteria.[56] This new probe technology achieved sensitive, stable labeling of single cells, applicable for flow cytometry/ cell counting experiments, viability assays, and sputum diagnostics.[98] A related application of this dual targeting anchor approach was more recently explored by the authors, employing a trehalose disaccharide as the secondary targeting moiety (**Figure 11**, CDG-Tre).[104] The trehalose anchor is conjugated to a Tokyo Green fluorophore masked by a cephalosporin promoiety, similar to a

previous approach employing tagged trehalose probes for *Mtb* detection in sputum samples.[105] BLase cleavage releases the conjugate, turning on fluorescence (as with CDG-DNB); the fluorescently tagged trehalose is then incorporated by Ag85 enzymes into arabinogalactans. The end result is highly selective and extremely stable fluorescent labelling of the mycobacterial envelope. An added benefit of the trehalose-BL combination was improved labelling of macrophage-engulfed mycobacteria, compared to fluorescent trehalose probes and the previously described CDG-DNB3; the disaccharide group appears to improve membrane permeability, and the addition of a second selection mechanism (the cephalosporin promoiety) enabled use of lower probe concentrations, reducing cytotoxicity.[104]

1.3.3 Other recent imaging applications of BLase-enabled probes

Following on the early advances reported by Tsien and others, several groups have more recently explored chemical biology applications of BLase-sensitive probes. One particularly promising approach is the fluorescent labeling of proteins of interest, using covalent labeling technologies such as HaloTag.[106] The Kikuchi group has developed a similar strategy, described as "BL-tag", using a FRET-based cephalosporin probe to achieve selective, "no wash" fluorescent labeling of fusion proteins containing a TEM-1 domain with an E166N mutation, which prevents deacylation and turnover of the probe.[107] Their coumarin-DABCYL reporter (CCD, **Table 1**) selectively labelled HEK293T cells expressing a ^{E166N}TEM-EGFR fusion protein, providing a powerful proof of concept for this technology; several follow-up studies highlighted other potential applications of this BL-tag technology in protein labeling and imaging experiments.[108-110] However, despite the authors' initial goals, a wash step was still required during sample preparation, due to slow turn-on fluorescence response and nonspecific probe accumulation in cell membranes. Fortunately, the authors were able to improve upon this technology in a subsequent report

describing novel FRET-based cephalosporin probes.[111] Replacement of the hydrophobic DABCYL quencher with an azopyridine resolved two limitations demonstrated in the initial probe design. First, the charged pyridinium linker reduced probe lipophilicity, limiting nonspecific accumulation due to hydrophobic interactions. Secondly, the reduced pKa of this linker also furnished faster C-3′ elimination following BLase cleavage, increasing the speed of fluorescence turn on and allowing for application in pulse-chase experiments visualizing rapid protein dynamics.[111] An S-oxidized probe, FCAPO2, was able to label BL-tag-fused cell surface proteins, while a diacetylated analogue, FCAPO2-DA, proved capable of visualizing intracellular proteins such as the nuclei-associating nuclear localization signal (**Table 1**).[111]

In their exploration of this nascent BL-tag technology, the Kikuchi lab also explored a similar system employing a fluoroscein fluorophore and a dinitrobenzene quencher (FCDNB, **Table 1**).[112-113] Unlike the previous FRET-based probes, this construct achieves fluorescence quenching through nonspecific π-stacking interactions between the electron-poor quencher and electron-rich fluorophore. This simplified quenching paradigm avoids the difficulties associated with selecting a suitable FRET donor-acceptor pair that retains acceptable membrane permeability and pharmacokinetic parameters.[112] Modification of the ethylene glycol linkage to the dinitrobenzene moiety allowed for optimization of fluorescence quenching. FCDNB successfully labeled HEK293T cells expressing TEM-EGFR fusion proteins but displayed a relatively slow fluorescence on rate. Fluorescence turn on was significantly faster for WT TEM-1 than the E166N mutant, suggesting spontaneous elimination of the DNB quencher was slower from the acyl-enzyme intermediate than the hydrolyzed probe.[112] Subsequent studies seeking to create a quencher linkage with improved elimination kinetics led to the discovery of a new DNB-based quencher (CC3DNB, **Table 1**) operating through a photoinduced electron transfer (PET) mechanism

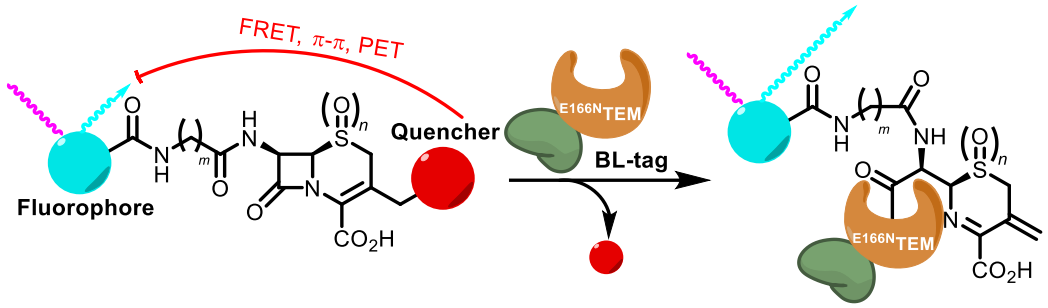

Table 1. Cephalosporin Fluorophore-Quencher Probes for BL-Tag Applications.

Probe Name	*Fluorophore*	*Quencher*	*m*	*n*	*Comment*	*Ref.*
CCD	Coumarin	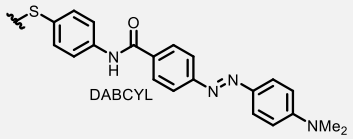 DABCYL	1	0	FRET quencher; poor release kinetics	Mizukami 2009
FCAPO2/ -DA	Fluorescein/ Diacetylfluorescein	 Azopyridinium	2	1	Pyridinium improves elimination rate and membrane penetration	Mizukami 2012
FCDNB	Fluorescein	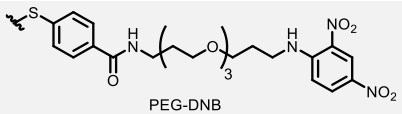 PEG-DNB	1	0	Non-FRET quencher; slow elimination	Sadhu 2010
CC3DNB	Coumarin	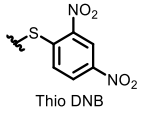 Thio DNB	1	0	PET quencher; reduced pKa improves release kinetics	Sadhu 2012

in which an electron-rich, fluorescently excited fluorophore donates to an electron-deficient acceptor, achieving non-radiative dissipation of this excited-state energy.[111, 114] This alternative quenching mechanism, which requires close association of the quencher and fluorophore, as well as the reduced pKa of the thio-DNB leaving group, results in significantly faster quencher elimination and fluorescence turn-on, overcoming the limitations noted with the previous generation probe.[111]

Another recent imaging application of a cephalosporin-based FRET probe was reported by Shao and Xing, featuring a bulky Ru(II)$(bpy)_3^{2+}$ complex as the fluorophore paired with a DABCYL-derived BHQ3 quencher (BLRu, **Table 2**).[115] The use of a transition metal complex fluorophore presents several advantages, including long emission lifetimes, broad absorption range into near-infrared wavelengths and, critically, the ability to catalyze production of reactive oxygen species (ROS) such as singlet oxygen upon white light irradiation. ROS cause damage to biomolecules and are highly cytotoxic, but are not produced while the Ru complex is stabilized by its FRET acceptor; the authors proposed BLRu as both a BLase-activated imaging agent and a selectively active antibiotic for BL-resistant organisms, depending upon the from of radiation applied. As evidence of this paradigm, the authors were able to achieve selective labeling of BLase-expressing organisms upon fluorescent excitation, and potent killing (MIC_{90} <1 μM) of these species upon white light irradiation.[115] The Xing group has published several other recent reports of BLase-selective imaging agents. Their 2013 report described a FRET-based probe with a self-immolating linker, which rearranges following C-3′ elimination from the cephalosporin backbone to release the FRET quencher and form a reactive quinone-methide electrophile capable of further reactions with cellular nucleophiles (LRBL1-3, **Table 2**); this secondary activation step achieves

not only BLase-triggered fluorescence turn-on but also covalent labelling of the resistant organism, achieving greater sensitivity and enabling identification and counting of single BLase-expressing cells.[116] Another probe (ERM-1, **Table 2**) makes use of a tetraphenylethylene (TPE) fluorophore for imaging of biofilms *in vitro*. Biofilms are a common feature among resistant organisms, and conventional fluorogenic probes in this densely populated microenvironment suffer from fluorescence quenching due to dye aggregation (ACQ).[117] Conversely, TPE demonstrates aggregation-induced emission (AIE), allowing for robust fluorescence at high local concentrations. Introduction of a bulky 7-methoxyimino group, as employed in later generation cephalosporins, conferred selectivity to the broader spectrum BLases commonly found in resistant colonies, such as AmpC.[117] The Xing group's most recent publication in this field employs another FRET-based probe (DFD-1, **Table 2**) that, like LRBL, also achieves covalent labelling for single-cell imaging and flow cytometry-enabled sorting. In this case, a more selective labeling mechanism is employed: cells are preincubated with fatty acids containing a terminal azide moiety. This group participates in a strain-promoted 1,3-cycloaddition (SPAAC, a "click" reaction) with a dibenzylcyclooctyne (DBCO) sidechain connected to the cephalosporin backbone. Following attachment to the cell surface, fluorescence is not activated unless BLase cleavage eliminates the C-3′ quencher; additionally, like the previous generation probe, placement of the fluorophore and bulky DBCO group at the N7 position prevent hydrolysis by class A BLases, providing a more selective probe for visualization of highly BL-resistant organisms such as *P. aeruginosa* and *Enterobacter cloacae*.[118]

Table 2. Cephalosporin Imaging Probes Developed by Xing *et al.*

Probe Name	*Structure*	*Fluorophore* 	*Quencher* 	*Comment*	*Ref.*
BLRu	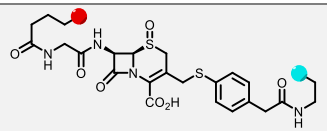	$Ru(II)(bpy)_3^{2+}$	BHQ3	Also produces ROS upon white light irradiation; applications as selective antibiotic	Shao 2012
LRBL1-3	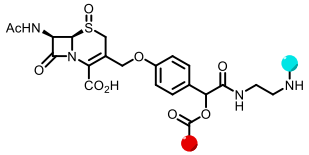	FITC / Cy3 / Cy5.5	DABCYL / BHQ2 / BHQ3	*p*-Hydroxybenzylic ester linker spontaneously degrades to quinone-methide nucleophilic trap for covalent labeling of proteins	Shao 2013
ERM-1	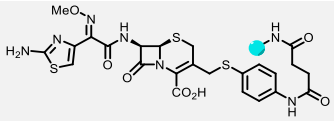	TRP	None (non-FRET)	Optimized for imaging in biofilms; fluorescence is enhanced following aggregation at high local concentrations	Aw 2017
DFD-1	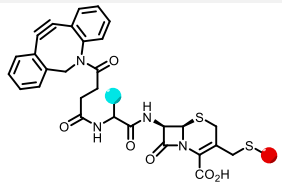	FITC	DABCYL	Click chemistry-enabled covalent labeling of cells; cephalosporin-ase expression activates fluorescence	Chan 2018

1.4 Antibiotics: Lactam Conjugates as Pro- and Co-Drugs

BLase-mediated fragmentation has been widely exploited for applications in diagnostics and imaging of resistant organisms. In tandem with these studies, researchers have also undertaken substantial effort to use this phenomenon for targeting of antibiotic-resistant organisms. In the early 1970s, O'Callaghan and colleagues published early reports characterizing enzymatic release of C-3′ leaving groups from cephaloridine and the 3′-azido cephalosporin BTCA, and investigating nitrocefin as a chromogenic BLase reporter. Soon after, the researchers described a strategy for using this release mechanism as a delivery vehicle for a cytotoxic warhead, in order to selectively target BL-resistant bacteria.[19, 37, 119] A known antiseptic small molecule, 2-mercaptopyridine-N-oxide (pyrithione), was installed at the 3′ position of a cephalosporin and evaluated against a variety of bacteria, including BL-resistant strains. The conjugate displayed similar activity to a first-generation cephalosporin, cephalothin, in BL-susceptible strains, such as MSSA, but was significantly more active against BLase-expressing organisms such as *Enterobacter cloacae* (class C, AmpC) and *Klebsiella oxytoca* (class A, OXY-1/2).[119] Subsequent experiments demonstrated that this cephalosporin conjugate, MCO, released pyrithione upon exposure to BLase, and retained antibacterial activity *in vitro* even after prior digestion by purified BLase. Additionally, MCO displayed greater activity against organisms lacking BLase expression, suggesting the conjugate could also act as a typical PBP inhibitor and was likely exerting a codrug effect.[119] Despite the authors' ultimate conclusions that MCO lacked therapeutic utility due to likely off-target toxicity associated with the pyrithione warhead, this proof of concept study established a novel paradigm for combating antibiotic resistance. In the subsequent decades, dozens of BL conjugates were reported with exciting activity against a variety of organisms. Many of these approaches involved codrugs featuring other classes of antibiotics, such as quinolones and glycopeptides, conjugated to

a cephalosporin scaffold;[119-128] several groups also examined conjugates with other BL scaffolds capable of BLase-mediated fragmentation, including penems and carbapenems.[129-131] Ultimately, cephalosporins appeared most effective for these applications, providing a combination of conjugate stability, spectrum of BLase susceptibility, and synthetic accessibility.[131] Early reports in this field have been reviewed previously;[28, 132] this chapter will focus on more recent advances in the field, summarizing several interesting reports within a few specific sub-classes.

1.4.1 Subclass: Nitric oxide donors

One recent group of antibacterial prodrugs with demonstrated success against resistant organisms have been nitric oxide (NO) donors, which selectively deliver reactive NO species to the site of infection. NO and its reactive byproducts damage a variety of cellular targets, such as DNA, metabolic enzymes, and membrane components; this pleiotropic and non-selective bioactivity essentially eliminates the possibility for resistance development.[133-134] In addition, NO has shown enhanced inhibition of biofilm formation, a powerful resistance mechanism that can reduce antibiotic efficacy by several orders of magnitude.[135] Biofilm formation and dispersal rely upon sensitive quorum sensing pathways in bacterial communities, which are sensitive to external stimuli such as NO levels and can be disrupted by exogenous NO delivery (**Figure 12A**).[134, 136-137] As a result, this therapeutic class represents a promising target for biofilm-reliant infections, such as *P. aeruginosa* respiratory infections in cystic fibrosis (CF) patients. NO is unfortunately not suitable for therapeutic use, due to its non-specific cytotoxicity and gaseous state. As a result, a number of NO-prodrug strategies have been developed and reviewed previously employing a variety of delivery vehicles, such as polymers,[138] small molecule pro-forms,[134] lipids,[139] or a combination of these strategies.[140] Delivery with a NO-BL prodrug is a particularly attractive strategy for biofilm elimination in organisms with BLases, such as *P. aeruginosa*, which expresses

an inducible, chromosomally-encoded class C BLase, PDC, frequently alongside plasmid-derived serine BLases such as TEM-1.[141]

This prodrug strategy was first investigated by Tang *et al* as a more general delivery vehicle for NO, which at the time had demonstrated antibacterial activity but had not yet been linked to biofilm formation.[142] The group designed two cephalosporins featuring 3′ NO donors— an aryl diazeniumdiolate conjugate, and a sydnonimine conjugate with a carbamate linker (**Figure 12B**). Synthetic difficulties prevented isolation of A, including a proposed radical-mediated nitro rearrangement, but conjugate B was successfully synthesized and demonstrated NO release upon BLase exposure.[142] Despite this successful synthesis, no biological results were reported for this conjugate, suggesting limitations were observed in subsequent experiments. Nearly a decade passed before another cephalosporin-NO donor conjugate (DEA-C3D, **Figure 12B**) was reported, this time by the Kelso and colleagues. This initial publication described a straightforward cephalosporin-N-diazeniumdiolate conjugate, which directly releases the unstable NO donor upon BLase cleavage.[143] The authors' background in biofilms research led to the explicit design of this conjugate as an antibiotic for *P. aeruginosa* and other biofilm-based infections. Amperometric assays confirmed production of NO upon BLase-mediated fragmentation; *in vitro* assays confirmed dose-dependent dispersal of *P. aeruginosa* biofilms, including moderate potentiation of conventional antibiotics. Pretreatment of bacteria with ampicillin also increased NO production, suggesting conjugate turnover was dependent upon induction of the chromosomally-encoded PDC BLase.[143] This study served as proof of concept for a novel NO prodrug strategy featuring a bacteria-selective release mechanism, a significant advantage over previous delivery vehicles. A subsequent report by this group proposed a similar prodrug (PYRRO-C3D, **Figure 12B**) employing pyrrolidine-N-diazeniumdiolate as the NO donor. PYRRO-C3D was investigated against

nontypeable *Haemophilus influenzae* (NTHI), a pathogen implicated in complications of pulmonary disorders such as COPD and CF.[144] Interestingly, the authors noted that PYRRO-C3D was moderately effective (MIC_{90} = 100 μM) against planktonic (non-biofilmed) NTHI but lacked activity against NTHI biofilms, including no observable biofilm dispersal. However, co-treatment with azithromycin demonstrated modest reductions in both biofilm size and cell viability; addition of an NO scavenger eliminated this synergy, suggesting NO release contributed to this observation. Subsequent assays in BLase-expressing and BLase-negative isolates showed significantly enhanced synergy against the PDC-producing organisms, providing further evidence for the proposed BLase-dependent NO release mechanism.[144] A subsequent study with PYRRO-C3D also demonstrated NO release and antibacterial efficacy in *Streptococcus pneumoniae*, a biofilm-producing organism that lacks BLases. The authors proposed the conjugate might serve as a dual-acting antibiotic in this context, inhibiting cell wall synthesis through labeling of PBPs/ transpeptidases while also subsequently releasing cytotoxic NO species (due to on-target cleavage of the BL bond); however, further experiments suggested the bioactivity was due to BL-derived inhibition of cell wall synthesis alone.[145] Finally, a recent follow-up study with DEA-C3D demonstrated successful dispersion of biofilms from multiple *P. aeruginosa* clinical isolates, activity that was further confirmed via fluorescent microscopy following SYTO9 staining.[146] DEA-C3D also demonstrated excellent synergy with antipseudomonals, nearly eliminating *P. aeruginosa* biofilms when used in combination with colistin.[147] These studies highlight the promise of BL conjugates for selective delivery of non-selective and potentially toxic molecular payloads, enabling application of powerful antibacterials without off-target effects.

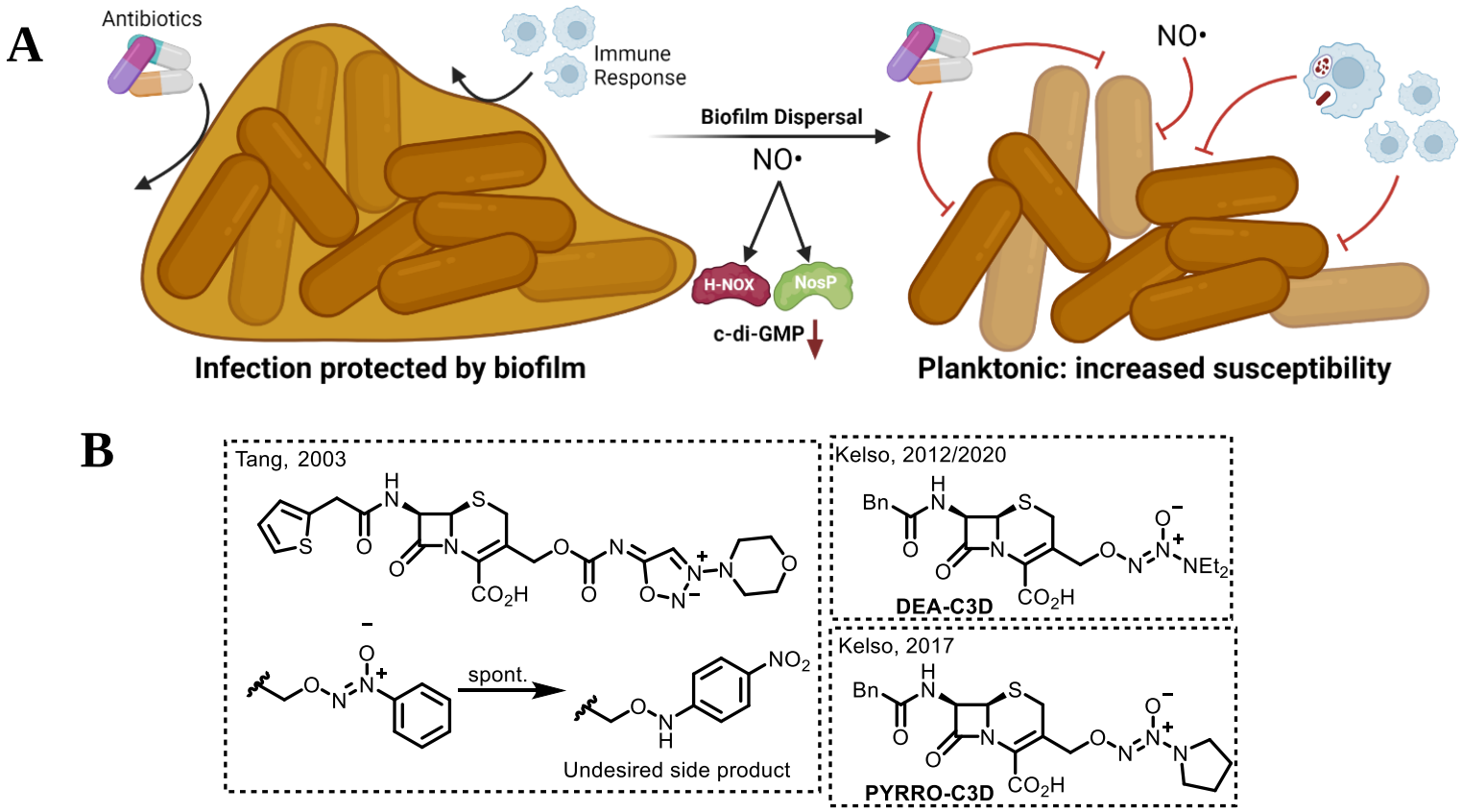

Figure 12. Cephalosporin-NO Donors for Targeted Biofilm Dispersal. **A.** NO-mediated biofilm dispersal restores susceptibility to therapeutics and host immune response. NO-sensitive signaling proteins stimulate cyclic di-GMP (c-di-GMP) hydrolysis and subsequent dispersal. Created with BioRender.com. **B.** BLase-activated cephalosporin NO prodrugs.

1.4.2 Subclass: β-Lactamase Inhibitors

Since the discovery of the earliest pencillinases in the 1940s, researchers have sought strategies to circumvent this resistance mechanism. Initially, the primary approach to avoiding BLase activity was the identification and application of novel BLs with reduced susceptibility to these enzymes, incorporating different ring structures and side chain modifications to prevent BLase binding or slow enzymatic hydrolysis. More recently, a different practice has proven successful at targeting these resistant organisms—co-therapy combining conventional BL antibiotics with BLase inhibitors (BLIs). The first of these, clavulanic acid, was identified in the late 1970s from *Streptomyces clavuligerus* cultures.[148] Subsequent studies identified the compound as a mechanism-based inhibitor capable of covalently inactivating serine BLases. Several synthetic penicillinate sulfone BLIs, sulbactam and tazobactam, were quickly developed a few years later.[149-150] Following the early discovery of these inhibitors, and their successful application in co-therapy with BL antibiotics, an entire field of BLI discovery has produced hundreds of putative therapeutics, including BL-based inhibitors (penicillin/cephalosporin sulfones, monobactams, methylidene penems, oxapenems) and more recently non-BL inactivators (boronic acids, phosphonates, diazabicycloctanes (DBOs)).[151-152] This field has been reviewed extensively in the literature, including historical perspectives as well as recent developments.[12, 151-155] This section will focus on recent explorations of BLase-mediated fragmentation for the development of novel BLIs, including conjugates targeting Ambler class B enzymes (MBLs).

The earliest example of an approach combining a BLI with a BL delivery vehicle was reported in 2002 by Hakimelahi and colleagues. Inspired by previous approaches using “dual action cephems,” the authors proposed a strategy conjugating a conventional BL antibiotic, amoxicillin, to a BL-derived BLI, such as clavulanic acid or 7-phenoxyacetamido-1-oxo-cephalosporin.[156]

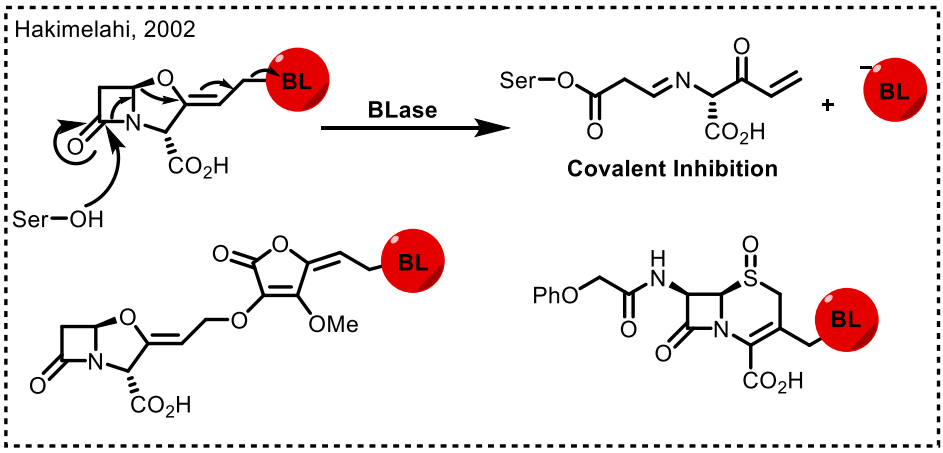

Figure 13. Early BL-BLI Conjugates from Hakimelahi *et al.* (2002).

BLase attack of the inhibitor moiety would yield covalent inhibition of the enzyme, with subsequent release of the amoxicillin warhead, which could evade enzymatic degradation and go on to successfully block cell wall synthesis. The cephalosporin-derived conjugates employed a traditional C-3′ release mechanism, while the clavulanic acid conjugates used allyl ether and butenolide linkers, which take advantage of an oxapenem ring-opening mechanism that occurs spontaneously following BLase acylation (**Figure 13**). Both the clavulanic acid and cephalosporin conjugates displayed dual-target activity, achieving BL inhibition comparable to clavulanic acid and potent antibacterial activity against a panel of BLase-expressing organisms, even surpassing amoxicillin-clavulanic acid combination therapy *in vitro*.[156]

Despite this promising early report, as well as a 2004 mechanistic study by Mercuri *et al* suggesting C-3′ elimination from conventional cephalosporins furnished covalent inhibition of BLase mutants,[157] further exploration of BL prodrugs as BLIs was not reported until over 15 years later, when Jackson and colleagues investigated this strategy for development of novel MBL inhibitors.[158] Despite the clinical success of Augmentin (amoxicillin + clavulanic acid), Zosyn (piperacillin + tazobactam), and other BL-BLI co-therapies against organisms expressing Ambler

class A, C, and D BLases, no inhibitors have been approved for use against the class B MBLs.[151, 158] Unlike these other classes, which rely upon a nucleophilic serine residue that can be covalently inactivated by deacylation-resistant electrophiles, MBLs achieve hydrolysis through a nucleophilic water molecule, activated through interactions with one or two zinc ions. This lack of a distinct target residue, combined with broad structural diversity and similarity to eukaryotic proteins, poses a unique challenge for inhibitor design.[153, 159] Jackson *et al* sought to address this challenge by designing a cephalosporin-chelator conjugate, which upon BLase cleavage releases a metal-binding pyrithione moiety capable of interfering with the active site zinc ions of MBLs such as NDM-1.[158] A number of putative MBL inhibitors contain metal-binding pharmacophores; unfortunately, such molecules typically lack selectivity and interfere with a wide variety of eukaryotic enzymes as well, causing off-target toxicity.[153] As noted for many of the other approaches in this review, caging this chelator in a cephalosporin prodrug provides a selectivity mechanism, ensuring the toxic warhead is released only at the site of BLase activity. This conjugate (PcephPT, **Table 3**) displayed low micromolar NDM-1 inhibition and successfully re-sensitized NDM-1-expressing *E. coli* to meropenem. Mechanistic studies suggested the conjugate inhibits the enzyme through formation of a ternary complex within the active site; further activity assays showed PcephPT monotherapy was also antibacterial, suggesting the pyrithione warhead exerts additional biological effects beyond MBL inhibition.[158]

Following this initial study, two more recent reports have further demonstrated the promise of this approach in MBL inhibitor design. Van Haren and colleagues described another series of cephalosporin conjugates (CS-TQ and CS-DPA, **Table 3**) featuring metal-binding warheads 8-thioquinoline (TQ) and dipicolinic acid (DPA). Both series of conjugates demonstrated potent inhibition of NDM-1 but had more varied activity against other MBLs, including VIM-2, IMP-1,

and IMP-28.[160] Stability assays indicated the ester linkage present in the DPA conjugates was unstable, but the thiol-linked TQ conjugates displayed good aqueous stability and were evaluated against a panel of MBL-expressing strains. CS-TQ-6 strongly potentiated the activity of meropenem against resistant *K. pneumoniae* and *E. coli* strains, but failed to re-sensitize *P. aeruginosa* strains, a feature the authors attribute to this organism's relatively impermeable outer membrane.[160] Another recent study described cephalosporin-thiol conjugates (CS-TH, **Table 3**) as potent inhibitors of IMP-type MBLs.[161] Initially, the authors designed these inhibitors in the same vein as the previous examples: a known metal-binding inhibitor conjugated to a cephalosporin promoiety, which would release upon cleavage to deliver the chelator to the enzyme active site. Featuring simple thiol acids the authors previously identified as synergistic with carbapenems against MBL-expressing organisms,[162] the conjugates achieved sub-micromolar inhibition of IMP-28, with more modest activity observed against other MBLs. Interestingly, mechanistic studies suggested the thiol acid was not released upon BL cleavage, but instead the thiazine ring undergoes Δ3-Δ4 tautomerization to yield a relatively stable hydrolysis product.[161] Coincidentally, this mechanism resembles the inhibition of serine BLases by imipenem, whereby the Δ1-pyrroline tautomer formed is significantly more stable to deacylation (which is not relevant for MBLs).[152] Follow-up experiments confirmed hydrolyzed conjugates retained inhibitory activity and were capable of binding zinc with low-micromolar affinities; docking studies predicted that both the C4 carboxylate and the carboxylate of the hydrolyzed BL ring are important for zinc binding.[161] Though this inhibitor ultimately does not rely on the fragmentation mechanism explored in this chapter, this study nonetheless provides an additional example of how this approach can lead to discoveries that are both scientifically interesting and therapeutically relevant.

Table 3. MBL Inhibitors Employing Selectively Released Chelators.

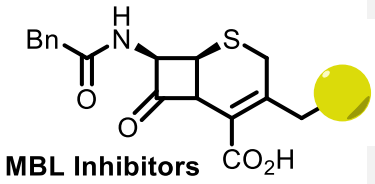

Inhibitor	*Chelator*	*Comment*	*Ref.*
PcephPT	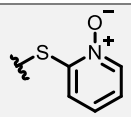	Also inhibits bacterial growth; similar to several previous approaches	Jackson, 2020
CS-TQ	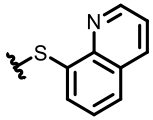	Favorable stability profile; re-sensitize MBL-expressing organisms to meropenem	Van Haren, 2021
CS-DPA	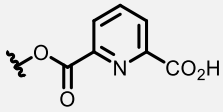	Poor aqueous stability improved through oxidation of thiazine sulfur	Van Haren, 2021
CS-TH	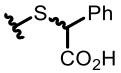	Thiol is not released following cleavage; thiazine undergoes Δ3-Δ4 tautomerization	Tehrani, 2021

1.4.3 Other Recent Applications

This section will focus on highlighting a number of other interesting recent applications of BLase-mediated fragmentation in antibiotic design. One intriguing report has been previously described in this review for its application as a photoactivated reporter of BLase activity (β-LEAF, **Figure 5**).[53-54] Hasan and coworkers had originally developed this technology as a light-activated antibiotic, employing an earlier conjugate design (β-LEAP, **Figure 14**) containing dual EtNBS photosensitizers. In the uncleaved conjugate, the moieties silence one another through static quenching, which requires close proximity; following BLase cleavage and release of the C-3′ photosensitizer, quenching is lost and, upon photoactivation, each forms active molecular species toxic to cells.[163] β-LEAP demonstrated selectivity for BL-resistant organisms, killing several MRSA strains with low toxicity towards both eukaryotic cells and MSSA. This specificity for only BLase-expressing organisms likely motivated the group to further pursue this approach as a diagnostic tool with β-LEAF. A follow up *in vivo* study demonstrated promising results as well, providing useful proof of concept for photosensitizers as warheads in a cephalosporin prodrug approach.[164]

A more recent application reported by the Miller lab described a cephalosporin-oxazolidinone conjugate featuring a novel N7 siderophore group for improved delivery to Gram negative organisms.[165] Siderophores are iron-sequestering molecules produced by bacteria to scavenge scarce iron from their microenvironment. Membrane transporters recognize these siderophore-iron complexes and furnish delivery into the cell. This siderophore-specific delivery mechanism has been exploited via a "Trojan Horse" approach, whereby the siderophore is conjugated to a cytotoxic warhead; first observed in natural antibiotics produced by *Actinomyces* and *Streptomyces,* this strategy has more recently been applied for the development of synthetic

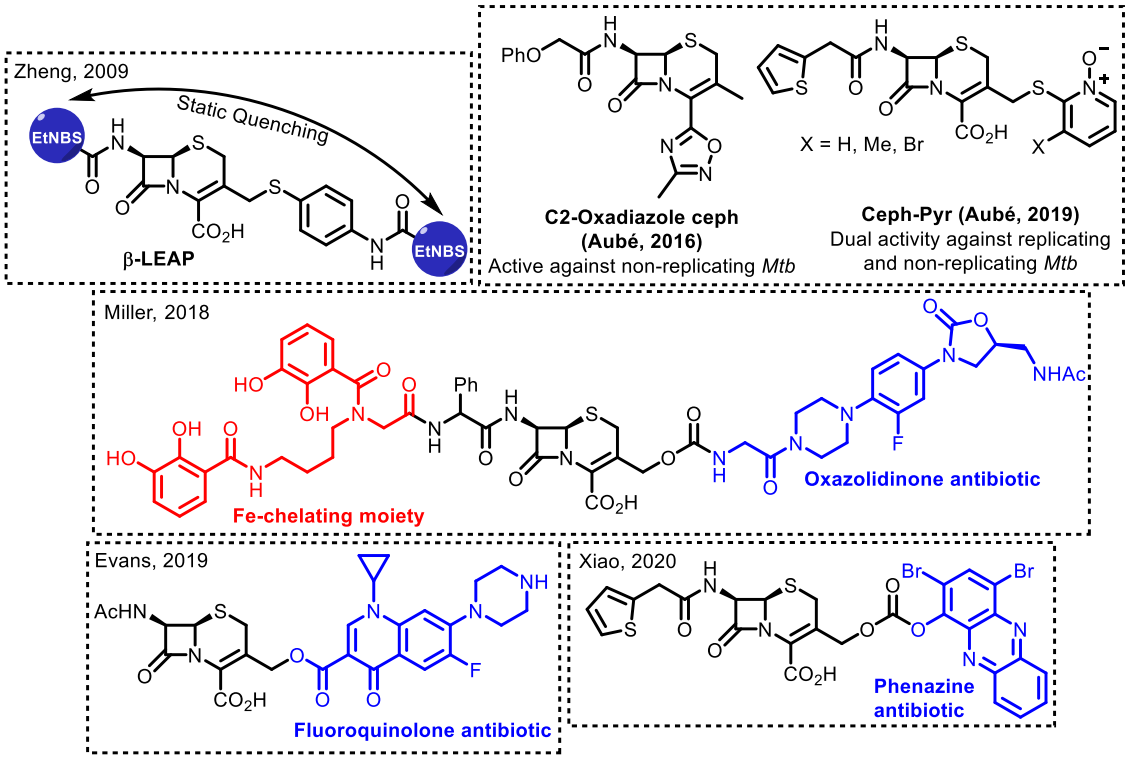

Figure 14. Recent Cephalosporin-Antibiotic Conjugates Employing BLase-Mediated Fragmentation.

siderophore-antibiotic conjugates with a wide variety of antibacterial warheads (as recently reviewed by Negash *et al* and Kong *et al*).[166-171] This strategy has also previously been exploited for the design of novel BL antibiotics, including the recently FDA-approved cefiderocol (Fetroja), which possesses an excellent spectrum of activity against highly resistant strains.[172-175] Liu *et al* combined this strategy with BLase-mediated fragmentation to create a novel siderophore-cephalosporin-antibiotic hybrid. The Miller group had previously developed cephalosporin-oxazolidione conjugates, which demonstrated intriguing antibacterial activity and robust stability.[176] The researchers endeavored to combine this approach with their previous work developing siderophore-carbacephalosporin conjugates, leading to the synthesis of a novel "triple warhead" cephalosporin (**Figure 14**).[165, 177-178] The conjugate demonstrated excellent, broad-spectrum activity against a panel of *A. baumannii* and *P. aeruginosa* strains resistant to not only BLs but also oxazolidinones, which are typically ineffective against Gram negative organisms due to their inability to cross the outer membrane. The siderophore side chain provides an intracellular delivery mechanism that bypasses this defense, while the cephalosporin promoiety enables subsequent BLase-mediated release of the oxazolidinone, which remains inactive while attached to the siderophore group.[165]

A few recent applications of this strategy have been employed for targeting of *Mtb*, which expresses a chromosomally-encoded BLase and traditionally lacks susceptibility to BL antibiotics (as described previously in the Diagnostics section of this review). A report by Pereira *et al* detailed peptide-methotrexate conjugates employing a BLase-sensitive cephalosporin linker (dpMtx-ceph-E_5) for selective targeting of macrophage-engulfed *Mtb*.[179] Methotrexate (Mtx) is a potent inhibitor of dihydrofolate reductase (DHFR), an essential enzyme involved in the production of folate cofactors and one-carbon metabolism. While DHFR inhibition has shown promise previously as an

antitubercular strategy, several limitations impede clinical use of Mtx, including poor mycobacterial envelope permeability and the presence of DHFR in eukaryotic cells.[179-180] Pereira and coworkers resolved to overcome this limitation by conjugating Mtx to a cationic, hydrophobic delivery peptide, which improves penetration into mycobacteria and, in eukaryotic cells, prevents access to mitochondrially-associated DHFR. However, this charged peptide would unfortunately limit penetration into phagosomes, the home of *Mtb* infection *in vivo*; thus, the researchers paired the cationic delivery peptide with an anionic masking peptide, neutralizing the overall molecular charge and improving membrane permeability. Mycobacteria-selective delivery is further enhanced through the use of a cephalosporin linker connecting the delivery and masking peptides: once inside the phagosome, secreted or envelope-associated mycobacterial BLase cleaves the linker and releases the C-3′ dpMtx moiety. The delivery peptide then enables penetration through the mycolic acid barrier, allowing the Mtx warhead to reach its intracellular target. dpMtx-ceph-E_5 was effective at clearing engulfed *M. smegmatis* after 72 hours with little cytotoxicity to macrophages observed; subsequent imaging experiments with TAMRA-labelled conjugate confirmed localization to mycobacteria following intramacrophage delivery and BLase cleavage.[179] Another recent approach targeting mycobacterial infections has been described by Aubé and colleagues. In an earlier work, the authors had identified cephalosporins selectively active against nonreplicating *Mtb* (C2-oxadiazole ceph, **Figure 14**).[181] In search of compounds with greater breadth of activity, the researchers undertook a high-throughput screening campaign with a large library of BLs, identifying dozens of hits active against *Mtb* under both normal (replicating) conditions and in a nonreplicating model. After further screening hits for on-target activity and plasma stability, a handful of lead BLs were identified.[182] Interestingly, several of these were cephalosporins featuring a pyrithione (Pyr) moiety at the C-3′ position (Ceph-Pyr, **Figure 14**), similar to the first- generation

dual action cephalosporin MCO and the recently reported MBL inhibitor PcephPT (**Table 3**).[119, 158] Release assays confirmed Pyr was expelled upon exposure to mycobacterial BlaC, and analogues replacing the thioether and Δ3 double bond with release-incompatible methylene and Δ2 moieties ablated Pyr release, confirming reliance upon BLase-mediated fragmentation. Further biological assays illustrated a few interesting trends. First, studies with Pyr and the cephalosporin promoiety alone suggested that both groups contributed to the observed activity (dual-acting) under replicating conditions, while Pyr alone was active in nonreplicating cells. Next, biochemical studies with a *blaC* knockout strain suggested that BlaC activity was largely (although perhaps not exclusively) responsible for Pyr release. Finally, microbiological evaluation of the *blaC* knockout demonstrated increased susceptibility to the Pyr conjugate against replicating organisms and similar to WT activity under nonreplicating conditions; potentiation of BLs against *Mtb ΔblaC* under actively replicating conditions has been demonstrated previously and is likely due to increased inhibition of PBPs, while the retained activity against nonreplicating *Mtb* (for which PBP inhibition is not toxic) suggests the possibility of an alternative release mechanism independent of BLase or PBP activity.[182-183] These recent reports, as well as a few other recent papers exploring BLase fragmentation with fluoroquinolone and phenazine conjugates, demonstrate the continued promise of this approach in circumventing limitations such as off-target effects or resistance mechanisms to repurpose known antibiotics for new antibacterial applications.[184-185] Many more examples of BL-antibiotic conjugates can be found in several recent reviews on this subject.[186-188]

1.5 Conclusions and Thesis Goals

Since it was first reported in the early 1960s, BLase-mediated fragmentation has expanded from a curious mechanistic observation into an entire field of research. Some of the most lasting innovations came in the form of new diagnostic tools for BLase-expressing organisms, allowing

for the rapid and sensitive identification of antibiotic-resistant organisms with the discovery of nitrocefin, PADAC, and CENTA in the 1970s and ‘80s; the same reactivity exploited by these early chromogenic reporters has now been extrapolated into a great diversity of probes, employing powerful reporter moieties for applications in diagnostics as well as cellular imaging and chemical biology approaches. This paradigm of BLase-specific release has also been harnessed for the development of new pro- and codrugs to combat the growing trend of antibiotic resistance. The proliferation of recent reports employing this technology demonstrates its great therapeutic potential for creating new treatments and repurposing old ones, overcoming therapeutic limitations by imparting an exquisitely selective release mechanism. Inspired by this elegant strategy (and particularly by its recent applications against *Mtb*),[56, 93, 105, 181-182] we sought to create new antituberculars employing BLase-mediated fragmentation. After investigating several warheads, we identified BL conjugates featuring pyrazinoic acid (POA, the active form of first-line TB drug pyrazinamide, PZA) as promising new leads for drug-resistant strains.

This dissertation will describe two projects centered around POA. In **Chapter 2**, we report the design, synthesis, and assessment of new cephem-POA conjugates that circumvent a frequently observed resistance mechanism that threatens the future use of PZA/POA. We find that these conjugates function as codrugs, with both the POA warhead and BL scaffold contributing to the observed antimycobacterial activity; this dual mechanism impedes resistance development and confers activity against strains/ conditions where just one of the therapeutic modalities would be ineffective. In **Chapter 3**, we describe efforts toward a next-generation POA, including design and synthesis of a small library of substituted POA analogues. After identifying new compounds with improved antimycobacterial activity, we employ biochemical techniques to query their mechanism and discover intriguing differences between the activity of the most active lead and POA. Guided

by these findings and recent structural insights into a putative POA target, *Mtb* PanD, we design new analogues that recapitulate this potent inhibition, providing important insights into PanD-POA SAR.

Chapter 2. Cephem-Pyrazinoic Acid Conjugates: Circumventing Resistance in *Mycobacterium tuberculosis*.

Malcolm S. Cole, Michael D. Howe, Joseph A. Buonomo, Sachin Sharma, Elise A. Lamont, Scott I. Brody, Neeraj K. Mishra, Yusuke Minato, Joshua M. Thiede, Anthony D. Baughn, Courtney C. Aldrich

This work was performed in collaboration with Michael D. Howe, Dr. Joseph A. Buonomo, Dr. Sachin Sharma, Dr. Elise A. Lamont, Scott I. Brody, Dr. Neeraj K. Mishra, Dr. Yusuke Minato, Dr. Joshua M. Thiede, Dr. Anthony D. Baughn, Dr. Courtney C. Aldrich, Pooja Hegde, Dr. Bruce A. Witthuhn, Dr. Surendra Dawadi, Eric Hess, Dr. Ryan C. Hunter, and Dr. Ryan A. Langlois.

MSC synthesized all compounds, produced *Mtb* BlaC, developed and performed enzymatic release assays, assisted in kinetics assays and antibacterial evaluation (in *M. bovis* BCG), developed and performed intracellular accumulation assays and pantothenate antagonism assays, and wrote the chapter. MDH (primary) YM, and JMT performed the MIC assays. MDH assisted in the accumulation assays and performed the FoR determination experiments. JAB helped conceive of the project and design conjugate syntheses, synthesized intermediates, and performed the stability assays. SS (primary) and NKM produced BlaC and CTX-M-1, and designed and performed the kinetics experiments. EAL performed the macrophage experiments. SIB performed the MIC assays with nonmycobacterial pathogens. ADB and CCA conceived of

the project and provided significant input and guidance. PH assisted with compound characterization. BAW assisted with LC-MS/MS operation and method development. SD provided support with HPLC purification and LC-MS/MS experiments. EH synthesized intermediates. RCH and RAL provided access to critical lab equipment. All listed authors assisted in writing protocols and contributed to editing of the chapter.

Chapter 2. Cephem-Pyrazinoic Acid Conjugates: Circumventing Resistance in *Mycobacterium tuberculosis*.

Tuberculosis (TB) is a leading source of infectious disease mortality globally. Antibiotic-resistant strains comprise an estimated 10% of new TB cases and present an urgent need for novel therapeutics. β-lactam antibiotics have traditionally been ineffective against *M. tuberculosis* (*Mtb*), the causative agent of TB, due to the organism's inherent expression of β-lactamases that destroy the electrophilic β-lactam warhead; we have developed novel β-lactam conjugates which exploit this inherent β-lactamase activity to achieve selective release of pyrazinoic acid (POA), the active form of a first-line antitubercular. These conjugates are selectively active against Mtb H37Rv, and activity is retained or even potentiated in multiple resistant strains and models. Preliminary mechanistic investigations suggest that both the POA "warhead" as well as the β-lactam "promoiety" contribute to the observed activity, demonstrating a "codrug" strategy with important implications for future TB therapy.

2.1 Introduction

Tuberculosis (TB), caused by *Mycobacterium tuberculosis*, was (until 2020) the leading cause of death by an infectious agent globally, killing 1.5 million in 2018.[189] This distinction exists in spite of the exhaustive efforts of biomedical and pharmaceutical research, which has developed an extremely successful first-line treatment regimen as well as a litany of second- and third-line agents. TB's tenacity is exemplified in the emergence of drug-resistant strains, which accounted for an estimated 500,000 new cases in 2018.[189] This corresponds to approximately 3.4% of all novel cases, but incidence is significantly higher in certain regions; parts of Eastern Europe and Russia have many fewer new cases than harder-hit regions, such as sub-Saharan Africa, but more than

20% of these new infections are by multidrug-resistant (MDR) strains (defined by resistance to two of the first line agents, isoniazid and rifampicin).[189] Drug resistance in TB has shifted the previously successful treatment paradigm: first-line therapy (consisting of combination therapy employing isoniazid, rifampicin, pyrazinamide and ethambutol for the first 8 weeks, then reducing to isoniazid and rifampicin for an additional 18 weeks) is effective in clearing diseases for greater than 85% of drug-susceptible cases, but only 56% for MDR-TB and below 40% for extensively drug-resistant (XDR) strains (defined as MDR-TB with additional resistance to multiple second-line agents).[189] A growing number of second- and third-line agents have been developed for these challenging strains, including Pretomanid, a novel nitroimidazole antitubercular, which was FDA-approved in 2019 for use against MDR-TB in combination therapy with two other second-line agents, bedaquiline and linezolid.[189-190] Despite these options, there remains an urgent therapeutic need to develop novel antituberculars effective against MDR- and XDR-TB in order to combat this rising trend of drug resistance.

Pyrazinamide (PZA) is a first-line antitubercular used under WHO standard treatment guidelines for the first two months of TB therapy. Despite its low activity *in vitro*, PZA is potentiated under stress conditions, such as acidity and oxidative stress; this potentiation allows PZA to efficiently clear *Mtb* from macrophages, the last bastion of infection after the active disease has been controlled.[191-192] This sterilizing activity *in vivo* reduces the required duration of TB treatment from 9 to 6 months.[193-194] Because of its tolerability and unique effects, PZA is arguably the most important therapeutic among the current first-line agents, and also the most likely to be used in future treatment regimens (as demonstrated by its synergy with novel antituberculars such as bedaquiline and pretomanid).[195] Despite its clinical importance, the mechanisms behind PZA action are poorly understood. PZA requires activation within *Mtb* via pyrazinamidase, an enzyme

within the NAD^+ salvage pathway encoded by *pncA*, to the carboxylic acid form pyrazinoic acid (POA). Upon activation, POA appears to interact with the aspartate decarboxylase PanD and inhibit the downstream Coenzyme A (CoA) biosynthetic pathway; recent evidence suggests that POA binding to PanD triggers native protease degradation, in a manner similar to the PROTAC strategy recently developed for eukaryotic cells.[196-199] Additionally, supplementation of attenuated strain *Mtb* mc^{2}7000 with some CoA pathway metabolites downstream of PanD, such as β-alanine and pantotheine, fails to antagonize POA/PZA, suggesting there is more to the mechanistic story left to be discovered.[200]

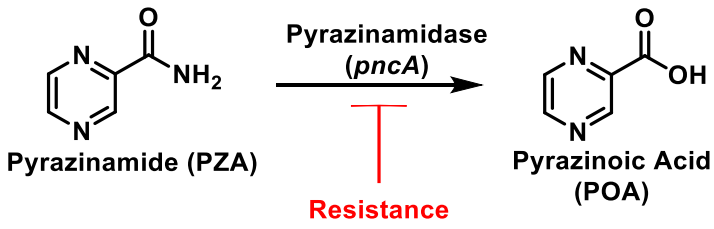

Figure 15. Resistance to PZA Through *pncA* Mutations

Given its importance to current and future TB therapy, resistance to PZA is an emerging cause for concern. PZA resistance appears to be on the rise clinically, including within a large proportion of MDR-TB patients.[201-202] Among these cases, the most commonly observed resistance mechanism is point mutations in *pncA* and its promoter region, which prevent activation of PZA (**Figure 15**). A number of options have previously been explored to overcome this limitation. The simplest would be direct treatment with POA, which would avoid the need for activation; unfortunately, POA is inactive *in vivo* due to poor pharmacokinetic (PK) properties, which limit penetration into epithelial lung fluid.[203] Simple prodrugs such as alkyl esters demonstrate improved PK but have also proven unsuccessful and are cleaved nonspecifically by serum esterases; Lanoix *et al*. have suggested that a site-selective release strategy may prove more fruitful by increasing

POA concentrations locally at the site of infection rather than throughout the serum.[203-205] In pursuit of this goal, we envisioned using a β-lactam as a delivery vehicle for the POA "warhead", taking advantage of the natively expressed BlaC, a Class A β-lactamase chromosomally encoded within the *Mtb* genome. Cleavage of the β-lactam bond liberates the lone pair on the nitrogen, which can then donate into a leaving group at the C-3′ position, triggering elimination of the POA moiety (**Figure 16**).

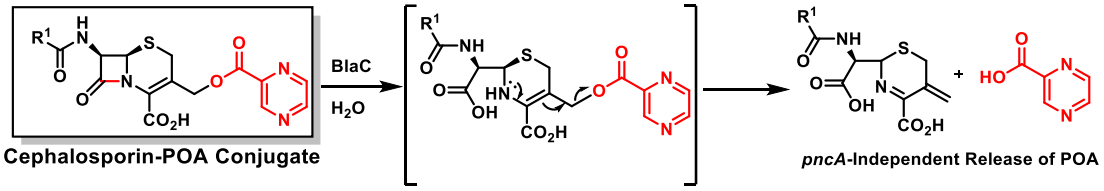

Figure 16. *pncA*-Independent Release Strategy Employing a β-Lactamase-Activated Cephalosporin Moiety.

This strategy has previously been explored as both a prodrug and codrug strategy for a number of bacterial pathogens, and was recently demonstrated by Aubé et al. as a viable strategy for targeting both active and nonreplicating models of *Mtb*.[120-121, 129, 156, 176, 182] Because β-lactamases are not expressed by eukaryotic cells and are rare in commensal organisms, this release mechanism is selective for the site of infection, enabling establishment of high local concentrations of POA; additional selectivity for BlaC over commensal β-lactamases can potentially be imparted through modifications to the cephalosporin backbone, as demonstrated by Rao et al. in developing selective β-lactamase diagnostics employing this same release mechanism.[56, 60, 98] This prodrug approach allows for pyrazinamidase-independent POA delivery, which circumvents the most common resistance mechanism to this important antitubercular. In addition, if we are able to achieve a codrug effect through the inherent β-lactam activity of the cephalosporin scaffold, resistance development should prove difficult for challenged organisms. Mechanisms which reduce POA

release, such as mutations to or reduced expression of BlaC, will confer increased susceptibility to the β-lactam component; PncA-independent resistance mechanisms, such as mutations to PanD, should also retain, and in certain cases even potentiate this β-lactam activity.[206]

2.2 Results

2.2.1 Synthesis of cephalosporin-pyrazinoic acid conjugate CS-POA.

Previous strategies employing cephalosporins in β-lactamase-targeted delivery strategies have typically relied upon functionalization of a free alcohol at the C-3′ position, as in **3**.[156, 176] We prepared this intermediate via a synthetic route developed by Yu and coworkers.[207] Commercially available 7-aminocephalosporanic acid (**7-ACA**) is functionalized at the N-7 position with phenyl acetyl chloride under Schotten-Baumann conditions to yield **CS Pro**; this molecule, dubbed the cephalosporin "promoiety", was also selected as a control cephalosporin for comparison to the POA conjugates in subsequent studies, due to its structural similarity and synthetic accessibility. **CS Pro** was then converted to the benzhydryl-protected alcohol **3** via a one-pot hydrolysis-esterification reaction developed by Yu et al.[207] With this intermediate in hand, a number of options were explored to achieve esterification at this position, which had little literature precedent compared to other, more well-explored conjugate linkers such as carbamates. We initially envisioned using a Mitsunobu reaction to install the POA warhead; this strategy would circumvent the need for challenging activation of the electron-deficient POA carboxylate and also avoid the use of base, which poses stability challenges via hydrolysis of the labile β-lactam bond as well as isomerization of the Δ3 double bond, a required component of the proposed release mechanism (**Figure 16**). Our initial attempts using traditional Mitsunobu conditions produced low yields, in part due to significant formation of a highly stable lactone side product (**Scheme 1A**). We hypothesized

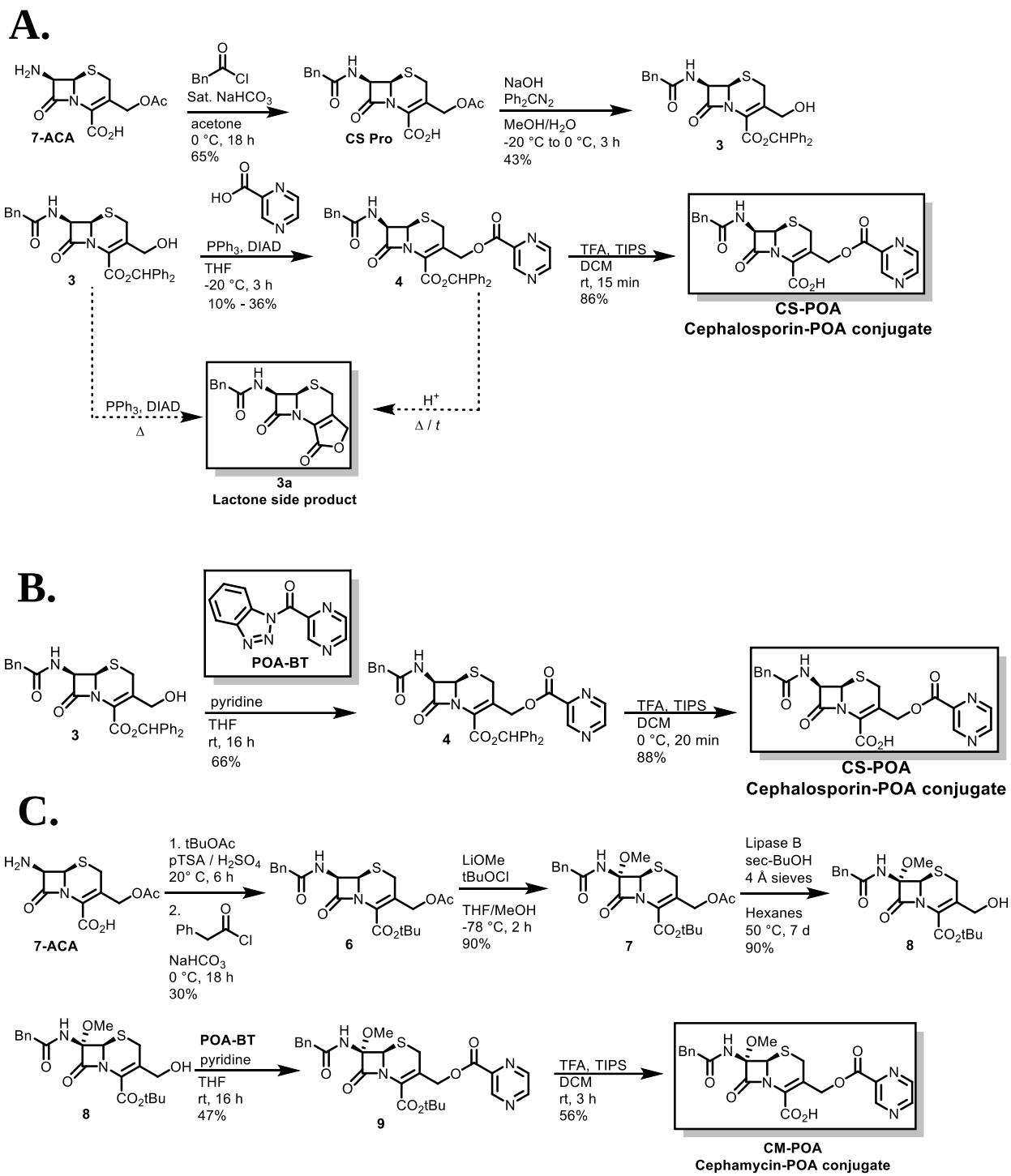

Scheme 1. Syntheses of Cephem-POA Conjugates **A.** Synthesis of cephalosporin-POA conjugate utilizing Mitsunobu esterification leads to significant production of lactone side product. **B.** Improved synthesis of CS-POA using POA-BT avoid activation of C-3′ alcohol. **C.** Synthesis of cephamycin-POA conjugate using POA-BT.

activation of the C-3′ alcohol to the phosphonium ion, normally required for nucleophilic attack by the carboxylic acid, was also priming the molecule for this intramolecular lactonization with subsequent spontaneous deprotection of the C-4 carboxylate. This lactonization has been observed previously following activation of the C-3′ position.[207-208] With an understanding of the probable mechanism behind this undesired reactivity, we theorized that reducing the reaction temperature would minimize this side reaction. A small temperature screen identified a narrow range of desired reactivity; temperatures too low failed to reach completion, likely due to the poor nucleophilicity of the pyrazine carboxylate. -20 °C was identified as ideal for these reaction conditions, although yields above 50% proved elusive. This problematic reactivity also presented itself in the subsequent acid-mediated carboxylate deprotection; it appears the basicity of the pyrazine ring allows for Bronsted acid-activated lactonization, especially in combination with the increased nucleophilicity of the freshly-deprotected C-4 carboxylate. Fortunately, optimization of this reaction proved more fruitful, with the key parameter in this instance being reaction time; halting the reaction after 15 min appears to allow for the deprotection reaction to run to near completion, while minimizing the opportunity for the free carboxylate to displace the activated pyrazine ester.

While we were excited to identify conditions capable of producing our desired product, we desired to further optimize the esterification reaction in order to aid in future compound scale-up. Based on our experiences developing Mitsunobu conditions, we hypothesized that activating the C-3′ alcohol would necessarily risk undesired lactonization and lower reaction yields. With this in mind, we turned to more typical esterification reactions involving activation of the partner carboxylate. Previous work by Katritzky and coworkers have identified activating conditions employing benzotriazole chemistry developed by their lab.[209-210] We prepared the activated pyrazinamide-benzotriazole (**POA-BT**, **Scheme 1B**) and were pleased to achieve robust

esterification under these conditions. Fortuitously, Δ3 isomerization, which has been previously observed by our lab and others as a common side product of base treatment, did not occur.[120, 176, 207] During the course of reaction development, we also identified slightly improved deprotection conditions. This newly developed reactivity affords the desired product from the precedented alcohol **3** in two steps with 58% yield and has proven fairly amenable to modest scale up, allowing for the production of grams of product necessary for detailed biological studies.

2.2.2 Synthesis of cephamycin-pyrazinoic acid conjugate CM-POA.

In addition to cephalosporin conjugates, we were also interested in exploring different classes of β-lactam scaffolds, such as the cephamycins, which contain a C-7 methoxy group neighboring the amide sidechain. Rao and coworkers have previously designed chromo- and fluorogenic cephamycin probes demonstrating exquisite selectivity for BlaC over similar class A β-lactamases; this selectivity is imparted through mutations in the substrate-specificity (omega) region near the active site, which garner significantly increased flexibility to the β-lactam-binding site.[56, 60] In the context of our prodrug approach, we envisioned a cephamycin scaffold might impart desirable selectivity and limit off-target release triggered from β-lactamases expressed by commensal organisms. Our synthetic route to these analogues was largely based off precedented work by Miller and coworkers, whose chemoenzymatic deprotection proved significantly more effective with a *tert*-butyl protecting group masking the C4 carboxylate (**Scheme 1C**).[211] 7-ACA was again employed as the starting material; Fischer esterification in a pressure vessel followed by amide formation under Schotten-Baumann conditions yielded the protected intermediate **6**. Methoxylation was accomplished using conditions developed by Koehler.[212] N-chlorination followed by deprotonation furnishes an activated imine intermediate, which is intercepted at the C-7 position by a methoxide anion; attack occurs stereoselectively due to the geometry of the

neighboring cephem ring, which forces approach from the back face of the molecule.[212] Next we employed a chemoenzymatic reaction developed by Miller and coworkers to liberate the C-3′ acetoxy group, yielding the C-3′ alcohol **8**; this intermediate is analogous to intermediate **3** from the cephalosporin scaffold approach.[211] We also attempted to access benzhydryl-protected cephamycin alcohols in order to employ the protecting group chemistry developed for the cephalosporins; however, we discovered that the chemoenzymatic reaction was particularly sensitive to protecting group variation, with yields <10% for the benzhydryl-protected analogues. From alcohol **8**, our previously explored application of Katritzky's benzotriazole chemistry proved fruitful, granting a significantly higher yield than observed using our Mitsunobu chemistry (26% over two steps, including the deprotection, as compared to 4% for the Mitsunobu).[209]

2.2.3 Initial Biochemical Characterization of POA Conjugates.

We performed several experiments to assess the potential viability of our conjugates as therapeutic candidates. Stability assays were performed with cephalosporin conjugate **1** using simulated serum and gastric fluid (SGF), as well as samples of mouse, rat, and human serum, and assessed using LC-MS.[213] Conjugate **1** demonstrated good stability at neutral pH but rapidly degraded in acidic SGF (**Table 4**). This finding correlates with our difficulties in developing deprotection conditions for acid-labile protecting groups; it appears protonation can catalyze intramolecular lactonization in this context as well.

Next, we performed a simple enzymatic assay to verify POA release upon β-lactamase exposure. His_6-tagged BlaC was cloned into and overexpressed in *E. coli* BL21/DE3 cells. Isolated and purified protein was incubated with **CS-POA**, quenched at varying endpoints and analyzed by HPLC. Time- and enzyme concentration-dependent degradation of conjugate and release of POA

Table 4. CS-POA Stability in Media and Serum.

Aqueous Stability (% remaining)[a]		Serum Stability (% remaining)[a]		
SGF[b]	*HEPES buffer*[c]	*Mouse*[c]	*Rat*[c]	*Human*[c]
50	>99	>95	>95	>95

Abbreviations: SGF = simulated gastric fluid; HEPES = 4-(2-hydroxyethyl)-1-piperazineethanesulfonic acid
[a] Determined by LC-MS with single ion monitoring ([M-H]$^-$=453 m/z). [b] pH 1.2; 60 min. [c] pH 7.4, 240 min

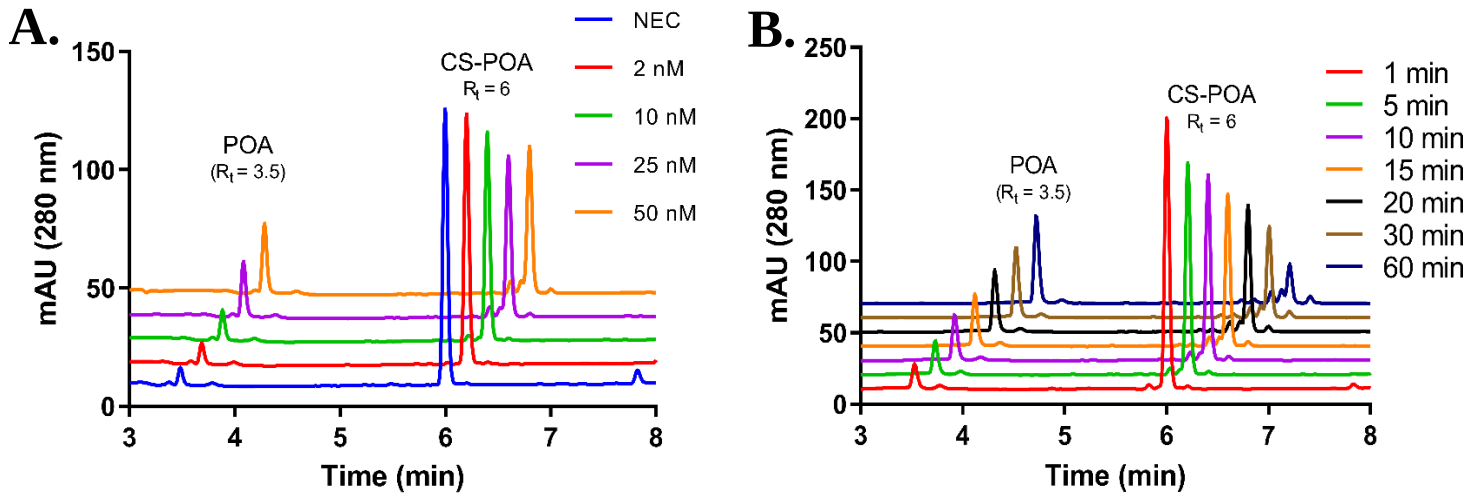

Figure 17. Enzymatic Release Assays. **A.** BlaC concentration-dependence release assay. Replicates were prepared as described with the indicated enzyme concentration and quenched at 10 min with TCA. 25 nM was chosen for time-dependence assay. **B.** Time-dependence release assay. Replicates were prepared as described with 25 nM BlaC and aliquots were quenched at the indicated timepoint with TCA.

were observed, confirming **CS-POA** is a substrate for BlaC and validating our strategy as a *pncA*-independent, TB-selective POA delivery vehicle (**Figure 17**). A minor amount of POA release was observed in the no enzyme control, suggesting a small amount of unspecific compound degradation, perhaps due to the acidic quench used to halt the enzymatic reaction.

Having verified β-lactamase-dependent release of POA, we next sought to further characterize this activity through spectrophotometry-based kinetics assays. Analogues **CS-POA**, **CM-POA**, and **CS Pro** were assessed against BlaC, and turnover was quantified through UV-vis spectrophotometry as previously described (Table 5).[214] All three β-lactams are substrates for BlaC, validating our initial findings that these conjugates are susceptible to BlaC hydrolysis, and thus compatible with a β-lactamase-targeted prodrug strategy. We also evaluated the conjugates against CTX-M-1, an Ambler class A extended spectrum β-lactamase (ESBL) capable of hydrolyzing many β-lactam classes, including oxyimino-cephalosporins.[215] This enzyme retains activity against the cephalosporin substrates but is incapable of hydrolyzing the bulkier cephamycin substrate (**Table 5**), validating our hypothesis that this scaffold could provide enhanced TB selectivity and avoid undesired release by commensal β-lactamases. To our knowledge, this study represents the first application of this paradigm for the design of an antitubercular.

Table 5. Kinetic Parameters for Beta-Lactamase Turnover of Cephem Substrates.

Com-pounds	Molar Extinction Coefficient (M^{-1} cm^{-1})	Wavelength (nm)	BlaC			CTX-M-1		
			K_M (μM)	k_{cat} (s^{-1})	k_{cat}/K_M (μM^{-1} s^{-1})	K_M (μM)	k_{cat} (s^{-1})	k_{cat}/K_M (μM^{-1} s^{-1})
CS-POA	3939	269	199.3 ± 26.2	13.5	6.77×10^{-2}	143.2 ± 17.4	99.3	$6.93*10^{-1}$
CS Pro	5827	263	594.3 ± 50.1	32.5	5.47×10^{-2}	150.0 ± 6.7	88.8	$5.92*10^{-1}$
CM-POA	4605	270	35.7 ± 0.9	0.51	1.45×10^{-2}	n.d.[b]	n.d.[b]	n.d.[b]

Abbreviations: n.d. = not determined

[a] Determined by UV-vis spectrophotometry in HEPES buffer (50 mM, pH 7.5), monitoring at the indicated wavelengths; [b] Parameters could not be determined due to lack of enzymatic hydrolysis over the observed time period.

2.2.4 Biological Activity Evaluation.

Compounds were evaluated for minimum inhibitory concentrations (**MIC)** against a panel of organisms, including *M. tuberculosis* H37Rv, along with several non-mycobacterial organisms representative of commensal species. The β-lactam-POA conjugates demonstrated intriguing activity against *Mtb*, imparting four-fold increased activity compared to POA alone. Compound **2**, the cephalosporin "promoiety", displayed even greater activity against *Mtb*, suggesting the β-lactam backbone may play a role in the observed activity. Of particular interest is the selective antimycobacterial activity observed for **CS-POA**, a feature shared by PZA/POA. This selectivity would prove particularly useful in avoiding nonspecific killing of commensal organisms and related gastrointestinal dysbiosis, a common cause for antibacterial side effects *in vivo*.[216]

To probe the antimicrobial mechanism behind these molecules, as well as to assess their potential therapeutic utility against drug-resistant strains, a number of *Mtb* mutants were prepared and challenged in additional MIC assays (**Table 6 & 7**, **Figure 18A**). The POA conjugates displayed increased activity over the parent PZA in *Mycobacterium bovis* BCG, an attenuated strain containing a point mutation in *pncA* that is completely resistant to PZA. Accordingly, we also found

that a *Mtb pncA* knockout mutant fully resisted PZA but was retained susceptiblity to **CS-Pro**. Silencing of *blaC* resulted in even greater potentiation of conjugate activity; susceptibility was partially recovered with *blaC* complementation. Transposon-mediated disruption of *panD*, encoding aspartate decarboxylase, a putative target of POA, conferred resistance to POA while also retaining susceptibility to the conjugate These results point towards a greater biological significance for the β-lactam backbone, which appears to impart added antimycobacterial activity under conditions where it evades hydrolysis or where the parent molecule, POA, is inactive.

Table 6. MIC_{90} Data for Nonmycobacterial Pathogens (μg/mL).

Compound	*M. tuberculosis* (*H37Rv*)[a]	*S. aureus* (*USA300*)[b]	*P. aeruginosa* (*PAO1*)[b]	*A. baumannii* (*AB5075*)[b]	*E. coli* (*K12*)[b]
PZA	50	>800	>800	>800	>800
POA	400	>800	>800	>800	>800
CS-POA	400	>730	>730	>730	>730
CS-Pro	100	**80**	>630	>630	>630
CM-POA	800	>780	>780	>780	>780

[a] 7H9 liquid medium, pH 5.8. [b] MHB 2 broth, pH 7.4.

Table 7. MIC_{90} Data for Select *Mycobacterium* Strains and Mutants (μg/mL)

Compound	*Mtb* (H37Rv)	*M. bovis* (BCG)	*Mtb ΔpncA*	*Mtb ΔblaC*	*Mtb ΔblaC::blaC*	*Mtb panD::Tn*
PZA	25-50	>800	>800	50	50	>800
POA	100	100	100	100	100	>800
CS-POA	100	100	100	25	100	200
CS Pro	200	50	100-200	12.5	50	100
CM-POA	100	200	200	100	100	(n.d.)[b]

a] Assays were performed in Middlebrook 7H9 liquid medium at pH 5.8, as described in the Supporting Information; [b] not determined.

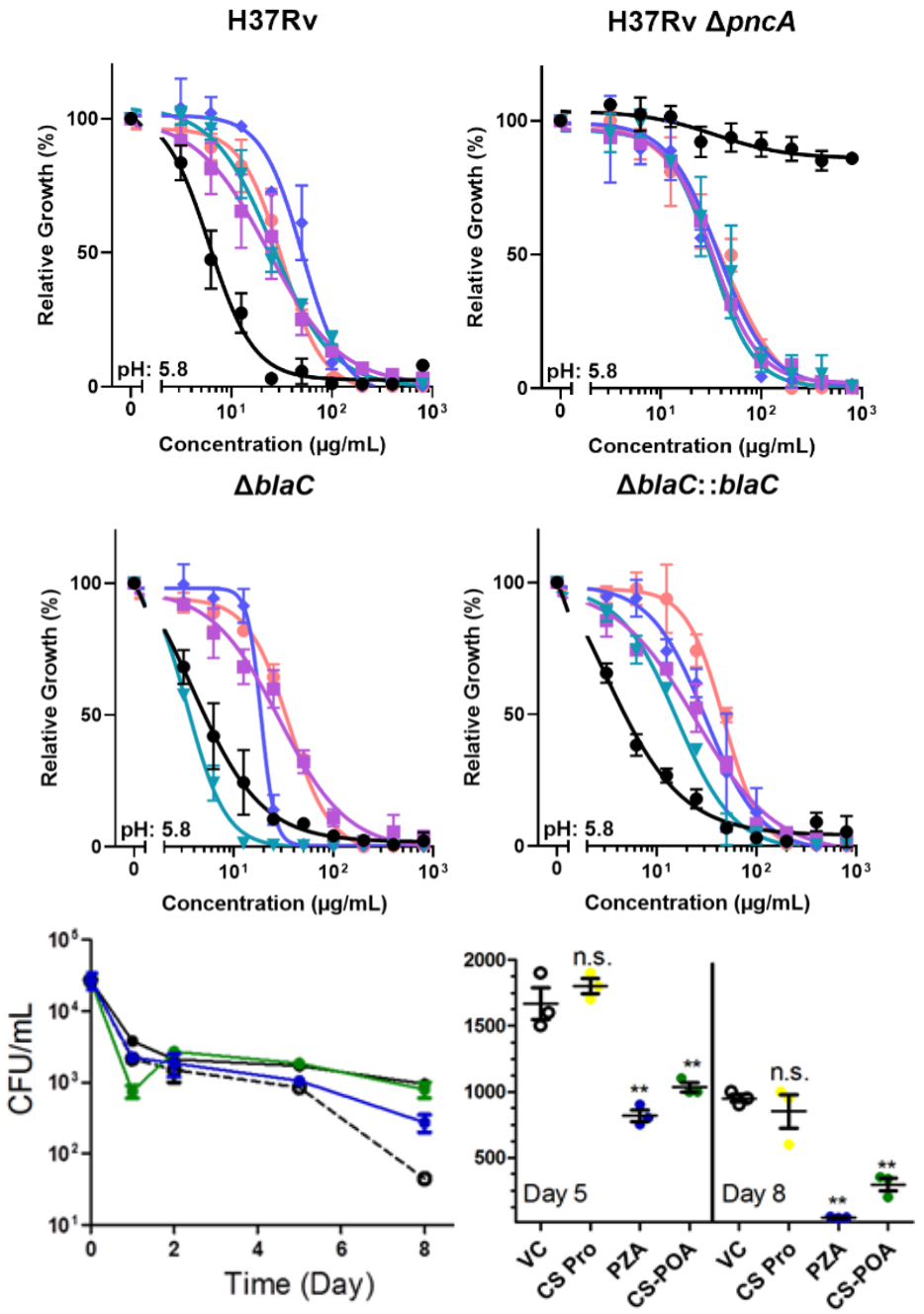

Figure 18. Antimycobacterial Evaluation of POA Conjugates.A. Evaluation of conjugates against *Mycobacterium* strains and mutants. ● = PZA; ■ = POA; ♦ = CS-POA; ▼ = CS Pro; ● = CM-POA. **B.** Activity of PZA and cephalosporins at 1.6 mM against *Mtb* in IFN-γ activated THP-1 macrophages. Abbreviations: VC =vehicle control (DMSO). ● = VC; ○ = PZA; ● = CS-POA; ● = CS Pro.

The cephalosporins were also assessed in IFN-γ activated THP-1 macrophages, a model for *in vivo Mtb* infection (**Figure 18B**).[217] Cephalosporins (and most β-lactams) are typically thwarted by phenotypic resistance in non-replicating infection models, as demonstrated by the lack of activity for **CS Pro**.[218-219] Conversely, the efficacy of PZA *in vivo* is largely due to its sterilizing activity against non-replicating *Mtb*, presenting in this study as a tenfold reduction in bacterial load by day 8.[192, 220] Interestingly, **CS-POA** also appears capable of achieving moderate killing in this infection model, demonstrating a fourfold reduction in colony-forming units(CFU)/mL at the same endpoint. Other lone β-lactams active in a macrophage model have only recently been identified by Aube *et al* through a high-throughput screening campaign.[221] Our conjugates also possess activity against actively replicating organisms, highlighting a potential advantage of our strategy over these previously-identified compounds. This sterilizing activity also demonstrates the benefit of the POA warhead, which appears to impart the traditional cephalosporin scaffold with novel activity against intracellular TB.

2.2.5 POA Accumulation Assays.

In our initial experimental design, we had conceived of a cephalosporin-POA conjugate as a prodrug strategy, with the β-lactam component merely imparting a mechanism for selective drug delivery. However, the activity of **1** *in vitro* against a variety of *Mtb* strains and growth conditions suggests a potential codrug effect, wherein both components of the molecule play a role in its observed activity. In order to further investigate the mechanism behind this activity, we next sought to assess POA delivery by measuring levels of intracellular POA accumulation in response to conjugate treatment (**Figure 19**). We incubated *M. bovis* BCG cells with **CS-POA** and POA and harvested the intracellular component; cultures were lysed and metabolites were extracted as

described previously.[222-223] Using LC-MS/MS, we analyzed samples to assess the ability of **CS-POA** to deliver POA into cells. After 24 h incubation, conjugate-treated cells displayed comparable intracellular POA concentrations when compared to POA-treated cells (approximately 80 nmol/mg protein for 800 μM **1**, compared to 180 nmol/mg protein for 1 mM POA). These results, taken with the observed activity in a nonreplicating infection model, provide evidence that these conjugates are codrugs, with both the β-lactam and POA components contributing to the observed biological activity.[1, 196]

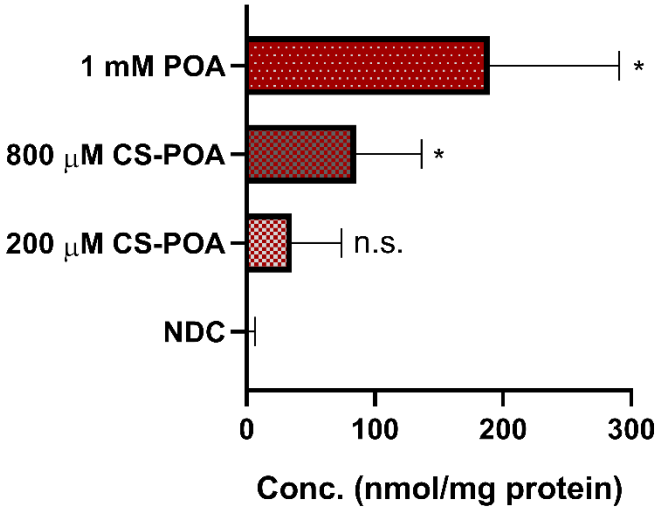

Figure 19. Intracellular POA Concentrations. Concentrations assessed 24 h after treatment with indicated compound concentrations. Abbreviations: NDC = no drug control; * = p-value < 0.05; n.s. = not significant.

2.2.6 Pantothenate antagonism investigation.

In order to further assess the role of POA in conjugate activity, we next sought to investigate the effect of pantothenate supplementation in *M. bovis* BCG. Previous work by Dillon *et al.* has demonstrated that pantothenate, a CoA pathway metabolite downstream of PanD, is able to strongly antagonize POA *in vitro*.[200] We hypothesized that our POA conjugates, which appear partially dependent on POA action, would also be antagonized by this supplementation. We grew

M. bovis BCG cultures in the presence of 100 μM pantothenate and investigated the action of both POA and **CS-POA** (**Figure 20**). Similar to the results observed by Dillon *et al*., POA was antagonized in the pantothenate culture, with a more than four-fold shift in MIC_{90} compared to the unsupplemented control. In contrast, **CS-POA** was completely agnostic to pantothenate supplementation, with nearly identical inhibition curves for both growth conditions. This finding suggests that **CS-POA** is exerting a co-drug effect, where both the cephalosporin scaffold and POA warhead contribute to the observed biological activity. This result also supports our finding that **CS-POA** remains active in the *panD* transposon-insertion mutant, which is POA resistant.

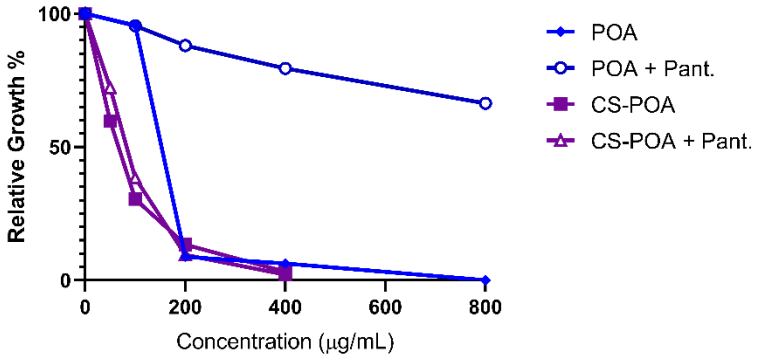

Figure 20. Pantothenate Antagonism Growth Kinetics. Abbreviations: Pant. = pantothenate.

2.2.7 Frequency of resistance (FoR) determination.

As stated previously, a primary goal of our project was to develop a new form of PZA that would be less susceptible to conventional resistance mechanisms. In order to evaluate the success of this goal, we next performed assays to determine the frequency of resistance (FoR) for our compounds against *Mtb* H37Rv. Using large bioassay trays, we were able to plate approximately 2 x 10^7 colony-forming units (CFU) in duplicate at pH 5.8. These cultures were challenged with 4X MIC concentrations of PZA, POA, **CS-POA** and **CS Pro**. Relatively high levels of resistance were

observed for PZA, equating to an FoR of approximately 1.2 x 10^{-5}; resistance to POA was less frequent, but a few colonies were identified, yielding an FoR of approximately 2.9 x 10^{-7}. These values are in line with literature reports for PZA but lower than reported for POA (likely due to the use of reduced pH to align with our previously described MIC assays).[196, 224] Gratifyingly, no resistant colonies were observed for POA conjugate **1**, suggesting this strategy is less susceptible to resistance development than the first line therapy. Resistant colonies were also not observed for the cephalosporin promoiety **2**, providing limited evidence that the decreased FoR for the POA conjugate may result from the biological effect of the β-lactam scaffold.

2.3 Discussion

β-Lactam antibiotics, a widely employed and wildly successful therapeutic class, have had little clinical success against *Mtb*. The lack of inhibitory effect *in vitro*, determined to result in part from expression of chromosomally encoded β-lactamases, led to the general abandonment of this chemical arsenal in the battle against TB.[225] Fortunately, discovery of β-lactamase inhibitors (BLIs) such as clavulanic acid in the 1970s, coupled with a growing prevalence of resistant strains, revitalized interest in the β-lactams as potential TB therapeutics.[226-227] Early *in vitro* studies suggested BLI co-treatment of penicillins and cephalosporins was effective against *Mtb*.[228-231] More recent results have indicated the promise of carbapenems such as meropenem and imipenem, which have demonstrated potent activity in combination with clavulanate *in vivo*, as well as unique activity against resistant (MDR/XDR) and nonreplicating bacteria.[219, 232-236] Another recent, less-explored approach seeks to exploit, rather than inhibit, this resistance mechanism, employing these molecules as β-lactamase-activated delivery vehicles of antitubercular warheads. Cephalosporin conjugates bearing a variety of payloads have been previously developed for *Mtb*.[176, 182, 184, 237-240] Our novel strategy, inspired by these earlier approaches, aims to exploit this TB resistance

mechanism towards circumvention of a second, through pyrazinamidase-independent delivery of POA.

Our conjugates demonstrated promising activity *in vitro* against *Mtb*. The reported MICs appear higher than typically observed for β-lactam antibiotics but compared favorably with the parent drugs PZA/POA, which also exhibit relatively high MICs. Pyrazinamide activity, despite its robust sterilizing effect *in vivo*, is difficult to accurately measure *in vitro* and typically requires additional stressors, such as reduced pH, hypoxia or nutrient deprivation.[200] Particularly encouraging were the results observed for the *Mtb* mutant strains, which demonstrate the potential utility of this approach in combatting resistance. Improved activity of **CS-POA** against the *pncA* knockout suggests this strategy is effective against the most common form of PZA resistance observed clinically (as demonstrated by a >100-fold increase in MIC compared to PZA). Retention of activity against a *panD* transposon insertion mutant was also promising; this mutation confers selective and paradoxical resistance to POA, and the gene product PanD has been identified as a putative target of pyrazinamide.[196-199] Retention of activity against this mutant may be imparted by the cephalosporin backbone itself. Increased activity was observed for both the conjugates and the cephalosporin promoiety in a *blaC* knockout, suggesting these analogues are still able to modify tubercular PBPs and $_{L,D}$-transpeptidases; similar potentiation of cephalosporins has been observed in *blaC* knockout strains previously.[241] Finally, selectivity for *Mtb* over other bacterial strains was achieved, with both conjugates lacking activity against any of the nontubercular strains. This was an encouraging result: given the relatively high concentrations required for killing in *Mtb*, we were concerned about the potential for off-target killing of commensal organisms, which are known to cause GI distress in contemporary β-lactam therapy.[216] Nevertheless, to avoid potential gut

dysbiosis and circumvent the molecules' observed acid instability, intravenous administration is likely the optimal therapeutic route for these first-generation molecules.

While the conjugates demonstrated promising *in vitro* activity, the cephalosporin promoiety **CS Pro** was also equipotent (or even slightly more active) against these strains. Motivated by a desire to understand the role of the POA warhead in compound activity, we devised several experiments to answer these fundamental questions. Following assays confirming POA release in the presence of BlaC activity and POA accumulation in conjugate-treated cells, we explored activity in cultures supplemented with pantothenate. Pantothenate is a metabolite in the CoA biosynthetic pathway downstream of PanD; pantothenate-mediated inhibition of POA provides evidence for PanD as the target of these drugs. Intriguingly, supplementation failed to antagonize conjugate **CS-POA** at any concentration tested. This result, like the bioactivity against the *panD* transposon insertion mutant, suggests that these molecules can inhibit *Mtb* independently of PanD, likely due (at least in part) to the inherent activity of the cephalosporin scaffold.

Following this inconclusive result, we next explored our molecules in a macrophage infection model. These experiments more faithfully replicate an *in vivo* system where mycobacteria are engulfed in acidified macrophages and subjected to a host of cellular stressors, such as hypoxia, nutrient limitation and reactive oxygen species. PZA shines in this system, demonstrating potent sterilizing activity; conversely, β-lactams are typically ineffective against these nonreplicating cells.[182, 191, 219, 242] Accordingly, the cephalosporin promoiety **2** wholly lacked activity, demonstrating no difference with the vehicle control. Fascinatingly, conjugate **1** was active in this model, conferring a fourfold reduction in growth by day 8. Other lone β-lactams active in a macrophage model have only recently been identified by Aube et al in a high-throughput screening campaign.[181-182] Interestingly, our conjugates also possess activity against actively replicating

organisms, highlighting a potential advantage of our strategy over these previously identified compounds. Regardless, activity in this model is best explained by the POA warhead, which is released and inhibits cell growth under conditions that would normally render the β-lactam scaffold ineffective.

Additional studies characterizing the conjugates provided several interesting observations. Hydrolysis kinetics confirmed all three β-lactams are substrates for BlaC, with affinity and turnover rates comparable to other cephalosporin and cephamycin antibiotics.[243-244] We were pleased to find that the bulkier cephamycin conjugate **CM-POA** was hydrolysable by BlaC, validating significant previous work by Rao and coworkers.[56, 60, 98, 104] The enhanced flexibility present in the BlaC active site is due to mutations within the substrate-specificity (omega) loop, particularly R164A, which eliminates stabilizing salt bridges with neighboring aspartate and glutamate residues.[56] This feature has been explored in the development of diagnostic and fluorescent probes for studying TB, but to our knowledge this study represents the first proposed therapeutic application of this paradigm. Selectivity for BlaC-mediated hydrolysis is crucial for the development of orally available β-lactam conjugates, particularly those containing warheads with non-specific antibacterial activity, in order to reduce side effects caused by gut dysbiosis. The presented conjugates are not amenable to oral dosing (due to their acid instability) and contain a warhead with exquisite selectivity for *Mtb*; nonetheless, these observations provide a valuable proof-of-concept for this strategy, and BlaC selectivity will be evaluated in a future manuscript.

Finally, FoR studies supported our initial hypothesis that a dual pharmacophore approach would hinder resistance development, as no resistant mutants were isolated for cephalosporin conjugate **CS-POA**. This result proved superior to both PZA and POA, which displayed FoRs of 1.2×10^{-5} and 2.9×10^{-7}, respectively. Unfortunately, resistant mutants could not be isolated for the

cephalosporin promoiety **CS Pro** under these conditions, indicating an FoR lower than 5 x 10^{-8}; experimental evidence for β-lactam resistance development in *Mtb* is scarce, likely due to the perceived limitations of β-lactam therapy for TB (given the organism's constitutive expression of a resistance-conferring enzyme). Nonetheless, the macrophage studies described previously demonstrate that conventional β-lactams like **CS Pro** are susceptible to phenotypic resistance under conditions simulating the *Mtb* infection *in vivo*, and that our conjugates circumvent this form of resistance as well.

2.4 Conclusion

We have presented a novel strategy for targeted delivery of POA which circumvents the most common resistance mechanism blocking the parent drug. A cephalosporin-based POA conjugate (**CS-POA**) displays comparable activity to PZA/POA and retains activity against resistant mutants and in a macrophage infection model. A cephamycin-based approach (**CM-POA**) achieves selective release by the mycobacterial β-lactamase, a new proof of concept for the therapeutic potential of this strategy. Mechanistic studies have suggested **CS-POA** acts as a co-drug, with the β-lactam scaffold and pyrazinoic acid warhead both contributing to the observed activity. This dual approach is superior to either class alone, conferring both reduced resistance susceptibility and activity against non-replicating organisms. This study contributes to a growing trend demonstrating the utility of the previously neglected β-lactams as a viable treatment option against the growing threat of drug-resistant TB.[219, 244-248]

2.5 Experimentals

2.5.1 General Remarks

Chemical reagents and solvents were purchased from Alfa Aesar, Acros, Fisher Scientific, SigmaAldrich, TCI America or Oakwood Chemical and used without additional purification unless otherwise indicated. For anhydrous reactions, dichloromethane (DCM), methanol (MeOH), and tetrahydrofuran (THF) were dispensed under Argon (Ar) using an Inert solvent purification system (MBRAUN). Ethyl acetate (EtOAc), acetone, hexanes (Fisher Scientific), and tert-butyl acetate (tBuOAc, Acros) were purchased and used without additional purification. Anhydrous reactions were performed under inert gas (Ar or N_2) in flame-dried glassware. Thin-layer chromatography (TLC) was performed on TLC silica gel 60F254 plates from EMD Chemical Inc. and visualized using UV light and ninhydrin or I_2 staining. Reaction purification was performed via column chromatography employing a Teledyne ISCO RF-200 CombiFlash system with the indicated solvent gradient; flash column silica gel cartridges were used for purifying intermediates, while RediSep® Rf Gold® Cyano cartridges (Teledyne ISCO) were used for purification of final carboxylic acid products. Percent purity analysis was performed using analytical high pressure liquid chromatography (HPLC) with a reversed-phase Eclipse® XDB 5 μm C-8 4.6 × 150 mm LC column (Agilent), with detection at 250 nm. A gradient method of 5% to 95% acetonitrile (MeCN) + 0.1% formic acid (FA) in water + 0.1% FA over 10 min at a flow rate of 1.0 ml/min was employed. Nuclear magnetic resonance (NMR) spectroscopy was performed using a Bruker 500 MHz spectrometer at 500 MHz for 1H and 126 MHz for 13C and calibrating to known chemical shifts for residual solvent peaks. Data for 1 H NMR are reported as follows: chemical shift (multiplicity, coupling constant in Hertz (Hz), number of hydrogens). Abbreviations are as follows: s = singlet, d = doublet, t = triplet, q = quartet, dd = doublet of doublets, td = triplet of doublets, m

= multiplet, ABq = AB quartet. High resolution mass spectrometry (HRMS) analysis was performed using BioTOF II Mass Spectrometer (Bruker). Statistical analysis was performed using the unpaired t-test function of Graphpad Prism 8.0 software..

2.5.2 Synthesis of CS-POA

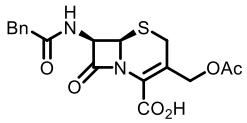

(6*R*,7*R*)-3-(acetoxymethyl)-8-oxo-7-(2-phenylacetamido)-5-thia-1-azabicyclo[4.2.0]oct-2-ene-2-carboxylic acid (CS Pro).[207] 7-aminocephalosporanic acid (7-ACA, 8.00 g, 29.4 mmol) was dissolved in a solution of acetone (67 mL) and saturated aqueous $NaHCO_3$ (200 mL) and cooled to 0 ºC with vigorous stirring under ambient atmosphere. Phenyl acetyl chloride (4.4 mL, 32 mmol, 1.1 equiv) was added dropwise and the reaction was gradually warmed to room temperature overnight. After 18 h, the reaction mixture was diluted with EtOAc (100 mL), then acidified to pH 0 with aqueous 2N HCl. The layers were separated, and the aqueous layer was extracted with EtOAc (2 × 50 mL). The organic layers were combined and washed with saturated aqueous NaCl (100 mL), dried with $MgSO_4$, and concentrated *in vacuo* to afford a wet brown solid. This crude product was washed Et_2O (3 × 50 mL) and filtered, furnishing the desired product (10.0 g, 87%) as a tan solid, which was taken on without additional purification: HPLC purity: 97.4% (t_R = 7.7 min, k' = 4.3); ^{1}H NMR (500 MHz, DMSO-d_6) δ 13.67 (s, 1H), 9.10 (d, J = 8.3 Hz, 1H), 7.32–7.20 (m, 5H), 5.68 (dd, J = 8.3, 4.8 Hz, 1H), 5.08 (d, J = 4.9 Hz, 1H), 5.00 (d, J = 12.8 Hz, 1H), 4.69 (d, J = 12.8 Hz, 1H), 3.64-3.46 (ABqd, J = 64.1, 18.1 Hz, 2H), 3.59-3.47 (ABqd, J = 38.2, 13.6 Hz, 2H), 2.03 (s, 3H); ^{13}C NMR (126 MHz, DMSO-d_6) δ 171.0, 170.2, 164.8, 162.8, 135.8, 129.0, 128.2, 126.56, 126.49, 123.4, 62.7, 59.1, 57.4, 41.6, 25.5, 20.6; HRMS (ESI–

) calcd for $C_{18}H_{17}N_2O_6S^-$ [M-H]$^-$: 389.0813, found: 389.0798 (error = 3.7 ppm); Mp: decomposed at 150 ºC.

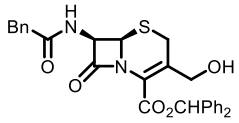

Benzhydryl (6*R*,7*R*) -3-(hydroxymethyl)-8-oxo-7-(2-phenylacetamido)-5-thia-1-azabicyclo[4.2.0]oct-2-ene-2-carboxylate (3).[207] *Caution! Diphenyldiazomethane is hazardous and potentially explosive. See safety note in Javed et al. for more information.*[249] Intermediate **2** (8.2 g, 19 mmol) was dissolved in MeOH (32 mL) and H_2O (38 mL) and cooled to -20 ºC with stirring. Aqueous NaOH solution (15% w/v, 8.2 mL, 31 mmol, 1.6 equiv) was added dropwise over 40 minutes; occasional warming was required to prevent the reaction slurry from freezing completely. Following this addition, the reaction was stirred for an additional 15 min, then warmed to 0 ºC and acidified to pH 6 with aqueous 2N HCl (2.5 mL). Diphenyldiazomethane[249] (8.0 g, 41 mmol, 2.2 equiv) was dissolved in THF (19 mL) and added to the reaction in one portion. Additional aqueous 2N HCl (8.2 mL) was added dropwise over 15 min, and the reaction was stirred for an additional 90 min at 0 ºC; as the reaction proceeded, product and diphenyldiazomethane gradually separated out of solution as purple oily globs. After warming to room temperature, the reaction was filtered and the resultant viscous purple filtrant was washed with excess EtOAc and then limited Et_2O, yielding the desired product (4.12 g, 43%) as a light pink powder: ^{1}H NMR (500 MHz, DMSO-d_6) δ 9.12 (d, J = 8.4 Hz, 1H), 7.50 (d, J = 7.2 Hz, 2H), 7.42 (d, J = 7.1 Hz, 2H), 7.40–7.19 (m, 11H), 6.90 (s, 1H), 5.72 (dd, J = 8.3, 4.7 Hz, 1H), 5.15 (t, J = 5.7 Hz, 1H), 5.11 (d, J = 4.7 Hz, 1H), 4.26–4.15 (m, 2H), 3.61 (s, 2H), 3.54 (dd, J = 32.0, 13.9 Hz, 2H); ^{13}C NMR (126 MHz, DMSO-d_6) δ 171.0, 165.2, 160.9, 140.1, 140.0, 135.8, 134.4, 129.0, 128.5, 128.4, 128.2, 127.84, 127.77, 126.8, 126.6, 126.5, 122.0, 78.3, 59.8, 58.9, 57.7, 41.6, 25.6;

HRMS (ESI+) calcd for $C_{29}H_{26}N_2O_5SNa$ $[M+Na]^+$: 537.1455, found: 537.1435 (error = 3.7 ppm); Mp: 175 ºC.

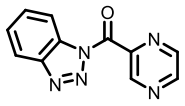

1*H*-1,2,3-Benzotriazol-1-yl(2-pyrazinyl)methanone (POA-BT).[250] 1-H-benzotriazole (19.4 g, 163 mmol, 4.00 equiv) was dissolved in CH_2Cl_2 (200 mL) at room temperature. Thionyl chloride (3.54 mL, 48.8 mmol, 1.20 equiv) was added slowly, inducing a color change towards dark yellow. This mixture was stirred for 30 min, then cooled to -15 ºC and pyrazinoic acid (5.0 g, 41 mmol) was added portion-wise under positive pressure over several minutes. This cloudy mixture was stirred at -15 ºC for 4 h, then warmed to 0 ºC and quenched slowly with aqueous 5% $NaHCO_3$ solution to pH 7. The layers were separated, and the aqueous layer was washed with additional portions of CH_2Cl_2 (3 × 50 mL). The combined organic layers were washed with saturated aqueous NaCl, dried with $MgSO_4$ and concentrated *in vacuo* to yield a yellow solid. The crude product was triturated with hot Et_2O and filtered, yielding a lighter yellow solid; trituration was repeated with Et_2O to remove remaining BTZ contaminant. Filtration yielded the desired product (2.95 g, 32%) as a white solid: ^{1}H NMR (500 MHz, DMSO-d_6) δ 9.34 (d, J = 1.4 Hz, 1H), 9.01 (d, J = 2.5 Hz, 1H), 8.95 (dd, J = 2.5, 1.5 Hz, 1H), 8.35 (obs t, J = 7.5 Hz, 2H), 7.89 (t, J = 8.0 Hz, 1H), 7.71 (t, J = 7.3 Hz, 1H);); ^{13}C NMR (126 MHz, DMSO-d_6) δ 163.7, 147.8, 146.6, 145.7, 145.2, 144.6, 131.22, 131.16, 127.1, 120.2, 114.1; Mp: 137-140 ºC.

General benzotriazole esterification: Intermediate **3**/**8** and **POA-BT** (1.1 equiv) were dissolved in THF (0.015M) at room temperature. Pyridine (1.1 equiv) was added slowly and the reaction was stirred at room temperature overnight. After 16 h, the reaction was diluted with EtOAc and H_2O and the layers were separated; the aqueous portion was washed with EtOAc (2×). The

combined organic layers were washed with saturated aqueous NaCl, dried with $MgSO_4$ and concentrated *in vacuo*.

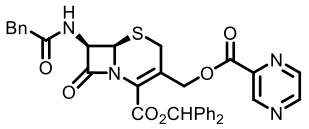

Benzhydryl (6*R*,7*R*)-8-oxo-7-(2-phenylacetamido)-3-(((pyrazine-2-carbonyl)oxy)methyl)-5-thia-1-azabicyclo[4.2.0]oct-2-ene-2-carboxylate (4). Intermediate **3** (200 mg, 0.39 mmol) was reacted following the general benzotriazole esterification procedure. The crude product was purified by flash chromatography (0-75% EtOAc/hexanes, stepwise gradient), furnishing the desired product (160 mg, 66%) as a yellow solid: R_f = 0.15 (50% EtOAc/ hexanes); ^{1}H NMR (500 MHz, DMSO-d_6) δ 9.21–9.14 (m, 2H), 8.91 (d, *J* = 2.4 Hz, 1H), 8.83 (dd, *J* = 2.4, 1.5 Hz, 1H), 7.51–7.46 (m, 2H), 7.44–7.38 (m, 2H), 7.35–7.19 (m, 12H), 6.94 (s, 1H), 5.81 (dd, *J* = 8.3, 4.8 Hz, 1H), 5.22 (d, *J* = 13.0 Hz, 1H), 5.18 (d, *J* = 4.9 Hz, 1H), 5.07–4.97 (m, 1H), 3.77 (dd, *J* = 39.4, 18.4 Hz, 2H), 3.54 (dd, *J* = 34.2, 13.7 Hz, 3H); ^{13}C NMR (126 MHz, DMSO-d_6) δ 171.0, 165.3, 163.1, 160.5, 148.2, 145.7, 144.9, 143.4, 142.6, 139.74, 139.65, 135.8, 129.0, 128.5, 128.4, 128.2, 127.9, 126.8, 126.51, 126.49, 125.51, 125.47, 78.9, 64.1, 59.1, 57.6, 41.6, 26.0; HRMS (ESI+) calcd for $C_{34}H_{29}N_4O_6S$ $[M+H]^+$: 621.1802, found: 621.1815 (error = 2.0 ppm); Mp: 90 ºC.

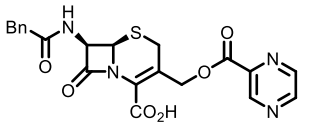

(6*R*,7*R*) -8-oxo-7-(2-phenylacetamido)-3-(((pyrazine-2-carbonyl)oxy)methyl)-5-thia-1-azabicyclo[4.2.0]oct-2-ene-2-carboxylic acid (CS-POA). Intermediate **4** (490 mg, 0.79 mmol) was dissolved in CH_2Cl_2 (34 mL) and cooled to 0 ºC. Triisopropylsilane (1.62 mL, 7.89 mmol, 10.0 equiv) and then trifluoroacetic acid (6.08 mL, 78.9 mmol, 100. equiv) were added and the mixture

was stirred for 20 min at 0 ºC. The reaction was warmed to room temperature and condensed *in vacuo*, then dissolved in toluene and condensed (10 mL × 3) to remove excess TFA. The crude product was loaded onto celite and purified by flash chromatography (0-90% MeOH/ CH_2Cl_2, gradient method) using a RediSep® Gold cyano-functionalized silica cartridge (Teledyne Isco), furnishing the desired product (317 mg, 88%) as a tan solid: HPLC purity: 96.9% (t_R = 7.3 min, k' = 4.1); ^{1}H NMR (500 MHz, DMSO-d_6) δ 13.79 (br s, 1H), 9.23 (d, J = 1.5 Hz, 1H), 9.12 (d, J = 8.4 Hz, 1H), 8.91 (d, J = 2.4 Hz, 1H), 8.84 (dd, J = 2.5, 1.5 Hz, 1H), 7.32–7.20 (m, 5H), 5.71 (dd, J = 8.3, 4.8 Hz, 1H), 5.36 (d, J = 12.8 Hz, 1H), 5.12 (d, J = 4.9 Hz, 1H), 5.06 (d, J = 12.8 Hz, 1H), 3.79-3.63 (dd, J = 50.2, 18.2 Hz, 2H), 3.60-3.48 (dd, J = 38.7, 13.8 Hz, 2H); ^{13}C NMR (126 MHz, DMSO-d_6) δ 170.1, 164.8, 163.2, 162.9, 148.2, 145.8, 144.9, 142.8, 135.8, 129.0, 128.2, 126.5, 64.4, 59.1, 57.5, 41.6, 25.6; HRMS (ESI–) calcd for $C_{21}H_{17}N_4O_6S$ [M-H]$^-$: 453.0874, found: 453.0831 (error = 9.4 ppm); Mp: decomposed at 150 ºC

2.5.3 Synthesis of CM-POA

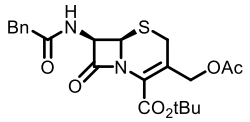

tert-Butyl (6R,7R)-3-(acetoxymethyl)-8-oxo-7-(2-phenylacetamido)-5-thia-1-azabicyclo[4.2.0]oct-2-ene-2-carboxylate (6).[211] 7-aminocephalosporanic acid (**7-ACA**, 4.00 g, 14.7 mmol) was dissolved in tert-butyl acetate (180 mL) in a large, screw-top pressure flask. p-Toluenesulfonic acid (3.10 g, 18.0 mmol) was added and the mixture was stirred for 15 min at room temperature. Sulfuric acid (4.5 mL, 84 mmol) was added slowly over 15 min, and the reaction flask was sealed and stirred at room temperature. The cloudy reaction mixture gradually cleared over the course of the reaction, and was assumed near completion when fully cleared. After 6 h, the reaction vessel was vented slowly, and the mixture was quenched with saturated aqueous $NaHCO_3$ to pH 8.

The organic layer was separated, and the aqueous layer was washed with additional portions (3 × 50 mL) of EtOAC. The combined organic layers were washed with saturated aqueous NaCl, dried with $MgSO_4$ and concentrated in vacuo. The crude product (yellow solid, 2.50 g, 7.61 mmol) was dissolved in a biphasic mixture of 50/50 CH_2Cl_2/ saturated aqueous $NaHCO_3$ (150 mL total) and stirred vigorously at room temperature. Phenyl acetyl chloride (2.01 mL, 15.2 mmol) was added dropwise over 5 min and the mixture was stirred for 2 h at room temperature. The reaction mixture was then diluted with CH_2Cl_2 (50 mL) and the layers were separated; the aqueous portion was washed with additional portions of CH_2Cl_2 (2 × 50 mL). The combined organic layers were washed with saturated aqueous $NaHCO_3$ and then saturated aqueous NaCl, dried with MgSO4 and concentrated in vacuo. The crude product was purified by flash chromatography (0-90% EtOAc/hexanes, stepwise gradient), furnishing the desired product (1.98 g, 30% over two steps) as a white-yellow solid: R_f = 0.65 (50% EtOAc/hexanes); ^{1}H NMR (500 MHz, DMSO-d_6) δ 9.10 (d, J = 8.3 Hz, 1H), 7.33–7.19 (m, 5H), 5.69 (dd, J = 8.4, 4.9 Hz, 1H), 5.10 (d, J = 4.9 Hz, 1H), 4.92 (d, J = 12.7 Hz, 1H), 4.63 (d, J = 12.7 Hz, 1H), 3.55 (dd, J = 63.8, 18.1 Hz, 2H), 3.53 (dd, J = 33.2, 13.9 Hz, 2H), 2.03 (s, 3H), 1.47 (s, 9H); ^{13}C NMR (126 MHz, DMSO) δ 171.4, 170.6, 165.1, 160.8, 136.3, 129.5, 128.7, 127.4, 127.0, 122.7, 83.2, 63.0, 59.6, 58.0, 42.1, 27.9, 26.2, 21.0; HRMS (ESI–) calcd for $C_{22}H_{25}N_2O_6S$ [M-H]$^-$: 445.1439, found: 445.1449 (error = 2.2 ppm); Mp: decomposed at 170 ºC.

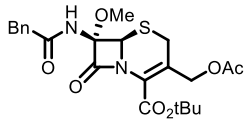

***tert*-Butyl (6*R*,7*S*)-3-(acetoxymethyl)-7-methoxy-8-oxo-7-(2-phenylacetamido)-5-thia-1-azabicyclo[4.2.0]oct-2-ene-2-carboxylate (7).**[251] Intermediate **6** (1.5 g, 3.4 mmol) was dissolved in THF (54 mL) and cooled to -78 °C. LiOMe (315 mg, 8.40 mmol) was dissolved in MeOH (12.3 mL) and added dropwise over 5 min. *tert*-Butyl hypochlorite (675 μL, 6.01 mmol) was added

dropwise over 5 min and the reaction mixture was stirred at -78 °C. After 2 h, the reaction was diluted with 30 mL THF and quenched by pouring into an ice-cold aqueous solution of 5% $NaHSO_3$ / 5% NH_4Cl (100 mL). After stirring for 10 min, the mixture was diluted with 50 mL EtOAc and the layers were separated. The aqueous layer was washed with additional portions (2 × 50 mL) of EtOAc. The combined organic layers were washed with saturated aqueous NaCl, dried with $MgSO_4$ and concentrated *in vacuo*. The crude product was purified by flash chromatography (0-75% EtOAc/hexanes, stepwise gradient), furnishing the desired product (1.43 g, 90%) as a wet yellow solid: R_f = 0.50 (50% EtOAc/hexanes); ^{1}H NMR (500 MHz, DMSO-d_6) δ 9.44 (s, 1H), 7.33–7.20 (m, 5H), 5.16 (s, 1H), 4.86 (d, *J* = 12.7 Hz, 1H), 4.60 (d, *J* = 12.7 Hz, 1H), 3.64–3.52 (m, 4H), 3.35 (s, 3H), 2.02 (s, 3H), 1.48 (s, 9H); ^{13}C NMR (126 MHz, DMSO-d_6) δ 172.0, 170.6, 160.6, 160.4, 136.0, 129.6, 128.7, 127.1, 127.0, 123.4, 95.6, 83.4, 63.0, 62.7, 52.9, 42.2, 27.8, 26.4, 21.0; HRMS (ESI–) calcd for $C_{23}H_{27}N_2O_7S$ $[M-H]^-$: 475.1544, found: 475.1561 (error = 3.6 ppm); Mp: 65 ºC.

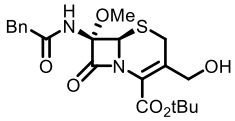

***tert*-Butyl (6*R*,7*S*)-3-(hydroxymethyl)-7-methoxy-8-oxo-7-(2-phenylacetamido)-5-thia-1-azabicyclo[4.2.0]oct-2-ene-2-carboxylate (8).**[252] Intermediate **7** (965 mg, 2.01 mmol) was dissolved in THF (20 mL) in a 500 mL Erlenmeyer flask. Hexanes (150 mL) was added, resulting in precipitation of a portion of the starting material; gentle sonication was used to resolubilize **7**. Lipase B from *Candida antartica* (CALB) immobilized on beads (480 mg, ≥960 U), *sec*-butanol (6 mL), and activated 4 Å molecular sieves were added to the reaction vessel, which was sealed with a Suba•Seal rubber septum and shaken in an incubator at 50 °C, 120 rpm for 5 d. At this point, a small amount of white solid was observed adherent to the sides of the flask; the reaction was cooled to room temperature and this solid was scraped back into the reaction mixture. TLC

monitoring (50% EtOAc/hexanes) suggested the reaction was near completion; the vessel was resealed and continued shaking at 50 °C for an additional 2 d. After a total of 7 d, the reaction was cooled to room temperature and diluted with CH_2Cl_2, then filtered to remove CALB beads and molecular sieves and concentrated *in vacuo*. The crude product (790 mg, 90%) was obtained as a wet, yellow solid and was taken forward without additional purification: R_f = 0.25 (40% EtOAc/hexanes); ^{1}H NMR (500 MHz, DMSO-d_6) δ 9.40 (s, 1H), 7.35–7.20 (m, 5H), 5.10 (s, 1H), 5.08 (t, *J* = 5.7 Hz, 1H), 4.16 (d, *J* = 5.6 Hz, 2H), 3.62–3.51 (m, 4H), 3.35 (s, 3H), 1.48 (s, 9H); ^{13}C NMR (126 MHz, DMSO-d_6) δ 171.4, 160.4, 160.2, 135.6, 130.6, 129.1, 128.2, 126.5, 123.6, 95.0, 82.3, 62.7, 59.6, 52.4, 41.7, 27.4, 25.6; HRMS (ESI–) calcd for $C_{21}H_{25}N_2O_6S$ [M-H]$^-$: 433.1439, found: 433.1482 (error = 9.9 ppm); Mp: 80 ºC.

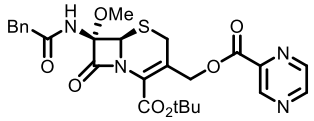

***tert*-Butyl (6*R*,7*S*)-7-methoxy-8-oxo-7-(2-phenylacetamido)-3-(((pyrazine-2-carbonyl)oxy)methyl)-5-thia-1-azabicyclo[4.2.0]oct-2-ene-2-carboxylate (9). 9** was prepared from intermediate **8** (600. mg, 1.38 mmol) and **POA-BT** (342 mg, 1.52 mmol, 1.10 equiv) using the general benzotriazole esterification procedure from the synthesis of intermediate 4. The crude product was purified by flash chromatography (0-75% EtOAc/hexanes, stepwise gradient), furnishing the desired product (350 mg, 47%) as a fluffy yellow solid: R_f = 0.50 (50% EtOAc/ hexanes); ^{1}H NMR (500 MHz, DMSO-d_6) δ 9.46 (s, 1H), 9.23 (d, *J* = 1.5 Hz, 1H), 8.91 (d, *J* = 2.4 Hz, 1H), 8.83 (dd, *J* = 2.5, 1.5 Hz, 1H), 7.33–7.20 (m, 5H), 5.25 (d, *J* = 12.7 Hz, 1H), 5.19 (s, 1H), 4.97 (d, *J* = 12.7 Hz, 1H), 3.75-3.49 (ABqd, *J* = 103.6, 18.2 Hz, 2H), 3.59 (d, *J* = 4.8 Hz, 2H), 3.36 (s, 3H), 1.49 (s, 9H); ^{13}C NMR (126 MHz, DMSO) δ 171.5, 163.2, 160.2, 159.9, 148.3, 145.8, 144.9, 142.8, 135.6, 129.1, 128.2, 127.1, 126.5, 122.6, 95.2, 83.1, 63.8, 62.6, 52.5, 41.7, 27.4, 26.0;

HRMS (ESI–) calcd for $C_{26}H_{27}N_4O_7S$ [M-H]$^-$: 539.1606, found: 539.1619 (error = 2.4 ppm); Mp: 85 ºC.

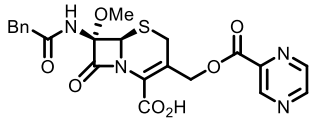

(6*R*,7*S*)-7-Methoxy-8-oxo-7-(2-phenylacetamido)-3-(((pyrazine-2-carbonyl)oxy)methyl)-5-thia-1-azabicyclo[4.2.0]oct-2-ene-2-carboxylic acid (CM-POA). Intermediate **9** (400 mg, 0.74 mmol) was dissolved in CH_2Cl_2 (32 mL) at room temperature. Triisopropylsilane (1.5 mL, 7.4 mmol, 10. equiv) and then trifluoroacetic acid (5.7 mL, 74 mmol, 100 equiv) were added slowly and the mixture was stirred at room temperature for 3 h. Following completion, the reaction was condensed *in vacuo*, then redissolved in toluene and condensed (10 mL × 3) to remove excess TFA. The crude product was loaded onto celite and purified by flash chromatography (0-90% MeOH/ CH_2Cl_2, gradient method) using a RediSep® Gold cyano-functionalized silica cartridge (Teledyne Isco), furnishing the desired product (202 mg, 56%) as a brown solid: HPLC purity: 93.1% (t_R = 7.4 min, k' = 4.1); ^{1}H NMR (500 MHz, DMSO-d_6) δ 13.87 (br s, 1H), 9.45 (s, 1H), 9.22 (s, 1H), 8.91 (d, J = 2.4 Hz, 1H), 8.83 (obs s, 1H), 7.34–7.20 (m, 5H), 5.29 (d, J = 12.8 Hz, 1H), 5.16 (s, 1H), 5.02 (d, J = 12.8 Hz, 1H), 3.61 (ABqd, J = 111.4, 18.1 Hz, 2H), 3.59 (ABqd, J = 20.2, 14.1 Hz, 2H), 3.35 (s, 3H); 13C NMR (126 MHz, DMSO-d_6) δ 171.5, 163.2, 162.5, 160.4, 148.2, 145.8, 144.9, 142.8, 135.6, 129.2, 128.2, 126.8, 126.5, 123.3, 95.1, 64.0, 62.7, 52.5, 41.7, 25.9; HRMS (ESI+) calcd for $C_{22}H_{21}N_4O_7S$ [M+H]$^+$: 485.1125, found: 485.1130 (error = 0.9 ppm); Mp: decomposed at 120 ºC.

2.5.4 Stability Assays

CS-POA was incubated in simulated gastric fluid (pH 1.2) and HEPES buffer (pH 7.4) to assess aqueous stability, and in CD-1 female pooled mouse plasma, Sprague-Dawley female pooled rat plasma, and female pooled human plasma (BioChemed, Winchester, VA) to assess plasma stability, as described previously.[253] 20 μL of compound stock (10.0 mM in DMSO) was added to 980 μL buffer or plasma in triplicate, briefly vortexed and incubated for 60 to 240 min at 37 °C. 100 μL aliquots were removed at 0 min and endpoints and placed on ice; an equivalent volume of MeCN containing 10 μM internal standard (2-hydroxynicotinic acid) was added to plasma samples to precipitate proteins, which were removed via centrifugation (18,000 *x g*, 5 minutes). Samples were filtered through a 0.2 mm PVDF syringe cartridge and analyzed using LC-MS with single ion monitoring. Stability was calculated as the percentage of conjugate remaining at the endpoint. Quantitation was performed using an Agilent 1260 Infinity analytical HPLC system and an Agilent 6120 single quadrupole mass spectrometer. LC separation was performed using a Kinetex C18 column (3.0 x 100 mm, 2.6 μm particle size, Phenomenex) eluting with H_2O/MeCN +0.1% formic acid. **CS-POA** was observed using single ion monitoring ($[M-H]^-$= 453 m/z) and normalized to internal standard ($[M-H]^-$= 138 m/z).

2.5.5. β-Lactamase Overexpression and Purification

2.5.5.1 BlaC: Enzymatic Release Assays

A pET28 plasmid containing truncated *blaC* (codons 41-307) with *N*-terminal His_6-tagged BlaC from *M. tuberculosis* was received as a gift from Dr. John S. Blanchard. *E. coli* BL21(DE3) cells were transformed with this plasmid and cultured in LB broth (37 ºC, 250 rpm) supplemented with 50 μg/mL kanamycin to OD_{600} = 0.5. At this point, 1 mM aqueous IPTG solution was used to induce overexpression, and the culture was cooled to 16 °C and shaken for 18 h. Following

overexpression, the culture was clarified by centrifugation and the pellet was suspended in Tris buffer (75 mL 25 mM Tris + 300 mM NaCl, pH 7.5). The cells were lysed via sonication, debris removed with centrifugation, and the supernatant was incubated onto Ni-NTA agarose resin for 1 h at 4 °C. The resin was then loaded onto a gravity column and eluted using Tris buffer with a gradient up to 200 mM imidazole. The combined 200 mM imidazole fractions were dialyzed to remove imidazole, then repurified by size-exclusion chromatography (SEC) using a Superdex® 200 gel filtration column eluting with 25 mM Tris-HCl buffer containing 300 mM NaCl (pH 7.5). Fractions were assessed by SDS-PAGE, and fractions containing BlaC (MW ~35 kDa) were pooled and transferred to a storage solution (10mM MES/ 50 mM NaCl in 10% glycerol) for long-term storage at -80 ºC. Protein concentration in pooled fractions was determined using a NanoDrop 2000 UV-vis spectrophotometer (Thermo Scientfic) as described previously.[244]

2.5.5.2 BlaC and CTX-M-1: Kinetics Assays

MtbBlaC and *blaCTX-M-1* were codon optimized for *E. coli* and cloned into pET-28b(+) expression vectors, which were used to transform *E. coli* BL21 (DE3) cells. Single colonies were picked and allowed to grow in 50 mL LB (37 ºC, 250 rpm) supplemented with desired antibiotic overnight. Overnight cultures were transferred to 1 L LB broth with kanamycin 50 µg/mL and grown to OD_{600} = 0.6 (37 ºC, 250 rpm). Protein expression was induced by adding 0.5 mM IPTG and reducing the temperature to 20 °C for 16 hours. Cells were harvested by centrifugation at 8000*g* for 10 minutes and resuspended in lysis buffer (50 mM Tris pH 7.5, 150 mM NaCl, and 1.0 M sorbitol) containing cOmplete Protease Inhibitor Tablet (Roche), PMSF (5 mM) and hen egg white lysozyme (0.5 mg/ml). Cells were lysed with an Emulsiflex C3 ultra high-pressure liquidizer (Avestin) at 15000-20000 psi for 15 minutes. Supernatants were obtained after high-speed

centrifugation and incubated with equilibrated Ni-NTA beads for 90 mins at 4 °C on rotator. Both proteins were purified by gravity column and SEC, as described in the previous section.

2.5.6 Enzymatic Release Assays

Mtb BlaC was diluted in buffer (50 mM aqueous NH_4OAc, pH 6.5) to the target concentration (total volume for time course studies = 500 µL). Clavulanate cellulose (Apollo Scientific, 5 mM in DMSO) was added to indicated samples to 100 µM final concentration and all replicates were pre-incubated for 30 min at rt. **CS-POA** was added to 250 µM final concentration at 23 ºC to initiate the reaction. Aliquots of samples were quenched at indicated time points with addition of an equivalent volume of ice cold (aq. 8% TCA soln or MeCN, as indicated). 100 uL was taken on to analysis by analytical HPLC with UV/vis spectrophotometry, monitoring at 280 nm.

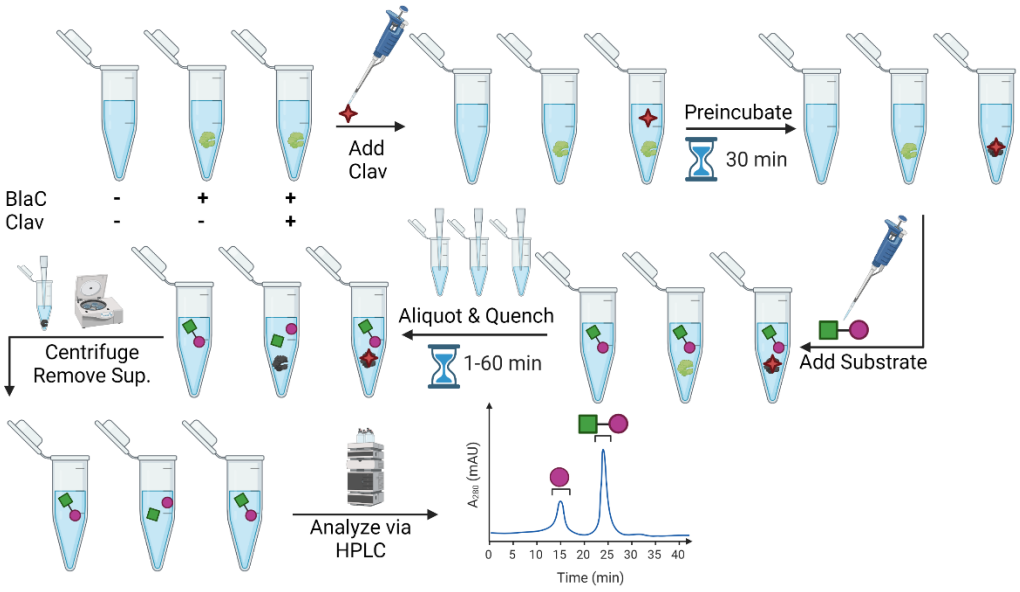

Figure 21. Enzymatic Release Assay Workflow. ♦ = Clavulanate; ■-● = CS-POA; ● = POA. Created with BioRender.com.

2.5.7 Kinetics Assays

Kinetic parameters of **CS-POA**, **CS Pro**, and **CM-POA** were determined for BlaC and CTX-M-1 using a continuous assay measuring the hydrolysis-induced change in absorbance at the indicated wavelengths (**Table 5**). Molar extinction coefficients for hydrolysis were also calculated in order to determine substrate concentrations at measured timepoints, as described previously.[214] Initial velocities were determined for a range of substrate concentrations in order to determine apparent steady-state kinetic parameters. All initial velocity experiments were conducted in buffer (50 mM HEPES, pH 7.5) at 25 °C using enzyme concentrations ranging from 1-50 nM.

2.5.8 Antibacterial Evaluation

2.5.8.1 Nonmycobacterial pathogens

Non-*Mtb* MICs were assessed in *E. coli* K12, *S. aureus* USA300, *A. baumannii* AB5075, and *P. aeruginosa* PAO1 using established methods.[254] These four pathogens were tested for susceptibility against the indicated compounds via broth microdilution in Mueller-Hinton Broth 2 (pH 7.4) in triplicate using 96-well microplates. Each plate was run with a known control antibiotic, as well as each column containing both positive and negative growth controls. In brief, an overnight culture of each bacterium was used to inoculate a range of six concentrations, from 1,600 μM to 50 μM, prepared by serial 2-fold dilutions. The plates were then incubated at 37 ºC for 16-24 hours. After the incubation period, the OD_{600} was determined on a plate reader. The MIC_{90} was identified as the wells that showed less than 90% growth when compared to positive growth control.

2.5.8.2 Mycobacterial Strains

Strains and Media: *M. tuberculosis* H37Rv and *M. bovis* BCG Pasteur were gifts from W. R. Jacobs, Jr., of the Albert Einstein College of Medicine. *M. tuberculosis* H37Rv and *M. bovis*

BCG Pasteur, unless otherwise stated, were grown in Middlebrook 7H9 liquid medium or on Middlebrook 7H10 agar plates supplemented with oleate-albumin-dextrose-catalase (OADC; Becton Dickinson 10% vol/vol), and glycerol (0.2% vol/vol). When grown in liquid format, tyloxapol (0.05% vol/vol) was also added.

Generation of Δ*pncA* Deletion Strain: *M. tuberculosis* H37Rv Δ*pncA* was constructed using the ORBIT recombineering method as described previously.[255-256] In brief, 100 ml of *M. tuberculosis* cells previously transformed with pKM461, the plasmid expressing the Che9c RecT annealase and Bxb1 integrase functions required for ORBIT, was grown from frozen to an OD_{600} of ~0.8. Upon reaching the desired OD_{600}, anhydrotetracycline (ATc; Alfa Aesar) was added at a concentration of 500 ng/ml for induction of RecT and the Bxb1 integrase and allowed to incubate with shaking at 37°C for ~8 h. Following this incubation, 2M glycine was added and incubated with shaking overnight (~16 h). The next day, cells were collected by centrifugation at 4000 RPM in 50-ml conical tubes and the cell pellets were washed with equal-volume 10% glycerol. The centrifugation and washing steps were repeated twice. A final resuspension in 3.2 ml final volume 10% glycerol was completed. Cells were then taken and electroporated with 1 µg of the *pncA* targeting oligo harboring an *attP* attachment site core and 200 ng of the suicide deletion vector pKM464 containing an *attB* core and hygromycin resistance cassette. Plasmid only and no DNA negative controls were also performed in conjunction. Transformed cells were recovered in 2 ml of supplemented 7H9 medium and shaken overnight at 37 °C. The following day, all cells were plated on supplemented 7H10 plates containing 50 µg/ml of hygromycin and 2% sucrose to select for site-specific integration of pKM464 and curing of pKM464 utilizing the counter-selectable marker *sacB*, respectively. Successful deletion of *pncA* was confirmed by PCR using *pncA* specific primers (F and R primers listed) and sequencing of the 5' junction of the pKM464 integrated plasmid. The

targeting oligo sequence used for deletion of *pncA* was 5'-CGGGCAGTCGCCCGAACGTATGGTGGACGTATGCGGGCGTTGATCATCGTCGACGTGCAGGGTTTGTCTGGTCAACCACCGCGGTCTCAGTGGTGTACGGTACAAACCGCCAGCGTCGAGTTGGTTTGCAGCTCCTGATGGCACCGCCGAACCGGGATGAACTGTTGG-3′.

Antimicrobial Susceptibility Determination: Assessment of antimycobacterial susceptibility was completed as previously described.[257] The indicated compounds were assessed in medium adjusted to either low pH (5.8) or neutral (6.8). Mycobacterial strains were grown exponentially to mid-log phase (OD_{600} of ~0.8) and then inoculated into 30-ml Nalgene square-bottles with 5 ml of supplemented 7H9 liquid medium added containing antimycobacterial compounds to a starting OD_{600} of 0.01. Antimycobacterial compounds were added to the final concentrations as indicated in the figures and text. Cultures were incubated with shaking at 100 rpm at 37°C for 7 (*M. bovis* BCG only) or 14 days and following this incubation period, antimicrobial susceptibility was determined by measuring the optical density OD_{600} of each respective bottle. When described, the MIC_{90} of compounds tested was defined as the minimum inhibitory concentration required to inhibit at least 90% of growth relative to no drug control bottles.

2.5.9 Evaluation in THP-1 Activated Macrophages

Adapted from previously described reports.[258-260] Unless noted, macrophages were cultured in RPMI 1640 (ATCC modification) containing 10% heat-inactivated fetal bovine serum (FBS) and 0.05mM 2-mercaptoethanol, herein referred to as RPMI 1640 complete, and incubated in a humidified chamber containing 5% CO_2 at 37°C. THP-1 cells were seeded at a density of 2.0×10^4 cells/mL and treated with phorbol 12-myristate 13-acetate (100 nM) in RPMI complete medium for 72 h to achieve differentiation to macrophages. Macrophages were rinsed thrice using Hank's

Buffered Saline (HBSS) and incubated for an addition 24 h in fresh RPMI 1640 complete medium. Macrophages were later activated with IFN-γ (5 ng/mL) for 16 h prior to infection. Cells were infected with *M. tuberculosis* strain H37Rv at a MOI of 1 for 2 h. Cells were subsequently washed thrice in HBSS and treated separately with DMSO (vehicle control), CS-Pro, PZA, and CS-POA (all at 1.62 mM) in RPMI 1640 complete medium. Medium containing appropriate treatments were refreshed daily throughout the entire length of the study. Upon days 5 and 8 post-infection, cells were washed thrice in HBSS, lysed in 0.01% Triton-X 100, serial diluted, and plated on Middlebrook 7H10 agar supplemented with oleate-albumin-dextrose-catalase (OADC; Becton Dickinson 10% vol/vol), and glycerol (0.2% vol/vol). Plates were incubated for 3 weeks at 37 ºC and colonies were counted to determine CFU/mL measurements.

2.5.10 Intracellular Accumulation Assays

Adapted from the protocol by Chakraborty *et al*.[261-262] Briefly, *M. bovis* (BCG) cells were cultured to mid-log phase (OD_{600} ~0.4) and challenged with 1X/4X MIC concentrations of **CS-POA** and 1X MIC POA. 500 µL culture aliquots were taken immediately prior to compound addition and after 24 h. Aliquots were centrifuged (3.2k RPM) for 10 min at 4 ºC, and pellets were washed twice with 1X PBS. Washed pellets were suspended in 1 mL metabolite extraction buffer (40:40:20 ACN:MeOH:H_2O) in 2 mL screw-top vials charged with 0.1 mm zirconia/silica beads (BioSpec Products). Suspensions were lysed using a BeadBlaster homogenizer (Benchmark Scientific; 2x1 min cycles, chill for 5 min, repeat once) and centrifuged (3.2k RPM) for 10 min at 4 ºC. Supernatants from lysed cultures were filtered through a 0.22 µm filter (Millipore), and approximately 100 µL was saved for protein quantitation. The remaining filtrate was filtered using a 3 kDa Amicon® filtration unit, centrifuging (12k RPM) for 30 min at 4 ºC. Following extraction, 300 µL of each sample was concentrated *in vacuo* and reconstituted in 100 µL of 10 mM

ammonium acetate (90:10 ACN:H_2O; pH 7) containing 10 μM internal standard (POA-d_3, Toronto Research Chemicals). Quantitation was performed using a Shimadzu UFLC-XR system and an AB SciEx QTRAP 5500 mass spectrometer. LC separation was performed using a Zorbax Eclipse XDB-C8 column (4.6 x 150 mm, 5 μm particle size; Agilent), eluting with 5 mM aqueous NH_4OAc (pH unadjusted) in 2% MeCN (solvent A) and 100% MeCN (solvent B) at a flow rate of 0.5 mL/min using the following method: 5% B for 1 min, increase to 95% B over 3 min, 95% B for 3 min, 5% B for 4 min. MS/MS was performed with ESI set to ± 4500 V using the following parameters:

ANALYTE	R_T (MIN)	POLARITY	DP (V)	CE (V)	CXP (V)	Q1	Q3
POA	2.50	Negative	-35	-20	-17	123	79
CS-POA	2.29	Positive	+49	+10	+17	485	333
POA-D_3 (I.S.)	2.51	Negative	-35	-20	-17	126	82
AMPICILLIN (I.S.)	1.72	Positive	+35	+20	+17	350	106

DP: declustering potential; CE: collision energy; CXP: exit potential

Analyte and internal standard peak areas were quantitated using MultiQuant software (Sciex); analyte peak areas were normalized to internal standard peak areas. A standard curve was prepared for POA with 2-fold serial dilutions from 10.00 to 0.08 μM and used to determine concentrations of POA in samples. Zero concentration standards were also prepared and used to determine the lower limits of detection and quantitation, which were defined as 3:1 and 10:1 signal-to-noise ratios, respectively. Concentrations of POA were normalized to the protein concentration of each sample as determined using a BCA protein assay kit (Pierce Biotechnology).

2.5.11 Pantothenate Antagonism Assays

Assays were performed following the reported method, and generally described in the procedure for Mycobacterial Strains: Antibacterial Susceptibility Determination, using *M. bovis* (BCG) in 7H9 liquid medium (pH 6.8).[257] Indicated cultures were supplemented with 0.1 mM

pantothenate, and OD_{600} at day 5 was compared with the untreated control to determine relative growth percentage.

2.5.12 Frequency of Resistance Determination

The frequency of resistance (FoR) for PZA, POA, CS-POA and CS Pro at acidic pH (5.8) was determined by plating of approximately 2 X 10^7 cells onto large supplemented 7H10 agar plates (Corning 245mm Square BioAssay Dish) containing OADC and containing drugs at a concentration of 4X their previously determined MIC values. Following incubation at 37°C for 4 weeks in a standing incubator at atmospheric CO_2, resistant colonies were enumerated. The FoR was calculated as the CFUs counted divided by the total number of bacteria plated for each compound after plating serial-dilutions of the initial culture.

2.6 Acknowledgements

This work was supported by a grant (5R21AI144501-02 to C.C.A. and A.D.B.) from the National Institutes of Health. Mass spectrometry was carried out with the assistance of Dr. Bruce A. Witthuhn (College of Biological Sciences, University of Minnesota). The pET28-*blaC* plasmid used for *E. coli* transformation was a gift from Dr. John S. Blanchard (Department of Biochemistry, Albert Einstein College of Medicine). M.S.C. received funding from The 3M Company and the National Institutes of Health (5T32GM008700-18).

Chapter 3. Synthesis, Biological Evaluation, and Structure-Activity Relationships of Novel Pyrazinoic Acid Analogues for *Mycobacterium tuberculosis*.

Adapted in Part and with Permission from:

Ragunathan P, Cole M, Latka C, Aragaw WW, Hegde P, Shin J, Subramanian Manimekalai MS, Rishikesan S, Aldrich CC, Dick T, Grüber G. *Mycobacterium tuberculosis* PanD Structure-Function Analysis and Identification of a Potent Pyrazinoic Acid-Derived Enzyme Inhibitor. *ACS Chem Biol.* **2021**, *16* (6), 1030-1039.

This work was performed in collaboration with Dr. Priya Ragunathan, Dr. Chitra Latka, Dr. Wassihun Wedajo Aragaw, Pooja Hegde, Dr. Joon Shin, Dr. Malathy Sony Subramanian Manimekalai, Dr. Sankaranarayanan Rishikesan, Dr. Courtney C. Aldrich, Dr. Thomas Dick, Dr. Gerhard Grüber, Dr. Gorakhnath Jachak, and Eric Hess.

MSC designed the library, developed reaction conditions and LC methods, synthesized compounds (POAA008-010, 012, 015-018, 020-029, 060-061), assisted with PanD production and ^{1}H-NMR assays, edited the original manuscript and wrote the chapter. PR wrote the original manuscript; PR, CL, JS, MSSM, and SR produced PanD, performed the ITC and ^{1}H-NMR assays, analyzed the previously reported PanD-POA crystal structure (6OYY) as part of the rational inhibitor design, and edited the original manuscript. PH designed the library, synthesized compounds (POAA031-059), assisted in compound characterization, and edited the original

manuscript. WWA constructed the *M. bovis* L132R PanD and *M. bovis* RFP-PanD mutant strains, performed all MIC assays, and performed the reporter degradation assays. CCA, TD, and GG conceived of the project, provided feedback and edited the original manuscript. GJ provided technical support on compound synthesis and provided valuable insight on the saponification reaction. EH synthesized intermediates.

3.1 Introduction

The previous section described one strategy to overcome PZA resistance- an alternative, non-PZase dependent form of the active metabolite, POA. This chapter will cover another approach: developing new POA analogues featuring modifications to the pyrazine ring and its substituents. To provide context to this approach, the history of PZA, including its discovery and serendipitous success, and the continued, unresolved efforts to determine its mechanism of action, will be described.

3.1.1 Pyrazinamide: Discovery and Adoption

Following its initial reporting in 1936 at Merck, the development of PZA as an antitubercular began in the early 1950s, when two pharmaceutical companies independently identified the molecule, through screening of nicotinamide analogues, as a potent inhibitor of TB in a murine infection model.[263-265] Previous studies by Chorine and colleagues suggested nicotinamide possessed inhibitory activity against another mycobacterium, *M. leprae*, the causative organism of leprosy, and researchers were eager to determine whether a similar molecule could be used to treat *Mtb* as well.[192, 266] Following this initial identification, a number of studies confirmed potent *in vivo* inhibition, including seminal reports by McCune *et al* describing the unique sterilizing activity of PZA, which cleared infection from mouse lung and spleen infections with comparable activity to the first-line isoniazid (INH).[267-268] Unfortunately, resistant organisms were observed after several months of treatment, highlighting a limitation of pyrazinamide monotherapy; importantly, this limitation was overcome when PZA was used in combination therapy with INH, rapidly clearing bacteria from both pulmonary and systemic infections to undetectable levels within six weeks. Furthermore, no resistant strains were observed after over three months of observation (and even to nine months when tissue homogenates were cultured *in vitro*), demonstrating the

viability of this strategy in clearing both active and latent TB from the host.[268] A similar six month treatment course in guinea pigs determined PZA achieved persistent clearing of TB lesions following eight to twelve weeks of treatment.[268] This promising study was, amazingly, preceded by small trials in human patients, and was followed by more widespread adoption into clinical use in the subsequent decades.[192, 263, 269-271] Despite this success, PZA's use was limited primarily to second-line therapy due to hepatotoxicity observed at the extremely high dosages used for treatment (3g/day).[263] Fortunately, additional dosage trials in the 1970s exploring PZA in combination with rifampicin (RIF) and INH confirmed efficacy could be maintained at lower doses, eliminating the observed long-term effects and allowing PZA to enter clinical use as a first line antitubercular.[263]

Since its incorporation, PZA has remained a staple of TB therapy, in large part due to its unique activity clearing latent, non-replicating *Mtb*, which is frequently missed by the other, more potent first-line agents. Following McCune's early reports demonstrating the sterilizing effect of PZA co-therapy in mice, subsequent studies on its use in humans have suggested PZA shortens the duration of first-line therapy substantially.[267-268] First line therapy without PZA, consisting of RIF, INH and ethambutol (EMB) requires an estimated 9-12 months to clear latent TB; addition of PZA shortens this duration to 6 months, and PZA treatment is only required for the first 8 weeks of this regimen.[263, 272-273] PZA is also critical for the treatment of multidrug-resistant (MDR) TB in combination with second-line agents; MDR-TB with additional resistance to PZA requires a significantly longer treatment course (24 months, as compared to 9-12 months for PZA-susceptible MDR-TB), and treatment failure/relapse are more common for these cases.[274-275] Furthermore, PZA has demonstrated excellent synergy with emerging TB therapeutics, including bedaquiline (approved in 2012) and pretomanid (approved in 2019), and is considered the most likely of the first-line antituberculars to remain essential in future treatment regimens.[195, 276-277]

3.1.2 A Mysterious Mechanism

Despite its importance in TB therapy, PZA's mechanism of action is still poorly understood over 70 years after its first use in human patients. One particularly striking feature is its extremely weak *in vitro* activity under normal growth conditions: at pH 6.8, PZA is essentially inactive, with an MIC over 1000 μg/mL. Indeed, had the original nicotinamide drug discovery program employed more typical *in vitro* testing, PZA may have never been identified. Fortunately, this study directly assessed *in vivo* efficacy, a setting in which PZA activity is substantially improved. In fact, a number of conditions have been identified that potentiate the activity of PZA. In the mid-1950s, McDermott and others discovered that reduced pH potentiated PZA; acidified media is now typically used to assess PZA in *in vitro* experiments, and it was long believed that acidic conditions were required for PZA activity (though recent reports have disproven this theory, as will be discussed in the following section).[278-283] A number of other conditions have also been found to potentiate the activity of PZA, including anaerobic conditions,[284] nutrient limitation,[285] oxidative stress,[286-287] and the infection microenvironment produced by the host's immunopathology.[192, 277, 288] These observations suggest environmental stressors, along with *Mtb*'s response to this stress, somehow enhance PZA's cell killing ability. This important clue has not yet led to a definitive mechanism of action for PZA, although several putative targets have been suggested over the years.

One accepted facet of PZA's pharmacology is that the molecule acts as a prodrug, and conversion to the corresponding acid POA is required for activity. PZA is hydrolyzed by an amidase, PZase, encoded by *pncA*. PZase is an enzyme in the NAD+ salvage pathway and is responsible for catalyzing the analogous conversion of nicotinamide to nicotinic acid (**Figure 22**). The NAD+ salvage pathway is one method by which *Mtb* biosynthesizes NAD+, an essential co-factor involved in biological redox and ADP-ribose transfer reactions.[289] Through the salvage

pathway, *Mtb* can resynthesize NAD+ from other nicotinamide pathway metabolites, which can be scavenged from neighboring bacteria or from the host itself.[289-290] *Mtb* is also able to produce NAD+ *de novo* from Asp, but the salvage pathway is thought to be activated in response to environmental stressors, such as nutrient limitation or hypoxia, which are commonly encountered by *Mtb* during the course of an infection (**Figure 22**).[289-290] Critically, despite this stress-induced preference, the salvage pathway is not essential for survival *in vivo*, and in fact does not appear to impact *Mtb* fitness when silenced. *Mtb*'s ability to hydrolyze PZA was observed soon after its discovery, and this activity was even used in a diagnostic capacity to distinguish the organism from the bovine mycobacterium *M. bovis*, which is genetically similar to *Mtb* but lacks PZase activity due to a C to G point mutation within *pncA*.[291-292] However, the relationship between *pncA* and PZA action was only gradually untangled over several decades, culminating in a seminal 1996 paper by Scorpio and Zhang identifying PZA-resistant mutants harboring mutations in *pncA*.[291-294] It is now estimated that 70% of PZA-resistant clinical isolates carry *pncA* mutations, underscoring the critical role PZase holds in maintaining PZA susceptibility.[224, 295]

So if POA, not PZA, is the active metabolite toxic to *Mtb*, how does it exert its antitubercular effect? This question has been explored over decades of research, and still lacks a satisfying conclusion. One early theory postulated that POA acts as a protonophore, disrupting the electrochemical gradient required for ATP production.[281, 296] POA, a weak acid (pKa = 2.9), could act as a proton shuttle, carrying protons from the acidic microenvironment inside the granuloma into TB. This process would acidify the cytoplasm, depolarizing the proton-dependent membrane potential required for oxidative phosphorylation.[281, 296] Several key early pieces of

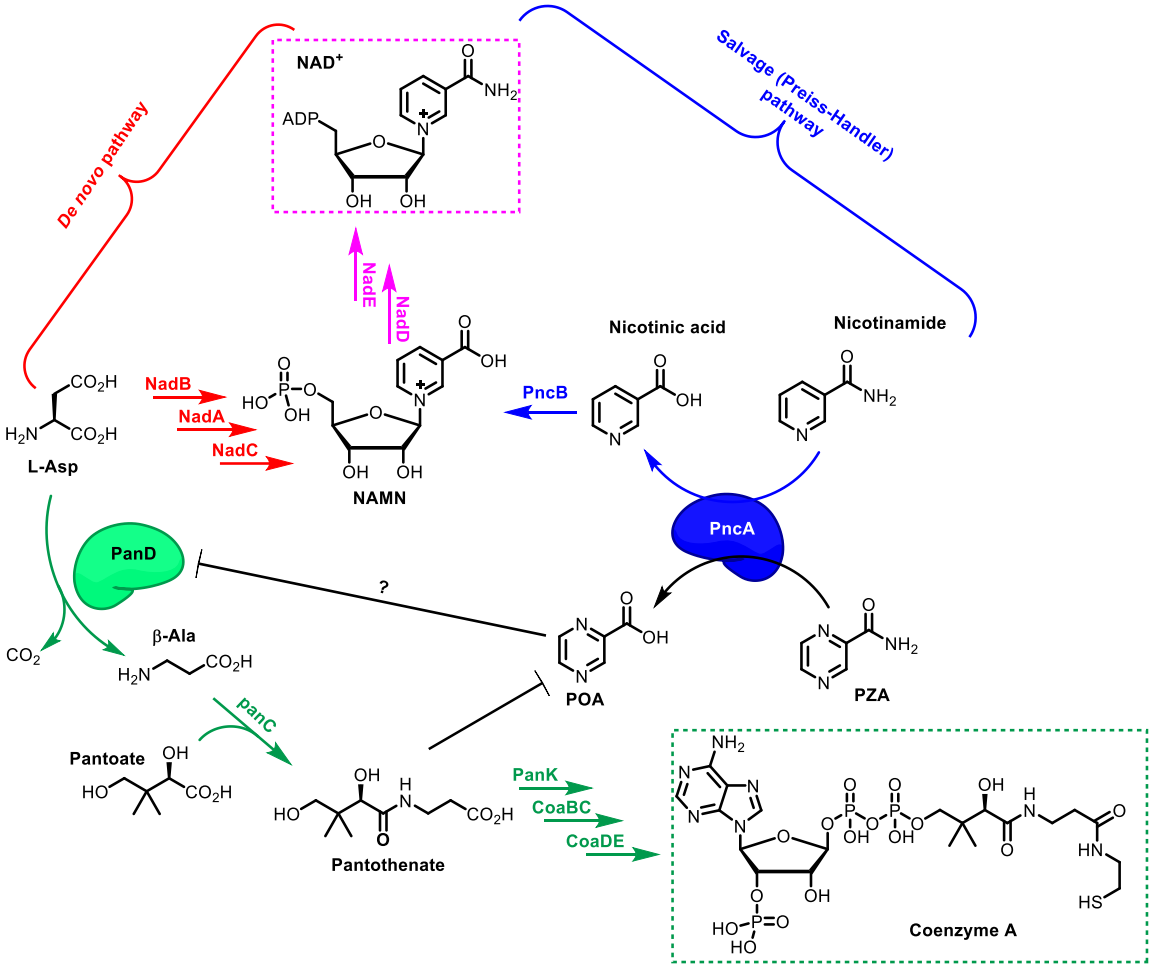

Figure 22. Interactions Between PZA/POA and Biosynthetic Pathways in *Mtb*. [197, 290]

evidence provided support to this theory: PZA/POA appeared to require acidic pH for activity *in vitro*, and pH correlation to antibacterial activity is very similar to the relationship between pH and protonation state predicted by the Henderson-Hasselbach equation for POA;[297] PZA is potentiated by known inhibitors of ATP synthesis, providing evidence of a shared target;[281] and POA has been shown to decrease ATP synthesis and the proton motive force (PMF) in *Mtb* membrane vesicles *in vitro*.[298] However, more recent reports called this theory into question, demonstrating that PZA retains activity *in vitro* at neutral pH in the presence of other activating factors, including nutrient limitation, *pncA* overexpression, reduced culture temperature, or the use of minimal medium.[282-283, 299] Additionally, the ability of PZA/POA to acidify the cytoplasm and collapse membrane potential in the whole cell remains controversial, and conflicting reports exist regarding this activity.[282, 300] Another early theory proposed fatty acid synthase I (FAS-I) as a putative target, citing evidence that a close analogue, 5-Cl PZA inhibited purified *Mtb* FAS-I in biochemical assays, as well as *Mtb* fatty acid production *in vitro* (**Figure 23**).[301] Other 5-substituted PZA analogues, as well as simple POA esters have also been shown to inhibit FAS-I, and 5-Cl PZA has been proposed as a potential alternative treatment for PZA-resistant TB.[302-303] An early disputing report by Boshoff *et al* has largely undermined this theory by demonstrating that, while 5-Cl PZA does indeed inhibit fatty acid production *in vitro*, POA fails to recapitulate this activity and does not inhibit purified enzyme in biochemical assays;[304] however, an intriguing recent report has provided evidence that both PZA and POA inhibit FAS-I, but each molecule binds the enzyme at a different site and functions through differing inhibitory paradigms.[305] A more recently proposed and highly controversial theory, first proposed by Shi and colleagues, suggests that POA interferes with *trans*-translation through inhibition of ribosomal protein S1 (RpsA) (**Figure 23**).[306] *Trans*-translation is a cellular process by which stalled ribosomes are rescued and erroneous polypeptides are degraded following

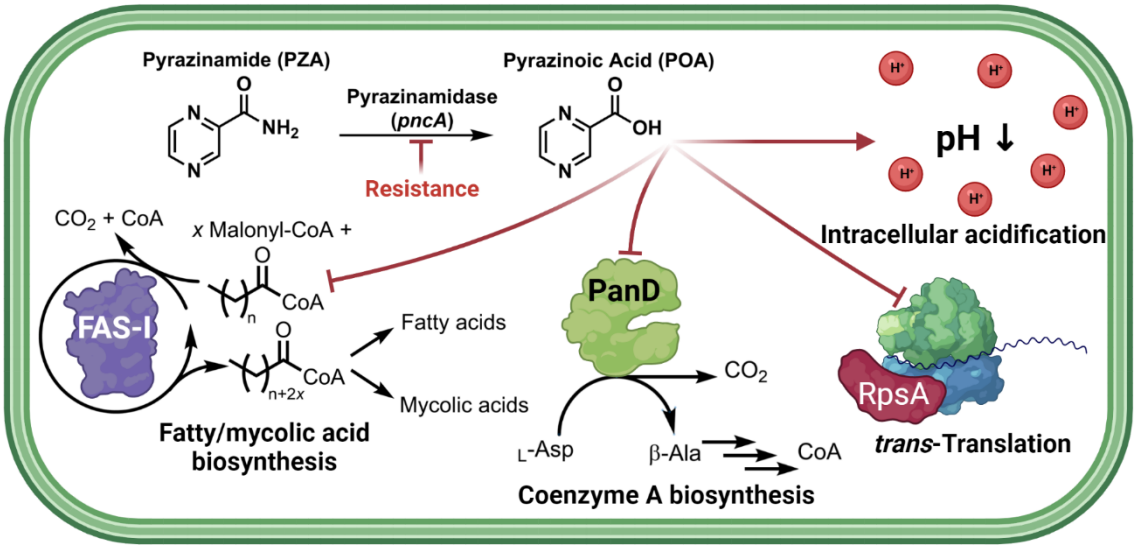

Figure 23. PZA Activation and Proposed Mechanisms of POA Activity. As reviewed by Lamont *et al.*, 2020.[307] Created with BioRender.com.

errors in translation. This process allows translation to proceed efficiently and has been shown to be critical to *Mtb* virulence and stress response. In the seminal study, researchers identified RpsA through pull-down assays with another close POA analogue, 5-OH POA; subsequent experiments determined that *rpsA* overexpression conferred fivefold resistance to PZA *in vitro*, and a PZA-resistant clinical isolate without *pncA* mutations was confirmed to have a point mutation in *rpsA*. Follow-up studies suggested *rpsA* mutations were not useful for identifying PZA resistance in clinical isolates, and mutants with deleted *smpB*, another important *trans*-translation enzyme, did not show altered susceptibility to PZA.[308-309] Two more recent reports have found little evidence of POA-RpsA interactions with a variety of biophysical techniques, while also making the point that the PZA-resistant *rpsA* mutant identified by the authors retains PZA susceptibility *in vivo*;[310-312] Shi and colleagues have also published a follow-up report that provides some light refutations to these

disputing studies, including evidence that *rpsA* point mutations in WT *Mtb* cause mild PZA resistance.[118]

3.1.3 New Theory on the Block: PanD and PZA

The most recent and arguably best-supported hypothesis suggests POA exerts its antitubercular effect through inhibition of PanD, an aspartate decarboxylase essential for *de novo* Coenzyme A (CoA) biosynthesis in *Mtb* (**Figure 22 & 23**). CoA is an acyl carrier moiety present is a wide variety of enzymes, and is an essential co-factor for central metabolism, including metabolism of fatty acids (which may in part explain some of the early results indicating FAS-I as a target of POA).[313-314] In 2013, Zhang and colleagues identified PZA-resistant mutants with WT *pncA* and *rpsA* that contained point mutations in *panD*, previously uncharacterized for its effect on PZA activity.[315] Early supportive evidence of this theory included further screens confirming *panD* mutants with PZA/POA resistance,[310, 313] as well as the presence of *panD* point mutations in *Mtb* clinical isolates,[315] and the finding that supplementation with β-Ala (the product of PanD-catalyzed Asp decarboxylation) and pantothenate (a downstream CoA pathway metabolite) antagonize both PZA and POA *in vitro* (**Figure 22**).[200] The study by Gopal *et al* introduced several new findings, including the discovery that POA-resistant mutations specifically mapped to the C-terminus of PanD and that POA treatment induced depletion of CoA biosynthesis intermediates (a trend ameliorated in the resistant mutants).[313] Two subsequent reports by this group in 2017 presented new insights, including confirmations of the *in vivo* viability of *panD* mutants, binding of POA (but not PZA) to PanD through ITC, and loss of binding in C- and N-terminal mutants.[316-317] These studies also introduced a new player into the PanD-PZA paradigm: mutations to *ClpC1* were also found to confer POA resistance. ClpC1 is an unfoldase/ATPase and a key component of the caseinolytic protease complex, an enzyme responsible for proteome regulation and maintenance.[317]

While the authors initially speculated ClpC1 was inhibited by POA, the most recent study in this sequence has provided a more intriguing explanation: POA binding to PanD is only weakly inhibitory to β-Ala production, but binding at the C-terminal tail triggers recognition and degradation by the ClpC1-ClpP caseinolytic protease complex.[318] This interesting targeted degradation mechanism has been previously exploited for anticancer therapies, such as the PROTAC strategy employing E3 ubiquitin ligase. Despite strong experimental support for this mechanistic theory, several conflicting pieces of evidence remain, such as the lack of *panD* mutations in clinical isolates or the fact that a pantothenate auxotrophic strain, *Mtb* $mc^2$7000, retains susceptibility to PZA at sub-antagonistic levels of pantothenate.[192, 257, 317, 319] A recent report by Sun and colleagues provided structural evidence that POA binds to PanD, but near the active site at the interface between subunits of the tetrameric complex, functioning alone as a competitive inhibitor, a model conflicting with the proposed degradation mechanism by Gopal *et al*.[320] Additionally, several other minor theories for molecular targets of PZA/POA have been proposed over the years, as recently reviewed by Gopal.[321] Thus, despite significant efforts and experimental evidence, a conclusive mechanistic explanation for the confounding activity of this important antitubercular remains elusive.

3.1.4 Research Goals: Designing Next-Generation POA Analogues

Given the previously described urgent need for novel treatments for antibiotic-resistant TB, our lab has undertaken efforts to design next-generation analogues of PZA/POA with increased potency and improved activity against resistant organisms. In collaboration with the Dick and Gruber labs, who have pioneered the recent insights into POA action, we have also endeavored to use these analogues to further probe the relationship between POA structure and PanD inhibition. In strategizing for a structure-activity relationship (SAR) campaign with PZA/POA, we came to

several realizations about the existing SAR knowledge present in the literature (**Figure 24A)**. Modifications to PZA have largely focused on functionalization of the amide, from simple alkyl and aryl groups to co-drug approaches conjugating a second antibiotic.[322-328] Substitutions off the pyrazine ring have generally involved simple functional groups, most commonly at the 5 position, and have generally reported relatively narrow SAR.[329-335] However, from the outset we were less interested in pursuing PZA analogues than the corresponding acids. PZA requires activation to POA, a trait that would likely be shared by analogues with a shared mechanism of action. Amide-functionalized analogues would thus be converted to normal POA, which would remove the potential for new mechanistic insights as a result of our studies. Additionally, modifications to either the amide or pyrazine ring of PZA would need to not only retain on-target activity, but also remain substrates for PZase. In our view, an SAR campaign with amides would potentially miss key SAR insights by selecting for PZase-activatable analogues. Therefore, we endeavored to focus our campaign on analogues of POA, which has been explored significantly less in existing literature. Many reports focus on preparing POA esters, which circumvent *pncA*-mediated resistance and have been explored as alternative PZA proforms (as described in Chapter 2).[204-205, 325, 336-342] Comparatively few reports have described POA analogues with functionalization off the pyrazine ring, and most of these reports precede any mechanistic understanding of PZA/POA activity (**Figure 24A**).[320, 343-348] Finally, isosteres of the pyrazine ring have been well characterized (PZA is itself an isostere of a previously discovered antitubercular, nicotinamide), but only a few reports describe activity of isosteres of the carboxylic acid group.[349-350] Ultimately, we designed our SAR campaign to cover some of the existing knowledge gaps in the literature, primarily focusing on 3-, 5-, and 6-substituted POA analogues, as well as limited evaluation of analogues featuring isosteric replacement of the pyrazine or carboxylic acid (**Figure 24B**). The aims of our

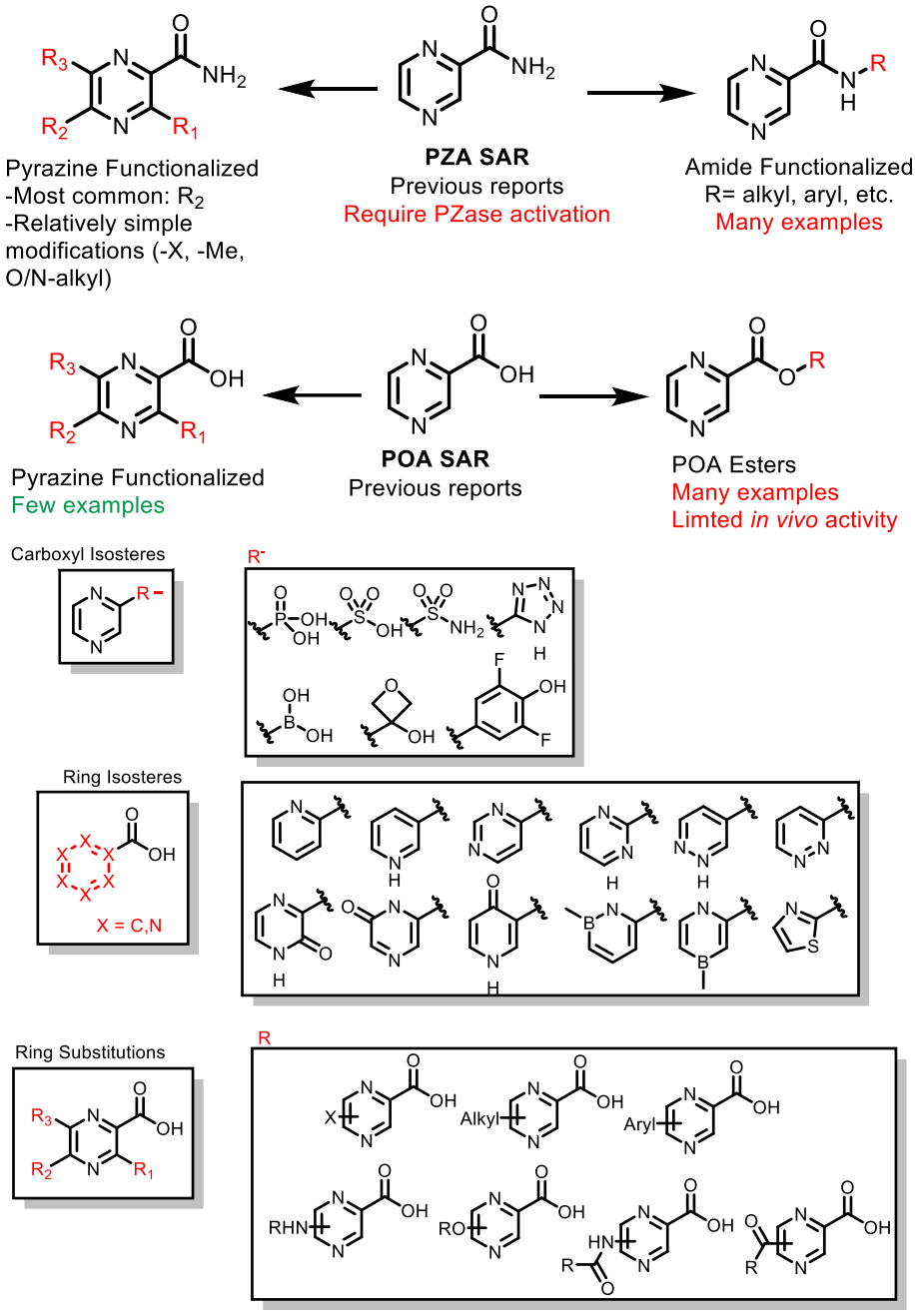

Figure 24. Designing an SAR Campaign for POA. A. Summary of previous reports on PZA/POA analogues. **B.** Initial proposed library of POA analogues.

study were to: 1) synthesize novel POA analogues using robust chemical techniques; 2) evaluate the activity of these analogues *in vitro* against *Mtb* H37Rv, as well as several POA-resistant mutants; and to 3) query interesting analogues with biophysical techniques, such as ITC and ^{1}H NMR, to further investigate interactions between the new analogues and PanD.

3.2 Results and Discussion

3.2.1 Synthesis of POA Analogues

Synthetic routes to the substituted POA analogues are described in the Experimentals section. We employed robust synthetic methods toward diversity-oriented synthesis of a small library for biological experiments, allowing for straightforward preparation of approximately 40 analogues from several common intermediates. Amino-substituted analogues were prepared through S_NAr reactions with a variety of amines, taking advantage of the electron-deficient pyrazine ring to achieve robust yields. This reaction proved more challenging for the 6-substituted analogues; a small screen was able to identify relatively forcing conditions that achieved moderate success, but this increase in reaction yield was not worth the impracticalities of running reactions in DMSO (**Table 8**). The use of 3/5/6-Cl POA esters in preparation of the amino analogues was advantageous, as this substrate could also be used in Suzuki couplings to prepare biaryl POA analogues. Another screen identified suitable conditions for achieving moderate yields with a variety of aryl boronic acids, although it was noted that nitrogen-containing boronates performed more poorly (**Table 9**). Finally, amido-functionalized analogues were prepared from condensation of 3-NH_2 POA methyl ester and acid chlorides; variations in reaction time were required to achieve completion for some of the bulkier substrates, likely due to steric clash between the large aryl substituents and the neighboring POA methyl ester. We employed methyl esters as starting substrates in order to simplify reaction purification; functionalized analogues were deprotected

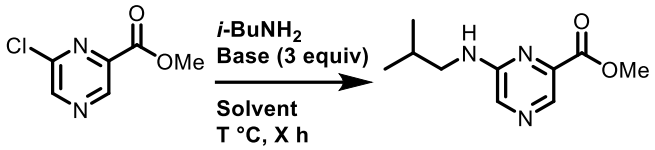

Table 8. S_NAr Optimization for 6-Amino Analogues.

Entry	Base	Solvent	T	X	%Yield
A	DIPEA	1,4-dioxanes	95	24	34
B	TEA	toluene	110	18	trace
C	TEA	DMF	110	18	trace
D	TEA	DMSO	110	18	**50**
E	TEA	1,4-dioxanes	95	18	amide form. preferred
F	TEA	DMSO	60	48	trace
G	TEA	DMSO	80	15	4
H	TEA	DMSO	100	15	34

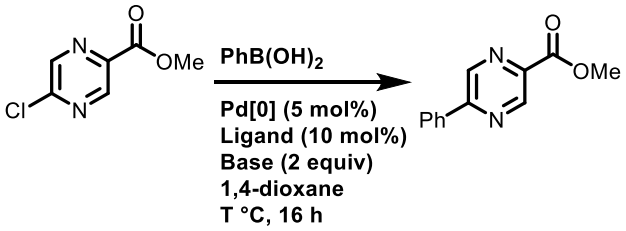

Table 9. Suzuki-Miyaura Coupling Optimization.

Entry	Pd[0]	Ligand	Base	T	%Yield
A	$Pd(PPh_3)_4$	-	K_3PO_4	80	61
B	$PdCl_2(PPh_3)_2$	-	K_3PO_4	80	**68**
C	$Pd(OAc)_2$	*t*-Bu Brett Phos	K_3PO_4	80	trace
D	$Pd(OAc)_2$	SPhos	K_3PO_4	80	**71**
E	$PdCl_2(PPh_3)_2$	-	K_3PO_4	100	56
F	$PdCl_2(PPh_3)_2$	-	Na_2CO_3	100	38
G	$Pd(OAc)_2$	SPhos	K_3PO_4	100	61

using simple saponification conditions (which had to be carefully monitored for the potentially labile 3-amido analogues) and purified as sodium salts for synthetic simplicity.

3.2.2 *In Vitro* Evaluation Against *Mycobacterium bovis*

Analogues were evaluated *in vitro* against *Mycobacterium bovis* (BCG), an attenuated species with inherent PZA resistance (due to a point mutation in *pncA* preventing activation).[291-292] Activity was also assessed using a mutant strain, *M. bovis* PanD L132R, containing a mutation in *panD* previously shown to confer POA resistance.[313, 318] This mutation is located in the PanD C-terminus and has been demonstrated to be important for POA binding to PanD; we planned to use this strain as a control for distinguishing between on-target (i.e. PanD-targeted) binding and non-specific cytotoxicity. The expected result is shown for POA, which demonstrates a five-fold decrease in inhibition of this mutant (**Table 10**); analogues which bind in a similar fashion should thus demonstrate reduced activity against the L132R mutant, while off-target analogues will retain activity. MIC assays revealed several insights regarding POA SAR. Modifications at the 3-position appear well-tolerated, with all but one of the most active analogues (*M. bovis* BCG $MIC_{50} < 0.50$ mM; red highlights) bearing substituents at this position (**Table 10**). Bulkier groups were tolerated at this position, although the presence of a hydrogen bond donor appears important, as both the C-C linked biaryl analogues and the analogues bearing tertiary amine linkages displayed decreased activity compared to POA. Substitutions at the 6 position also appeared to negatively affect activity, contradicting the findings of an earlier report employing 6-Cl POA (**Table 12**);[320] isosteric replacement of the pyrazine ring and carboxylate also decreased activity, although closer carboxylate isosteres will need to be evaluated prior to making claims about its essentiality to activity (**Table 13**). Unfortunately, solubility was an issue with many of the compounds assessed, exacerbated by the extremely high concentrations required for achieving antimycobacterial activity

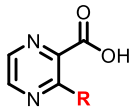

Table 10. MIC_{50} data (mM) for 3-substituted POA analogues.

Compound	*R* =	*M. bovis* (BCG)	*M. bovis* PanD L132R
POA	H	1.0	5.0
POAA008	NH_2	0.80	0.90
POAA010		1.1	1.4
POAA012		**0.22**	**0.31**
POAA017		1.5	2.7
POAA021[a]		n.d.	n.d.
POAA023	NEt_2	3.6	6.5
POAA024	NH*i*-Bu	**0.18**	**0.46**
POAA026	Ph	1.5	3.2
POAA027	(4-F)Ph	3.4	3.5
POAA028	(4-SMe)Ph	1.8	3.6
POAA029	(*o*-Me)Ph	10	>10
POAA031		4.7	7.5
POAA032		>2.5	>2.5
POAA033	NHBn	**0.23**	**0.23**
POAA034	NHPh	**0.40**	**0.50**
POAA035		**0.40**	**0.40**
POAA036		**0.40**	**0.40**
POAA037		>5	>5
POAA038		8.0	>10
POAA039	NHEt	**0.40**	**0.50**
POAA040	NH*n*-Bu	0.60	0.60
POAA041		>2.5	>2.5
POAA060	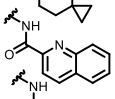	**0.30**	**0.26**
POAA061	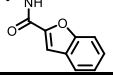	1.0	0.80

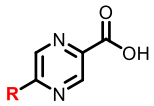

Table 11. MIC_{50} data (mM) for 5-substituted POA analogues.

Compound	*R* =	*M. bovis* (BCG)	*M. bovis* PanD L132R
POA	H	1.0	5.0
POAA001	Cl	1.7	3.7
POAA002	Me	3.2	5.4
POAA009	NH_2	0.78	0.75
POAA018	NEt_2	1.0	1.7
POAA020[a]	Ph	n.d.	n.d.
POAA022	NH*i*-Bu	**0.36**	**0.57**
POAA025[a]	(*o*-Me)Ph	n.d.	n.d.
POAA042[a]		n.d.	n.d.
POAA043[a]		n.d.	n.d.
POAA044[a]		n.d.	n.d.

POAA045		1.5	2.8
POAA046		>2.5	>2.5
POAA047[a]	NHPh	n.d.	n.d.
POAA048[a]		n.d.	n.d.

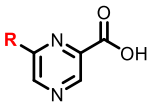

Table 12. MIC_{50} data (mM) for 6-substituted POA analogues.

Compound	*R* =	*M. bovis* (BCG)	*M. bovis* PanD L132R
POA	H	1.0	5.0
POAA003	OMe	2.0	2.6
POAA049		2.0	>2.5
POAA050[a]		n.d.	n.d.
POAA051		>2.5	>2.5
POAA052		>2.5	>2.5
POAA053	NHEt	>2.5	>2.5
POAA054		1.0	1.2
POAA055	NH*i*-Bu	>2.5	>2.5
POAA056	Ph	1.7	1.7
POAA057	(4-F)Ph	2.8	3.5
POAA058	(*o*-Me)Ph	>2.5	>2.5
POAA059[a]	(4-SMe)Ph	n.d.	n.d.

Table 13. MIC_{50} data (mM) for POA isosteres.

Compound	Structure	*M. bovis* (BCG)	*M. bovis* PanD L132R
POA		1.0	5.0
POAA004[a]		n.d.	n.d.
POAA005		10	>10
POAA006		7.0	7.5
POAA007	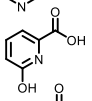	9.0	7.0
POAA011	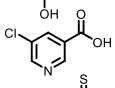	1.6	2.6
POAA013	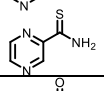	2.7	3.8
POAA014		>10	>10
POAA015	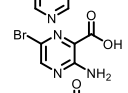	2.1	3.1
POAA016	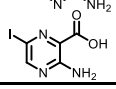	1.6	1.8

[a] Compound was insufficiently soluble to determine MIC. n.d. = not determined.

in vitro. Solubility issues limited the upper concentration usable for certain analogues and disallowed evaluation of others entirely including a large number of the 5-substituted analogues, limiting our ability to make claims about modifications at this position (**Table 11**). We attempted unsuccessfully to solvate troublesome compounds with a variety of solvents and cosolvents, as well as heating and sonication. Efforts are currently underway to evaluate alternative forms of these analogues with potentially improved solubility, including simple esters and salts featuring different counterions; hopefully, these modifications will allow for evaluation of POA SAR at the 5-position as well.

3.2.3 Biochemical Evaluation Against *Mtb* PanD: ITC and ^{1}H NMR Assays

Analogues with promising antimycobacterial activity were further evaluated for inhibition of PanD using biochemical techniques. First, binding to *Mtb* PanD was assessed using isothermal titration calorimetry (ITC). Due to the solubility issues noted previously, primarily the 3-substituted analogues were evaluated in these assays. In addition to the most potent analogues, we also selected for evaluation compounds with apparent on-target activity (indicated by decreased activity against the L132R mutant), such as POAA015, 023, and 026. General trends were difficult to identify for these results, and selective activity against the WT strain appeared to poorly predict PanD binding. Nonetheless, several analogues were identified with PanD binding affinities comparable to POA (**Table 14**). Similar to the antimicrobial results, the presence of a hydrogen bond donor and bulky substituent appears preferred at the 3 position (with a few exceptions, as in the case of POAA033). Some of the more potent binders, such as POAA015, displayed poor activity in the antimicrobial assays, suggesting PanD binding alone may be insufficient for growth inhibition. To further assess this hypothesis, a select few analogues were assessed in ^{1}H nuclear magnetic resonance (NMR)

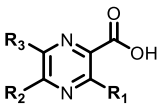

Table 14. Biochemical Evaluation of PanD Binding and Inhibition.

Compound	R_1	R_2	R_3	K_D (μM)[a]	PanD % Inhibition[b]
POA	H	H	H	20 ±0.2	4.8
POAA001	H	Cl	H	47	-
POAA002	H	Me	H	22	-
POAA003	H	H	OMe	26	-
POAA008	NH_2	H	H	40 ±1.8	13.5
POAA009	H	NH_2	H	37.3	-
POAA010		H	H	50 ±3.2	64.3
POAA012		H	H	**20 ±0.5**	**95.5**
POAA015	NH_2	H	Br	**14 ±0.9**	15.1
POAA016	NH_2	H	I	100 ±4.8	-
POAA017		H	H	200 ±0.9	-
POAA022	H	NH*i*-Bu	H	n.d.[c]	-
POAA023	NEt_2	H	H	n.d.[c]	-
POAA024	NH*i*-Bu	H	H	265 ±4.5	-
POAA026	Ph	H	H	n.d.[c]	-
POAA027	(4-F)Ph	H	H	550 ±20	-
POAA028	(4-SMe) Ph	H	H	n.d.[c]	-
POAA029	(*o*-Me)Ph	H	H	n.d.[c]	-
POAA033	NHBn	H	H	n.d.[c]	-
POAA034	NHPh	H	H	**27 ±2.5**	25.3
POAA035		H	H	n.d.[c]	-
POAA036		H	H	286 ±17	-
POAA039	NHEt	H	H	200 ±2.1	-
POAA040	NH*n*-Bu	H	H	265 ±4.5	-
POAA060	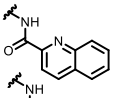	H	H	-	**74.6**
POAA061	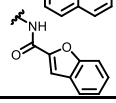	H	H	-	**69.9**

a) Determined by ITC with *Mtb* PanD; b) Determined by ^{1}H NMR monitoring of conversion of L-Asp to β-Ala.

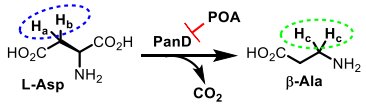

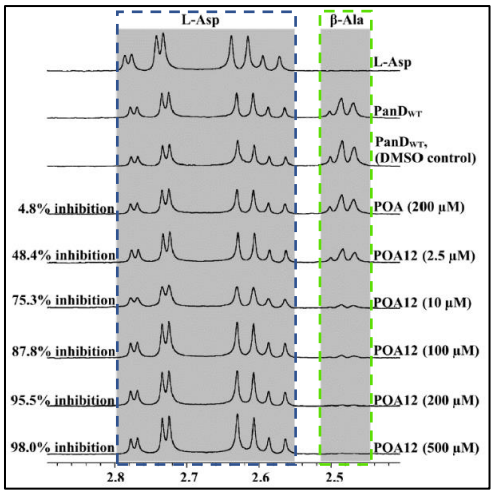

Figure 25. ^{1}H NMR Evaluation of PanD Inhibition. % Inhibition was calculated using peak areas for the indicated protons and comparing to the untreated control. From Ragunathan *et al.*, 2021.[314] Copyright 2021 American Chemical Society.

assays to determine their ability to inhibit PanD enzymatic activity *in vitro*. By monitoring for the consumption of L-Asp and production of β-Ala (using peaks corresponding to the indicated protons), relative PanD inhibition can be quantified at varying inhibitor concentrations (**Figure 25**).[318] As demonstrated previously by the authors, despite its relatively potent binding affinity, POA is only weakly inhibitory to PanD enzymatic activity, displaying approximately 5% inhibition at concentrations tenfold greater than K_D.[318] Gopal *et al* have proposed that this discrepancy between moderate binding affinity, poor inhibitory effect, and relatively potent antimycobacterial activity is explained through the action of the caseinolytic protease complex (ClpC1-ClpP), which recognizes and degrades POA-bound PanD and potentiates its activity in whole cell assays.[317-318] Interestingly, unlike POA, a number of our analogues displayed potent inhibition of PanD in these enzymatic assays, absent the activity of ClpC1-ClpP. The most active compound, POAA012, displayed an IC_{50} of 2.5 μM, approximately a three-log increase in potency compared to POA (**Figure 25**).

3.2.4 Degradation Assays: Evaluating Mechanism of Action

The ability of POAA012 to inhibit PanD activity without the need for targeted degradation by ClpC1-ClpP, as required by POA, led us to question whether this inhibitor could act through a similar mechanism in the presence of the complex. To answer this question, we employed a *M. bovis* strain expressing a red fluorescent protein-PanD fusion protein (RFP-PanD), as described previously.[321] Upon treatment with increasing concentrations of POA, *M. bovis* RFP-PanD cells exhibit a dose-dependent decrease in fluorescence relative to *M. bovis* cells expressing non-fused RFP (**Figure 26**), indicating ClpC1-ClpP-mediated degradation of the fusion protein following POA binding. Conversely, POAA012 treatment failed to achieve a significant decrease in relative

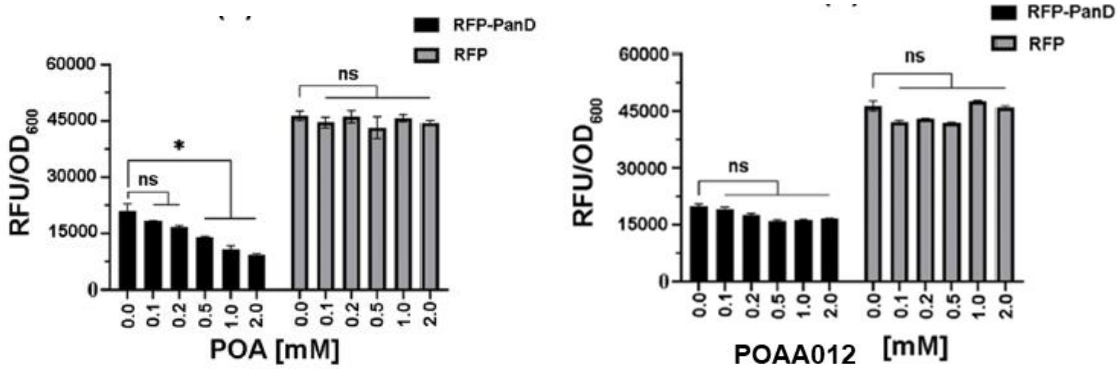

Figure 26. PanD Degradation Assay Using a PanD-RFP Fusion Protein.

From Ragunathan *et al.*, 2021.[314] Copyright 2021 American Chemical Society.

fluorescence (**Figure 26**), suggesting this analogue does not induce degradation of PanD and instead functions through direct inhibition of the enzyme.

3.2.5 Rational Design of New PanD Inhibitors

Despite their relative structural similarity, POA and POAA012 appear to achieve PanD inhibition and antimycobacterial activity through strikingly different mechanisms. Desiring a rationale for this observed activity, we examined the crystal structure of *Mtb* PanD bound to POA, as recently reported by Sun *et al*.[320] PanD is known to form barrel-shaped tetramers in solution, and this oligomerization is required for substrate binding and enzymatic activity. In this crystal structure (6OYY), POA binds at the interface of two PanD monomers, near residues K9 and H11. Previous mutagenesis studies performed by our collaborators have suggested that residues K9 and H11 are important for enzymatic activity and PanD oligomer formation.[314] Intriguingly, further inspection identified the presence of a gap between POA and the enzymatically critical H11 residue; introduction of a bulky group at the 3-position of POA (such as the 1-naphthamido substituent of POAA012) could allow for interactions with both K9 and H11, perturbing important interactions between these residues or with the neighboring PanD subunit (**Figure 27**).[314] To test this theory,

we synthesized two additional analogues featuring similar bulky 3-amido substituents, POAA060 and 061, and evaluated the new compounds with our biological and biochemical assays. Both compounds displayed similar antimycobacterial potency to POAA012 (**Table 10**), and subsequent evaluation in ^{1}H NMR PanD inhibitory assays confirmed both analogues were also potent PanD inhibitors (though weaker than POAA012) (**Table 14**). These molecules represent the first rationally designed mycobacterial PanD inhibitors, exploiting recently discovered structural and mechanistic insights into both PanD and POA.

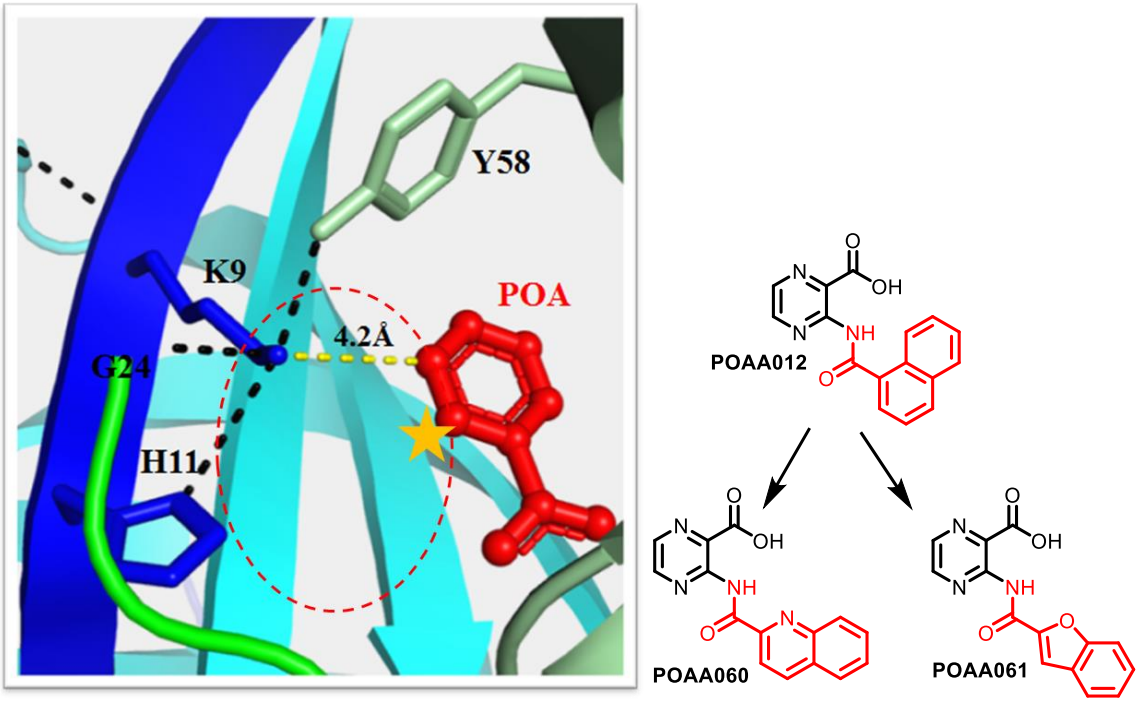

Figure 27. Rational Design of PanD Inhibitors. Image created from PanD-POA crystal structure (6OYY).[320] Adapted from Ragunathan *et al.*, 2021.[314] Copyright 2021 American Chemical Society.

3.3 Conclusion

Inspired by recent developments illuminating a new possible mechanism for PZA/POA, we designed and synthesized a small library of next-generation POA analogues. Assessment against two strains of *M. bovis* provided preliminary insights into POA-PanD SAR, suggesting the presence of a hydrogen bond donor and bulky group at the 3 position provide additional antimycobacterial activity. Further analysis in biochemical assays confirmed binding to PanD and, interestingly, suggested a novel mechanism of action distinct from the targeted degradation paradigm proposed for POA. The potent inhibitory activity of POAA012, combined with careful examination of recent structural insights into POA binding to PanD, guided the rational design of new and potent PanD inhibitors, providing a promising proof-of-concept for future antitubercular design.

3.4 Experimentals

3.4.1 General Remarks

Chemical reagents and solvents were purchased from Alfa Aesar, Fisher Scientific, Sigma- Aldrich, TCI America or Oakwood Chemical and used without additional purification. Dichloromethane (DCM), methanol (MeOH), and tetrahydrofuran (THF) were dispensed under Argon (Ar) using an Inert solvent purification system. 1,4-dioxanes was purchased from Fisher Scientific and degassed via sonification under vacuum for Suzuki-Miyaura reactions. Ethyl acetate (EtOAc) and hexanes were purchased from Fisher Scientific and used without additional purification. Anhydrous reactions were performed under inert gas (Ar or N_2) in flame-dried glassware. Thin-layer chromatography (TLC) was performed on TLC silica gel 60F254 plates from EMD Chemical Inc. and visualized using UV light or I_2 staining. Reaction purification was performed via column chromatography employing a Teledyne ISCO RF-200

CombiFlash system with the indicated solvent gradient; flash column silica gel cartridges were used for purifying intermediates, while RediSep® Rf Gold® Cyano cartridges (Teledyne ISCO) were used for purification of final carboxylic acid products. Percent purity analysis was performed using analytical high pressure liquid chromatography (HPLC) with a reversed-phase XSelect® CSH 5 μm C-18 4.6 x 150 mm LC column, with detection at 250 nm. A gradient method of 5% to 95% acetonitrile (MeCN) in water over 15 min at a flow rate of 1.0 ml/min was employed; both solvents were treated with either 0.1% formic acid (most analyses) or 20 mM ammonium acetate (analogs **9** and **20** only) to assist resolution. Nuclear magnetic resonance (NMR) spectroscopy was performed using a 500 or 600 MHz spectrometer (Bruker) and calibrating to known chemical shifts for residual solvent peaks. High resolution mass spectrometry (HRMS) analysis was performed using an automated 6230 TOF LC/MS system (Agilent).

3.4.2 POA Analogue Syntheses

3.4.2.1 Common Intermediates

Esterification of 3-chloro and 3-aminopyrazinoic acid

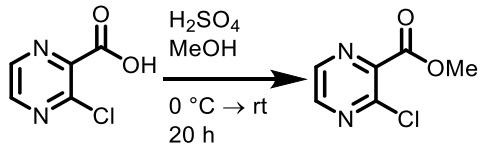

Methyl 3-chloropyrazine-2-carboxylate. 3-chloropyrazinoic acid (3 g, 18.9 mmol) was dissolved in MeOH (18.9 ml, 1 M) and cooled to 0 °C. Concentrated sulfuric acid (3.8 ml, 70 mmol) was added slowly, and the mixture was gradually warmed to room temperature (rt) with stirring overnight. After 20 h, the reaction was neutralized to pH ~8 with saturated aqueous sodium

bicarbonate solution, then extracted into several portions of EtOAc (3x 50 ml). The organic layers were combined, washed with brine, dried with $MgSO_4$ and condensed onto silica gel. The crude reaction was purified by flash column chromatography (hexanes/ EtOAc, 0% to 75% EtOAc over 20 min) and the major peak was collected and condensed, yielding the product as a thick yellow oil which crystallized into a white solid upon cooling (1.65 g, 51% yield). R_f = 0.25 (25:75 EtOAc:hexanes); ^{1}H NMR ($CDCl_3$) δ 8.58 (d, J = 2.3 Hz, 1H), 8.52 (d, J = 2.4 Hz, 1H), 4.03 (s, 3H); ^{13}C NMR (126 MHz, CDCl3) δ 163.81, 147.94, 145.80, 144.31, 141.95, 53.58; HRMS (ESI) calcd for $C_6H_6ClN_2O_2$ $[M+H]^+$: 173.0112, found: 173.0101 (error = 6.4 ppm). Spectral data matched previously reported values for the compound.[351]

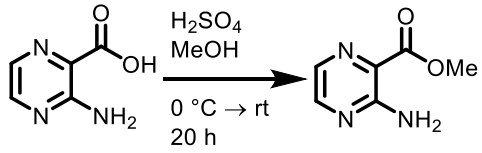

Methyl 3-aminopyrazine-2-carboxylate (POAA008-OMe). An identical procedure was employed for the preparation of methyl 3-aminopyrazine-2-carboxylate, yielding 1.53 g of crude product from 3 g of the starting acid (46% yield) as a brown solid, which was taken on without additional purification. R_f = 0.20 (50:50 EtOAc:hexanes); ^{1}H NMR ($CDCl_3$) δ 8.21 (d, J = 2.2 Hz, 1H), 8.00 (d, J = 2.2 Hz, 1H), 3.99 (s, 3H); ^{13}C NMR (126 MHz, $CDCl_3$) δ 163.78, 152.91, 145.84, 144.58, 141.42, 53.47; HRMS (ESI) calcd for $C_6H_8N_3O_2$ $[M+H]^+$: 154.0611, found: 154.0603 (error = 5.2 ppm); Mp: 150 ºC. Spectral data matched previously reported values for this compound.[352]

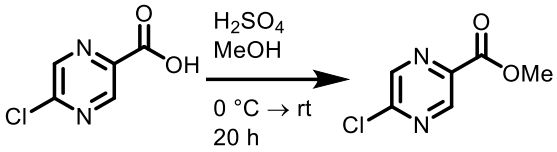

Methyl 5-chloropyrazine-2-carboxylate (POAA001-OMe). The same procedure was employed for the preparation of methyl 5-chloropyrazine-2-carboxylate. Upon neutralization, a thick white precipitate was observed, which was filtered, yielding 1.41 g of the desired product from 3 g of the starting acid (43% yield) as a white solid, which was taken on without additional purification. R_f = 0.65 (50:50 EtOAc:hexanes); ^{1}H NMR (500 MHz, $CDCl_3$) δ 9.08 (d, J = 1.3 Hz, 2H), 8.70 (d, J = 1.4 Hz, 2H), 4.04 (s, 7H).; ^{13}C NMR (126 MHz, CDCl3) δ 163.76, 152.89, 145.83, 144.57, 141.41, 53.45; HRMS (ESI) calcd for $C_6H_5ClN_2O_2$ [M+Na]+: 194.9932, found: 194.9937 (error = 2.6 ppm); Mp: 90 ºC.

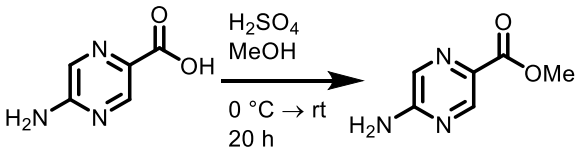

Methyl 5-aminopyrazine-2-carboxylate (POAA009-OMe). The same procedure was employed for the preparation of methyl 5-aminopyrazine-2-carboxylate. Upon neutralization, a thick white precipitate was observed, which was filtered, yielding 450 mg of product from 500 mg of starting acid (89% yield) as a yellow solid, which was taken on without additional purification. R_f = 0.10 (75:25 EtOAc:hexanes); ^{1}H NMR (500 MHz, $CDCl_3$) δ 8.78 (d, J = 1.4 Hz, 1H), 8.02 (d, J = 1.4 Hz, 1H), 3.97 (s, 3H); ^{13}C NMR (126 MHz, $CDCl_3$) δ 165.07, 155.95, 145.87, 133.20, 131.69, 52.59; HRMS (ESI) calcd for $C_6H_7N_3O_2Na$ $[M+Na]^+$: 176.0436, found: 176.0382 (error = 30.7 ppm); decomposed at 220 ºC.

3.4.2.2 Synthesis of Amido-POA Analogues

General amidation procedure

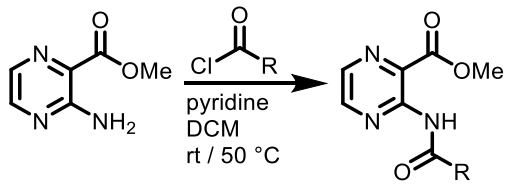

Methyl 3-amino-2-pyrazinecarboxylate (1 equiv) was dissolved in DCM (0.5 M) in a two dram vial equipped with a pressure release cap. Acid chloride (2.0 equiv) was added slowly and the reaction mixture was stirred at rt (50 °C for hindered acid chlorides noted) and monitored for completion by TLC (50-75% ETOAC/hexanes). Following consumption of starting material, the crude mixture was diluted with DCM, washed with saturated aqueous Na_2CO_3 solution and brine, dried with $MgSO_4$ and condensed onto silica gel. Purification was performed using column chromatography (ETOAC/hexanes, gradient method) and the major peak was collected.

Methyl 3-benzaamidopyrazine-2-carboxylate (POAA010-OMe). The title compound was obtained from benzoyl chloride in 29% yield (rt, 24 h reaction time) as an orange solid. R_f = 0.10 (50:50 EtOAc:hexanes); ^{1}H NMR (DMSO-d_6) δ 11.39 (s, 1H), 8.73 (d, J = 2.3 Hz, 1H), 8.57 (d, J = 2.4 Hz, 1H), 8.05 – 7.98 (m, 2H), 7.69 – 7.61 (m, 1H), 7.56 (dd, J = 8.3, 7.0 Hz, 2H), 3.76 (s, 3H); ^{13}C NMR (DMSO-d_6) δ 166.15, 164.88, 145.89, 145.22, 139.85, 138.47, 132.89, 132.54, 128.57, 128.05, 52.37; HRMS (ESI) for $C_{13}H_{10}N_3O_3$ $[M-H]^-$ calcd: 256.0728, found: 256.0736 (error = 3.1 ppm); Mp: 122 ºC.

Methyl 3-(1-naphthamido)pyrazine-2-carboxylate (POAA012-OMe). The title compound was obtained from 1-naphthoyl chloride in 31% yield (50 °C, 72 h reaction time) as a yellow-orange solid. R_f = 0.15 (50:50 EtOAc:hexanes); ^{1}H NMR (DMSO-d_6) δ 11.61 (s, 1H), 8.73 (d, J = 2.4 Hz, 1H), 8.59 (d, J = 2.4 Hz, 1H), 8.31 – 8.25 (m, 1H), 8.13 (d, J = 8.2 Hz, 1H), 8.07 – 8.01 (m, 1H), 7.81 (dd, J = 7.1, 1.2 Hz, 1H), 7.68 – 7.57 (m, 3H), 3.84 (s, 3H); ^{13}C NMR (DMSO-d_6) δ 168.07, 165.06, 145.35, 140.03, 138.66, 133.15, 132.48, 131.10, 129.75, 128.39, 127.18, 126.47, 126.43, 124.98, 52.51; HRMS (ESI) calcd for $C_{17}H_{12}N_3O_3$ [M-H]$^-$: 306.0884, found: 306.0894 (error = 3.3 ppm); Mp: 90 ºC.

Methyl 3-propionamidopyrazine-2-carboxylate (POAA017-OMe). The title compound was obtained from propionyl chloride in 77% yield (rt, 24 h reaction time) as a crystalline yellow solid. R_f = 0.20 (75:25 EtOAc:hexanes); ^{1}H NMR (DMSO-d_6) δ 10.90 (s, 1H), 8.62 (d, J = 2.4 Hz, 1H), 8.47 (d, J = 2.3 Hz, 1H), 3.76 (s, 3H), 2.39 (q, J = 7.6 Hz, 2H), 1.06 (t, J = 7.5 Hz, 3H); ^{13}C NMR (DMSO-d_6) δ 172.90, 164.83, 145.03, 144.93, 139.33, 138.01, 52.14, 28.76, 9.20; HRMS (ESI) for $C_9H_{11}N_3O_3$ [M-H]$^-$ calcd: 208.0728, found: 208.0731 (error = 1.4 ppm); Mp: 80 ºC.

Methyl 3-(2-naphthamido)pyrazine-2-carboxylate (POAA021-OMe). The title compound was obtained from 2-naphthoyl chloride in 64% yield (rt, 48 h reaction time) as a red solid. R_f = 0.25 (75:25 EtOAc:hexanes); ^{1}H NMR (DMSO-d_6) δ 11.86 (s, 1H), 8.75 (d, J = 2.3 Hz, 1H), 8.60 (d, J = 1.7 Hz, 1H), 8.46 (d, J = 2.3 Hz, 1H), 8.11 (dd, J = 8.6, 1.9 Hz, 1H), 8.05 (d, J = 7.4 Hz, 1H), 8.00 (d, J = 8.6 Hz, 1H), 7.93 (d, J = 7.6 Hz, 1H), 7.67 – 7.55 (m, 2H), 4.12 (s, 3H); ^{13}C NMR (DMSO-d_6) δ 167.22, 164.79, 150.55, 147.38, 138.63,

135.49, 132.82, 131.39, 129.61, 129.11, 128.96, 128.92, 128.52, 127.97, 127.13, 123.83, 53.97; HRMS (ESI) for $C_{17}H_{13}N_3O_3$ $[M-H]^-$ calcd: 306.0884, found: 306.0889 (error = 1.6 ppm); Mp: 145 ºC.

Methyl 3-(quinoline-2-carboxamido)pyrazine-2-carboxylate (POAA060-OMe). The title compound was obtained from quinaldoyl chloride in 58% yield (50 °C, 72 h reaction time) as a reddish solid. R_f = 0.20 (75:25 EtOAc:hexanes); ^{1}H NMR (DMSO-d_6) δ 13.18 (s, 1H), 8.75 (d, J = 2.3 Hz, 1H), 8.48 (d, J = 2.2 Hz, 1H), 8.41 (q, J = 8.5 Hz, 2H), 8.35 (d, J = 8.5 Hz, 1H), 7.94 (d, J = 8.2 Hz, 1H), 7.85 (ddd, J = 8.4, 6.8, 1.5 Hz, 1H), 7.69 (ddd, J = 8.1, 6.9, 1.2 Hz, 1H), 4.17 (s, 3H).; ^{13}C NMR (DMSO-d_6) δ 166.14, 162.86, 149.64, 149.30, 146.93, 146.65, 138.68, 138.05, 130.57, 130.41, 130.24, 129.85, 128.78, 127.88, 119.27, 53.75; HRMS (ESI) for $C_{16}H_{12}N_4O_3$ $[M-H]^-$ calcd: 307.0837, found: 307.0845 (error = 2.6 ppm); decomposed at 120 ºC.

Methyl 3-(benzofuran-2-carboxamido)pyrazine-2-carboxylate (POAA061-OMe). The title compound was obtained from benzofuran-2-carbonyl chloride in 56% yield (50 °C, 72 h reaction time) as a yellow-brown solid. R_f = 0.20 (75:25 EtOAc:hexanes); ^{1}H NMR δ 11.68 (s, 1H), 8.76 (d, J = 2.4 Hz, 1H), 8.60 (d, J = 2.4 Hz, 1H), 7.97 (d, J = 0.9 Hz, 1H), 7.86 (dd, J = 7.8, 1.1 Hz, 1H), 7.78 – 7.72 (m, 1H), 7.55 (ddd, J = 8.4, 7.2, 1.3 Hz, 1H), 7.43 – 7.35 (m, 1H), 3.83 (s, 3H); ^{13}C NMR (DMSO-d_6) δ 164.96, 156.96, 154.70, 147.33, 145.55, 145.34, 140.16, 137.47, 127.82, 126.89, 124.07, 123.29, 112.30, 112.08, 52.57.

3.4.2.3 Synthesis of Amino-POA Analogues

General Amination Procedure

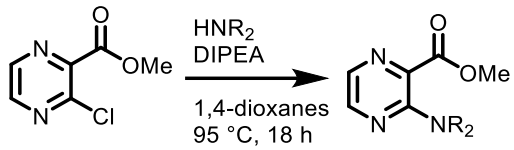

Methyl 3-chloro-2-pyrazinecarboxylate (1 equiv), diisopropylethylamine (3 equiv) and amine (2 equiv) were combined in a sealed round bottom flask, dissolved in 1,4-dioxanes (0.2 M), heated to 95 °C and stirred overnight. The reaction was monitored by TLC (50% EtOAc/hexanes) for consumption of starting material. Upon completion, the crude reaction mixture was diluted with DCM and condensed onto celite. The dry load was purified by column chromatography (EtOAc/hexanes, gradient method) and the major peak was collected.

Methyl 3-(diethylamino)pyrazine-2-carboxylate(POAA023-OMe). The title compound was obtained from diethylamine in 59% yield as a yellow oil. R_f = 0.70 (75:25 EtOAc:hexanes); ^{1}H NMR ($CDCl_3$) δ 8.11 (d, J = 2.1 Hz, 1H), 7.85 (d, J = 2.2 Hz, 1H), 3.95 (s, 3H), 3.45 (q, J = 7.1 Hz, 4H), 1.19 (t, J = 7.1 Hz, 6H); ^{13}C NMR ($CDCl_3$) δ 167.23, 153.17, 143.18, 131.16, 130.08, 52.94, 43.85, 12.58; HRMS (ESI) calcd for $C_{10}H_{15}N_3O_2$ $[M+H]^+$: 210.1237, found: 210.1257 (error = 9.5 ppm).

Methyl 3-(isobutylamino)pyrazine-2-carboxylate (POAA024-OMe). The title compound was obtained from isobutylamine in 64% yield as a yellow oil. R_f = 0.35 (35:65 EtOAc:hexanes); ^{1}H NMR ($CDCl_3$) δ 8.21 (d, J = 2.2 Hz, 1H), 8.08 (s, 1H), 7.84 (d, J = 2.2 Hz, 1H), 3.97 (s, 3H), 3.34 (dd, J = 6.9, 5.6 Hz, 2H), 1.98 – 1.88 (m, 1H), 0.99 (d, J = 6.7 Hz, 6H); ^{13}C NMR (DMSO-d_6) δ 166.85, 154.85, 147.38, 131.13, 123.75, 52.24, 52.10, 47.32, 27.53, 20.03.

Methyl 3-pyrrolidine-2-pyrazinoate (POAA031-OMe): The title compound was obtained from Methyl 3-chloropyrazinoate and pyrrolidine in 87% yield as an off-white solid. R_f = 0.49 (50:50 EtOAc:hexanes); ^{1}H NMR (500 MHz, $CDCl_3$) δ 8.14–8.03 (m, 1H), 7.81 (d, *J* = 2.1 Hz, 1H), 3.91 (s, 3H), 3.44–3.31 (m, 4H), 2.02–1.83 (m, 4H); ^{13}C NMR ($CDCl_3$) δ 166.7, 151.4, 143.9, 130.7, 128.4, 52.8, 49.2, 25.5; HRMS (EI) calcd for $C_{10}H_{13}N_3O_2$ [M+H]+ 207.1002, found: 207.0990 (error = 5.99 ppm).

Methyl 3-piperidine-2-pyrazinoate (POAA032-OMe): The title compound was obtained from Methyl 3-chloropyrazinoate and piperidine in 89% yield as a yellow oil. R_f = 0.56 (50:50 EtOAc:hexanes); ^{1}H NMR (500 MHz, $CDCl_3$) δ 8.07 (d, *J* = 2.3 Hz, 1H), 7.85 (d, *J* = 2.3 Hz, 1H), 3.90 (s, 3H), 3.38 (dd, *J* = 6.1, 3.8 Hz, 4H), 1.62–1.57 (m, 6H); ^{13}C NMR ($CDCl_3$) δ 166.6, 154.7, 143.4, 132.2, 130.4, 52.8, 49.2, 25.7, 24.3; HRMS (ESI) calcd for $C_{11}H_{15}N_3O_2$ $[M+Na]^+$ 244.1056, found: 244.1096 (error = 16.39 ppm).

Methyl 3-(benzylamino)pyrazine-2-carboxylate(POAA033-OMe): The title compound was obtained from benzylamine in 86% yield as an off-white solid. R_f = 0.51 (50:50 EtOAc:hexanes); ^{1}H NMR ($CDCl_3$) δ 8.37 (s, 1H), 8.28 (d, *J* = 2.9 Hz, 1H), 8.04–7.90 (m, 1H), 7.38 (t, *J* = 5.5 Hz, 4H), 7.32–7.22 (m, 2H), 4.77 (t, *J* = 4.6 Hz, 2H), 4.00 (d, *J* = 3.7 Hz, 3H); ^{13}C NMR ($CDCl_3$) δ 167.3, 155.3, 147.5, 138.6, 131.8, 128.7, 127.5, 124.4, 52.8, 44.6; HRMS (EI) calcd for $C_{13}H_{13}N_3O_2$[M+H]+ 243.1002, found: 243.0990 (error = 4.9 ppm).

Methyl 3-(phenylamino)pyrazine-2-carboxylate (POAA034-OMe). The title compound was obtained from aniline in 63% yield as a white solid. R_f = 0.38 (50:50 EtOAc:hexanes); ^{1}H NMR ($CDCl_3$) δ 8.81 (d, *J* = 1.5 Hz, 1H), 8.16 (d, *J* = 1.5 Hz, 1H), 7.43 (d, *J* = 7.9 Hz, 2H), 7.33 (t, *J* = 7.9 Hz, 2H), 7.12 (dd, *J* = 8.1, 6.6 Hz, 1H), 7.01 (d, *J* = 4.5 Hz, 1H),

3.91 (s, 3H); ^{13}C NMR ($CDCl_3$) δ 164.9, 153.6, 145.4, 137.8, 133.3, 132.1, 129.6, 125.0, 121.2, 52.4; HRMS (EI) calcd for $C_{12}H_{11}N_3O_2$[M+H]+: 229.0846 , found: 229.0826 (error = 8.79 ppm).

Methyl 3-(cyclopentylamino)pyrazine-2-carboxylate(POAA035-OMe): The title compound was obtained from cyclopentylamine in 96% yield as a yellow oil. R_f = 0.60 (50:50 EtOAc:hexanes); ^{1}H NMR ($CDCl_3$) δ 8.16 (d, *J* = 2.1 Hz, 1H), 7.94 (s, 1H), 7.78 (t, *J* = 1.7 Hz, 1H), 4.33 (h, *J* = 6.7 Hz, 1H), 3.90 (d, *J* = 1.3 Hz, 3H), 2.01 (dq, *J* = 12.7, 6.6 Hz, 2H), 1.77–1.65 (m, 2H), 1.65–1.52 (m, 2H), 1.46 (dq, *J* = 14.0, 7.6, 7.1 Hz, 2H); ^{13}C NMR ($CDCl_3$) δ 167.4, 155.1, 147.5, 131.1, 124.0, 52.7, 52.3, 33.2, 23.8; HRMS (EI) calcd for $C_{11}H_{15}N_3O_2$[M+H]+: 221.1159 , found: 221.1148 (error = 4.97 ppm).

Methyl 3-(cyclobutylamino)pyrazine-2-carboxylate (POAA036-OMe). The title compound was obtained from cyclobutylamine 67% yield as an off-white solid. R_f = 0.55 (50:50 EtOAc:hexanes); ^{1}H NMR ($CDCl_3$) δ 8.15 (d, *J* = 2.3 Hz, 1H), 7.80 (d, *J* = 2.3 Hz, 1H), 4.54–4.43 (m, 1H), 3.91 (s, 3H), 2.43–2.33 (m, 2H), 1.97–1.85 (m, 2H), 1.83–1.67 (m, 2H); ^{13}C NMR ($CDCl_3$) δ 167.3, 154.5, 147.5, 131.5, 124.0, 52.7, 45.9, 31.3, 15.4; HRMS (EI) calcd for $C_{10}H_{13}N_3O_2$[M+H]+ 207.1002, found: 207.0999 (error = 1.55 ppm).

Methyl 3-morpholino-2-pyrazinoate (POAA037-OMe): The title compound was obtained from Methyl 3-chloropyrazinoate and morpholine in 77% yield as a light yellow solid. R_f = 0.36 (50:50 EtOAc:hexanes); ^{1}H NMR (500 MHz, $CDCl_3$) δ 8.13 (d, *J* = 2.3 Hz, 1H), 7.96 (d, *J* = 2.3 Hz, 1H), 3.91 (s, 3H), 3.81–3.71 (m, 3H), 3.53–3.38 (m, 3H) ; ^{13}C NMR ($CDCl_3$) δ 166.3, 154.6, 143.7, 133.5, 130.7, 66.7, 52.9, 48.5; HRMS (EI) calcd for $C_{10}H_{13}N_3O_3$[M+H]+ 223.0951, found: 223.0933 (error = 8.08 ppm).

Methyl 3-thiomorpholino-2-pyrazinoate (POAA038-OMe): The title compound was obtained from Methyl 3-chloropyrazinoate and thiomorpholine in 86% yield as a yellow oil. R_f =

0.60 (50:50 EtOAc:hexanes); ^{1}H NMR (500 MHz, $CDCl_3$) δ 8.12 (d, *J* = 2.2 Hz, 1H), 7.94 (d, *J* = 2.3 Hz, 1H), 3.91 (s, 3H), 3.71–3.67 (m, 4H), 2.69–2.66 (m, 4H); ^{13}C NMR ($CDCl_3$) δ 166.3, 154.9, 143.5, 133.4, 131.2, 52.9, 50.9, 27.1; HRMS (EI) calcd for $C_{10}H_{13}N_3O_2S$[M+H]+: 239.0723, found: 239.0715 (error = 3.43 ppm).

Methyl 3-(ethylamino)-2-pyrazine-2-carboxylate (POAA039-OMe). The title compound was obtained from ethylamine in 40% yield as a yellow solid. R_f = 0.18 (25:75 EtOAc:hexanes); ^{1}H NMR ($CDCl_3$) δ 8.17 (d, *J* = 2.2 Hz, 1H), 7.79 (d, *J* = 2.2 Hz, 1H), 3.90 (s, 3H), 3.47 (qd, *J* = 7.1, 5.1 Hz, 2H), 1.22 (d, *J* = 7.2 Hz, 3H); ^{13}C NMR ($CDCl_3$) δ 167.3, 155.4, 147.5, 131.2, 52.7, 35.6, 14.7; HRMS (EI) calcd for $C_8H_{11}N_3O_2$[M+H]+: 181.0846, found: 181.0843 (error = 1.75 ppm).

Methyl 3-butylamino-2-pyrazinoate (POAA040-OMe): The title compound was obtained from Methyl 3-chloropyrazinoate and n-butylamine in 45% yield as a white solid. R_f = 0.6 (50:50 EtOAc:hexanes); ^{1}H NMR (500 MHz, $CDCl_3$) δ 8.16 (d, *J* = 2.2 Hz, 1H), 7.92 (s, 1H), 7.79 (d, *J* = 2.3 Hz, 1H), 3.91 (s, 3H), 3.44 (td, *J* = 7.1, 5.4 Hz, 2H), 1.61–1.55 (m, 2H), 1.38 (dt, *J* = 15.0, 7.4 Hz, 2H), 0.90 (t, *J* = 7.4 Hz, 3H); ^{13}C NMR ($CDCl_3$) δ 167.4, 155.6, 147.5, 131.1, 124.1, 52.71, 40.5, 31.4, 20.2, 13.8; HRMS (EI) calcd for $C_{10}H_{15}N_3O_2$[M+H]+: 209.1132, found: 209.1142 (error = 4.56 ppm).

Methyl 3-(6-azaspiro[2,5] octano)-2-pyrazinoate (POAA041-OMe): The title compound was obtained from Methyl 3-chloropyrazinoate and 6-azaspiro[2,5] octane in 72% yield as a yellow oil. R_f = 0.30 (25:75 EtOAc:hexanes); ^{1}H NMR (500 MHz, $CDCl_3$) δ 8.17 (t, *J* = 2.5 Hz, 1H), 7.95 (t, *J* = 2.5 Hz, 1H), 4.05–3.92 (m, 3H), 3.66–3.49 (m, 4H), 1.49 (dq, *J* = 5.4, 2.9 Hz, 4H), 0.40 (d, *J* = 2.7 Hz, 4H); ^{13}C NMR ($CDCl_3$) δ 166.7, 154.8, 143.5, 132.3, 130.5, 52.8, 48.2,

34.9, 17.6, 11.4; HRMS (EI) calcd for $C_{13}H_{17}N_3O_2$[M+H]+: 247.1315, found: 247.1304 (error = 4.44 ppm).

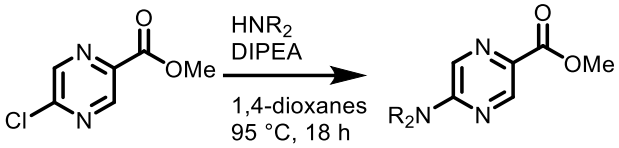

5-aminopyrazines were prepared using the general amination procedure.

Methyl 5-(diethylamino)pyrazine-2-carboxylate (POAA018-OMe): The title compound was obtained from diethylamine in 91% yield as a yellow oil. R_f = 0.30 (50:50 EtOAc:hexanes); ^{1}H NMR (500 MHz, $CDCl_3$) δ 8.78 (d, *J* = 1.4 Hz, 1H), 7.97 (d, *J* = 1.4 Hz, 1H), 3.94 (s, 3H), 3.60 (q, *J* = 7.1 Hz, 4H), 1.23 (t, *J* = 7.1 Hz, 6H); ^{13}C NMR (126 MHz, $CDCl_3$) δ 165.65, 154.16, 146.01, 129.73, 128.88, 52.27, 43.01, 12.83; HRMS (ESI) calcd for $C_{10}H_{16}N_3O_2$ [M+H]+: 210.1237, found: 210.1232 (error = 2.2 ppm).

Methyl 5-(4-(*tert*-butoxycarbonyl)piperazin-1-yl)pyrazine-2-carboxylate (POAA019-Boc-OMe): The title compound was obtained from N-Boc-piperazine in 74% yield as a yellow solid. R_f = 0.30 (50:50 EtOAc:hexanes); ^{1}H NMR (500 MHz, $CDCl_3$) δ 8.80 (d, *J* = 1.4 Hz, 1H), 8.13 (d, *J* = 1.4 Hz, 1H), 3.96 (s, 3H), 3.77 – 3.72 (m, 4H), 3.60 – 3.55 (m, 4H), 1.49 (s, 9H); ^{13}C NMR (126 MHz, $CDCl_3$) δ 165.25, 155.14, 154.72, 145.42, 131.35, 129.48, 80.60, 52.49, 44.13, 28.53; HRMS (ESI) calcd for $C_{15}H_{23}N_4O_4$ $[M+H]^+$: 323.1714, found: 323.1696 (error = 5.6 ppm); Mp: 163 ºC.

Methyl 5-(isobutylamino)pyrazine-2-carboxylate (POAA022-OMe): The title compound was obtained from isobutylamine in 59% yield as an off-white solid. R_f = 0.20 (50:50 EtOAc:hexanes); ^{1}H NMR (500 MHz, $CDCl_3$) δ 8.76 (d, *J* = 1.3 Hz, 1H), 7.91 (d,

J = 1.3 Hz, 1H), 3.95 (s, 3H), 3.28 (t, *J* = 6.4 Hz, 2H), 1.93 (dt, *J* = 13.4, 6.7 Hz, 1H), 1.00 (d, *J* = 6.7 Hz, 6H); ^{13}C NMR (126 MHz, $CDCl_3$) δ 165.28, 155.81, 145.89, 52.27, 48.97, 28.33, 20.18; HRMS (ESI) for $C_{10}H_{15}N_3O_2$ $[M-H]^-$ calcd: 208.1092, found: 208.1099 (error = 3.4 ppm); Mp: 120 ºC.

Methyl 5-morpholino-2-pyrazinoate (POAA042-OMe): The title compound was obtained from Methyl 5-chloropyrazinoate and morpholine in 60% yield as a white solid. R_f = 0.21 (50:50 EtOAc:hexanes); ^{1}H NMR (500 MHz, $CDCl_3$) δ 8.74 (d, *J* = 1.4 Hz, 1H), 8.06 (d, *J* = 1.4 Hz, 1H), 3.89 (s, 3H), 3.76 (t, *J* = 4.8 Hz, 4H), 3.68–3.64 (m, 4H); ^{13}C NMR ($CDCl_3$) δ 145.3, 129.2, 77.2, 66.4, 52.4 (d, *J* = 2.3 Hz), 44.4; HRMS (ESI) calcd for $C_{10}H_{13}N_3O_3[M+Na]^+$: 246.0849, found: 246.0874 (error = 10.16 ppm).

Methyl 5-thiomorpholino-2-pyrazinoate (POAA043-OMe): The title compound was obtained from Methyl 5-chloropyrazinoate and thiomorpholine in 63% yield as a white solid. R_f = 0.44 (50:50 EtOAc:hexanes); ^{1}H NMR (500 MHz, $CDCl_3$) δ 8.73 (d, *J* = 1.5 Hz, 1H), 8.05 (d, *J* = 1.4 Hz, 1H), 4.03 (dd, *J* = 6.4, 3.8 Hz, 4H), 3.89 (s, 3H), 2.67–2.62 (m, 4H); ^{13}C NMR ($CDCl_3$) δ 145.4, 129.4, 77.2, 52.3, 47.3, 26.7; HRMS (EI) calcd for $C_{10}H_{13}N_3O_2S[M+H]$+: 239.0723 , found: 239.0713 (error = 4.26 ppm).

Methyl 5-pyrrolidine-2-pyrazinoate (POAA044-OMe): The title compound was obtained from Methyl 5-chloropyrazinoate and pyrrolidine in 67% yield as a white solid. R_f = 0.23 (50:50 EtOAc:hexanes); ^{1}H NMR (500 MHz, $CDCl_3$) δ 8.74 (s, 1H), 7.83 (s, 1H), 3.88 (s, 3H), 3.52 (s, 4H), 2.01 (s, 4H) ; ^{13}C NMR ($CDCl_3$) δ 146.0, 129.9, 77.2, 52.2, 46.5; HRMS (EI) calcd for $C_{10}H_{13}N_3O_2[M+H]$+: 207.1002, found: 207.0997 (error = 2.36 ppm).

Methyl 5-cyclopentylamino-2-pyrazinoate (POAA045-OMe): The title compound was obtained from Methyl 5-chloropyrazinoate and cyclopentylamine in 66% yield as a yellow solid. R_f = 0.34 (50:50 EtOAc:hexanes); ^{1}H NMR (500 MHz, $CDCl_3$) δ 8.77–8.60 (m, 1H), 7.83 (d, *J* = 1.5 Hz, 1H), 5.38 (dt, *J* = 17.0, 7.1 Hz, 1H), 4.17 (q, *J* = 6.9 Hz, 1H), 3.87 (d, *J* = 2.4 Hz, 3H), 2.12–1.97 (m, 2H), 1.72–1.60 (m, 4H), 1.44 (dq, *J* = 12.7, 6.3 Hz, 2H); ^{13}C NMR ($CDCl_3$) δ 165.4, 155.3, 146.0, 131.2 (d, *J* = 76.8 Hz), 53.0, 52.2, 33.2, 23.7; HRMS (EI) calcd for $C_{11}H_{15}N_3O_2$[M+H]+: 221.1159, found: 221.1148 (error = 4.99 ppm).

Methyl 5-cyclobutylamino-2-pyrazinoate (POAA046-OMe): The title compound was obtained from Methyl 5-chloropyrazinoate and cyclobutylamine in 70% yield as a white solid. R_f = 0.33 (50:50 EtOAc:hexanes); ^{1}H NMR (500 MHz, $CDCl_3$) δ 8.68 (d, *J* = 1.4 Hz, 1H), 7.79 (d, *J* = 1.5 Hz, 1H), 5.72 (d, *J* = 7.6 Hz, 1H), 4.41–4.19 (m, 1H), 3.87 (s, 3H), 2.39 (dddd, *J* = 11.8, 10.1, 7.5, 2.9 Hz, 2H), 1.90 (qd, *J* = 9.5, 2.8 Hz, 2H), 1.79–1.66 (m, 2H); ^{13}C NMR ($CDCl_3$) δ 165.3, 154.7, 145.9, 131.2, 52.2, 46.6, 31.0, 15.2; HRMS (EI) calcd for $C_{10}H_{13}N_3O_2$[M+H]+: 207.1002, found: 207.1004 (error = 0.97 ppm).

Methyl 5-anilino-2-pyrazinoate (POAA047-OMe): The title compound was obtained from Methyl 5-chloropyrazinoate and aniline in 63% yield as a white solid. R_f = 0.38 (50:50 EtOAc:hexanes); ^{1}H NMR (500 MHz, $CDCl_3$) δ 8.81 (d, *J* = 1.5 Hz, 1H), 8.16 (d, *J* = 1.5 Hz, 1H), 7.43 (d, *J* = 7.9 Hz, 2H), 7.33 (t, *J* = 7.9 Hz, 2H), 7.12 (dd, *J* = 8.1, 6.6 Hz, 1H), 7.01 (d, *J* = 4.5 Hz, 1H), 3.91 (s, 3H); ^{13}C NMR ($CDCl_3$) δ 164.9, 153.6, 145.4,

137.8, 133.3, 132.1, 129.6, 125.0, 121.2, 52.4; HRMS (ESI) calcd for $C_{12}H_{11}N_3O_2[M+Na]^+$: 252.0743, found: 252.0771 (error = 11.11 ppm)

Methyl 5-piperidine-2-pyrazinoate (POAA048-OMe): The title compound was obtained from Methyl 5-chloropyrazinoate and piperidine in 80% yield as a white solid. R_f = 0.18 (33:67 EtOAc:hexanes); ^{1}H NMR (500 MHz, $CDCl_3$) δ 8.75–8.69 (m, 1H), 8.10–8.03 (m, 1H), 3.88 (s, 3H), 3.65 (t, *J* = 5.5 Hz, 4H), 1.66 (q, *J* = 6.0, 4.9 Hz, 2H), 1.62–1.57 (m, 4H); ^{13}C NMR ($CDCl_3$) δ 165.4, 155.0, 145.5, 129.8, 129.4, 52.2, 45.5, 25.5, 24.3; HRMS (EI) calcd for $C_8H_{11}N_3O_2[M+H]+$: 221.1159, found: 221.1153 (error = 2.77 ppm).

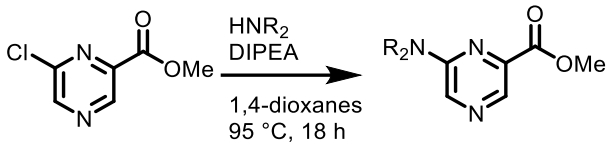

6-aminopyrazines were prepared using the general amination procedure.

Methyl 6-pyrrolidine-2-pyrazinoate (POAA049-OMe): The title compound was obtained from Methyl 6-chloropyrazinoate and pyrrolidine in 43% yield as a yellow solid. R_f = 0.49 (50:50 EtOAc:hexanes); ^{1}H NMR (500 MHz, $CDCl_3$) δ 8.40 (s, 1H), 7.95 (s, 1H), 3.89 (s, 3H), 3.52–3.47 (m, 4H), 2.01–1.94 (m, 4H); ^{13}C NMR ($CDCl_3$) δ 165.8, 152.3, 140.7, 134.0, 132.5, 52.6, 46.6, 30.9, 25.4; HRMS (EI) calcd for $C_{10}H_{13}N_3O_2[M+H]+$: 207.0427, found: 207.0426 (error = 0.39 ppm)

Methyl 6-morpholino-2-pyrazinoate (POAA050-OMe): The title compound was obtained from Methyl 6-chloropyrazinoate and morpholine in 48% yield as a yellow solid. R_f = 0.34 (50:50 EtOAc:hexanes); ^{1}H NMR (500 MHz, $CDCl_3$) δ 8.50 (s, 1H), 8.21 (s, 1H), 3.90 (s, 3H), 3.77 (t, *J* = 4.9 Hz, 4H), 3.59 (t, *J* = 4.9 Hz, 4H); ^{13}C NMR ($CDCl_3$) δ 165.2,

154.1, 140.3, 134.4, 133. 8, 66.5, 52.7, 44.6; HRMS (EI) calcd for $C_{10}H_{13}N_3O_3$[M+H]+: 223.0951, found: 223.0945 (error = 3.1 ppm)

Methyl 6-piperidine-2-pyrazinoate (POAA051-OMe): The title compound was obtained from Methyl 6-chloropyrazinoate and piperidine in 39% yield as a yellow solid. R_f = 0.56 (50:50 EtOAc:hexanes); ^{1}H NMR (500 MHz, $CDCl_3$) δ 8.39 (s, 1H), 8.20 (s, 1H), 3.89 (s, 3H), 3.59 (t, *J* = 5.1 Hz, 4H), 1.60 (dd, *J* = 9.6, 4.7 Hz, 6H); ^{13}C NMR ($CDCl_3$) δ 165.6, 154.1, 140.2, 134.0, 132.9, 52.6, 45.4, 25.4, 24.4; HRMS (EI) calcd for $C_{10}H_{13}N_3O_2$[M+H]+: 206.0924 , found: 206.0916 (error = 3.77 ppm)

Methyl 6-cyclobutylamino-2-pyrazinoate (POAA052-OMe): The title compound was obtained from Methyl 6-chloropyrazinoate and cyclobutylamine in 31% yield as a yellow solid. R_f = 0.19 (33:67 EtOAc:hexanes); ^{1}H NMR (500 MHz, $CDCl_3$) δ 8 8.54 (s, 1H), 7.96 (s, 1H), 5.15 (d, *J* = 6.9 Hz, 1H), 4.23 (h, *J* = 7.5 Hz, 1H), 3.97 (s, 3H), 2.52–2.43 (m, 2H), 1.96–1.75 (m, 4H); ^{13}C NMR ($CDCl_3$) δ 159.4, 142.6, 136.9, 134.0, 131.5, 52.9, 47.0, 31.0, 15.1.; HRMS (EI) calcd for $C_{10}H_{13}N_3O_2[M+H]^+$ 208.1081, found: 208.1078 (error = 1.44 ppm)

Methyl 6-ethylamino-2-pyrazinoate (POAA053-OMe): The title compound was obtained from Methyl 6-chloropyrazinoate and ethylamine in 34% yield as a yellow solid. R_f = 0.33 (33:67 EtOAc:hexanes); ^{1}H NMR (500 MHz, $CDCl_3$) δ 8.50 (s, 1H), 8.03 (s, 1H), 3.95 (s, 3H), 3.41 (q, *J* = 7.2 Hz, 2H), 1.27 (t, *J* = 7.2 Hz, 3H); ^{13}C NMR ($CDCl_3$) δ 165.2, 153.7, 140.3, 134.3, 133.9, 52.8, 36.6, 14.5; HRMS (EI) calcd for $C_8H_{11}N_3O_2$[M+H]+: 181.0846, found: 181.0851 (error = 2.62 ppm)

Methyl 6-cyclopentylamino-2-pyrazinoate (POAA054-OMe): The title compound was obtained from Methyl 6-chloropyrazinoate cyclopentylamine in 20% yield as a yellow solid. R_f = 0.21 (33:67 EtOAc:hexanes); ^{1}H NMR (500 MHz, $CDCl_3$) δ 8.47 (s, 1H), 8.03 (s, 1H), 5.14 (s, 1H), 3.91 (s, 3H), 2.02 (dq, *J* = 13.5, 6.6 Hz, 2H), 1.73–1.58 (m, 4H), 1.50–1.40 (m, 2H); ^{13}C NMR ($CDCl_3$) δ 165.3, 153.5, 140.7, 134.0, 130.1, 53.1 (d, *J* = 63.4 Hz), 33.4, 23.8; HRMS (EI) calcd for $C_{11}H_{15}N_3O_2$[M+H]+: 221.1237, found: 221.1221 (error = 7.01 ppm)

Methyl 6-isobutylamino-2-pyrazinoate (POAA055-OMe): The title compound was obtained from Methyl 6-chloropyrazinoate and isobutylamine in 31% yield as a yellow solid. R_f = 0.12 (25:75 EtOAc:hexanes); ^{1}H NMR (500 MHz, $CDCl_3$) δ 8.50 (d, *J* = 2.8 Hz, 1H), 8.04 (d, *J* = 2.8 Hz, 1H), 5.07 (s, 1H), 3.98–3.91 (m, 3H), 3.21–3.09 (m, 2H), 1.90 (dtd, *J* = 13.8, 6.9, 2.9 Hz, 1H), 1.02–0.92 (m, 6H); ^{13}C NMR ($CDCl_3$) δ 165.2, 154.0, 140.2, 134.0 (d, *J* = 15.6 Hz), 52.8, 49.4, 28.3, 20.2; HRMS (EI) calcd for $C_{10}H_{15}N_3O_2$[M+H]+: 209.1159, found: 209.1147 (error = 5.57 ppm)

3.4.2.4 Synthesis of Biaryl POA Analogues

General Suzuki-Miyaura coupling procedure

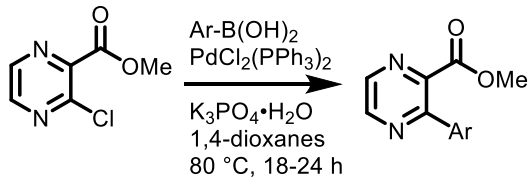

Methyl 3-chloro-2-pyrazinecarboxylate (1 equiv), aryl boronic acid (2.0 equiv), bis(triphenylphosphine)palladium(II) dichloride (10 mol%), and potassium phosphate

monohydrate (2.0 equiv) were combined in a 2 dram vial, which was purged under vacuum and degassed with N_2. Degassed 1,4-dioxanes (sonicated under vacuum) was added under positive pressure, and vial cap was replaced with a pressure release cap. Vial was heated to 80 °C and stirred overnight. Reaction progress was monitored by TLC (50% EtOAc/hexanes) to completion, then condensed *in vacuo*, redissolved in EtOAc and extracted from water, washing with additional EtOAc (3 portions). Combined organics were condensed onto silica and purified by column chromatography (EtOAc/hexanes).

Methyl 3-phenylpyrazine-2-carboxylic acid (POAA026-OMe). The title compound was obtained from phenylboronic acid in 86% yield as a yellow-brown oil. R_f = 0.95 (50:50 EtOAc:hexanes); ^{1}H NMR ($CDCl_3$) δ 8.76 (d, *J* = 2.3 Hz, 1H), 8.60 (d, *J* = 2.4 Hz, 1H), 7.63 (ddd, *J* = 5.5, 2.9, 1.6 Hz, 2H), 7.51 – 7.45 (m, 3H), 3.84 (s, 3H); ^{13}C NMR (126 MHz, $CDCl_3$) δ 166.87, 153.83, 145.48, 144.55, 141.87, 137.17, 129.91, 128.76, 128.66, 53.14. Spectral data matched previously reported values for this compound.[353]

Methyl 3-(4-fluorophenyl)pyrazine-2-carboxylate (POAA027-OMe). The title compound was obtained from 4-fluorophenyl boronic acid in 84% yield as a red solid. R_f = 0.60 (25:75 EtOAc:hexanes); ^{1}H NMR ($CDCl_3$) δ 8.75 (d, J = 2.4 Hz, 1H), 8.60 (d, J = 2.4 Hz, 1H), 7.67 – 7.59 (m, 2H), 7.23 – 7.13 (m, 2H), 3.87 (s, 3H); ^{13}C NMR ($CDCl_3$); δ 166.71, 164.95, 152.80, 145.48, 144.27, 141.95, 133.27, 130.75, 130.69, 115.99, 115.82, 53.22; ^{19}F NMR ($CDCl_3$) δ -111.06.

Methyl 3-(4-(Methylthio)phenyl)pyrazine-2-carboxylate (POAA028-OMe). The title compound was obtained from 4-(methylthio)phenylboronic acid in 94% yield as a yellow oil. R_f = 0.55 (25:75 EtOAc:hexanes); ^{1}H NMR ($CDCl_3$) δ 8.74 (d, J = 2.4 Hz, 1H), 8.57 (d, J = 2.4 Hz, 1H),

7.60 – 7.54 (m, 2H), 7.36 – 7.30 (m, 2H), 3.88 (s, 3H), 2.53 (s, 3H); ^{13}C NMR ($CDCl_3$) δ 166.88, 152.97, 145.23, 144.31, 141.69, 141.65, 133.20, 129.77, 129.07, 126.03, 123.89, 53.23, 15.37.

Methyl 3-(*o*-Tolyl)pyrazine-2-carboxylate (POAA029-OMe). The title compound was obtained from *o*-tolylboronic acid in 75% yield as an off-white solid. R_f = 0.60 (25:75 EtOAc:hexanes); ^{1}H NMR ($CDCl_3$) δ 8.80 (d, J = 2.4 Hz, 1H), 8.67 (d, J = 2.4 Hz, 1H), 7.36 (td, J = 7.4, 1.4 Hz, 1H), 7.32 – 7.25 (m, 2H), 7.18 (dd, J = 7.6, 1.3 Hz, 1H), 3.77 (s, 3H), 2.19 (s, 3H); ^{13}C NMR ($CDCl_3$) δ 155.86, 145.74, 144.46, 142.39, 137.37, 135.92, 130.50, 129.28, 128.62, 125.83, 53.08, 19.79.

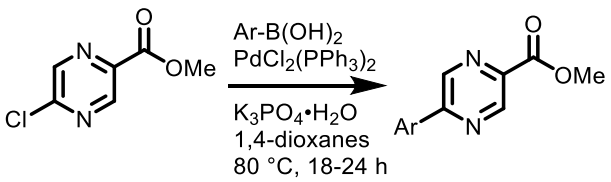

5-arylpyrazines were prepared using the general Suzuki-Miyaura coupling procedure.

Methyl 5-phenylpyrazine-2-carboxylate (POAA020-OMe): The title compound was obtained from phenylboronic acid in quantitative yield as a white solid. R_f = 0.50 (50:50 EtOAc:hexanes); ^{1}H NMR (500 MHz, $CDCl_3$) δ 9.34 (d, *J* = 1.5 Hz, 1H), 9.13 (d, *J* = 1.5 Hz, 1H), 8.14 – 8.07 (m, 2H), 7.59 – 7.50 (m, 3H), 4.06 (s, 3H); ^{13}C NMR (126 MHz, $CDCl_3$) δ 164.72, 155.41, 145.82, 141.53, 141.10, 135.42, 131.16, 129.40, 127.66, 53.20; HRMS (ESI) calcd for $C_{12}H_{11}N_2O_2$ $[M+H]^+$: 215.0815, found: 215.0805 (error = 4.6 ppm); Mp: 128 ºC.

Methyl 5-(o-tolyl)pyrazine-2-carboxylate (POAA025-OMe): The title compound was obtained from *o*-tolylboronic acid in 60% yield as a white solid. R_f = 0.35 (25:75 EtOAc:hexanes); ^{1}H NMR (500 MHz, $CDCl_3$) δ 9.38 (d, *J* = 1.4 Hz, 1H), 8.85 (d, *J* = 1.4 Hz, 1H), 7.49 (dd, *J* = 7.8, 1.5 Hz, 1H), 7.44 – 7.38 (m, 1H), 7.38 – 7.32 (m, 2H), 4.08 (s, 3H), 2.43 (s, 3H); ^{13}C NMR (126

MHz, $CDCl_3$) δ 164.76, 158.61, 145.37, 144.63, 140.69, 136.80, 135.94, 131.57, 130.15, 126.54, 53.26, 20.52.

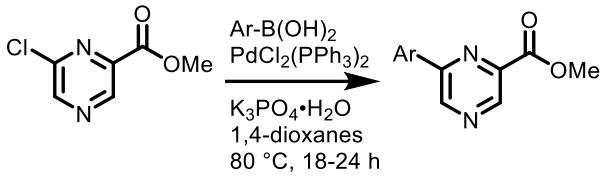

6-arylpyrazines were prepared using the general Suzuki-Miyaura coupling procedure.

Methyl 6-phenylpyrazine-2-carboxylate (POAA056-OMe): The title compound was obtained from Methyl 6-chloropyrazinoate and phenyl boronic acid in 87% yield as a yellow solid. R_f = 0.52 (33:67 EtOAc:hexane); ^{1}H NMR (500 MHz, $CDCl_3$) δ 9.18 (d, *J* = 13.5 Hz, 2H), 8.10–8.02 (m, 2H), 7.57–7.47 (m, 3H), 4.04 (s, 3H); ^{13}C NMR ($CDCl_3$) δ 164.7, 152.5, 144.8, 143.9, 142.6, 135.4, 130.5, 129.2, 127.3, 53.1; HRMS (EI) calcd for $C_{12}H_{10}N_2O_2$[M+H]+ 214.0737 , found: 214.0740 (error = 1.44 ppm)

Methyl 6-(4-fluorophenyl) pyrazine-2-carboxylate (POAA057-OMe): The title compound was obtained from Methyl 6-chloropyrazinoate and 4-fluorophenyl boronic acid in 81% yield as a yellow solid. R_f = 0.48 (33:67 EtOAc:hexane); ^{1}H NMR (500 MHz, $CDCl_3$) δ 9.21 (s, 1H), 9.15 (s, 1H), 8.10 (ddd, *J* = 8.6, 5.4, 2.7 Hz, 2H), 4.06 (s, 3H); ^{13}C NMR ($CDCl_3$) δ 165.6, 163.1, 144.4, 143.8, 136.9, 129.3, 116.2, 115.2, 115.0, 53.1; HRMS (EI) calcd for $C_{12}H_9FN_2O_2$[M+H]+ 234.0751 , found: 234.0743 (error = 3.75 ppm)

Methyl 6-(o-tolyl) pyrazine-2-carboxylate (POAA058-OMe): The title compound was obtained from Methyl 6-chloropyrazinoate and o-tolyl boronic acid in 83% yield as a yellow solid. R_f = 0.57 (33:67 EtOAc:hexane); ^{1}H NMR (500 MHz, $CDCl_3$) δ 9.24 (d, *J* = 2.2 Hz, 1H), 8.86 (d, *J* = 2.2 Hz, 1H), 7.47–7.40 (m, 1H), 7.37–7.32 (m, 1H), 7.33–7.28 (m, 2H), 4.03 (d, *J* = 2.1 Hz, 3H), 2.39 (d, *J* = 2.2 Hz, 3H); ^{13}C NMR ($CDCl_3$) δ 164.7, 155.2, 147.8, 143.6, 142.2, 136.5, 131.2,

130.0, 129.7, 126.3, 53.1, 20.2; HRMS (EI) calcd for $C_{13}H_{12}N_2O_2$[M+H]+ 228.0893, found: 228.0906 (error = 5.50 ppm)

Methyl 6-(4-(methylthio) phenyl)pyrazine-2-carboxylate (POAA059-OMe): The title compound was obtained from Methyl 6-chloropyrazinoate and (4-methylthio) phenyl boronic acid in 86% yield as a yellow solid. R_f = 0.5 (33:67 EtOAc:hexane); ^{1}H NMR (500 MHz, $CDCl_3$) δ 9.14 (dd, *J* = 9.5, 2.4 Hz, 2H), 8.04–7.96 (m, 2H), 7.39–7.31 (m, 2H), 4.06–4.01 (m, 3H), 2.55–2.50 (m, 3H); ^{13}C NMR ($CDCl_3$) δ 164.7, 151.9, 144.3, 143.6, 142.6, 142.3, 131.7, 127.5, 126.3, 53.0, 15.2; HRMS (EI) calcd for $C_{13}H_{12}N_2O_2S$[M+H]+ 261.0692 , found: 261.0686 (error = 2.41 ppm)

3.4.2.5 Saponification of Methyl Ester Intermediates

General saponification procedure

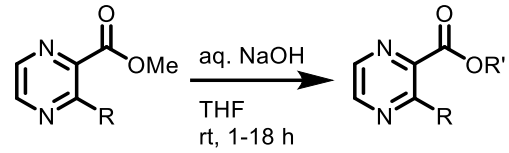

R = Ar, NR_2, NHCOR
R' = H, Na

Methyl ester (1 equiv) was dissolved in THF (0.1 M) at rt. Aqueous NaOH solution (0.25 N, 2.5 equiv) was added slowly over 5 min, and the reaction was stirred at rt until completion as determined by TLC (25% MeOH in DCM; 1-18 h). The crude reaction mixture was condensed to dryness *in vacuo*, then resolubilized in DCM/MeOH, condensed onto celite and purified by column chromatography using a cyano-functionalized silica cartridge (Teledyne Isco) with a gradient of 0-70% MeOH in DCM. A small number of products were isolated as the free acid.

Sodium 3-(benzaamido)pyrazine-2-carboxylate (POAA010). The title compound was obtained from the methyl ester in 90% yield as a white powder. HPLC purity: 98.3%; ^{1}H NMR (DMSO-d_6) δ 15.22 (s, 1H), 8.37 (d, J = 2.5 Hz, 1H), 8.25 (d, J = 2.5 Hz, 1H), 8.05 – 7.98 (m, 2H),

7.66 – 7.59 (m, 1H), 7.59 – 7.53 (m, 2H); ^{13}C NMR (DMSO-d_6) δ 166.59, 163.37, 149.61, 142.58, 138.12, 137.53, 135.04, 131.97, 128.78, 127.33; HRMS (ESI) calcd for $C_{12}H_8N_3O_3$ [M-H]$^-$: 242.0571, found: 242.0584 (error = 5.37 ppm); decomposed at 280 °C.

Sodium 3-(1-naphthamido)pyrazine-2-carboxylate (POAA012). The title compound was obtained from the methyl ester in quantitative yield as an off-white solid. HPLC purity: 93.5%; ^{1}H NMR (DMSO-d_6) δ 14.81 (s, 1H), 8.42 – 8.32 (m, 2H), 8.27 (d, J = 2.5 Hz, 1H), 8.10 (d, J = 8.2 Hz, 1H), 8.06 – 7.99 (m, 1H), 7.87 (dd, J = 7.2, 1.2 Hz, 1H), 7.65 – 7.56 (m, 3H); ^{13}C NMR (MeOD) δ 170.49, 169.25, 150.86, 144.54, 139.49, 138.26, 135.43, 135.05, 132.80, 131.64, 129.55, 128.34, 127.61, 127.14, 126.39, 126.00; HRMS (ESI) calcd for $C_{16}H_{11}N_3O_3$ [M-H]$^-$: 292.0728, found: 292.0746 (error = 6.16 ppm); decomposed at 200 °C.

3-Amino-6-bromopyrazine-2-carboxylate (POAA015). The title compound was obtained from the methyl ester in 73% yield as a yellow solid. HPLC purity: 92.8%; ^{1}H NMR (500 MHz, MeOD) δ 8.32 (s, 1H); ^{13}C NMR (126 MHz, MeOD) δ 168.32, 156.82, 151.43, 124.59, 124.22; HRMS (ESI) calcd for $C_5H_3BrN_3O_2$ [M-H]$^-$: 215.9414, found: 215.9425 error = 5.1 ppm); decomposed at 160 ºC. Spectra and other analytical data matched previously reported values for this compound.[354]

3-Amino-2-iodopyrazine-2-carboxylic acid (POAA016). The title compound was obtained from the methyl ester in 83% yield as a yellow solid. HPLC purity: 97.0%; ^{1}H NMR (DMSO-d_6) δ 13.32 (s, 1H), 8.44 (s, 1H), 7.49 (s, 2H); ^{13}C NMR (126 MHz, DMSO) δ 167.11, 155.25, 154.45, 125.70, 97.49; HRMS (ESI) calcd for $C_5H_3IN_3O_2$ [M-H]$^-$: 263.9275, found: 263.9291 (error = 6.1 ppm); decomposed at 185 °C. Spectra and other analytical data matched previously reported values for this compound.[355]

Sodium 3-(propionamido)pyrazine-2-carboxylate (POAA017). The title compound was obtained from the methyl ester in 38% yield as a white solid. HPLC purity: 99.2%; ^{1}H NMR (DMSO-d_6) δ 13.71 (s, 1H), 8.26 (d, J = 2.4 Hz, 1H), 8.16 (d, J = 2.5 Hz, 1H), 2.56 (q, J = 7.5 Hz, 2H), 1.09 (t, J = 7.5 Hz, 3H); ^{13}C NMR (DMSO-d_6) δ 172.21, 166.40, 148.96, 141.99, 141.99, 138.02, 136.87, 136.87, 30.90, 9.19; HRMS (ESI) calcd for $C_8H_8N_3O_3$ [M-H]$^-$: 194.0571, found: 194.0579 (error = 4.12 ppm); decomposed at 260 °C.

Sodium 3-(2-naphthamido)pyrazine-2-carboxylate (POAA021). The title compound was obtained from the methyl ester in 44% yield as an off-white solid. HPLC purity: 96.7%; ^{1}H NMR (MeOD) δ 8.68 (s, 1H), 8.45 (d, J = 2.5 Hz, 1H), 8.39 (d, J = 2.5 Hz, 1H), 8.16 (dd, J = 8.6, 1.9 Hz, 1H), 8.12 (d, J = 7.9 Hz, 1H), 8.03 (d, J = 8.6 Hz, 1H), 7.97 (d, J = 7.9 Hz, 1H), 7.62 (dqd, J = 8.2, 6.9, 1.4 Hz, 2H); ^{13}C NMR (MeOD) δ 170.70, 166.76, 151.02, 144.53, 139.24, 136.73, 134.20, 132.96, 130.50, 129.78, 129.62, 129.36, 128.78, 128.01, 124.92; HRMS (ESI) calcd for $C_{16}H_{10}N_3O_3$ [M-H]$^-$: 292.0728, found: 292.0742 (error = 4.79 ppm); decomposed at 230 °C.

Sodium 3-(diethylamino)pyrazine-2-carboxylate (POAA023). The title compound was obtained from the methyl ester in quantitative yield as a yellow solid. HPLC purity: 95.8%; ^{1}H NMR (MeOD) δ 7.95 (d, J = 2.6 Hz, 1H), 7.58 (d, J = 2.6 Hz, 1H), 3.58 (q, J = 7.0 Hz, 4H), 1.20 (t, J = 7.0 Hz, 6H).; ^{13}C NMR (MeOD) δ 175.42, 152.56, 142.88, 141.32, 130.13, 44.26, 13.22.; HRMS (ESI) calcd for $C_9H_{12}N_3O_2$ [M-H]$^-$: 194.0935, found: 194.0945 (error = 5.15 ppm); decomposed at 240 °C.

Sodium 3-(isobutylamino)pyrazine-2-carboxylate (POAA024). The title compound was obtained from the methyl ester in 97% yield as an off-white solid. HPLC purity: 99.7%; ^{1}H NMR (DMSO-d_6) δ 10.06 (t, J = 5.7 Hz, 1H), 7.88 (d, J = 2.6 Hz, 1H), 7.53 (d, J = 2.6 Hz, 1H), 3.19 – 3.11 (m, 2H), 1.87 – 1.76 (m, 1H), 0.91 (d, J = 6.7 Hz, 6H); ^{13}C NMR (DMSO-d_6) δ 168.06, 155.46,

142.21, 135.59, 128.80, 47.40, 27.75, 20.28; HRMS (ESI) calcd for $C_9H_{12}N_3O_2$ [M-H]$^-$: 194.0935, found: 194.0944 (error = 4.64 ppm); decomposition temperature greater than 280 °C.

Sodium 3-phenylpyrazine-2-carboxylate (POAA026). The title compound was obtained from the methyl ester in 66% yield as a white solid. HPLC purity: 97.6%; ^{1}H NMR (500 MHz, MeOD) δ 8.80 (d, J = 2.5 Hz, 1H), 8.62 (d, J = 2.5 Hz, 1H), 7.74 – 7.67 (m, 2H), 7.54 – 7.46 (m, 3H); ^{13}C NMR (126 MHz, MeOD) δ 153.98, 146.42, 142.97, 138.50, 130.70, 129.77, 129.51; HRMS (ESI) calcd for $C_{11}H_7N_2O_2$ [M-H]$^-$: 199.0513, found: 199.0526 (error = 6.5 ppm); Mp: 135 °C. Spectra and other analytical data matched previously reported values for this compound.[356]

Sodium 3-(4-fluorophenyl)pyrazine-2-carboxylate (POAA027). The title compound was obtained from the methyl ester in 90% yield as a tan solid. HPLC purity: 98.8%; ^{1}H NMR (DMSO-d_6) δ 8.45 (d, J = 2.5 Hz, 1H), 8.34 (d, J = 2.5 Hz, 1H), 8.07 – 7.98 (m, 2H), 7.27 – 7.18 (m, 2H; ^{13}C NMR (DMSO-d_6) δ 169.95, 163.43, 161.48, 155.74, 145.93, 141.47, 140.75, 134.90, 130.56, 130.50, 114.83, 114.66; ^{19}F NMR ($CDCl_3$) δ -112.97; HRMS (ESI) calcd for $C_{11}H_6FN_2O_2$ [M-H]$^-$: 217.0419, found: 217.0431 (error = 5.53 ppm); decomposition temperature greater than 280 °C.

Sodium 3-(4-(methylthio)phenyl)pyrazine-2-carboxylate (POAA028). The title compound was obtained from the methyl ester in 56% yield as an off-white solid. HPLC purity: 90.7%; ^{1}H NMR (MeOD) δ 8.56 (d, J = 2.6 Hz, 1H), 8.41 (d, J = 2.6 Hz, 1H), 7.87 – 7.80 (m, 2H), 7.35 – 7.30 (m, 2H), 2.51 (s, 3H); ^{13}C NMR (MeOD) δ 154.07, 150.64, 146.77, 143.87, 142.29, 142.14, 135.29, 130.90, 130.13, 126.75, 124.79, 15.19; HRMS (ESI) calcd for $C_{12}H_{10}N_2O_2S$ [M-H]$^-$: 245.0390, found: 245.0402 (error = 4.90 ppm); decomposed at 270 °C.

Sodium 3-(*o*-tolyl)pyrazine-2-carboxylate (POAA029). The title compound was obtained from the methyl ester in 92% yield as a tan solid. HPLC purity: 98.2%; ^{1}H NMR (MeOD)

δ 8.56 (d, J = 2.6 Hz, 1H), 8.50 (d, J = 2.6 Hz, 1H), 7.39 – 7.34 (m, 1H), 7.33 – 7.24 (m, 2H), 7.21 (td, J = 7.3, 1.7 Hz, 1H), 2.23 (s, 3H); ^{13}C NMR (MeOD) δ 173.55, 155.18, 153.26, 143.34, 142.98, 138.98, 137.84, 131.27, 130.34, 129.74, 126.35, 20.12; HRMS (ESI) calcd for $C_{12}H_9N_2O_2$ [M-H]$^-$: 213.0670, found: 213.0684 (error = 6.57 ppm); decomposition temperature greater than 280 °C.

Sodium 3-Pyrrolidine-2-Pyrazinoate (POAA031): The title compound was obtained from Methyl 6-chloropyrazinoate in 89% yield as a white solid. R_f = 0.09 (90:10 DCM:MeOH); HPLC purity: 98.6%; ^{1}H NMR (500 MHz, MeOD) δ 8.07 (d, *J* = 2.2 Hz, 1H), 7.69 (d, *J* = 2.2 Hz, 1H), 3.35 (d, *J* = 6.6 Hz, 4H), 1.91–1.82 (m, 4H); ^{13}C NMR (126 MHz, MeOD) δ 167.9, 151.2, 143.7, 129.5, 48.8, 25.0; HRMS (ESI) calcd for $C_9H_{11}N_3O_2$[M+2Na]$^+$: 238.0563 , found: 238.0558 (error = 2.10 ppm); Mp: 122–124 ℃.

Sodium 3-Piperidine-2-pyrazinoate (POAA032): The title compound was obtained from Methyl 6-chloropyrazinoate in 74% yield as a yellow solid. R_f = 0.31 (90:10 DCM:MeOH); HPLC purity: 97.2%; ^{1}H NMR (500 MHz, MeOD) δ 8.10 (d, *J* = 2.4 Hz, 1H), 7.78 (d, *J* = 2.4 Hz, 1H), 3.37 (t, *J* = 5.0 Hz, 4H), 1.63–1.51 (m, 6H); ^{13}C NMR (126 MHz, MeOD) δ 167.9, 154.5, 143.6, 131.8, 48.1, 25.3, 23.9; HRMS (EI) calcd for $C_{10}H_{13}N_3O_2$[M+H]+: 207.1008, found: 207.0316; Mp: 127–129 ℃.

Sodium 3-(benzylamino)pyrazine-2-carboxylate (POAA033): The title compound was obtained from Methyl 6-chloropyrazinoate in 74% yield as a white solid. HPLC purity: 98.8%; ^{1}H NMR (MeOD) δ 7.89 (d, *J* = 2.6 Hz, 1H), 7.62 (d, *J* = 2.6 Hz, 1H), 7.26 (d, *J* = 7.1 Hz, 2H), 7.22–7.18 (m, 2H), 7.15–7.10 (m, 1H), 4.54 (s, 2H); ^{13}C NMR (MeOD) δ 171.0, 155.0, 143.2, 139. 5, 129.7, 128.1, 127.0, 126.5, 43.9; HRMS (ESI) calcd for $C_{12}H_{11}N_3O_2$ [M+2Na]$^+$ 274.0563, found: 274.0564 (error = 0.08 ppm); decomposition temperature greater than 280 °C.

Sodium 3-(phenylamino)pyrazine-2-carboxylate (POAA034). The title compound was obtained from the methyl ester in 69% yield as a yellow solid. HPLC purity: 97.8%; ^{1}H NMR (MeOD) δ 8.04 (d, *J* = 2.5 Hz, 1H), 7.80 (d, *J* = 2.6 Hz, 1H), 7.60 (d, *J* = 8.0 Hz, 2H), 7.21–7.16 (m, 2H), 6.88 (td, *J* = 7.4, 1.2 Hz, 1H); ^{13}C NMR (MeOD) δ 119.29, 121.6, 128.4, 131.8, 140.0, 142.8, 152.7; HRMS (ESI) calcd for $C_{11}H_9N_3O_2$ $[M+2Na]^+$ 260.0406, found: 260.0404 (error = 0.16 ppm); decomposition temperature greater than 280 °C.

Sodium 3-(cyclopentylamino)pyrazine-2-carboxylate (POAA035): The title compound was obtained from the ester in 78% yield as an off- white solid. HPLC purity: 99.3%; ^{1}H NMR (MeOD) δ 8.16 (d, *J* = 2.2 Hz, 1H), 7.67 (d, *J* = 2.2 Hz, 1H), 4.27 (q, *J* = 6.5 Hz, 1H), 1.97 (dq, *J* = 12.9, 6.8 Hz, 2H), 1.71–1.62 (m, 2H), 1.58 (qd, *J* = 9.5, 7.7, 5.2 Hz, 2H), 1.47–1.36 (m, 2H); ^{13}C NMR (MeOD) δ 168.1, 155.0, 147.6, 129.9, 123.9, 52.0, 32.7, 23.3; HRMS (ESI) calcd for $C_{10}H_{13}N_3O_2$ $[M+2Na]^+$: 252.0719, found: 252.0701 (error = 6.85 ppm); Mp: 99–101 °C.

Sodium 3-(cyclobutylamino)pyrazine-2-carboxylate (POAA036): The title compound was obtained from the methyl ester in 86% yield as a white solid. HPLC purity: 95.8%; ^{1}H NMR (MeOD) δ 7.85 (d, *J* = 2.6 Hz, 1H), 7.58 (d, *J* = 2.6 Hz, 1H), 4.34 (p, *J* = 8.0 Hz, 1H), 2.32 (dtt, *J* = 12.8, 8.0, 2.6 Hz, 2H), 1.94–1.84 (m, 1H), 1.78–1.64 (m, 2H); ^{13}C NMR (MeOD) δ 170.9, 154.1, 143.2, 133.5, 129.4, 45.6, 30.8, 14.8; HRMS (ESI) calcd for $C_9H_{11}N_3O_2Na_2$$[M+2Na]^+$: 238.0563, found: 238.0566 (error = 1.46 ppm); decomposition temperature greater than 280 °C.

Sodium 3-Morpholino-2-pyrazinoate (POAA037): The title compound was obtained from the ester in 43% yield as a white solid. R_f = 0.12 (90:10 DCM:MeOH); HPLC purity: 99.9%; ^{1}H NMR (500 MHz, MeOD) δ 7.96 (d, *J* = 2.7 Hz, 1H), 7.69 (d, *J* = 2.9 Hz, 1H), 3.72–3.62 (m, 4H), 3.44 (t, *J* = 4.7 Hz, 4H); ^{13}C NMR (126 MHz, MeOD) δ 173.35, 152.5, 140.3, 131.8, 66.4;

HRMS (ESI) calcd for $C_9H_{11}N_3O_3$ $[M+2Na]^+$: 254.0512 , found: 254.0510 (error = 4.32 ppm); decomposition temperature beyond 280 ℃.

Sodium 3-Thiomorpholino-2-pyrazinoate (POAA038): The title compound was obtained from the ester in 66% yield as a yellow solid. R_f = 0.22 (90:10 DCM:MeOH); HPLC purity: 99.6%; ^{1}H NMR (500 MHz, MeOD) δ 8.15 (d, *J* = 2.2 Hz, 1H), 7.85 (d, *J* = 2.2 Hz, 1H), 3.70–3.65 (m, 4H), 2.63 (dd, *J* = 6.3, 3.8 Hz, 4H); ^{13}C NMR (126 MHz, MeOD) δ 167.5, 154.8, 132.4, 131.9, 50. 8, 26.4 ; HRMS (ESI) calcd for $C_{11}H_9N_3O_2$ $C_9H_{11}N_3O_2S$ $[M+2Na]^+$: 270.0284, found: 270.0250 (error = 12.46 ppm); Mp: 204–207 ℃.

Sodium 3-(ethylamino)pyrazine-2-carboxylate (POAA039): The title compound was obtained from the methyl ester in 87% yield as a white solid. HPLC purity: 99.1%; ^{1}H NMR (MeOD) δ 7.87 (d, *J* = 2.6 Hz, 1H), 7.57 (d, *J* = 2.6 Hz, 1H), 3.33 (q, *J* = 7.2 Hz, 2H), 1.16 (t, *J* = 7.2 Hz, 3H); ^{13}C NMR (MeOD) δ 171.0, 155.1, 143.1, 133.8, 129.1, 34.8, 13.5; HRMS (ESI) calcd for $C_7H_9N_3O_2$ $[M+2Na]^+$: 212.0456, found: 212.0471 (error = 8.02 ppm); Mp: 133–136 °C.

Sodium 3-Butylamino-2-pyrazinoate (POAA040): The title compound was obtained from the ester in 45% yield as a white solid. R_f = 0.60 (90:10 DCM:MeOH); HPLC purity: 99.4%; NMR (500 MHz, MeOD) δ 7.99 (d, *J* = 2.6 Hz, 1H), 7.68 (d, *J* = 2.6 Hz, 1H), 3.43 (t, *J* = 7.0 Hz, 2H), 1.65 (dd, *J* = 8.5, 6.4 Hz, 2H), 1.55–1.46 (m, 2H), 0.99 (t, *J* = 7.4 Hz, 3H); ^{13}C NMR (126 MHz, MeOD) δ 178.9, 143.2, 129.0, 39.8, 31.2, 22.9, 19.9, 12.8; HRMS (ESI) calcd for $C_{11}H_9N_3O_2$ $C_9H_{13}N_3O_2$ $[M+2Na]^+$: 240.0719, found: 240.0727 (error = 3.26 ppm); decomposition temperature between 268–272 ℃.

Sodium 3-(6-azaspiro[2,5] octano) 2-pyrazinoate (POAA041): The title compound was obtained from the ester in 57% yield as a yellow solid. HPLC purity: 95.7%; R_f = 0.28 (90:10 DCM:MeOH); ^{1}H NMR (500 MHz, MeOD) δ 7.89 (d, *J* = 2.8 Hz, 1H), 7.60 (d, *J* = 2.6 Hz, 1H),

3.55–3.47 (m, 4H), 1.40–1.34 (m, 4H), 0.26 (s, 4H); ^{13}C NMR (126 MHz, MeOD) δ 140.1, 130.5, 34.6, 22.8, 17.3, 10.6; HRMS (ESI) calcd for $C_{12}H_{15}N_3O_2$ $[M+2Na]^+$: 278.0878, found: 278.0866 (error = 4.26 ppm); decomposition temperature between 272–275 ℃.

Sodium 3-(quinoline-2-carboxamido)pyrazine-2-carboxylate (POAA060). The title compound was obtained from the methyl ester in 85% yield as a white solid. HPLC purity: 99.2%; ^{1}H NMR (MeOD) δ 8.51 (d, J = 8.5 Hz, 1H), 8.49 – 8.43 (m, 2H), 8.40 (d, J = 2.5 Hz, 1H), 8.35 (d, J = 8.4 Hz, 1H), 8.01 (dd, J = 8.3, 1.4 Hz, 1H), 7.86 (ddd, J = 8.4, 6.8, 1.4 Hz, 1H), 7.71 (ddd, J = 8.2, 6.9, 1.2 Hz, 1H); ^{13}C NMR (MeOD) δ 170.68, 164.99, 150.98, 150.15, 148.16, 144.21, 139.37, 139.00, 131.67, 131.46, 130.96, 129.69, 128.78, 119.72; HRMS (ESI) calcd for $C_{15}H_9N_4O_3$ $[M-H]^-$: 293.0680, found: 293.0693 (error = 4.44 ppm); decomposition temperature beyond 280 °C.

Sodium 3-(benzofuran-2-carboxamido)pyrazine-2-carboxylate (POAA061). The title compound was obtained from the methyl ester in 52% yield as a tan solid. HPLC purity: 89.9%; ^{1}H NMR (DMSO-d_6) δ 15.50 (s, 1H), 8.41 (d, J = 2.4 Hz, 1H), 8.28 (d, J = 2.5 Hz, 1H), 7.84 (d, J = 7.8 Hz, 1H), 7.74 – 7.65 (m, 2H), 7.56 – 7.49 (m, 1H), 7.38 (t, J = 7.5 Hz, 1H); ^{13}C NMR (DMSO-d_6) δ 167.00, 155.64, 155.01, 149.85, 149.66, 143.28, 138.44, 127.91, 127.72, 127.62, 124.45, 124.29, 123.52, 123.44, 112.54, 112.38, 111.18, 111.00; HRMS (ESI) calcd for $C_{14}H_8N_3O_4$ $[M-H]^-$: 282.0520, found: 282.0532 (error = 4.25 ppm) ; decomposed at 240 °C.

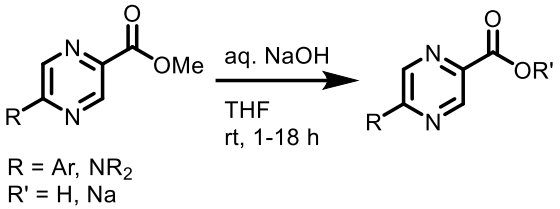

5-substituted pyrazinoates were prepared using the general saponification procedure.

Sodium 5-(diethylamino)pyrazine-2-carboxylate (POAA018): The title compound was obtained from the methyl ester in 60% yield as a tan solid. HPLC purity: 99.1%; ^{1}H NMR (500 MHz, MeOD) δ 8.69 (d, *J* = 1.4 Hz, 1H), 8.00 – 7.96 (m, 1H), 3.62 (q, *J* = 7.1 Hz, 4H), 1.23 (t, *J* = 7.1 Hz, 6H); ^{13}C NMR (126 MHz, MeOD) δ 172.70, 154.72, 145.12, 137.06, 129.16, 43.66, 13.04; HRMS (ESI) calcd for $C_9H_{12}N_3O_2$ [M-H]$^-$: 194.0935, found: 194.0941 (error = 3.1 ppm); Mp: 142 ºC.

Sodium 5-phenylpyrazine-2-carboxylate (POAA020): The title compound was obtained from the methyl ester in 64% as a white solid. HPLC purity: 99.6%; ^{1}H NMR (500 MHz, MeOD) δ 9.22 (d, *J* = 1.5 Hz, 1H), 9.10 (d, *J* = 1.6 Hz, 1H), 8.15 – 8.09 (m, 2H), 7.59 – 7.48 (m, 3H); ^{13}C NMR (126 MHz, MeOD) δ 169.47, 155.23, 149.93, 145.82, 141.85, 137.38, 131.23, 130.13, 128.25; HRMS (ESI) calcd for $C_{11}H_7N_2O_2$ [M-H]$^-$: 199.0513, found: 199.0522 (error = 4.5 ppm); decomposition temperature greater than 230 ºC.

Sodium 5-(isobutylamino)pyrazine-2-carboxylate (POAA022): The title compound was obtained from the methyl ester in 91% yield as an orange solid. ^{1}H NMR (500 MHz, MeOD) δ 8.62 (s, 1H), 7.90 (s, 1H), 3.22 (d, *J* = 6.9 Hz, 2H), 1.92 (hept, *J* = 6.7 Hz, 1H), 0.98 (d, *J* = 6.7 Hz, 6H); ^{13}C NMR (126 MHz, MeOD) δ 170.12, 157.53, 145.83, 133.72, 29.26, 20.56; HRMS (ESI) calcd for $C_9H_{12}N_3O_2$ [M-H]$^-$: 194.0935, found: 194.0948 (error = 6.7 ppm); Mp: 125 ºC.

Sodium 5-(o-tolyl)pyrazine-2-carboxylate (POAA025): The title compound was obtained from the methyl ester in 34% yield as a white solid. HPLC purity: 99.1%; ^{1}H NMR (500 MHz, MeOD) δ 9.25 (d, *J* = 1.5 Hz, 1H), 8.73 (d, *J* = 1.5 Hz, 1H), 7.45 (dd, *J* = 7.5, 1.5 Hz, 1H), 7.42 – 7.32 (m, 3H), 2.38 (s, 3H); ^{13}C NMR (126 MHz, MeOD) δ 170.89, 157.18, 148.87, 145.32, 144.86, 137.77, 137.69, 132.10, 130.85, 130.55, 127.26, 20.34; HRMS (ESI) calcd for $C_{12}H_9N_2O_2$ $[M-H]^-$: 213.0670, found: 213.0680 (error = 4.7 ppm); decomposition temperature greater than 230 ºC.

Sodium 5-Morpholino-2-pyrazinoate (POAA042): The title compound was obtained from the ester in 75% yield as an off-white solid. HPLC purity: 96.0%; R_f = 0.01 (90:10 DCM:MeOH); ^{1}H NMR (500 MHz, MeOD) δ 8.76 (d, *J* = 1.4 Hz, 1H), 8.16 (d, *J* = 1.4 Hz, 1H), 3.89–3.78 (m, 4H), 3.73–3.63 (m, 4H); ^{13}C NMR (126 MHz, MeOD) δ 154.8, 143.4, 137.5, 128.7, 66.2, 44.4; HRMS (ESI) calcd for $C_9H_{11}N_3O_3[M+2Na]^+$: 254.0512, found: 254.0502 (error = 4.00 ppm); decomposition temperature beyond 280 ºC.

Sodium 5-Thiomorpholino-2-pyrazinoate (POAA043): The title compound was obtained from the ester in 83% yield as a white solid. HPLC purity: 99.3%; R_f = 0.01 (90:10 DCM:MeOH); ^{1}H NMR (500 MHz, MeOD) δ 8.61 (d, *J* = 1.3 Hz, 1H), 8.04 (d, *J* = 1.5 Hz, 1H), 4.09–3.93 (m, 4H), 2.70–2.51 (m, 4H); ^{13}C NMR (126 MHz, MeOD) δ 143.4, 137.2, 128.9, 25.7; HRMS (ESI) calcd for $C_9H_{11}N_3O_2S$ $[M+2Na]^+$: 270.0284, found: 270.0289 (error = 2.01 ppm); decomposition temperature beyond 280 ºC.

Sodium 5-Pyrrolidine-2-Pyrazinoate (POAA044): The title compound was obtained from the ester in 75% yield as a white solid. HPLC purity: 98.4%; R_f = 0.19 (90:10 DCM:MeOH); ^{1}H NMR (500 MHz, MeOD) δ 8.65 (d, *J* = 1.4 Hz, 1H), 7.89 (d, J = 1.5 Hz, 1H), 4.24 (h, *J* = 6.5 Hz, 1H), 2.06 (dt, *J* = 13.0, 6.3 Hz, 2H), 1.83–1.76 (m, 2H), 1.72–1.63 (m, 2H), 1.57 (dt, *J* = 12.8,

6.2 Hz, 2H); ^{13}C NMR (126 MHz, MeOD) δ 171.3, 152.4, 143.6, 136.0, 129.1, 46.3, 24.9, 17.0; HRMS (ESI) calcd for $C_9H_{11}N_3O_2$[M+2Na]$^+$: 238.0563, found: 238.0559 (error = 1.78 ppm); decomposition temperature beyond 280 ℃.

Sodium 5-Cyclopentylamino-2-pyrazinoate (POAA045): The title compound was obtained from the ester in 75% yield as a yellow solid. HPLC purity: 95.1%; R_f = 0.15 (90:10 DCM:MeOH); ^{1}H NMR (500 MHz, MeOD) δ 8.65 (d, *J* = 1.4 Hz, 1H), 7.89 (d, *J* = 1.5 Hz, 1H), 4.24 (h, *J* = 6.5 Hz, 1H), 2.06 (dt, *J* = 13.0, 6.3 Hz, 2H), 1.83–1.76 (m, 2H), 1.72–1.63 (m, 2H), 1.57 (dt, *J* = 12.8, 6.2 Hz, 2H); ^{13}C NMR (126 MHz, MeOD) δ 171.30, 155.11, 143.48, 135.72, 132.11, 52.25, 32.33, 23.37; HRMS (ESI) calcd for $C_{10}H_{13}N_3O_2$[M+2Na]$^+$: 252.0719, found: 252.0729 (error = 3.82 ppm); decomposition temperature between 204–207 ℃.

Sodium 5-Cyclobutylamino-2-pyrazinoate (POAA046): The title compound was obtained from the ester in 84% yield as a yellow solid. HPLC purity: 96.3%; R_f = 0.12 (90:10 DCM:MeOH); ^{1}H NMR (500 MHz, MeOD) δ 8.64 (d, *J* = 1.3 Hz, 1H), 7.87 (d, *J* = 1.3 Hz, 1H), 4.41 (q, *J* = 8.0 Hz, 1H), 2.43 (dtd, *J* = 13.2, 7.4, 3.0 Hz, 2H), 2.16–1.98 (m, 2H), 1.89–1.75 (m, 2H); ^{13}C NMR (126 MHz, MeOD) δ 171.2, 154.4, 143.6, 136.1, 131.7, 46.1, 30.3, 14.6 HRMS (ESI) calcd for $C_9H_{11}N_3O_2$[M+2Na]$^+$: 238.0563, found: 238.0545 (error = 7.72 ppm); decomposition temperature beyond 280 ℃.

Sodium 5-Anilino-2-pyrazinoate (POAA047): The title compound was obtained from the ester in 75% yield as a yellow solid. HPLC purity: 87.1%; R_f = 0.10 (90:10 DCM:MeOH); ^{1}H NMR (500 MHz, MeOD) δ 8.80–8.73 (m, 1H), 8.21–8.12 (m, 1H), 7.69 (d, *J* = 8.0 Hz, 2H), 7.33 (t, *J* = 7.9 Hz, 2H), 7.04 (t, *J* = 7.2 Hz, 1H); ^{13}C NMR (126 MHz, MeOD) δ 170.8, 153.2, 143.1, 140.0, 138.3, 132.7, 128.5, 122. 3, 119.2; HRMS (ESI) calcd for $C_{11}H_9N_3O_2$ [M+2Na]$^+$: 260.0406, found: 260.0404; decomposition temperature beyond 280 ℃.

Sodium 5- Piperidine-2-pyrazinoate (POAA048): The title compound was obtained from the ester in 69% yield as a yellow solid. HPLC purity: 98.2%; R_f = 0.84 (90:10 DCM:MeOH); ^{1}H NMR (500 MHz, MeOD) δ 8 8.59 (s, 1H), 8.00–7.97 (m, 1H), 3.58 (t, *J* = 5.5 Hz, 4H), 1.62 (dt, *J* = 11.5, 5.2 Hz, 2H), 1.55 (q, *J* = 5.9 Hz, 4H); ^{13}C NMR (126 MHz, MeOD) δ 170.8, 160.2, 155.2, 143.4, 128.1, 29.3, 25.5, 24.3 HRMS (ESI) calcd for $C_{10}H_{13}N_3O_2$ $[M+2Na]^+$: 252.0719, found: 252.0722 (error = 1.16 ppm); Mp: 115–118 ℃.

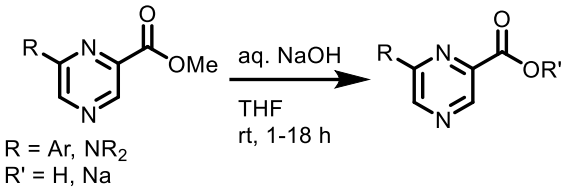

6-substituted pyrazinoates were prepared using the general saponification procedure.

Sodium 6-Pyrrolidine-2-Pyrazinoate (POAA049): The title compound was obtained from the ester in 79% yield as a white solid. HPLC purity: 97.1%; R_f = 0.36 (90:10 DCM:MeOH); ^{1}H NMR (500 MHz, MeOD) δ 8.25 (s, 1H), 7.95 (s, 1H), 3.48–3.45 (m, 4H), 1.99–1.93 (m, 4H); ^{13}C NMR (126 MHz, MeOD) δ 166.9, 152.5, 141.3, 133.5, 130.8, 46.2, 24.9; HRMS (ESI) calcd for $C_9H_{11}N_3O_2$[M+2Na]$^+$: 238.0563, found: 238.0559 (error = 1.80 ppm); decomposition temperature between 278–283 ℃.

Sodium 6-Morpholino-2-pyrazinoate (POAA050): The title compound was obtained from the ester in 85% yield as an off-white solid. HPLC purity: 95.1%; R_f = 0.34 (90:10 DCM:MeOH); ^{1}H NMR (500 MHz, MeOD) δ 8.29 (s, 1H), 8.07 (s, 1H), 3.70 (t, *J* = 4.9 Hz, 4H), 3.60–3.54 (m, 4H); ^{13}C NMR (126 MHz, MeOD) δ 171.0, 154.6, 147.4, 132.5, 130.4, 66.3, 44.6; HRMS (ESI) calcd for $C_9H_{11}N_3O_3$ $[M+2Na]^+$: 254.0512, found: 254.0525 (error = 5.33 ppm); decomposition temperature between 270–273 ℃.

Sodium 6-Piperidine-2-pyrazinoate (POAA051): The title compound was obtained from the ester in 81% yield as a white solid. HPLC purity: 98.5%; R_f = 0.07 (90:10 DCM:MeOH); ^{1}H NMR (500 MHz, MeOD) δ 9.14 (s, 0H), 8.73 (d, *J* = 6.5 Hz, 1H), 8.24 (s, 1H), 4.08 (s, 3H), 1.93 (s, 9H); ^{13}C NMR (126 MHz, MeOD) δ 179.1, 170.1, 160.1, 146.7, 136.3, 135.5, 48.0, 22.8; HRMS (ESI) calcd for $C_{10}H_{13}N_3O_2$[M+2Na]$^+$: 252.0719, found: 252.0736 (error = 6.42 ppm); decomposition temperature beyond 280 ℃.

Sodium 6-Cyclobutylamino-2-pyrazinoate (POAA052): The title compound was obtained from the ester in % yield as a off-white solid. HPLC purity: 94.2%; R_f = 0.08 (95:5 DCM:MeOH); ^{1}H NMR (500 MHz, MeOD) δ 8.25 (d, *J* = 1.3 Hz, 1H), 7.76 (d, *J* = 1.3 Hz, 1H), 4.39 (t, *J* = 7.9 Hz, 1H), 2.46 – 2.35 (m, 2H), 1.91 (td, *J* = 14.9, 12.5, 7.3 Hz, 2H), 1.84 – 1.73 (m, 2H); ^{13}C NMR (126 MHz, MeOD) δ 171.0, 153.8, 147.6, 131.2 (d, *J* = 53.6 Hz), 63.3, 30.5, 23.9, 14.4; HRMS (ESI) calcd for $C_9H_{11}N_3O_2$ [M-H]$^-$: 192.0779, found: 192.0777 (error = 1.04 ppm); decomposition temperature between 200–205 ℃.

Sodium 6-Ethylamino-2-pyrazinoate (POAA053): The title compound was obtained from the ester in 87% yield as a white solid. HPLC purity: 88.5%; R_f = 0.08 (95:5 DCM:MeOH); ^{1}H NMR (500 MHz, MeOD) δ 8.32 (s, 1H), 7.89 (s, 1H), 3.35 (d, *J* = 7.4 Hz, 2H), 1.27 (t, *J* = 7.3 Hz, 3H); ^{13}C NMR (126 MHz, MeOD) δ 170.2, 154.6, 131.6, 35.9, 13.3; HRMS (ESI) calcd for $C_7H_9N_3O_2$ [M-H]$^-$ 166.0622, found: 166.0625 (error = 1.80 ppm); decomposition temperature between 167–170 ℃.

Sodium 6-Cyclopentylamino-2-pyrazinoate (POAA054): The title compound was obtained from the ester in 75% yield as a yellow solid. HPLC purity: 97.7%; R_f = 0.43 (95:5 DCM:MeOH); ^{1}H NMR (500 MHz, MeOD) δ 8.22 (s, 1H), 7.82 (s, 1H), 4.23 (s, 1H), 2.04 (s, 2H), 1.68 (dd, *J* = 41.7, 9.5 Hz, 4H), 1.49 (d, *J* = 11.6 Hz, 2H); ^{13}C NMR (126 MHz, MeOD) δ 179.0,

160.1, 154.6, 147.7, 130.8, 53.3 – 50.9 (m), 32.5, 23.4; HRMS (ESI) calcd for $C_{10}H_{13}N_3O_2$[M-H]$^-$: 206.0935, found: 206.0946 (error = 5.33 ppm); decomposition temperature between 179–183 ℃.

Sodium 6-Isobutylamino-2-pyrazinoate (POAA055): The title compound was obtained from the ester in 45% yield as a white solid. HPLC purity: 88.3%; R_f = 0.33 (95:5 DCM:MeOH); ^{1}H NMR (500 MHz, MeOD) δ 8.20 (d, *J* = 1.8 Hz, 1H), 7.83 (d, *J* = 1.7 Hz, 1H), 3.21 (dd, *J* = 6.9, 1.7 Hz, 2H), 1.94 – 1.83 (m, 1H), 0.97 (dd, *J* = 6.7, 1.8 Hz, 6H).; ^{13}C NMR (126 MHz, MeOD) δ 171.3, 160.1, 155.1, 147.6, 130.7, 61.4, 28.0, 19.2; HRMS (ESI) calcd for $C_9H_{13}N_3O_2$[M-H]$^-$: 194.0935, found: 194.0937 (error = 1.03 ppm); decomposition temperature between 197–201 ℃.

Sodium 6-Phenylpyrazine-2-carboxylic acid (POAA056): The title compound was obtained from the ester in 45% yield as a white solid. HPLC purity: 98.8%; R_f = 0.86 (95:5 DCM:MeOH); ^{1}H NMR (500 MHz, MeOD) δ 9.03 (d, *J* = 23.3 Hz, 2H), 8.07 (d, *J* = 7.4 Hz, 2H), 7.44 (d, *J* = 9.0 Hz, 3H); ^{13}C NMR (126 MHz, MeOD) δ 169.9, 152.0, 149.4, 142.9, 142.0, 136.2, 129.6, 128.6, 127.0; HRMS (ESI) calcd for $C_{11}H_8N_2O_2$ [M-H]$^-$: 199.0513, found: 199.0521 (error = 4.01 ppm); decomposition temperature greater than 280 ℃.

Sodium 6-(4-Fluorophenyl) pyrazine-2-carboxylic acid (POAA057): The title compound was obtained from the ester in 45% yield as a white solid. HPLC purity: 99.3%; R_f = 0.88 (95:5 DCM:MeOH); ^{1}H NMR (500 MHz, MeOD) δ 9.05 (dd, *J* = 10.5, 1.7 Hz, 2H), 8.26 (ddd, *J* = 9.0, 5.3, 1.8 Hz, 2H), 7.23 (td, *J* = 8.8, 1.8 Hz, 2H); ^{13}C NMR (126 MHz, MeOD) δ 170.0, 165.0, 163.3, 150.8, 142.6, 141.3, 132.5 (d, *J* = 3.0 Hz), 129.3 (d, *J* = 8.5 Hz), 115.4 (d, *J* = 21.9 Hz); HRMS (ESI) calcd for $C_{11}H_7FN_2O_2$[M-H]$^-$: 217.0419, found: 217.0416 (error = 1.38 ppm); decomposition temperature between 198–201 ℃.

Sodium 6-(o-tolyl) pyrazine-2-carboxylic acid (POAA058): The title compound was obtained from the ester in 45% yield as a white solid. HPLC purity: 97.5%; R_f = 0.11 (95:5

DCM:MeOH); ^{1}H NMR (500 MHz, MeOD) δ 9.08 (s, 1H), 8.67 (s, 1H), 7.45 (d, *J* = 7.3 Hz, 1H), 7.32 (tt, *J* = 11.8, 7.3 Hz, 3H), 2.35 (s, 3H); ^{13}C NMR (126 MHz, MeOD) δ 169.8, 154.5, 149.3, 144.6, 142.4, 136.7, 136.3, 130.4, 129.6, 128.9, 125.7, 18.9; HRMS (ESI) calcd for $C_{12}H_{10}N_2O_2$[M-H]$^-$: 213.0670, found: 213.0664 (error = 2.82 ppm); decomposition temperature between 218–222 ℃.

Sodium 6-(4-(methylthio) phenyl)pyrazine-2-carboxylic acid (POAA059): The title compound was obtained from the ester in 45% yield as a white solid. HPLC purity: 97.3%; R_f = 0.69 (95:5 DCM:MeOH); ^{1}H NMR (500 MHz, MeOD) δ 9.02 (dd, *J* = 15.4, 1.9 Hz, 2H), 8.18 – 8.11 (m, 2H), 7.40 – 7.33 (m, 2H), 2.51 (d, *J* = 2.0 Hz, 3H); ^{13}C NMR (126 MHz, MeOD) δ 170.1, 151.4, 149.5, 142.2, 141.7, 141.1, 132.5, 127.3, 125.7, 13.6; HRMS (ESI) calcd for $C_{12}H_{10}N_2O_2S$[M-H]$^-$: 245.0390, found: 245.0384 (error = 2.45 ppm); decomposition temperature greater than 280 ℃.

3.4.3 Bacterial Strains and Media

M. bovis BCG cultures were grown at 37 °C in supplemented complete Middlebrook 7H9 medium (BD Difco), as described previously.[316, 318]

3.4.4 Cloning, Production, and Purification of *Mtb* PanD

The coding region of *panD* from *M. tuberculosis* was ligated into a pET9-d1-His6 vector, transformed into *E. coli* BL21 (DE3) cells, expressed via IPTG induction, and purified from lysed cultures by Ni^{2+}-NTA column and size exclusion chromatography, as described previously by Gopal *et al*.[316] *M. bovis panD* and *M. tuberculosis panD* are 100% identical.

3.4.5 MIC Determination and PanD Reporter Assay

The growth inhibition dose−response assay for *M. bovis* BCG (ATCC 35734) and *M. bovis* L132R PanD was performed using the broth microdilution method, as described previously.[357] Exponential phase cultures (OD_{600} = 0.05) were treated with increasing concentrations of POA or analogue 2 for 5 days and growth was measured by OD_{600} determination. Experiments were performed three times independently in duplicate. Analogues were dissolved in DMSO, or in another suitable solvent (MeOH/EtOH/H_2O) and filtered through a 0.22 μm syringe filter. The PanD reporter assay was performed according to Gopal *et al*, using a *M. bovis BCG* strain harboring a constitutively expressed RFP−PanD fusion.[318]

3.4.6 Isothermal Titration Calorimetry

ITC experiments were performed using a microcalorimeter (Model ITC200, MicroCal, Northampton, U.K.), to study the binding of PanD mutants with POA or binding of newly synthesized POA analogues, as recently described.[316]

3.4.7 ^{1}H NMR PanD Activity Assays

NMR samples containing 2 mM L-Asp and 10 μM *Mtb* PanD were prepared in 20 mM sodium phosphate buffer (pH 6.5) in deuterated water. Basic 1H-1D NMR spectra were collected with presaturation of solvent water (relaxation delay of 2 s; solvent presaturation applied during the relaxation delay) after 40 min of incubation of the NMR sample, using a Bruker Avance 400 MHz NMR spectrometer, equipped on a 5 mm BBI probe head at 298 K. The inhibitory effect of the analogues, dissolved in d6-DMSO or for comparison in buffer (20 mM sodium phosphate buffer (pH 6.5)) were added into the enzymatic reaction mixture at a final concentration of 0, 2.5, 10, 100, 200, and 500 μM of the respective analogue. After 40 min of incubation at 298 K, a series of ^{1}H-

^{1}D spectra were obtained and the inhibition rate at each concentration of the analogues was calculated by measuring the peak volume of the product β-Ala. In comparison, a ^{1}H-^{1}D NMR spectra was recorded in the presence of 200 μM of POA. 2,2-Dimethyl-2-silapentane-5-sulfonate (DSS) was used as an internal standard for the calibration of the NMR peaks.

3.5 Acknowledgements

Research reported in this chapter was supported by the National Institute of Allergy and Infectious Diseases of the National Institutes of Health, Award No. R01AI106398 (T.D., C.C.A., G.G.) the National Research Foundation (NRF) Singapore, NRF Competitive Research Programme (CRP), Grant Award No. NRF-CRP18-2017-01) to G.G., and the Singapore Ministry of Education Academic Research Fund Tier 1 (No. RG107/20) to G.G. M.S.C. received funding from The 3M Company and the National Institutes of Health (5T32GM008700-18).

4. Bibliography

1. Abraham, E. P., History of β-Lactam Antibiotics. In *Antibiotics Containing the Beta-Lactam Structure I*, Demain, A. L. S., N.A., Ed. Springer-Verlag: Berlin, 1983; Vol. 1, pp 1-13.
2. Ernest, I.; Gosteli, J.; Greengrass, C. W.; Holick, W.; Pfaendler, H. R.; Woodward, R. B., The penems, a new class of .beta.-lactam antibiotics: 6-acylaminopenem-3-carboxylic acids. *Journal of the American Chemical Society* **1978,** *100* (26), 8214-8222.
3. El-Lababidi, R. A.-O.; Rizk, J. A.-O., Cefiderocol: A Siderophore Cephalosporin. (1542-6270 (Electronic)).
4. Zhanel, G. G.; Chung, P.; Adam, H.; Zelenitsky, S.; Denisuik, A.; Schweizer, F.; Lagacé-Wiens, P. R. S.; Rubinstein, E.; Gin, A. S.; Walkty, A.; Hoban, D. J.; Lynch, J. P.; Karlowsky, J. A., Ceftolozane/Tazobactam: A Novel Cephalosporin/β-Lactamase Inhibitor Combination with Activity Against Multidrug-Resistant Gram-Negative Bacilli. *Drugs* **2014,** *74* (1), 31-51.
5. Papp-Wallace Krisztina, M.; Bethel Christopher, R.; Caillon, J.; Barnes Melissa, D.; Potel, G.; Bajaksouzian, S.; Rutter Joseph, D.; Reghal, A.; Shapiro, S.; Taracila Magdalena, A.; Jacobs Michael, R.; Bonomo Robert, A.; Jacqueline, C., Beyond Piperacillin-Tazobactam: Cefepime and AAI101 as a Potent β-Lactam−β-Lactamase Inhibitor Combination. *Antimicrobial Agents and Chemotherapy* **2019,** *63* (5), e00105-19.
6. Cluck, D.; Lewis, P.; Stayer, B.; Spivey, J.; Moorman, J., Ceftolozane–tazobactam: A new-generation cephalosporin. *American Journal of Health-System Pharmacy* **2015,** *72* (24), 2135-2146.
7. Abraham, E. P.; Chain, E., An Enzyme from Bacteria able to Destroy Penicillin. *Nature* **1940,** *146* (3713), 837-837.
8. Lohans, C. T.; Chan, H. T. H.; Malla, T. R.; Kumar, K.; Kamps, J. J. A. G.; McArdle, D. J. B.; van Groesen, E.; de Munnik, M.; Tooke, C. L.; Spencer, J.; Paton, R. S.; Brem, J.; Schofield, C. J., Non-Hydrolytic β-Lactam Antibiotic Fragmentation by l,d-Transpeptidases and Serine β-Lactamase Cysteine Variants. *Angewandte Chemie International Edition* **2019,** *58* (7), 1990-1994.
9. Tang, S. S.; Apisarnthanarak, A.; Hsu, L. Y., Mechanisms of β-lactam antimicrobial resistance and epidemiology of major community- and healthcare-associated multidrug-resistant bacteria. *Adv Drug Deliv Rev* **2014,** *78*, 3-13.
10. Georgopapadakou, N. H. S., R.B., Bacterial Enzymes Interacting with Beta-Lactam Antibiotics. In *Antibiotics Containing the Beta-Lactam Structure*, Demain, A. L. S., N.A., Ed. Springer-Verlag: Berlin, 1983; Vol. 2, pp 36-54.
11. Zeng, X.; Lin, J., Beta-lactamase induction and cell wall metabolism in Gram-negative bacteria. *Front Microbiol* **2013,** *4*, 128-128.
12. Bush, K.; Bradford Patricia, A., Epidemiology of β-Lactamase-Producing Pathogens. *Clinical Microbiology Reviews* **2020,** *33* (2), e00047-19.

13. Dawoud, T. M. S.; Syed, A.; Maurya, A. K.; Ahmad, S. S.; Rabbani, Q.; Alyousef, A. A.; Alqasim, A.; Arshad, M.; Khan, M. S.; Khalid, M.; Khan, H.; Daglia, M., Incidence and antimicrobial profile of extended-spectrum β-lactamase producing gram-negative bacterial isolates: An in-vitro and statistical analysis. *Journal of Infection and Public Health* **2020,** *13* (11), 1729-1733.
14. Jia, P.; Zhu, Y.; Li, X.; Kudinha, T.; Yang, Y.; Zhang, G.; Zhang, J.; Xu, Y.; Yang, Q., High Prevalence of Extended-Spectrum Beta-Lactamases in Escherichia coli Strains Collected From Strictly Defined Community-Acquired Urinary Tract Infections in Adults in China: A Multicenter Prospective Clinical Microbiological and Molecular Study. *Front Microbiol* **2021,** *12*, 1611.
15. Eggers, S. H.; Emerson, T. R.; Kane, V. V.; Lowe, G., The Synthesis of a New Fragmentation Product of a Cephalosporanic Acid Derivative. *Proc Chem Soc* **1963**, 248-249.
16. Research, C. o. M.; Council, M. R., Chemistry of Penicillin. *Science* **1945,** *102* (2660), 627-629.
17. Jago, M.; Migliacci, A.; Abraham, E. P., Production of a Cephalosporinase by Pseudomonas pyocyanea. *Nature* **1963,** *199* (4891), 375-375.
18. Sabath, L. D.; Jago, M.; Abraham, E. P., Cephalosporinase and penicillinase activities of a beta-lactamase from Pseudomonas pyocyanea. *Biochem J* **1965,** *96*, 739-752.
19. O'Callaghan, C. H.; Kirby, S. M.; Morris, A.; Waller, R. E.; Duncombe, R. E., Correlation between hydrolysis of the -lactam bond of the cephalosporin nucleus and expulsion of the 3-substituent. *J Bacteriol* **1972,** *110* (3), 988-991.
20. Hamilton-Miller, J. M. T.; Richards, E.; Abraham, E. P., Changes in proton-magnetic-resonance spectra during aminolysis and enzymic hydrolysis of cephalosporins. *Biochemical Journal* **1970,** *116* (3), 385-395.
21. Hamilton-Miller, J. M.; Newton, G. G.; Abraham, E. P., Products of aminolysis and enzymic hydrolysis of the cephalosporins. *The Biochemical journal* **1970,** *116* (3), 371-384.
22. Fountain, R. H.; Russell, A. D., Studies on the Mode of Action of Some Cephalosporin Derivatives. *Journal of Applied Bacteriology* **1969,** *32* (3), 312-321.
23. Russell, A. D.; Fountain, R. H., Aspects of the Mechanism of Action of Some Cephalosporins. *J Bacteriol* **1971,** *106* (1), 65-69.
24. Ogura, H.; Takeda, K.; Takahashi, H., Studies on Lactams. V. Nucleophilic Reaction of Benzylpenicillin with Lithiated Compounds. *CHEMICAL & PHARMACEUTICAL BULLETIN* **1975,** *23* (11), 2469-2473.
25. Boyd, D. B.; Hermann, R. B.; Presti, D. E.; Marsh, M. M., Electronic structures of cephalosporins and penicillins. 4. Modeling acylation by the .beta.-lactam ring. *Journal of Medicinal Chemistry* **1975,** *18* (4), 408-417.

26. Boyd, D. B.; Lunn, W. H. W., Electronic structures of cephalosporins and penicillins. 9. Departure of a leaving group in cephalosporins. *Journal of Medicinal Chemistry* **1979,** *22* (7), 778-784.
27. Murphy, J.; Walshe, R.; Devocelle, M., A Theoretical Analysis of the Prodrug Delivery System for Treating Antibiotic-Resistant Bacteria. *IEEE/ACM transactions on computational biology and bioinformatics / IEEE, ACM* **2011,** *8*, 650-8.
28. Xing, B.; Rao, J.; Liu, R., Novel Beta-Lactam Antibiotics Derivatives: Their New Applications as Gene Reporters, Antitumor Prodrugs and Enzyme Inhibitors. *Mini reviews in medicinal chemistry* **2008,** *8*, 455-71.
29. Pollock, M. R., The Cell-bound Penicillinase of Bacillus cereus. *Microbiology* **1956,** *15* (1), 154-169.
30. Henry, R. J.; Housewright, R. D., Studies on penicillinase; manometric method of assaying penicillinase and penicillin, kinetics of the penicillin-penicillinase reaction, and the effects of inhibitors on penicillinase. *J Biol Chem* **1947,** *167* (2), 559-571.
31. Foster Jackson, W., Acid Formation from Penicillin During Enzymatic Inactivation. *Science* **1945,** *101* (2617), 205-205.
32. Alicino, J. F., Iodometric Method for Assay of Penicillin Preparations. *Industrial & Engineering Chemistry Analytical Edition* **1946,** *18* (10), 619-620.
33. Perret, C. J., Iodometric Assay of Penicillinase. *Nature* **1954,** *174* (4439), 1012-1013.
34. Novick, R. P., Micro-iodometric assay for penicillinase. *The Biochemical journal* **1962,** *83* (2), 236-240.
35. Catlin, B. W., Iodometric detection of Haemophilus influenzae beta-lactamase: rapid presumptive test for ampicillin resistance. *Antimicrobial agents and chemotherapy* **1975,** *7* (3), 265-270.
36. Jorgensen, J. H.; Lee, J. C.; Alexander, G. A., Rapid penicillinase paper strip test for detection of beta-lactamase-producing Haemophilus influenzae and Neisseria gonorrhoeae. *Antimicrobial agents and chemotherapy* **1977,** *11* (6), 1087-1088.
37. O'Callaghan, C. H.; Morris, A.; Kirby, S. M.; Shingler, A. H., Novel method for detection of beta-lactamases by using a chromogenic cephalosporin substrate. *Antimicrobial agents and chemotherapy* **1972,** *1* (4), 283-288.
38. Lacroix, J. M.; Lamothe, F.; Malouin, F., Role of Bacteroides bivius beta-lactamase in beta-lactam susceptibility. *Antimicrobial agents and chemotherapy* **1984,** *26* (5), 694-698.
39. Chen, K. C.; Knapp, J. S.; Holmes, K. K., Rapid, inexpensive method for specific detection of microbial beta-lactamases by detection of fluorescent end products. *J Clin Microbiol* **1984,** *19* (6), 818-825.

40. Lamothe, F.; Auger, F.; Lacroix, J. M., Effect of clavulanic acid on the activities of ten beta-lactam agents against members of the Bacteroides fragilis group. *Antimicrobial agents and chemotherapy* **1984,** *25* (5), 662-665.
41. Boehle, K. E.; Gilliand, J.; Wheeldon, C. R.; Holder, A.; Adkins, J. A.; Geiss, B. J.; Ryan, E. P.; Henry, C. S., Utilizing Paper-Based Devices for Antimicrobial-Resistant Bacteria Detection. *Angew Chem Int Ed Engl* **2017,** *56* (24), 6886-6890.
42. Schindler, P.; Huber, G. DETECTION OF BETA-LACTAMASE UTILIZING A CHROMOPHORIC CEPHALOSPORIN COMPOSITION. 1980.
43. Jones, R. N.; Wilson, H. W.; Novick, W. J., Jr.; Barry, A. L.; Thornsberry, C., In vitro evaluation of CENTA, a new beta-lactamase-susceptible chromogenic cephalosporin reagent. *J Clin Microbiol* **1982,** *15* (5), 954-958.
44. Mikhnevich, T. A.; Vyatkina Turkova, A. V.; Grigorenko, V. G.; Rubtsova, M. Y.; Rukhovich, G. D.; Letarova, M. A.; Kravtsova, D. S.; Vladimirov, S. A.; Orlov, A. A.; Nikolaev, E. N.; Zherebker, A.; Perminova, I. V., Inhibition of Class A β-Lactamase (TEM-1) by Narrow Fractions of Humic Substances. *ACS Omega* **2021,** *6* (37), 23873-23883.
45. Raczynska, J. E.; Imiolczyk, B.; Komorowska, M.; Sliwiak, J.; Czyrko-Horczak, J.; Brzezinski, K.; Jaskolski, M., Flexible loops of New Delhi metallo-β-lactamase modulate its activity towards different substrates. *International Journal of Biological Macromolecules* **2020,** *158*, 104-115.
46. Grigorenko, V.; Uporov, I.; Rubtsova, M.; Andreeva, I.; Shcherbinin, D.; Veselovsky, A.; Serova, O.; Ulyashova, M.; Ishtubaev, I.; Egorov, A., Mutual influence of secondary and key drug-resistance mutations on catalytic properties and thermal stability of TEM-type β-lactamases. *FEBS Open Bio* **2017,** *8* (1), 117-129.
47. Gao, W.; Xing, B.; Tsien, R. Y.; Rao, J., Novel Fluorogenic Substrates for Imaging β-Lactamase Gene Expression. *Journal of the American Chemical Society* **2003,** *125* (37), 11146-11147.
48. Zlokarnik, G.; Negulescu Paul, A.; Knapp Thomas, E.; Mere, L.; Burres, N.; Feng, L.; Whitney, M.; Roemer, K.; Tsien Roger, Y., Quantitation of Transcription and Clonal Selection of Single Living Cells with β-Lactamase as Reporter. *Science* **1998,** *279* (5347), 84-88.
49. Zhang, J.; Shen, Y.; May, S. L.; Nelson, D. C.; Li, S., Ratiometric Fluorescence Detection of Pathogenic Bacteria Resistant to Broad-Spectrum β-Lactam Antibiotics. *Angewandte Chemie International Edition* **2012,** *51* (8), 1865-1868.
50. Mao, W.; Xia, L.; Wang, Y.; Xie, H., A Self-Immobilizing and Fluorogenic Probe for β-Lactamase Detection. *Chemistry – An Asian Journal* **2016,** *11* (24), 3493-3497.

51. Peng, L.; Xiao, L.; Ding, Y.; Xiang, Y.; Tong, A., A simple design of fluorescent probes for indirect detection of β-lactamase based on AIE and ESIPT processes. *Journal of Materials Chemistry B* **2018,** *6* (23), 3922-3926.
52. Thompson, R. B., *Fluorescence Sensors and Biosensors*. CRC Press: 2005.
53. Sultan Sibel, E.; Shazia, K.; Akilan, P.; Tayyaba, H., Rapid, low-cost fluorescent assay of β-lactamase-derived antibiotic resistance and related antibiotic susceptibility. *Journal of Biomedical Optics* **2014,** *19* (10), 1-11.
54. Sallum, U. W.; Zheng, X.; Verma, S.; Hasan, T., Rapid functional definition of extended spectrum β-lactamase activity in bacterial cultures via competitive inhibition of fluorescent substrate cleavage. *Photochem Photobiol* **2010,** *86* (6), 1267-1271.
55. Xie, J.; Mu, R.; Fang, M.; Cheng, Y.; Senchyna, F.; Moreno, A.; Banaei, N.; Rao, J., A dual-caged resorufin probe for rapid screening of infections resistant to lactam antibiotics. *Chemical Science* **2021,** *12* (26), 9153-9161.
56. Xie, H.; Mire, J.; Kong, Y.; Chang, M.; Hassounah, H. A.; Thornton, C. N.; Sacchettini, J. C.; Cirillo, J. D.; Rao, J., Rapid point-of-care detection of the tuberculosis pathogen using a BlaC-specific fluorogenic probe. *Nat Chem* **2012,** *4* (10), 802-9.
57. Dortet, L.; Poirel, L.; Nordmann, P., Rapid Identification of Carbapenemase Types in Enterobacteriaceae and Pseudomonas spp. by Using a Biochemical Test. *Antimicrobial Agents and Chemotherapy* **2012,** *56* (12), 6437-6440.
58. Xing, B.; Khanamiryan, A.; Rao, J., Cell-Permeable Near-Infrared Fluorogenic Substrates for Imaging β-Lactamase Activity. *Journal of the American Chemical Society* **2005,** *127* (12), 4158-4159.
59. Yao, H.; So, M. K.; Rao, J., A bioluminogenic substrate for in vivo imaging of beta-lactamase activity. *Angew Chem Int Ed Engl* **2007,** *46* (37), 7031-4.
60. Cheng, Y.; Xie, H.; Sule, P.; Hassounah, H.; Graviss, E. A.; Kong, Y.; Cirillo, J. D.; Rao, J., Fluorogenic probes with substitutions at the 2 and 7 positions of cephalosporin are highly BlaC-specific for rapid Mycobacterium tuberculosis detection. *Angew Chem Int Ed Engl* **2014,** *53* (35), 9360-4.
61. Lyu, F.; Xu, M.; Cheng, Y.; Xie, J.; Rao, J.; Tang, S. K. Y., Quantitative detection of cells expressing BlaC using droplet-based microfluidics for use in the diagnosis of tuberculosis. *Biomicrofluidics* **2015,** *9* (4), 044120.
62. Chen, Y.; Xianyu, Y.; Wu, J.; Zheng, W.; Rao, J.; Jiang, X., Point-of-Care Detection of β-Lactamase in Milk with a Universal Fluorogenic Probe. *Analytical Chemistry* **2016,** *88* (11), 5605-5609.
63. Song, A.; Cheng, Y.; Xie, J.; Banaei, N.; Rao, J., Intramolecular substitution uncages fluorogenic probes for detection of metallo-carbapenemase-expressing bacteria. *Chemical Science* **2017,** *8* (11), 7669-7674.

64. Thai, H. B. D.; Yu, J. K.; Park, B. S.; Park, Y.-J.; Min, S.-J.; Ahn, D.-R., A fluorogenic substrate of beta-lactamases and its potential as a probe to detect the bacteria resistant to the third-generation oxyimino-cephalosporins. *Biosensors and Bioelectronics* **2016,** *77*, 1026-1031.
65. Mao, W.; Xia, L.; Xie, H., Detection of Carbapenemase-Producing Organisms with a Carbapenem-Based Fluorogenic Probe. *Angewandte Chemie International Edition* **2017,** *56* (16), 4468-4472.
66. Kim, J.; Kim, Y.; Abdelazem, A. Z.; Kim, H. J.; Choo, H.; Kim, H. S.; Kim, J. O.; Park, Y.-J.; Min, S.-J., Development of carbapenem-based fluorogenic probes for the clinical screening of carbapenemase-producing bacteria. *Bioorganic Chemistry* **2020,** *94*, 103405.
67. Mao, W.; Wang, Y.; Qian, X.; Xia, L.; Xie, H., A Carbapenem-Based Off–On Fluorescent Probe for Specific Detection of Metallo-β-Lactamase Activities. *ChemBioChem* **2019,** *20* (4), 511-515.
68. Yang, Z.; Ho, P.-L.; Liang, G.; Chow, K. H.; Wang, Q.; Cao, Y.; Guo, Z.; Xu, B., Using β-Lactamase to Trigger Supramolecular Hydrogelation. *Journal of the American Chemical Society* **2007,** *129* (2), 266-267.
69. Alkekhia, D.; Safford, H.; Shukla, S.; Hopson, R.; Shukla, A., β-Lactamase triggered visual detection of bacteria using cephalosporin functionalized biomaterials. *Chemical Communications* **2020,** *56* (75), 11098-11101.
70. deBoer, T. R.; Tarlton, N. J.; Yamaji, R.; Adams-Sapper, S.; Wu, T. Z.; Maity, S.; Vesgesna, G. K.; Sadlowski, C. M.; DePaola, P. t.; Riley, L. W.; Murthy, N., An Enzyme-Mediated Amplification Strategy Enables Detection of β-Lactamase Activity Directly in Unprocessed Clinical Samples for Phenotypic Detection of β-Lactam Resistance. *Chembiochem : a European journal of chemical biology* **2018,** *19* (20), 2173-2177.
71. DeBoer, T. R. T., N.J.; Murthy, N.; Riley, L.W.; Resendez, A. Compounds to Identify Beta-Lactamases, and Methods of Use Thereof. 2021.
72. Maity, S.; Wang, X.; Das, S.; He, M.; Riley, L. W.; Murthy, N., A cephalosporin–chemiluminescent conjugate increases beta-lactamase detection sensitivity by four orders of magnitude. *Chemical Communications* **2020,** *56* (24), 3516-3519.
73. Richard, J.-A.; Jean, L.; Romieu, A.; Massonneau, M.; Noack-Fraissignes, P.; Renard, P.-Y., Chemiluminescent Probe for the in Vitro Detection of Protease Activity. *Organic Letters* **2007,** *9* (23), 4853-4855.
74. Roth-Konforti, M.; Green, O.; Hupfeld, M.; Fieseler, L.; Heinrich, N.; Ihssen, J.; Vorberg, R.; Wick, L.; Spitz, U.; Shabat, D., Ultrasensitive Detection of Salmonella and Listeria monocytogenes by Small-Molecule Chemiluminescence Probes. *Angewandte Chemie International Edition* **2019,** *58* (30), 10361-10367.
75. Son, S.; Won, M.; Green, O.; Hananya, N.; Sharma, A.; Jeon, Y.; Kwak, J. H.; Sessler, J. L.; Shabat, D.; Kim, J. S., Chemiluminescent Probe for the In Vitro

and In Vivo Imaging of Cancers Over-Expressing NQO1. *Angewandte Chemie International Edition* **2019,** *58* (6), 1739-1743.
76. Jain, V. K.; Magrath, I. T., A chemiluminescent assay for quantitation of β-galactosidase in the femtogram range: Application to quantitation of β-galactosidase in lacZ-transfected cells. *Analytical Biochemistry* **1991,** *199* (1), 119-124.
77. Wetherall, N. T.; Trivedi, T.; Zeller, J.; Hodges-Savola, C.; McKimm-Breschkin, J. L.; Zambon, M.; Hayden, F. G., Evaluation of Neuraminidase Enzyme Assays Using Different Substrates To Measure Susceptibility of Influenza Virus Clinical Isolates to Neuraminidase Inhibitors: Report of the Neuraminidase Inhibitor Susceptibility Network. *J Clin Microbiol* **2003,** *41* (2), 742-750.
78. Gholap, S. P.; Yao, C.; Green, O.; Babjak, M.; Jakubec, P.; Malatinský, T.; Ihssen, J.; Wick, L.; Spitz, U.; Shabat, D., Chemiluminescence Detection of Hydrogen Sulfide Release by β-Lactamase-Catalyzed β-Lactam Biodegradation: Unprecedented Pathway for Monitoring β-Lactam Antibiotic Bacterial Resistance. *Bioconjug Chem* **2021,** *32* (5), 991-1000.
79. Philippon, A.; Dusart, J.; Joris, B.; Frère, J. M., The diversity, structure and regulation of β-lactamases. *Cellular and Molecular Life Sciences CMLS* **1998,** *54* (4), 341-346.
80. Moore, J. T.; Davis, S. T.; Dev, I. K., The Development of β-Lactamase as a Highly Versatile Genetic Reporter for Eukaryotic Cells. *Analytical Biochemistry* **1997,** *247* (2), 203-209.
81. An, G.; Hidaka, K.; Siminovitch, L., Expression of Bacterial β-Galactosidase in Animal Cells. *Molecular and Cellular Biology* **1982,** *2* (12), 1628-1632.
82. Chalfie, M.; Tu, Y.; Euskirchen, G.; Ward William, W.; Prasher Douglas, C., Green Fluorescent Protein as a Marker for Gene Expression. *Science* **1994,** *263* (5148), 802-805.
83. Gould, S. J.; Subramani, S., Firefly luciferase as a tool in molecular and cell biology. *Analytical Biochemistry* **1988,** *175* (1), 5-13.
84. Zlokarnik, G., [15] Fusions to β-lactamase as a reporter for gene expression in live mammalian cells. In *Methods in Enzymology*, Academic Press: 2000; Vol. 326, pp 221-241.
85. Cavrois, M.; de Noronha, C.; Greene, W. C., A sensitive and specific enzyme-based assay detecting HIV-1 virion fusion in primary T lymphocytes. *Nature Biotechnology* **2002,** *20* (11), 1151-1154.
86. Galarneau, A.; Primeau, M.; Trudeau, L.-E.; Michnick, S. W., β-Lactamase protein fragment complementation assays as in vivo and in vitro sensors of protein–protein interactions. *Nature Biotechnology* **2002,** *20* (6), 619-622.

87. Spotts, J. M.; Dolmetsch, R. E.; Greenberg, M. E., Time-lapse imaging of a dynamic phosphorylation-dependent protein–protein interaction in mammalian cells. *Proceedings of the National Academy of Sciences* **2002,** *99* (23), 15142.
88. Wehrman, T.; Kleaveland, B.; Her, J.-H.; Balint, R. F.; Blau, H. M., Protein–protein interactions monitored in mammalian cells via complementation of β-lactamase enzyme fragments. *Proceedings of the National Academy of Sciences* **2002,** *99* (6), 3469.
89. Whitney, M.; Rockenstein, E.; Cantin, G.; Knapp, T.; Zlokarnik, G.; Sanders, P.; Durick, K.; Craig, F. F.; Negulescu, P. A., A genome-wide functional assay of signal transduction in living mammalian cells. *Nature Biotechnology* **1998,** *16* (13), 1329-1333.
90. Li, L.; Li, Z.; Shi, W.; Li, X.; Ma, H., Sensitive and Selective Near-Infrared Fluorescent Off–On Probe and Its Application to Imaging Different Levels of β-Lactamase in Staphylococcus aureus. *Analytical Chemistry* **2014,** *86* (12), 6115-6120.
91. Rukavishnikov, A.; Gee, K. R.; Johnson, I.; Corry, S., Fluorogenic cephalosporin substrates for β-lactamase TEM-1. *Analytical Biochemistry* **2011,** *419* (1), 9-16.
92. Zhang, Y.-L.; Xiao, J.-M.; Feng, J.-L.; Yang, K.-W.; Feng, L.; Zhou, L.-S.; Crowder, M. W., A novel fluorogenic substrate for dinuclear Zn(II)-containing metallo-β-lactamases. *Bioorganic & Medicinal Chemistry Letters* **2013,** *23* (6), 1676-1679.
93. Kong, Y.; Yao, H.; Ren, H.; Subbian, S.; Cirillo, S. L.; Sacchettini, J. C.; Rao, J.; Cirillo, J. D., Imaging tuberculosis with endogenous beta-lactamase reporter enzyme fluorescence in live mice. *Proc Natl Acad Sci U S A* **2010,** *107* (27), 12239-44.
94. Ehrt, S.; Schnappinger, D., Mycobacterial survival strategies in the phagosome: defence against host stresses. *Cellular Microbiology* **2009,** *11* (8), 1170-1178.
95. Flynn, J. L.; Chan, J., Immunology of Tuberculosis. *Annual Review of Immunology* **2001,** *19* (1), 93-129.
96. Kong, K. F.; Schneper, L.; Mathee, K., Beta-lactam antibiotics: from antibiosis to resistance and bacteriology. *APMIS* **2010,** *118* (1), 1-36.
97. Nooshabadi, F.; Yang, H.-J.; Cheng, Y.; Durkee, M. S.; Xie, H.; Rao, J.; Cirillo, J. D.; Maitland, K. C., Intravital excitation increases detection sensitivity for pulmonary tuberculosis by whole-body imaging with β-lactamase reporter enzyme fluorescence. *J Biophotonics* **2017,** *10* (6-7), 821-829.
98. Cheng, Y.; Xie, J.; Lee, K.-H.; Gaur, R. L.; Song, A.; Dai, T.; Ren, H.; Wu, J.; Sun, Z.; Banaei, N.; Akin, D.; Rao, J., Rapid and specific labeling of single live Mycobacterium tuberculosis with a dual-targeting fluorogenic probe. *Science Translational Medicine* **2018,** *10* (454), eaar4470.

99. Makarov, V.; Manina, G.; Mikusova, K.; Möllmann, U.; Ryabova, O.; Saint-Joanis, B.; Dhar, N.; Pasca Maria, R.; Buroni, S.; Lucarelli Anna, P.; Milano, A.; De Rossi, E.; Belanova, M.; Bobovska, A.; Dianiskova, P.; Kordulakova, J.; Sala, C.; Fullam, E.; Schneider, P.; McKinney John, D.; Brodin, P.; Christophe, T.; Waddell, S.; Butcher, P.; Albrethsen, J.; Rosenkrands, I.; Brosch, R.; Nandi, V.; Bharath, S.; Gaonkar, S.; Shandil Radha, K.; Balasubramanian, V.; Balganesh, T.; Tyagi, S.; Grosset, J.; Riccardi, G.; Cole Stewart, T., Benzothiazinones Kill Mycobacterium tuberculosis by Blocking Arabinan Synthesis. *Science* **2009,** *324* (5928), 801-804.
100. Trefzer, C.; Rengifo-Gonzalez, M.; Hinner, M. J.; Schneider, P.; Makarov, V.; Cole, S. T.; Johnsson, K., Benzothiazinones: Prodrugs That Covalently Modify the Decaprenylphosphoryl-β-d-ribose 2′-epimerase DprE1 of Mycobacterium tuberculosis. *Journal of the American Chemical Society* **2010,** *132* (39), 13663-13665.
101. Trefzer, C.; Škovierová, H.; Buroni, S.; Bobovská, A.; Nenci, S.; Molteni, E.; Pojer, F.; Pasca, M. R.; Makarov, V.; Cole, S. T.; Riccardi, G.; Mikušová, K.; Johnsson, K., Benzothiazinones Are Suicide Inhibitors of Mycobacterial Decaprenylphosphoryl-β-d-ribofuranose 2′-Oxidase DprE1. *Journal of the American Chemical Society* **2012,** *134* (2), 912-915.
102. Makarov, V.; Mikušová, K., Development of Macozinone for TB treatment: An Update. *Applied Sciences* **2020,** *10* (7).
103. Li, L.; Lv, K.; Yang, Y.; Sun, J.; Tao, Z.; Wang, A.; Wang, B.; Wang, H.; Geng, Y.; Liu, M.; Guo, H.; Lu, Y., Identification of N-Benzyl 3,5-Dinitrobenzamides Derived from PBTZ169 as Antitubercular Agents. *ACS Medicinal Chemistry Letters* **2018,** *9* (7), 741-745.
104. Dai, T.; Xie, J.; Zhu, Q.; Kamariza, M.; Jiang, K.; Bertozzi, C. R.; Rao, J., A Fluorogenic Trehalose Probe for Tracking Phagocytosed Mycobacterium tuberculosis. *Journal of the American Chemical Society* **2020,** *142* (36), 15259-15264.
105. Kamariza, M.; Shieh, P.; Ealand Christopher, S.; Peters Julian, S.; Chu, B.; Rodriguez-Rivera Frances, P.; Babu Sait Mohammed, R.; Treuren William, V.; Martinson, N.; Kalscheuer, R.; Kana Bavesh, D.; Bertozzi Carolyn, R., Rapid detection of Mycobacterium tuberculosis in sputum with a solvatochromic trehalose probe. *Science Translational Medicine* **2018,** *10* (430), eaam6310.
106. Los, G. V.; Encell, L. P.; McDougall, M. G.; Hartzell, D. D.; Karassina, N.; Zimprich, C.; Wood, M. G.; Learish, R.; Ohana, R. F.; Urh, M.; Simpson, D.; Mendez, J.; Zimmerman, K.; Otto, P.; Vidugiris, G.; Zhu, J.; Darzins, A.; Klaubert, D. H.; Bulleit, R. F.; Wood, K. V., HaloTag: A Novel Protein Labeling Technology for Cell Imaging and Protein Analysis. *ACS Chemical Biology* **2008,** *3* (6), 373-382.

107. Mizukami, S.; Watanabe, S.; Hori, Y.; Kikuchi, K., Covalent Protein Labeling Based on Noncatalytic β-Lactamase and a Designed FRET Substrate. *Journal of the American Chemical Society* **2009,** *131* (14), 5016-5017.
108. Watanabe, S.; Mizukami, S.; Hori, Y.; Kikuchi, K., Multicolor Protein Labeling in Living Cells Using Mutant ??-Lactamase-Tag Technology. *Bioconjug Chem* **2010,** *21*, 2320-6.
109. Yoshimura, A.; Mizukami, S.; Hori, Y.; Watanabe, S.; Kikuchi, K., Cell-Surface Protein Labeling with Luminescent Nanoparticles through Biotinylation by Using Mutant β-Lactamase-Tag Technology. *ChemBioChem* **2011,** *12* (7), 1031-1034.
110. Mizukami, S.; Yamamoto, T.; Yoshimura, A.; Watanabe, S.; Kikuchi, K., Covalent Protein Labeling with a Lanthanide Complex and Its Application to Photoluminescence Lifetime-Based Multicolor Bioimaging. *Angewandte Chemie International Edition* **2011,** *50* (37), 8750-8752.
111. Mizukami, S.; Watanabe, S.; Akimoto, Y.; Kikuchi, K., No-Wash Protein Labeling with Designed Fluorogenic Probes and Application to Real-Time Pulse-Chase Analysis. *Journal of the American Chemical Society* **2012,** *134* (3), 1623-1629.
112. Sadhu, K. K.; Mizukami, S.; Watanabe, S.; Kikuchi, K., Turn-on fluorescence switch involving aggregation and elimination processes for β-lactamase-tag. *Chemical Communications* **2010,** *46* (39), 7403-7405.
113. Sadhu, K. K.; Mizukami, S.; Lanam, C. R.; Kikuchi, K., Fluorogenic Protein Labeling through Photoinduced Electron Transfer-Based BL-Tag Technology. *Chemistry – An Asian Journal* **2012,** *7* (2), 272-276.
114. Doose, S.; Neuweiler, H.; Sauer, M., Fluorescence Quenching by Photoinduced Electron Transfer: A Reporter for Conformational Dynamics of Macromolecules. *ChemPhysChem* **2009,** *10* (9-10), 1389-1398.
115. Shao, Q.; Xing, B., Enzyme responsive luminescent ruthenium(ii) cephalosporin probe for intracellular imaging and photoinactivation of antibiotics resistant bacteria. *Chemical Communications* **2012,** *48* (12), 1739-1741.
116. Shao, Q.; Zheng, Y.; Dong, X.; Tang, K.; Yan, X.; Xing, B., A Covalent Reporter of β-Lactamase Activity for Fluorescent Imaging and Rapid Screening of Antibiotic-Resistant Bacteria. *Chemistry – A European Journal* **2013,** *19* (33), 10903-10910.
117. Aw, J.; Widjaja, F.; Ding, Y.; Mu, J.; Liang, Y.; Xing, B., Enzyme-responsive reporter molecules for selective localization and fluorescence imaging of pathogenic biofilms. *Chemical Communications* **2017,** *53* (23), 3330-3333.
118. Chan, H. L.; Lyu, L.; Aw, J.; Zhang, W.; Li, J.; Yang, H.-H.; Hayashi, H.; Chiba, S.; Xing, B., Unique Fluorescent Imaging Probe for Bacterial Surface Localization and Resistant Enzyme Imaging. *ACS Chemical Biology* **2018,** *13* (7), 1890-1896.

119. O'Callaghan, C. H.; Sykes, R. B.; Staniforth, S. E., A new cephalosporin with a dual mode of action. *Antimicrobial agents and chemotherapy* **1976,** *10* (2), 245-248.
120. Albrecht, H. A.; Beskid, G.; Chan, K. K.; Christenson, J. G.; Cleeland, R.; Deitcher, K. H.; Georgopapadakou, N. H.; Keith, D. D.; Pruess, D. L.; Sepinwall, J.; et al., Cephalosporin 3'-quinolone esters with a dual mode of action. *J Med Chem* **1990,** *33* (1), 77-86.
121. Mobashery, S.; Lerner, S. A.; Johnston, M., Conscripting .beta.-lactamase for use in drug delivery. Synthesis and biological activity of a cephalosporin C10-ester of an antibiotic dipeptide. *Journal of the American Chemical Society* **1986,** *108* (7), 1685-1686.
122. Veinberg, G.; Shestakova, I.; Petrulanis, L.; Grigan, N.; Musel, D.; Zeile, D.; Kanepe, I.; Domrachova, I.; Kalvinsh, I.; Strakovs, A.; Lukevics, E., Synthesis and evaluation of dual action cephalosporins as elastase inhibitors. *Bioorganic & Medicinal Chemistry Letters* **1997,** *7* (7), 843-846.
123. Demuth, T. P.; White, R. E.; Tietjen, R. A.; Storrin, R. J.; Skuster, J. R.; Andersen, J. A.; McOsker, C. C.; Freedman, R.; Rourke, F. J., SYNTHESIS AND ANTIBACTERIAL ACTIVITY OF NEW C-10 QUINOLONYL-CEPHEM ESTERS. *J Antibiot* **1991,** *44* (2), 200-209.
124. Albrecht, H. A.; Beskid, G.; Christenson, J. G.; Durkin, J. W.; Fallat, V.; Georgopapadakou, N. H.; Keith, D. D.; Konzelmann, F. M.; Lipschitz, E. R., Dual-action cephalosporins: cephalosporin 3'-quaternary ammonium quinolones. *Journal of Medicinal Chemistry* **1991,** *34* (2), 669-675.
125. Albrecht, H. A.; Beskid, G.; Christenson, J. G.; Deitcher, K. H.; Georgopapadakou, N. H.; Keith, D. D.; Konzelmann, F. M.; Pruess, D. L.; Chen Wei, C., Dual-Action Cephalosporins Incorporating a 3'-Tertiary-Amine-Linked Quinolone. *Journal of Medicinal Chemistry* **1994,** *37* (3), 400-407.
126. Fatheree, P. R.; Linsell, M. S.; Long, D. D.; Marquess, D.; Moran, E. J.; Nodwell, M. B.; Turner, S. D.; Aggen, J. Cross-Linked Glycopeptide-Cephalosporin Antibiotics. 2005.
127. Li, Q.; Lee Jean, Y.; Castillo, R.; Hixon Mark, S.; Pujol, C.; Doppalapudi Venkata, R.; Shepard, H. M.; Wahl Geoffrey, M.; Lobl Thomas, J.; Chan Ming, F., NB2001, a Novel Antibacterial Agent with Broad-Spectrum Activity and Enhanced Potency against β-Lactamase-Producing Strains. *Antimicrobial Agents and Chemotherapy* **2002,** *46* (5), 1262-1268.
128. Stone Geoffrey, W.; Zhang, Q.; Castillo, R.; Doppalapudi, V. R.; Bueno Analia, R.; Lee Jean, Y.; Li, Q.; Sergeeva, M.; Khambatta, G.; Georgopapadakou Nafsika, H., Mechanism of Action of NB2001 and NB2030, Novel Antibacterial Agents Activated by β-Lactamases. *Antimicrobial Agents and Chemotherapy* **2004,** *48* (2), 477-483.

129. Corraz, A. J.; Dax, S. L.; Dunlap, N. K.; Georgopapadakou, N. H.; Keith, D. D.; Pruess, D. L.; Rossman, P. L.; Then, R.; Unowsky, J.; Wei, C. C., Dual-action penems and carbapenems. *J Med Chem* **1992,** *35* (10), 1828-39.
130. Hershberger, P.; Switzer, A.; Yelm, K.; Coleman, M.; Devries, C.; Rourke, F.; Davis, B.; Kraft, W.; Twinem, T.; Koenigs, P.; Paule, S.; Siehnel, R.; Zoutendam, P.; Imbus, R.; Demuth, T. J., Preparation and antimicrobial assessment of 2-thioether-linked quinolonyl-carbapenems. *J Antibiot* **1998,** *51* (9), 857-71.
131. Ehrhardt, A. F.; Sanders, C. C., Structure-activity studies of quinolone-penems in genetically defined strains of Escherichia coli. *Antimicrobial Agents and Chemotherapy* **1997,** *41* (11), 2570-2572.
132. Bryskier, A., Dual β-lactam-fluoroquinolone compounds: a novel approach to antibacterial treatment. *Expert Opinion on Investigational Drugs* **1997,** *6* (10), 1479-1499.
133. Privett, B. J.; Broadnax, A. D.; Bauman, S. J.; Riccio, D. A.; Schoenfisch, M. H., Examination of bacterial resistance to exogenous nitric oxide. *Nitric Oxide* **2012,** *26* (3), 169-173.
134. Yang, L.; Feura, E. S.; Ahonen, M. J. R.; Schoenfisch, M. H., Nitric Oxide–Releasing Macromolecular Scaffolds for Antibacterial Applications. *Advanced Healthcare Materials* **2018,** *7* (13), 1800155.
135. Flemming, H.-C.; Wingender, J., The biofilm matrix. *Nature Reviews Microbiology* **2010,** *8* (9), 623-633.
136. Hossain, S.; Nisbett, L.-M.; Boon, E. M., Discovery of Two Bacterial Nitric Oxide-Responsive Proteins and Their Roles in Bacterial Biofilm Regulation. *Acc Chem Res* **2017,** *50* (7), 1633-1639.
137. Williams, D. E.; Boon, E. M., Towards Understanding the Molecular Basis of Nitric Oxide-Regulated Group Behaviors in Pathogenic Bacteria. *Journal of Innate Immunity* **2019,** *11* (3), 205-215.
138. Rong, F.; Tang, Y.; Wang, T.; Feng, T.; Song, J.; Li, P.; Huang, W., Nitric Oxide-Releasing Polymeric Materials for Antimicrobial Applications: A Review. *Antioxidants (Basel)* **2019,** *8* (11), 556.
139. Elnaggar, M. A.; Subbiah, R.; Han, D. K.; Joung, Y. K., Lipid-based carriers for controlled delivery of nitric oxide. *Expert Opinion on Drug Delivery* **2017,** *14* (12), 1341-1353.
140. Cheng, J.; He, K.; Shen, Z.; Zhang, G.; Yu, Y.; Hu, J., Nitric Oxide (NO)-Releasing Macromolecules: Rational Design and Biomedical Applications. *Front Chem* **2019,** *7*, 530-530.
141. Barnes, M. D.; Taracila, M. A.; Rutter, J. D.; Bethel, C. R.; Galdadas, I.; Hujer, A. M.; Caselli, E.; Prati, F.; Dekker, J. P.; Papp-Wallace, K. M.; Haider, S.; Bonomo, R. A., Deciphering the Evolution of Cephalosporin Resistance to Ceftolozane-Tazobactam in Pseudomonas aeruginosa. *mBio* **2018,** *9* (6), e02085-18.

142. Tang, X.; Cai, T.; Wang, P. G., Synthesis of beta-Lactamase activated nitric oxide donors. *Bioorganic & Medicinal Chemistry Letters* **2003,** *13* (10), 1687-1690.
143. Barraud, N.; Kardak, B. G.; Yepuri, N. R.; Howlin, R. P.; Webb, J. S.; Faust, S. N.; Kjelleberg, S.; Rice, S. A.; Kelso, M. J., Cephalosporin-3′-diazeniumdiolates: Targeted NO-Donor Prodrugs for Dispersing Bacterial Biofilms. *Angewandte Chemie International Edition* **2012,** *51* (36), 9057-9060.
144. Collins Samuel, A.; Kelso Michael, J.; Rineh, A.; Yepuri Nageshwar, R.; Coles, J.; Jackson Claire, L.; Halladay Georgia, D.; Walker Woolf, T.; Webb Jeremy, S.; Hall-Stoodley, L.; Connett Gary, J.; Feelisch, M.; Faust Saul, N.; Lucas Jane, S. A.; Allan Raymond, N., Cephalosporin-3′-Diazeniumdiolate NO Donor Prodrug PYRRO-C3D Enhances Azithromycin Susceptibility of Nontypeable Haemophilus influenzae Biofilms. *Antimicrobial Agents and Chemotherapy* **2017,** *61* (2), e02086-16.
145. Allan, R. N.; Kelso, M. J.; Rineh, A.; Yepuri, N. R.; Feelisch, M.; Soren, O.; Brito-Mutunayagam, S.; Salib, R. J.; Stoodley, P.; Clarke, S. C.; Webb, J. S.; Hall-Stoodley, L.; Faust, S. N., Cephalosporin-NO-donor prodrug PYRRO-C3D shows β-lactam-mediated activity against Streptococcus pneumoniae biofilms. *Nitric Oxide* **2017,** *65*, 43-49.
146. Rineh, A.; Soren, O.; McEwan, T.; Ravikumar, V.; Poh, W. H.; Azamifar, F.; Naimi-Jamal, M. R.; Cheung, C.-Y.; Elliott, A. G.; Zuegg, J.; Blaskovich, M. A. T.; Cooper, M. A.; Dolange, V.; Christodoulides, M.; Cook, G. M.; Rice, S. A.; Faust, S. N.; Webb, J. S.; Kelso, M. J., Discovery of Cephalosporin-3′-Diazeniumdiolates That Show Dual Antibacterial and Antibiofilm Effects against Pseudomonas aeruginosa Clinical Cystic Fibrosis Isolates and Efficacy in a Murine Respiratory Infection Model. *ACS Infectious Diseases* **2020,** *6* (6), 1460-1479.
147. Soren, O.; Rineh, A.; Silva, D. G.; Cai, Y.; Howlin, R. P.; Allan, R. N.; Feelisch, M.; Davies, J. C.; Connett, G. J.; Faust, S. N.; Kelso, M. J.; Webb, J. S., Cephalosporin nitric oxide-donor prodrug DEA-C3D disperses biofilms formed by clinical cystic fibrosis isolates of Pseudomonas aeruginosa. *Journal of Antimicrobial Chemotherapy* **2020,** *75* (1), 117-125.
148. Reading, C.; Cole, M., Clavulanic Acid: a Beta-Lactamase-Inhibiting Beta-Lactam from Streptomyces clavuligerus. *Antimicrobial Agents and Chemotherapy* **1977,** *11* (5), 852-857.
149. English, A. R.; Retsema, J. A.; Girard, A. E.; Lynch, J. E.; Barth, W. E., CP-45,899, a beta-lactamase inhibitor that extends the antibacterial spectrum of beta-lactams: initial bacteriological characterization. *Antimicrobial agents and chemotherapy* **1978,** *14* (3), 414-419.
150. Fisher, J. W.; Belasco, J. G.; Charnas, R. L.; Khosla, S.; Knowles, J. R.; Baddiley, J.; Abraham, E. P., β-Lactamase inactivation by mechanism-based

reagents. *Philosophical Transactions of the Royal Society of London. B, Biological Sciences* **1980,** *289* (1036), 309-319.
151. Bush, K.; Bradford, P. A., β-Lactams and β-Lactamase Inhibitors: An Overview. *Cold Spring Harb Perspect Med* **2016,** *6* (8), a025247.
152. Drawz, S. M.; Bonomo, R. A., Three Decades of β-Lactamase Inhibitors. *Clinical Microbiology Reviews* **2010,** *23* (1), 160-201.
153. Linciano, P.; Cendron, L.; Gianquinto, E.; Spyrakis, F.; Tondi, D., Ten Years with New Delhi Metallo-β-lactamase-1 (NDM-1): From Structural Insights to Inhibitor Design. *ACS Infectious Diseases* **2019,** *5* (1), 9-34.
154. Tooke, C. L.; Hinchliffe, P.; Bragginton, E. C.; Colenso, C. K.; Hirvonen, V. H. A.; Takebayashi, Y.; Spencer, J., β-Lactamases and β-Lactamase Inhibitors in the 21st Century. *J Mol Biol* **2019,** *431* (18), 3472-3500.
155. Bunyak, J. D., The Discovery and Development of Modified Penicillin- and Cephalosporin- Derived β-Lactamase Inhibitors. *Curr Med Chem* **2004,** *11* (14), 1951-64.
156. Hakimelahi, G. H.; Shia, K. S.; Xue, C.; Hakimelahi, S.; Moosavi-Movahedi, A. A.; Saboury, A. A.; Khalafi-Nezhad, A.; Soltani-Rad, M. N.; Osyetrov, V.; Wang, K.; Liao, J. H.; Luo, F. T., Design, synthesis, and biological evaluation of a series of beta-lactam-based prodrugs. *Bioorganic & medicinal chemistry* **2002,** *10* (11), 3489-98.
157. Mercuri, P. S.; García-Sáez, I.; De Vriendt, K.; Thamm, I.; Devreese, B.; Van Beeumen, J.; Dideberg, O.; Rossolini, G. M.; Frère, J.-M.; Galleni, M., Probing the Specificity of the Subclass B3 FEZ-1 Metallo-β-lactamase by Site-directed Mutagenesis*. *Journal of Biological Chemistry* **2004,** *279* (32), 33630-33638.
158. Jackson, A. C.; Zaengle-Barone, J. M.; Puccio, E. A.; Franz, K. J., A Cephalosporin Prochelator Inhibits New Delhi Metallo-β-lactamase 1 without Removing Zinc. *ACS Infectious Diseases* **2020,** *6* (5), 1264-1272.
159. Mojica, M. F.; Rossi, M.-A.; Vila, A. J.; Bonomo, R. A., The urgent need for metallo-β-lactamase inhibitors: an unattended global threat. *The Lancet Infectious Diseases* **2021**.
160. van Haren, M. J.; Tehrani, K. H. M. E.; Kotsogianni, I.; Wade, N.; Brüchle, N. C.; Mashayekhi, V.; Martin, N. I., Cephalosporin Prodrug Inhibitors Overcome Metallo-β-Lactamase Driven Antibiotic Resistance. *Chemistry – A European Journal* **2021,** *27* (11), 3806-3811.
161. Tehrani, K. H. M. E.; Wade, N.; Mashayekhi, V.; Brüchle, N. C.; Jespers, W.; Voskuil, K.; Pesce, D.; van Haren, M. J.; van Westen, G. J. P.; Martin, N. I., Novel Cephalosporin Conjugates Display Potent and Selective Inhibition of Imipenemase-Type Metallo-β-Lactamases. *Journal of Medicinal Chemistry* **2021,** *64* (13), 9141-9151.

162. Tehrani, K. H. M. E.; Martin, N. I., Thiol-Containing Metallo-β-Lactamase Inhibitors Resensitize Resistant Gram-Negative Bacteria to Meropenem. *ACS Infectious Diseases* **2017,** *3* (10), 711-717.
163. Zheng, X.; Sallum, U. W.; Verma, S.; Athar, H.; Evans, C. L.; Hasan, T., Exploiting a Bacterial Drug-Resistance Mechanism: A Light-Activated Construct for the Destruction of MRSA. *Angewandte Chemie International Edition* **2009,** *48* (12), 2148-2151.
164. Fu, X.-J.; Zhu, Y.-Q.; Peng, Y.-B.; Chen, Y.-S.; Hu, Y.-P.; Lu, H.-X.; Yu, W.-R.; Fang, Y.; Du, J.-Z.; Yao, M., Enzyme activated photodynamic therapy for methicillin-resistant Staphylococcus aureus infection both inv itro and in vivo. *Journal of Photochemistry and Photobiology B: Biology* **2014,** *136*, 72-80.
165. Liu, R.; Miller, P. A.; Vakulenko, S. B.; Stewart, N. K.; Boggess, W. C.; Miller, M. J., A Synthetic Dual Drug Sideromycin Induces Gram-Negative Bacteria To Commit Suicide with a Gram-Positive Antibiotic. *J Med Chem* **2018,** *61* (9), 3845-3854.
166. Bickel, H.; Gäumann, E.; Nussberger, G.; Reusser, P.; Vischer, E.; Voser, W.; Wettstein, A.; Zähner, H., Stoffwechselprodukte von Actinomyceten. 25. Mitteilung. Über die Isolierung und Charakterisierung der Ferrimycine A1 und A2, neuer Antibiotika der Sideromycin-Gruppe. *Helvetica Chimica Acta* **1960,** *43* (7), 2105-2118.
167. Gause, G. F., Recent studies on albomycin, a new antibiotic. *Br Med J* **1955,** *2* (4949), 1177-1179.
168. Kong, H.; Cheng, W.; Wei, H.; Yuan, Y.; Yang, Z.; Zhang, X., An overview of recent progress in siderophore-antibiotic conjugates. *European Journal of Medicinal Chemistry* **2019,** *182*, 111615.
169. Möllmann, U.; Heinisch, L.; Bauernfeind, A.; Köhler, T.; Ankel-Fuchs, D., Siderophores as drug delivery agents: application of the “Trojan Horse” strategy. *BioMetals* **2009,** *22* (4), 615-624.
170. Negash, K. H.; Norris, J. K. S.; Hodgkinson, J. T., Siderophore-Antibiotic Conjugate Design: New Drugs for Bad Bugs? *Molecules* **2019,** *24* (18), 3314.
171. Vértesy, L.; Aretz, W.; Fehlhaber, H.-W.; Kogler, H., Salmycin A–D, Antibiotika aus Streptomyces violaceus, DSM 8286, mit Siderophor-Aminoglycosid-Struktur. *Helvetica Chimica Acta* **1995,** *78* (1), 46-60.
172. Arisawa, M.; Sekine, Y.; Shimizu, S.; Takano, H.; Angehrn, P.; Then, R. L., In vitro and in vivo evaluation of Ro 09-1428, a new parenteral cephalosporin with high antipseudomonal activity. *Antimicrobial Agents and Chemotherapy* **1991,** *35* (4), 653-659.
173. Ghosh, A.; Ghosh, M.; Niu, C.; Malouin, F.; Moellmann, U.; Miller, M. J., Iron transport-mediated drug delivery using mixed-ligand siderophore-β-lactam conjugates. *Chemistry & Biology* **1996,** *3* (12), 1011-1019.
174. Kohira, N.; West, J.; Ito, A.; Ito-Horiyama, T.; Nakamura, R.; Sato, T.; Rittenhouse, S.; Tsuji, M.; Yamano, Y., In Vitro Antimicrobial Activity of a

Siderophore Cephalosporin, S-649266, against Enterobacteriaceae Clinical Isolates, Including Carbapenem-Resistant Strains. *Antimicrobial Agents and Chemotherapy* **2015,** *60* (2), 729-734.
175. Zhanel, G. G.; Golden, A. R.; Zelenitsky, S.; Wiebe, K.; Lawrence, C. K.; Adam, H. J.; Idowu, T.; Domalaon, R.; Schweizer, F.; Zhanel, M. A.; Lagacé-Wiens, P. R. S.; Walkty, A. J.; Noreddin, A.; Lynch Iii, J. P.; Karlowsky, J. A., Cefiderocol: A Siderophore Cephalosporin with Activity Against Carbapenem-Resistant and Multidrug-Resistant Gram-Negative Bacilli. *Drugs* **2019,** *79* (3), 271-289.
176. Yan, S.; Miller, M. J.; Wencewicz, T. A.; Moollmann, U., Syntheses and biological evaluation of new cephalosporin-oxazolidinone conjugates. *Medchemcomm* **2010,** *1* (2), 145-148.
177. Dolence, E. K.; Minnick, A. A.; Miller, M. J., N5-Acetyl-N5-hydroxy-L-ornithine-derived siderophore-carbacephalosporin .beta.-lactam conjugates: iron transport mediated drug delivery. *Journal of Medicinal Chemistry* **1990,** *33* (2), 461-464.
178. Wencewicz, T. A.; Miller, M. J., Biscatecholate–Monohydroxamate Mixed Ligand Siderophore–Carbacephalosporin Conjugates are Selective Sideromycin Antibiotics that Target Acinetobacter baumannii. *Journal of Medicinal Chemistry* **2013,** *56* (10), 4044-4052.
179. Pereira, M. P.; Shi, J.; Kelley, S. O., Peptide Targeting of an Antibiotic Prodrug toward Phagosome-Entrapped Mycobacteria. *ACS Infectious Diseases* **2015,** *1* (12), 586-592.
180. Kumar, A.; Zhang, M.; Zhu, L.; Liao, R. P.; Mutai, C.; Hafsat, S.; Sherman, D. R.; Wang, M.-W., High-throughput screening and sensitized bacteria identify an M. tuberculosis dihydrofolate reductase inhibitor with whole cell activity. *PLoS One* **2012,** *7* (6), e39961-e39961.
181. Gold, B.; Smith, R.; Nguyen, Q.; Roberts, J.; Ling, Y.; Lopez Quezada, L.; Somersan, S.; Warrier, T.; Little, D.; Pingle, M.; Zhang, D.; Ballinger, E.; Zimmerman, M.; Dartois, V.; Hanson, P.; Mitscher, L. A.; Porubsky, P.; Rogers, S.; Schoenen, F. J.; Nathan, C.; Aubé, J., Novel Cephalosporins Selectively Active on Nonreplicating Mycobacterium tuberculosis. *Journal of Medicinal Chemistry* **2016,** *59* (13), 6027-6044.
182. Lopez Quezada, L.; Li, K.; McDonald, S. L.; Nguyen, Q.; Perkowski, A. J.; Pharr, C. W.; Gold, B.; Roberts, J.; McAulay, K.; Saito, K.; Somersan Karakaya, S.; Javidnia, P. E.; Porras de Francisco, E.; Amieva, M. M.; SP, D. A.; Mendoza Losana, A.; Zimmerman, M.; Liang, H. H.; Zhang, J.; Dartois, V.; Sans, S.; Lagrange, S.; Goullieux, L.; Roubert, C.; Nathan, C.; Aubé, J., Dual-Pharmacophore Pyrithione-Containing Cephalosporins Kill Both Replicating and Nonreplicating Mycobacterium tuberculosis. *ACS Infect Dis* **2019,** *5* (8), 1433-1445.

183. Flores, A.; Parsons, L.; Pavelka, M., Genetic analysis of the β-lactamases of Mycobacterium tuberculosis and Mycobacterium smegmatis and susceptibility to β-lactam antibiotics. *Microbiology (Reading, England)* **2005,** *151*, 521-32.
184. Evans, L. A.-O.; Krishna, A.; Ma, Y.; Webb, T. E.; Marshall, D. C.; Tooke, C. L.; Spencer, J. A.-O.; Clarke, T. B.; Armstrong, A. A.-O.; Edwards, A. M., Exploitation of Antibiotic Resistance as a Novel Drug Target: Development of a β-Lactamase-Activated Antibacterial Prodrug. *J Med Chem* **2019,** *62*, 4411-25.
185. Xiao, T.; Liu, K.; Huigens, R. W., Progress towards a stable cephalosporin-halogenated phenazine conjugate for antibacterial prodrug applications. *Bioorganic & Medicinal Chemistry Letters* **2020,** *30* (22), 127515.
186. Abeylath, S. C.; Turos, E., Drug delivery approaches to overcome bacterial resistance to β-lactam antibiotics. *Expert Opinion on Drug Delivery* **2008,** *5* (9), 931-949.
187. De Rosa, M.; Verdino, A.; Soriente, A.; Marabotti, A., The Odd Couple(s): An Overview of Beta-Lactam Antibiotics Bearing More Than One Pharmacophoric Group. *Int J Mol Sci* **2021,** *22* (2), 617.
188. Jubeh, B.; Breijyeh, Z.; Karaman, R., Antibacterial Prodrugs to Overcome Bacterial Resistance. *Molecules* **2020,** *25* (7), 1543.
189. WHO *Global tuberculosis report 2021*; World Health Organization: Geneva, Switzerland, 2021.
190. FDA approves new drug for treatment-resistant forms of tuberculosis that affects the lungs. U.S. Food & Drug Administration: fda.gov, 2019.
191. Theus, S. A.; Cave, M. D.; Eisenach, K. D., Activated THP-1 cells: an attractive model for the assessment of intracellular growth rates of Mycobacterium tuberculosis isolates. *Infect Immun* **2004,** *72* (2), 1169-1173.
192. Lamont, E. A.; Baughn, A. D., Impact of the host environment on the antitubercular action of pyrazinamide. *EBioMedicine* **2019,** *49*, 374-380.
193. Ormerod, L. P.; Horsfield, N., Short-course antituberculous chemotherapy for pulmonary and pleural disease: 5 years' experience in clinical practice. *British journal of diseases of the chest* **1987,** *81* (3), 268-71.
194. Controlled clinical trial of four short-course regimens of chemotherapy for two durations in the treatment of pulmonary tuberculosis: first report: Third East African/British Medical Research Councils study. *The American review of respiratory disease* **1978,** *118* (1), 39-48.
195. Diacon, A. H.; Dawson, R.; von Groote-Bidlingmaier, F.; Symons, G.; Venter, A.; Donald, P. R.; van Niekerk, C.; Everitt, D.; Winter, H.; Becker, P.; Mendel, C. M.; Spigelman, M. K., 14-day bactericidal activity of PA-824, bedaquiline, pyrazinamide, and moxifloxacin combinations: a randomised trial. *The Lancet* **2012,** *380* (9846), 986-993.
196. Gopal, P.; Yee, M.; Sarathy, J.; Low, J. L.; Sarathy, J. P.; Kaya, F.; Dartois, V.; Gengenbacher, M.; Dick, T., Pyrazinamide Resistance Is Caused by

Two Distinct Mechanisms: Prevention of Coenzyme A Depletion and Loss of Virulence Factor Synthesis. *ACS Infect Dis* **2016,** *2* (9), 616-626.
197. Gopal, P.; Nartey, W.; Ragunathan, P.; Sarathy, J.; Kaya, F.; Yee, M.; Setzer, C.; Manimekalai, M. S. S.; Dartois, V.; Gruber, G.; Dick, T., Pyrazinoic Acid Inhibits Mycobacterial Coenzyme A Biosynthesis by Binding to Aspartate Decarboxylase PanD. *ACS Infect Dis* **2017,** *3* (11), 807-819.
198. Gopal, P.; Dick, T., Targeted protein degradation in antibacterial drug discovery? *Prog Biophys Mol Biol* **2020,** *152*, 10-14.
199. Gopal, P.; Sarathy, J. P.; Yee, M.; Ragunathan, P.; Shin, J.; Bhushan, S.; Zhu, J.; Akopian, T.; Kandror, O.; Lim, T. K.; Gengenbacher, M.; Lin, Q.; Rubin, E. J.; Gruber, G.; Dick, T., Pyrazinamide triggers degradation of its target aspartate decarboxylase. *Nat Commun* **2020,** *11* (1), 1661.
200. Dillon, N. A.; Peterson, N. D.; Rosen, B. C.; Baughn, A. D., Pantothenate and pantetheine antagonize the antitubercular activity of pyrazinamide. *Antimicrob Agents Chemother* **2014,** *58* (12), 7258-63.
201. Diacon, A. H.; Donald, P. R.; Pym, A.; Grobusch, M.; Patientia, R. F.; Mahanyele, R.; Bantubani, N.; Narasimooloo, R.; De Marez, T.; van Heeswijk, R.; Lounis, N.; Meyvisch, P.; Andries, K.; McNeeley, D. F., Randomized pilot trial of eight weeks of bedaquiline (TMC207) treatment for multidrug-resistant tuberculosis: long-term outcome, tolerability, and effect on emergence of drug resistance. *Antimicrob Agents Chemother* **2012,** *56* (6), 3271-6.
202. Whitfield, M. G.; Soeters, H. M.; Warren, R. M.; York, T.; Sampson, S. L.; Streicher, E. M.; van Helden, P. D.; van Rie, A., A Global Perspective on Pyrazinamide Resistance: Systematic Review and Meta-Analysis. *PLoS One* **2015,** *10* (7), e0133869.
203. Lanoix, J. P.; Tasneen, R.; O'Brien, P.; Sarathy, J.; Safi, H.; Pinn, M.; Alland, D.; Dartois, V.; Nuermberger, E., High Systemic Exposure of Pyrazinoic Acid Has Limited Antituberculosis Activity in Murine and Rabbit Models of Tuberculosis. *Antimicrob Agents Chemother* **2016,** *60* (7), 4197-205.
204. Cynamon, M. H.; Klemens, S. P.; Chou, T. S.; Gimi, R. H.; Welch, J. T., Antimycobacterial activity of a series of pyrazinoic acid esters. *Journal of Medicinal Chemistry* **1992,** *35* (7), 1212-1215.
205. Cynamon, M. H.; Gimi, R.; Gyenes, F.; Sharpe, C. A.; Bergmann, K. E.; Han, H. J.; Gregor, L. B.; Rapolu, R.; Luciano, G.; Welch, J. T., Pyrazinoic Acid Esters with Broad Spectrum in Vitro Antimycobacterial Activity. *Journal of Medicinal Chemistry* **1995,** *38* (20), 3902-3907.
206. Thiede, J. M.; Dillon, N. A.; Howe, M. D.; Aflakpui, R.; Modlin, S. J.; Hoffner, S. E.; Valafar, F.; Minato, Y.; Baughn, A. D., Pyrazinamide action is driven by the cell envelope stress response in Mycobacterium tuberculosis. *bioRxiv* **2021**, 2021.02.17.431758.
207. Yu, K.; Sun, N.; Fang, S.; Mo, W.; Hu, B.; Shen, Z.; Hu, X., An Improved Process for the Preparation of Diphenylmethyl 7β-Phenylacetamido-3-

hydroxymethyl-3-cephem-4-carboxylate. *Organic Process Research & Development* **2009,** *13* (4), 815-819.
208. Muller, B.; Peter, H.; Schneider, P.; Bickel, H., New Beta-Lactam-Antibiotics. Fluorinated Cephalosporins. Preliminary Communication. Modifikationen von Antibiotika. 15. Mitteilung. *Helvetica Chimica Acta* **1975,** *58*, 2469-2473.
209. Panda, S. S.; Detistov, O. S.; Girgis, A. S.; Mohapatra, P. P.; Samir, A.; Katritzky, A. R., Synthesis and molecular modeling of antimicrobial active fluoroquinolone-pyrazine conjugates with amino acid linkers. *Bioorg Med Chem Lett* **2016,** *26* (9), 2198-205.
210. Katritzky, A. R.; He, H.-Y.; Suzuki, K., N-Acylbenzotriazoles: Neutral Acylating Reagents for the Preparation of Primary, Secondary, and Tertiary Amides. *The Journal of Organic Chemistry* **2000,** *65* (24), 8210-8213.
211. Patterson, L. D.; Miller, M. J., Enzymatic deprotection of the cephalosporin 3'-acetoxy group using Candida antarctica lipase B. *J Org Chem* **2010,** *75* (4), 1289-92.
212. Koppel Ga Fau - Koehler, R. E.; Koehler, R. E., Functionalization of C 6(7) of penicillins and cephalosporins. A one-step stereoselective synthesis of 7- -methoxycephalosporin C. (0002-7863 (Print)).
213. Dawadi, S.; Kawamura, S.; Rubenstein, A.; Remmel, R.; Aldrich, C. C., Synthesis and pharmacological evaluation of nucleoside prodrugs designed to target siderophore biosynthesis in Mycobacterium tuberculosis. *Bioorganic & medicinal chemistry* **2016,** *24* (6), 1314-21.
214. Samuni, A., A direct spectrophotometric assay and determination of Michaelis constants for the β-lactamase reaction. *Analytical Biochemistry* **1975,** *63* (1), 17-26.
215. Bush, K.; Jacoby, G. A., Updated functional classification of beta-lactamases. *Antimicrobial agents and chemotherapy* **2010,** *54* (3), 969-976.
216. Holten, K. B.; Onusko, E. M., Appropriate prescribing of oral beta-lactam antibiotics. *Am Fam Physician* **2000,** *62* (3), 611-20.
217. Theus, S. A.; Cave, M. D.; Eisenach, K. D., Activated THP-1 cells: an attractive model for the assessment of intracellular growth rates of Mycobacterium tuberculosis isolates. *Infect Immun* **2004,** *72* (2), 1169-1173.
218. Tuomanen, E., Phenotypic Tolerance: The Search for β-Lactam Antibiotics That Kill Nongrowing Bacteria. *Rev Infect Dis* **1986,** *8* (Supplement_3), S279-S291.
219. Hugonnet, J.-E.; Tremblay, L. W.; Boshoff, H. I.; Barry, C. E.; Blanchard, J. S., Meropenem-Clavulanate Is Effective Against Extensively Drug-Resistant Mycobacterium tuberculosis. *Science* **2009,** *323* (5918), 1215.
220. McCune, R. M., Jr.; Tompsett, R., Fate of Mycobacterium tuberculosis in mouse tissues as determined by the microbial enumeration technique. I. The

persistence of drug-susceptible tubercle bacilli in the tissues despite prolonged antimicrobial therapy. *J Exp Med* **1956,** *104* (5), 737-62.
221. Gold, B.; Smith, R.; Nguyen, Q.; Roberts, J.; Ling, Y.; Lopez Quezada, L.; Somersan, S.; Warrier, T.; Little, D.; Pingle, M.; Zhang, D.; Ballinger, E.; Zimmerman, M.; Dartois, V.; Hanson, P.; Mitscher, L. A.; Porubsky, P.; Rogers, S.; Schoenen, F. J.; Nathan, C.; Aubé, J., Novel Cephalosporins Selectively Active on Nonreplicating Mycobacterium tuberculosis. *J Med Chem* **2016,** *59* (13), 6027-6044.
222. Chakraborty, S.; Gruber, T.; Barry, C. E., 3rd; Boshoff, H. I.; Rhee, K. Y., Para-aminosalicylic acid acts as an alternative substrate of folate metabolism in Mycobacterium tuberculosis. *Science* **2013,** *339* (6115), 88-91.
223. Howe, M. D.; Kordus, S. L.; Cole, M. S.; Bauman, A. A.; Aldrich, C. C.; Baughn, A. D.; Minato, Y., Methionine Antagonizes para-Aminosalicylic Acid Activity via Affecting Folate Precursor Biosynthesis in Mycobacterium tuberculosis. *Frontiers in cellular and infection microbiology* **2018,** *8*, 399.
224. Stoffels, K.; Mathys, V.; Fauville-Dufaux, M.; Wintjens, R.; Bifani, P., Systematic analysis of pyrazinamide-resistant spontaneous mutants and clinical isolates of Mycobacterium tuberculosis. *Antimicrobial agents and chemotherapy* **2012,** *56* (10), 5186-5193.
225. Kasik, J. E., Mycobacterial Beta-Lactamases. In *Beta-Lactamases*, Hamilton-Miller, J. M. T.; Smith, J. T., Eds. Academic Press: New York, 1979; pp 339-50.
226. Drawz, S. M.; Bonomo, R. A., Three decades of beta-lactamase inhibitors. (1098-6618 (Electronic)).
227. Kwon, H. H.; Tomioka H Fau - Saito, H.; Saito, H., Distribution and characterization of beta-lactamases of mycobacteria and related organisms. (0962-8479 (Print)).
228. Chambers, H. F.; Moreau D Fau - Yajko, D.; Yajko D Fau - Miick, C.; Miick C Fau - Wagner, C.; Wagner C Fau - Hackbarth, C.; Hackbarth C Fau - Kocagöz, S.; Kocagöz S Fau - Rosenberg, E.; Rosenberg E Fau - Hadley, W. K.; Hadley Wk Fau - Nikaido, H.; Nikaido, H., Can penicillins and other beta-lactam antibiotics be used to treat tuberculosis? (0066-4804 (Print)).
229. Cynamon Mh Fau - Palmer, G. S.; Palmer, G. S., In vitro activity of amoxicillin in combination with clavulanic acid against Mycobacterium tuberculosis. (0066-4804 (Print)).
230. Segura, C.; Salvadó M Fau - Collado, I.; Collado I Fau - Chaves, J.; Chaves J Fau - Coira, A.; Coira, A., Contribution of beta-lactamases to beta-lactam susceptibilities of susceptible and multidrug-resistant Mycobacterium tuberculosis clinical isolates. (0066-4804 (Print)).
231. Sorg Tb Fau - Cynamon, M. H.; Cynamon, M. H., Comparison of four beta-lactamase inhibitors in combination with ampicillin against Mycobacterium tuberculosis. (0305-7453 (Print)).

232. Hugonnet, J. E.; Blanchard, J. S., Irreversible inhibition of the Mycobacterium tuberculosis beta-lactamase by clavulanate. (0006-2960 (Print)).
233. Veziris, N.; Truffot C Fau - Mainardi, J.-L.; Mainardi Jl Fau - Jarlier, V.; Jarlier, V., Activity of carbapenems combined with clavulanate against murine tuberculosis. (1098-6596 (Electronic)).
234. Gurumurthy, M.; Verma, R.; Naftalin, C. M.; Hee, K. H.; Lu, Q.; Tan, K. H.; Issac, S.; Lin, W.; Tan, A.; Seng, K. Y.; Lee, L. S.; Paton, N. I., Activity of faropenem with and without rifampicin against Mycobacterium tuberculosis: evaluation in a whole-blood bactericidal activity trial. (1460-2091 (Electronic)).
235. Cohen, K. A.; El-Hay, T.; Wyres, K. L.; Weissbrod, O.; Munsamy, V.; Yanover, C.; Aharonov, R.; Shaham, O.; Conway, T. C.; Goldschmidt, Y.; Bishai, W. R.; Pym, A. S., Paradoxical Hypersusceptibility of Drug-resistant Mycobacteriumtuberculosis to β-lactam Antibiotics. (2352-3964 (Electronic)).
236. Solapure, S.; Dinesh N Fau - Shandil, R.; Shandil R Fau - Ramachandran, V.; Ramachandran V Fau - Sharma, S.; Sharma S Fau - Bhattacharjee, D.; Bhattacharjee D Fau - Ganguly, S.; Ganguly S Fau - Reddy, J.; Reddy J Fau - Ahuja, V.; Ahuja V Fau - Panduga, V.; Panduga V Fau - Parab, M.; Parab M Fau - Vishwas, K. G.; Vishwas Kg Fau - Kumar, N.; Kumar N Fau - Balganesh, M.; Balganesh M Fau - Balasubramanian, V.; Balasubramanian, V., In vitro and in vivo efficacy of β-lactams against replicating and slowly growing/nonreplicating Mycobacterium tuberculosis. (1098-6596 (Electronic)).
237. Zhao, G.; Miller Mj Fau - Franzblau, S.; Franzblau S Fau - Wan, B.; Wan B Fau - Möllmann, U.; Möllmann, U., Syntheses and studies of quinolone-cephalosporins as potential anti-tuberculosis agents. (0960-894X (Print)).
238. Majewski, M. W.; Tiwari, R.; Miller, P. A.; Cho, S.; Franzblau, S. G.; Miller, M. J., Design, syntheses, and anti-tuberculosis activities of conjugates of piperazino-1,3-benzothiazin-4-ones (pBTZs) with 2,7-dimethylimidazo [1,2-a]pyridine-3-carboxylic acids and 7-phenylacetyl cephalosporins. (1464-3405 (Electronic)).
239. Gold B Fau - Smith, R.; Smith R Fau - Nguyen, Q.; Nguyen, Q.; Roberts J Fau - Ling, Y.; Ling Y Fau - Lopez Quezada, L.; Lopez Quezada L Fau - Somersan, S.; Somersan S Fau - Warrier, T.; Warrier T Fau - Little, D.; Little D Fau - Pingle, M.; Pingle M Fau - Zhang, D.; Zhang D Fau - Ballinger, E.; Ballinger E Fau - Zimmerman, M.; Zimmerman, M.; Dartois, V.; Hanson P Fau - Mitscher, L. A.; Mitscher La Fau - Porubsky, P.; Porubsky P Fau - Rogers, S.; Rogers, S.; Schoenen Fj Fau - Nathan, C.; Nathan C Fau - Aubé, J.; Aubé, J., Novel Cephalosporins Selectively Active on Nonreplicating Mycobacterium tuberculosis. (1520-4804 (Electronic)).
240. Bianchet, M. A.; Pan, Y. H.; Basta, L. A. B.; Saavedra, H.; Lloyd, E. P.; Kumar, P.; Mattoo, R.; Townsend, C. A.; Lamichhane, G. A.-O., Structural insight into the inactivation of Mycobacterium tuberculosis non-classical transpeptidase Ldt(Mt2) by biapenem and tebipenem. (1471-2091 (Electronic)).

241. Flores, A. R.; Parsons, L. M.; Pavelka, M. S., Genetic analysis of the beta-lactamases of Mycobacterium tuberculosis and Mycobacterium smegmatis and susceptibility to beta-lactam antibiotics. (1350-0872 (Print)).
242. Tuomanen, E., Phenotypic Tolerance: The Search for β-Lactam Antibiotics That Kill Nongrowing Bacteria. *Reviews of Infectious Diseases* **1986,** *8* (Supplement_3), S279-S291.
243. Chow, C.; Xu, H.; Blanchard, J. S., Kinetic characterization of hydrolysis of nitrocefin, cefoxitin, and meropenem by beta-lactamase from Mycobacterium tuberculosis. *Biochemistry* **2013,** *52* (23), 4097-104.
244. Hugonnet, J.-E.; Blanchard, J. S., Irreversible inhibition of the Mycobacterium tuberculosis beta-lactamase by clavulanate. *Biochemistry* **2007,** *46* (43), 11998-12004.
245. Cohen, K. A.; El-Hay, T.; Wyres, K. L.; Weissbrod, O.; Munsamy, V.; Yanover, C.; Aharonov, R.; Shaham, O.; Conway, T. C.; Goldschmidt, Y.; Bishai, W. R.; Pym, A. S., Paradoxical Hypersusceptibility of Drug-resistant Mycobacteriumtuberculosis to β-lactam Antibiotics. *EBioMedicine* **2016,** *9*, 170-179.
246. Gurumurthy, M.; Verma, R.; Naftalin, C.; Hee, K.; Lu, Q.; Tan, K.; Issac, S.; Lin, W.; Tan, A.; Seng, K.-Y.; Lee, L.; Paton, N., Activity of faropenem with and without rifampicin against Mycobacterium tuberculosis: Evaluation in a whole-blood bactericidal activity trial. *The Journal of antimicrobial chemotherapy* **2017,** *72*.
247. Solapure, S.; Dinesh, N.; Shandil, R.; Ramachandran, V.; Sharma, S.; Bhattacharjee, D.; Ganguly, S.; Reddy, J.; Ahuja, V.; Panduga, V.; Parab, M.; Vishwas, K. G.; Kumar, N.; Balganesh, M.; Balasubramanian, V., In Vitro and In Vivo Efficacy of β-Lactams against Replicating and Slowly Growing/Nonreplicating Mycobacterium tuberculosis. *Antimicrobial agents and chemotherapy* **2013,** *57* (6), 2506-2510.
248. Veziris, N.; Truffot, C.; Mainardi, J.-L.; Jarlier, V., Activity of carbapenems combined with clavulanate against murine tuberculosis. *Antimicrobial agents and chemotherapy* **2011,** *55* (6), 2597-2600.
249. Javed, M. I.; Brewer, M., Diphenyldiazomethane. *Org. Synth.* **2008,** *85*, 189.
250. Panda, S. S.; Detistov, O. S.; Girgis, A. S.; Mohapatra, P. P.; Samir, A.; Katritzky, A. R., Synthesis and molecular modeling of antimicrobial active fluoroquinolone–pyrazine conjugates with amino acid linkers. *Bioorganic & Medicinal Chemistry Letters* **2016,** *26* (9), 2198-2205.
251. Koppel, G. A.; Koehler, R. A., Functionalization of C6(7) of penicillins and cephalosporins. One-step stereoselective synthesis of 7-.alpha.-methoxycephalosporin C. *Journal of the American Chemical Society* **1973,** *95* (7), 2403-2404.

252. Patterson, L. D.; Miller, M. J., Enzymatic Deprotection of the Cephalosporin 3′-Acetoxy Group Using Candida antarctica Lipase B. *The Journal of Organic Chemistry* **2010,** *75* (4), 1289-1292.
253. Dawadi, S.; Kawamura, S.; Rubenstein, A.; Remmel, R.; Aldrich, C. C., Synthesis and pharmacological evaluation of nucleoside prodrugs designed to target siderophore biosynthesis in Mycobacterium tuberculosis. *Bioorganic & Medicinal Chemistry* **2016,** *24* (6), 1314-1321.
254. Wiegand, I.; Hilpert, K.; Hancock, R. E. W., Agar and broth dilution methods to determine the minimal inhibitory concentration (MIC) of antimicrobial substances. *Nature Protocols* **2008,** *3* (2), 163-175.
255. Murphy Kenan, C.; Nelson Samantha, J.; Nambi, S.; Papavinasasundaram, K.; Baer Christina, E.; Sassetti Christopher, M.; Nacy Carol, A., ORBIT: a New Paradigm for Genetic Engineering of Mycobacterial Chromosomes. *mBio* **2018,** *9* (6), e01467-18.
256. Murphy, K. C., Oligo-Mediated Recombineering and its Use for Making SNPs, Knockouts, Insertions, and Fusions in Mycobacterium tuberculosisMycobacterium tuberculosis (M. tuberculosis). In *Mycobacteria Protocols*, Parish, T.; Kumar, A., Eds. Springer US: New York, NY, 2021; pp 301-321.
257. Dillon Nicholas, A.; Peterson Nicholas, D.; Rosen Brandon, C.; Baughn Anthony, D., Pantothenate and Pantetheine Antagonize the Antitubercular Activity of Pyrazinamide. *Antimicrobial Agents and Chemotherapy* **2014,** *58* (12), 7258-7263.
258. Bai, X.; Kim, S.-H.; Azam, T.; McGibney, M. T.; Huang, H.; Dinarello, C. A.; Chan, E. D., IL-32 Is a Host Protective Cytokine against Mycobacterium tuberculosis in Differentiated THP-1 Human Macrophages. *The Journal of Immunology* **2010,** *184* (7), 3830.
259. DesJardin, L. E.; Kaufman, T. M.; Potts, B.; Kutzbach, B.; Yi, H.; Schlesinger, L. S., Mycobacterium tuberculosis-infected human macrophages exhibit enhanced cellular adhesion with increased expression of LFA-1 and ICAM-1 and reduced expression and/or function of complement receptors, FcγRII and the mannose receptor. *Microbiology* **2002,** *148* (10), 3161-3171.
260. Kelly, D. M.; ten Bokum, A. M. C.; O'Leary, S. M.; O'Sullivan, M. P.; Keane, J., Bystander macrophage apoptosis after Mycobacterium tuberculosis H37Ra infection. *Infect Immun* **2008,** *76* (1), 351-360.
261. Chakraborty, S.; Gruber, T.; Barry, C. E., 3rd; Boshoff, H. I.; Rhee, K. Y., Para-aminosalicylic acid acts as an alternative substrate of folate metabolism in Mycobacterium tuberculosis. *Science* **2013,** *339* (6115), 88-91.
262. Howe, M. D.; Kordus, S. L.; Cole, M. S.; Bauman, A. A.; Aldrich, C. C.; Baughn, A. D.; Minato, Y., Methionine Antagonizes para-Aminosalicylic Acid Activity via Affecting Folate Precursor Biosynthesis in Mycobacterium tuberculosis. *Front Cell Infect Microbiol* **2018,** *8*, 399-399.

263. Zhang, Y.; Shi, W.; Zhang, W.; Mitchison, D.; Hatfull Graham, F.; Jacobs Jr. William, R., Mechanisms of Pyrazinamide Action and Resistance. *Microbiology Spectrum* **2014,** *2* (4), 2.4.03.
264. Kushner, S.; Dalalian, H.; Sanjurjo, J. L.; Bach, F. L.; Safir, S. R.; Smith, V. K.; Williams, J. H., Experimental Chemotherapy of Tuberculosis. II. The Synthesis of Pyrazinamides and Related Compounds1. *Journal of the American Chemical Society* **1952,** *74* (14), 3617-3621.
265. Solotorovsky, M.; Gregory, F. J.; Ironson, E. J.; Bugie, E. J.; O'Neill, R. C.; Pfister, K., Pyrazinoic Acid Amide-An Agent Active Against Experimental Murine Tuberculosis. *Proceedings of the Society for Experimental Biology and Medicine* **1952,** *79* (4), 563-565.
266. Chorine, V., Action De l'Amide Nicotinique Sur Les Bacilles Du Genre Mycobacterium. *Compt Rendu Acad Sci* **1945,** *220*, 150-51.
267. McCune, R. M., Jr.; Tompsett, R., FATE OF MYCOBACTERIUM TUBERCULOSIS IN MOUSE TISSUES AS DETERMINED BY THE MICROBIAL ENUMERATION TECHNIQUE : I. THE PERSISTENCE OF DRUG-SUSCEPTIBLE TUBERCLE BACILLI IN THE TISSUES DESPITE PROLONGED ANTIMICROBIAL THERAPY. *Journal of Experimental Medicine* **1956,** *104* (5), 737-762.
268. McCune, R. M., Jr.; Tompsett, R.; McDermott, W., THE FATE OF MYCOBACTERIUM TUBERCULOSIS IN MOUSE TISSUES AS DETERMINED BY THE MICROBIAL ENUMERATION TECHNIQUE : II. THE CONVERSION OF TUBERCULOUS INFECTION TO THE LATENT STATE BY THE ADMINISTRATION OF PYRAZINAMIDE AND A COMPANION DRUG. *Journal of Experimental Medicine* **1956,** *104* (5), 763-802.
269. Geiter, L. J.; O'Brien, R. J.; Combs, D. L.; Snider, D. E., United states public health service tuberculosis therapy trial 21: Preliminary results of an evaluation of a combination tablet of isoniazid, rifampin and pyrazinamide. *Tubercle* **1987,** *68* (2, Supplement 1), 41-46.
270. Muschenheim, C.; McDermott, W.; McCune, R.; Deuschle, K.; Ormond, L.; Tompsett, R., Pyrazinamide-Isoniazid in Tuberculosis. I. Results in 58 patients with pulmonary lesions one year after the start of therapy. *Am Rev Tuberc* **1954,** *70* (4), 743-47.
271. Yeager, R. L.; Munroe, W. G.; Dessau, F. I., Pyrazinamide (Aldinamide) in the Treatment of Pulmonary Tuberculosis. *Am Rev Tuberc* **1952,** *65* (5), 523-46.
272. Fox, W.; Ellard, G. A.; Mitchison, D. A., Studies on the treatment of tuberculosis undertaken by the British Medical Research Council tuberculosis units, 1946-1986, with relevant subsequent publications. *Int J Tuberc Lung Dis* **1999,** *3*, S231-S279.
273. Ormerod, L. P.; Horsfield, N., Short-course antituberculous chemotherapy for pulmonary and pleural disease: 5 years' experience in clinical practice. *British Journal of Diseases of the Chest* **1987,** *81*, 268-271.

274. Falzon, D.; Schünemann, H. J.; Harausz, E.; González-Angulo, L.; Lienhardt, C.; Jaramillo, E.; Weyer, K., World Health Organization treatment guidelines for drug-resistant tuberculosis, 2016 update. *European Respiratory Journal* **2017,** *49* (3), 1602308.
275. Sun, F.; Li, Y.; Chen, Y.; Guan, W.; Jiang, X.; Wang, X.; Ren, P.; Li, J.; Shi, J.; He, G.; Wu, M.; Tang, P.; Wang, F.; Sheng, Y.; Huang, F.; Zhou, Z.; Huang, H.; Hong, L.; Liu, Q.; Zhang, Y.; Zhang, W., Introducing molecular testing of pyrazinamide susceptibility improves multidrug-resistant tuberculosis treatment outcomes: a prospective cohort study. *European Respiratory Journal* **2019,** *53* (3), 1801770.
276. Nuermberger, E.; Tyagi, S.; Tasneen, R.; Williams Kathy, N.; Almeida, D.; Rosenthal, I.; Grosset Jacques, H., Powerful Bactericidal and Sterilizing Activity of a Regimen Containing PA-824, Moxifloxacin, and Pyrazinamide in a Murine Model of Tuberculosis. *Antimicrobial Agents and Chemotherapy* **2008,** *52* (4), 1522-1524.
277. Santucci, P.; Greenwood, D. J.; Fearns, A.; Chen, K.; Jiang, H.; Gutierrez, M. G., Intracellular localisation of Mycobacterium tuberculosis affects efficacy of the antibiotic pyrazinamide. *Nature Communications* **2021,** *12* (1), 3816.
278. Tarshis, M. S.; Weed, W. A., Lack of Significant in Vitro Sensitivity of Mycobacterium Tuberculosis to Pyrazinamide on Three Different Solid Media. *American Review of Tuberculosis* **1953,** *67* (3), 391-395.
279. McDermott, W.; Tompsett, R., Activation of Pyrazinamide and Nicotinamide in Acidic Environments in Vitro. *American Review of Tuberculosis* **1954,** *70* (4), 748-754.
280. Salfinger, M.; Heifets, L. B., Determination of pyrazinamide MICs for Mycobacterium tuberculosis at different pHs by the radiometric method. *Antimicrobial agents and chemotherapy* **1988,** *32* (7), 1002-1004.
281. Zhang, Y.; Wade, M. M.; Scorpio, A.; Zhang, H.; Sun, Z., Mode of action of pyrazinamide: disruption of Mycobacterium tuberculosis membrane transport and energetics by pyrazinoic acid. *Journal of Antimicrobial Chemotherapy* **2003,** *52* (5), 790-795.
282. Peterson Nicholas, D.; Rosen Brandon, C.; Dillon Nicholas, A.; Baughn Anthony, D., Uncoupling Environmental pH and Intrabacterial Acidification from Pyrazinamide Susceptibility in Mycobacterium tuberculosis. *Antimicrobial Agents and Chemotherapy* **2015,** *59* (12), 7320-7326.
283. Shi, W., Activity of Pyrazinamide against Mycobacterium tuberculosis at Neutral pH in PZA-S1 Minimal Medium. *Antibiotics (Basel)* **2021,** *10* (8), 909.
284. Wade, M. M.; Zhang, Y., Anaerobic incubation conditions enhance pyrazinamide activity against Mycobacterium tuberculosis. *Journal of Medical Microbiology* **2004,** *53* (8), 769-773.

285. Huang, Q.; Chen, Z. F.; Li, Y. Y.; Zhang, Y.; Ren, Y.; Fu, Z.; Xu, S. Q., Nutrient-starved incubation conditions enhance pyrazinamide activity against Mycobacterium tuberculosis. *Chemotherapy* **2007,** *53* (5), 338-43.
286. Somoskovi, A.; Wade, M. M.; Sun, Z.; Zhang, Y., Iron enhances the antituberculous activity of pyrazinamide. *Journal of Antimicrobial Chemotherapy* **2004,** *53* (2), 192-196.
287. Wade, M. M.; Zhang, Y., Effects of weak acids, UV and proton motive force inhibitors on pyrazinamide activity against Mycobacterium tuberculosis in vitro. *Journal of Antimicrobial Chemotherapy* **2006,** *58* (5), 936-941.
288. Blanc, L.; Sarathy, J. P.; Alvarez Cabrera, N.; O'Brien, P.; Dias-Freedman, I.; Mina, M.; Sacchettini, J.; Savic, R. M.; Gengenbacher, M.; Podell, B. K.; Prideaux, B.; Ioerger, T.; Dick, T.; Dartois, V., Impact of immunopathology on the antituberculous activity of pyrazinamide. *Journal of Experimental Medicine* **2018,** *215* (8), 1975-1986.
289. Vilchèze, C.; Weinrick, B.; Wong, K.-W.; Chen, B.; Jacobs, W. R., Jr., NAD+ auxotrophy is bacteriocidal for the tubercle bacilli. *Mol Microbiol* **2010,** *76* (2), 365-377.
290. Boshoff, H. I. M.; Xu, X.; Tahlan, K.; Dowd, C. S.; Pethe, K.; Camacho, L. R.; Park, T.-H.; Yun, C.-S.; Schnappinger, D.; Ehrt, S.; Williams, K. J.; Barry, C. E., 3rd, Biosynthesis and recycling of nicotinamide cofactors in mycobacterium tuberculosis. An essential role for NAD in nonreplicating bacilli. *The Journal of biological chemistry* **2008,** *283* (28), 19329-19341.
291. Konno, K.; Feldmann, F. M.; McDermott, W., Pyrazinamide Susceptibility and Amidase Activity of Tubercle Bacilli. *American Review of Respiratory Disease* **1967,** *95* (3), 461-469.
292. Scorpio, A.; Zhang, Y., Mutations in pncA, a gene encoding pyrazinamidase/nicotinamidase, cause resistance to the antituberculous drug pyrazinamide in tubercle bacillus. *Nature Medicine* **1996,** *2* (6), 662-667.
293. Butler, W. R.; Kilburn, J. O., Susceptibility of Mycobacterium tuberculosis to pyrazinamide and its relationship to pyrazinamidase activity. *Antimicrobial agents and chemotherapy* **1983,** *24* (4), 600-601.
294. McClatchy, J. K.; Tsang, A. Y.; Cernich, M. S., Use of pyrazinamidase activity on Mycobacterium tuberculosis as a rapid method for determination of pyrazinamide susceptibility. *Antimicrobial agents and chemotherapy* **1981,** *20* (4), 556-557.
295. Bhuju, S.; Fonseca, L. d. S.; Marsico, A. G.; de Oliveira Vieira, G. B.; Sobral, L. F.; Stehr, M.; Singh, M.; Saad, M. H. F., Mycobacterium tuberculosis isolates from Rio de Janeiro reveal unusually low correlation between pyrazinamide resistance and mutations in the pncA gene. *Infection, Genetics and Evolution* **2013,** *19*, 1-6.

296. Zhang, Y.; Scorpio, A.; Nikaido, H.; Sun, Z., Role of acid pH and deficient efflux of pyrazinoic acid in unique susceptibility of Mycobacterium tuberculosis to pyrazinamide. *J Bacteriol* **1999,** *181* (7), 2044-2049.
297. ZHANG, Y.; PERMAR, S.; SUN, Z., Conditions that may affect the results of susceptibility testing of Mycobacterium tuberculosis to pyrazinamide. *Journal of Medical Microbiology* **2002,** *51* (1), 42-49.
298. Lu, P.; Haagsma, A. C.; Pham, H.; Maaskant, J. J.; Mol, S.; Lill, H.; Bald, D., Pyrazinoic acid decreases the proton motive force, respiratory ATP synthesis activity, and cellular ATP levels. *Antimicrobial agents and chemotherapy* **2011,** *55* (11), 5354-5357.
299. den Hertog, A. L.; Menting, S.; Pfeltz, R.; Warns, M.; Siddiqi, S. H.; Anthony, R. M., Pyrazinamide Is Active against Mycobacterium tuberculosis Cultures at Neutral pH and Low Temperature. *Antimicrobial agents and chemotherapy* **2016,** *60* (8), 4956-4960.
300. Fontes, F. L.; Peters, B. J.; Crans, D. C.; Crick, D. C., The Acid–Base Equilibrium of Pyrazinoic Acid Drives the pH Dependence of Pyrazinamide-Induced Mycobacterium tuberculosis Growth Inhibition. *ACS Infectious Diseases* **2020,** *6* (11), 3004-3014.
301. Zimhony, O.; Cox, J. S.; Welch, J. T.; Vilchèze, C.; Jacobs, W. R., Pyrazinamide inhibits the eukaryotic-like fatty acid synthetase I (FASI) of Mycobacterium tuberculosis. *Nature Medicine* **2000,** *6* (9), 1043-1047.
302. Baughn Anthony, D.; Deng, J.; Vilchèze, C.; Riestra, A.; Welch John, T.; Jacobs William, R.; Zimhony, O., Mutually Exclusive Genotypes for Pyrazinamide and 5-Chloropyrazinamide Resistance Reveal a Potential Resistance-Proofing Strategy. *Antimicrobial Agents and Chemotherapy* **2010,** *54* (12), 5323-5328.
303. Ngo Silvana, C.; Zimhony, O.; Chung Woo, J.; Sayahi, H.; Jacobs William, R.; Welch John, T., Inhibition of Isolated Mycobacterium tuberculosis Fatty Acid Synthase I by Pyrazinamide Analogs. *Antimicrobial Agents and Chemotherapy* **2007,** *51* (7), 2430-2435.
304. Boshoff Helena, I.; Mizrahi, V.; Barry Clifton, E., Effects of Pyrazinamide on Fatty Acid Synthesis by Whole Mycobacterial Cells and Purified Fatty Acid Synthase I. *J Bacteriol* **2002,** *184* (8), 2167-2172.
305. Sayahi, H.; Zimhony, O.; Jacobs, W. R.; Shekhtman, A.; Welch, J. T., Pyrazinamide, but not pyrazinoic acid, is a competitive inhibitor of NADPH binding to Mycobacterium tuberculosis fatty acid synthase I. *Bioorganic & Medicinal Chemistry Letters* **2011,** *21* (16), 4804-4807.
306. Shi, W.; Zhang, X.; Jiang, X.; Yuan, H.; Lee Jong, S.; Barry Clifton, E.; Wang, H.; Zhang, W.; Zhang, Y., Pyrazinamide Inhibits Trans-Translation in Mycobacterium tuberculosis. *Science* **2011,** *333* (6049), 1630-1632.
307. Lamont, E. A.; Dillon, N. A.; Baughn, A. D., The Bewildering Antitubercular Action of Pyrazinamide. *Microbiol Mol Biol Rev* **2020,** *84* (2), e00070-19.

308. Alexander David, C.; Ma Jennifer, H.; Guthrie Jennifer, L.; Blair, J.; Chedore, P.; Jamieson Frances, B., Gene Sequencing for Routine Verification of Pyrazinamide Resistance in Mycobacterium tuberculosis: a Role for pncA but Not rpsA. *J Clin Microbiol* **2012,** *50* (11), 3726-3728.
309. Personne, Y.; Parish, T., Mycobacterium tuberculosis possesses an unusual tmRNA rescue system. *Tuberculosis* **2014,** *94* (1), 34-42.
310. Dillon, N. A.; Peterson, N. D.; Feaga, H. A.; Keiler, K. C.; Baughn, A. D., Anti-tubercular Activity of Pyrazinamide is Independent of trans-Translation and RpsA. *Scientific Reports* **2017,** *7* (1), 6135.
311. Klemens, S. P.; Sharpe, C. A.; Cynamon, M. H., Activity of pyrazinamide in a murine model against Mycobacterium tuberculosis isolates with various levels of in vitro susceptibility. *Antimicrobial Agents and Chemotherapy* **1996,** *40* (1), 14-16.
312. Vallejos-Sánchez, K.; Lopez, J. M.; Antiparra, R.; Toscano, E.; Saavedra, H.; Kirwan, D. E.; Amzel, L. M.; Gilman, R. H.; Maruenda, H.; Sheen, P.; Zimic, M., Mycobacterium tuberculosis ribosomal protein S1 (RpsA) and variants with truncated C-terminal end show absence of interaction with pyrazinoic acid. *Scientific Reports* **2020,** *10* (1), 8356.
313. Gopal, P.; Yee, M.; Sarathy, J.; Low, J. L.; Sarathy, J. P.; Kaya, F.; Dartois, V.; Gengenbacher, M.; Dick, T., Pyrazinamide Resistance Is Caused by Two Distinct Mechanisms: Prevention of Coenzyme A Depletion and Loss of Virulence Factor Synthesis. *ACS Infectious Diseases* **2016,** *2* (9), 616-626.
314. Ragunathan, P.; Cole, M.; Latka, C.; Aragaw, W. W.; Hegde, P.; Shin, J.; Subramanian Manimekalai, M. S.; Rishikesan, S.; Aldrich, C. C.; Dick, T.; Grüber, G., Mycobacterium tuberculosis PanD Structure–Function Analysis and Identification of a Potent Pyrazinoic Acid-Derived Enzyme Inhibitor. *ACS Chemical Biology* **2021,** *16* (6), 1030-1039.
315. Zhang, S.; Chen, J.; Shi, W.; Liu, W.; Zhang, W.; Zhang, Y., Mutations in panD encoding aspartate decarboxylase are associated with pyrazinamide resistance in Mycobacterium tuberculosis. *Emerging Microbes & Infections* **2013,** *2* (1), 1-5.
316. Gopal, P.; Nartey, W.; Ragunathan, P.; Sarathy, J.; Kaya, F.; Yee, M.; Setzer, C.; Manimekalai, M. S. S.; Dartois, V.; Grüber, G.; Dick, T., Pyrazinoic Acid Inhibits Mycobacterial Coenzyme A Biosynthesis by Binding to Aspartate Decarboxylase PanD. *ACS Infectious Diseases* **2017,** *3* (11), 807-819.
317. Gopal, P.; Tasneen, R.; Yee, M.; Lanoix, J.-P.; Sarathy, J.; Rasic, G.; Li, L.; Dartois, V.; Nuermberger, E.; Dick, T., In Vivo-Selected Pyrazinoic Acid-Resistant Mycobacterium tuberculosis Strains Harbor Missense Mutations in the Aspartate Decarboxylase PanD and the Unfoldase ClpC1. *ACS Infectious Diseases* **2017,** *3* (7), 492-501.
318. Gopal, P.; Sarathy, J. P.; Yee, M.; Ragunathan, P.; Shin, J.; Bhushan, S.; Zhu, J.; Akopian, T.; Kandror, O.; Lim, T. K.; Gengenbacher, M.; Lin, Q.; Rubin,

E. J.; Grüber, G.; Dick, T., Pyrazinamide triggers degradation of its target aspartate decarboxylase. *Nature Communications* **2020,** *11* (1), 1661.
319. Maslov, D. A.; Zaĭchikova, M. V.; Chernousova, L. N.; Shur, K. V.; Bekker, O. B.; Smirnova, T. G.; Larionova, E. E.; Andreevskaya, S. N.; Zhang, Y.; Danilenko, V. N., Resistance to pyrazinamide in Russian Mycobacterium tuberculosis isolates: pncA sequencing versus Bactec MGIT 960. *Tuberculosis* **2015,** *95* (5), 608-12.
320. Sun, Q.; Li, X.; Perez, L. M.; Shi, W.; Zhang, Y.; Sacchettini, J. C., The molecular basis of pyrazinamide activity on Mycobacterium tuberculosis PanD. *Nature Communications* **2020,** *11* (1), 339.
321. Gopal, P.; Grüber, G.; Dartois, V.; Dick, T., Pharmacological and Molecular Mechanisms Behind the Sterilizing Activity of Pyrazinamide. *Trends in Pharmacological Sciences* **2019,** *40* (12), 930-940.
322. Orlewska, C.; Foks, H.; Janowiec, M.; Zwolskakwiek, Z., Studies on pyrazine derivatives, XXIX: Synthesis of N1-thioamido substituted pyrazincarboxyamidrazones with expected tuberculostatic activity. *Die Pharmazie* **1995,** *50*, 565-6.
323. Li, L.; Jin, Y.; Wang, B.; Yang, Z.; Liu, M.; Guo, H.; Zhang, J.; Lu, Y., A structure-based strategy toward the development of novel candidates for antimycobacterial activity: Synthesis, biological evaluation, and docking study. *Chemical Biology & Drug Design* **2018,** *91* (3), 769-780.
324. Shindikar, A. V.; Viswanathan, C. L., Novel fluoroquinolones: design, synthesis, and in vivo activity in mice against Mycobacterium tuberculosis H37Rv. *Bioorganic & Medicinal Chemistry Letters* **2005,** *15* (7), 1803-1806.
325. Simões, M. F.; Valente, E.; Gómez, M. J. R.; Anes, E.; Constantino, L., Lipophilic pyrazinoic acid amide and ester prodrugs: Stability, activation and activity against M. tuberculosis. *European Journal of Pharmaceutical Sciences* **2009,** *37* (3), 257-263.
326. Sriram, D.; Yogeeswari, P.; Reddy, S. P., Synthesis of pyrazinamide Mannich bases and its antitubercular properties. *Bioorganic & Medicinal Chemistry Letters* **2006,** *16* (8), 2113-2116.
327. Zhou, S.; Yang, S.; Huang, G., Design, synthesis and biological activity of pyrazinamide derivatives for anti-Mycobacterium tuberculosis. *J Enzyme Inhib Med Chem* **2017,** *32* (1), 1183-1186.
328. Zitko, J.; Barbora, S.-V.; Paterová, P.; Navrátilová, L.; Trejtnar, F.; Kuneš, J.; Doležal, M., Design, synthesis and anti-mycobacterial evaluation of some new iV-phenylpyrazine-2-carboxamides. *Chemical Papers* **2016,** *70* (5), 649-657.
329. Cynamon Michael, H.; Speirs Robert, J.; Welch John, T., In Vitro Antimycobacterial Activity of 5-Chloropyrazinamide. *Antimicrobial Agents and Chemotherapy* **1998,** *42* (2), 462-463.
330. Dolezal, M.; Miletin, M.; Kunes, J.; Kralova, K., Substituted Amides of Pyrazine-2-carboxylic acids: Synthesis and Biological Activity. *Molecules : A*

Journal of Synthetic Chemistry and Natural Product Chemistry **2002,** *7* (3), 363-373.
331. Markad, S. D.; Kaur, P.; Kishore Reddy, B. K.; Chinnapattu, M.; Raichurkar, A.; Nandishaiah, R.; Panda, M.; Iyer, P. S., Novel lead generation of an anti-tuberculosis agent active against non-replicating mycobacteria: exploring hybridization of pyrazinamide with multiple fragments. *Medicinal Chemistry Research* **2015,** *24* (7), 2986-2992.
332. Servusová, B.; Paterová, P.; Mandíková, J.; Kubíček, V.; Kučera, R.; Kuneš, J.; Doležal, M.; Zitko, J., Alkylamino derivatives of pyrazinamide: Synthesis and antimycobacterial evaluation. *Bioorganic & Medicinal Chemistry Letters* **2014,** *24* (2), 450-453.
333. Zitko, J.; Servusová, B.; Janoutová, A.; Paterová, P.; Mandíková, J.; Garaj, V.; Vejsová, M.; Marek, J.; Doležal, M., Synthesis and antimycobacterial evaluation of 5-alkylamino-N-phenylpyrazine-2-carboxamides. *Bioorganic & medicinal chemistry* **2015,** *23* (1), 174-183.
334. Juhás, M.; Pallabothula, V. S. K.; Grabrijan, K.; Šimovičová, M.; Janďourek, O.; Konečná, K.; Bárta, P.; Paterová, P.; Gobec, S.; Sosič, I.; Zitko, J., Design, synthesis and biological evaluation of substituted 3-amino-N-(thiazol-2-yl)pyrazine-2-carboxamides as inhibitors of mycobacterial methionine aminopeptidase 1. *Bioorganic Chemistry* **2022,** *118*, 105489.
335. Jandourek, O.; Tauchman, M.; Paterova, P.; Konecna, K.; Navratilova, L.; Kubicek, V.; Holas, O.; Zitko, J.; Dolezal, M., Synthesis of Novel Pyrazinamide Derivatives Based on 3-Chloropyrazine-2-carboxamide and Their Antimicrobial Evaluation. *Molecules* **2017,** *22* (2), 223.
336. Bergmann, K. E.; Cynamon, M. H.; Welch, J. T., Quantitative Structure−Activity Relationships for the in Vitro Antimycobacterial Activity of Pyrazinoic Acid Esters. *Journal of Medicinal Chemistry* **1996,** *39* (17), 3394-3400.
337. Dolezal, M.; Kesetovic, D.; Zitko, J., Antimycobacterial Evaluation of Pyrazinoic Acid Reversible Derivatives. *Current Pharmaceutical Design* **2011,** *17* (32), 3506-3514.
338. Fernandes, J. P.-D. S.; Pavan, F. R.; Leite, C. Q. F.; Felli, V. M. A., Synthesis and evaluation of a pyrazinoic acid prodrug in Mycobacterium tuberculosis. *Saudi Pharm J* **2014,** *22* (4), 376-380.
339. Hassan, N. W.; Saudi, M. N.; Abdel-Ghany, Y. S.; Ismail, A.; Elzahhar, P. A.; Sriram, D.; Nassra, R.; Abdel-Aziz, M. M.; El-Hawash, S. A., Novel pyrazine based anti-tubercular agents: Design, synthesis, biological evaluation and in silico studies. *Bioorganic Chemistry* **2020,** *96*, 103610.
340. Khani-Meinagh, H.; Mostafavi, H.; Reiling, N.; Mahdavi, M.; Zarrini, G., Design, synthesis and evaluation of biological activities of some novel anti-TB agents with bio-reducible functional group. *Bioimpacts* **2019,** *9* (4), 199-209.

341. Krátký, M.; Vinšová, J.; Novotná, E.; Stolaříková, J., Salicylanilide pyrazinoates inhibit in vitro multidrug-resistant Mycobacterium tuberculosis strains, atypical mycobacteria and isocitrate lyase. *European Journal of Pharmaceutical Sciences* **2014,** *53*, 1-9.
342. Seitz, L. E.; Suling, W. J.; Reynolds, R. C., Synthesis and Antimycobacterial Activity of Pyrazine and Quinoxaline Derivatives. *Journal of Medicinal Chemistry* **2002,** *45* (25), 5604-5606.
343. Dolezal, M.; Jampílek, J.; Osicka, Z.; Kuneš, J.; Buchta, V.; Víchová, P., Substituted 5-aroylpyrazine-2-carboxylic acid derivatives: synthesis and biological activity. *Il Farmaco* **2003,** *58* (11), 1105-1111.
344. Foks, Polish journal of pharmacology and pharmacy. *Polish journal of pharmacology and pharmacy.* **1976,** *28* (3), 295.
345. Foks; Janowiec; Pilarski, Studies on pyrazine derivatives. Part X. Synthesis and tuberculostatic activity of some 6-cyclamino-, 6-imidazolyl--and triazolylpyrazine-2-carboxylic acids derivatives. *Polish journal of pharmacology and pharmacy.* **1978,** *30* (1), 105.
346. Novácek, L.; Celadník, M.; Palát, K.; Kubala, E., [Antitubercular agents. X. The action of derivatives of 3-substituted 2 pyrazinecarboxylic acid]. *Ceskoslovenská farmacie* **1969,** *18*, 385-7.
347. Pancechowska-Ksepko, D.; Foks, H.; Janowiec, M., [Studies on pyrazine derivatives. XIX. Synthesis and tuberculostatic activity of various 3-phenoxy-2-pyrazinecarboxylic acid derivatives]. *Acta poloniae pharmaceutica* **1983,** *40*, 15-9.
348. Pancechowska-Ksepko, D.; Sawlewicz, J.; Samulska, J.; Janowiec, M., [Synthesis and tuberculostatic activity of various derivatives of 3-alkylthio- and 3-phenylthiopyrazine-2-carboxylic acids and thieno[2,3-b]pyrazine]. *Acta poloniae pharmaceutica* **1979,** *36 3*, 289-94.
349. Gangarapu, N. R.; Ranganatham, A.; Reddy, E. K.; Surendra, H. D.; Sajith, A. M.; Yellappa, S.; Chandrasekhar, K. B., Design, Synthesis, and Biological Evaluation of 3,5-Disubstituted 2-Pyrazineamide Derivatives as Antitubercular Agents. *Journal of Heterocyclic Chemistry* **2019,** *56* (3), 1117-1126.
350. Wächter, G. A.; Davis, M. C.; Martin, A. R.; Franzblau, S. G., Antimycobacterial Activity of Substituted Isosteres of Pyridine- and Pyrazinecarboxylic Acids. *Journal of Medicinal Chemistry* **1998,** *41* (13), 2436-2438.
351. Norcott, P.; Rayner, P. J.; Green, G. G. R.; Duckett, S. B., Achieving High 1H Nuclear Hyperpolarization Levels with Long Lifetimes in a Range of Tuberculosis Drug Scaffolds. *Chemistry – A European Journal* **2017,** *23* (67), 16990-16997.
352. Duan, H.; Ning, M.; Chen, X.; Zou, Q.; Zhang, L.; Feng, Y.; Zhang, L.; Leng, Y.; Shen, J., Design, Synthesis, and Antidiabetic Activity of 4-

Phenoxynicotinamide and 4-Phenoxypyrimidine-5-carboxamide Derivatives as Potent and Orally Efficacious TGR5 Agonists. *Journal of Medicinal Chemistry* **2012,** *55* (23), 10475-10489.
353. Komeyama, K.; Nagao, Y.; Abe, M.; Takaki, K., Scope and Limitation for FeSO4-Mediated Direct Arylation of Heteroarenes with Arylboronic Acids and Its Synthetic Applications. *Bulletin of the Chemical Society of Japan* **2014,** *87*, 301-313.
354. Dai, X.; Liu, H.; Palani, S. H.; Nargund, R.; Xiao, D.; Zorn, N.; Dang, Q.; McComas, C. C.; Peng, X.; Li, P.; Soll, R. Substituted benzofuran compounds and methods of use thereof for the treatment of viral diseases. 2014.
355. Arnold, W. D.; Gosberg, A.; Li, Z.; Steensma, R. W.; Wilson, M. E. Fused ring heterocycle kinase modulators. 2006.
356. Barlin, G. B., Heterocyclic amplifiers of phleomycin. II. Thiazol-4'-ylpyrazines with phenyl substituents and strongly basic side chains. *Aus J Chem* **1984,** *37* (5), 1049-56.
357. Gengenbacher, M.; Rao, S. P. S.; Pethe, K.; Dick, T., Nutrient-starved, non-replicating Mycobacterium tuberculosis requires respiration, ATP synthase and isocitrate lyase for maintenance of ATP homeostasis and viability. *Microbiology* **2010,** *156* (1), 81-87.

Appendix A. NMR Spectra

(6*R*,7*R*)-3-(acetoxymethyl)-8-oxo-7-(2-phenylacetamido)-5-thia-1-azabicyclo[4.2.0]oct-2-ene-2-carboxylic acid (CS Pro)

^{1}H NMR (500 MHz, DMSO) δ 13.65 (s, 1H), 9.10 (d, *J* = 8.3 Hz, 1H), 7.34 – 7.19 (m, 6H), 5.68 (dd, *J* = 8.3, 4.8 Hz, 1H), 5.08 (d, *J* = 4.8 Hz, 1H), 5.00 (d, *J* = 12.8 Hz, 1H), 4.69 (d, *J* = 12.8 Hz, 1H), 3.65 – 3.46 (m, 5H), 2.03 (s, 3H).

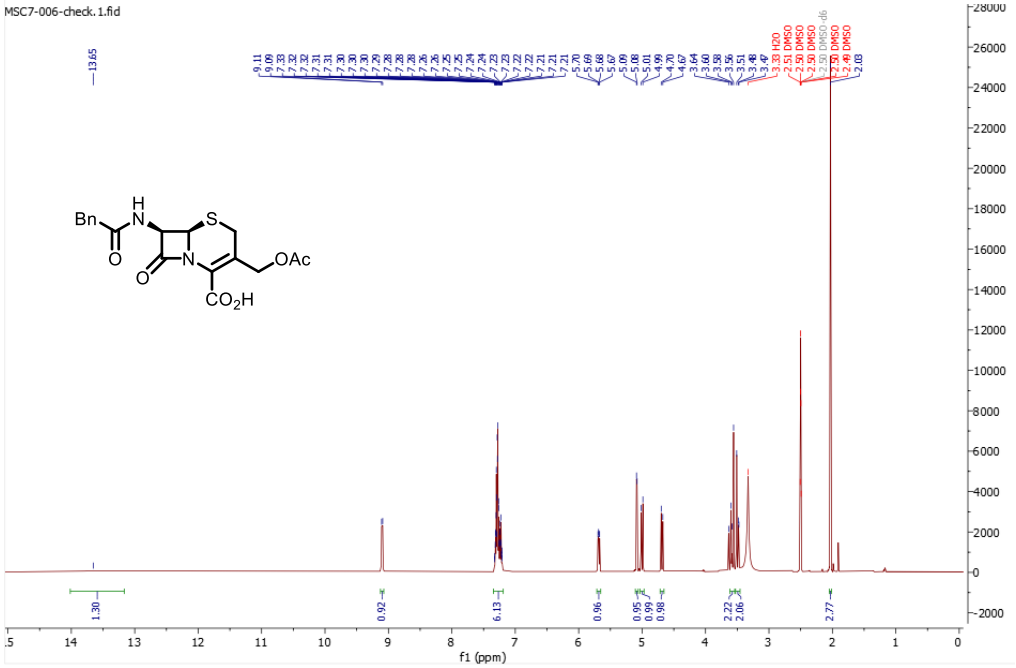

^{13}C NMR (126 MHz, DMSO) δ 173.15, 171.43, 170.67, 165.26, 163.31, 136.27, 135.49, 129.82, 129.48, 128.70, 127.04, 126.97, 126.81, 123.84, 63.16, 59.56, 57.90, 42.04, 41.15, 26.01, 21.04.

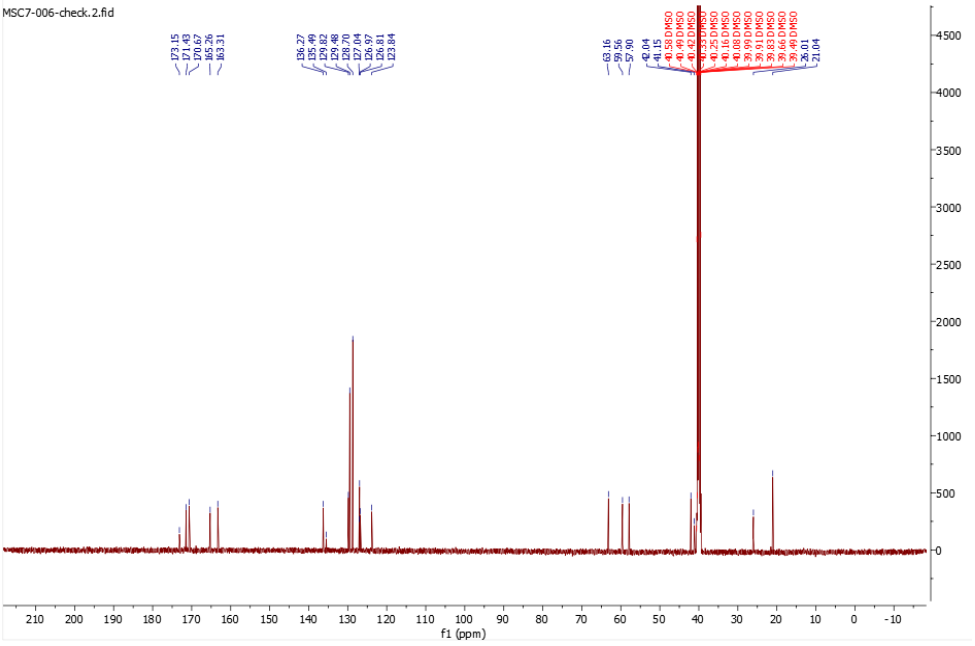

Benzhydryl (6*R*,7*R*) -3-(hydroxymethyl)-8-oxo-7-(2-phenylacetamido)-5-thia-1-azabicyclo[4.2.0]oct-2-ene-2-carboxylate (3)

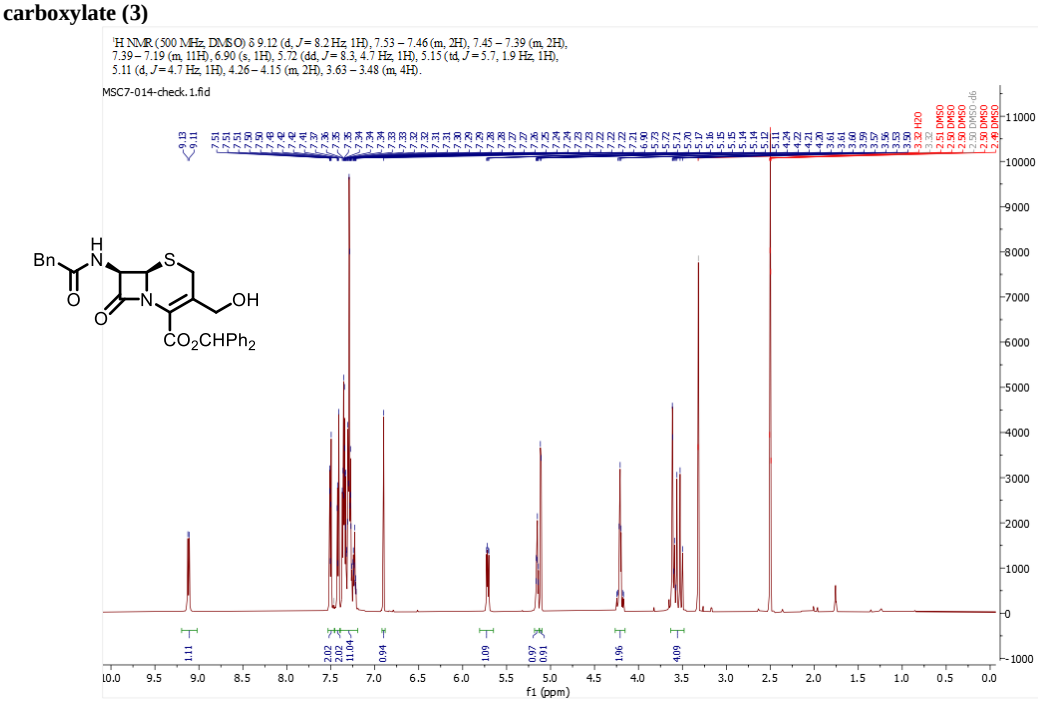

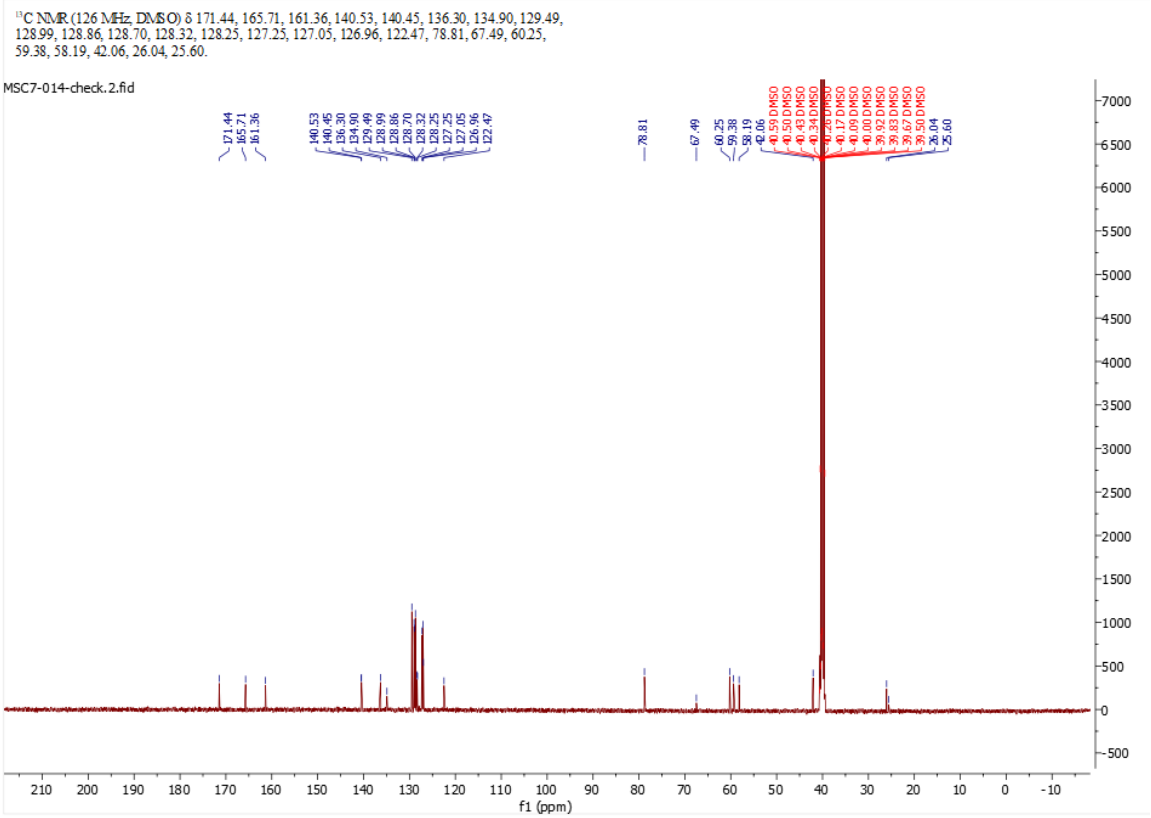

(1H-benzo[d][1,2,3]triazol-1-yl)(pyrazin-2-yl)methanone (POA-BT)

^{1}H NMR (500 MHz, DMSO) δ 9.34 (d, J = 1.4 Hz, 1H), 9.01 (d, J = 2.5 Hz, 1H), 8.95 (dd, J = 2.5, 1.5 Hz, 1H), 8.35 (dd, J = 8.3, 6.7 Hz, 2H), 7.93 – 7.86 (m, 1H), 7.74 – 7.68 (m, 1H).

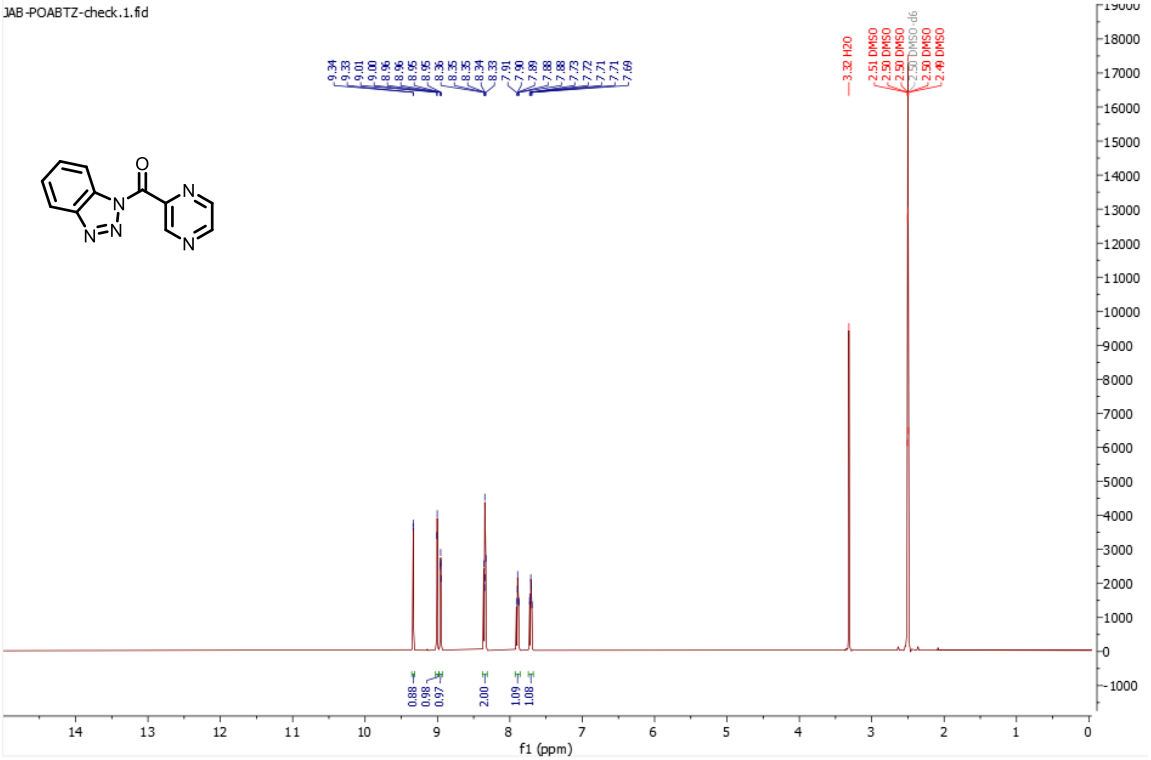

Benzhydryl (6*R*,7*R*)-8-oxo-7-(2-phenylacetamido)-3-(((pyrazine-2-carbonyl)oxy)methyl)-5-thia-1-azabicyclo[4.2.0]oct-2-ene-2-carboxylate (4)

^{1}H NMR (500 MHz, DMSO) δ 9.21 – 9.14 (m, 2H), 8.91 (d, *J* = 2.4 Hz, 1H), 8.83 (dd, *J* = 2.4, 1.5 Hz, 1H), 7.51 – 7.46 (m, 2H), 7.44 – 7.38 (m, 2H), 7.35 – 7.19 (m, 12H), 6.94 (s, 1H), 5.81 (dd, *J* = 8.3, 4.8 Hz, 1H), 5.22 (d, *J* = 13.0 Hz, 1H), 5.18 (d, *J* = 4.9 Hz, 1H), 5.07 – 4.97 (m, 1H), 3.77 (dd, *J* = 39.4, 18.4 Hz, 2H), 3.54 (dd, *J* = 34.2, 13.7 Hz, 3H).

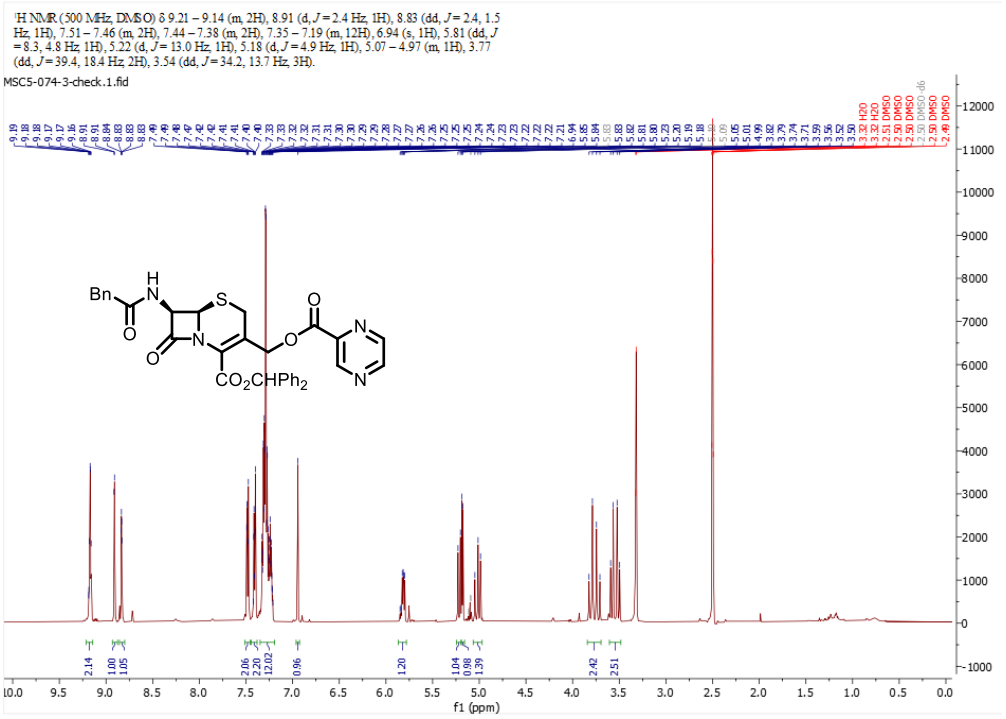

^{13}C NMR (126 MHz, DMSO) δ 171.44, 165.80, 163.60, 161.02, 148.72, 146.20, 145.35, 143.85, 143.12, 140.22, 140.14, 136.25, 129.49, 128.95, 128.84, 128.71, 128.33, 127.31, 126.99, 126.97, 125.99, 125.95, 79.40, 71.85, 64.57, 60.20, 59.57, 58.11, 57.82, 42.08, 42.01, 26.46, 22.86.

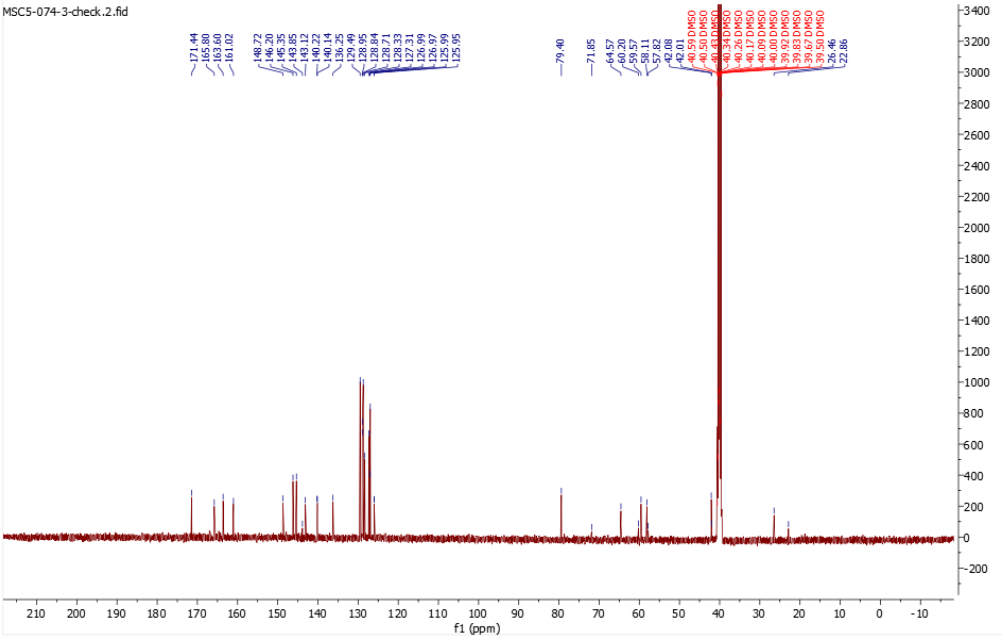

(6*R*,7*R*) -8-oxo-7-(2-phenylacetamido)-3-(((pyrazine-2-carbonyl)oxy)methyl)-5-thia-1-azabicyclo[4.2.0]oct-2-ene-2-carboxylic acid (CS-POA)

^{1}H NMR (500 MHz, DMSO) δ 13.78 (s, 1H), 9.23 (d, *J* = 1.5 Hz, 1H), 9.12 (d, *J* = 8.4 Hz, 1H), 8.91 (d, *J* = 2.4 Hz, 1H), 8.84 (dd, *J* = 2.5, 1.5 Hz, 1H), 7.34 – 7.19 (m, 6H), 5.71 (dd, *J* = 8.3, 4.8 Hz, 1H), 5.36 (d, *J* = 12.8 Hz, 1H), 5.12 (d, *J* = 4.9 Hz, 1H), 5.06 (d, *J* = 12.8 Hz, 1H), 3.71 (d, *J* = 32.2 Hz, 2H), 3.61 – 3.48 (m, 2H).

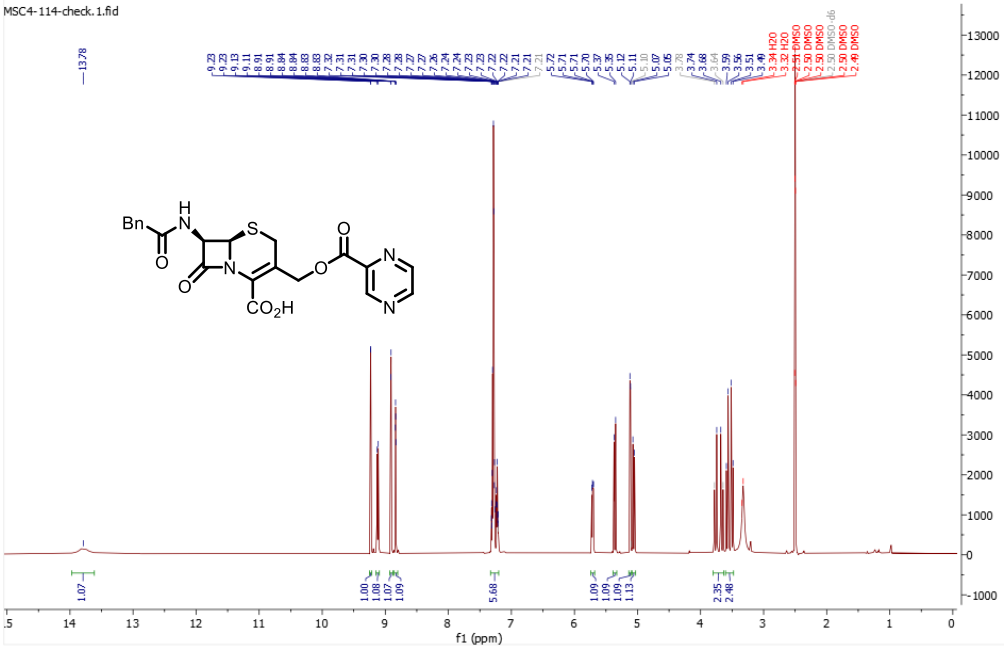

^{13}C NMR (126 MHz, DMSO) δ 170.95, 164.83, 163.24, 162.89, 148.22, 145.76, 144.88, 142.81, 135.80, 129.01, 128.22, 126.49, 64.37, 59.10, 57.45, 41.57, 25.62.

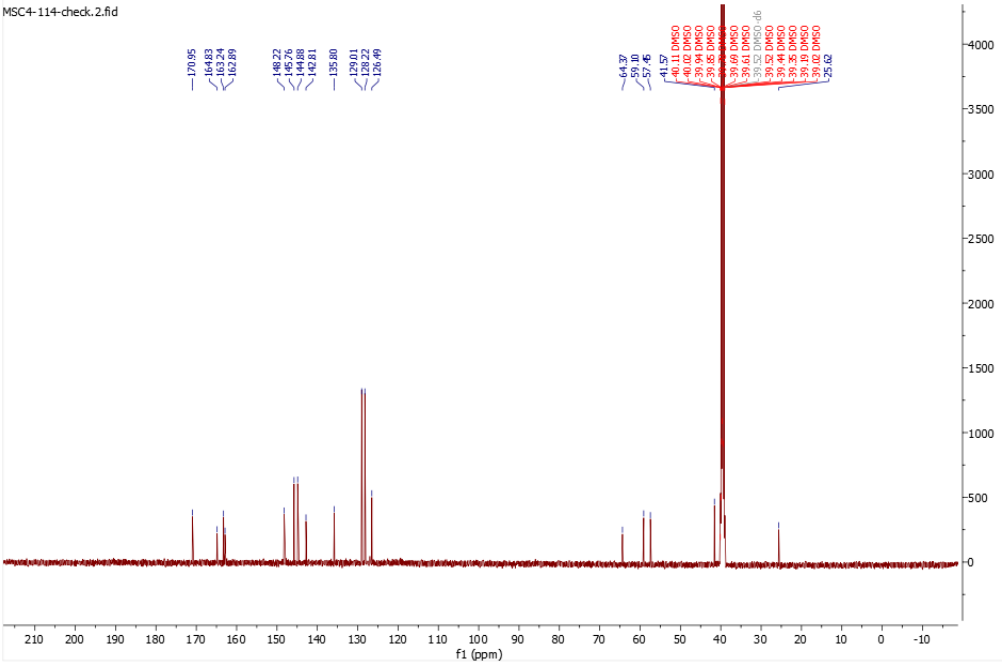

***tert*-Butyl (6*R*,7*R*)-3-(acetoxymethyl)-8-oxo-7-(2-phenylacetamido)-5-thia-1-azabicyclo[4.2.0]oct-2-ene-2-carboxylate (6)**

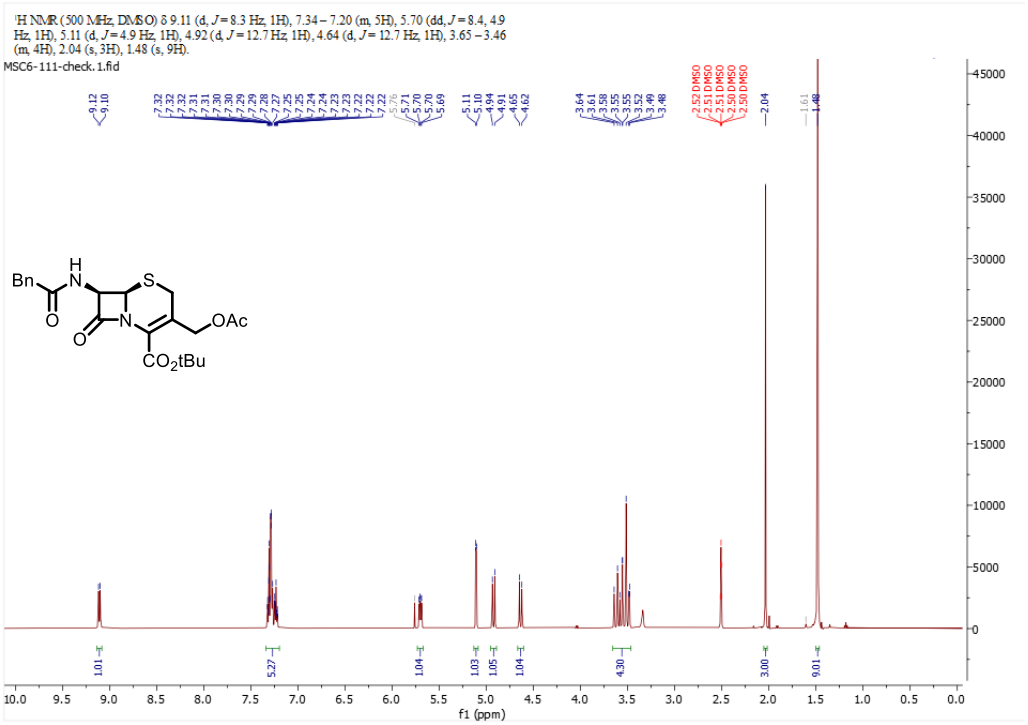

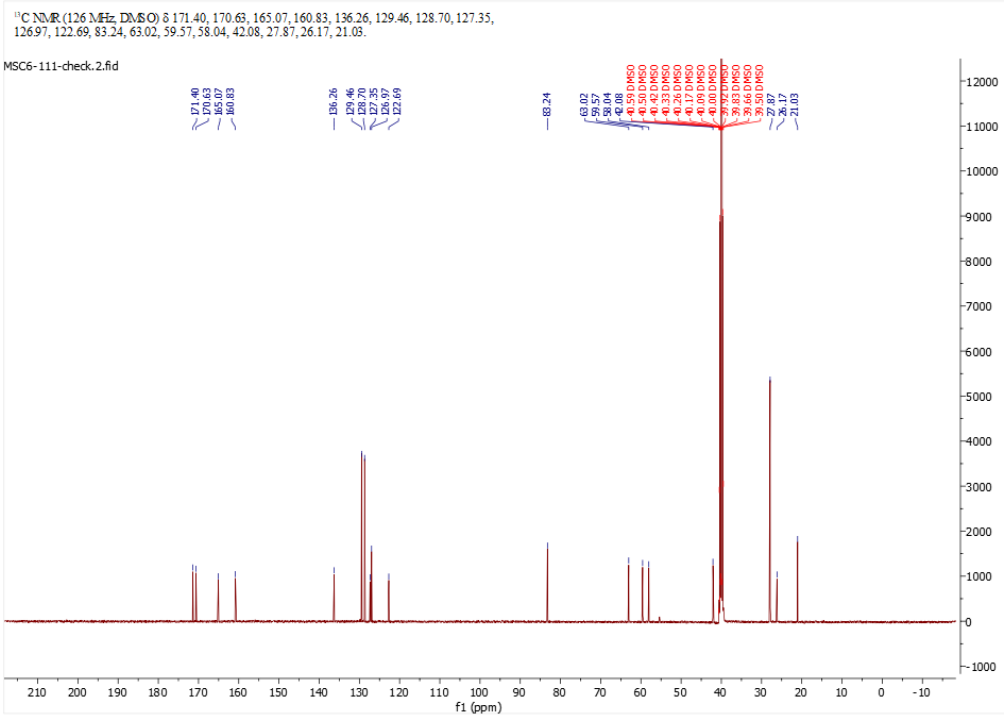

***tert*-Butyl (6*R*,7*S*)-3-(acetoxymethyl)-7-methoxy-8-oxo-7-(2-phenylacetamido)-5-thia-1-azabicyclo[4.2.0]oct-2-ene-2-carboxylate (7)**

^{1}H NMR (500 MHz, DMSO) δ 9.44 (s, 1H), 7.33 – 7.20 (m, 5H), 5.16 (s, 1H), 4.86 (d, *J* = 12.7 Hz, 1H), 4.60 (d, *J* = 12.7 Hz, 1H), 3.64 – 3.52 (m, 4H), 3.35 (s, 3H), 2.02 (s, 3H), 1.48 (s, 9H).

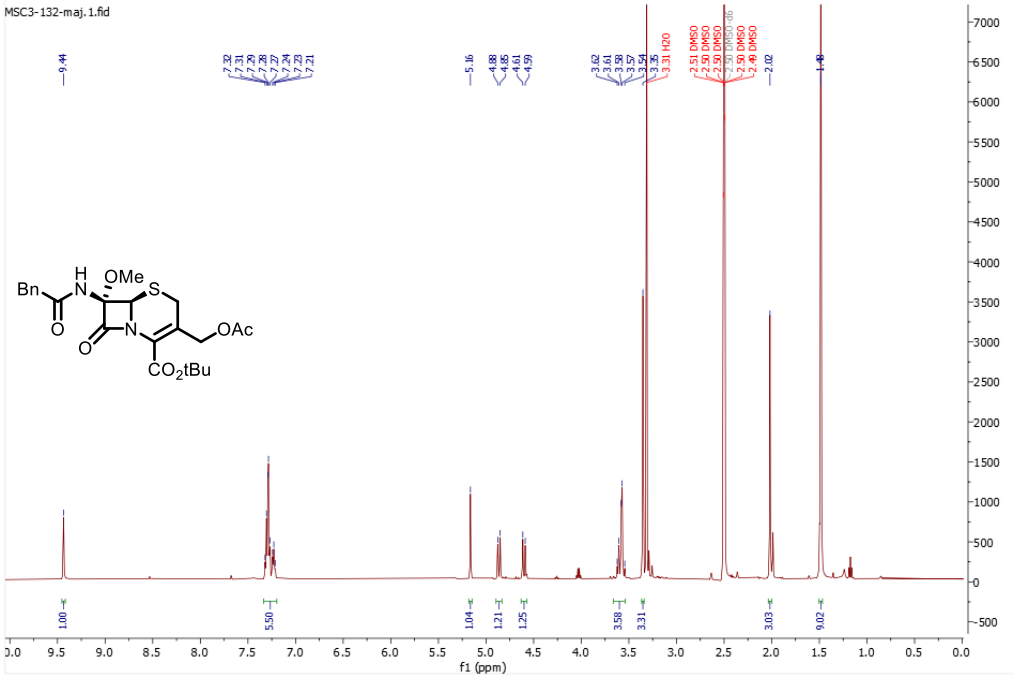

^{13}C NMR (126 MHz, DMSO) δ 171.49, 170.12, 160.15, 135.56, 129.13, 128.22, 126.67, 126.51, 122.96, 95.15, 82.96, 62.50, 62.24, 52.46, 41.67, 27.36, 25.93, 20.54.

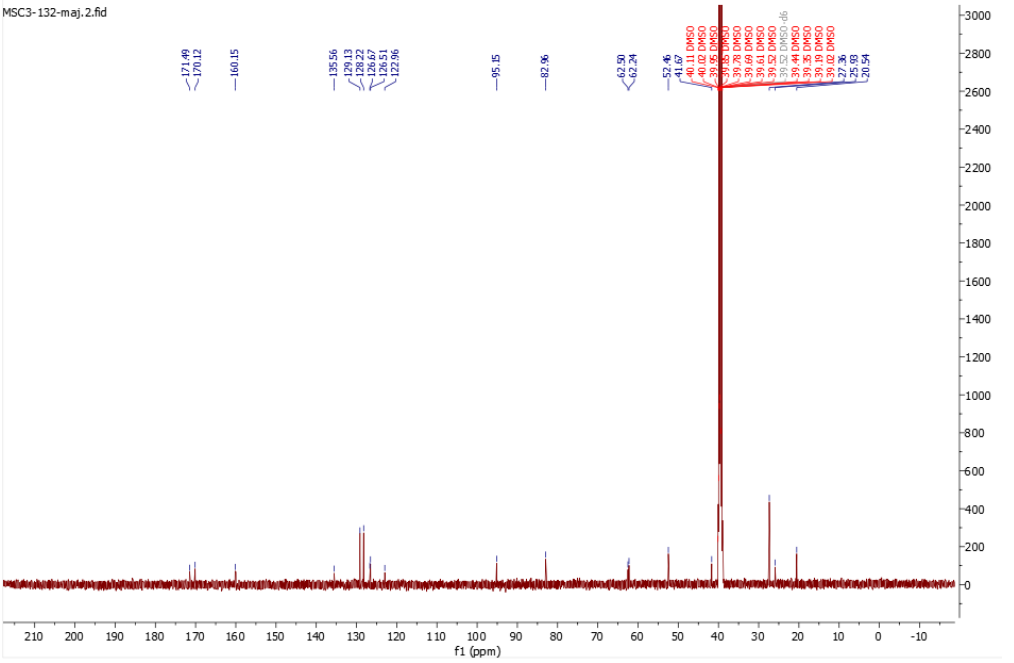

***tert*-Butyl (6*R*,7*S*)-3-(hydroxymethyl)-7-methoxy-8-oxo-7-(2-phenylacetamido)-5-thia-1-azabicyclo[4.2.0]oct-2-ene-2-carboxylate (8)**

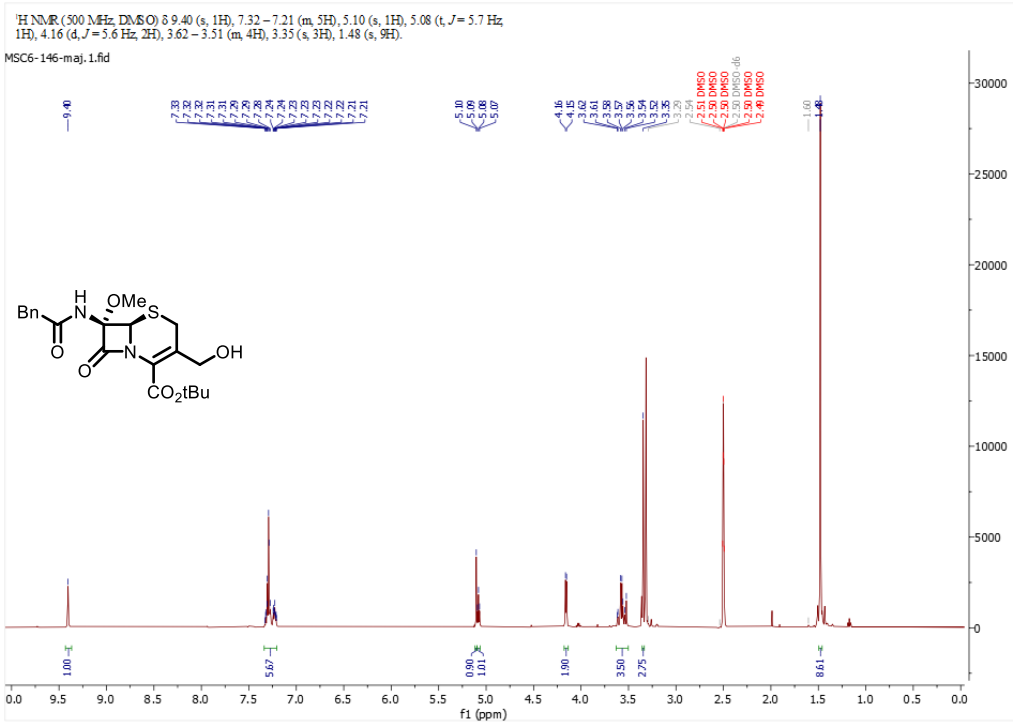

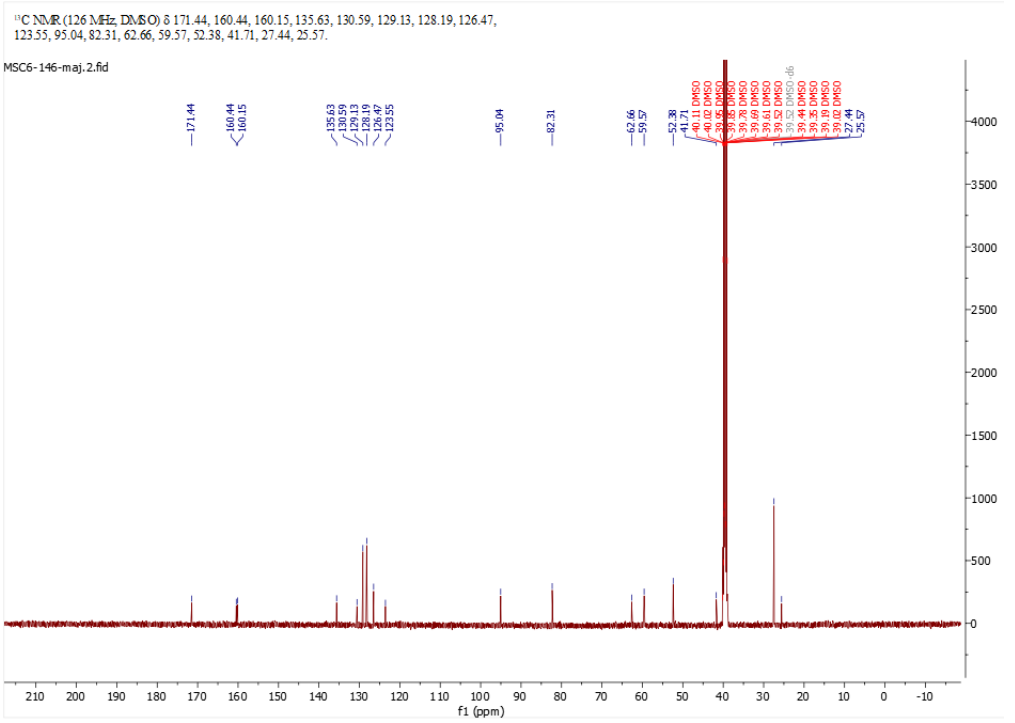

***tert*-Butyl (6*R*,7*S*)-7-methoxy-8-oxo-7-(2-phenylacetamido)-3-(((pyrazine-2-carbonyl)oxy)methyl)-5-thia-1-azabicyclo[4.2.0]oct-2-ene-2-carboxylate (9)**

^{1}H NMR (500 MHz, DMSO) δ 9.46 (s, 1H), 9.22 (d, *J* = 1.5 Hz, 1H), 8.91 (d, *J* = 2.4 Hz, 1H), 8.83 (dd, *J* = 2.5, 1.5 Hz, 1H), 7.34 – 7.20 (m, 5H), 5.25 (d, *J* = 12.7 Hz, 1H), 5.19 (s, 1H), 4.97 (d, *J* = 12.7 Hz, 1H), 3.76 – 3.48 (m, 4H), 3.36 (s, 3H), 1.49 (s, 9H).

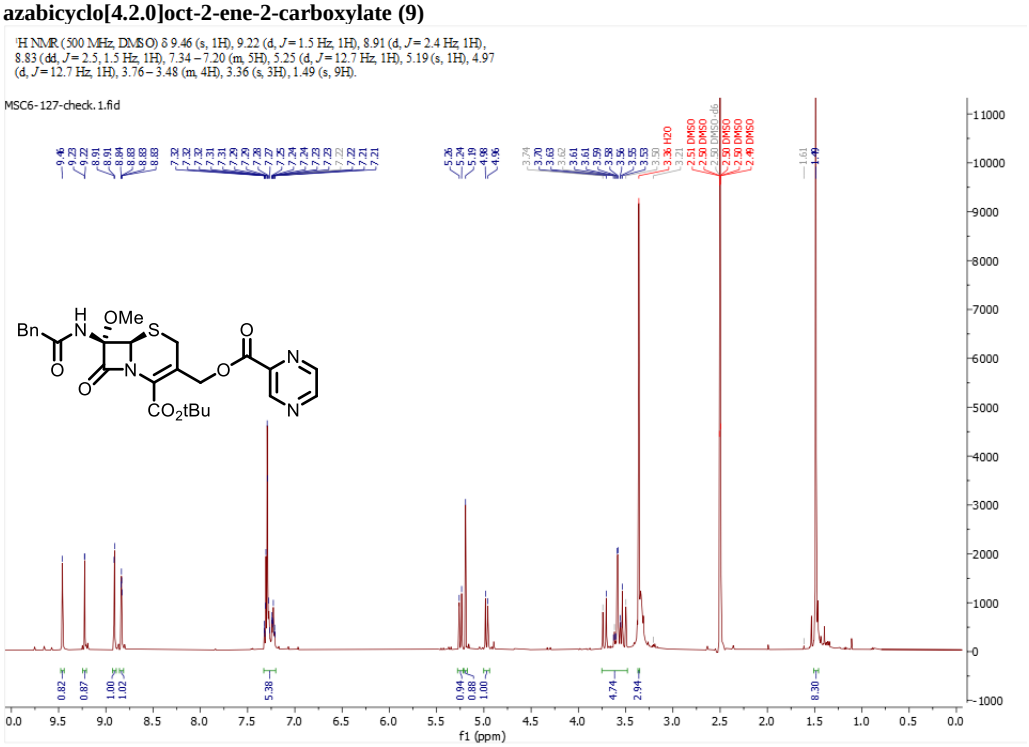

^{13}C NMR (126 MHz, DMSO) δ 171.51, 163.19, 160.20, 159.94, 148.25, 145.76, 144.88, 142.75, 135.56, 129.13, 128.21, 127.06, 126.50, 122.63, 95.15, 83.13, 63.80, 62.55, 52.47, 41.67, 27.36, 26.02.

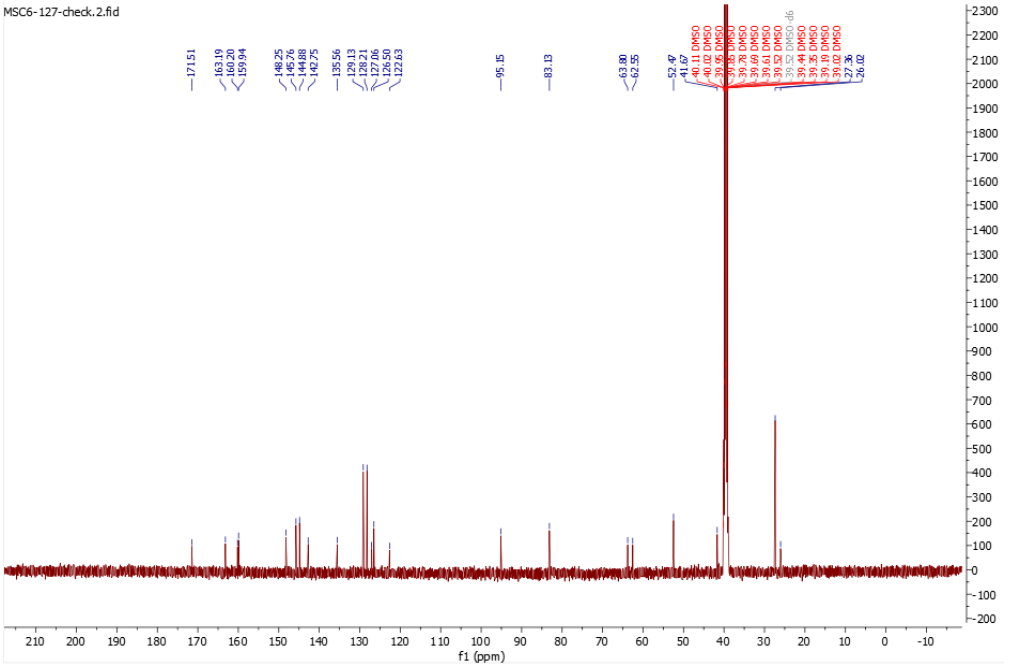

(6*R*,7*S*)-7-Methoxy-8-oxo-7-(2-phenylacetamido)-3-(((pyrazine-2-carbonyl)oxy)methyl)-5-thia-1-azabicyclo[4.2.0]oct-2-ene-2-carboxylic acid (CM-POA)

^{1}H NMR (500 MHz, DMSO-d_6) δ 13.87 (s, 1H), 9.45 (s, 1H), 9.22 (s, 1H), 8.91 (d, J = 2.4 Hz, 1H), 8.83 (t, J = 1.9 Hz, 1H), 7.36 – 7.19 (m, 6H), 5.29 (d, J = 12.8 Hz, 1H), 5.16 (s, 1H), 5.02 (d, J = 12.8 Hz, 1H), 3.72 (d, J = 18.2 Hz, 1H), 3.64 – 3.54 (m, 2H), 3.50 (d, J = 18.1 Hz, 1H), 3.35 (s, 3H).

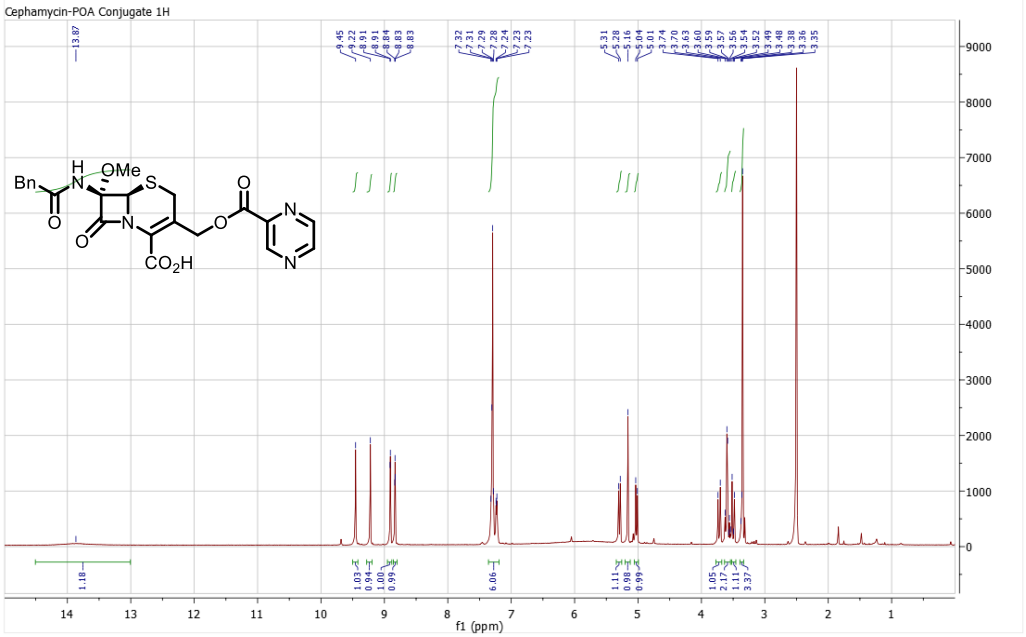

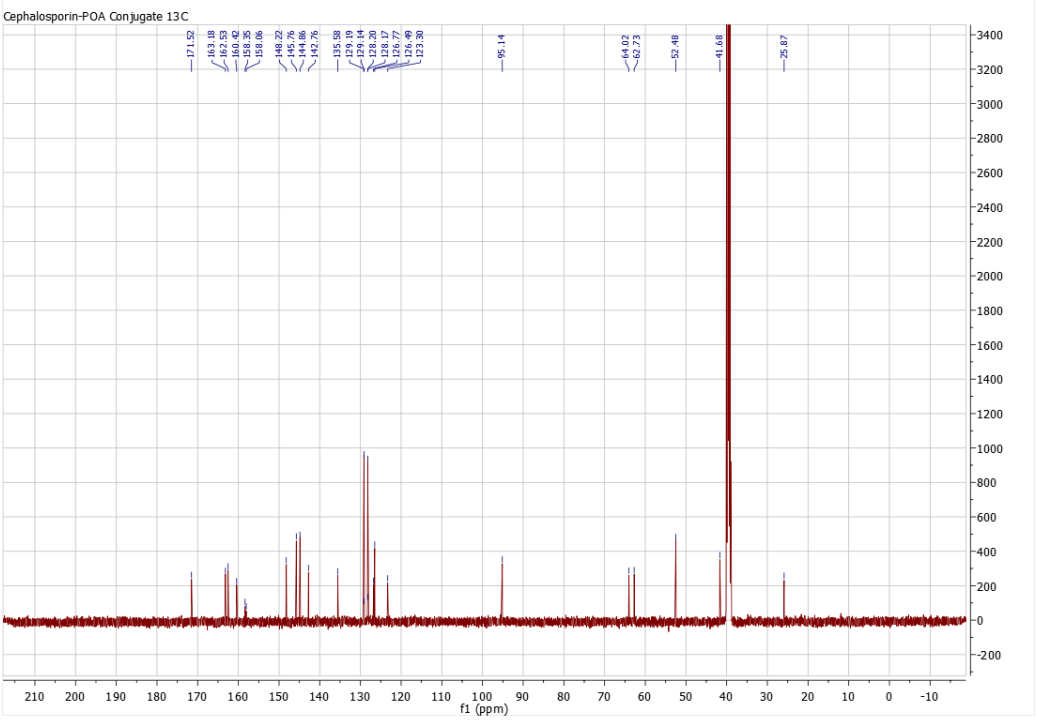

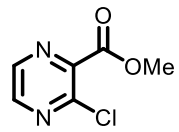

Methyl 3-chloropyrazine-2-carboxylate

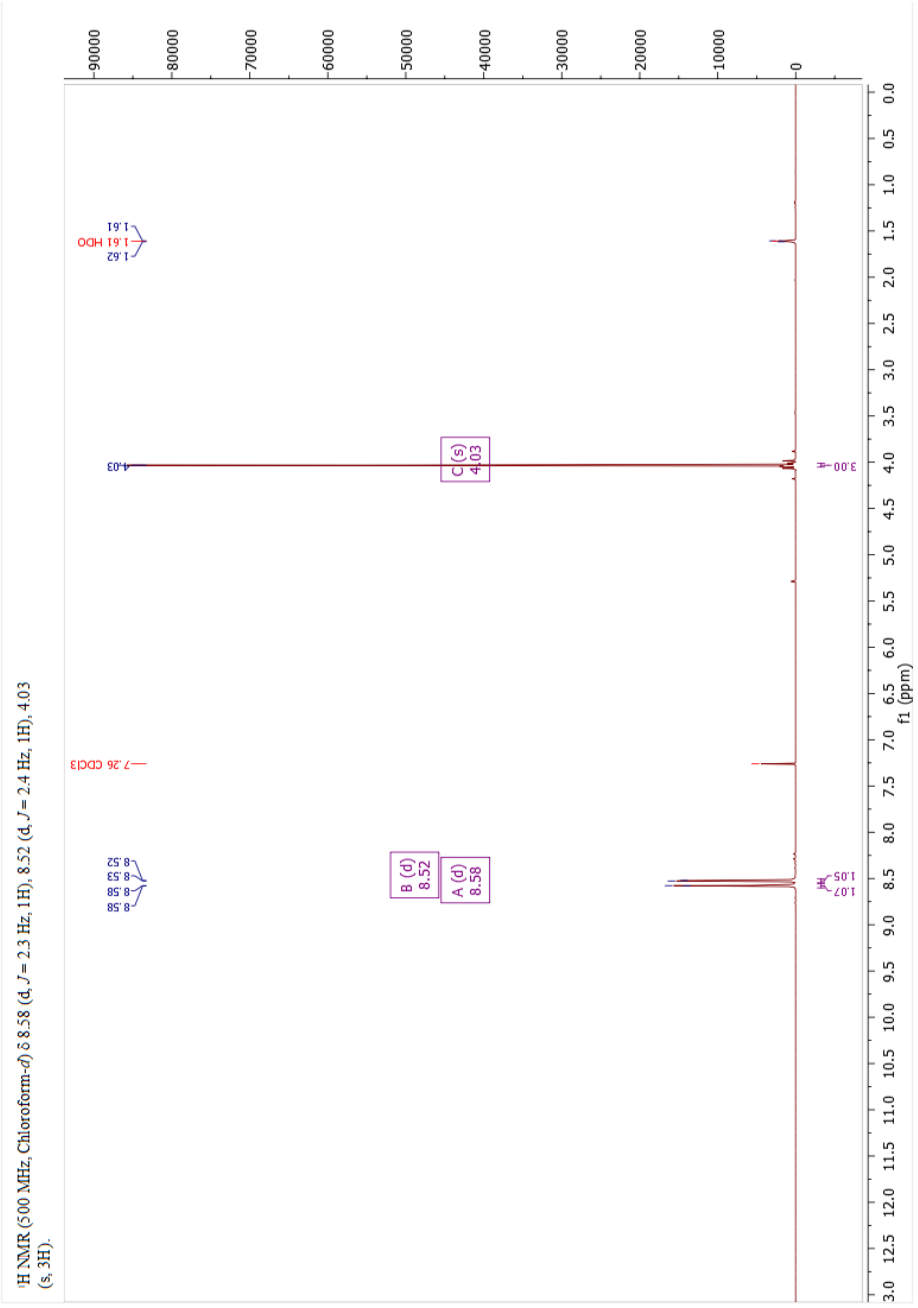

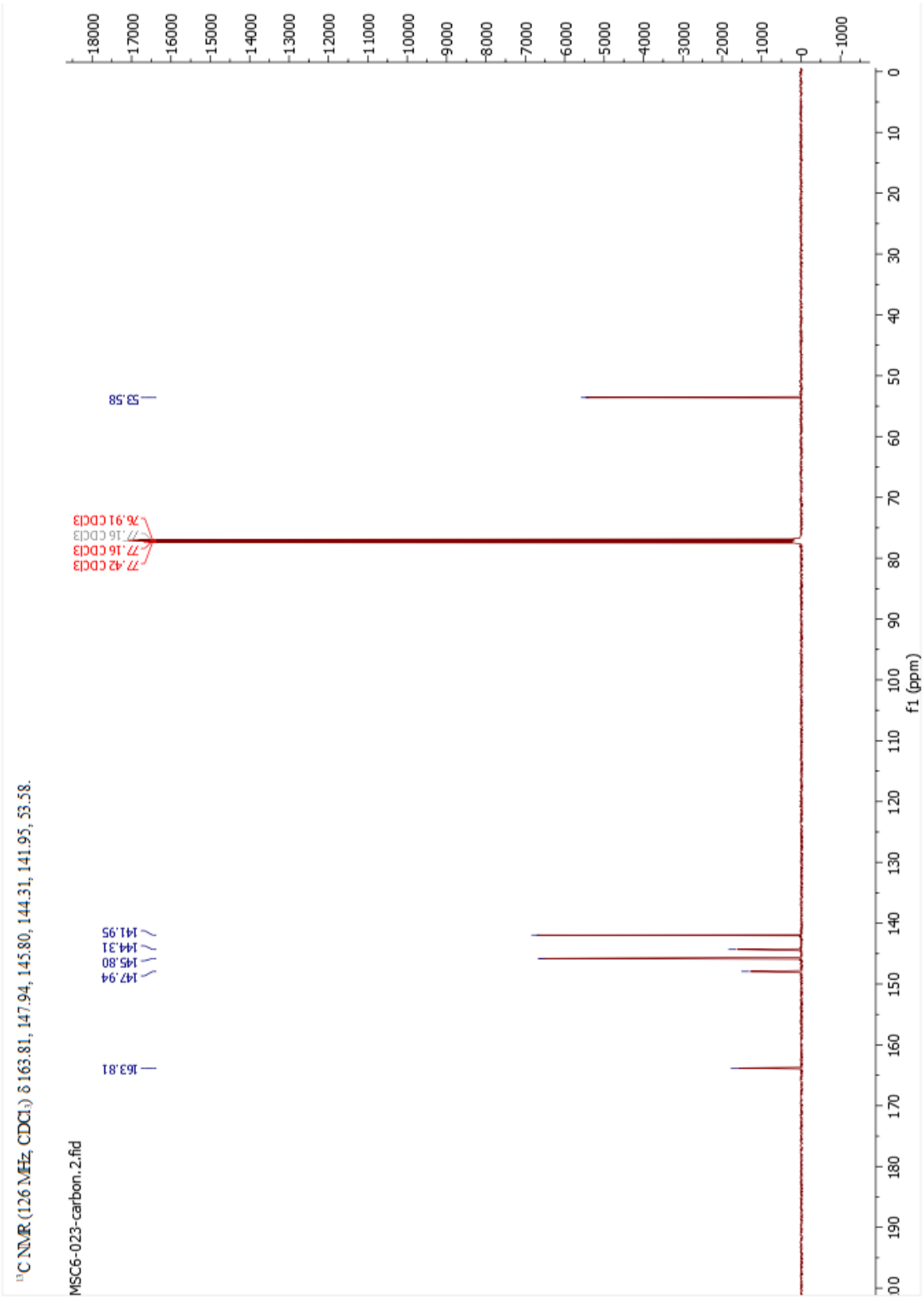
MSC6-023-carbon.2.fid
^{13}C NMR (126 MHz, CDCl$_3$) δ 163.81, 147.94, 145.80, 144.31, 141.95, 53.58.
163.81
147.94
145.80
144.31
141.95
77.42 CDCl3
77.16 CDCl3
76.91 CDCl3
53.58
f1 (ppm)

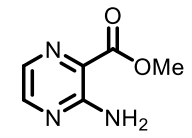
O
OMe
N
N
NH2

POAA008-OMe

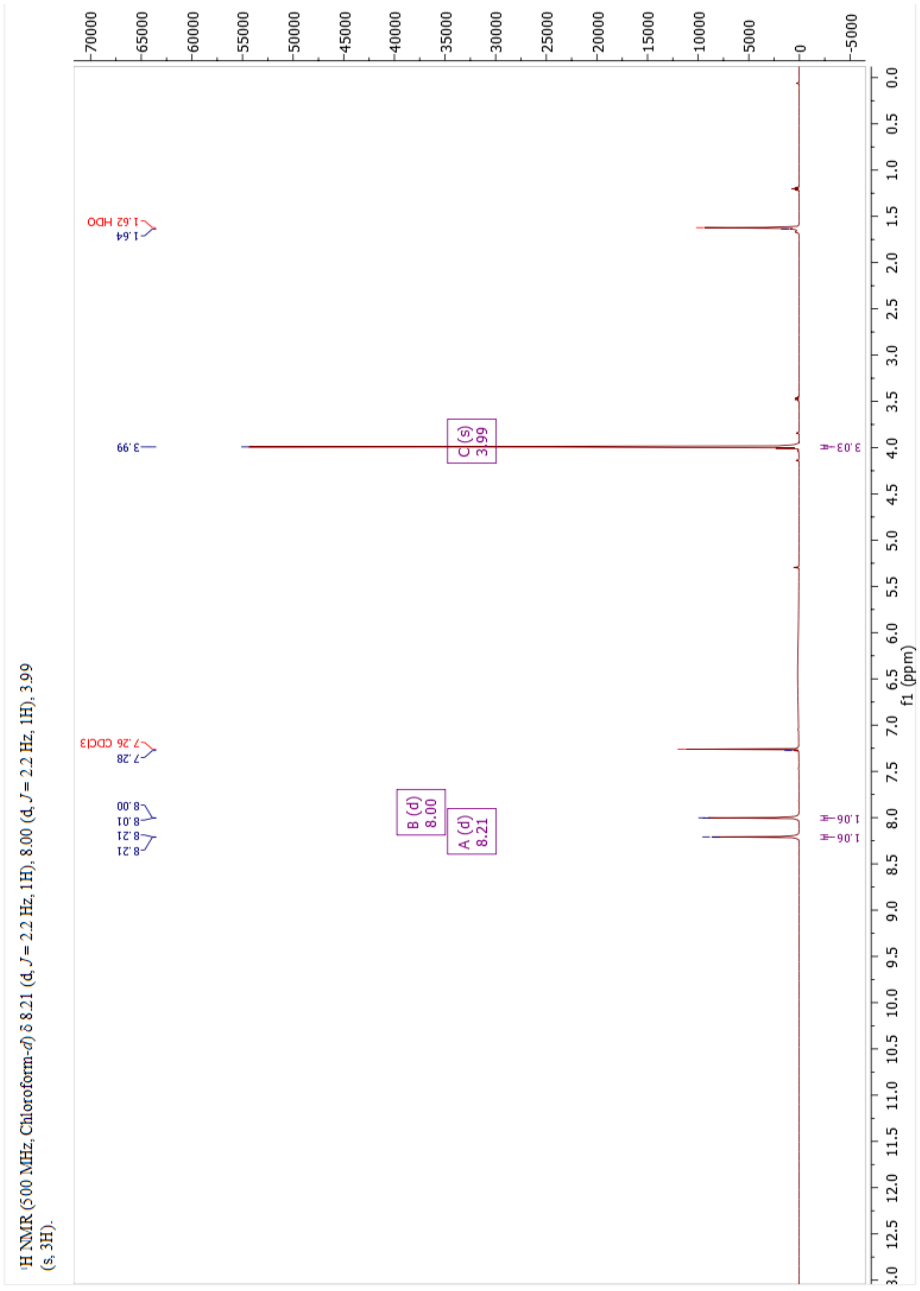
1H NMR (500 MHz, Chloroform-d) δ 8.21 (d, J = 2.2 Hz, 1H), 8.00 (d, J = 2.2 Hz, 1H), 3.99 (s, 3H).
1.64
1.62 HDO
3.99
7.28
7.26 CDCl3
8.21
8.01
8.21
8.00
C (s) 3.99
B (d) 8.00
A (d) 8.21
3.03
1.06
1.06
f1 (ppm)

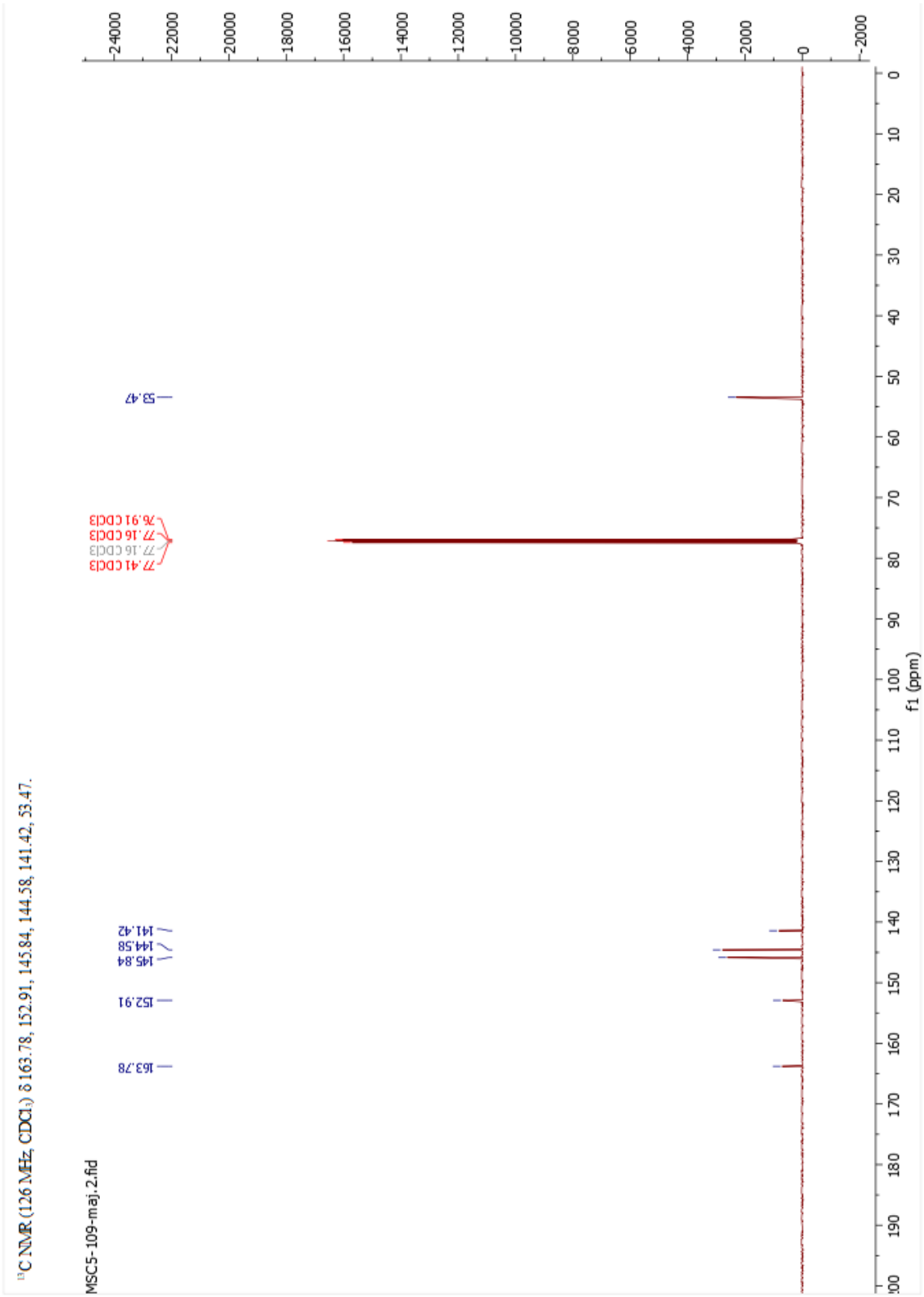

^{13}C NMR (126 MHz, $CDCl_3$) δ 163.78, 152.91, 145.84, 144.58, 141.42, 53.47.

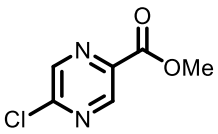
O
N
OMe
Cl
N

POAA001-OMe

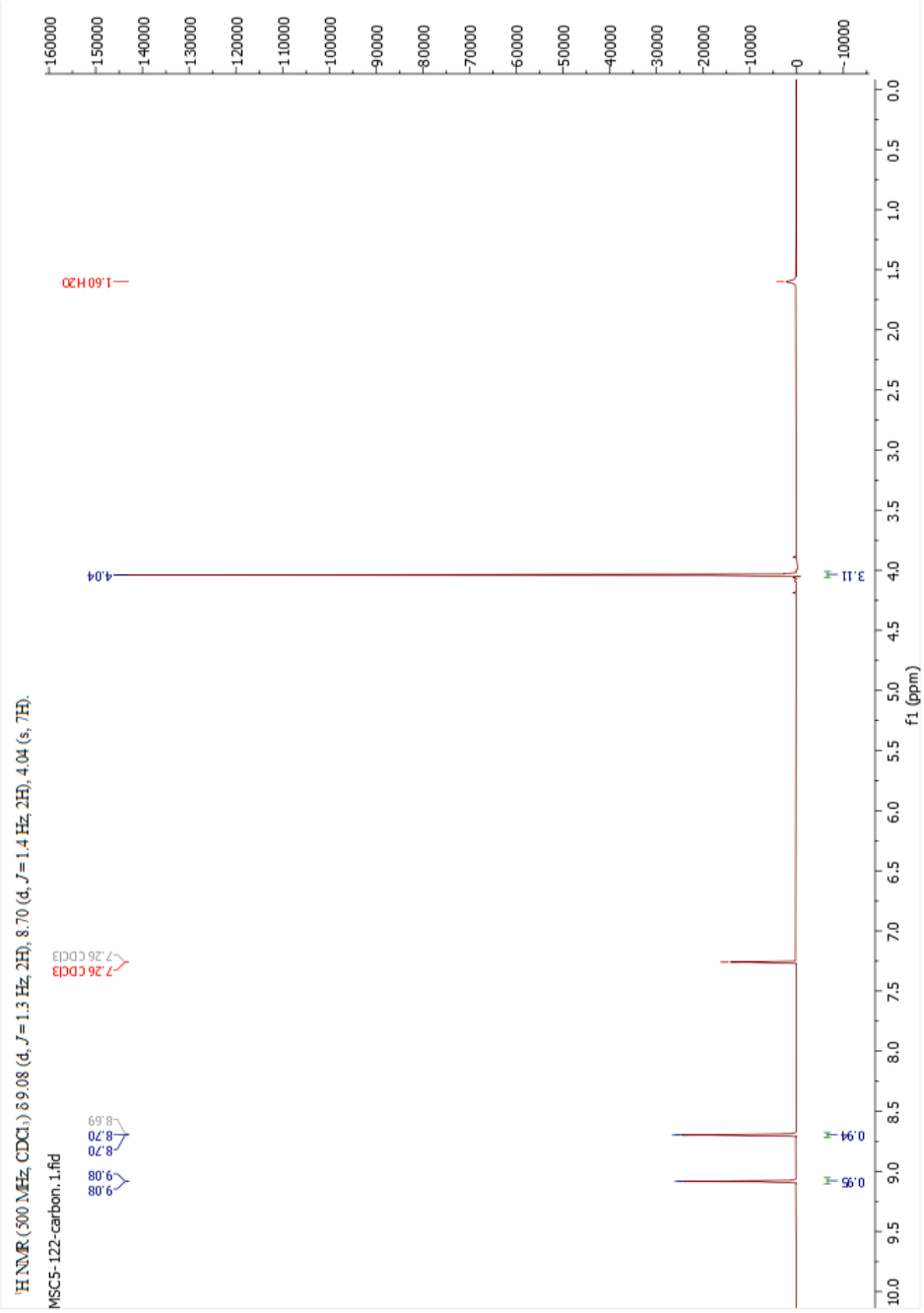
MSC5-122-carbon.1.fid
f1 (ppm)
1.60 H2O
4.04
7.26 CDCl3
8.70
8.69
9.08
3.11
0.94
0.95

^{13}C NMR (126 MHz, $CDCl_3$) δ 163.76, 152.89, 145.83, 144.57, 141.41, 53.45.

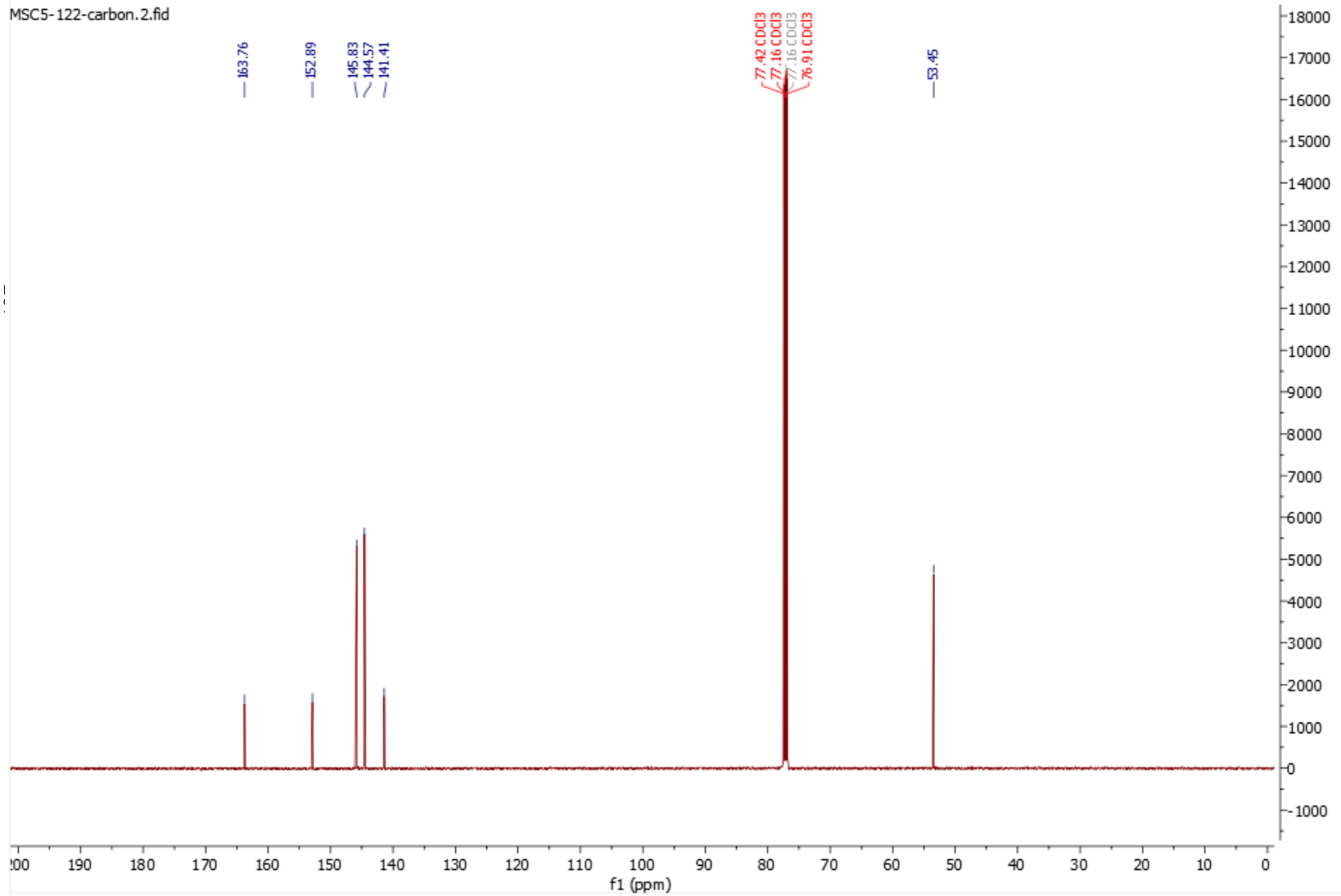

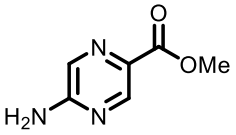
O
N
OMe
H2N
N

POAA009-OMe

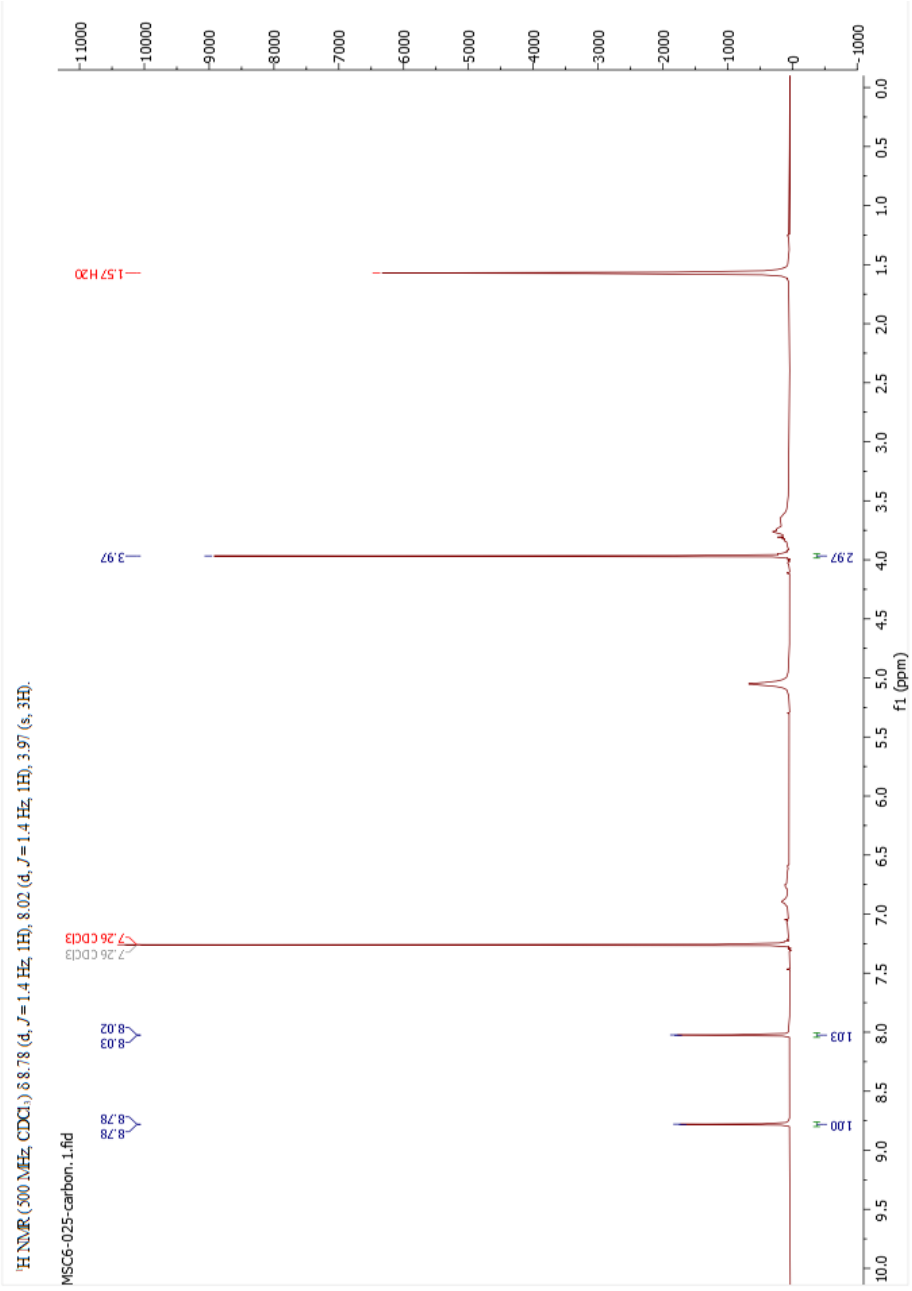
1.57 H2O
3.97
2.97
7.26 CDCl3
8.03
8.02
8.78
8.78
1.03
1.00
f1 (ppm)
MSC6-025-carbon.1.fid
¹H NMR (500 MHz, CDCl3) δ 8.78 (d, J = 1.4 Hz, 1H), 8.02 (d, J = 1.4 Hz, 1H), 3.97 (s, 3H).

^{13}C NMR (126 MHz, $CDCl_3$) δ 165.07, 155.95, 145.87, 133.20, 131.69, 52.59.

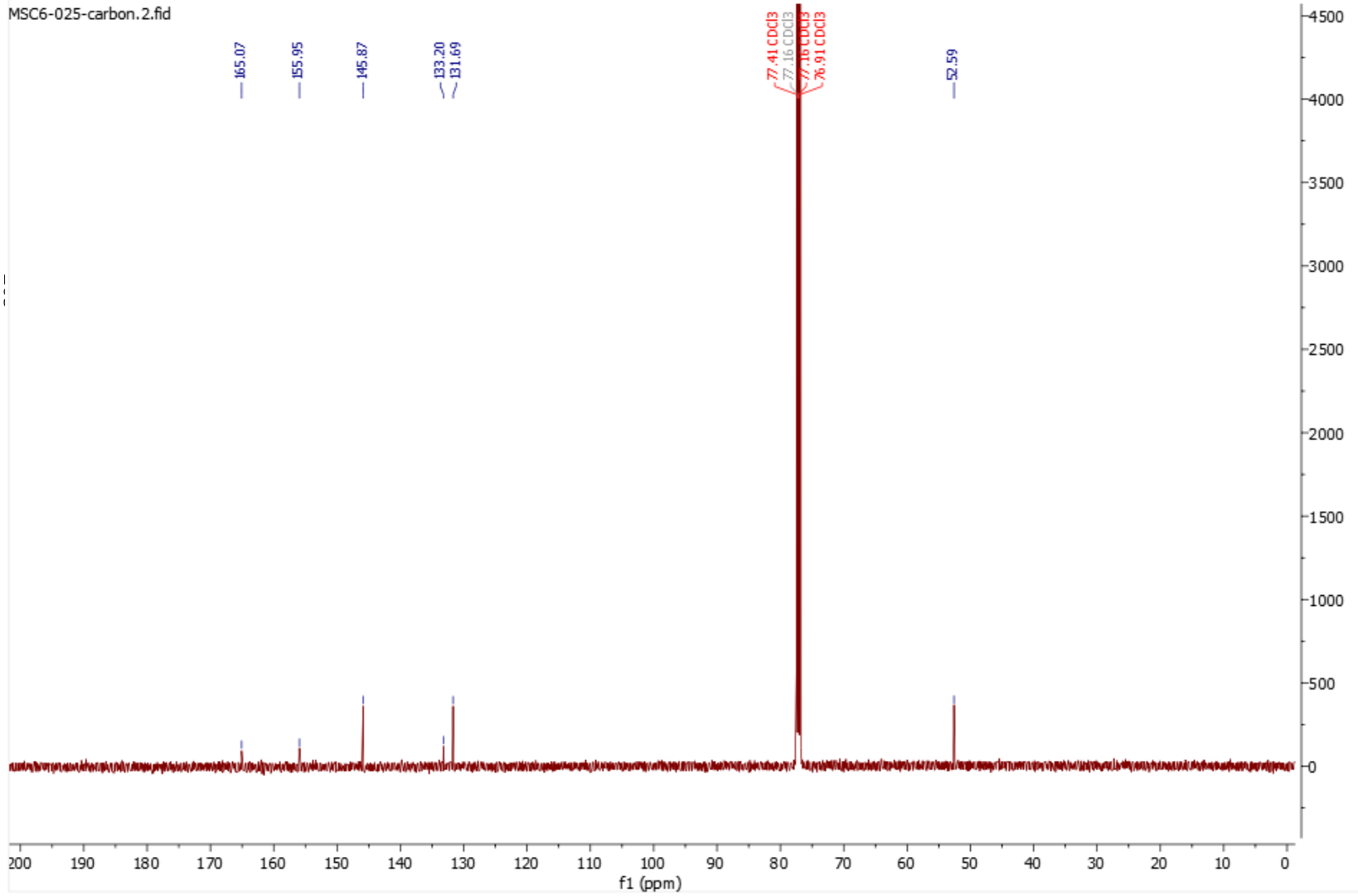

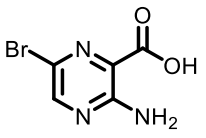
Br
N
O
OH
N
NH2

POAA015

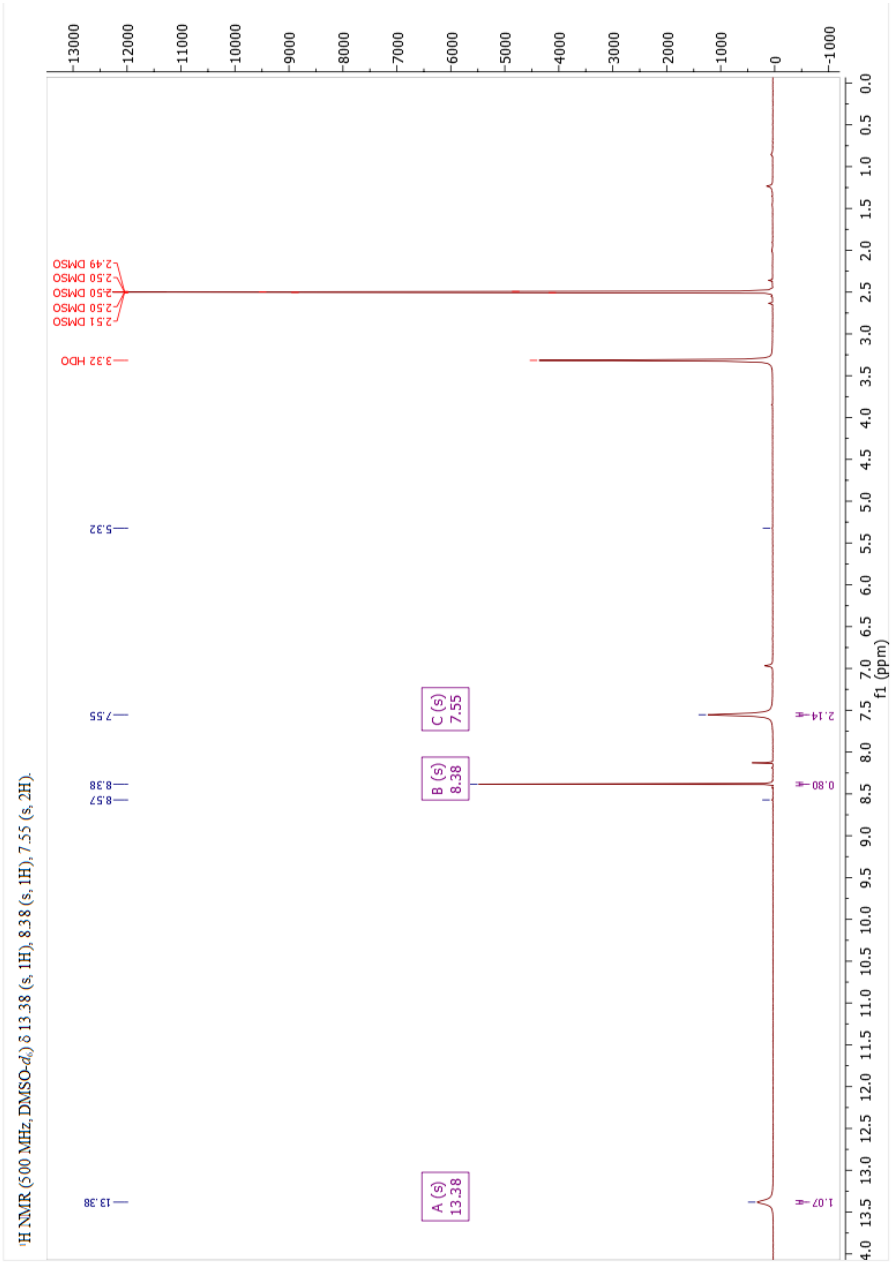
^{1}H NMR (500 MHz, DMSO-d_6) δ 13.38 (s, 1H), 8.38 (s, 1H), 7.55 (s, 2H).
A (s) 13.38
B (s) 8.38
C (s) 7.55
f1 (ppm)

^{13}C NMR (126 MHz, MeOD) δ 168.32, 156.82, 151.43, 124.59, 124.22.

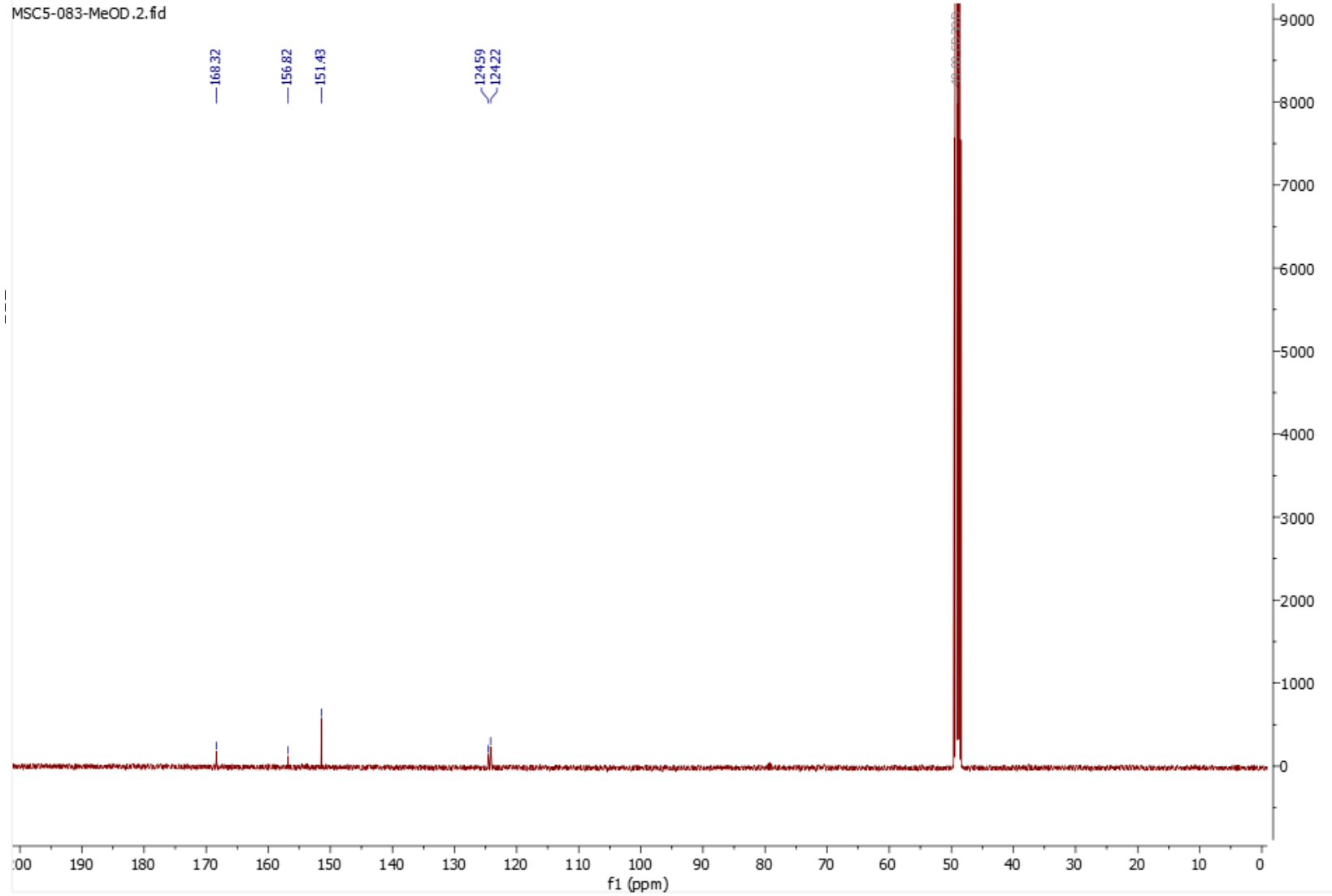

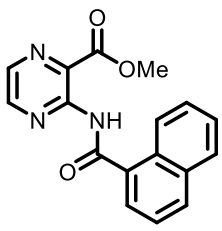

POAA012-OMe

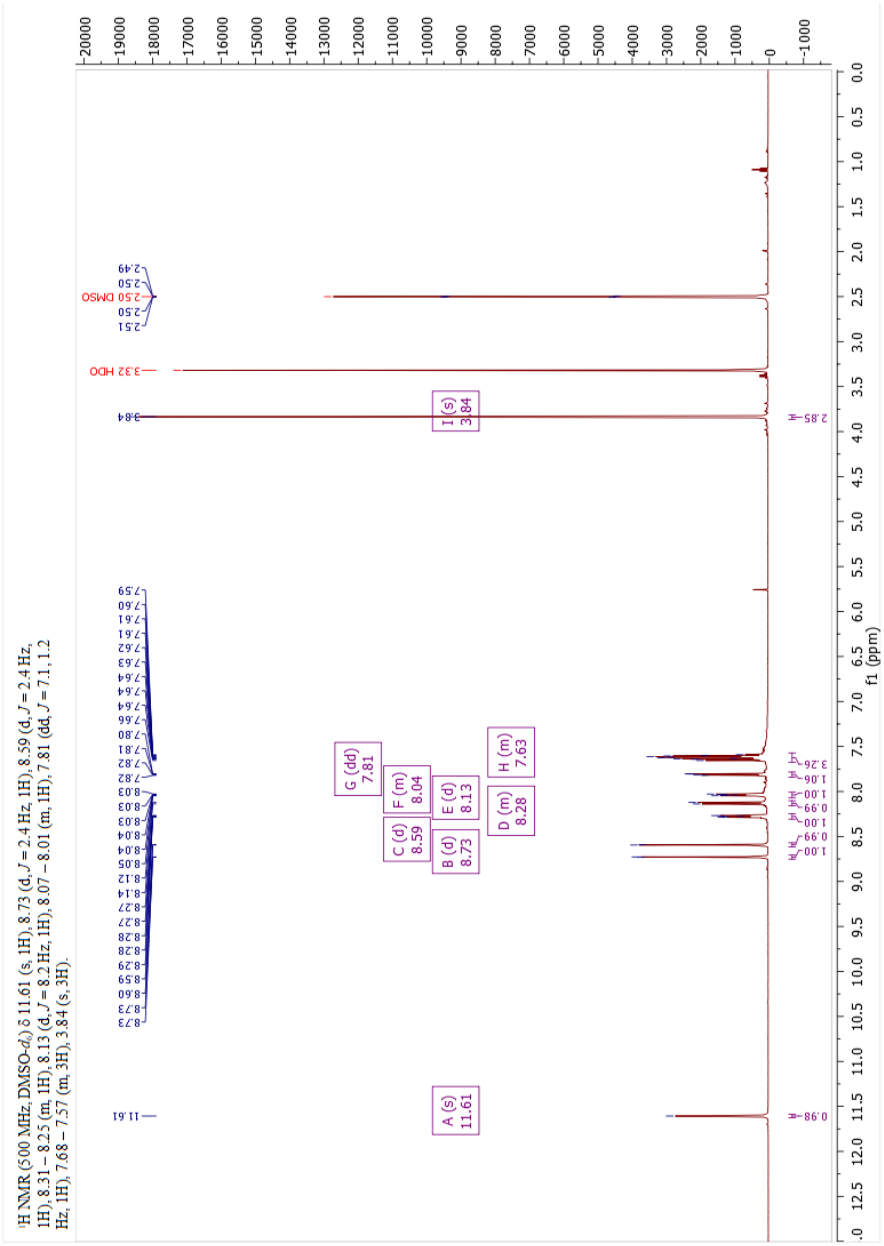

^{1}H NMR (500 MHz, DMSO-d_6) δ 11.61 (s, 1H), 8.73 (d, J = 2.4 Hz, 1H), 8.59 (d, J = 2.4 Hz, 1H), 8.31 – 8.25 (m, 1H), 8.13 (d, J = 8.2 Hz, 1H), 8.07 – 8.01 (m, 1H), 7.81 (dd, J = 7.1, 1.2 Hz, 1H), 7.68 – 7.57 (m, 3H), 3.84 (s, 3H).

^{13}C NMR (126 MHz, DMSO) δ 168.07, 165.06, 145.35, 140.03, 138.66, 133.15, 132.48, 131.10, 129.75, 128.39, 127.18, 126.47, 126.43, 124.98, 52.51.

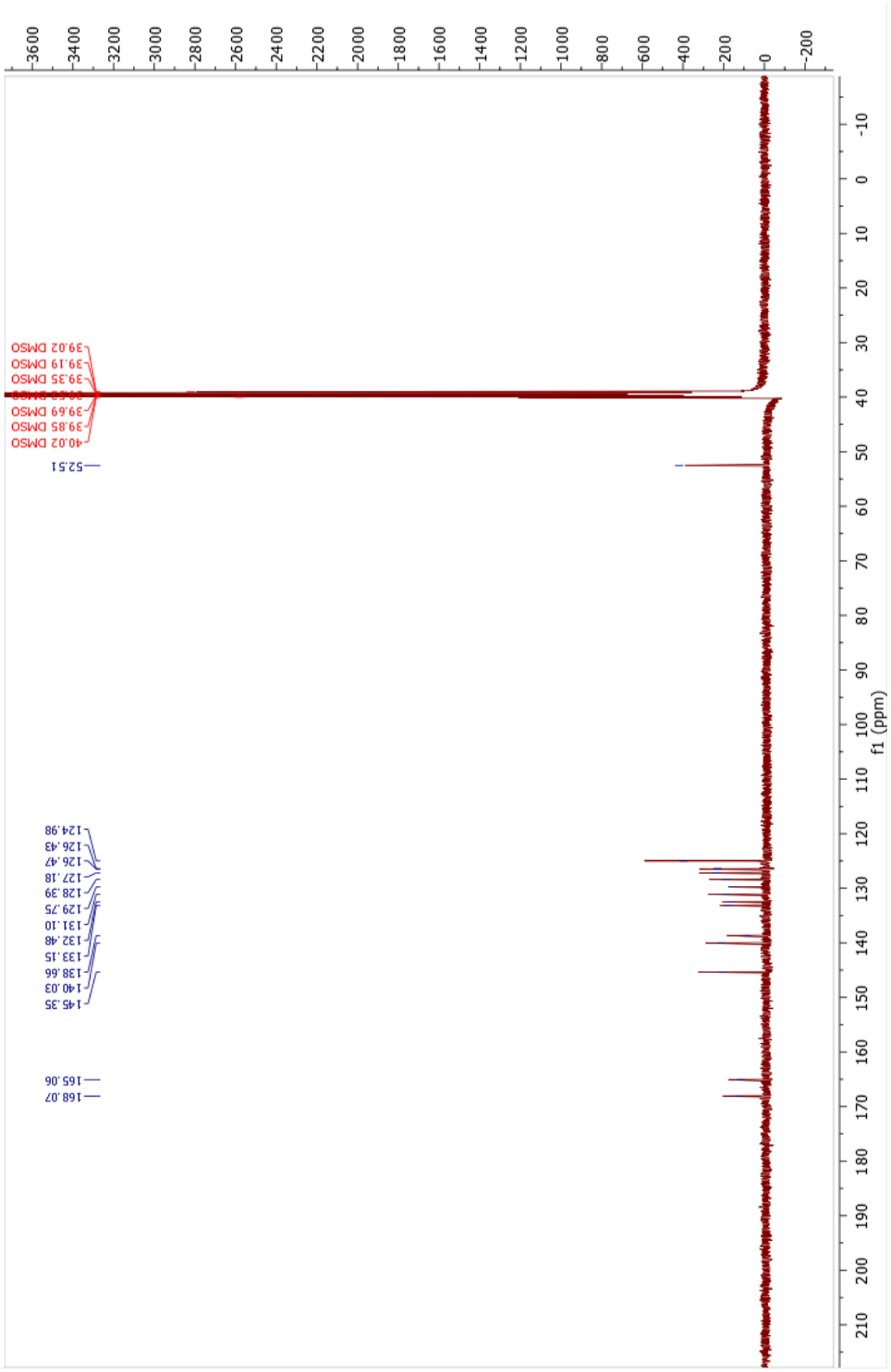

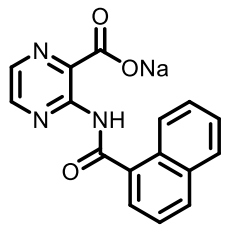
O
ONa
N
N
NH
O

POAA012

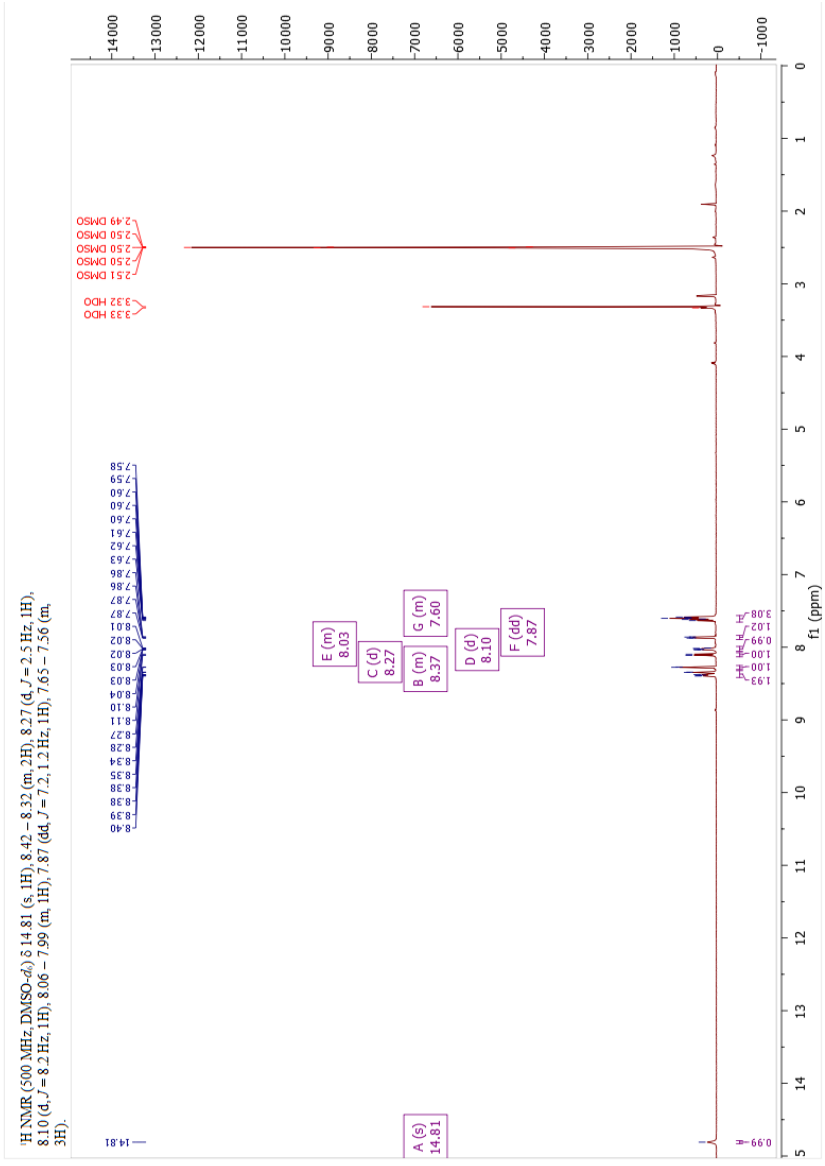
^{1}H NMR (500 MHz, DMSO-d_6) δ 14.81 (s, 1H), 8.42 – 8.32 (m, 2H), 8.27 (d, J = 2.5 Hz, 1H), 8.10 (d, J = 8.2 Hz, 1H), 8.06 – 7.99 (m, 1H), 7.87 (dd, J = 7.2, 1.2 Hz, 1H), 7.65 – 7.56 (m, 3H).
A (s) 14.81
B (m) 8.37
C (d) 8.27
D (d) 8.10
E (m) 8.03
F (dd) 7.87
G (m) 7.60
f1 (ppm)

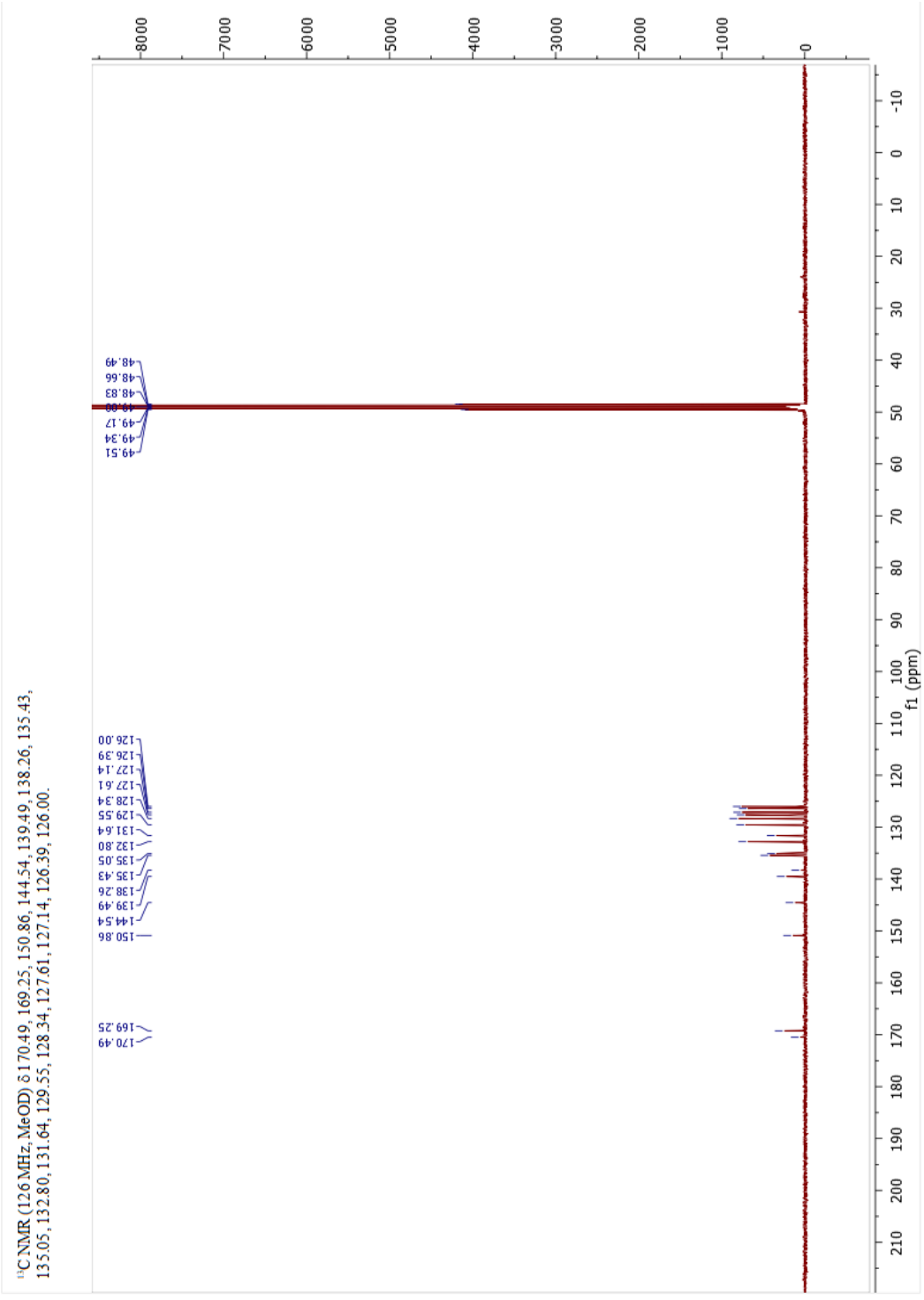
^{13}C NMR (126 MHz, MeOD) δ 170.49, 169.25, 150.86, 144.54, 139.49, 138.26, 135.43, 135.05, 132.80, 131.64, 129.55, 128.34, 127.61, 127.14, 126.39, 126.00.
170.49
169.25
150.86
144.54
139.49
138.26
135.43
135.05
132.80
131.64
129.55
128.34
127.61
127.14
126.39
126.00
49.51
49.34
49.17
48.83
48.66
48.49
f1 (ppm)

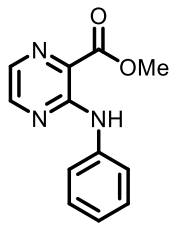
O
OMe
N
N
NH

POAA034-OMe

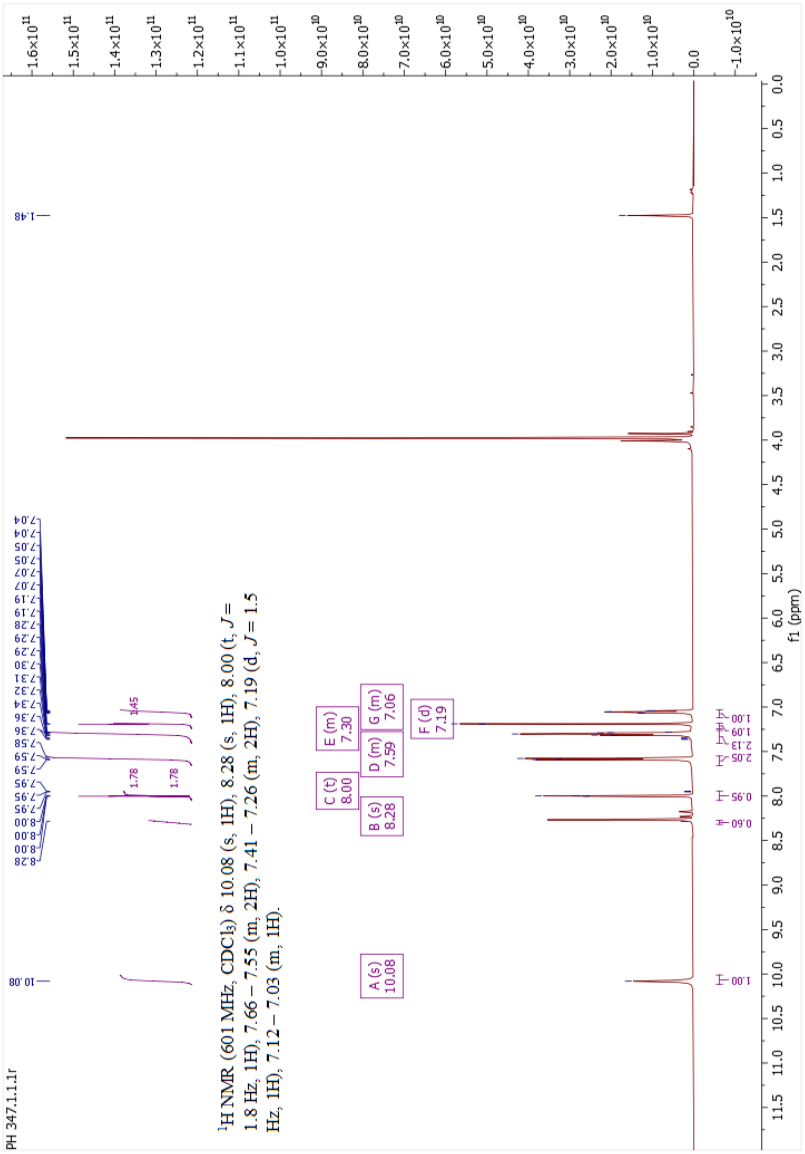
PH 347.1.1.1r
^{1}H NMR (601 MHz, $CDCl_3$) δ 10.08 (s, 1H), 8.28 (s, 1H), 8.00 (t, J = 1.8 Hz, 1H), 7.66 – 7.55 (m, 2H), 7.41 – 7.26 (m, 2H), 7.19 (d, J = 1.5 Hz, 1H), 7.12 – 7.03 (m, 1H).
A (s) 10.08
B (s) 8.28
C (t) 8.00
D (m) 7.59
E (m) 7.30
F (d) 7.19
G (m) 7.06
f1 (ppm)

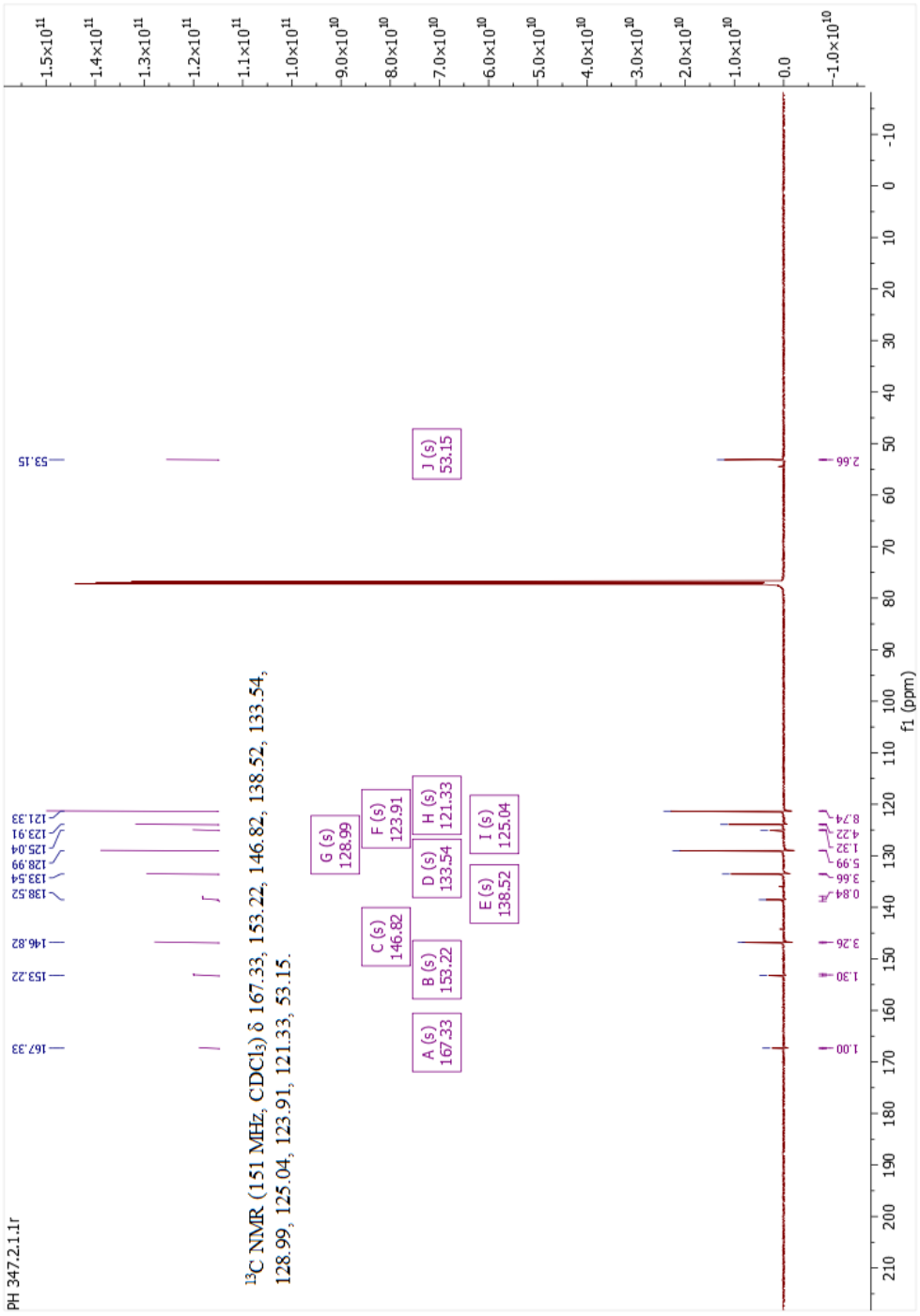
PH 347.2.1.1r
^{13}C NMR (151 MHz, $CDCl_3$) δ 167.33, 153.22, 146.82, 138.52, 133.54, 128.99, 125.04, 123.91, 121.33, 53.15.
A (s) 167.33
B (s) 153.22
C (s) 146.82
D (s) 133.54
E (s) 138.52
F (s) 123.91
G (s) 128.99
H (s) 121.33
I (s) 125.04
J (s) 53.15
f1 (ppm)

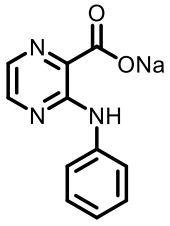
O
ONa
N
N
NH

POAA034

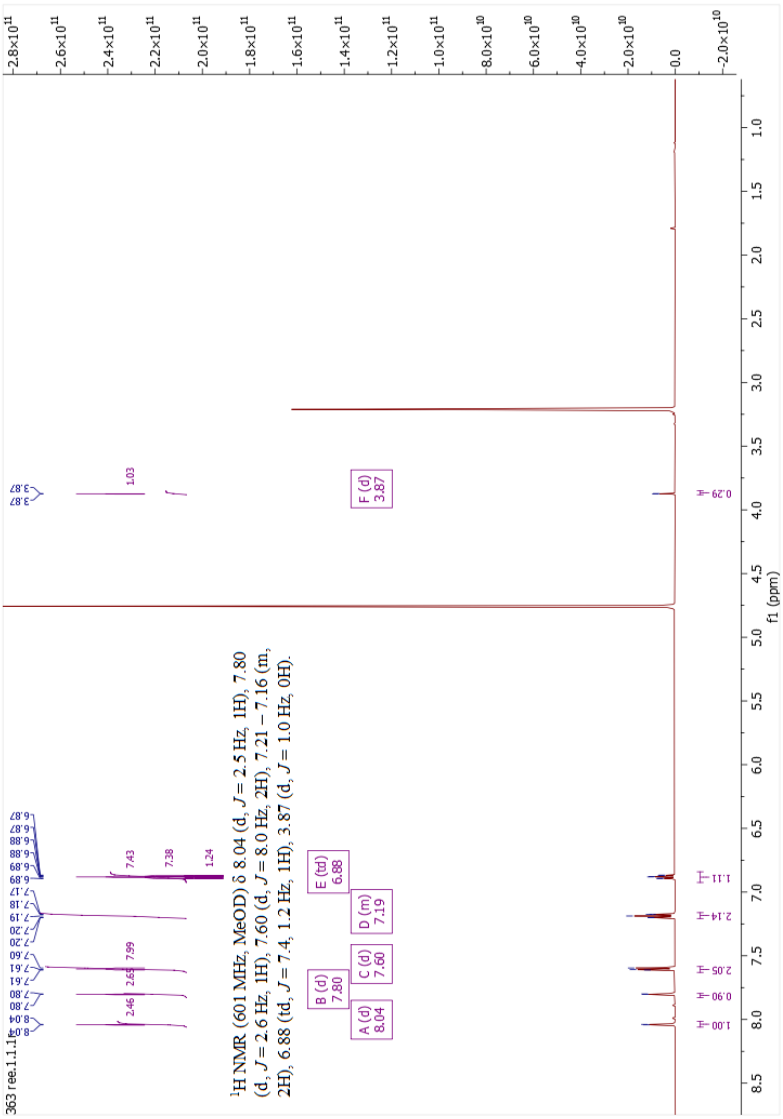
^{1}H NMR (601 MHz, MeOD) δ 8.04 (d, J = 2.5 Hz, 1H), 7.80 (d, J = 2.6 Hz, 1H), 7.60 (d, J = 8.0 Hz, 2H), 7.21 – 7.16 (m, 2H), 6.88 (td, J = 7.4, 1.2 Hz, 1H), 3.87 (d, J = 1.0 Hz, 0H).
A (d) 8.04
B (d) 7.80
C (d) 7.60
D (m) 7.19
E (td) 6.88
F (d) 3.87
f1 (ppm)

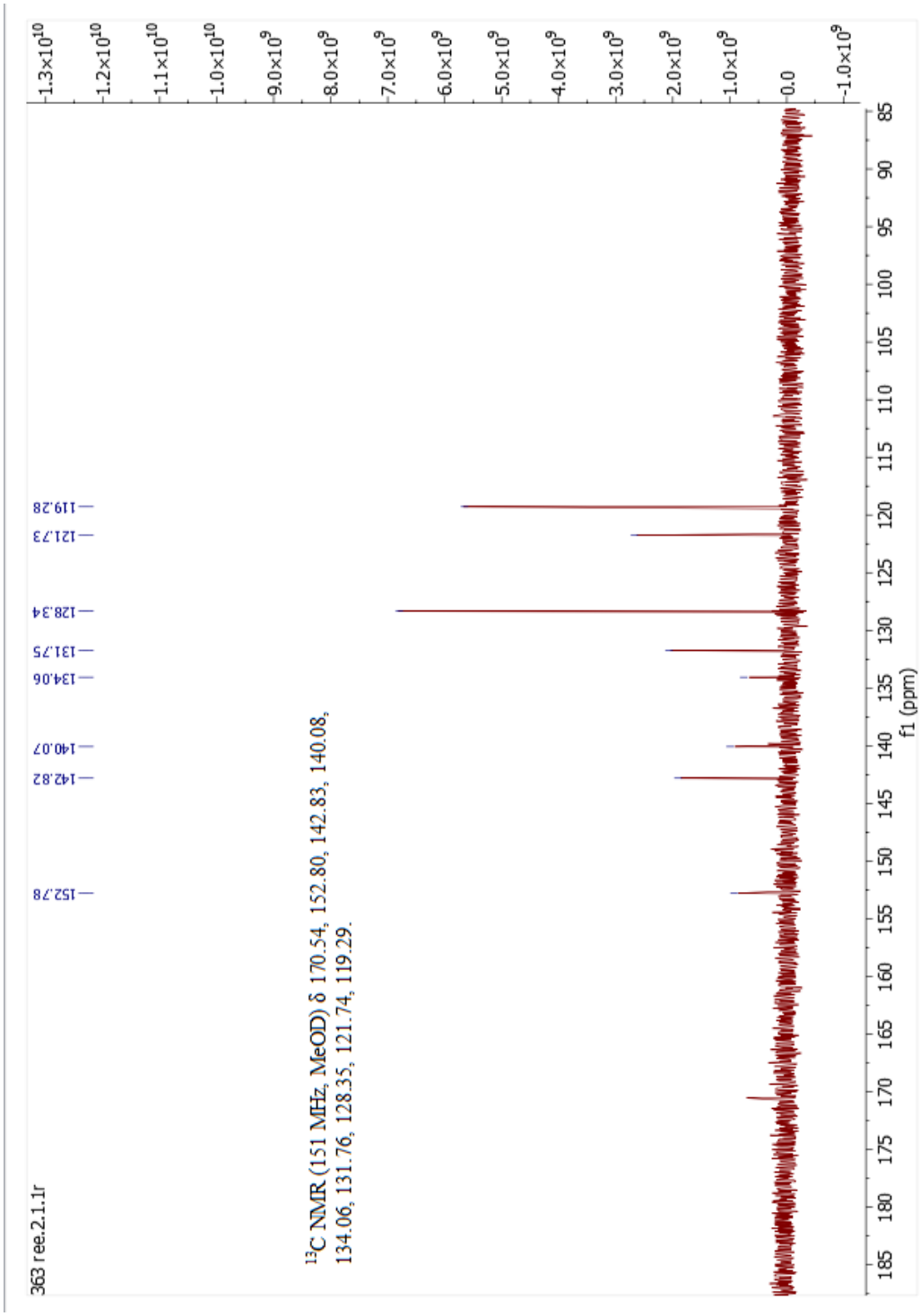
363 ree.2.1.1r
^{13}C NMR (151 MHz, MeOD) δ 170.54, 152.80, 142.83, 140.08, 134.06, 131.76, 128.35, 121.74, 119.29.
119.28
121.73
128.34
131.75
134.06
140.07
142.82
152.78
f1 (ppm)

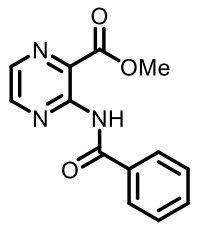
O
OMe
N
N
NH
O

POAA010-OMe

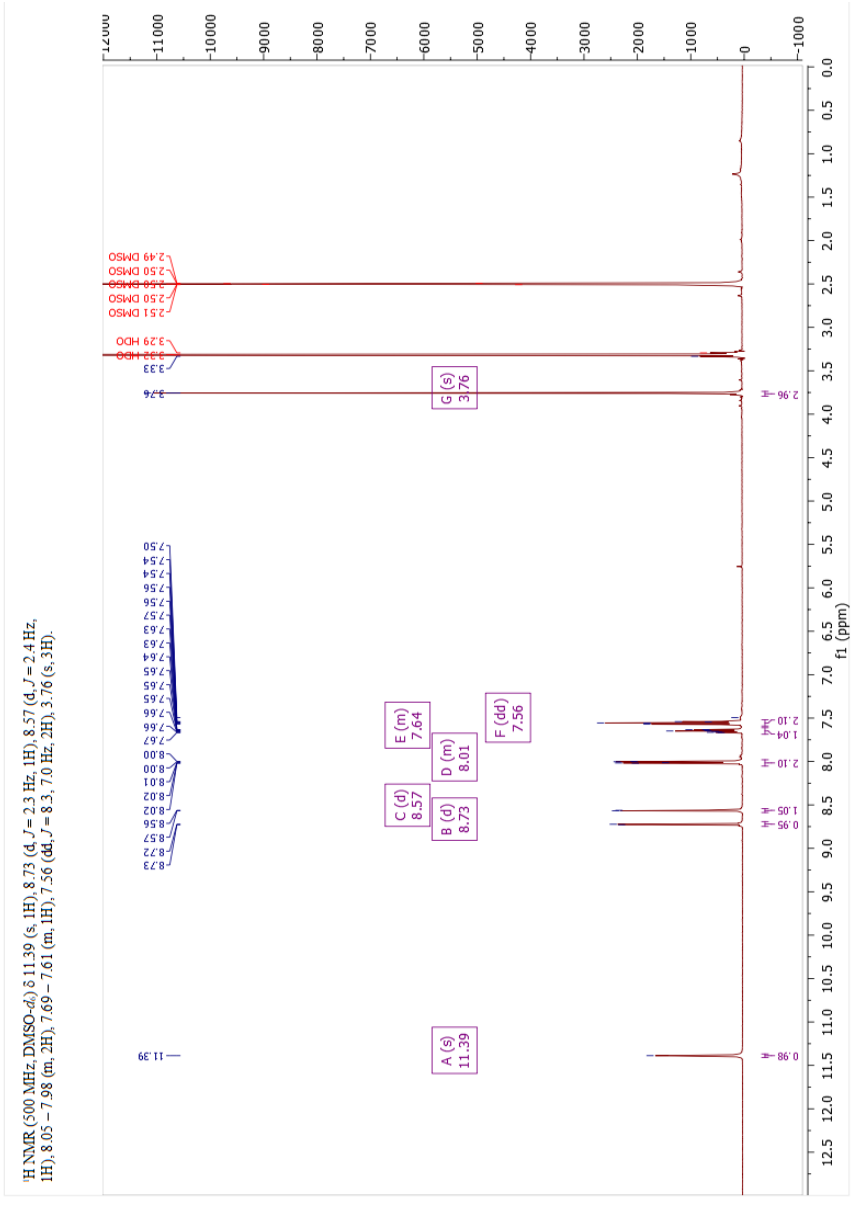
^{1}H NMR (500 MHz, DMSO-d_6) δ 11.39 (s, 1H), 8.73 (d, J = 2.3 Hz, 1H), 8.57 (d, J = 2.4 Hz, 1H), 8.05 – 7.98 (m, 2H), 7.69 – 7.61 (m, 1H), 7.56 (dd, J = 8.3, 7.0 Hz, 2H), 3.76 (s, 3H).
A (s) 11.39
B (d) 8.73
C (d) 8.57
D (m) 8.01
E (m) 7.64
F (dd) 7.56
G (s) 3.76
f1 (ppm)

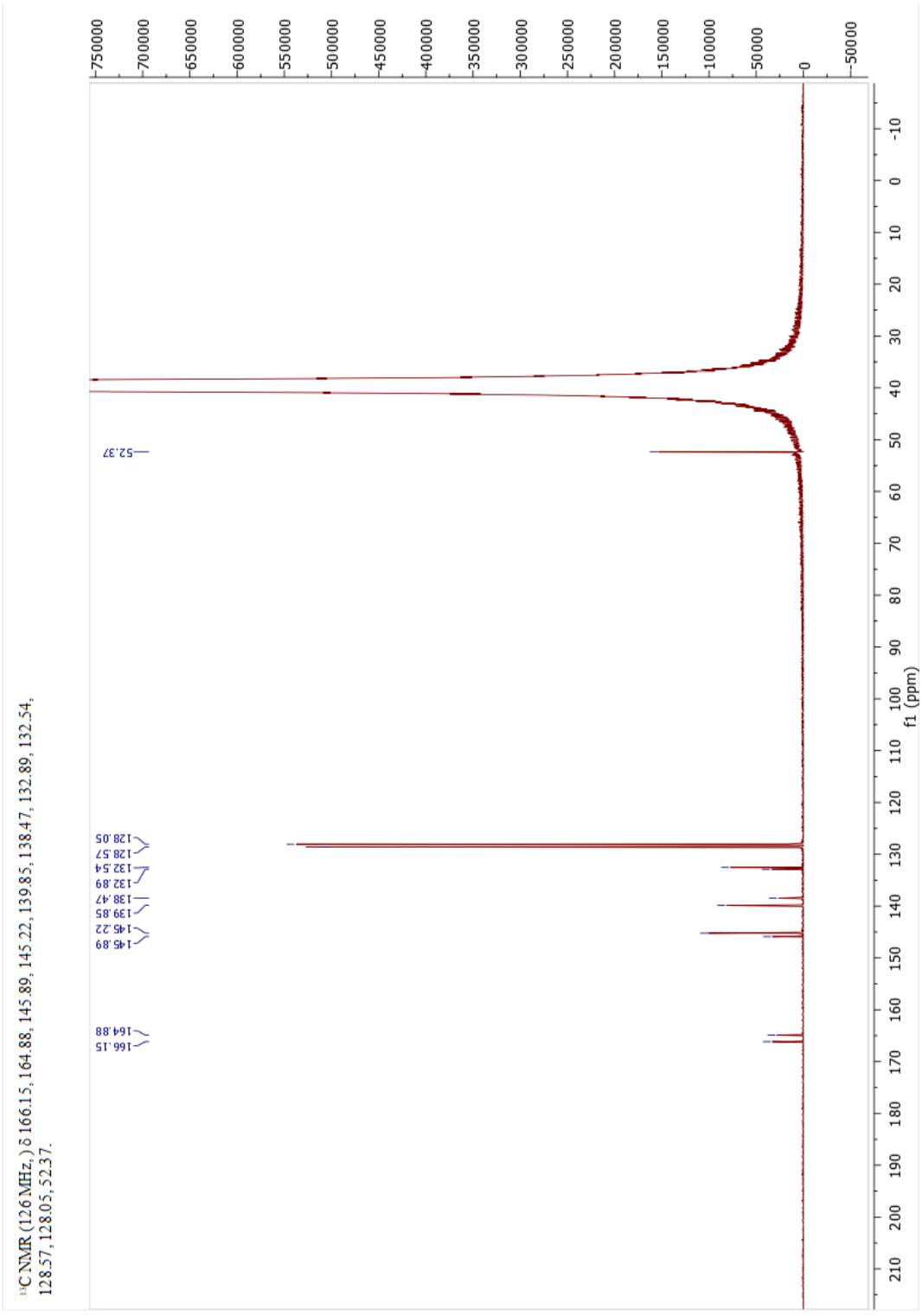

^{13}C NMR (126 MHz,) δ 166.15, 164.88, 145.89, 145.22, 139.85, 138.47, 132.89, 132.54, 128.57, 128.05, 52.37.

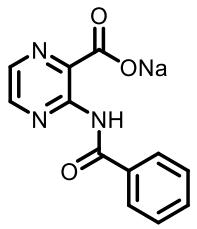
O
ONa
N
N
NH
O

POAA010

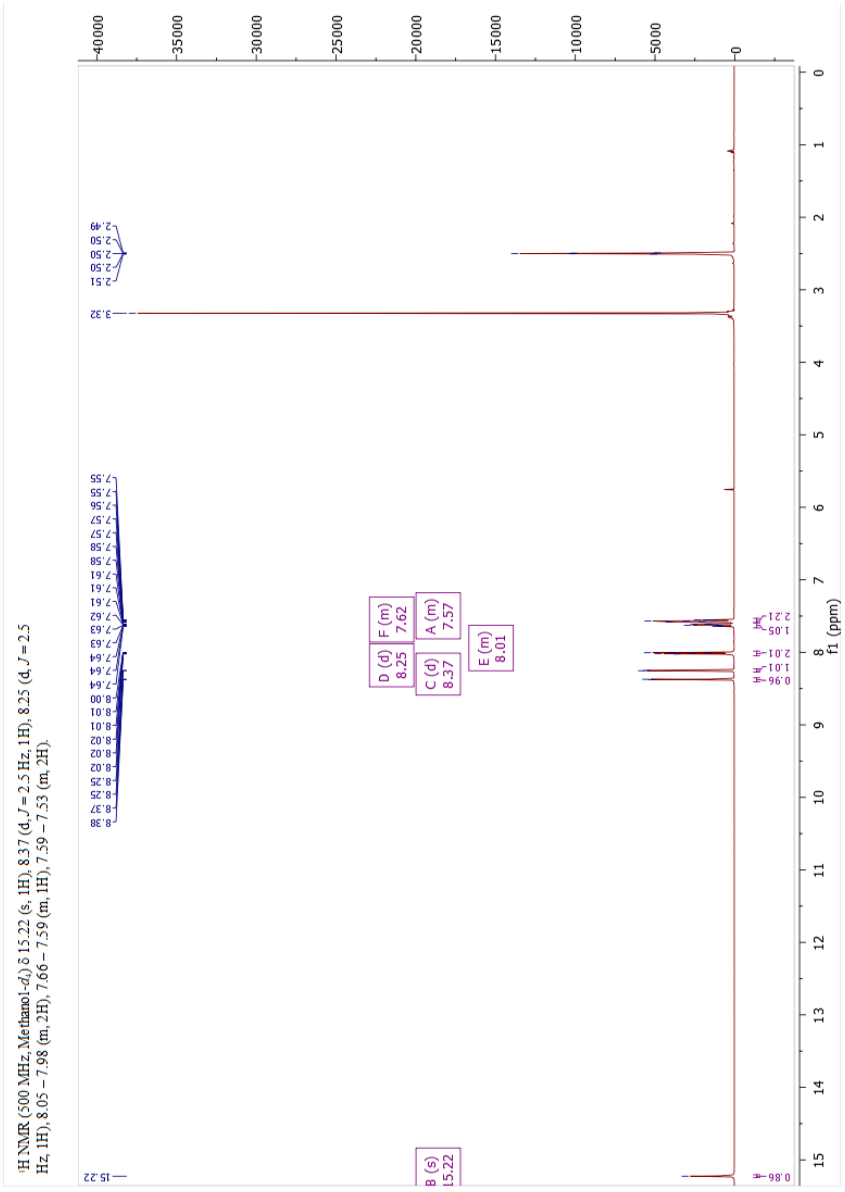
^{1}H NMR (500 MHz, Methanol-d_4) δ 15.22 (s, 1H), 8.37 (d, J = 2.5 Hz, 1H), 8.25 (d, J = 2.5 Hz, 1H), 8.05 – 7.98 (m, 2H), 7.66 – 7.59 (m, 1H), 7.59 – 7.53 (m, 2H).
B (s) 15.22
D (d) 8.25
C (d) 8.37
F (m) 7.62
A (m) 7.57
E (m) 8.01
f1 (ppm)

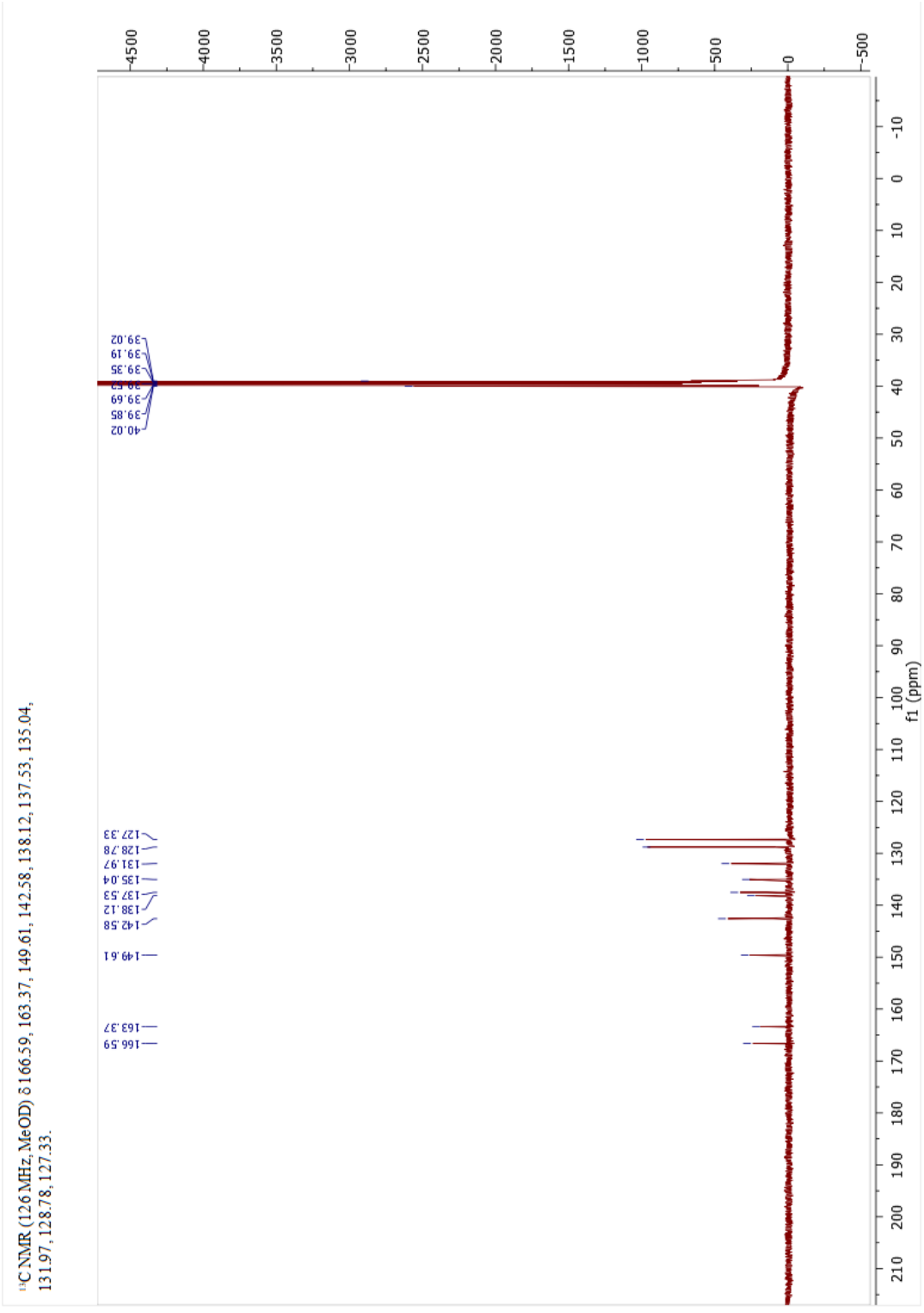
13C NMR (126 MHz, MeOD) δ 166.59, 163.37, 149.61, 142.58, 138.12, 137.53, 135.04, 131.97, 128.78, 127.33.
166.59
163.37
149.61
142.58
138.12
137.53
135.04
131.97
128.78
127.33
40.02
39.85
39.69
39.52
39.35
39.19
39.02
f1 (ppm)

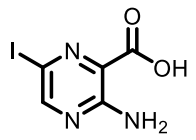
O
I
N
OH
N
NH2

POAA016

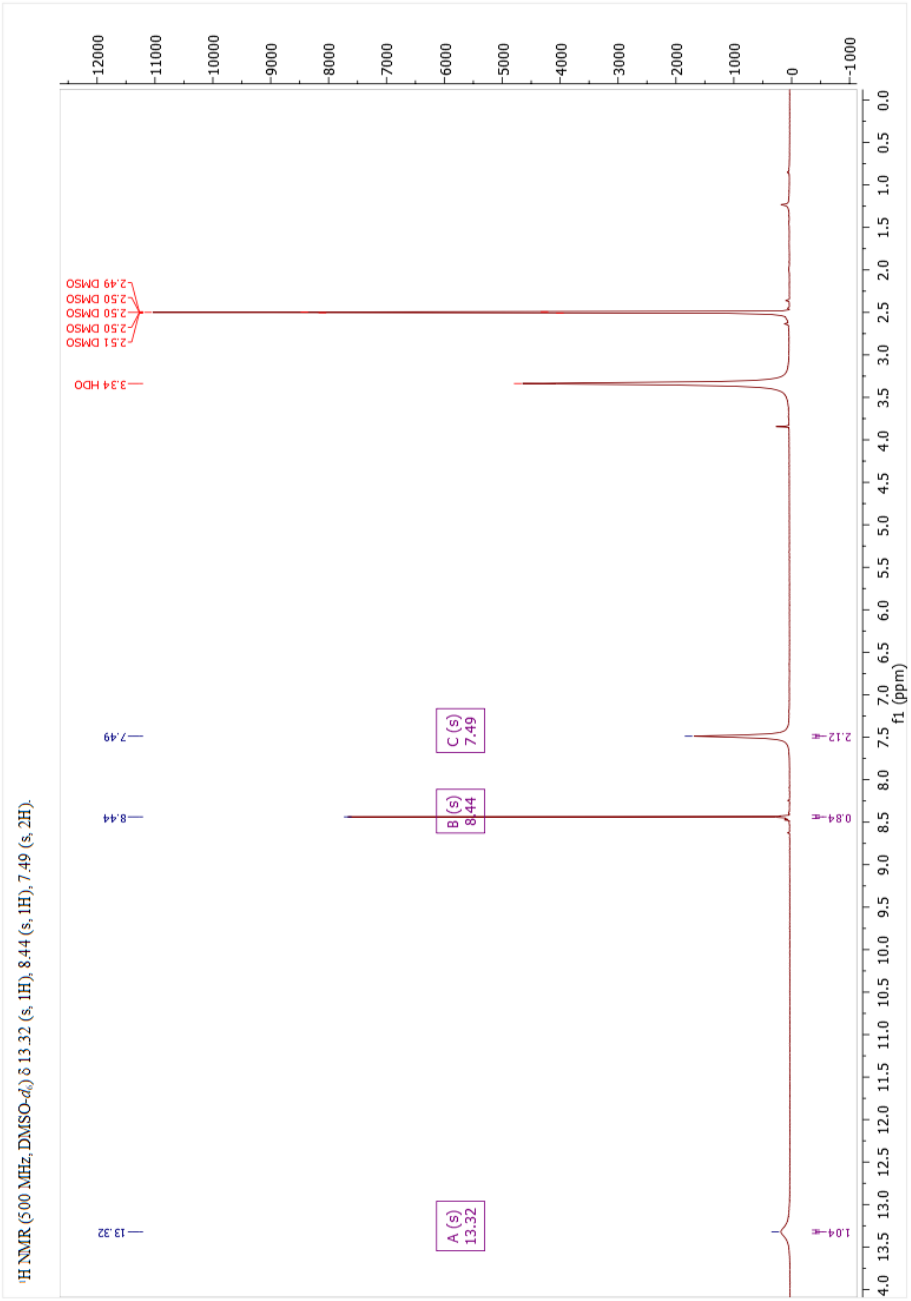
12000
11000
10000
9000
8000
7000
6000
5000
4000
3000
2000
1000
0
-1000
0.0
0.5
1.0
1.5
2.0
2.5
3.0
3.5
4.0
4.5
5.0
5.5
6.0
6.5
7.0
7.5
8.0
8.5
9.0
9.5
10.0
10.5
11.0
11.5
12.0
12.5
13.0
13.5
14.0
f1 (ppm)
2.51 DMSO
2.50 DMSO
2.50 DMSO
2.50 DMSO
2.49 DMSO
3.34 HDO
7.49
8.44
13.32
2.12
0.84
1.04
C (s) 7.49
B (s) 8.44
A (s) 13.32
¹H NMR (500 MHz, DMSO-d6) δ 13.32 (s, 1H), 8.44 (s, 1H), 7.49 (s, 2H).

^{13}C NMR (126 MHz, DMSO) δ 167.11, 155.25, 154.45, 125.70, 97.49.

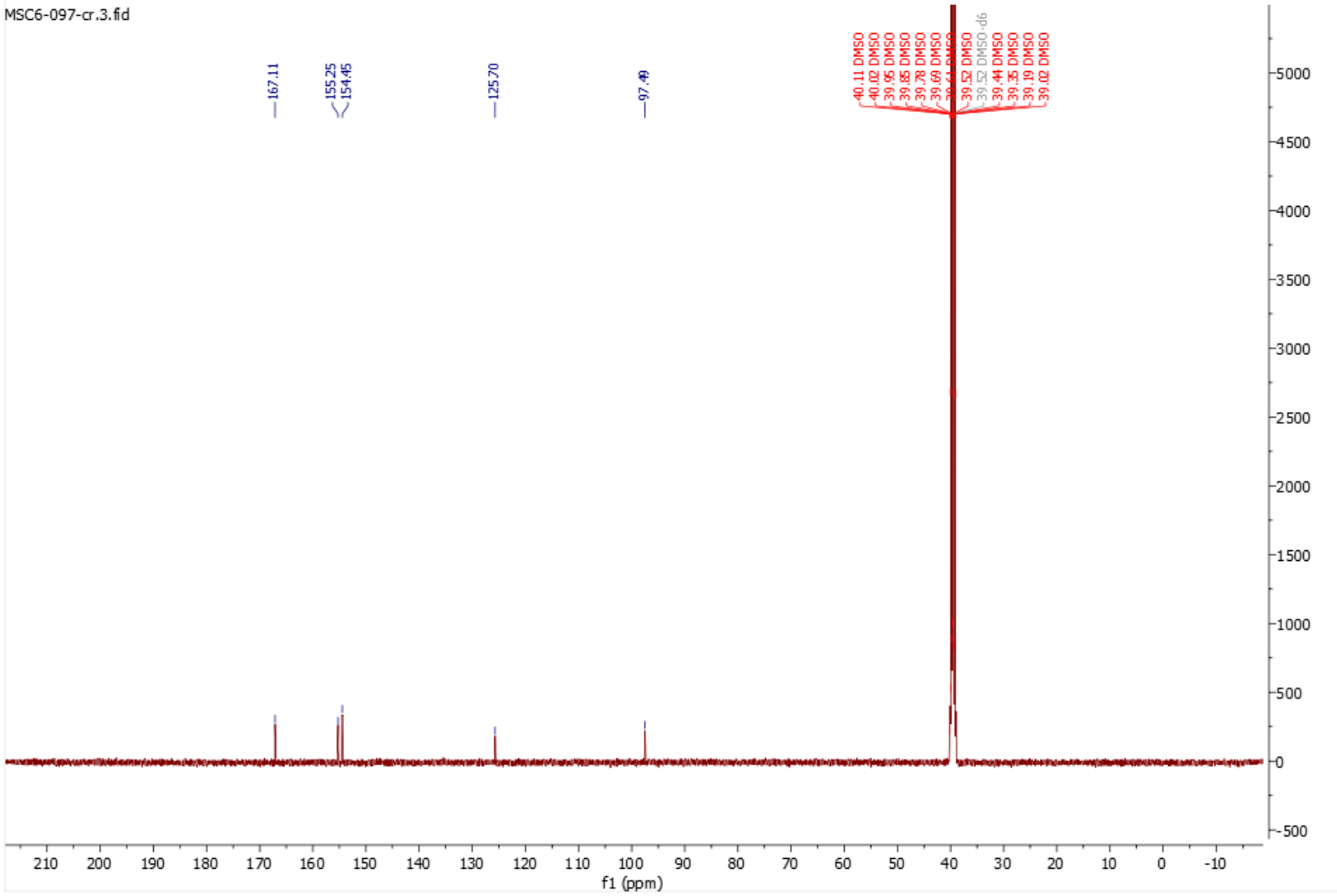

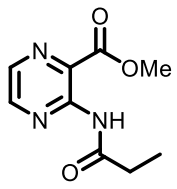
O
OMe
N
N
NH
O

POAA017-OMe

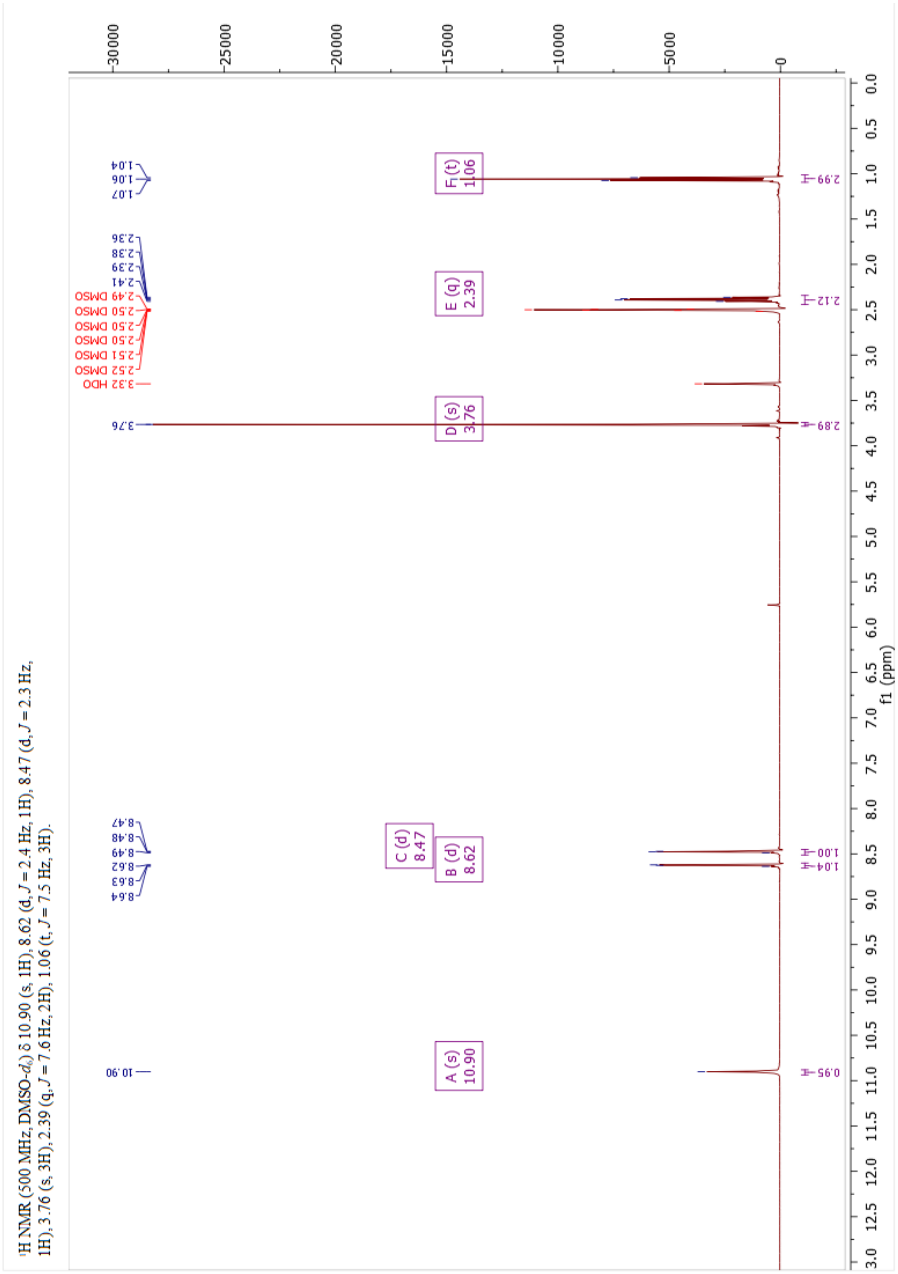
^{1}H NMR (500 MHz, DMSO-d_6) δ 10.90 (s, 1H), 8.62 (d, J = 2.4 Hz, 1H), 8.47 (d, J = 2.3 Hz, 1H), 3.76 (s, 3H), 2.39 (q, J = 7.6 Hz, 2H), 1.06 (t, J = 7.5 Hz, 3H).
A (s) 10.90
B (d) 8.62
C (d) 8.47
D (s) 3.76
E (q) 2.39
F (t) 1.06
f1 (ppm)

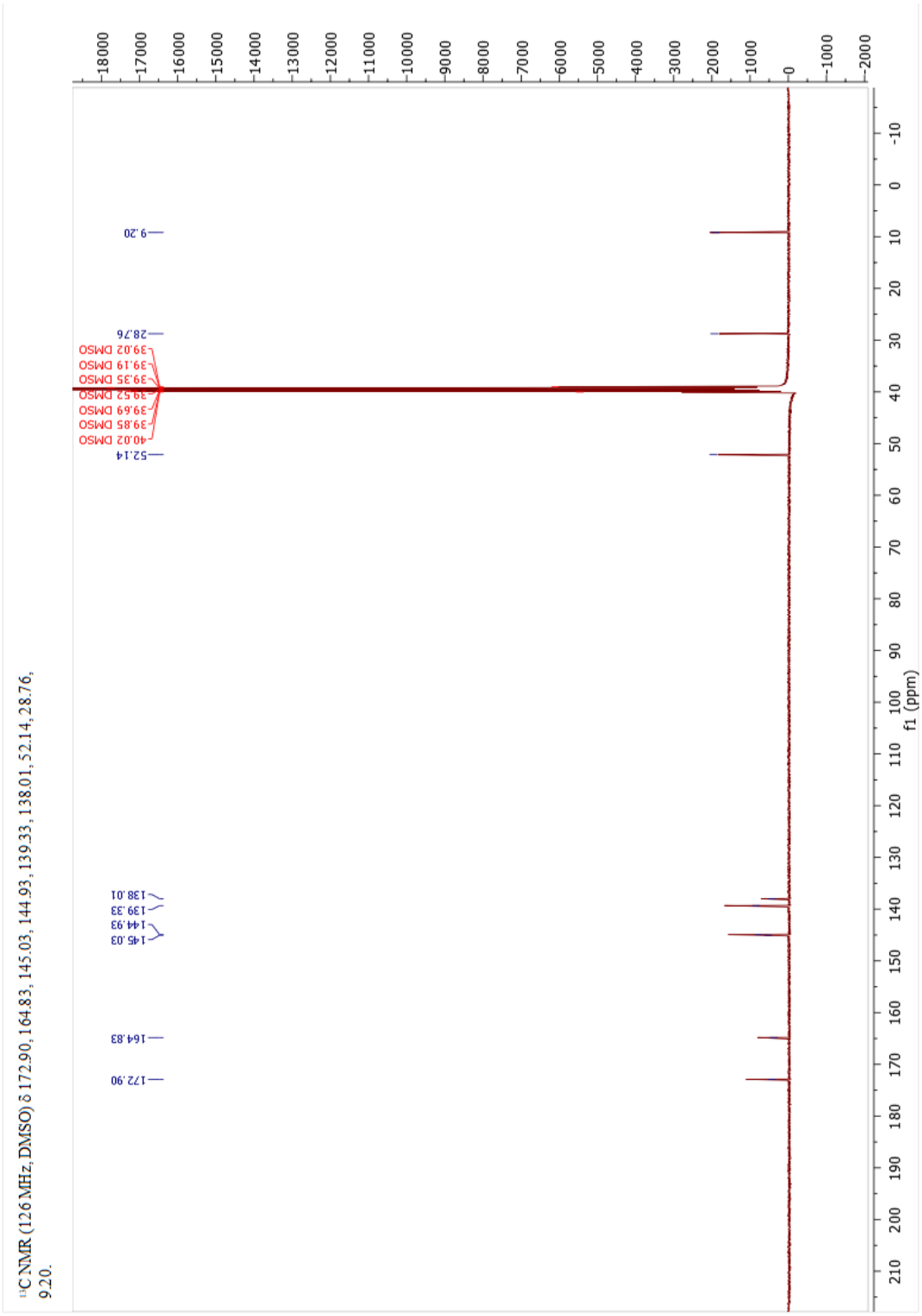

^{13}C NMR (126 MHz, DMSO) δ 172.90, 164.83, 145.03, 144.93, 139.33, 138.01, 52.14, 28.76, 9.20.

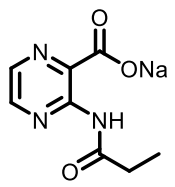

POAA017

^{1}H NMR (500 MHz, DMSO-d_6) δ 13.71 (s, 1H), 8.26 (d, J = 2.4 Hz, 1H), 8.16 (d, J = 2.5 Hz, 1H), 2.56 (q, J = 7.5 Hz, 2H), 1.09 (t, J = 7.5 Hz, 3H).

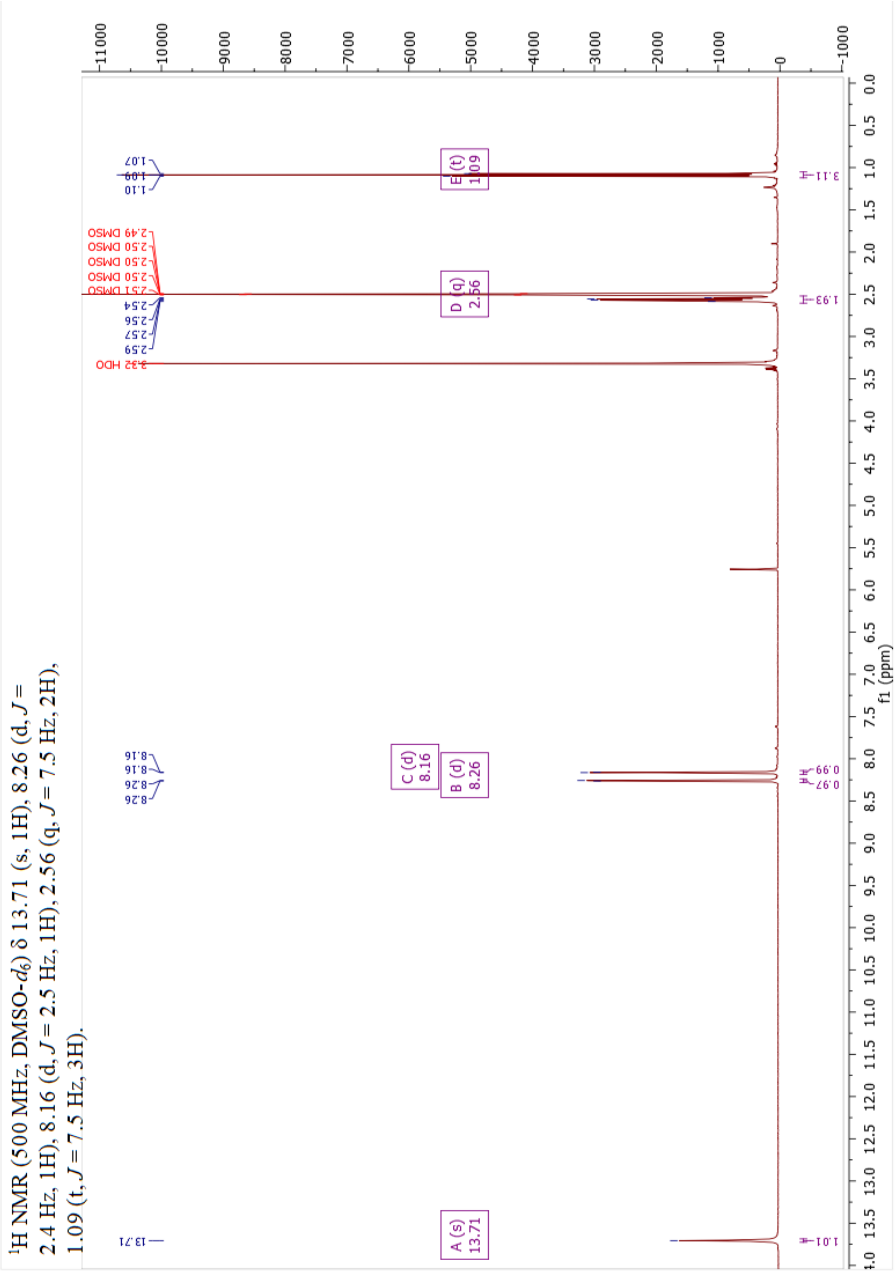

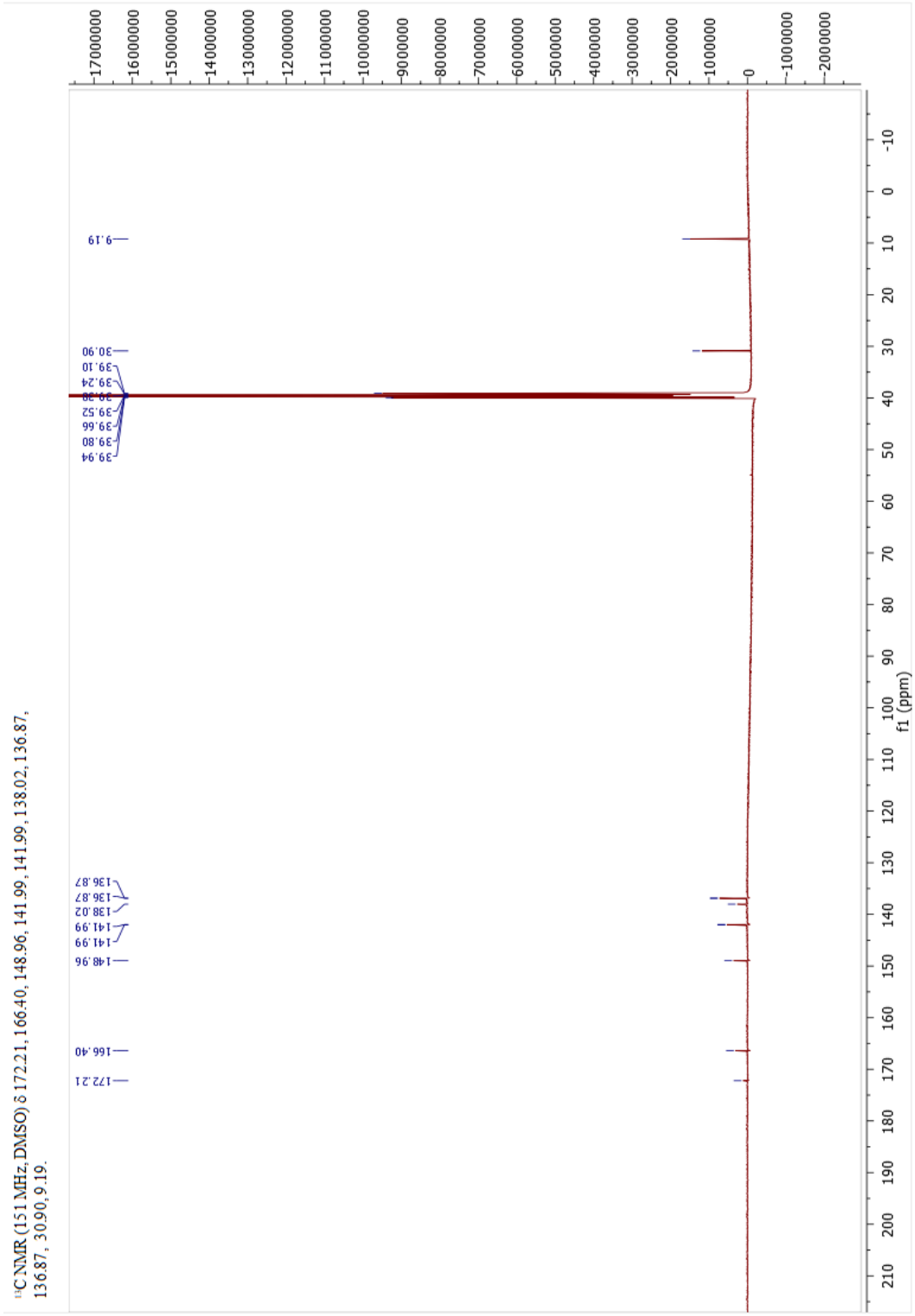

^{13}C NMR (151 MHz, DMSO) δ 172.21, 166.40, 148.96, 141.99, 141.99, 138.02, 136.87, 136.87, 30.90, 9.19.

^{1}H NMR (500 MHz, $CDCl_3$) δ 8.78 (d, J = 1.4 Hz, 1H), 7.97 (d, J = 1.4 Hz, 1H), 3.94 (s, 3H), 3.60 (q, J = 7.1 Hz, 4H), 1.23 (t, J = 7.1 Hz, 6H).

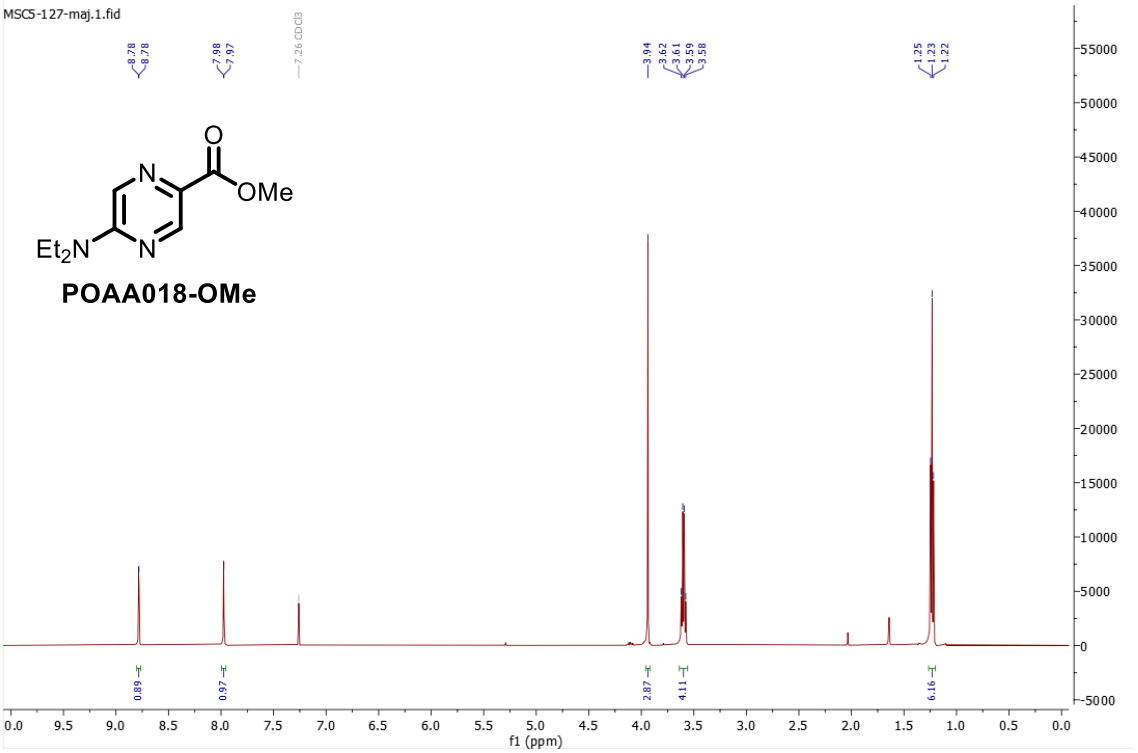

^{13}C NMR (126 MHz, $CDCl_3$) δ 165.65, 154.16, 146.01, 129.73, 128.88, 52.27, 43.01, 12.83.

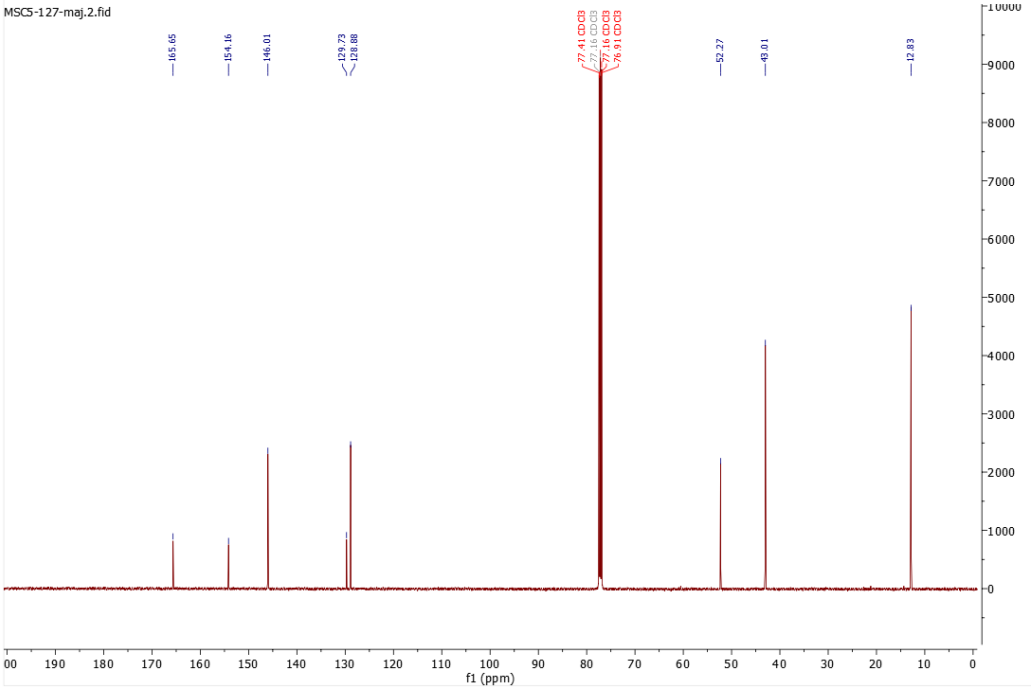

^{13}C NMR (126 MHz, MeOD) δ 172.70, 154.72, 145.12, 137.06, 129.16, 43.66, 13.04.

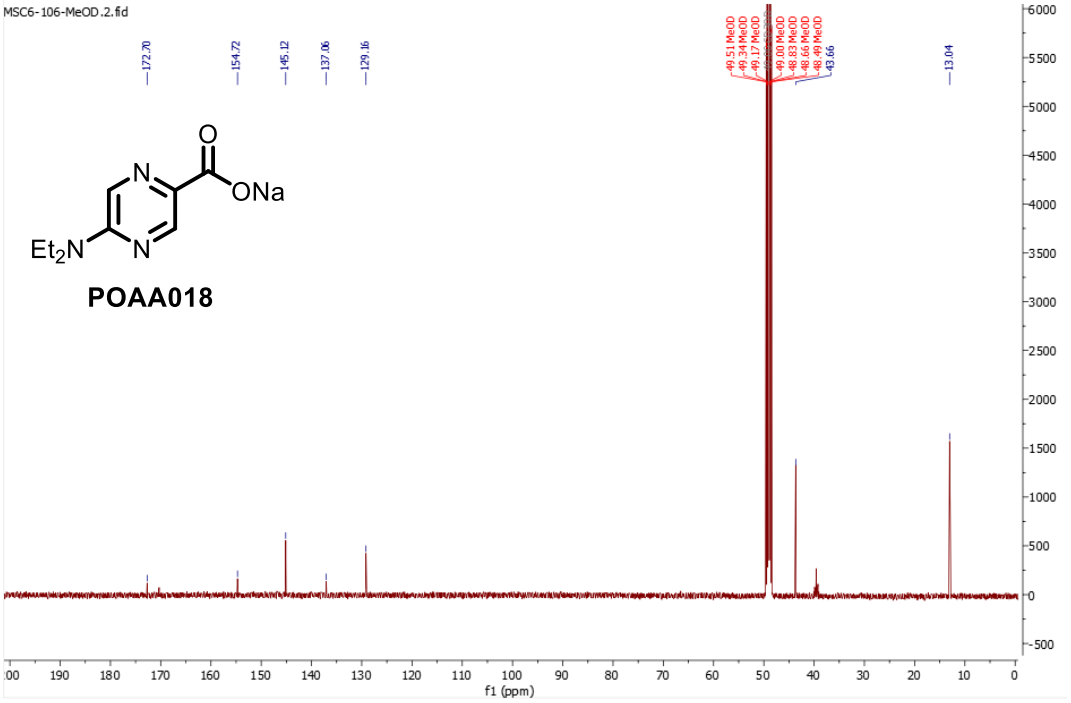

^{1}H NMR (500 MHz, MeOD) δ 8.69 (d, J = 1.4 Hz, 1H), 8.00 – 7.96 (m, 1H), 3.62 (q, J = 7.1 Hz, 4H), 1.23 (t, J = 7.1 Hz, 6H).

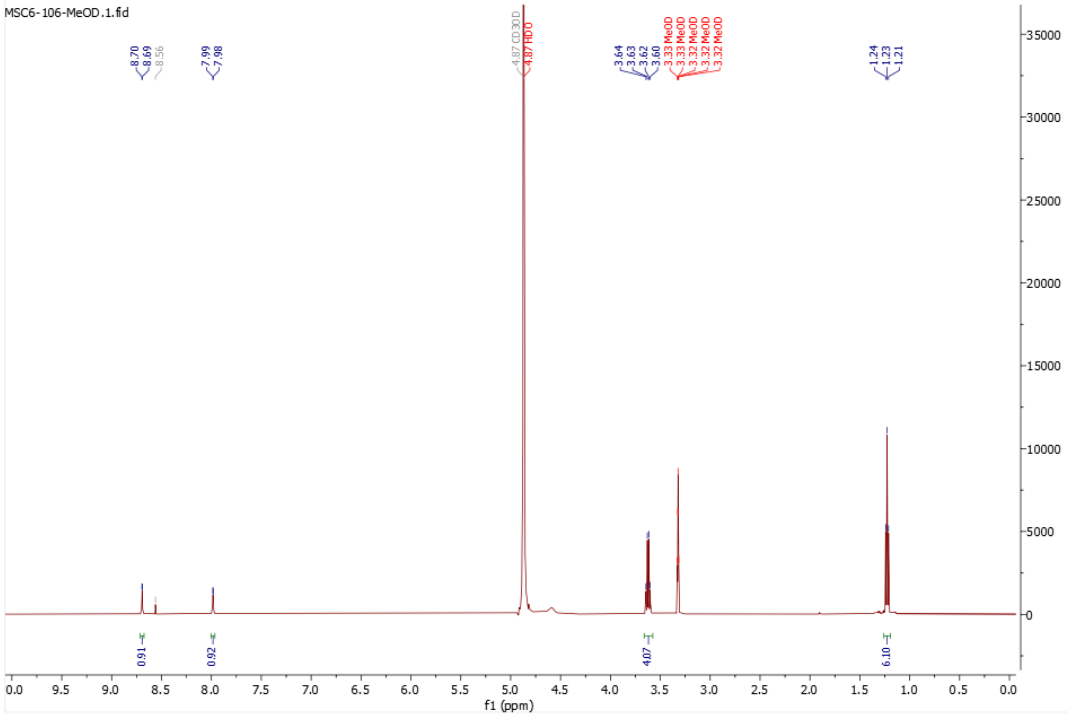

^{1}H NMR (500 MHz, $CDCl_3$) δ 9.34 (d, J = 1.5 Hz, 1H), 9.13 (d, J = 1.5 Hz, 1H), 8.14 – 8.07 (m, 2H), 7.59 – 7.50 (m, 3H), 4.06 (s, 3H).

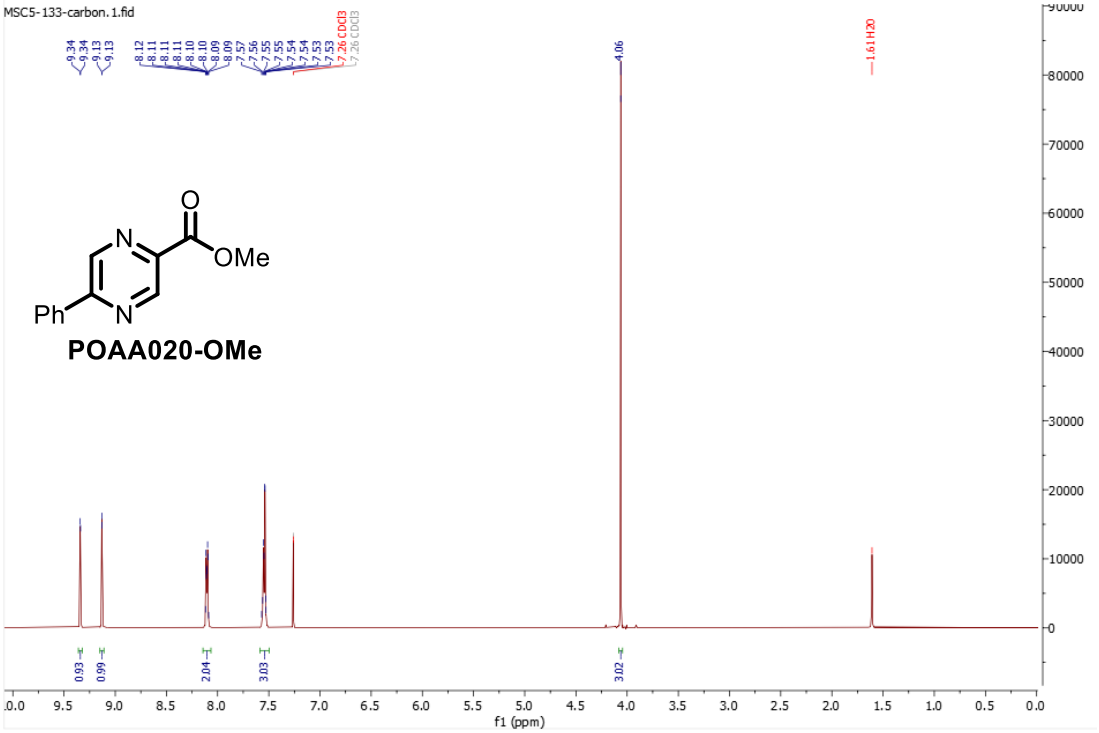

POAA020-OMe

^{13}C NMR (126 MHz, $CDCl_3$) δ 164.72, 155.41, 145.82, 141.53, 141.10, 135.42, 131.16, 129.40, 127.66, 53.20.

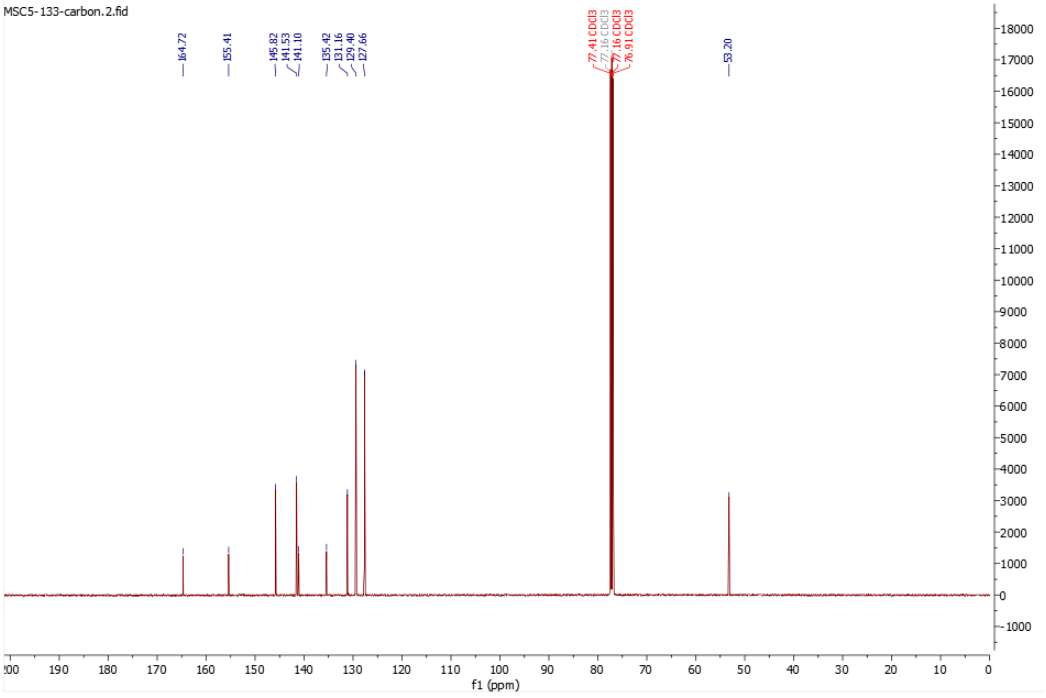

^{1}H NMR (500 MHz, MeOD) δ 9.22 (d, J = 1.5 Hz, 1H), 9.10 (d, J = 1.6 Hz, 1H), 8.15 – 8.09 (m, 2H), 7.59 – 7.48 (m, 3H).

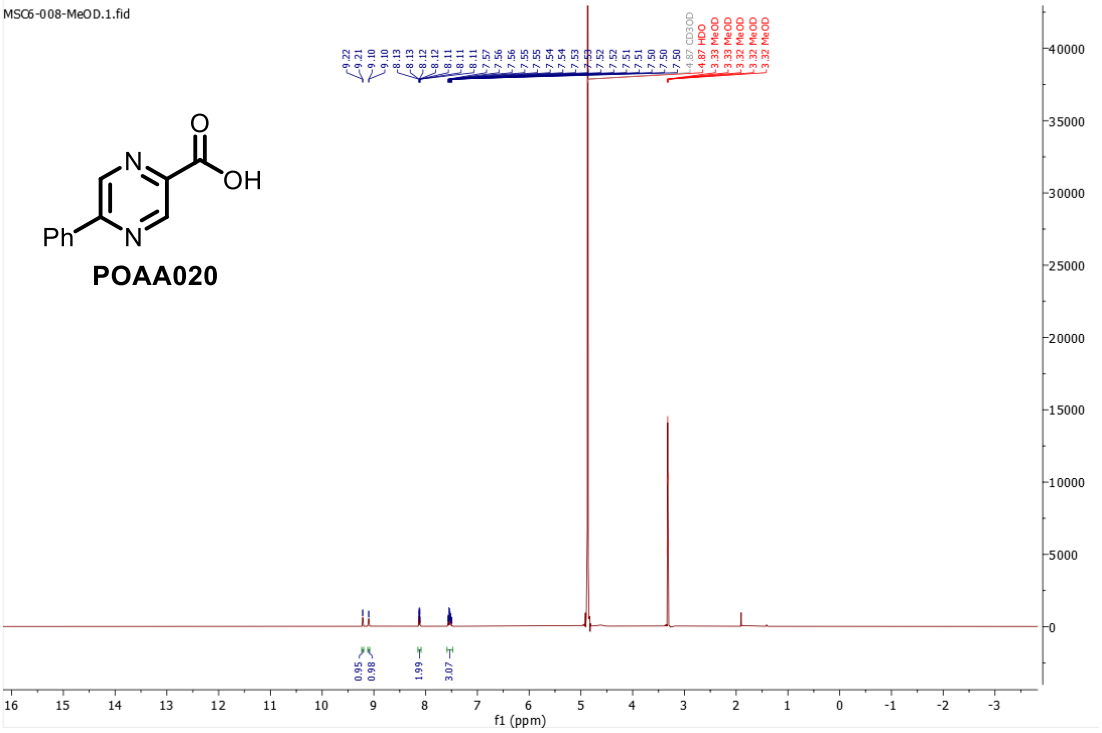

^{13}C NMR (126 MHz, MeOD) δ 169.47, 155.23, 149.93, 145.82, 141.85, 137.38, 131.23, 130.13, 128.25.

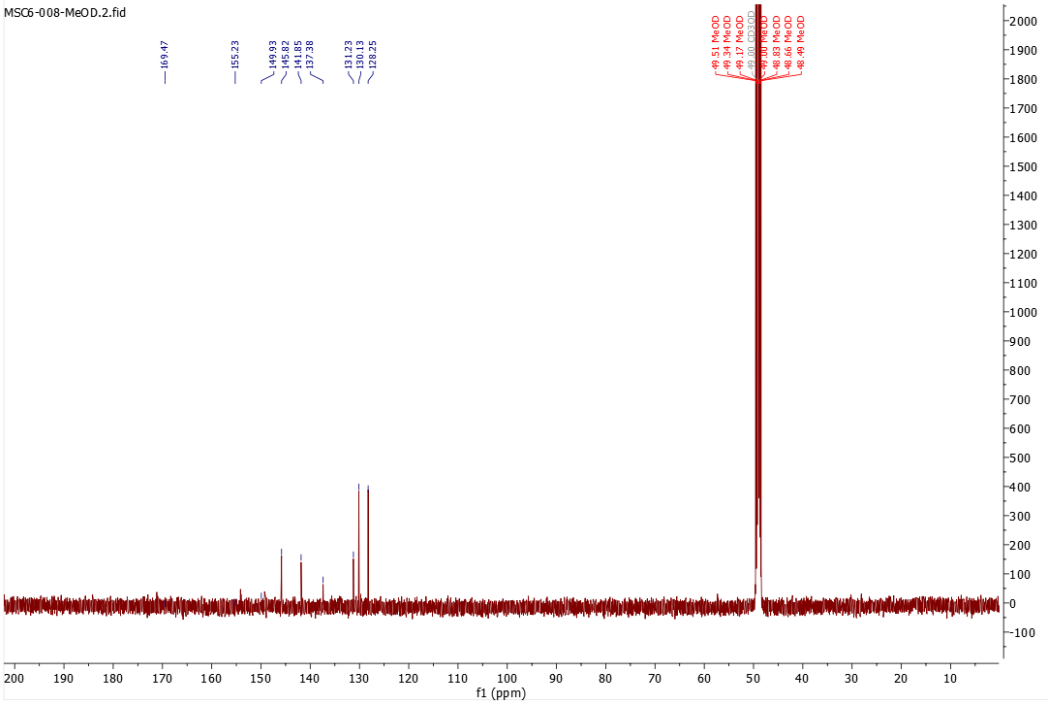

^{1}H NMR (500 MHz, $CDCl_3$) δ 8.76 (d, J = 1.3 Hz, 1H), 7.91 (d, J = 1.3 Hz, 1H), 3.95 (s, 3H), 3.28 (t, J = 6.4 Hz, 2H), 1.93 (dt, J = 13.4, 6.7 Hz, 1H), 1.00 (d, J = 6.7 Hz, 6H).

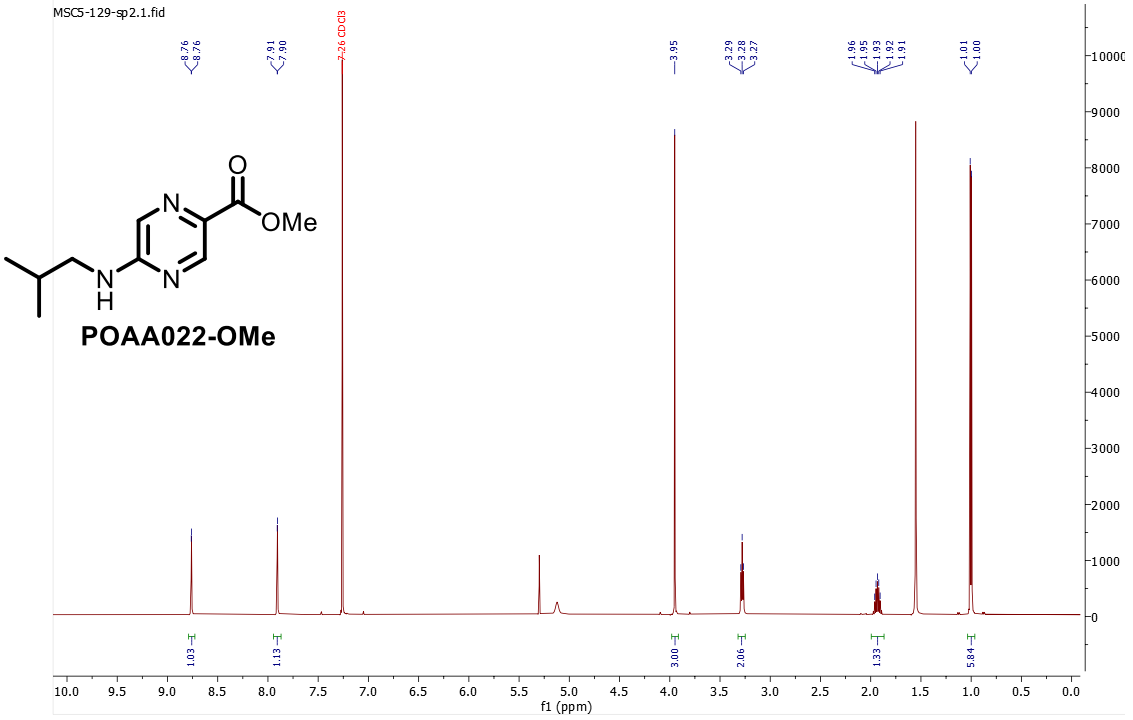

POAA022-OMe

^{13}C NMR (126 MHz, $CDCl_3$) δ 165.28, 155.81, 145.89, 52.27, 48.97, 28.33, 20.18.

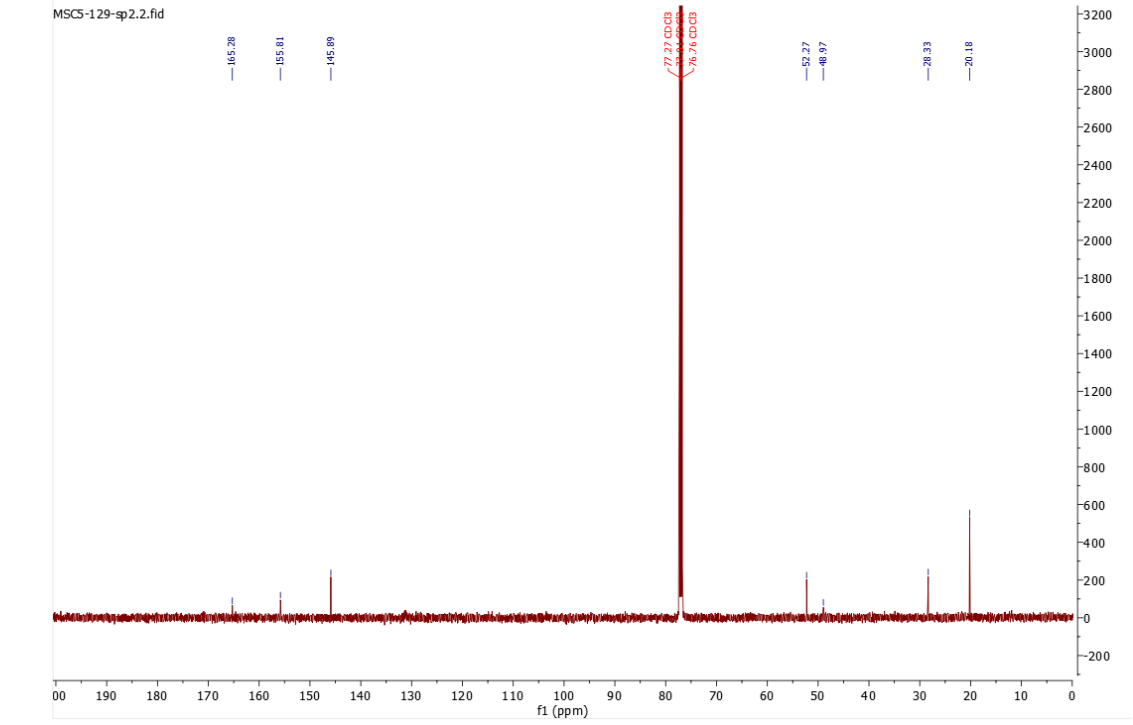

^{1}H NMR (500 MHz, MeOD) δ 8.62 (s, 1H), 7.90 (s, 1H), 3.22 (d, J = 6.9 Hz, 2H), 1.92 (hept, J = 6.7 Hz, 1H), 0.98 (d, J = 6.7 Hz, 6H).

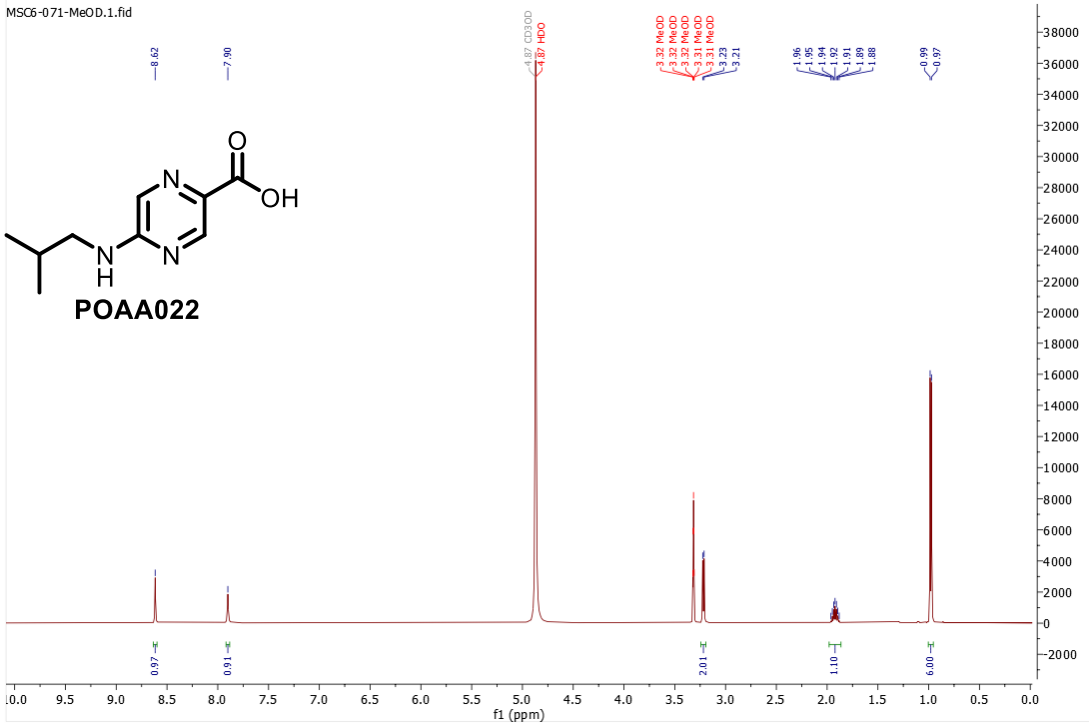

^{13}C NMR (126 MHz, MeOD) δ 170.12, 157.53, 145.83, 133.72, 29.26, 20.56.

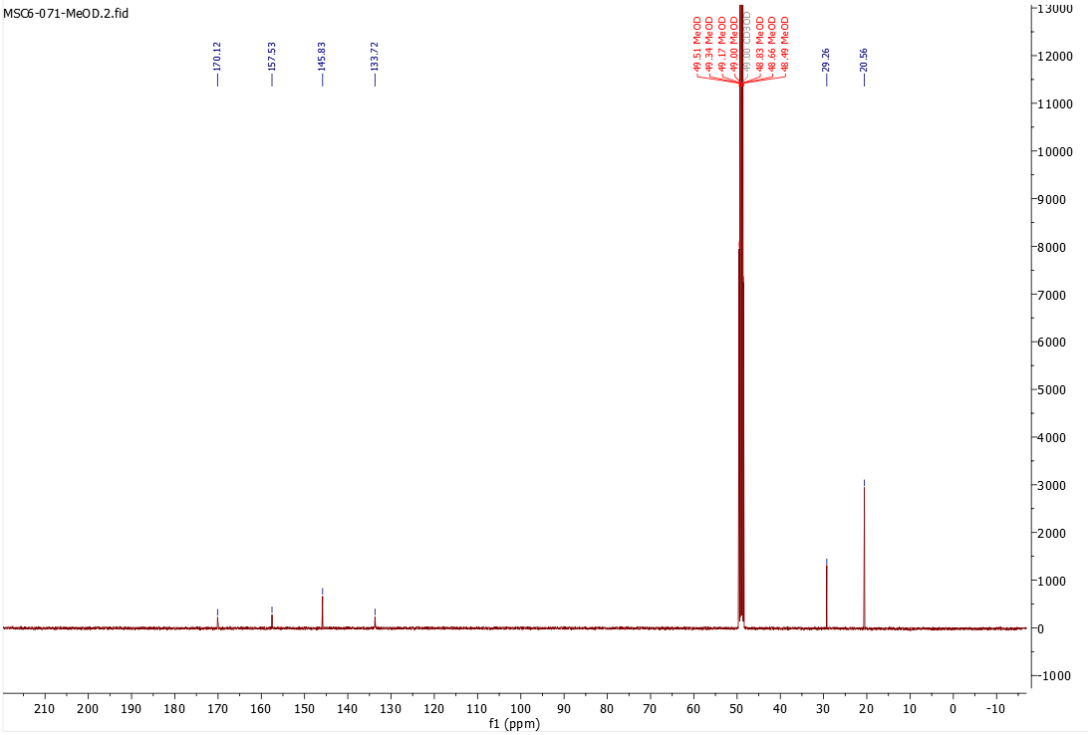

^{1}H NMR (500 MHz, $CDCl_3$) δ 9.38 (d, J = 1.4 Hz, 1H), 8.85 (d, J = 1.4 Hz, 1H), 7.49 (dd, J = 7.8, 1.5 Hz, 1H), 7.44 – 7.38 (m, 1H), 7.38 – 7.32 (m, 2H), 4.08 (s, 3H), 2.43 (s, 3H).

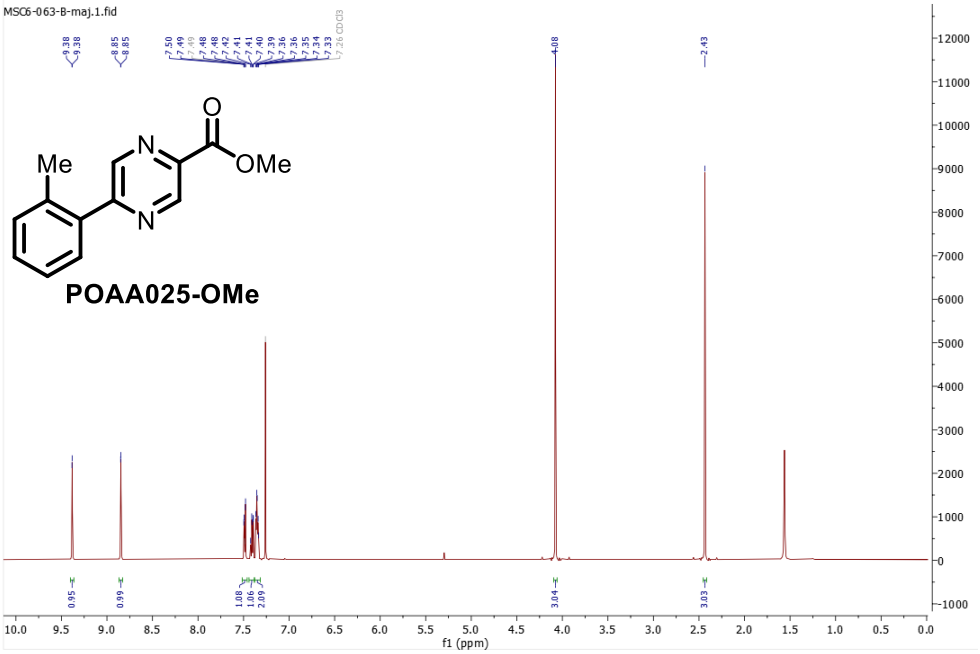

^{13}C NMR (126 MHz, $CDCl_3$) δ 164.76, 158.61, 145.37, 144.63, 140.69, 136.80, 135.94, 131.57, 130.15, 126.54, 53.26, 20.52.

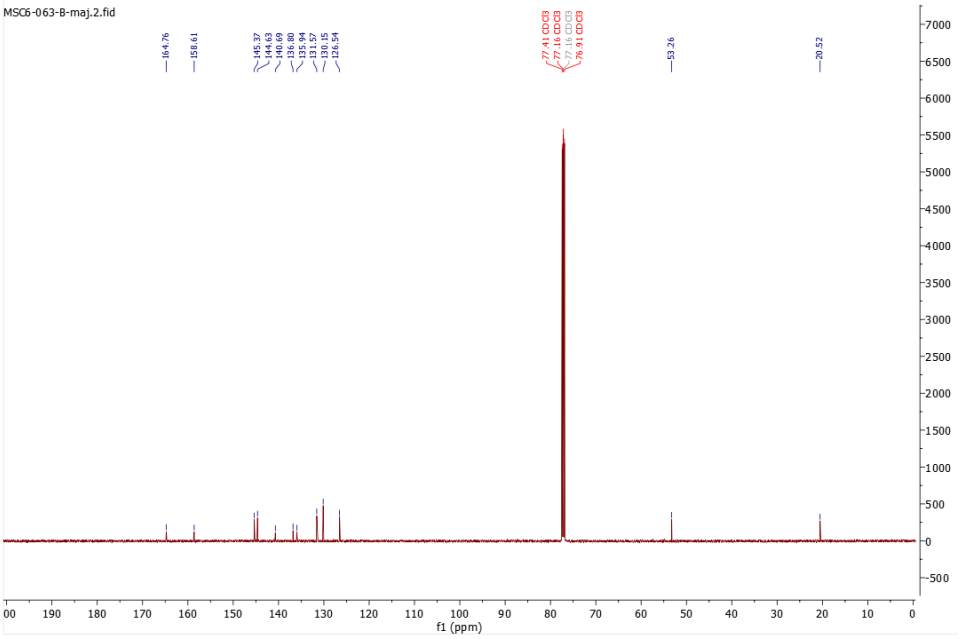

^{1}H NMR (500 MHz, MeOD) δ 9.25 (d, J = 1.5 Hz, 1H), 8.73 (d, J = 1.5 Hz, 1H), 7.45 (dd, J = 7.5, 1.5 Hz, 1H), 7.42 – 7.32 (m, 3H), 2.38 (s, 3H).

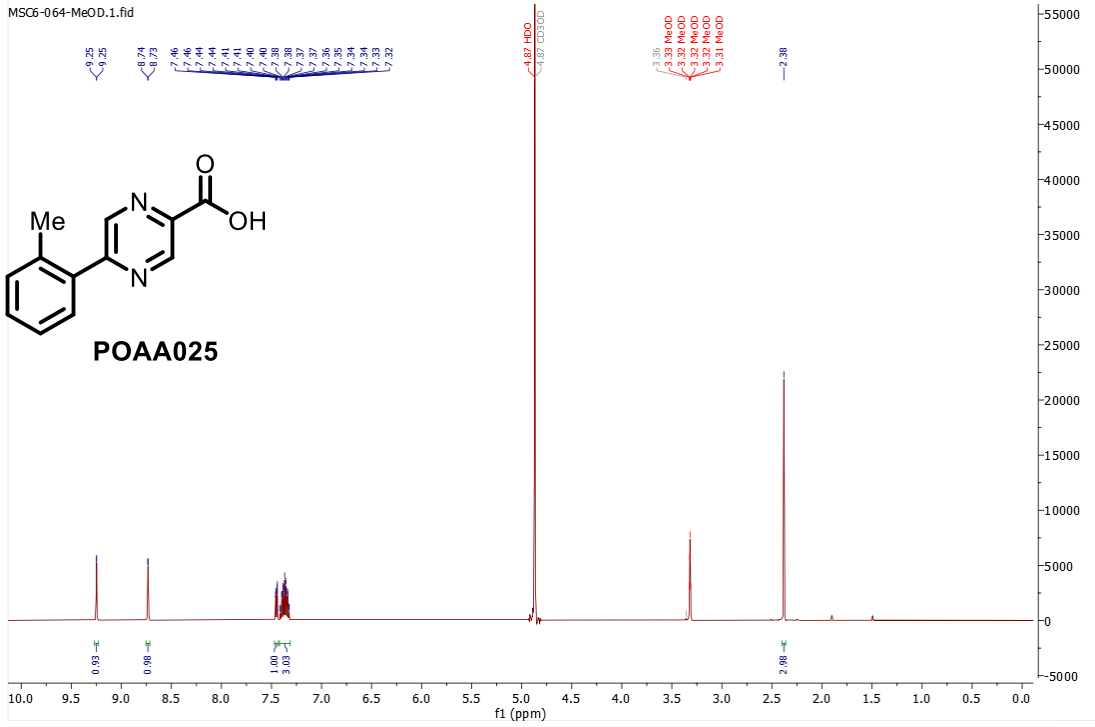

^{13}C NMR (126 MHz, MeOD) δ 170.89, 157.18, 148.87, 145.32, 144.86, 137.77, 137.69, 132.10, 130.85, 130.55, 127.26, 20.34.

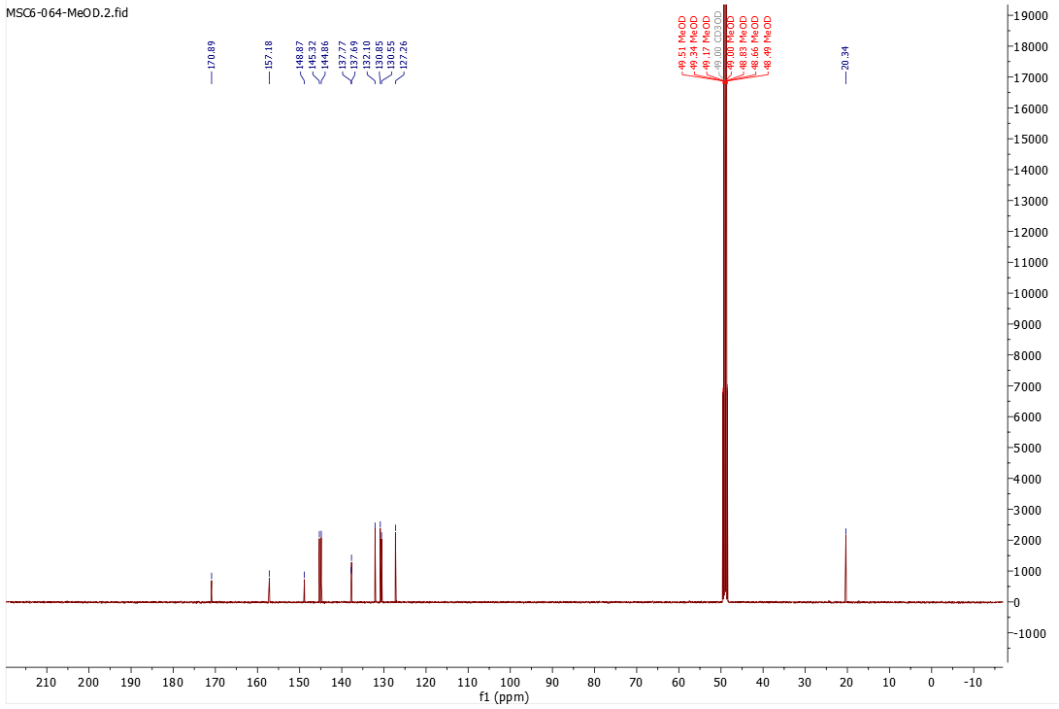

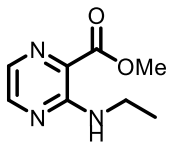

POAA039-OMe

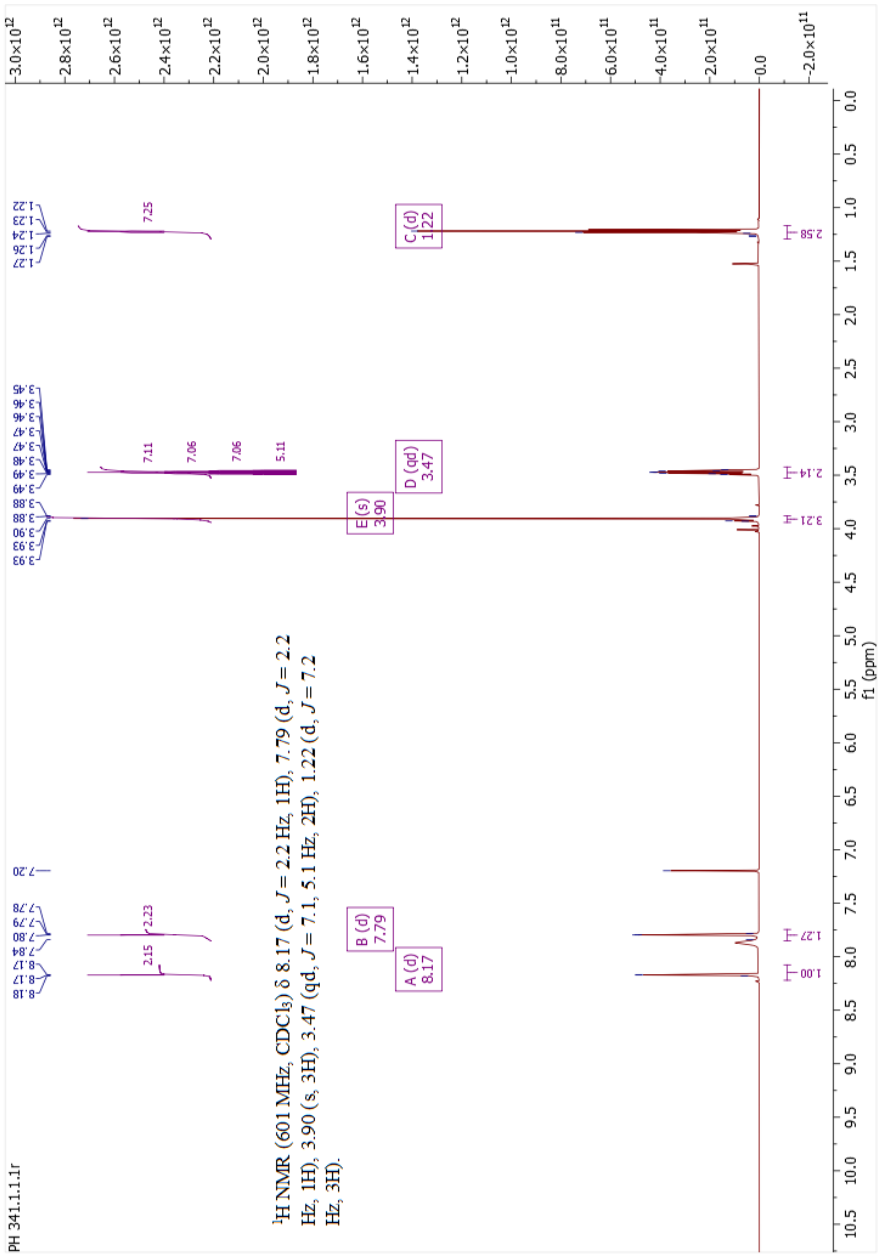
PH 341.1.1.1r
^{1}H NMR (601 MHz, $CDCl_3$) δ 8.17 (d, J = 2.2 Hz, 1H), 7.79 (d, J = 2.2 Hz, 1H), 3.90 (s, 3H), 3.47 (qd, J = 7.1, 5.1 Hz, 2H), 1.22 (d, J = 7.2 Hz, 3H).
A (d) 8.17
B (d) 7.79
E (s) 3.90
D (qd) 3.47
C (d) 1.22
f1 (ppm)

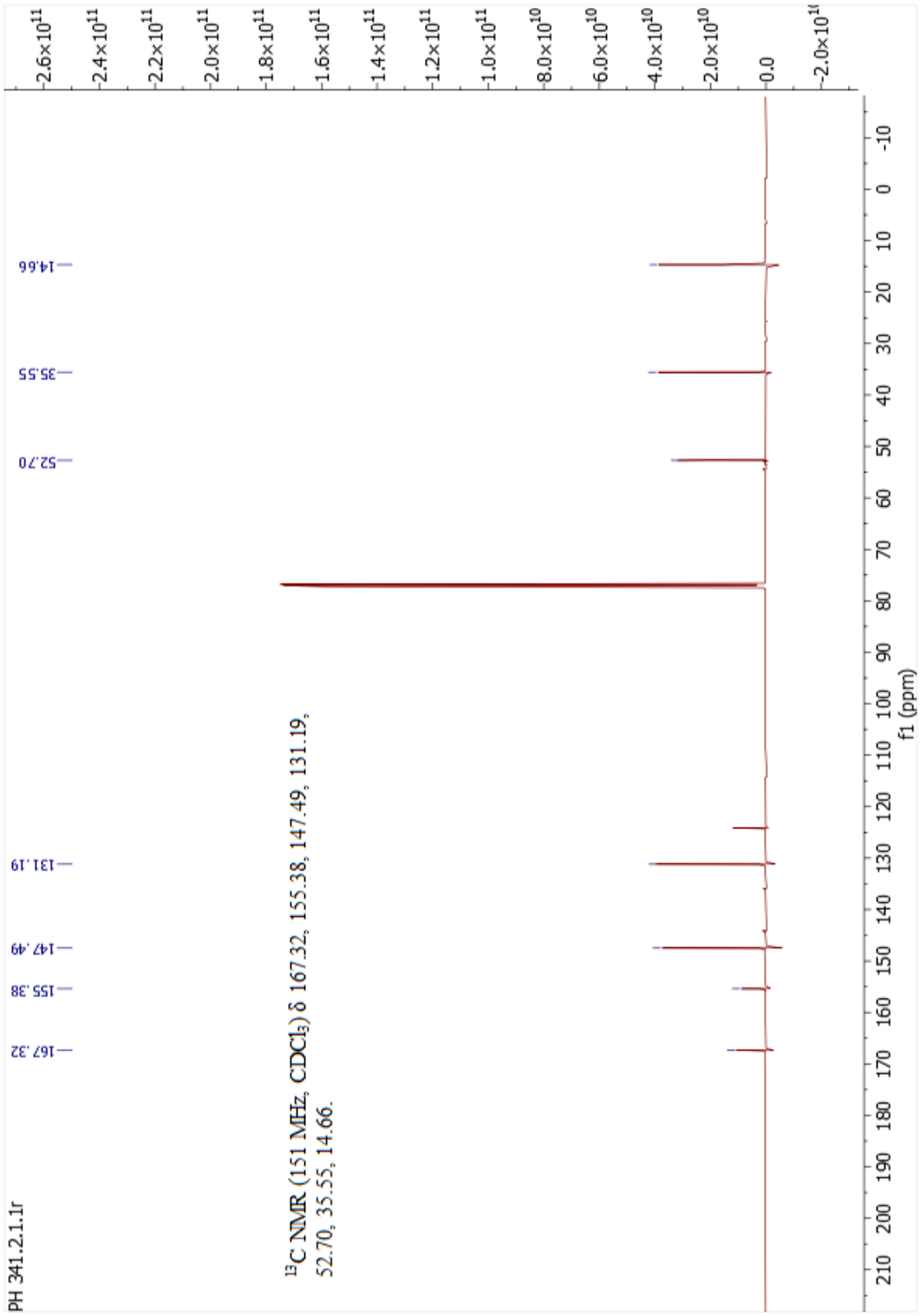
PH 341.2.1.1r
^{13}C NMR (151 MHz, $CDCl_3$) δ 167.32, 155.38, 147.49, 131.19, 52.70, 35.55, 14.66.
167.32
155.38
147.49
131.19
52.70
35.55
14.66
f1 (ppm)

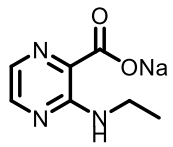
O
ONa
N
N
N
H

POAA039

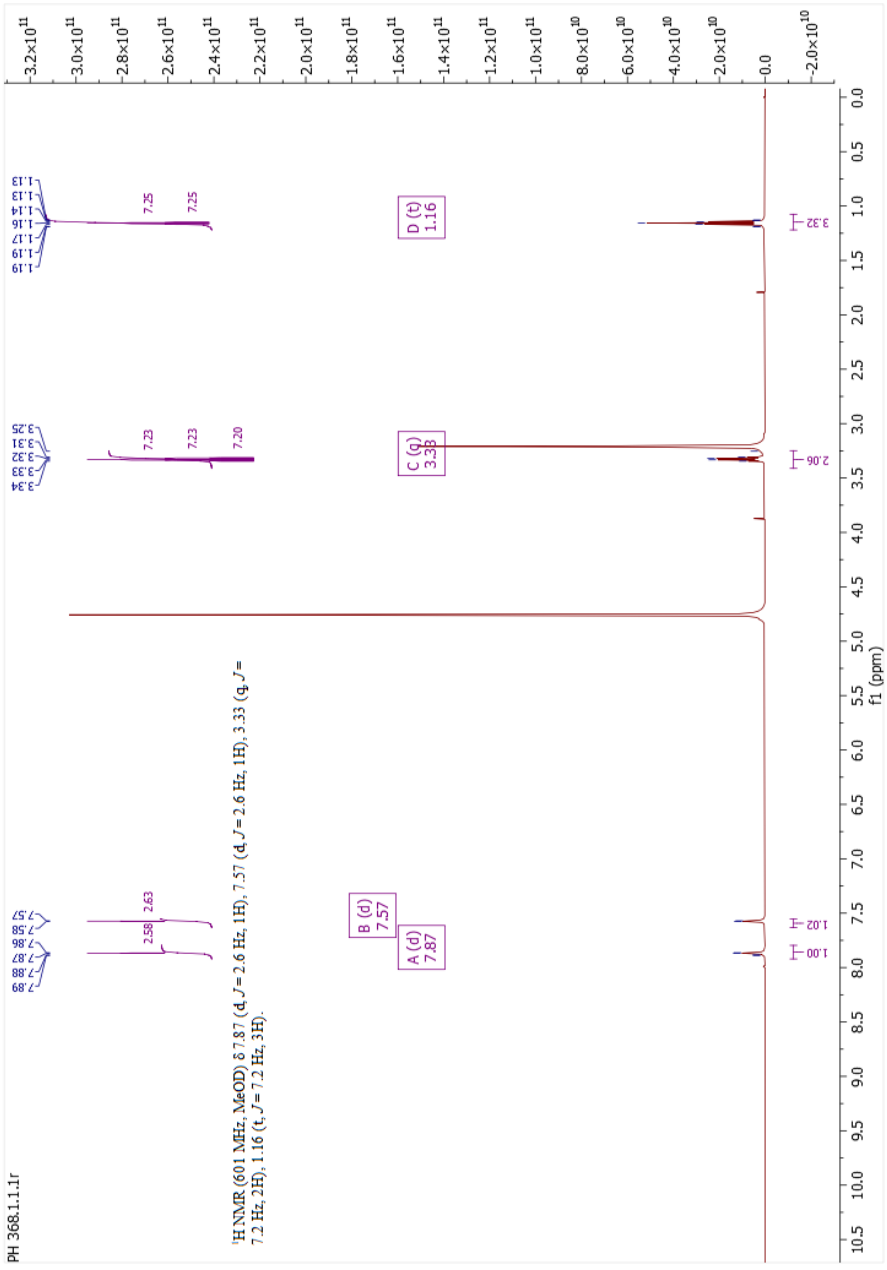
PH 368.1.1.1r
^{1}H NMR (601 MHz, MeOD) δ 7.87 (d, J = 2.6 Hz, 1H), 7.57 (d, J = 2.6 Hz, 1H), 3.33 (q, J = 7.2 Hz, 2H), 1.16 (t, J = 7.2 Hz, 3H).
A (d) 7.87
B (d) 7.57
C (q) 3.33
D (t) 1.16
f1 (ppm)

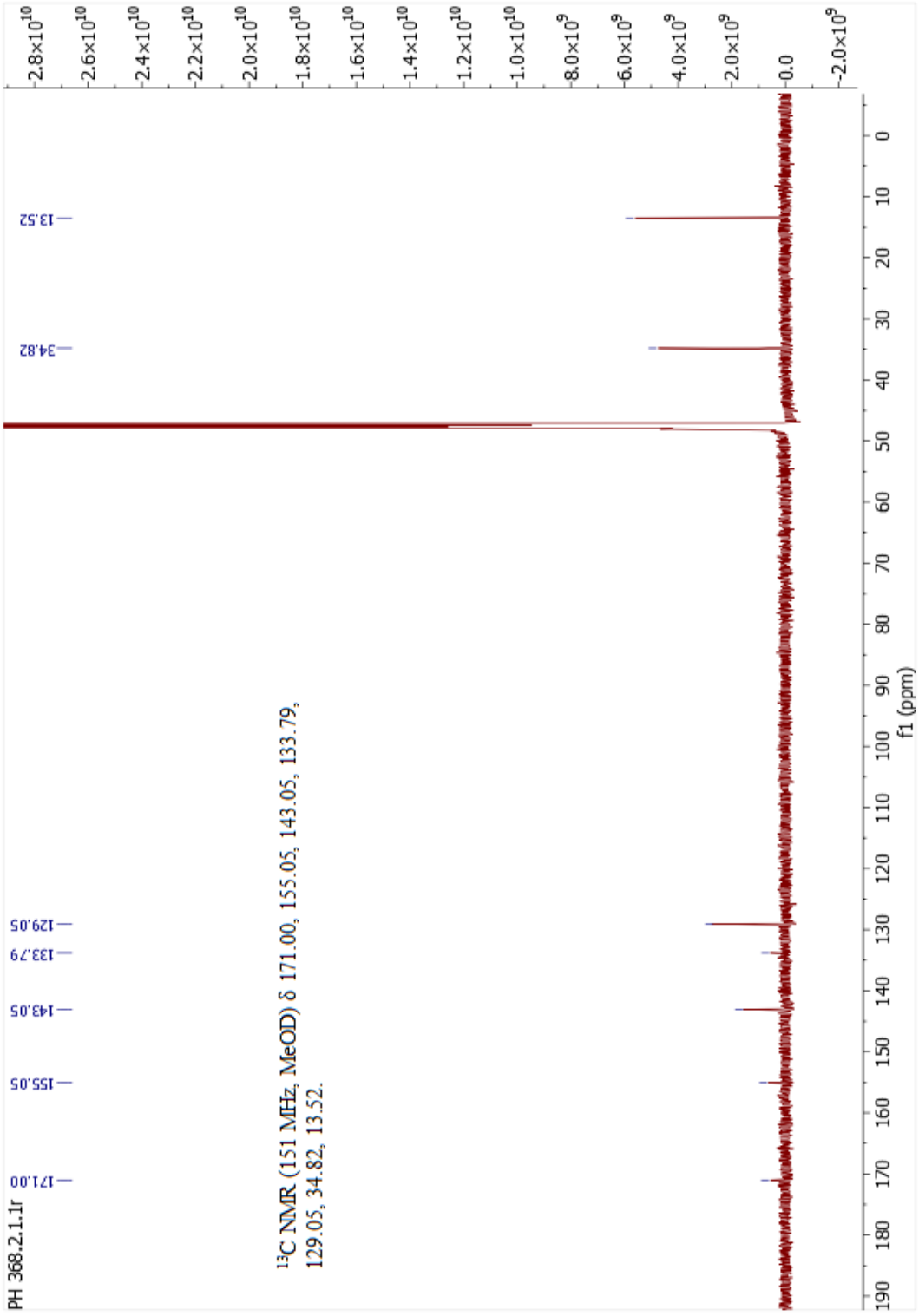
PH 368.2.1.1r
171.00
155.05
143.05
133.79
129.05
34.82
13.52
^{13}C NMR (151 MHz, MeOD) δ 171.00, 155.05, 143.05, 133.79, 129.05, 34.82, 13.52.
f1 (ppm)

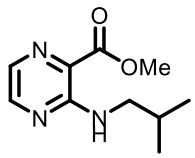

POAA024-OMe

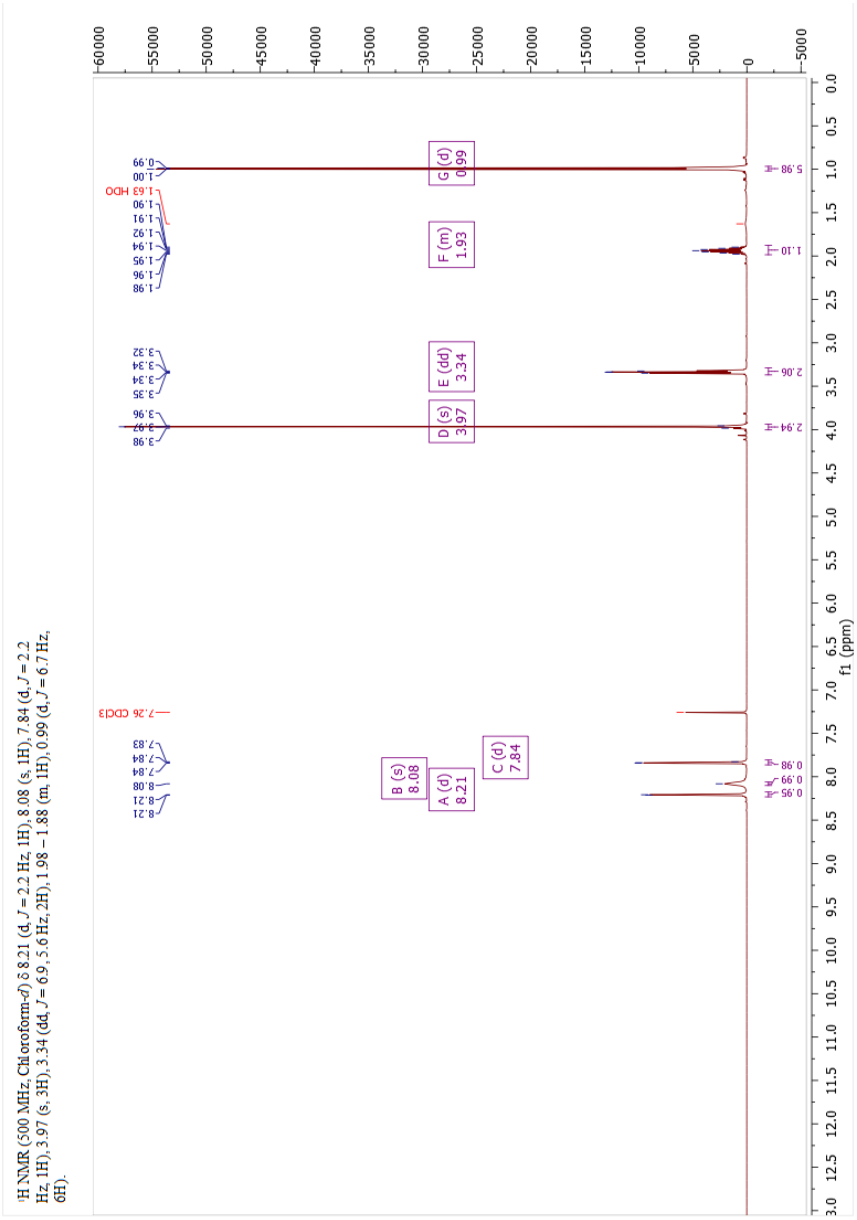
1H NMR (500 MHz, Chloroform-d) δ 8.21 (d, J = 2.2 Hz, 1H), 8.08 (s, 1H), 7.84 (d, J = 2.2 Hz, 1H), 3.97 (s, 3H), 3.34 (dd, J = 6.9, 5.6 Hz, 2H), 1.98 – 1.88 (m, 1H), 0.99 (d, J = 6.7 Hz, 6H).
G (d) 0.99
F (m) 1.93
E (dd) 3.34
D (s) 3.97
B (s) 8.08
A (d) 8.21
C (d) 7.84
7.26 CDCl3
1.63 HDO
f1 (ppm)

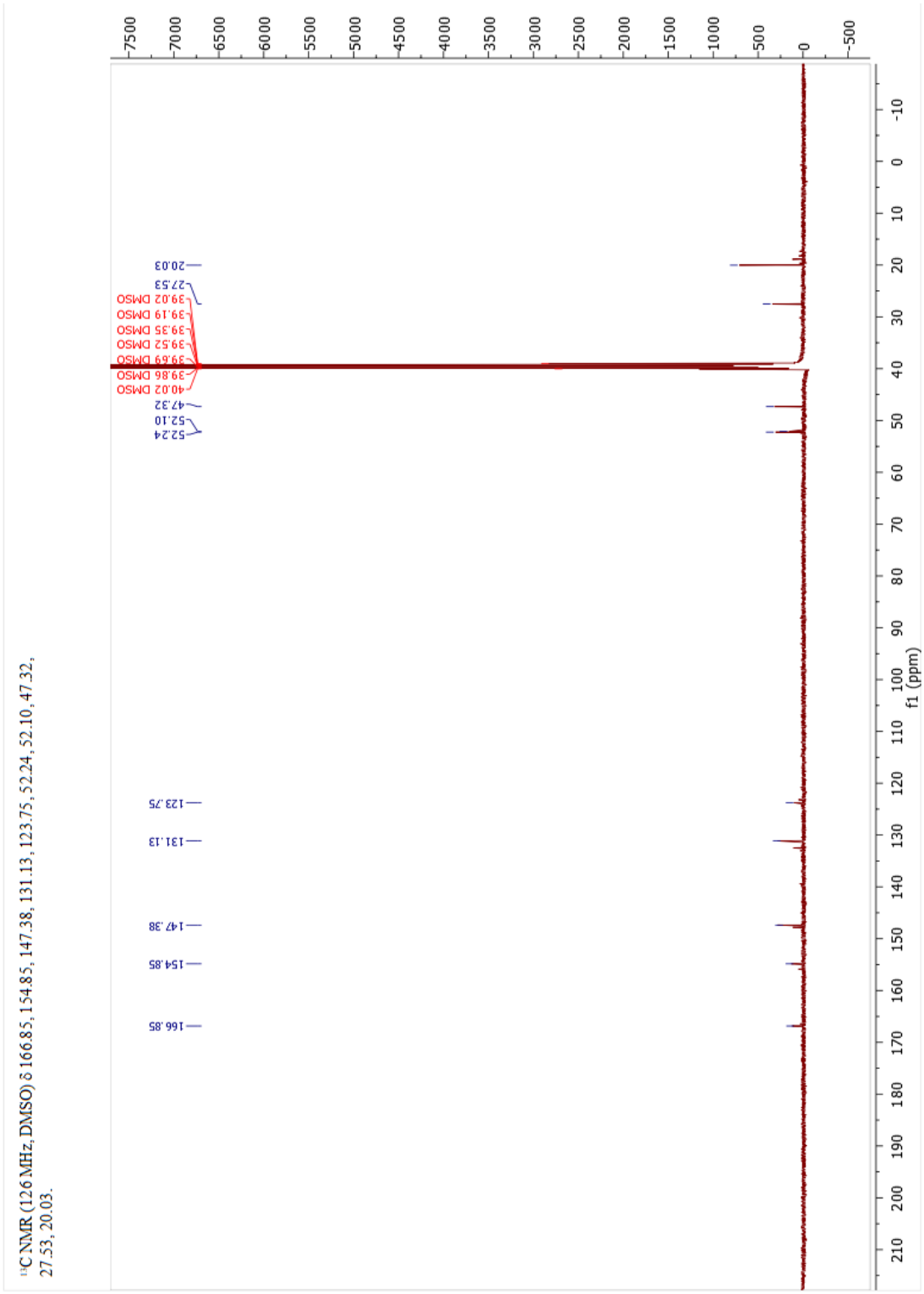

^{13}C NMR (126 MHz, DMSO) δ 166.85, 154.85, 147.38, 131.13, 123.75, 52.24, 52.10, 47.32, 27.53, 20.03.

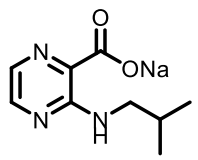
O
ONa
N
N
N
H

POAA024

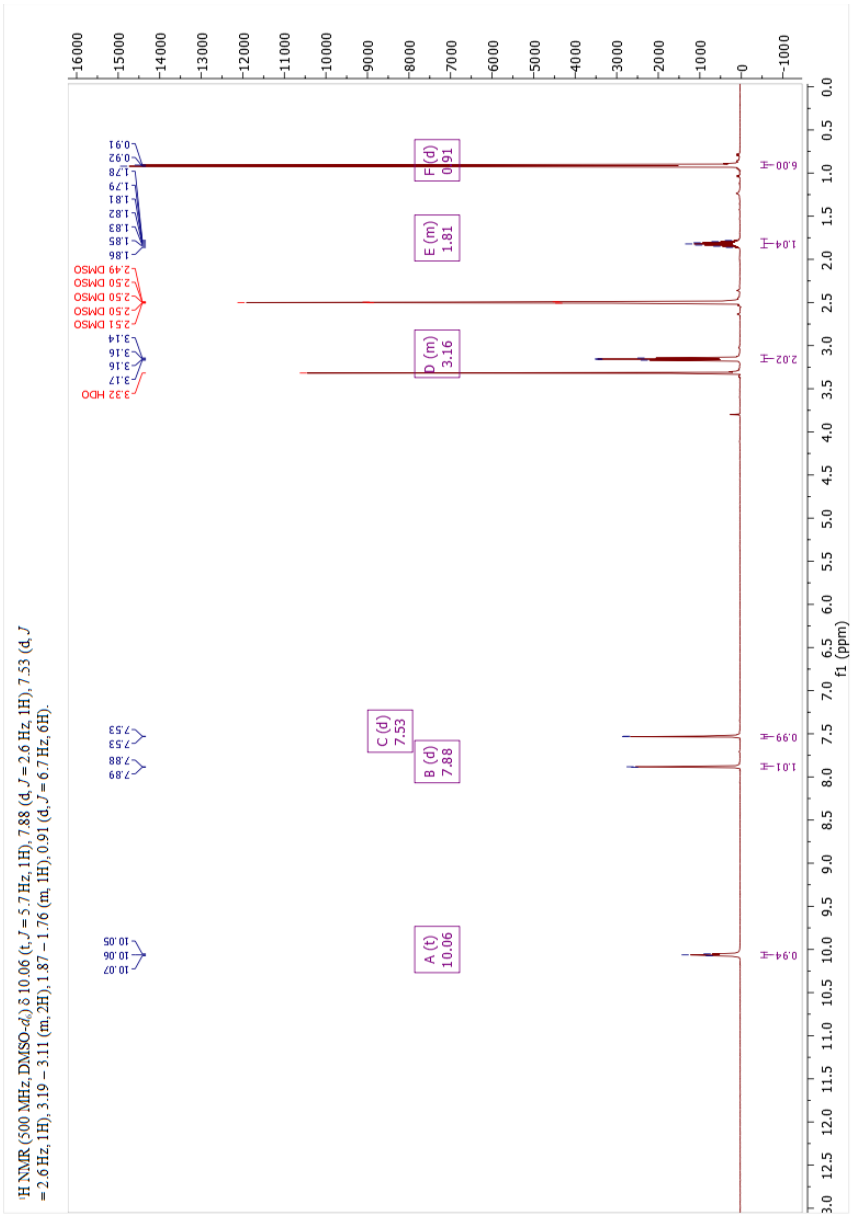
^{1}H NMR (500 MHz, DMSO-d_6) δ 10.06 (t, J = 5.7 Hz, 1H), 7.88 (d, J = 2.6 Hz, 1H), 7.53 (d, J = 2.6 Hz, 1H), 3.19 – 3.11 (m, 2H), 1.87 – 1.76 (m, 1H), 0.91 (d, J = 6.7 Hz, 6H).
A (t) 10.06
B (d) 7.88
C (d) 7.53
D (m) 3.16
E (m) 1.81
F (d) 0.91
f1 (ppm)

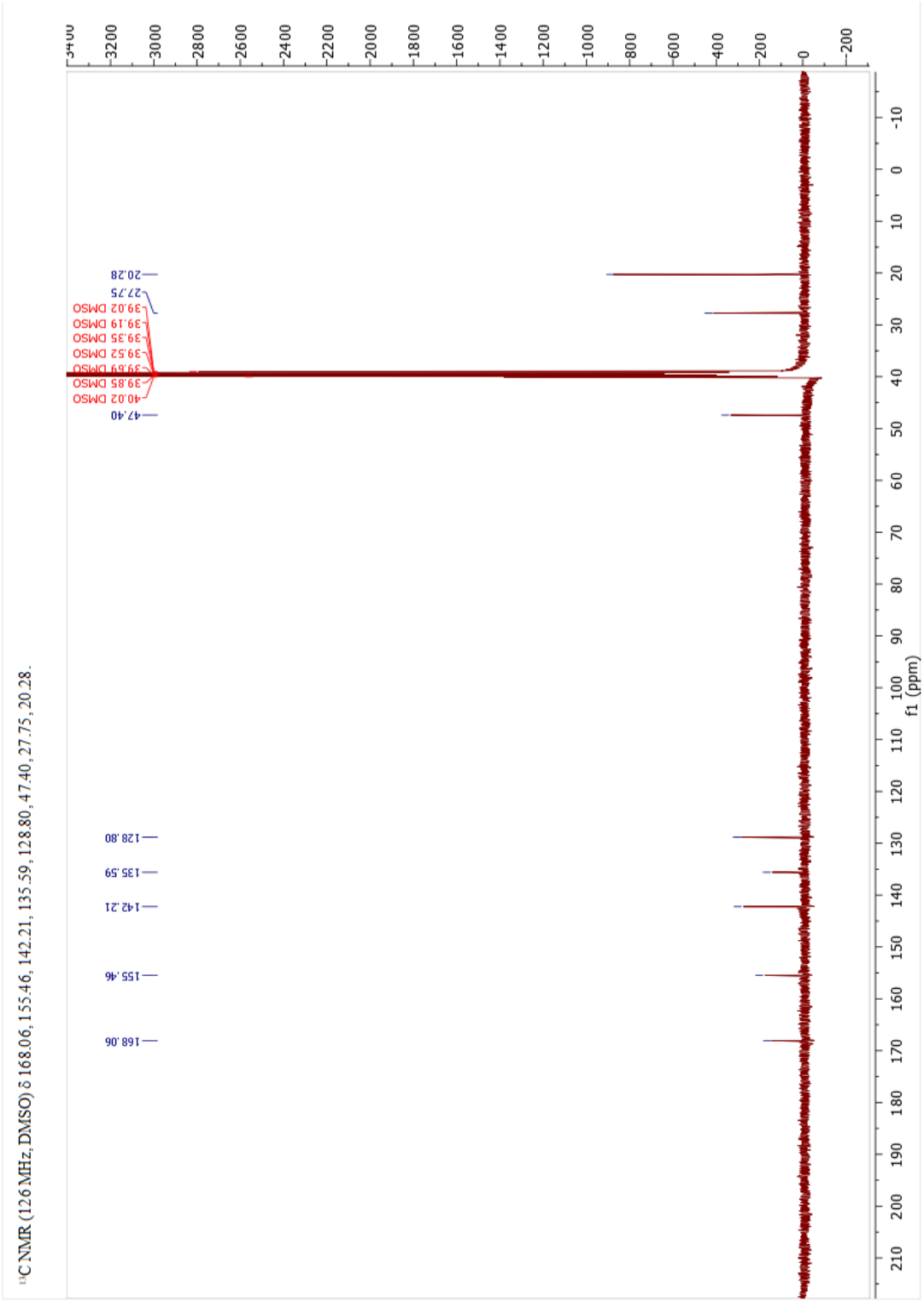
^{13}C NMR (126 MHz, DMSO) δ 168.06, 155.46, 142.21, 135.59, 128.80, 47.40, 27.75, 20.28.
f1 (ppm)

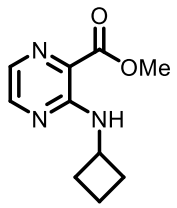
O
OMe
N
N
NH

POAA036-OMe

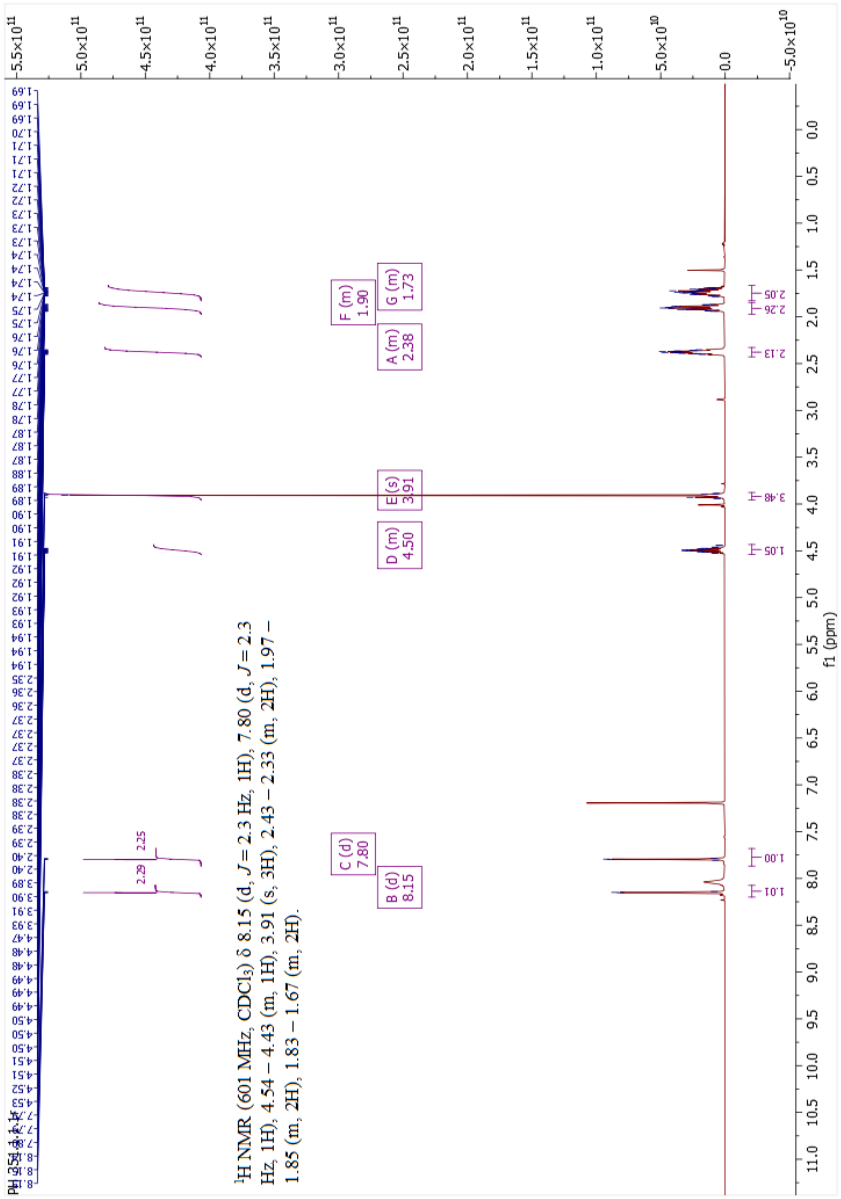
^{1}H NMR (601 MHz, $CDCl_3$) δ 8.15 (d, J = 2.3 Hz, 1H), 7.80 (d, J = 2.3 Hz, 1H), 4.54 – 4.43 (m, 1H), 3.91 (s, 3H), 2.43 – 2.33 (m, 2H), 1.97 – 1.85 (m, 2H), 1.83 – 1.67 (m, 2H).
B (d) 8.15
C (d) 7.80
D (m) 4.50
E (s) 3.91
A (m) 2.38
F (m) 1.90
G (m) 1.73
f1 (ppm)

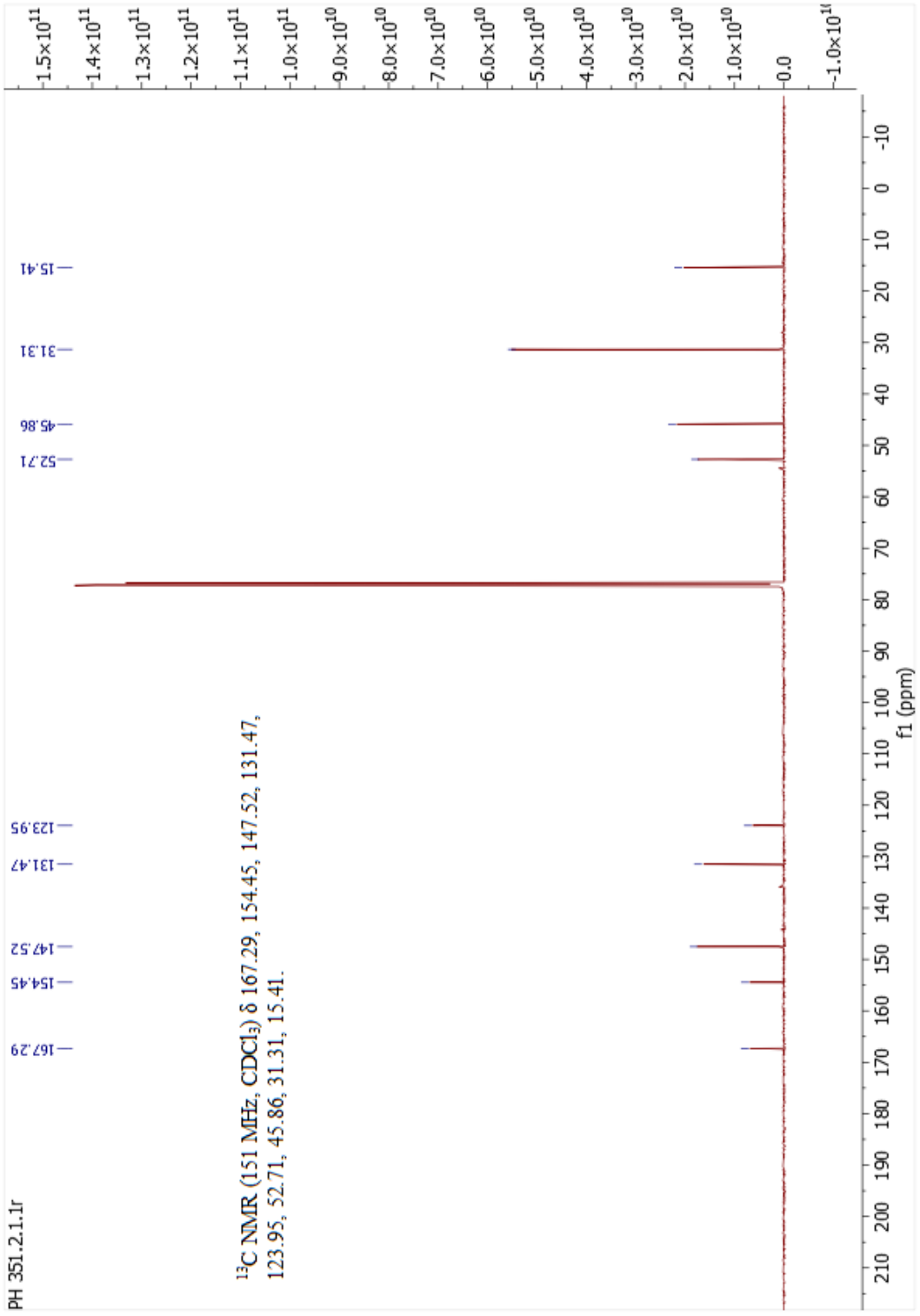
PH 351.2.1.1r
^{13}C NMR (151 MHz, $CDCl_3$) δ 167.29, 154.45, 147.52, 131.47, 123.95, 52.71, 45.86, 31.31, 15.41.
167.29
154.45
147.52
131.47
123.95
52.71
45.86
31.31
15.41
f1 (ppm)

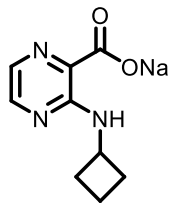
O
ONa
N
N
NH

POAA036

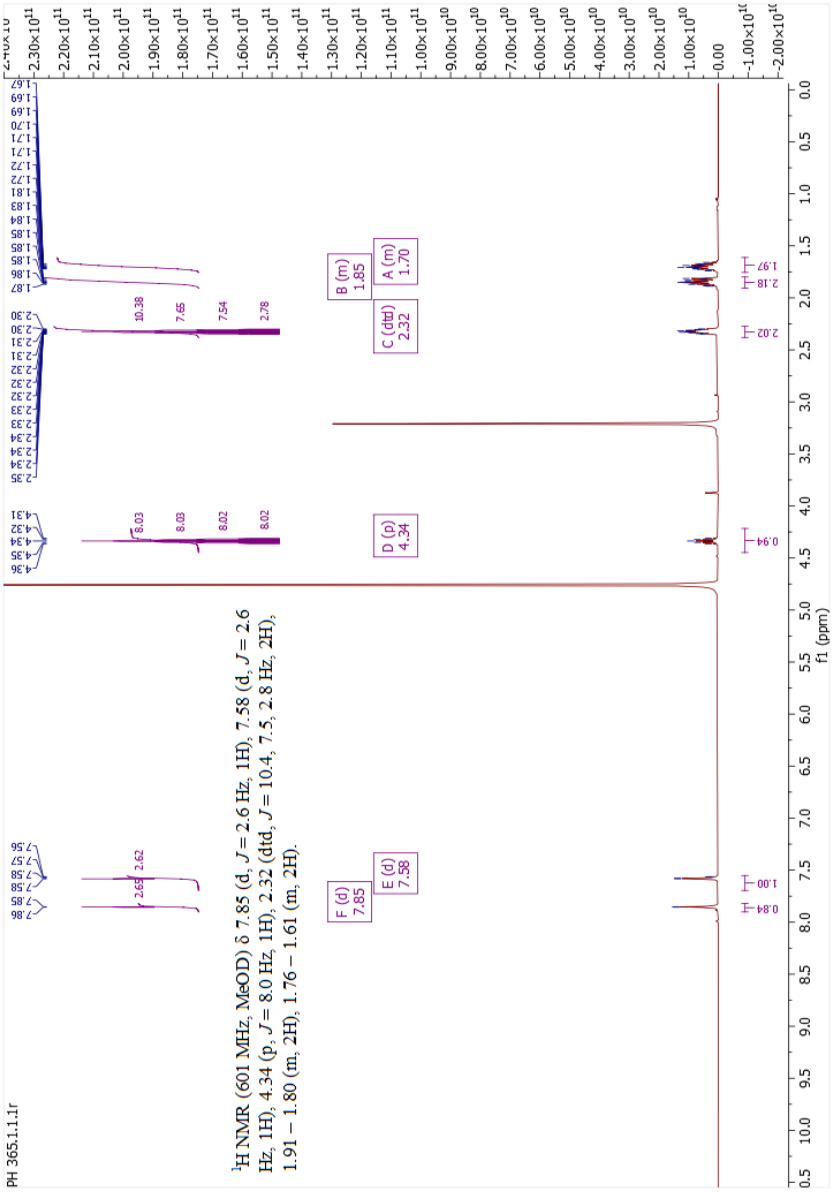
PH 365.1.1.1r
^{1}H NMR (601 MHz, MeOD) δ 7.85 (d, J = 2.6 Hz, 1H), 7.58 (d, J = 2.6 Hz, 1H), 4.34 (p, J = 8.0 Hz, 1H), 2.32 (dtd, J = 10.4, 7.5, 2.8 Hz, 2H), 1.91 – 1.80 (m, 2H), 1.76 – 1.61 (m, 2H).
F (d) 7.85
E (d) 7.58
D (p) 4.34
C (dtd) 2.32
B (m) 1.85
A (m) 1.70
f1 (ppm)

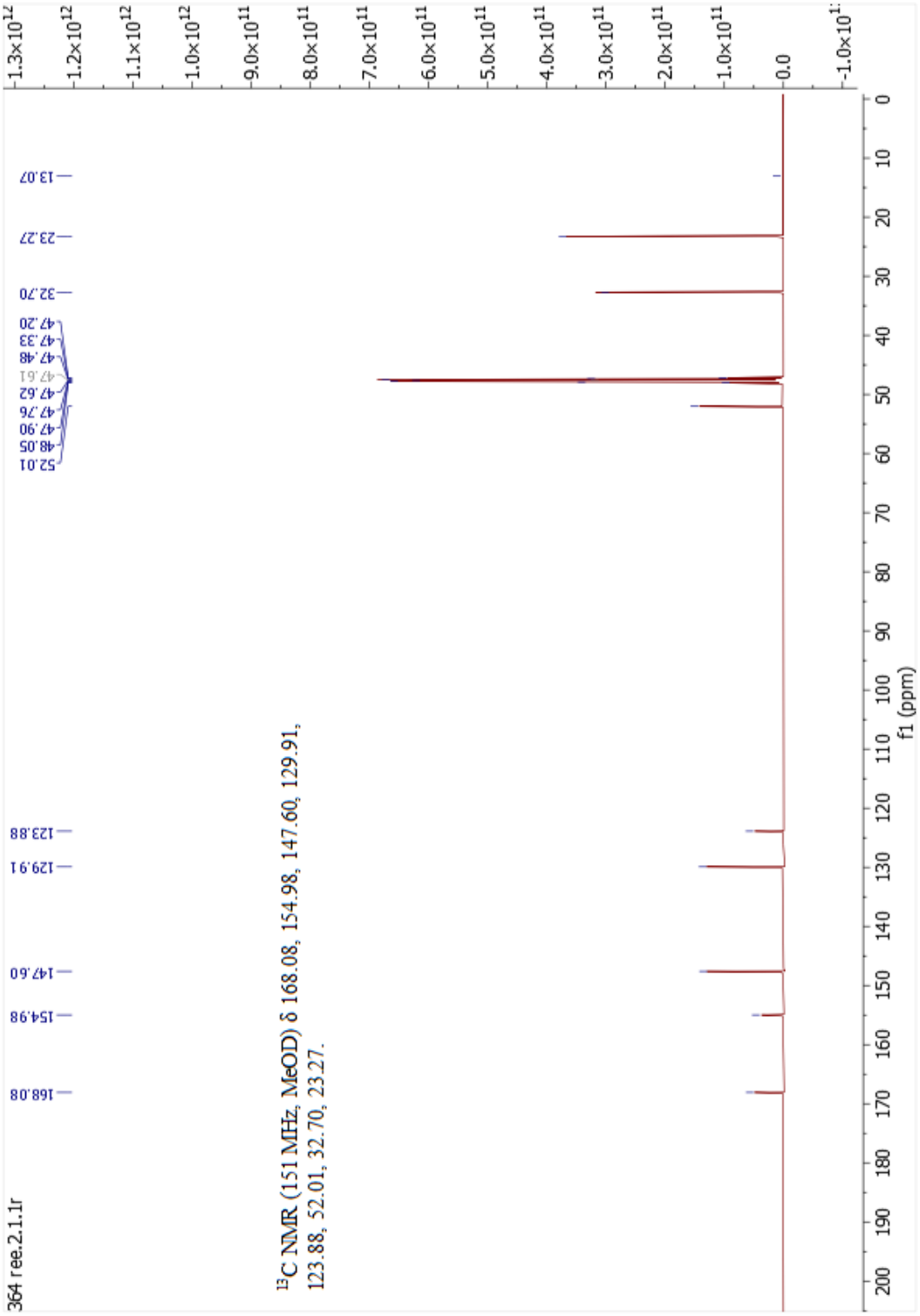
364 ree.2.1.1r
^{13}C NMR (151 MHz, MeOD) δ 168.08, 154.98, 147.60, 129.91, 123.88, 52.01, 32.70, 23.27.
168.08
154.98
147.60
129.91
123.88
52.01
48.05
47.90
47.76
47.62
47.61
47.48
47.33
47.20
32.70
23.27
13.07
f1 (ppm)

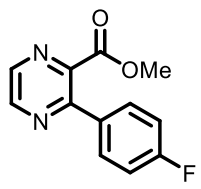
O
OMe
N
N
F

POAA027-OMe

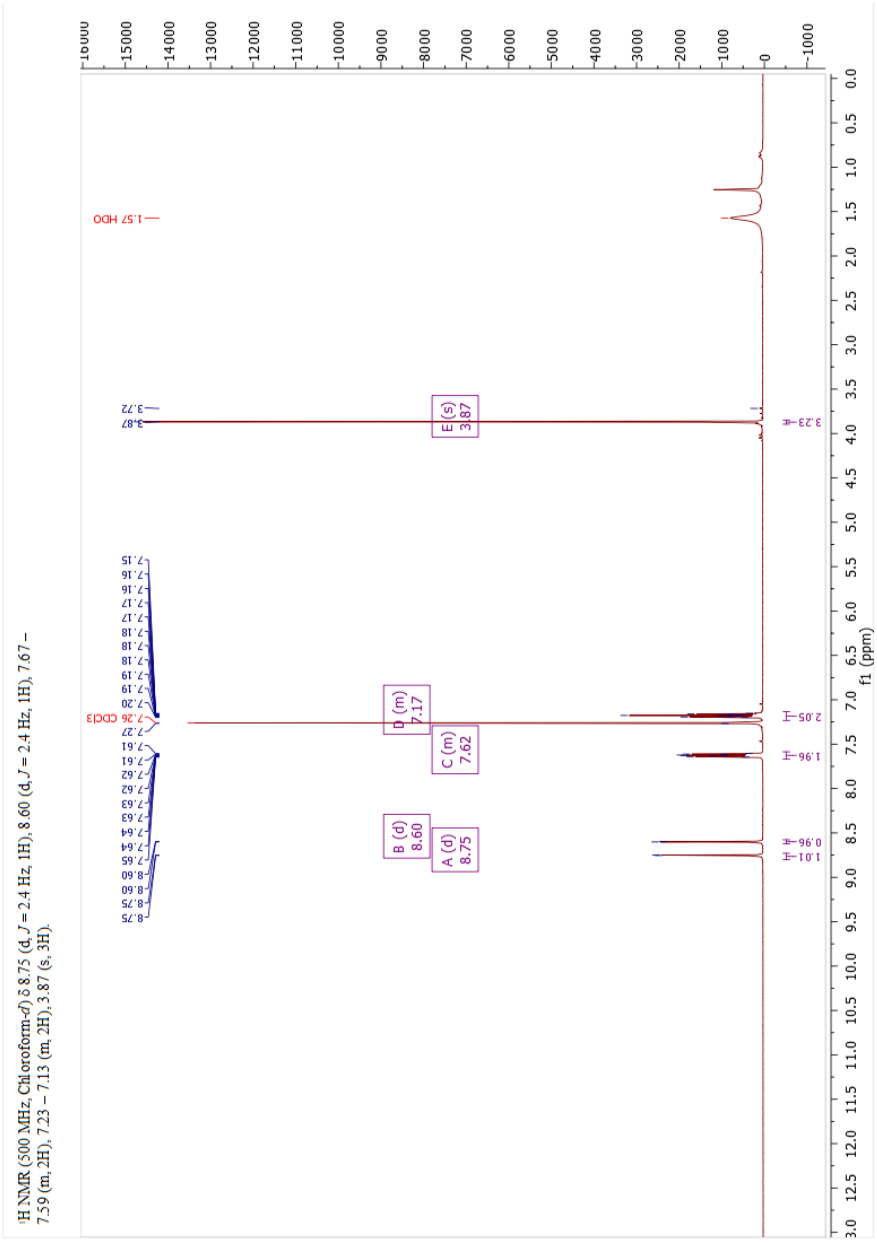
^{1}H NMR (500 MHz, Chloroform-d) δ 8.75 (d, J = 2.4 Hz, 1H), 8.60 (d, J = 2.4 Hz, 1H), 7.67 – 7.59 (m, 2H), 7.23 – 7.13 (m, 2H), 3.87 (s, 3H).
1.57 HDO
3.87
3.72
7.26 CDCl3
E (s) 3.87
D (m) 7.17
C (m) 7.62
B (d) 8.60
A (d) 8.75
3.23
2.05
1.96
1.01
0.96
f1 (ppm)

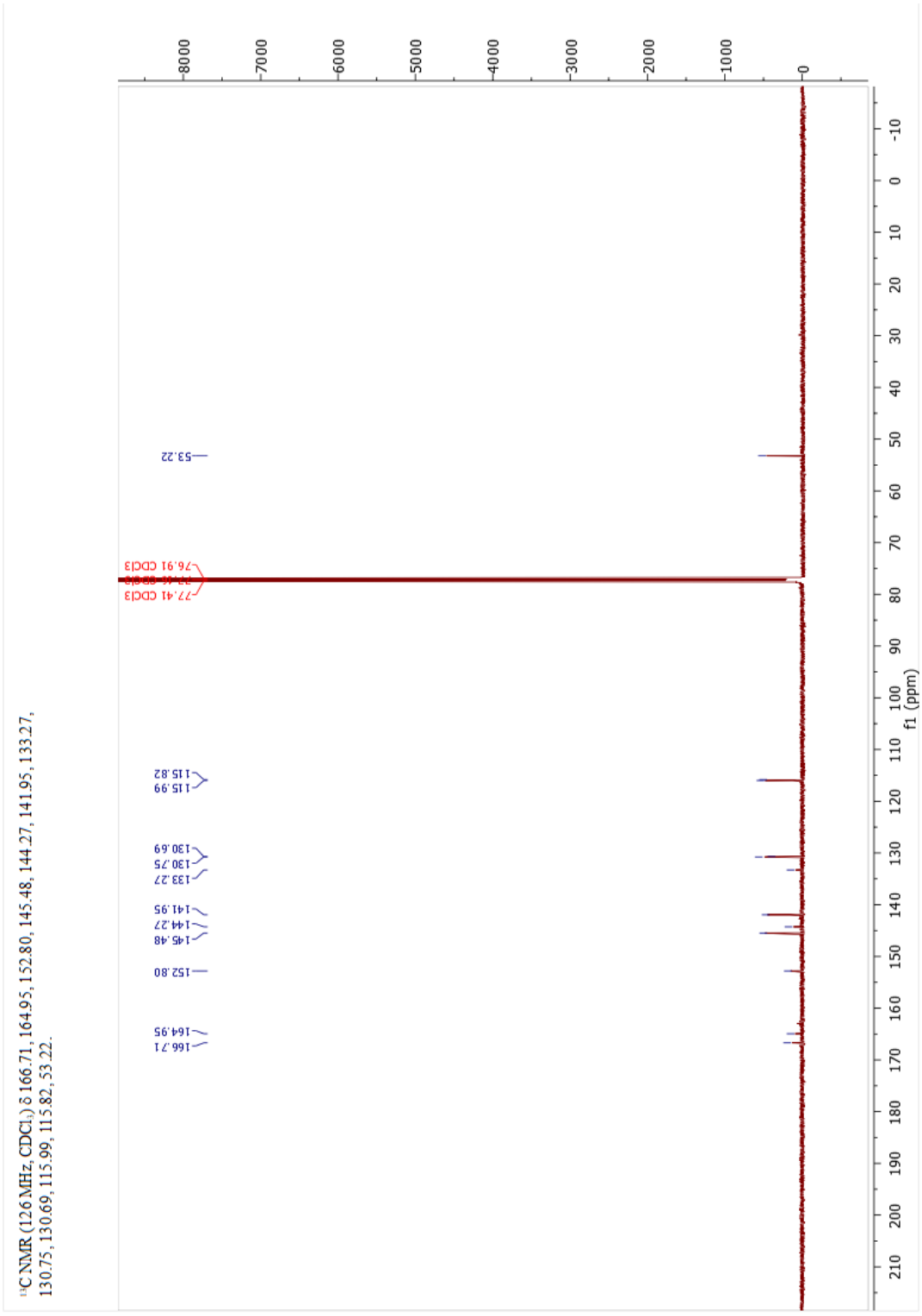
^{13}C NMR (126 MHz, CDCl$_3$) δ 166.71, 164.95, 152.80, 145.48, 144.27, 141.95, 133.27, 130.75, 130.69, 115.99, 115.82, 53.22.
53.22
77.41 CDCl3
76.91 CDCl3
115.99
115.82
130.69
130.75
133.27
141.95
144.27
145.48
152.80
164.95
166.71
f1 (ppm)

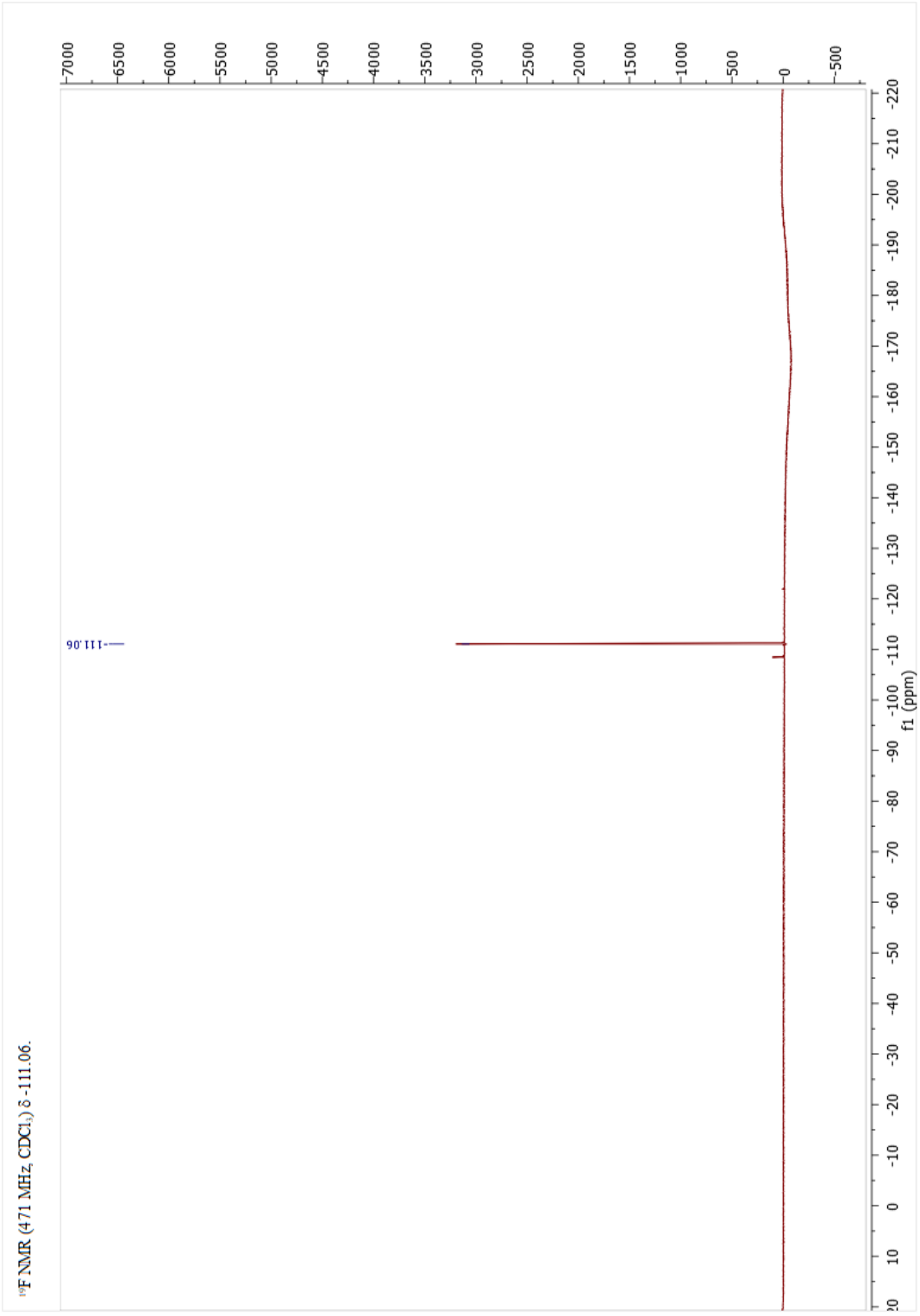

^{19}F NMR (471 MHz, $CDCl_3$) δ -111.06.

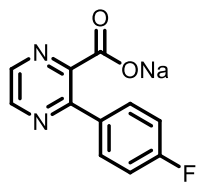
O
ONa
N
N
F

POAA027

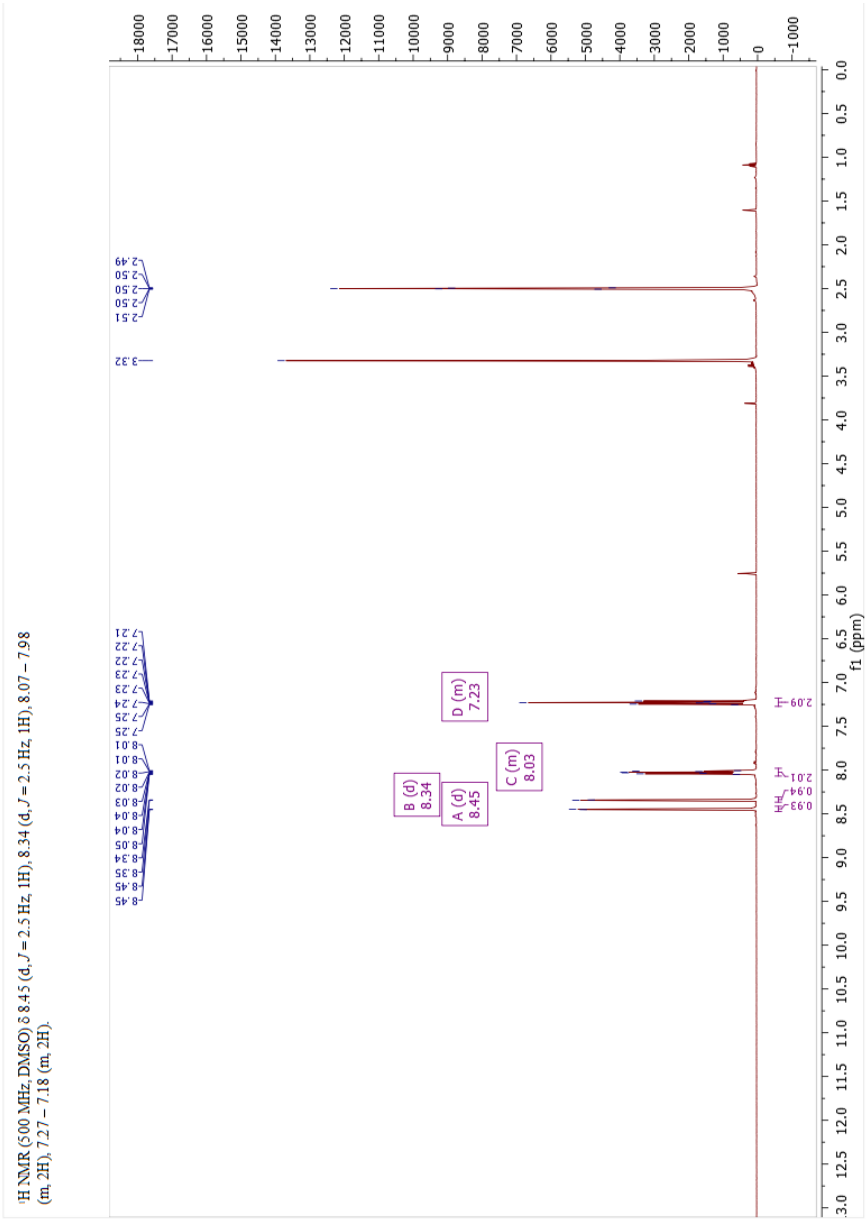
^{1}H NMR (500 MHz, DMSO) δ 8.45 (d, J = 2.5 Hz, 1H), 8.34 (d, J = 2.5 Hz, 1H), 8.07 – 7.98 (m, 2H), 7.27 – 7.18 (m, 2H).
B (d) 8.34
A (d) 8.45
C (m) 8.03
D (m) 7.23
f1 (ppm)

^{13}C NMR (126 MHz, DMSO) δ 169.95, 163.43, 161.48, 155.74, 145.93, 141.47, 140.75, 134.90, 130.56, 130.50, 114.83, 114.66.

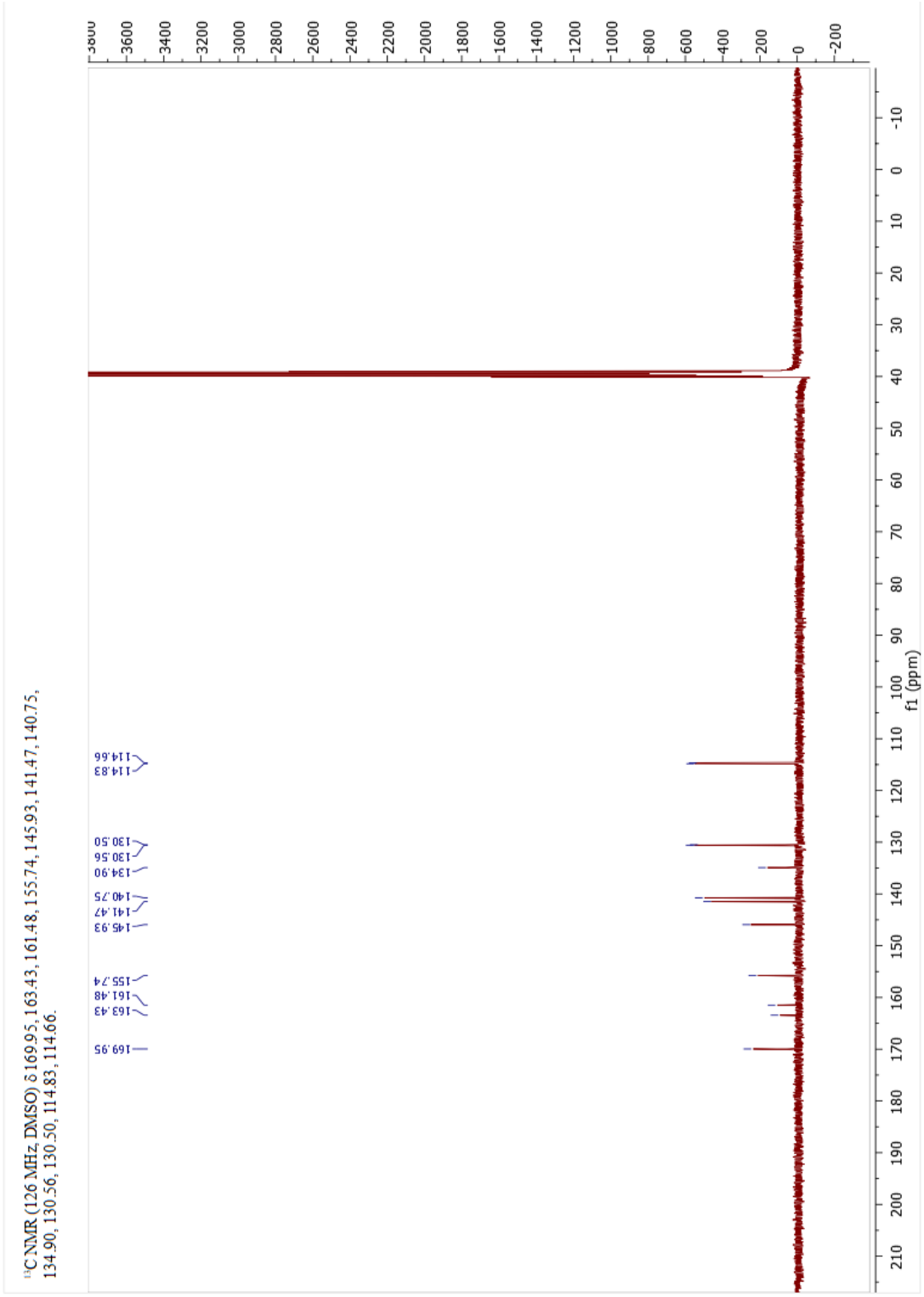

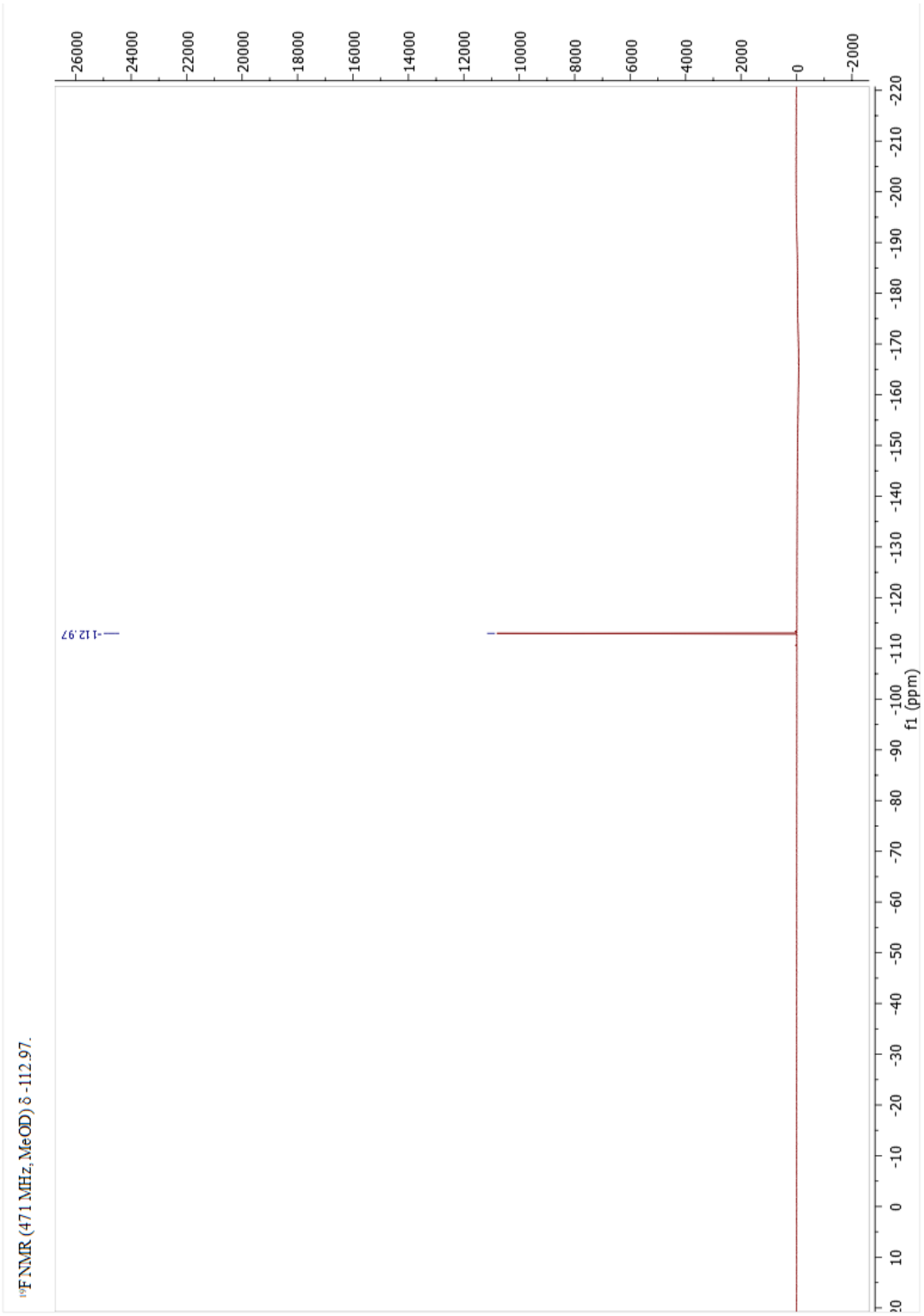

^{19}F NMR (471 MHz, MeOD) δ -112.97.

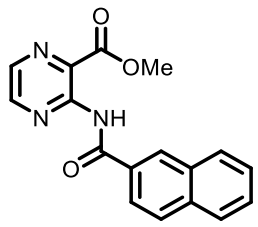
O
OMe
N
N
NH
O

POAA021-OMe

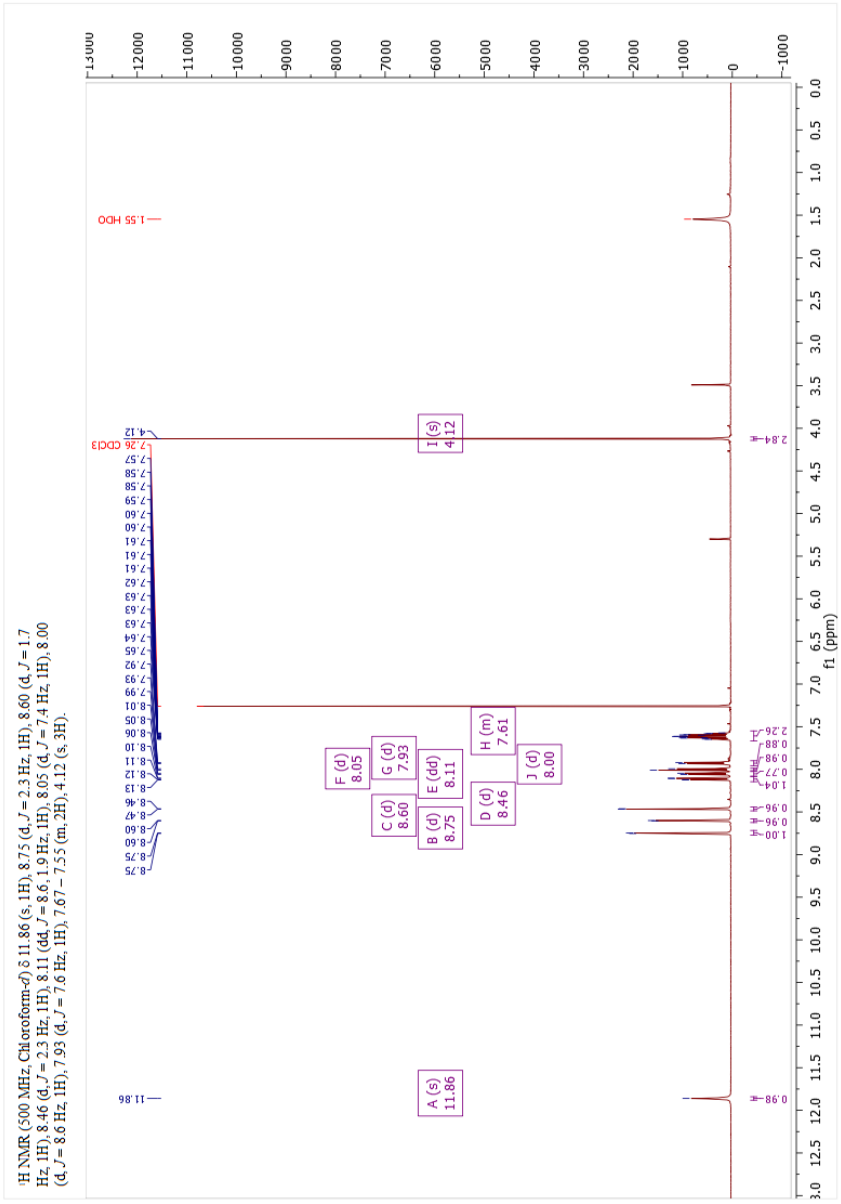
¹H NMR (500 MHz, Chloroform-d) δ 11.86 (s, 1H), 8.75 (d, J = 2.3 Hz, 1H), 8.60 (d, J = 1.7 Hz, 1H), 8.46 (d, J = 2.3 Hz, 1H), 8.11 (dd, J = 8.6, 1.9 Hz, 1H), 8.05 (d, J = 7.4 Hz, 1H), 8.00 (d, J = 8.6 Hz, 1H), 7.93 (d, J = 7.6 Hz, 1H), 7.67 – 7.55 (m, 2H), 4.12 (s, 3H).
A (s) 11.86
B (d) 8.75
C (d) 8.60
D (d) 8.46
E (dd) 8.11
F (d) 8.05
G (d) 7.93
H (m) 7.61
I (s) 4.12
J (d) 8.00
1.55 HDO
7.26 CDCl3
f1 (ppm)

^{13}C NMR (126 MHz, $CDCl_3$) δ 167.22, 164.79, 150.55, 147.38, 138.63, 135.49, 132.82, 131.39, 129.61, 129.11, 128.96, 128.92, 128.52, 127.97, 127.13, 123.83, 53.97.

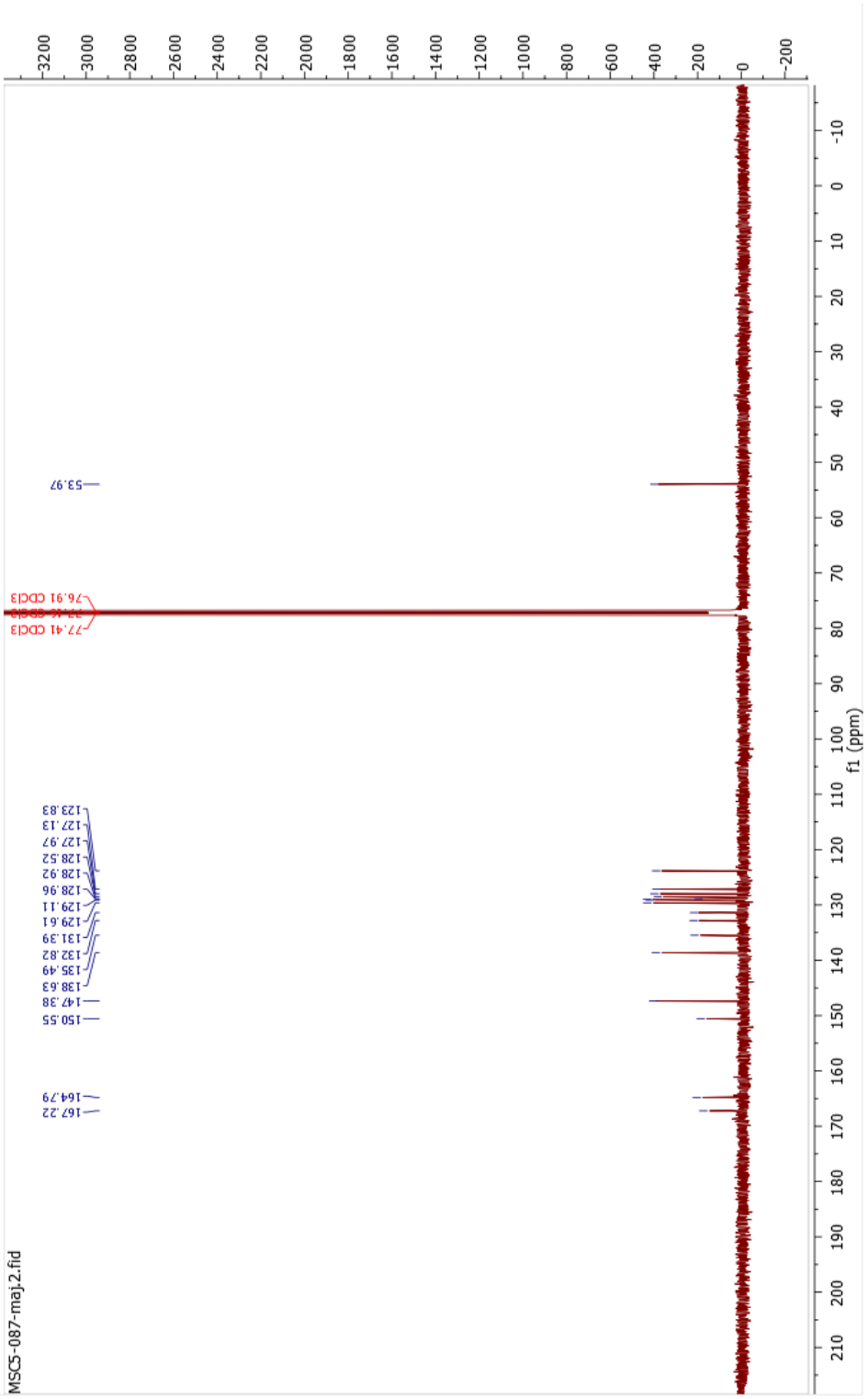

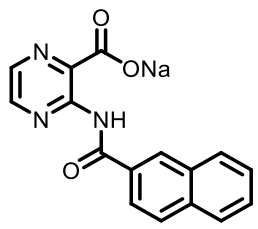
O
ONa
N
N
NH
O

POAA021

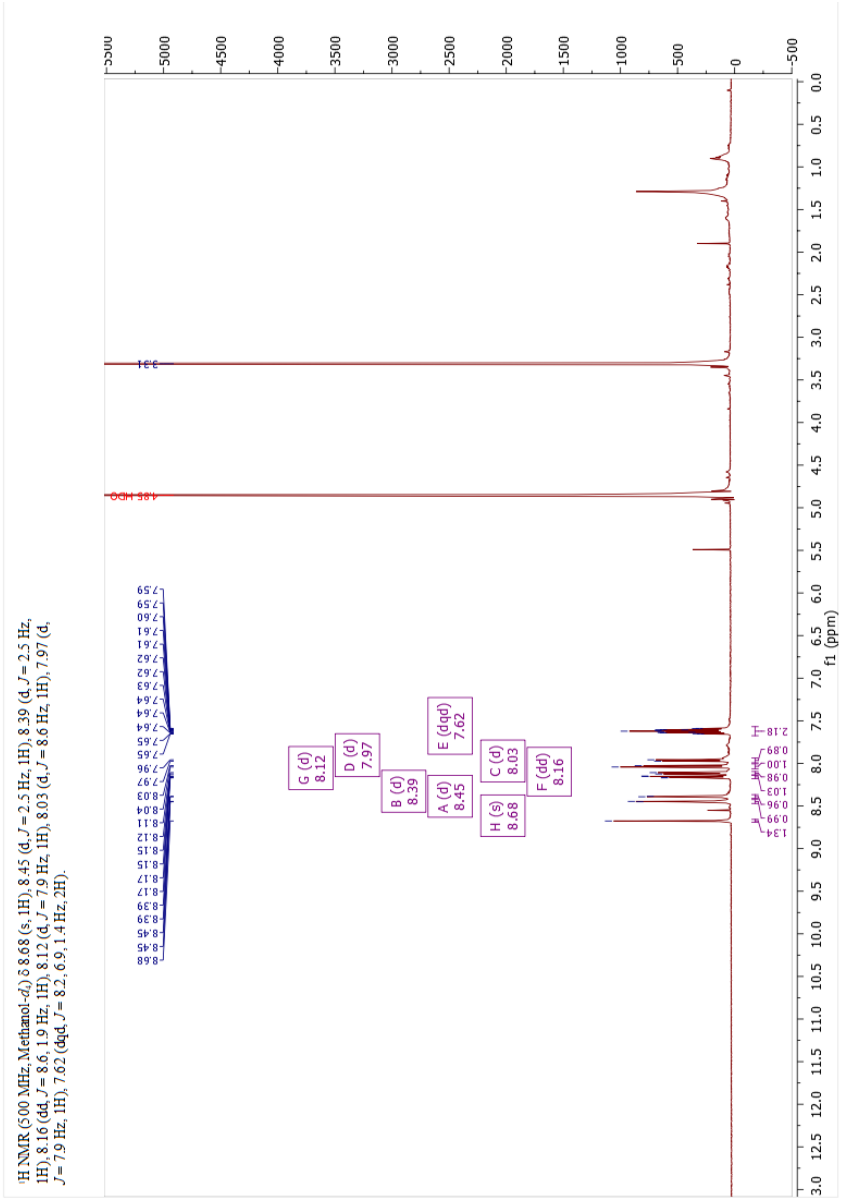
^{1}H NMR (500 MHz, Methanol-d_4) δ 8.68 (s, 1H), 8.45 (d, J = 2.5 Hz, 1H), 8.39 (d, J = 2.5 Hz, 1H), 8.16 (dd, J = 8.6, 1.9 Hz, 1H), 8.12 (d, J = 7.9 Hz, 1H), 8.03 (d, J = 8.6 Hz, 1H), 7.97 (d, J = 7.9 Hz, 1H), 7.62 (dqd, J = 8.2, 6.9, 1.4 Hz, 2H).
G (d) 8.12
D (d) 7.97
B (d) 8.39
E (dqd) 7.62
A (d) 8.45
C (d) 8.03
H (s) 8.68
F (dd) 8.16
f1 (ppm)

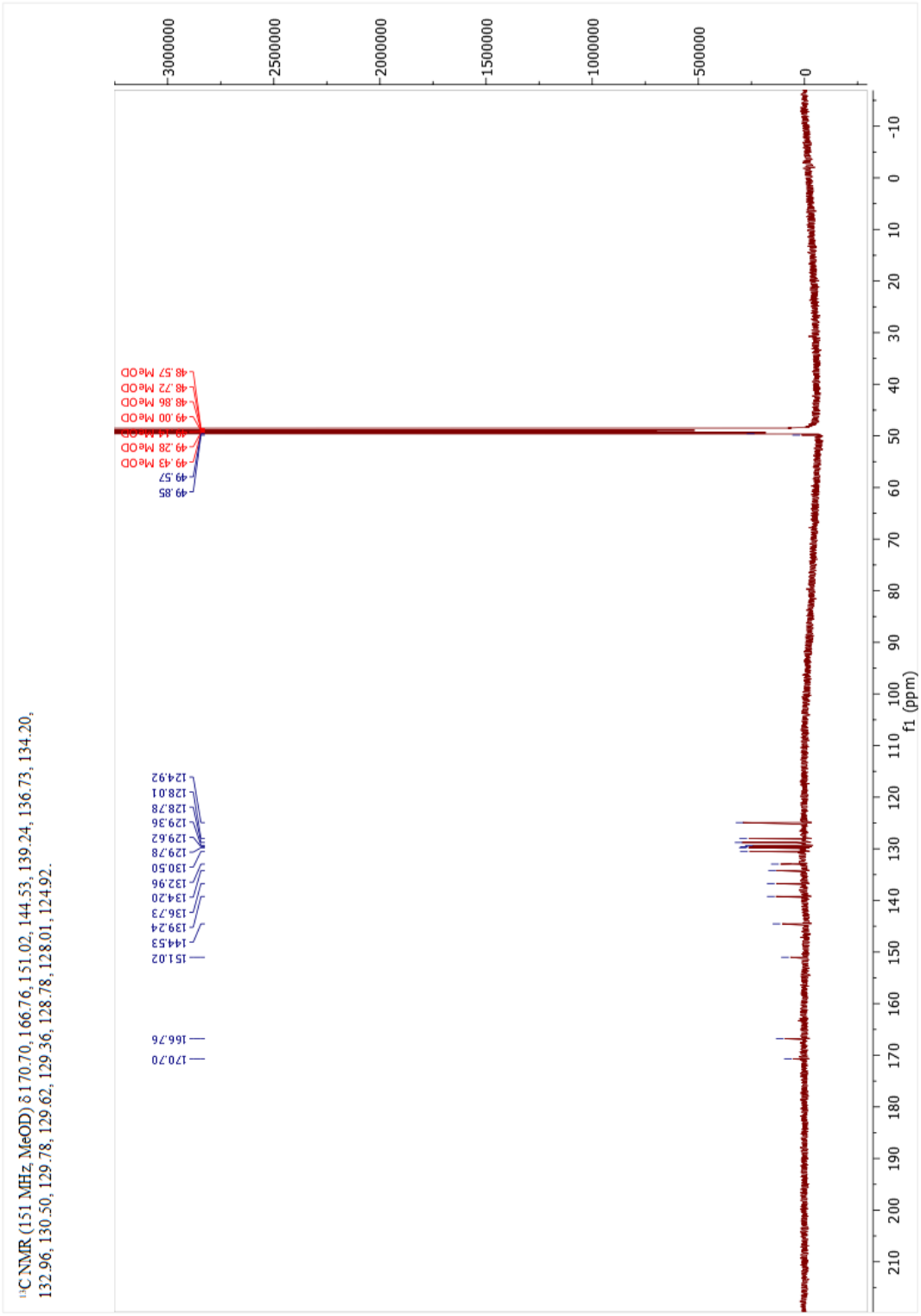
^{13}C NMR (151 MHz, MeOD) δ 170.70, 166.76, 151.02, 144.53, 139.24, 136.73, 134.20, 132.96, 130.50, 129.78, 129.62, 129.36, 128.78, 128.01, 124.92.
f1 (ppm)

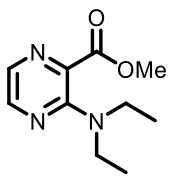
O
OMe
N
N
N

POAA023-OMe

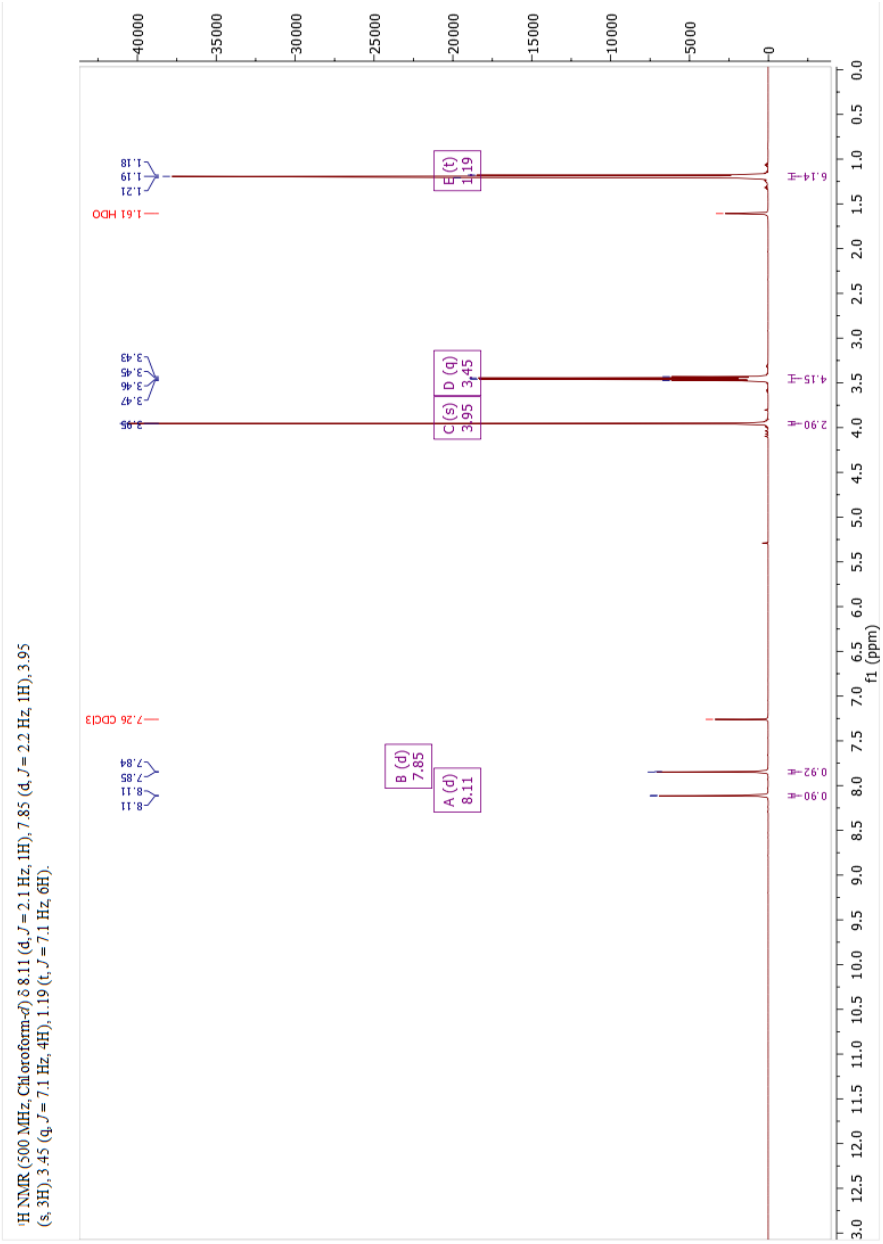
^{1}H NMR (500 MHz, Chloroform-d) δ 8.11 (d, J = 2.1 Hz, 1H), 7.85 (d, J = 2.2 Hz, 1H), 3.95 (s, 3H), 3.45 (q, J = 7.1 Hz, 4H), 1.19 (t, J = 7.1 Hz, 6H).
f1 (ppm)
A (d) 8.11
B (d) 7.85
C (s) 3.95
D (q) 3.45
E (t) 1.19
7.26 CDCl3
1.61 HDO

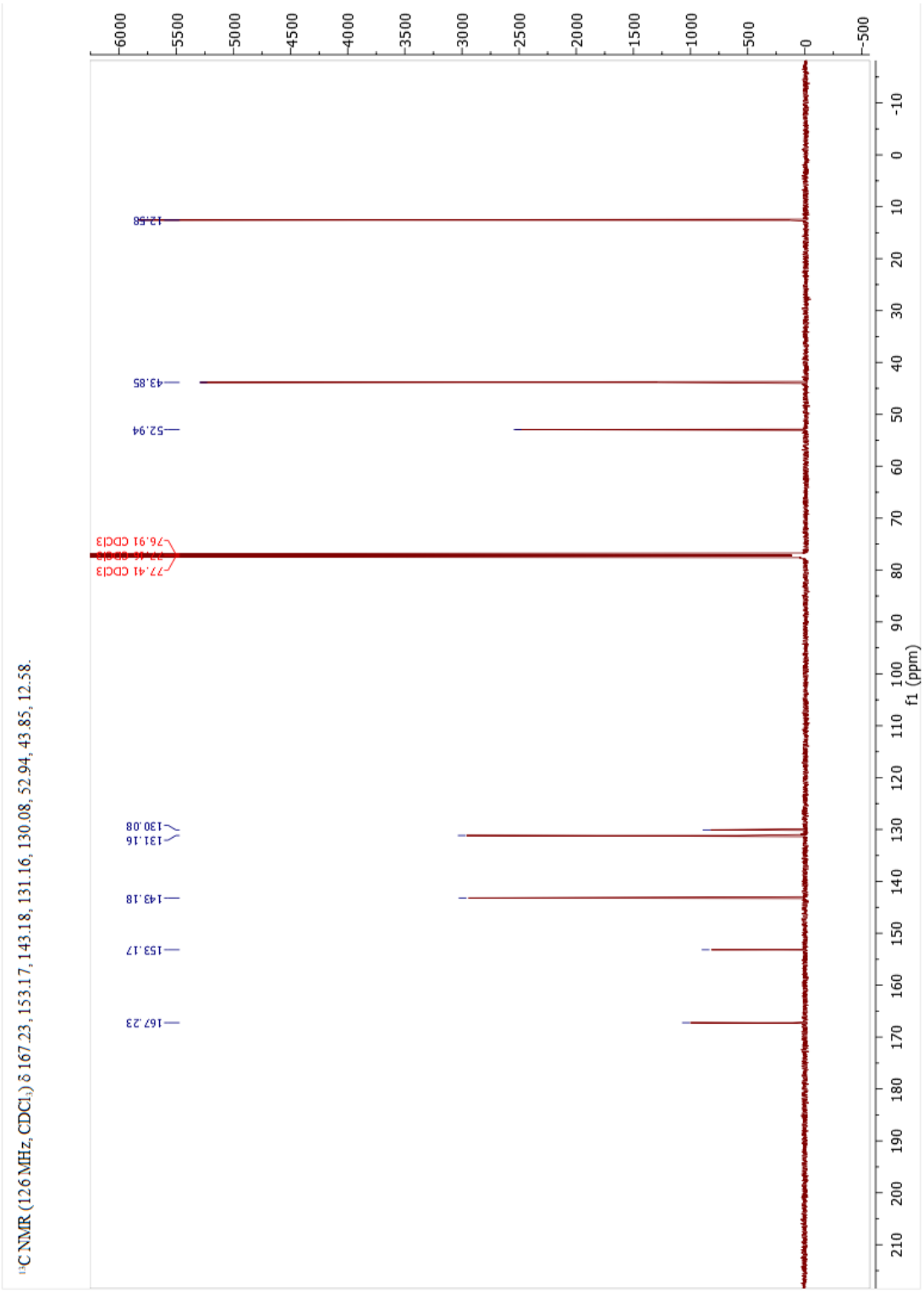

^{13}C NMR (126 MHz, $CDCl_3$) δ 167.23, 153.17, 143.18, 131.16, 130.08, 52.94, 43.85, 12.58.

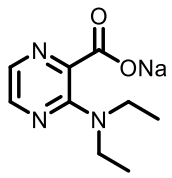
O
ONa
N
N
N

POAA023

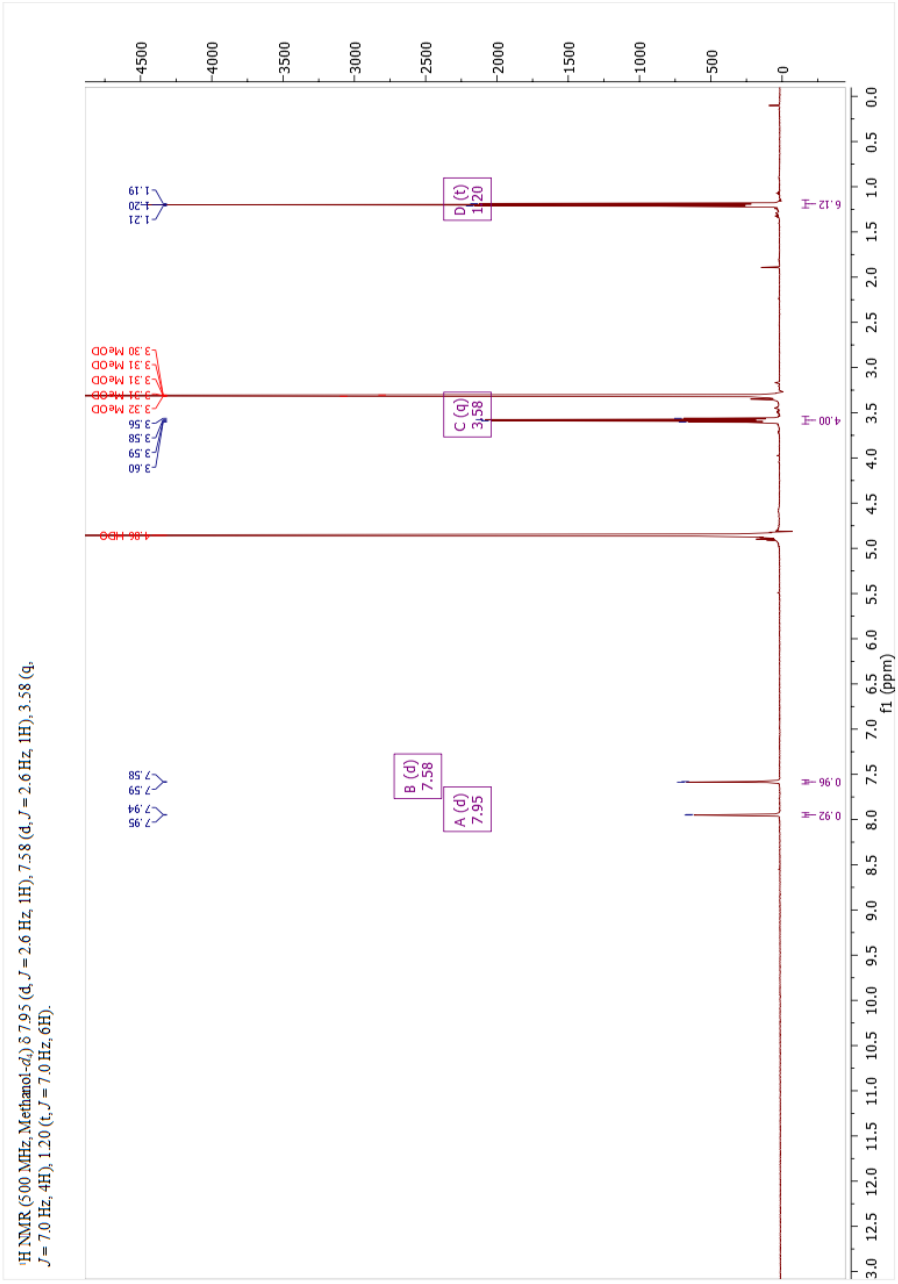
^{1}H NMR (500 MHz, Methanol-d_4) δ 7.95 (d, J = 2.6 Hz, 1H), 7.58 (d, J = 2.6 Hz, 1H), 3.58 (q, J = 7.0 Hz, 4H), 1.20 (t, J = 7.0 Hz, 6H).
A (d) 7.95
B (d) 7.58
C (q) 3.58
D (t) 1.20
f1 (ppm)

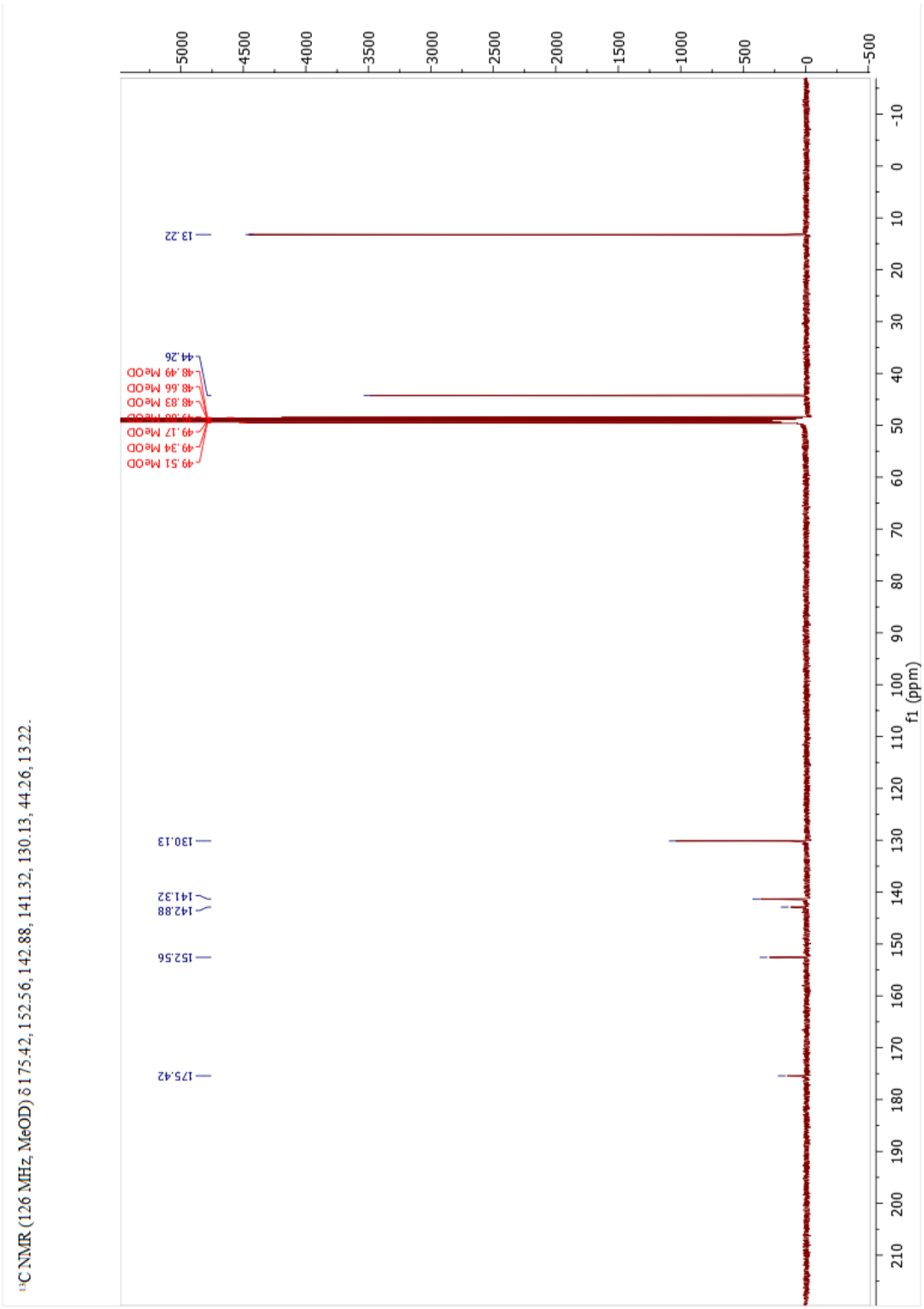

^{13}C NMR (126 MHz, MeOD) δ 175.42, 152.56, 142.88, 141.32, 130.13, 44.26, 13.22.

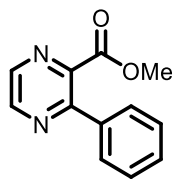
O
OMe
N
N

POAA026-OMe

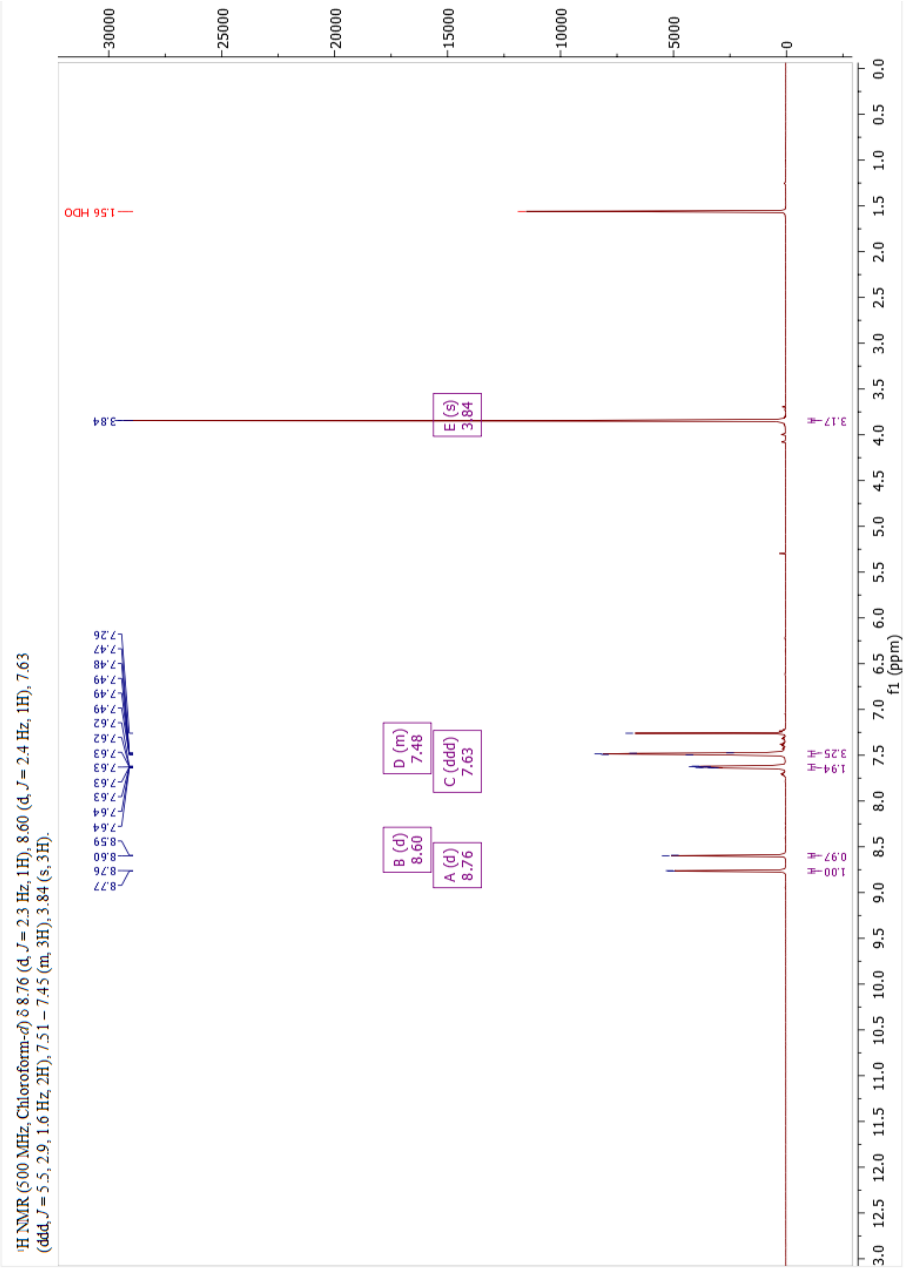
^{1}H NMR (500 MHz, Chloroform-*d*) δ 8.76 (d, *J* = 2.3 Hz, 1H), 8.60 (d, *J* = 2.4 Hz, 1H), 7.63 (ddd, *J* = 5.5, 2.9, 1.6 Hz, 2H), 7.51 – 7.45 (m, 3H), 3.84 (s, 3H).
1.56 HDO
3.84
E (s) 3.84
D (m) 7.48
C (ddd) 7.63
B (d) 8.60
A (d) 8.76
3.17
1.94
3.25
1.00
0.97
f1 (ppm)

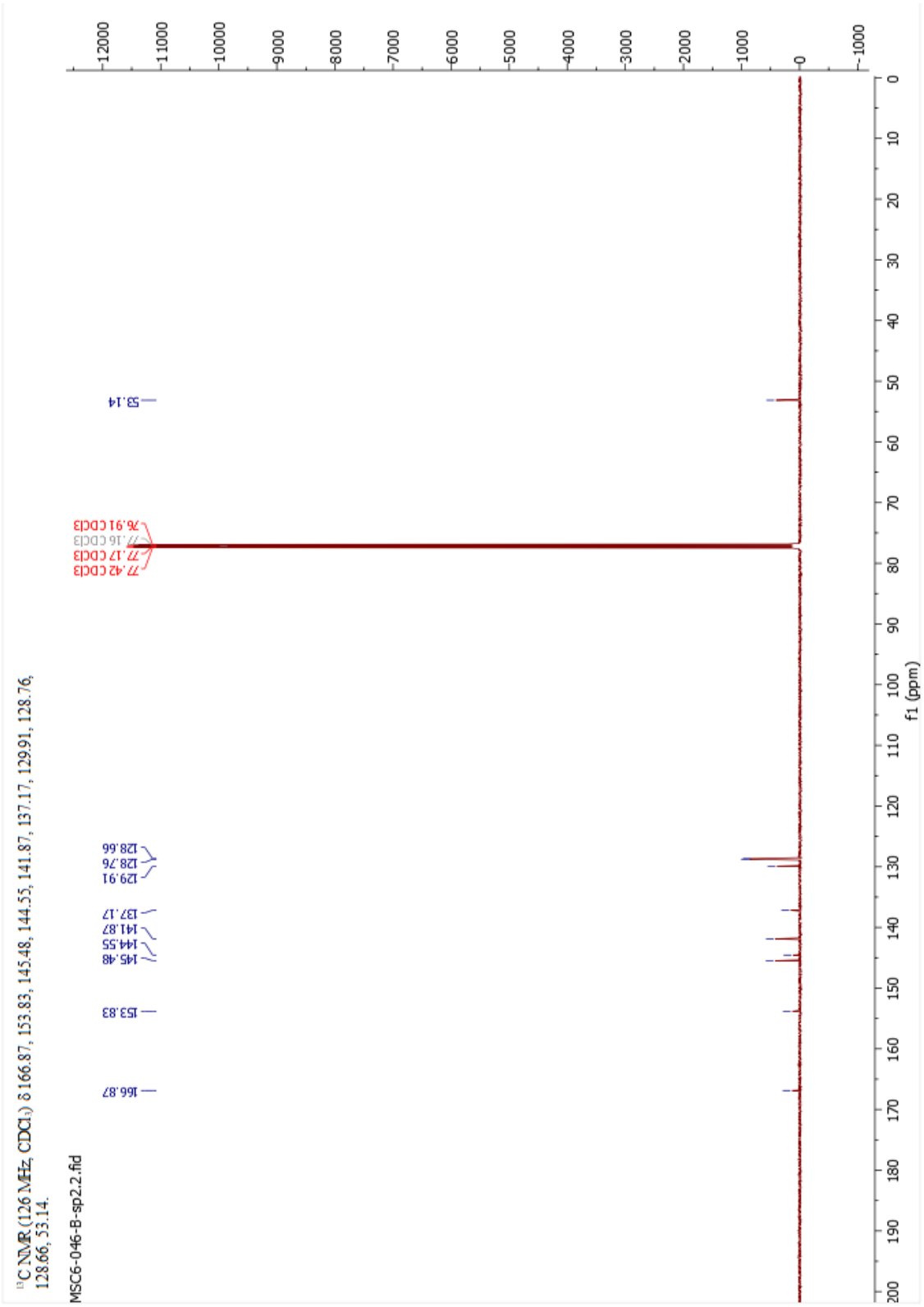

^{13}C NMR (126 MHz, $CDCl_3$) δ 166.87, 153.83, 145.48, 144.55, 141.87, 137.17, 129.91, 128.76, 128.66, 53.14.

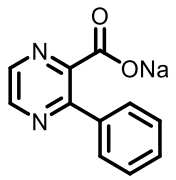
O
N
ONa
N

POAA026

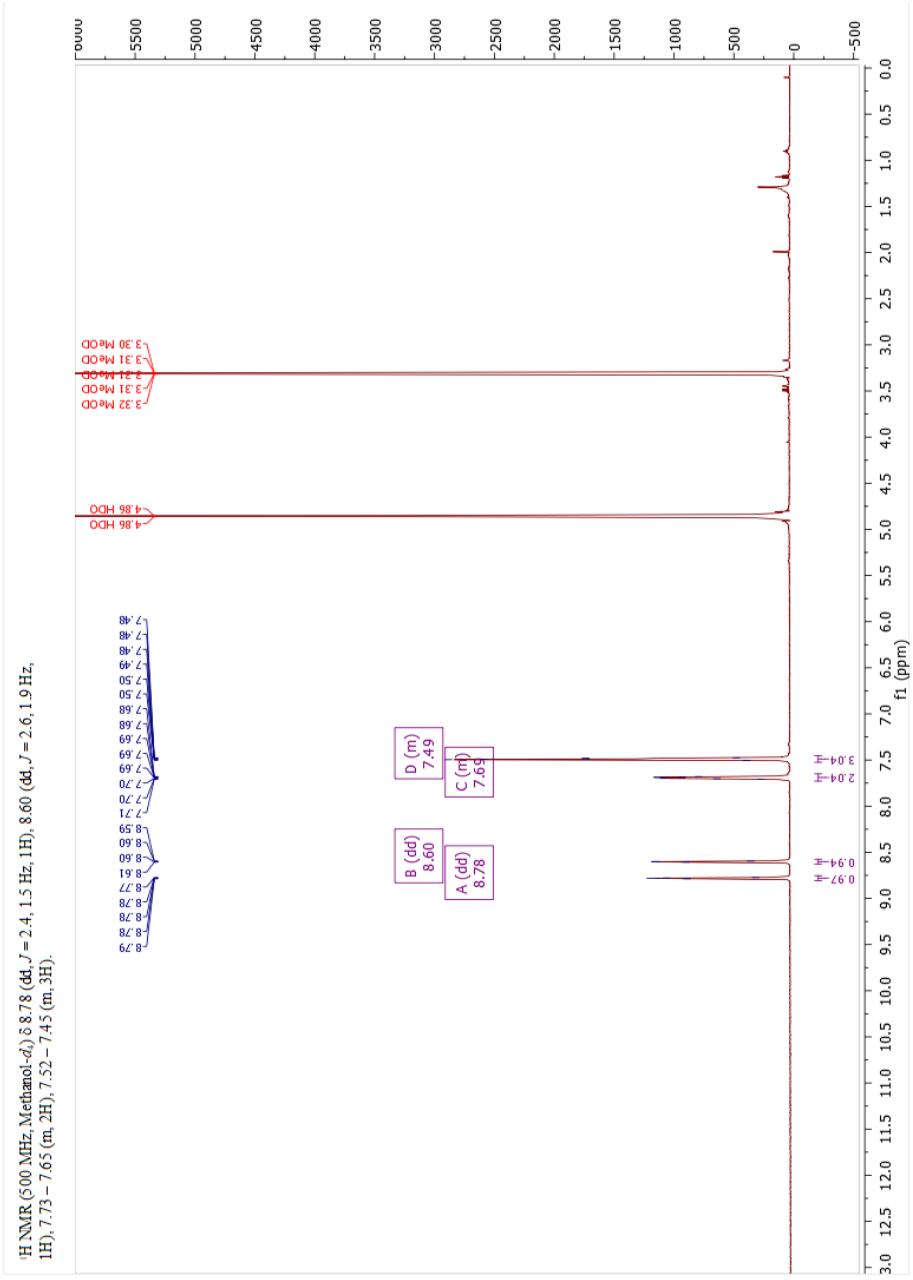
^{1}H NMR (500 MHz, Methanol-d_4) δ 8.78 (dd, J = 2.4, 1.5 Hz, 1H), 8.60 (dd, J = 2.6, 1.9 Hz, 1H), 7.73 – 7.65 (m, 2H), 7.52 – 7.45 (m, 3H).
A (dd) 8.78
B (dd) 8.60
C (m) 7.69
D (m) 7.49
4.86 HDO
3.32 MeOD
3.31 MeOD
3.31 MeOD
3.31 MeOD
3.30 MeOD
0.97
0.94
2.04
3.04
f1 (ppm)

^{13}C NMR (126 MHz, MeOD) δ 153.98, 146.42, 142.97, 138.50, 130.70, 129.77, 129.51.

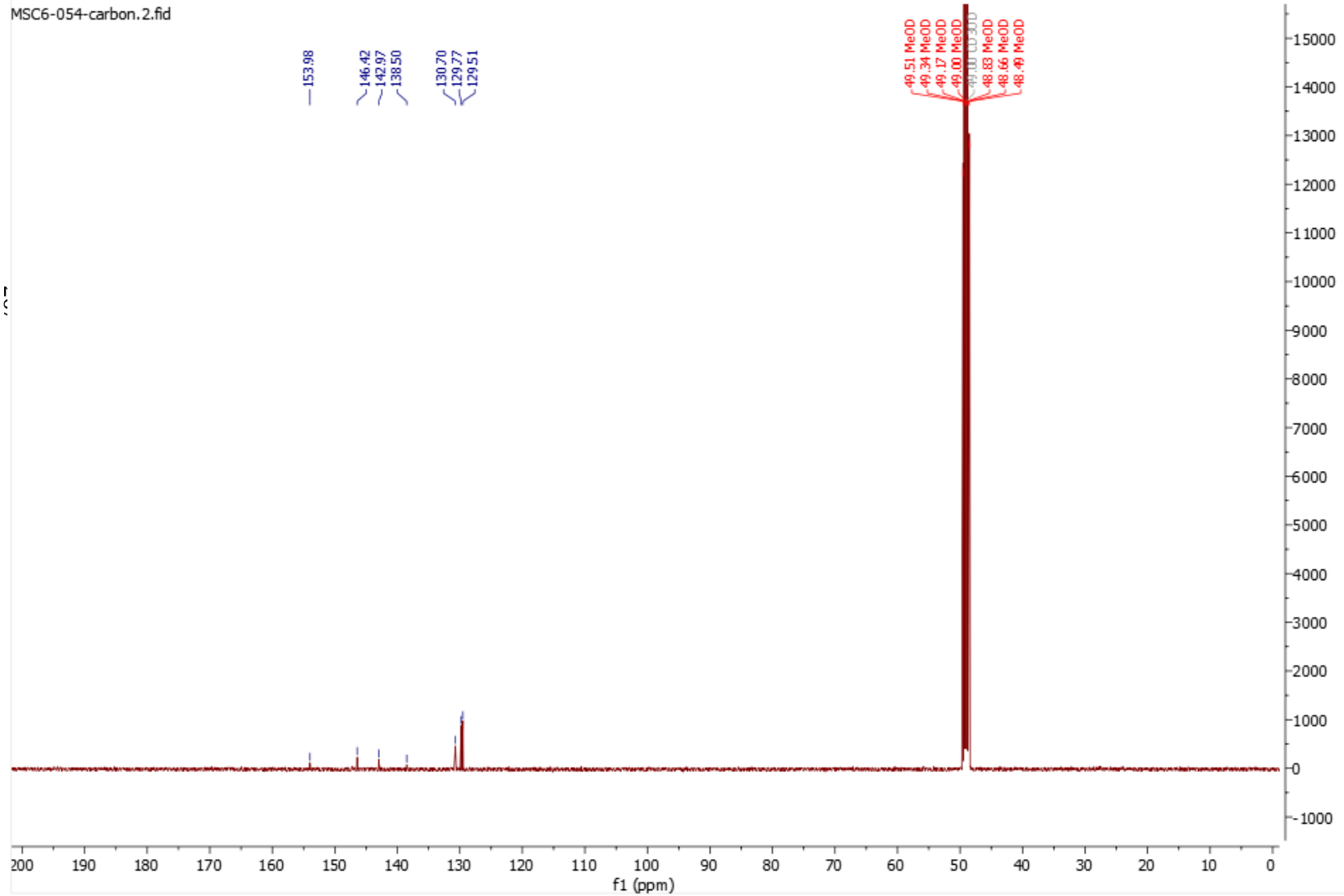

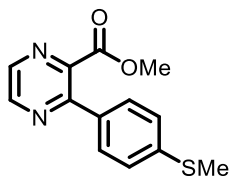

POAA028-OMe

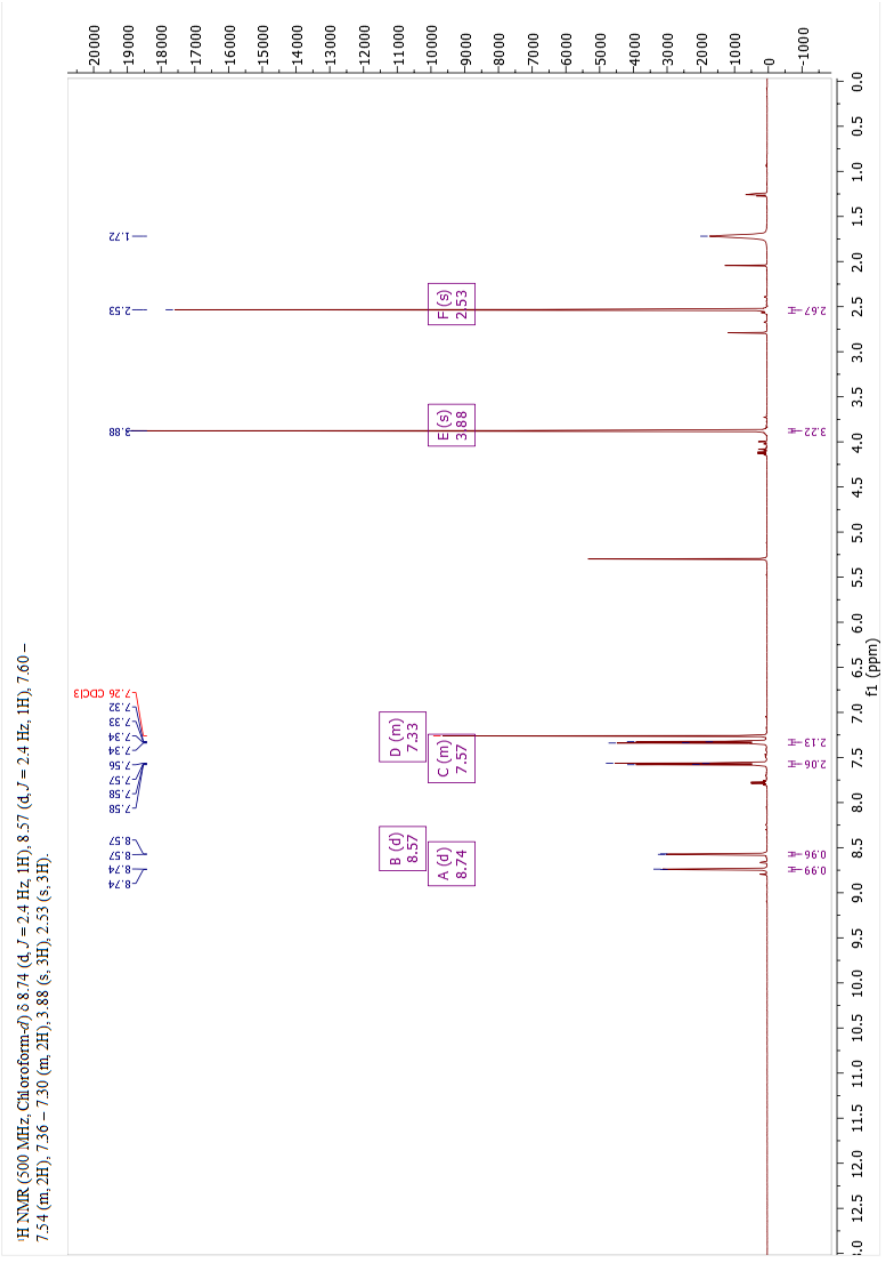

^{1}H NMR (500 MHz, Chloroform-d) δ 8.74 (d, J = 2.4 Hz, 1H), 8.57 (d, J = 2.4 Hz, 1H), 7.60 – 7.54 (m, 2H), 7.36 – 7.30 (m, 2H), 3.88 (s, 3H), 2.53 (s, 3H).

^{13}C NMR (126 MHz, $CDCl_3$) δ 166.88, 152.97, 145.23, 144.31, 141.69, 141.65, 133.20, 129.77, 129.07, 126.03, 123.89, 53.23, 15.37.

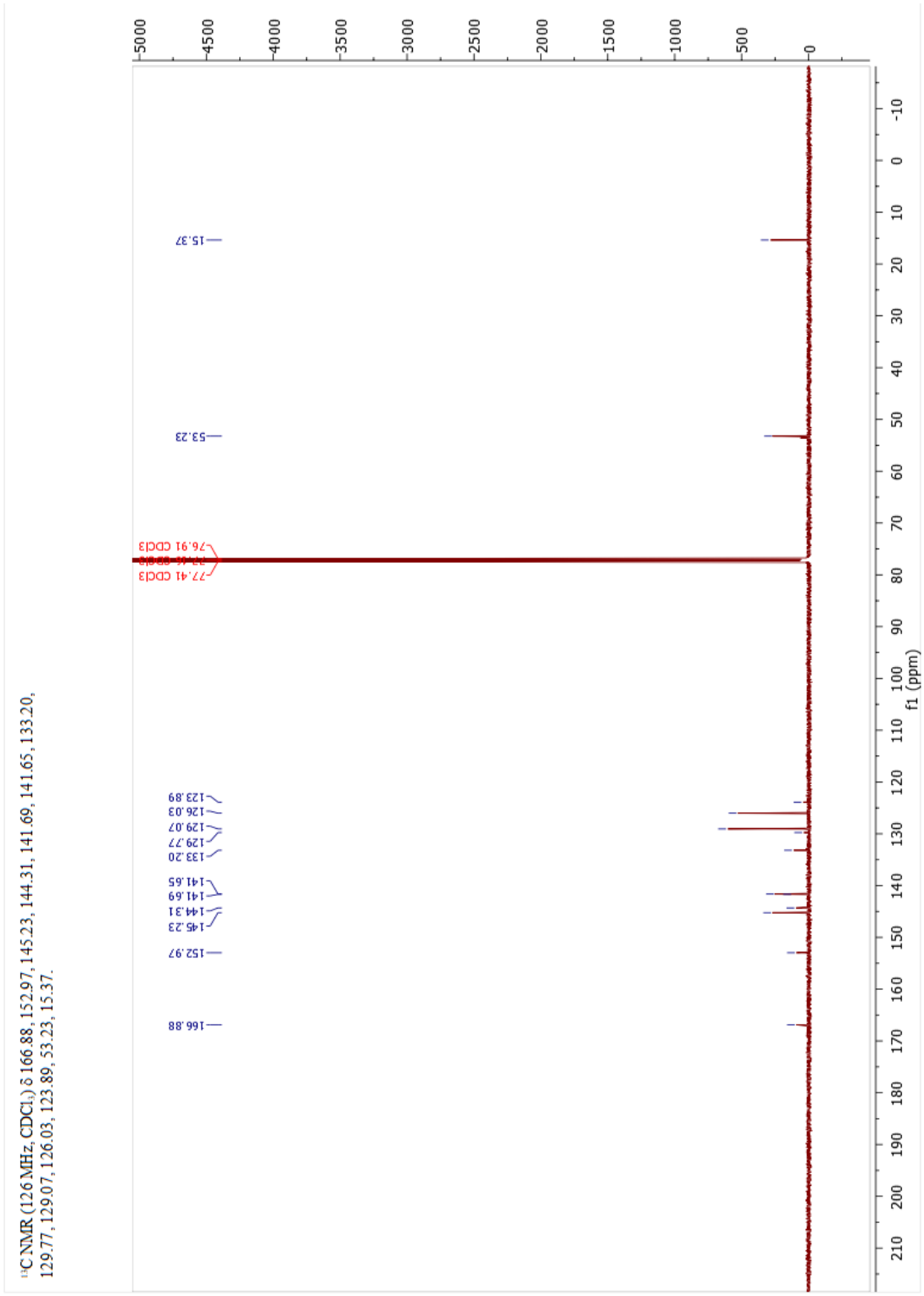

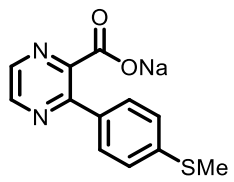
O
ONa
N
N
SMe

POAA028

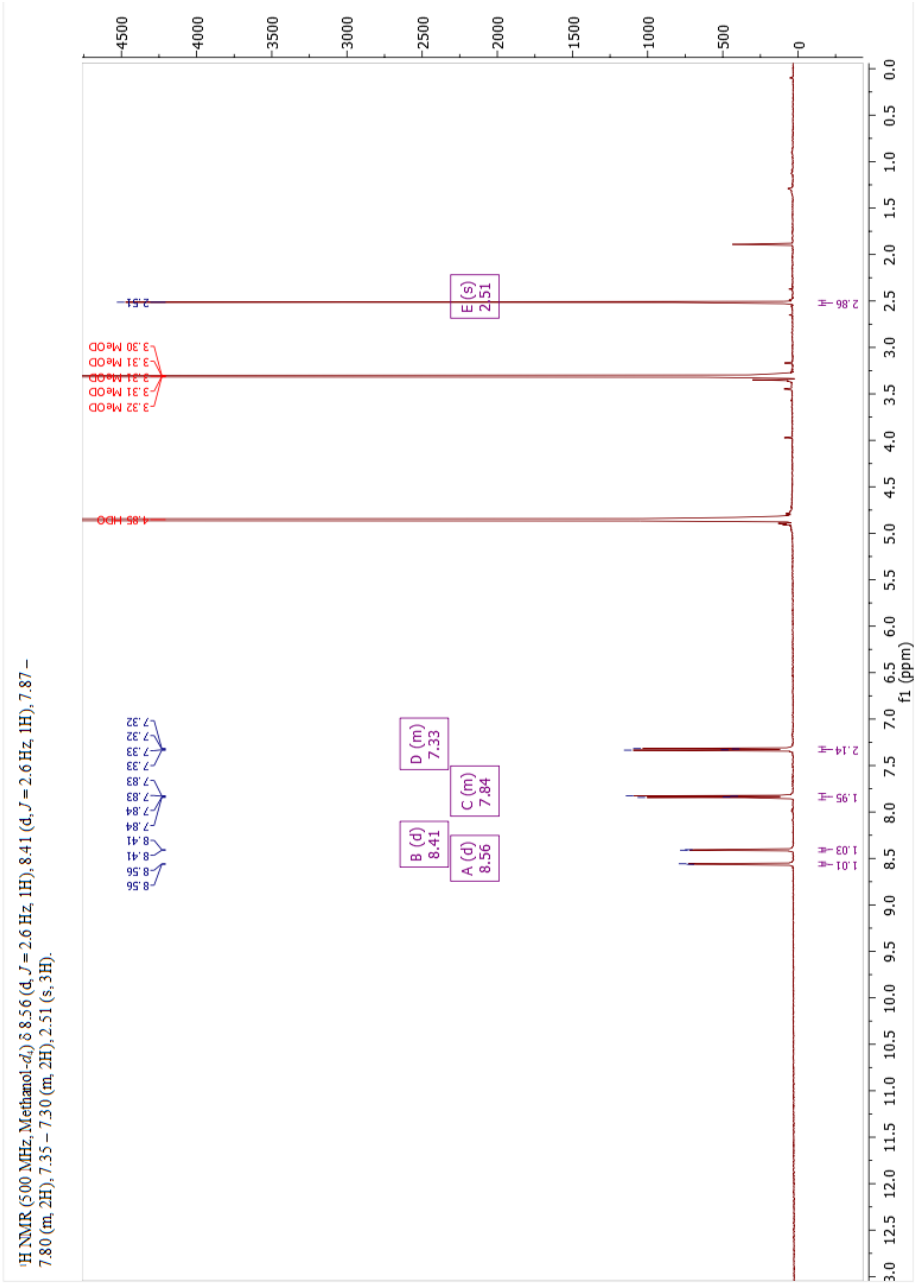
^{1}H NMR (500 MHz, Methanol-d_4) δ 8.56 (d, J = 2.6 Hz, 1H), 8.41 (d, J = 2.6 Hz, 1H), 7.87 – 7.80 (m, 2H), 7.35 – 7.30 (m, 2H), 2.51 (s, 3H).
E (s) 2.51
D (m) 7.33
C (m) 7.84
B (d) 8.41
A (d) 8.56
f1 (ppm)

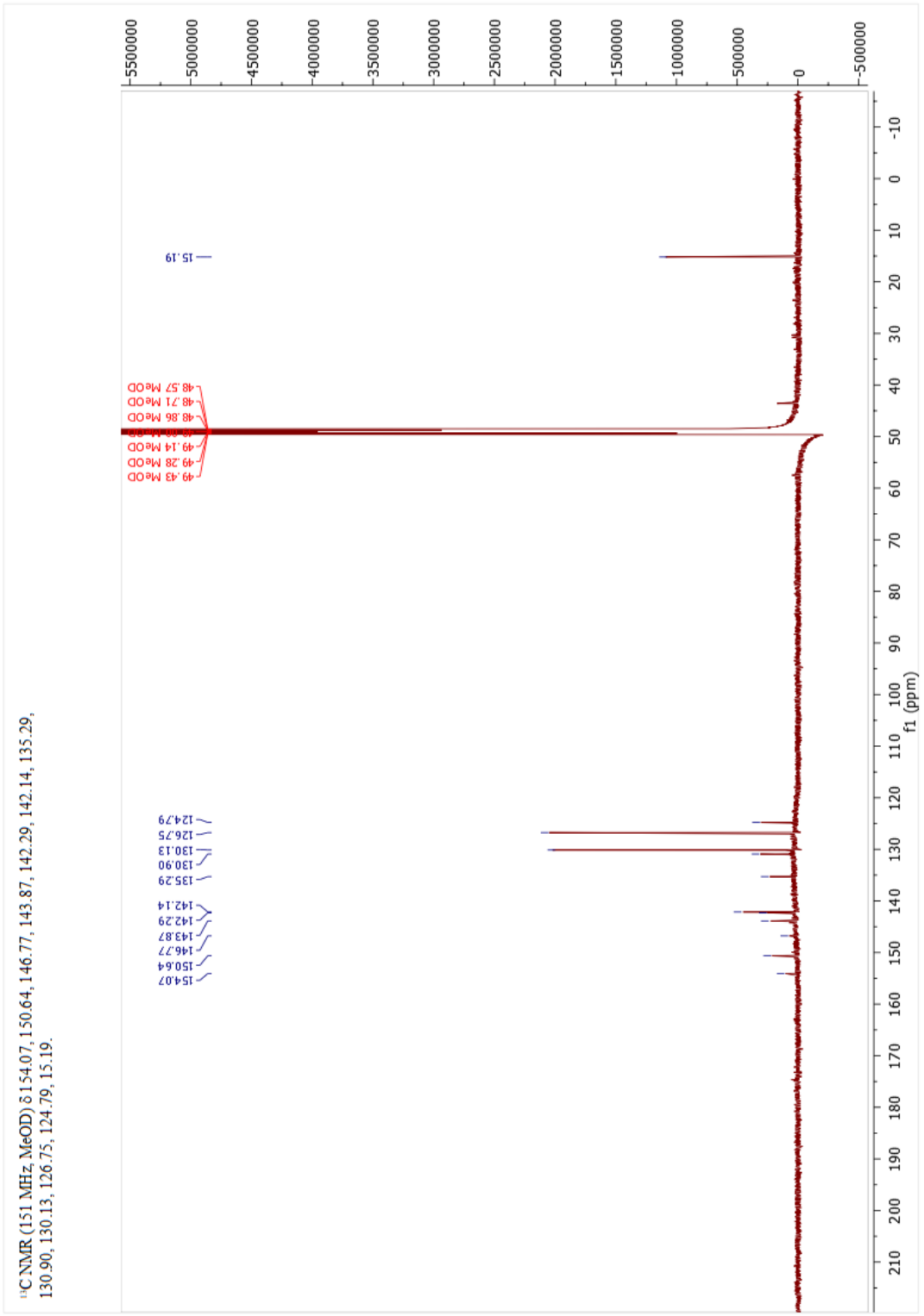

^{13}C NMR (151 MHz, MeOD) δ 154.07, 150.64, 146.77, 143.87, 142.29, 142.14, 135.29, 130.90, 130.13, 126.75, 124.79, 15.19.

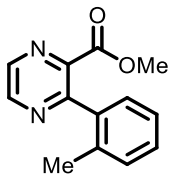
O
OMe
N
N
Me

POAA029-OMe

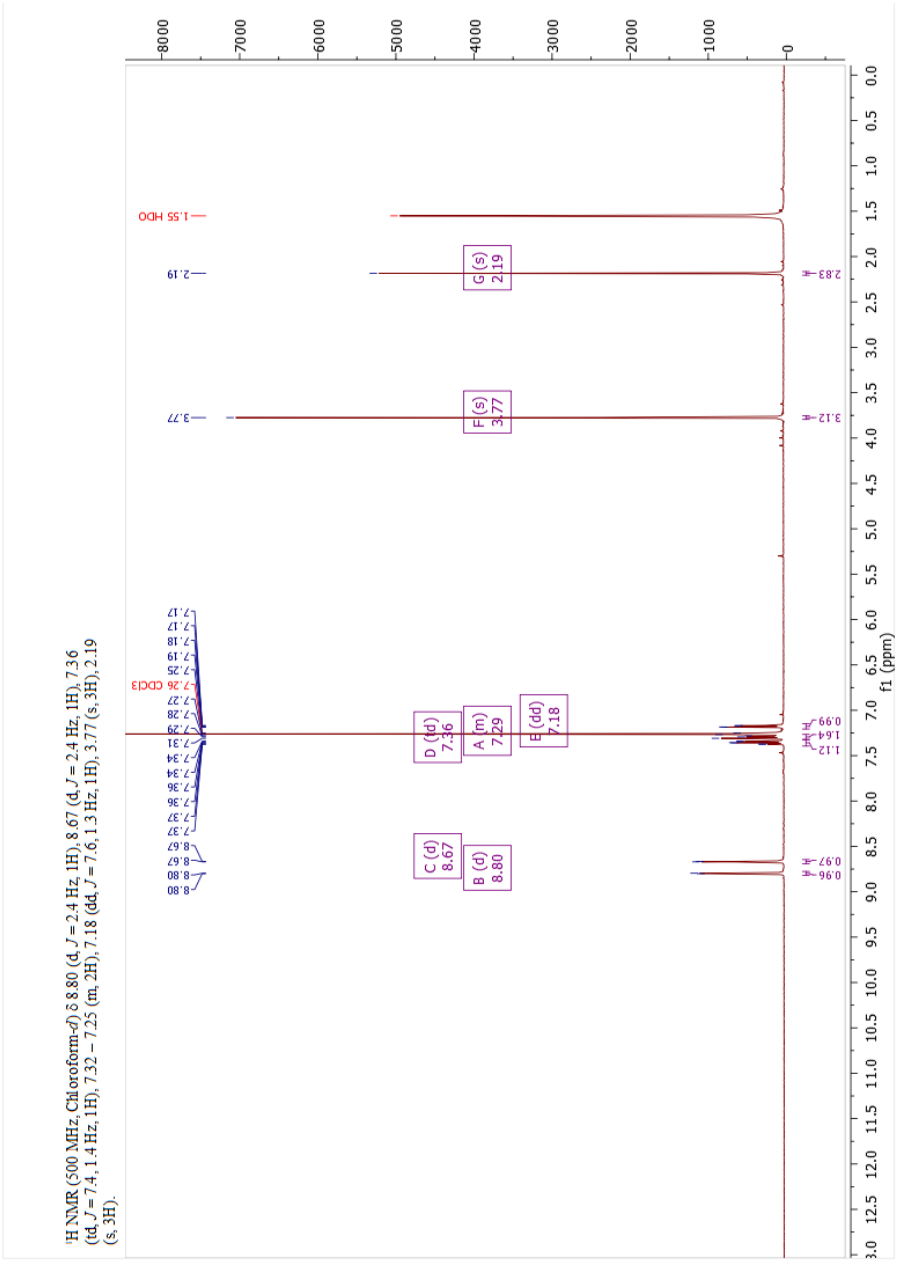
^{1}H NMR (500 MHz, Chloroform-*d*) δ 8.80 (d, *J* = 2.4 Hz, 1H), 8.67 (d, *J* = 2.4 Hz, 1H), 7.36 (td, *J* = 7.4, 1.4 Hz, 1H), 7.32 – 7.25 (m, 2H), 7.18 (dd, *J* = 7.6, 1.3 Hz, 1H), 3.77 (s, 3H), 2.19 (s, 3H).
C (d) 8.67
B (d) 8.80
D (td) 7.36
A (m) 7.29
E (dd) 7.18
F (s) 3.77
G (s) 2.19
CDCl3
HDO
f1 (ppm)

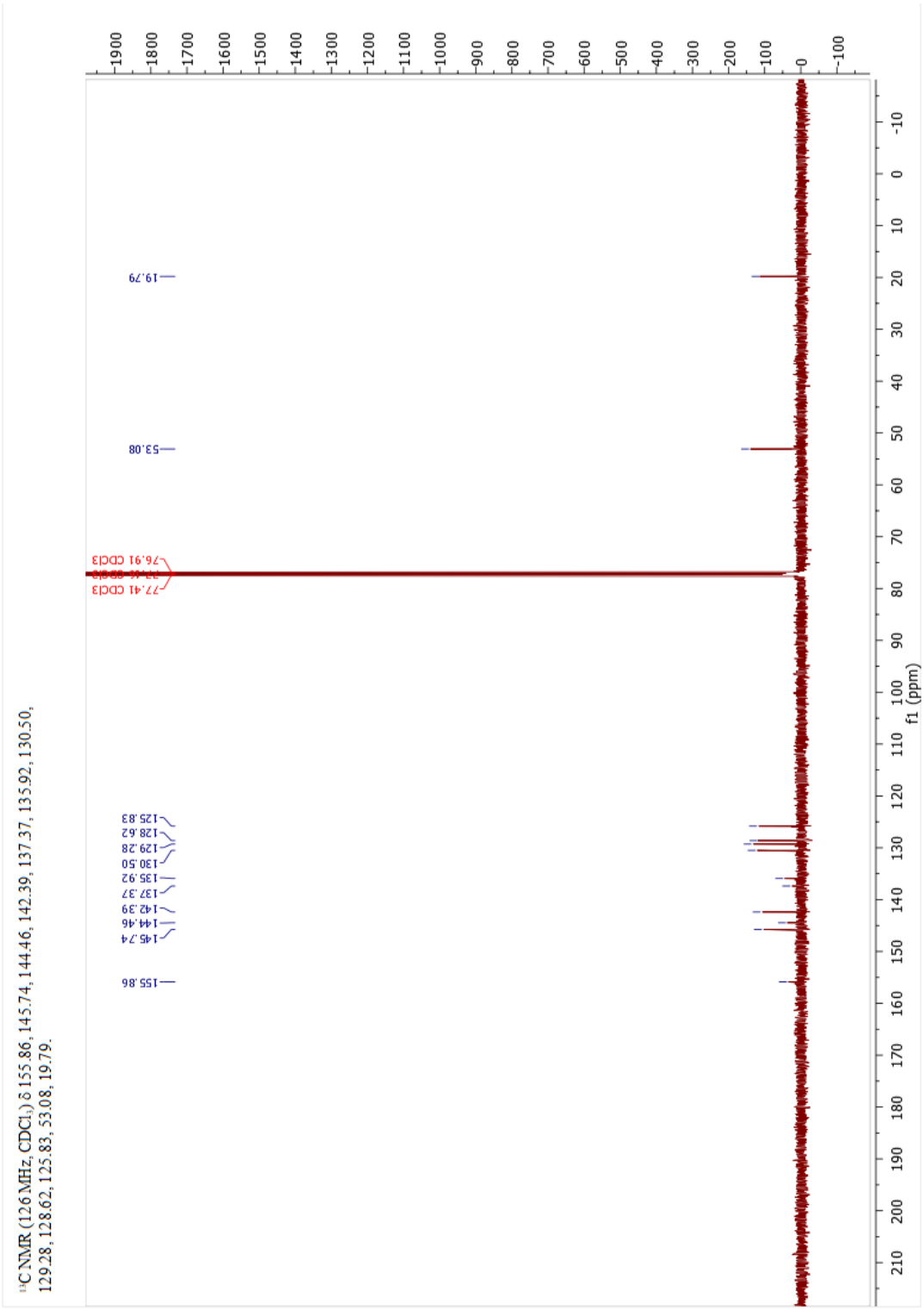
^{13}C NMR (126 MHz, CDCl$_3$) δ 155.86, 145.74, 144.46, 142.39, 137.37, 135.92, 130.50, 129.28, 128.62, 125.83, 53.08, 19.79.
155.86
145.74
144.46
142.39
137.37
135.92
130.50
129.28
128.62
125.83
77.41 CDCl3
76.91 CDCl3
53.08
19.79
f1 (ppm)

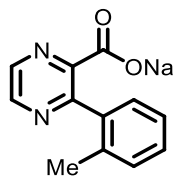
O
N
ONa
N
Me

POAA029

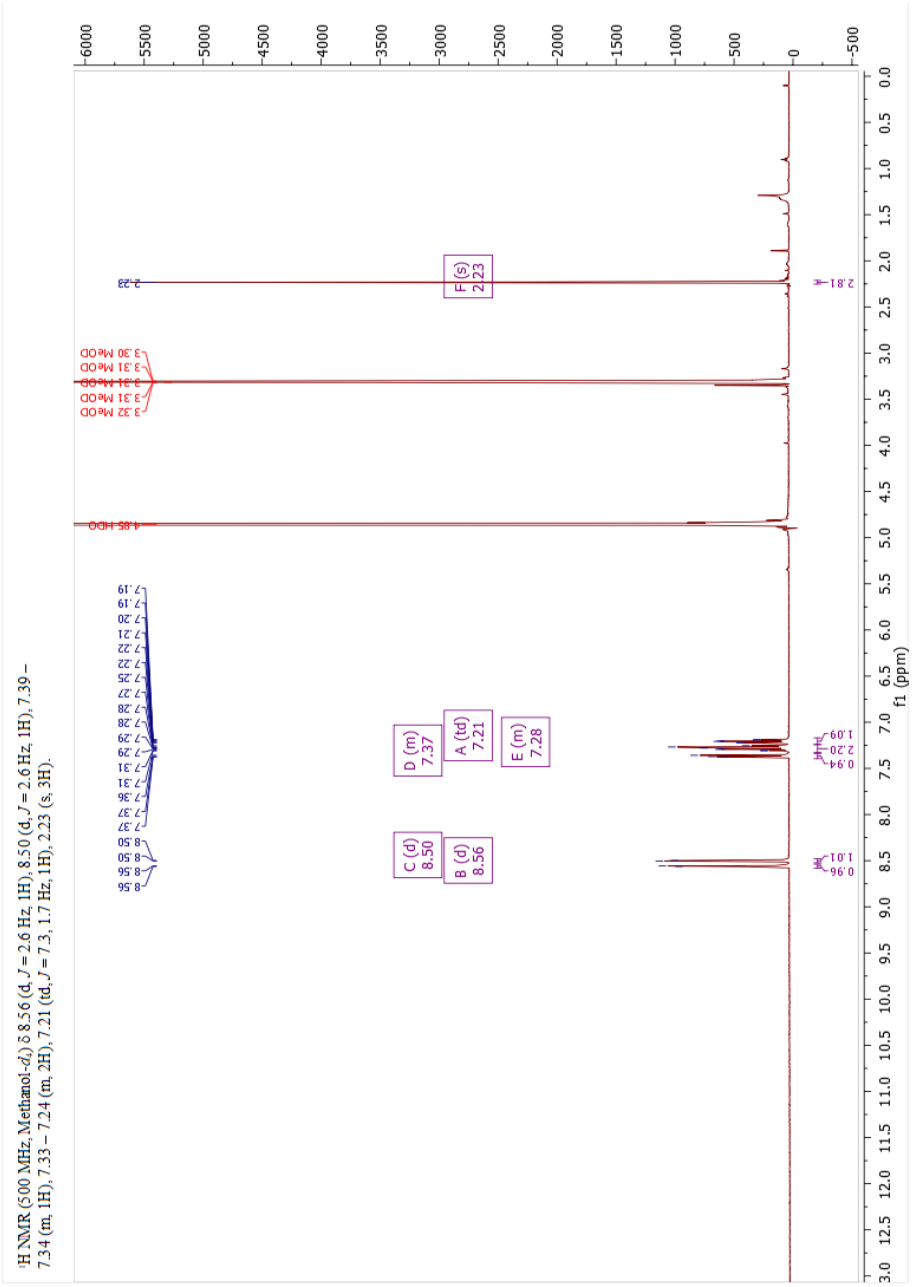
^{1}H NMR (500 MHz, Methanol-d_4) δ 8.56 (d, J = 2.6 Hz, 1H), 8.50 (d, J = 2.6 Hz, 1H), 7.39 – 7.34 (m, 1H), 7.33 – 7.24 (m, 2H), 7.21 (td, J = 7.3, 1.7 Hz, 1H), 2.23 (s, 3H).
F (s) 2.23
D (m) 7.37
A (td) 7.21
E (m) 7.28
C (d) 8.50
B (d) 8.56
f1 (ppm)

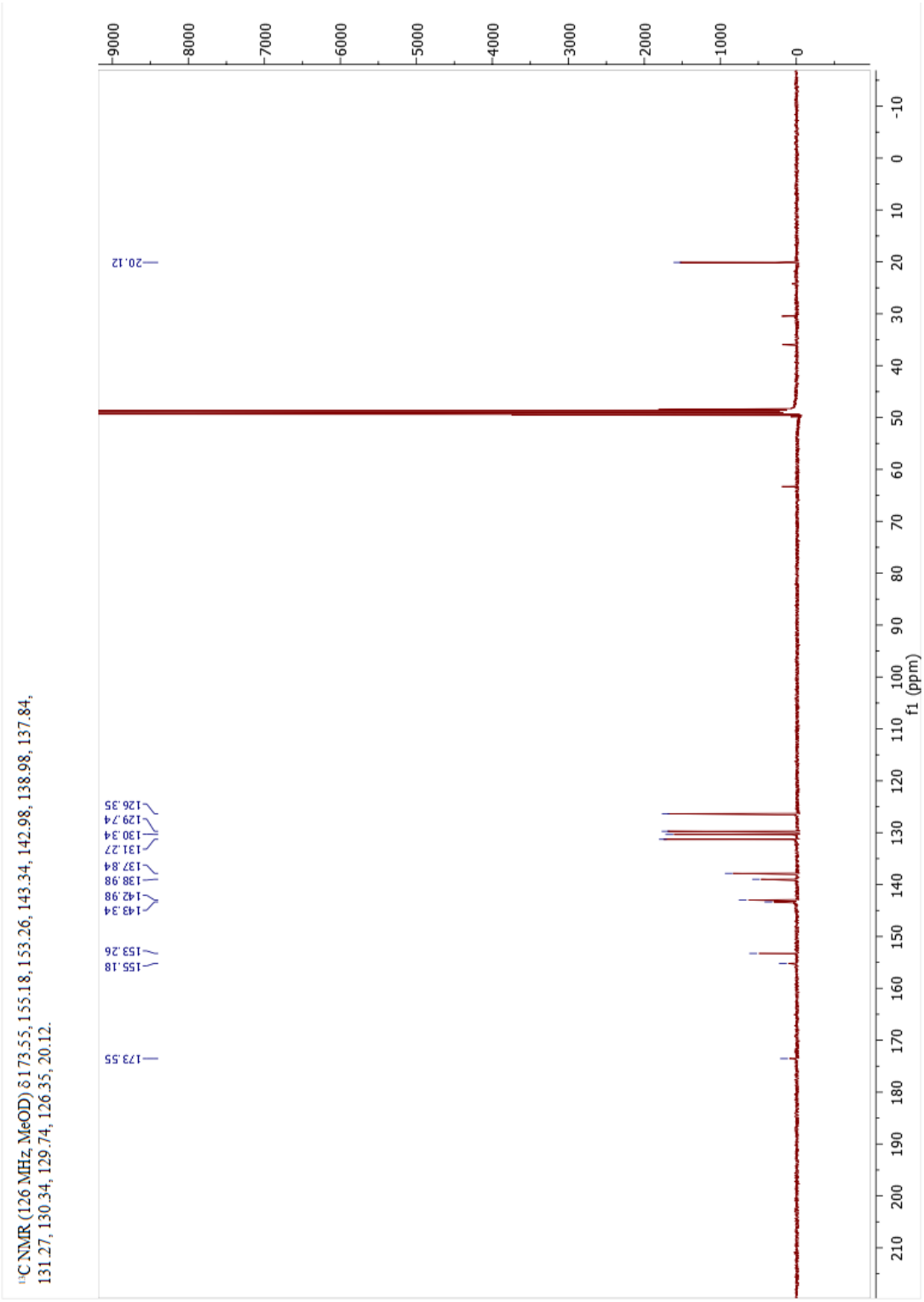
^{13}C NMR (126 MHz, MeOD) δ 173.55, 155.18, 153.26, 143.34, 142.98, 138.98, 137.84, 131.27, 130.34, 129.74, 126.35, 20.12.
20.12
126.35
129.74
130.34
131.27
137.84
138.98
142.98
143.34
153.26
155.18
173.55
f1 (ppm)

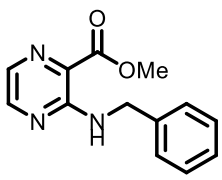

POAA033-OMe

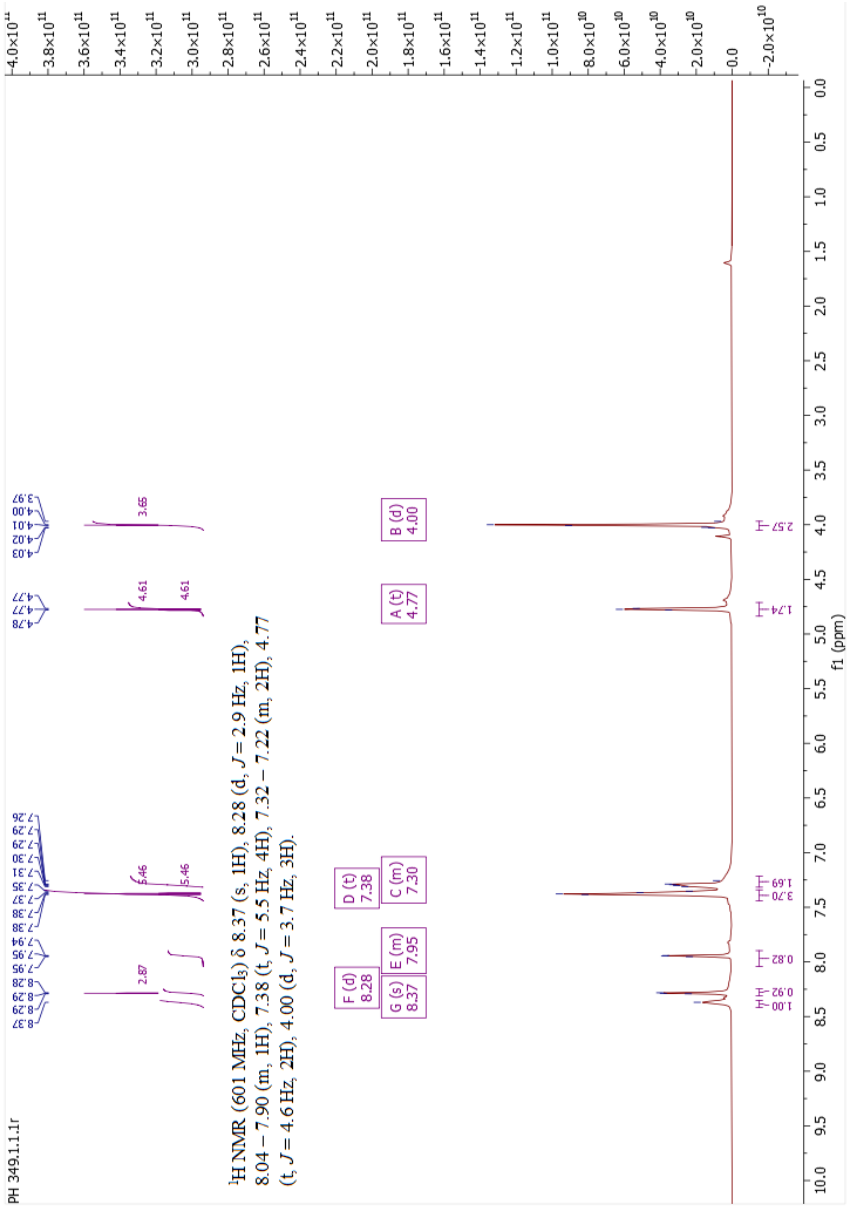
PH 349.1.1.1r
^{1}H NMR (601 MHz, $CDCl_3$) δ 8.37 (s, 1H), 8.28 (d, J = 2.9 Hz, 1H), 8.04 – 7.90 (m, 1H), 7.38 (t, J = 5.5 Hz, 4H), 7.32 – 7.22 (m, 2H), 4.77 (t, J = 4.6 Hz, 2H), 4.00 (d, J = 3.7 Hz, 3H).
F (d) 8.28
G (s) 8.37
E (m) 7.95
D (t) 7.38
C (m) 7.30
A (t) 4.77
B (d) 4.00
f1 (ppm)

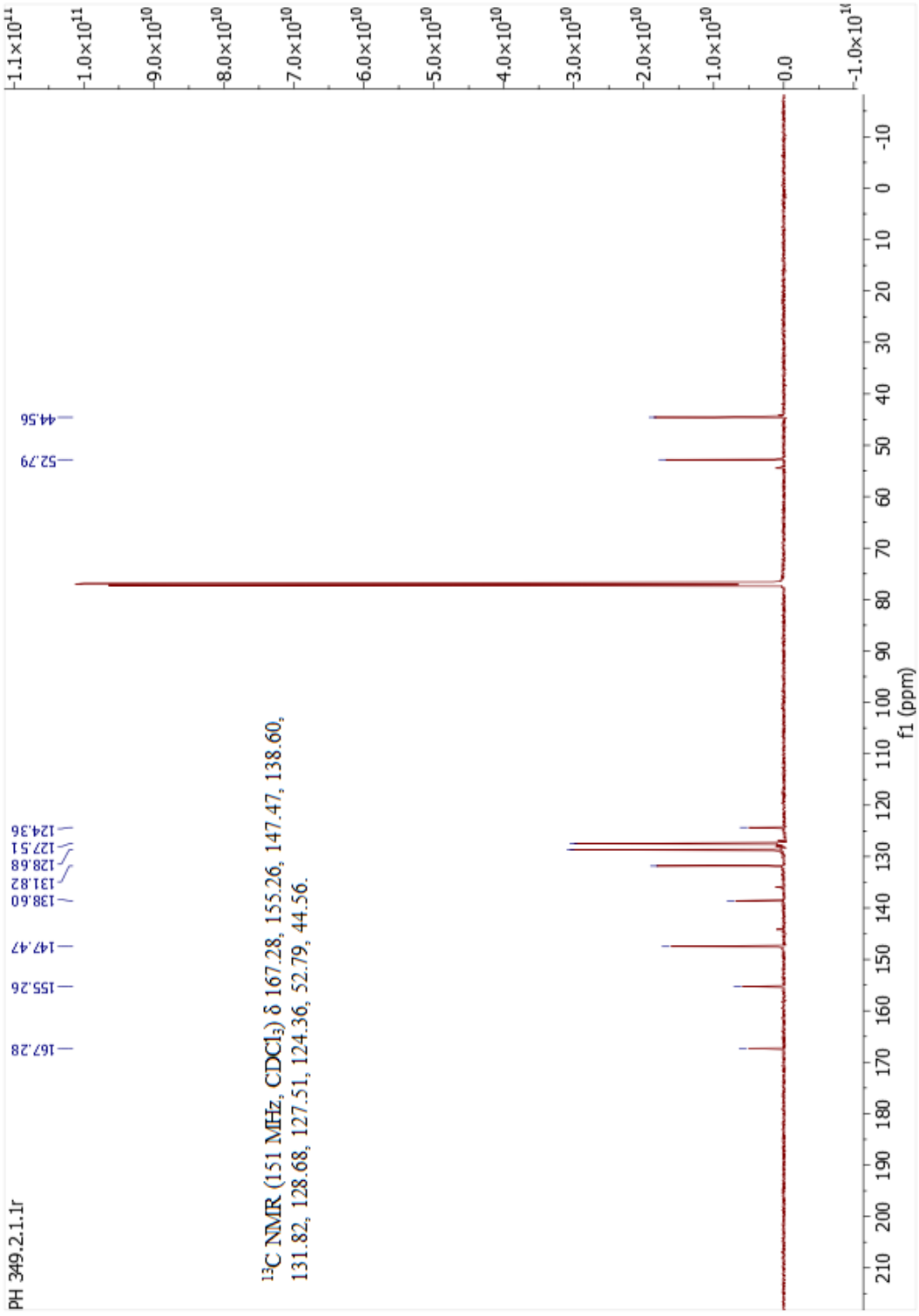
PH 349.2.1.1r
^{13}C NMR (151 MHz, CDCl$_3$) δ 167.28, 155.26, 147.47, 138.60, 131.82, 128.68, 127.51, 124.36, 52.79, 44.56.
167.28
155.26
147.47
138.60
131.82
128.68
127.51
124.36
52.79
44.56
f1 (ppm)

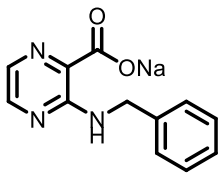
O
ONa
N
N
N
H

POAA033

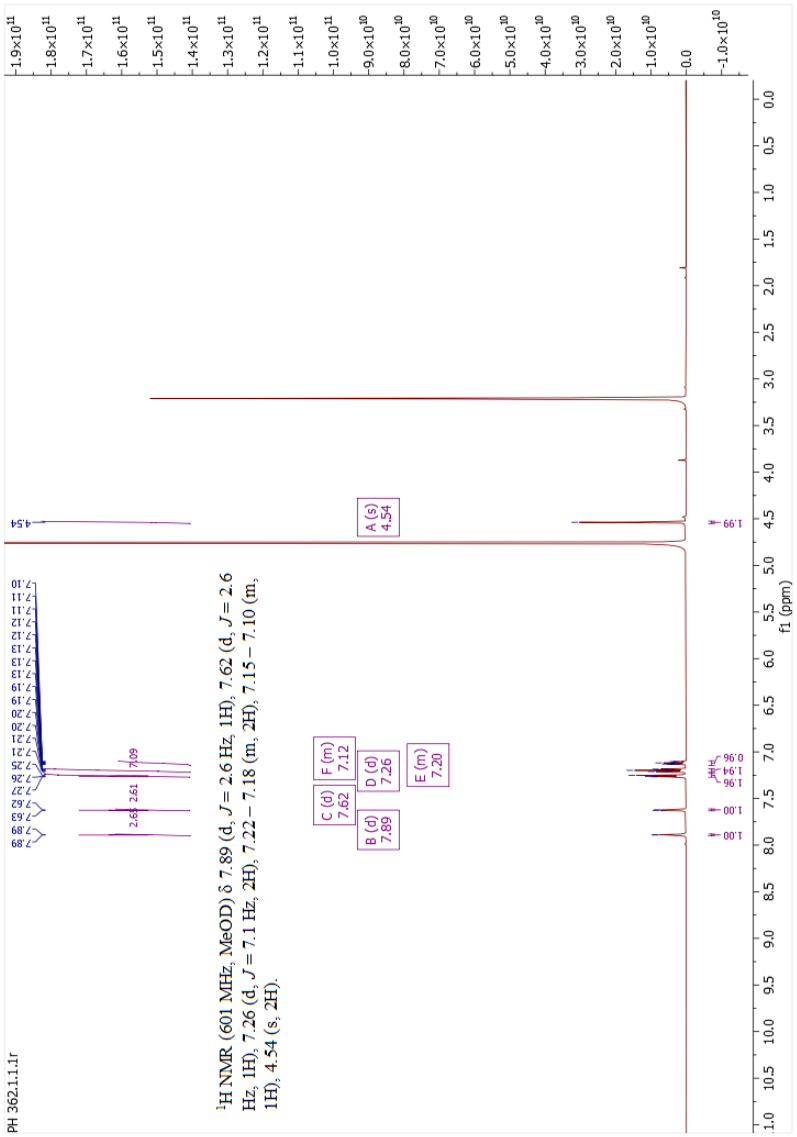
PH 362.1.1.1r
^{1}H NMR (601 MHz, MeOD) δ 7.89 (d, J = 2.6 Hz, 1H), 7.62 (d, J = 2.6 Hz, 1H), 7.26 (d, J = 7.1 Hz, 2H), 7.22 – 7.18 (m, 2H), 7.15 – 7.10 (m, 1H), 4.54 (s, 2H).
A (s) 4.54
B (d) 7.89
C (d) 7.62
D (d) 7.26
E (m) 7.20
F (m) 7.12
f1 (ppm)

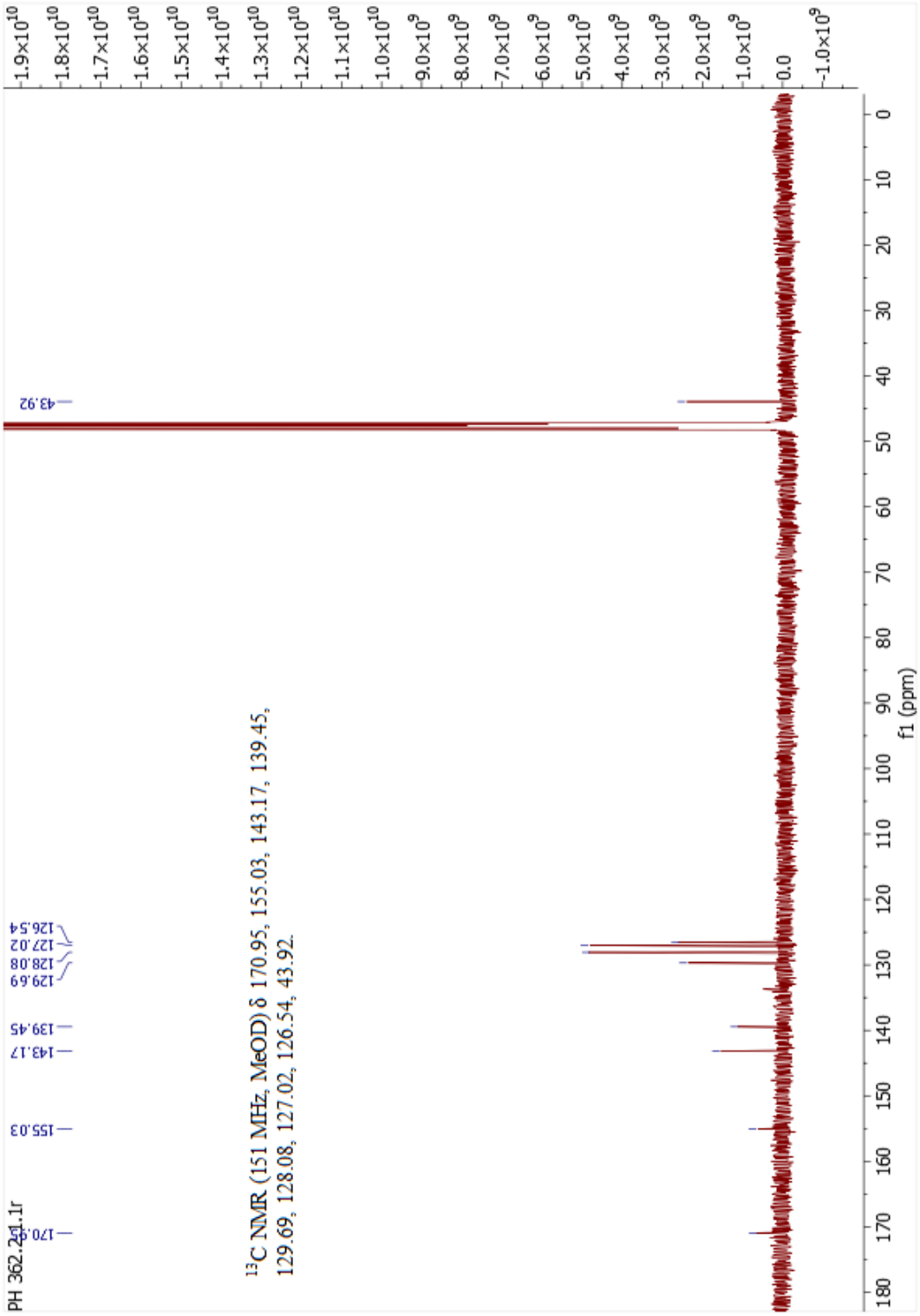
PH 362.2d1.1r
170.95
155.03
143.17
139.45
129.69
128.08
127.02
126.54
43.92
^{13}C NMR (151 MHz, MeOD) δ 170.95, 155.03, 143.17, 139.45, 129.69, 128.08, 127.02, 126.54, 43.92.
f1 (ppm)

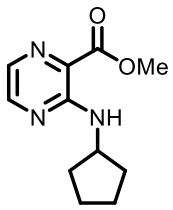

POAA035-OMe

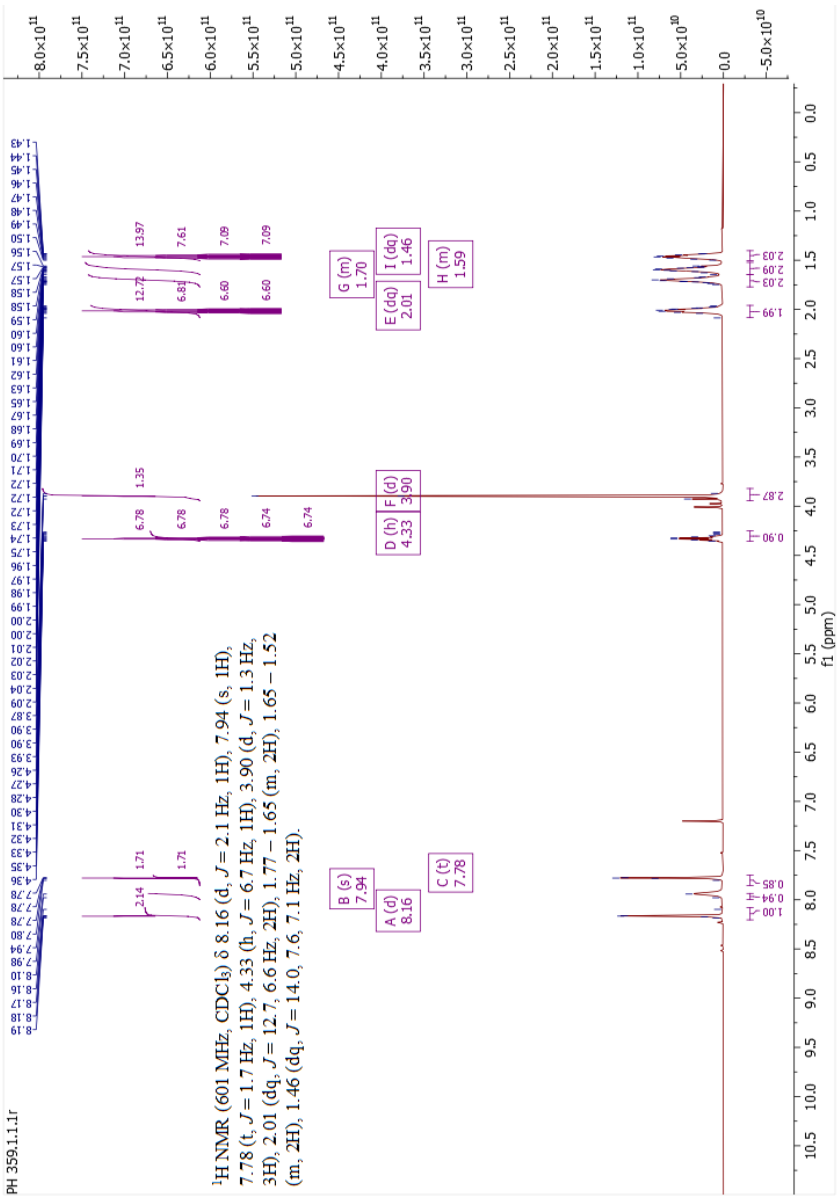
PH 359.1.1.1r
^{1}H NMR (601 MHz, $CDCl_3$) δ 8.16 (d, J = 2.1 Hz, 1H), 7.94 (s, 1H), 7.78 (t, J = 1.7 Hz, 1H), 4.33 (h, J = 6.7 Hz, 1H), 3.90 (d, J = 1.3 Hz, 3H), 2.01 (dq, J = 12.7, 6.6 Hz, 2H), 1.77 – 1.65 (m, 2H), 1.65 – 1.52 (m, 2H), 1.46 (dq, J = 14.0, 7.6, 7.1 Hz, 2H).
A (d) 8.16
B (s) 7.94
C (t) 7.78
D (h) 4.33
E (dq) 2.01
F (d) 3.90
G (m) 1.70
H (m) 1.59
I (dq) 1.46
f1 (ppm)

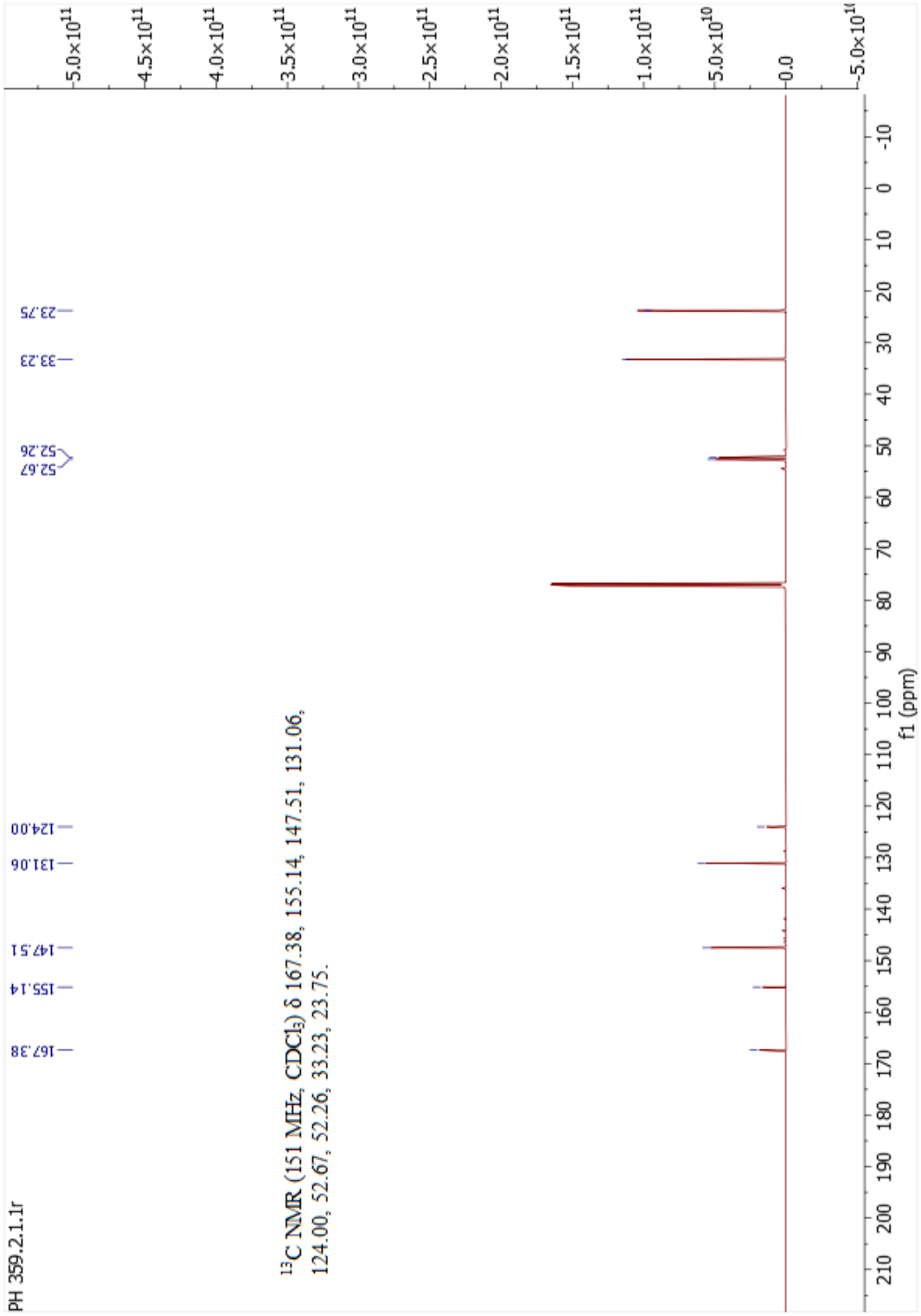
PH 359.2.1.1r
^{13}C NMR (151 MHz, $CDCl_3$) δ 167.38, 155.14, 147.51, 131.06, 124.00, 52.67, 52.26, 33.23, 23.75.
167.38
155.14
147.51
131.06
124.00
52.67
52.26
33.23
23.75
f1 (ppm)

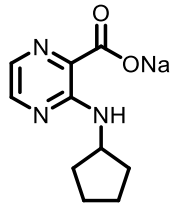
O
ONa
N
N
NH

POAA035

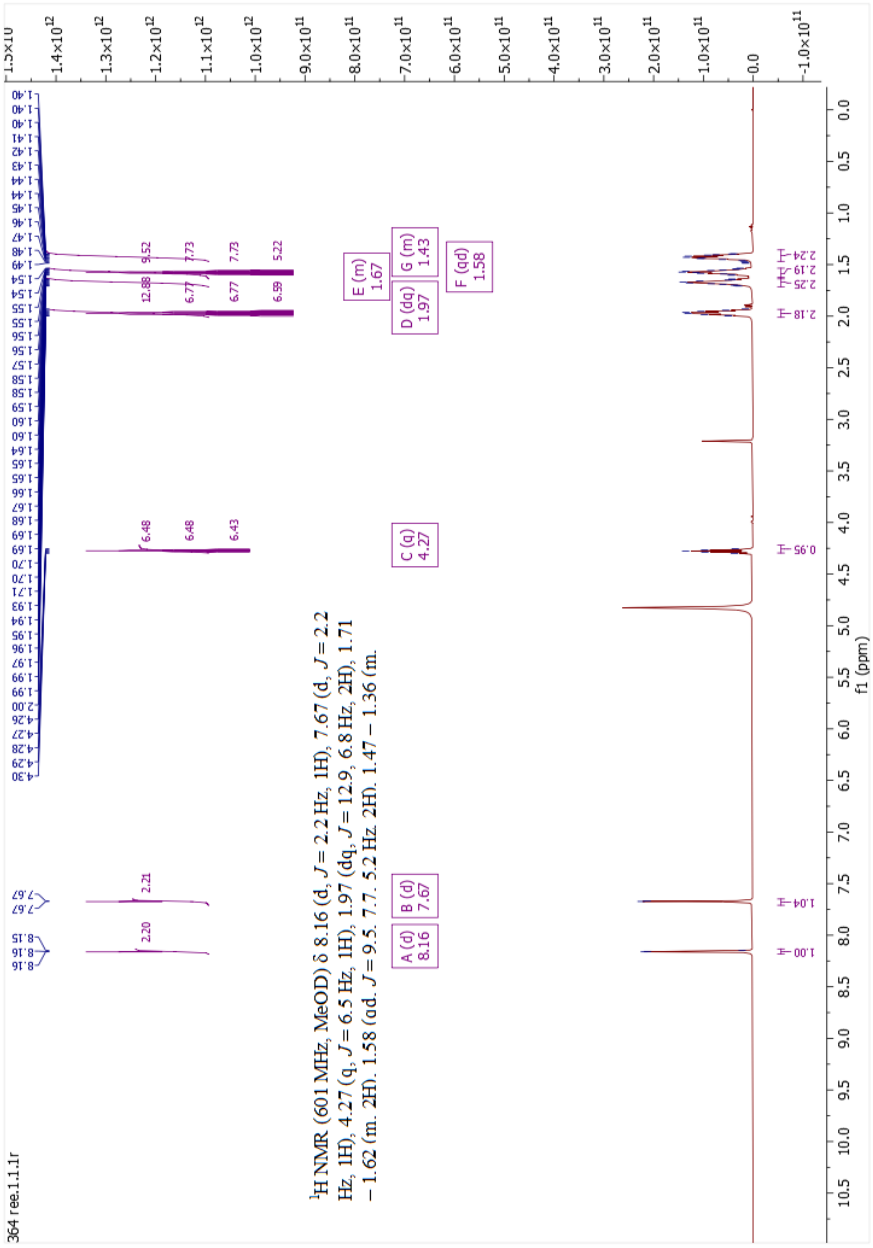
^{1}H NMR (601 MHz, MeOD) δ 8.16 (d, J = 2.2 Hz, 1H), 7.67 (d, J = 2.2 Hz, 1H), 4.27 (q, J = 6.5 Hz, 1H), 1.97 (dq, J = 12.9, 6.8 Hz, 2H), 1.71 – 1.62 (m, 2H), 1.58 (qd, J = 9.5, 7.7, 5.2 Hz, 2H), 1.47 – 1.36 (m,
A (d) 8.16
B (d) 7.67
C (q) 4.27
D (dq) 1.97
E (m) 1.67
F (qd) 1.58
G (m) 1.43
f1 (ppm)

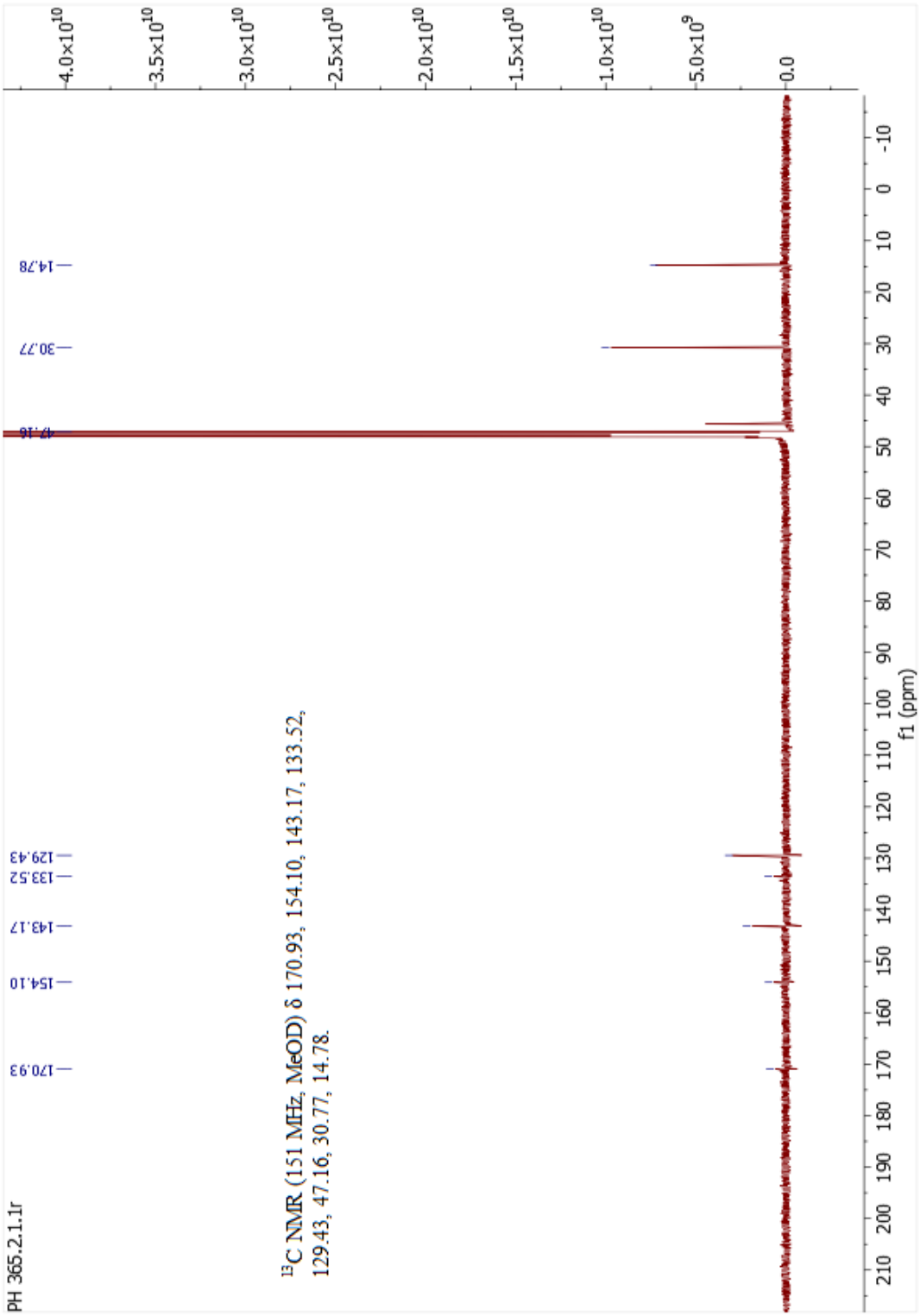
PH 365.2.1.1r
^{13}C NMR (151 MHz, MeOD) δ 170.93, 154.10, 143.17, 133.52, 129.43, 47.16, 30.77, 14.78.
170.93
154.10
143.17
133.52
129.43
47.16
30.77
14.78
f1 (ppm)

Sodium 3-pyrrolidinepyrazine-2-carboxylate (POA 31)

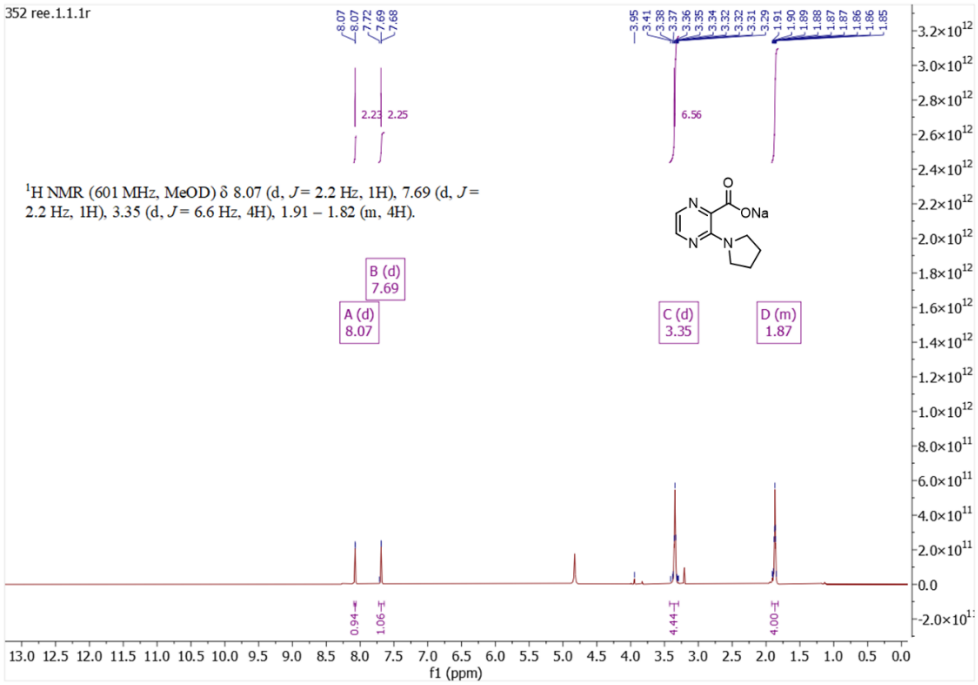

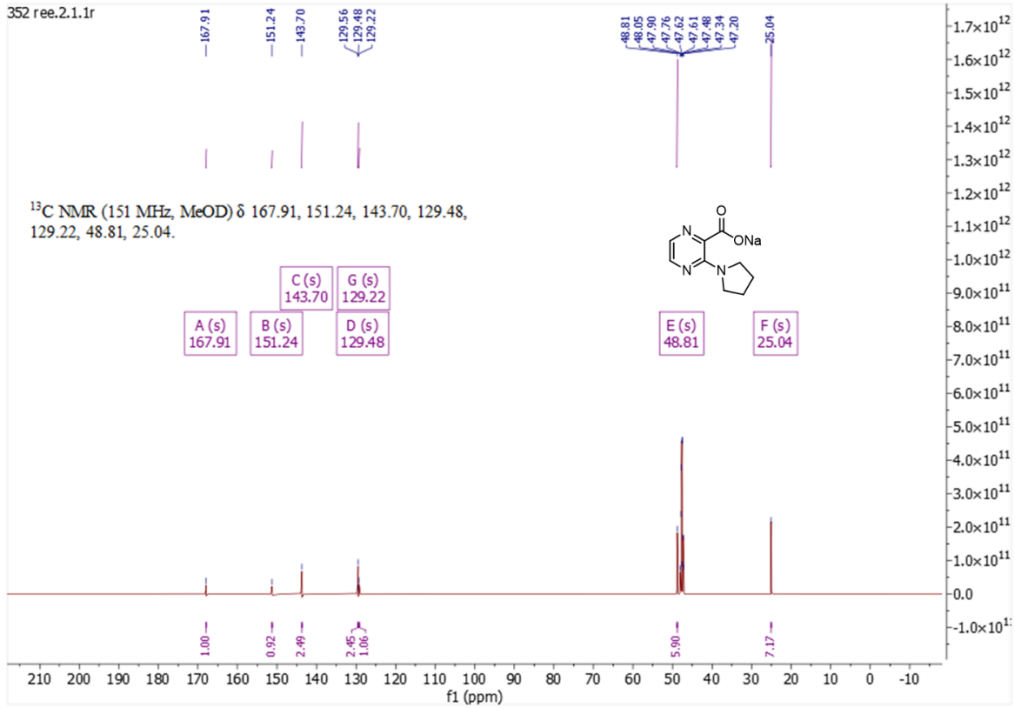

Sodium 3-piperidinepyrazine-2-carboxylate (POA 32)

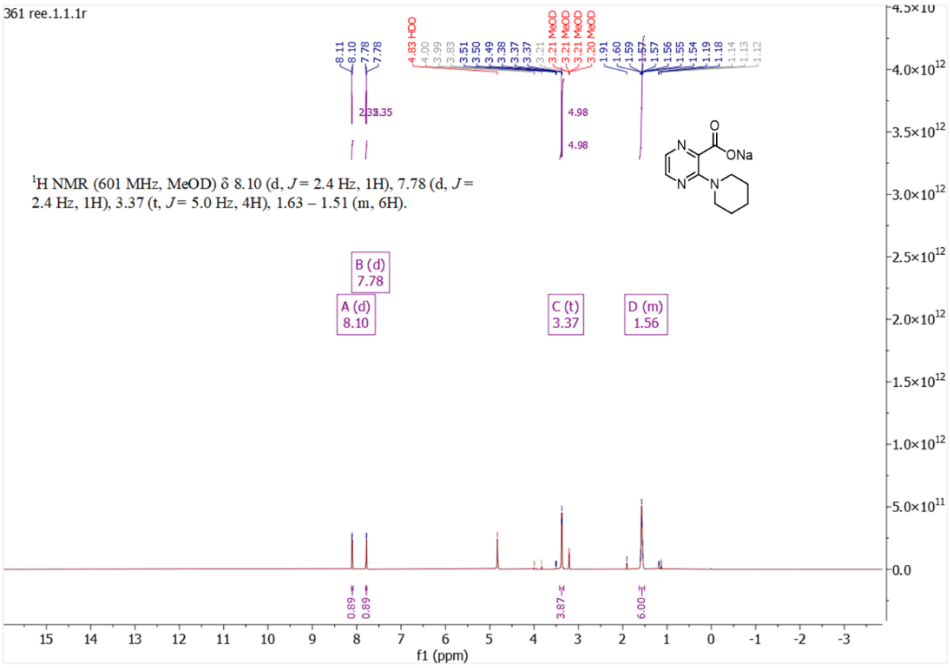

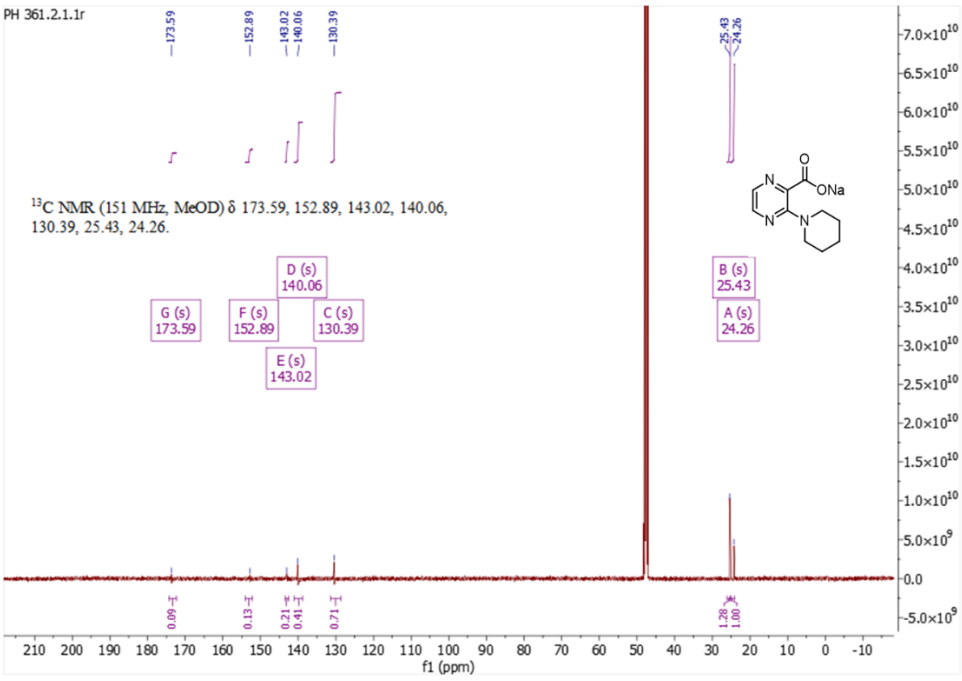

Sodium 3-morpholinopyrazine-2-carboxylate (POA 37)

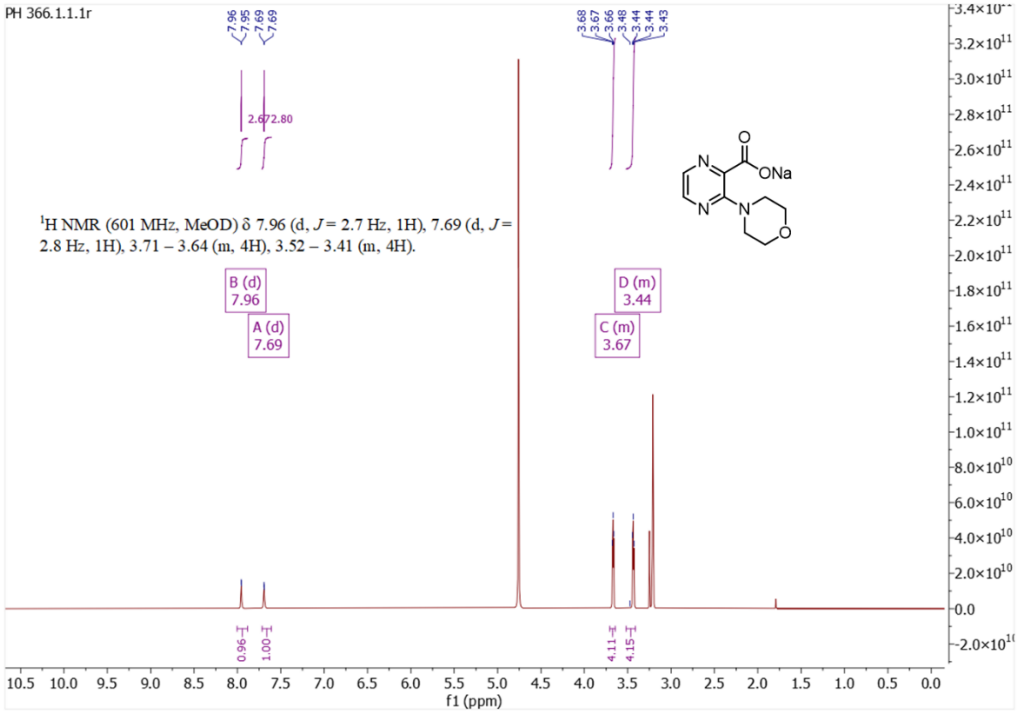

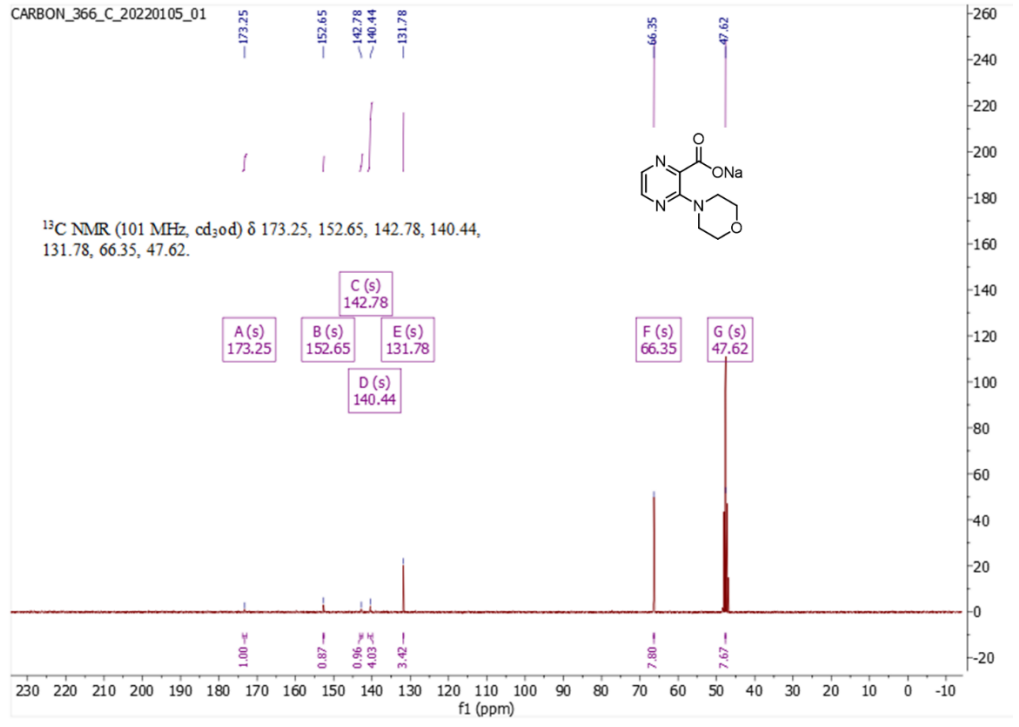

Sodium 3-thiomorpholinopyrazine-2-carboxylate (POA 38)

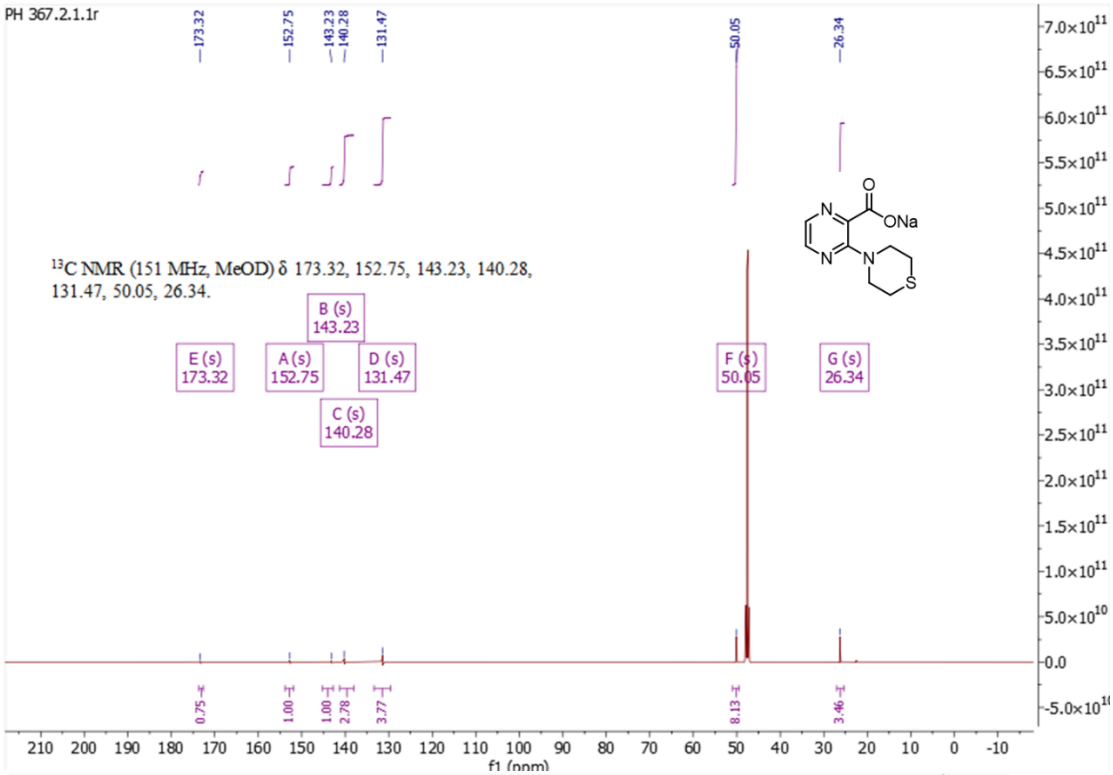

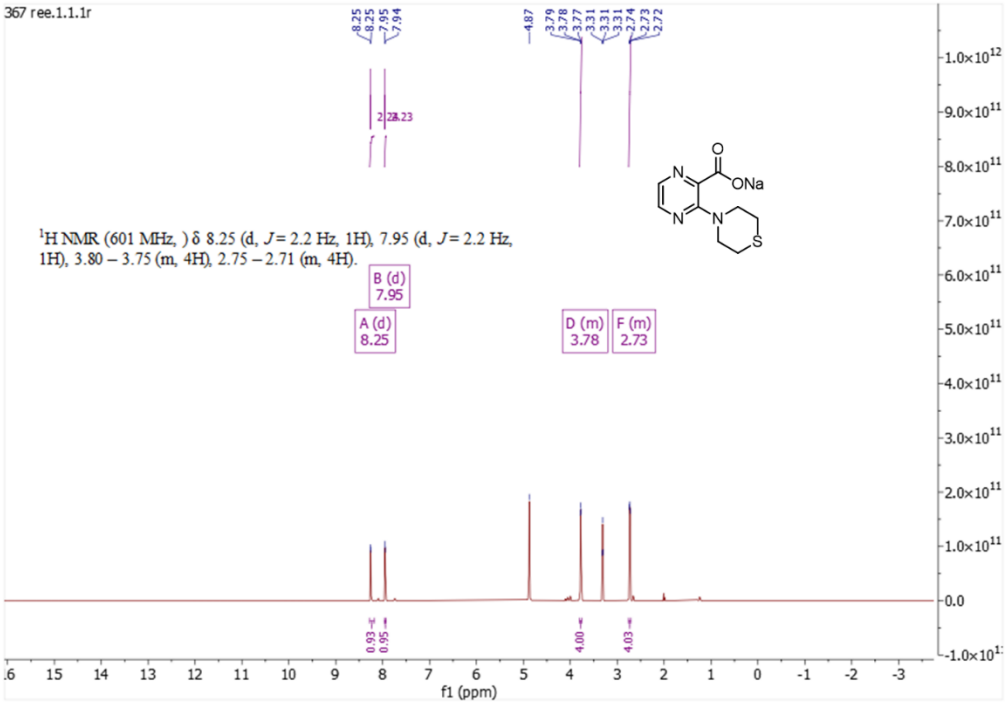

3-(6-azaspiro[2,5] octano) 2-pyrazinoic acid (POA 41)

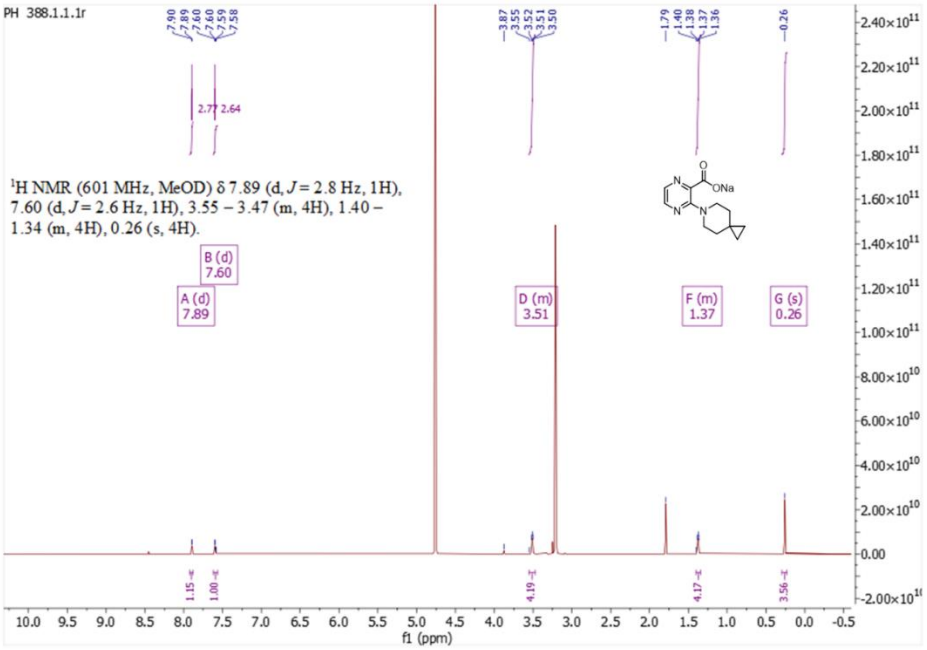

^{1}H NMR (601 MHz, MeOD) δ 7.89 (d, J = 2.8 Hz, 1H), 7.60 (d, J = 2.6 Hz, 1H), 3.55 – 3.47 (m, 4H), 1.40 – 1.34 (m, 4H), 0.26 (s, 4H).

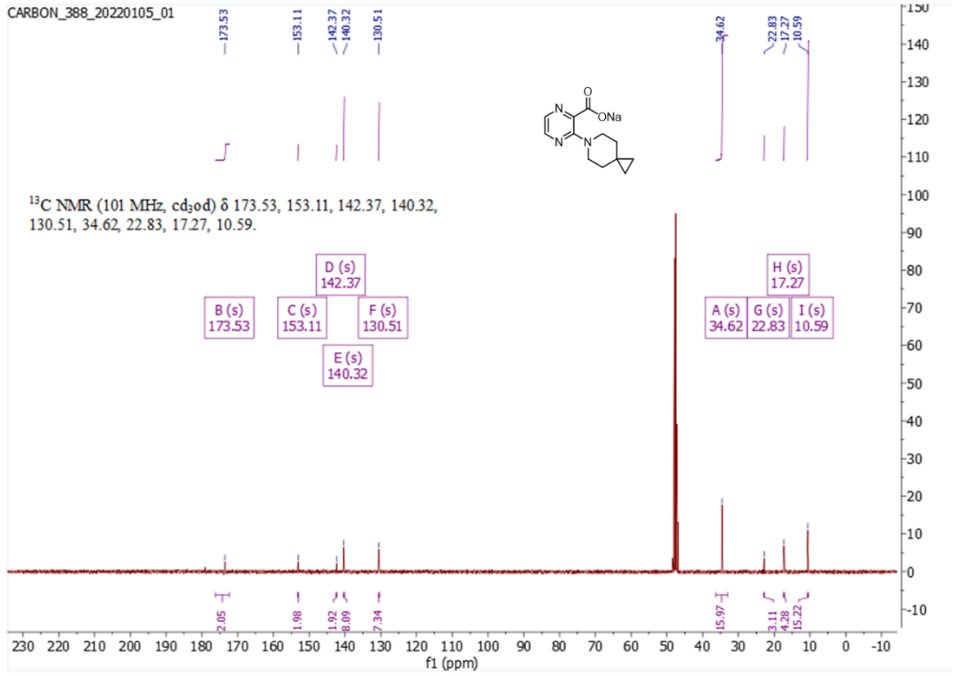

^{13}C NMR (101 MHz, cd_3od) δ 173.53, 153.11, 142.37, 140.32, 130.51, 34.62, 22.83, 17.27, 10.59.

Sodium 5-Pyrrolidine-2-Pyrazinoate (POAA 044)

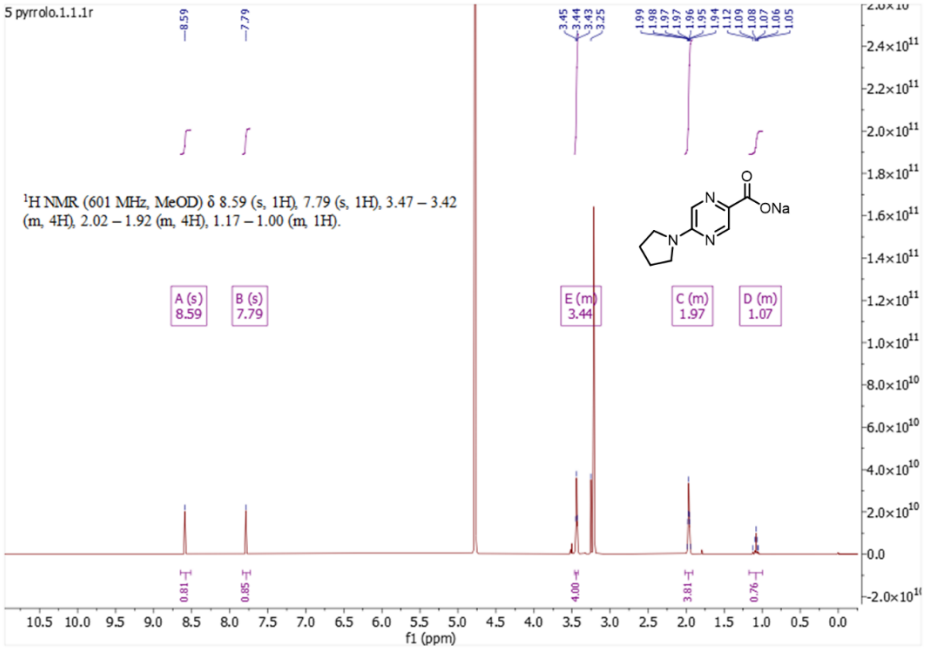

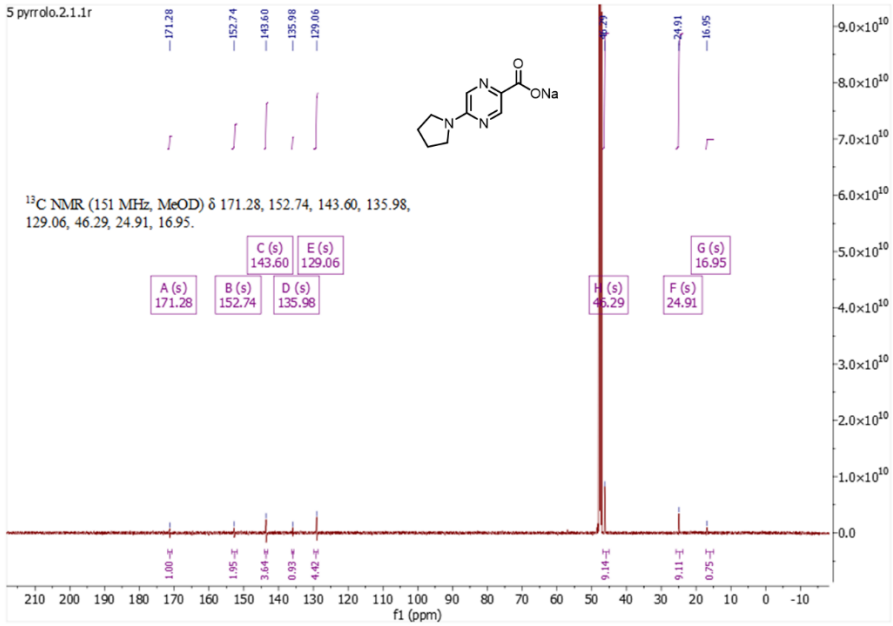

Sodium 5-cyclopentylaminopyrazine-2-carboxylate (POA 45)

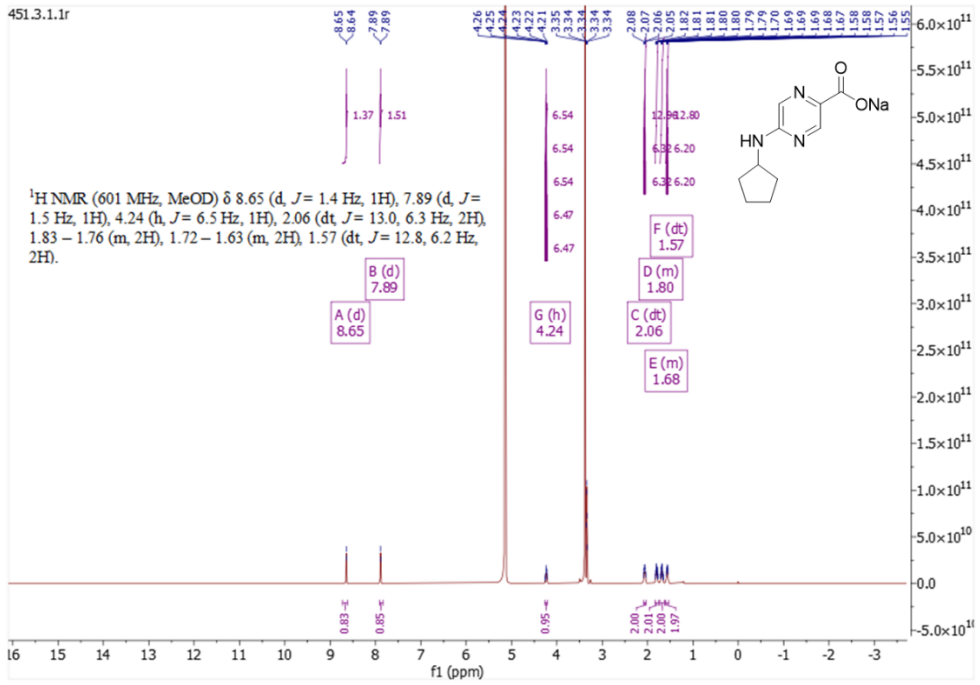

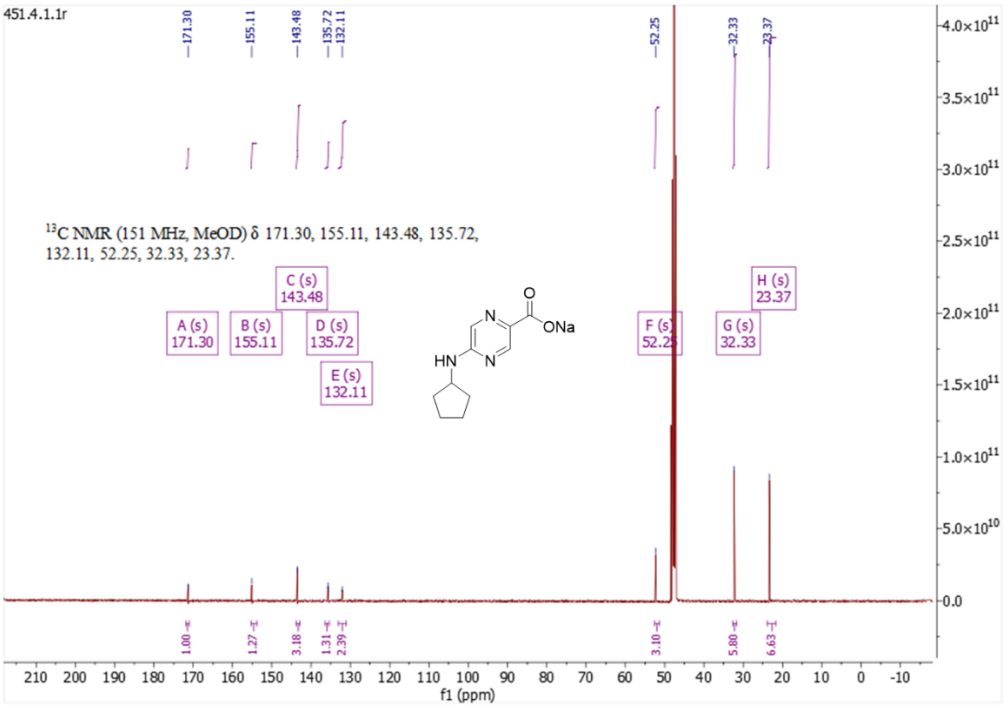

Sodium 5-cyclobutylaminopyrazine-2-carboxylate (POA 46)

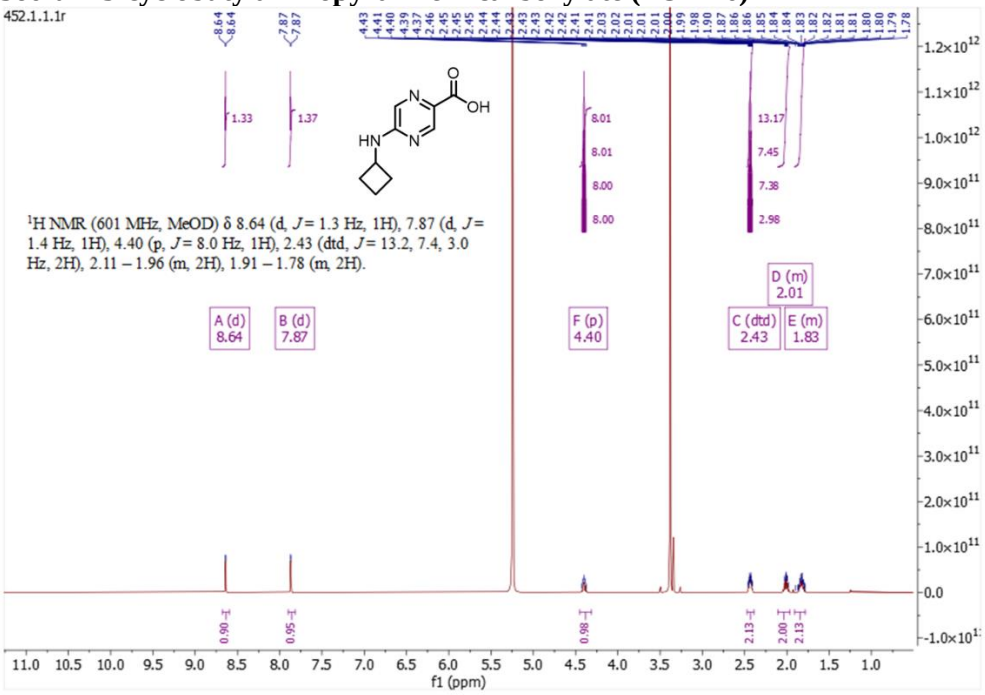

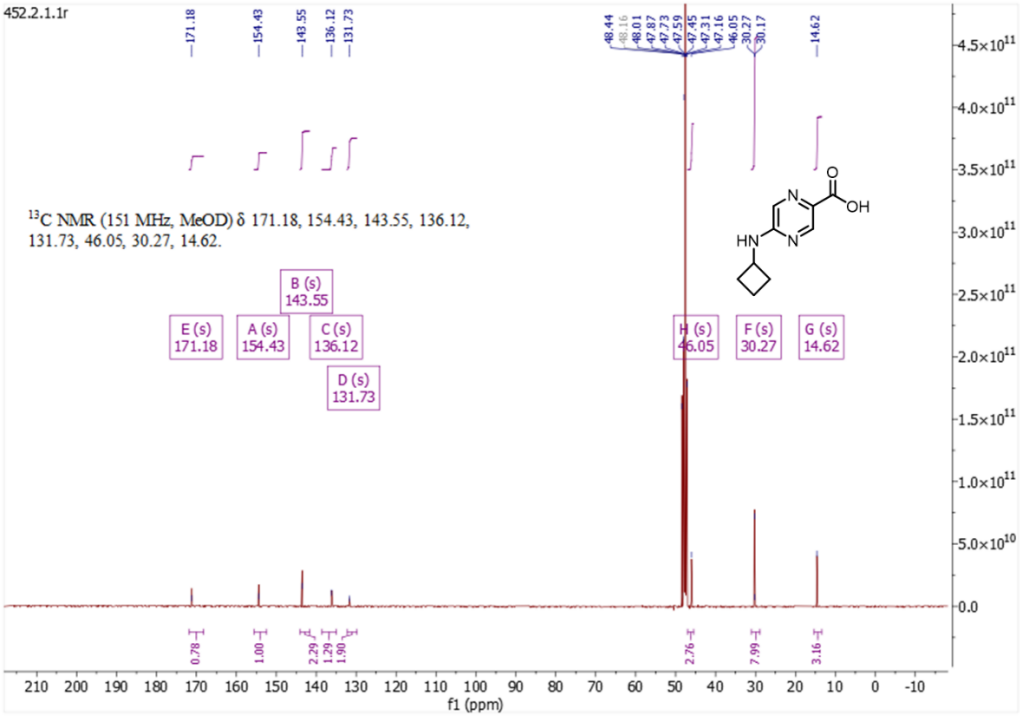

Sodium 5-Anilino-2-pyrazinoate (POAA 047)

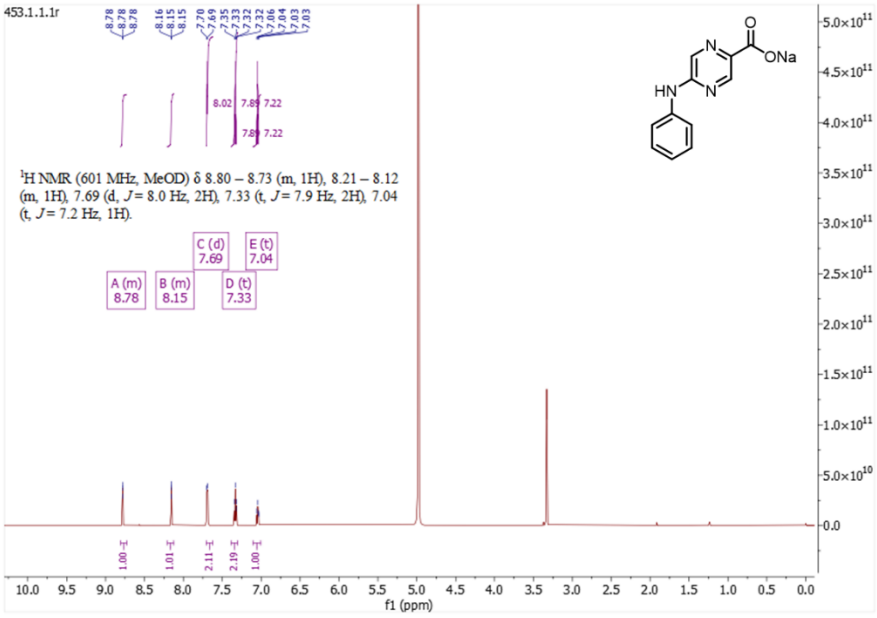

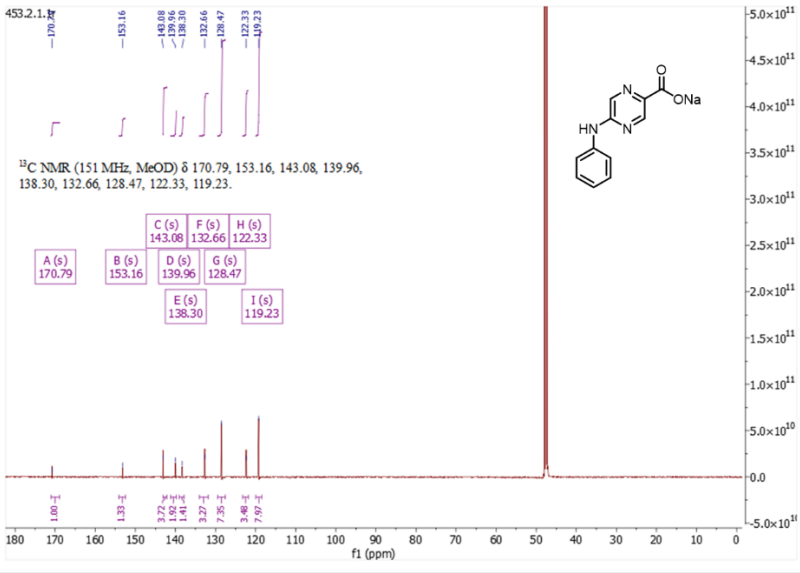

Sodium 6-cyclobutylaminopyrazine-2-carboxylate (POA 52)

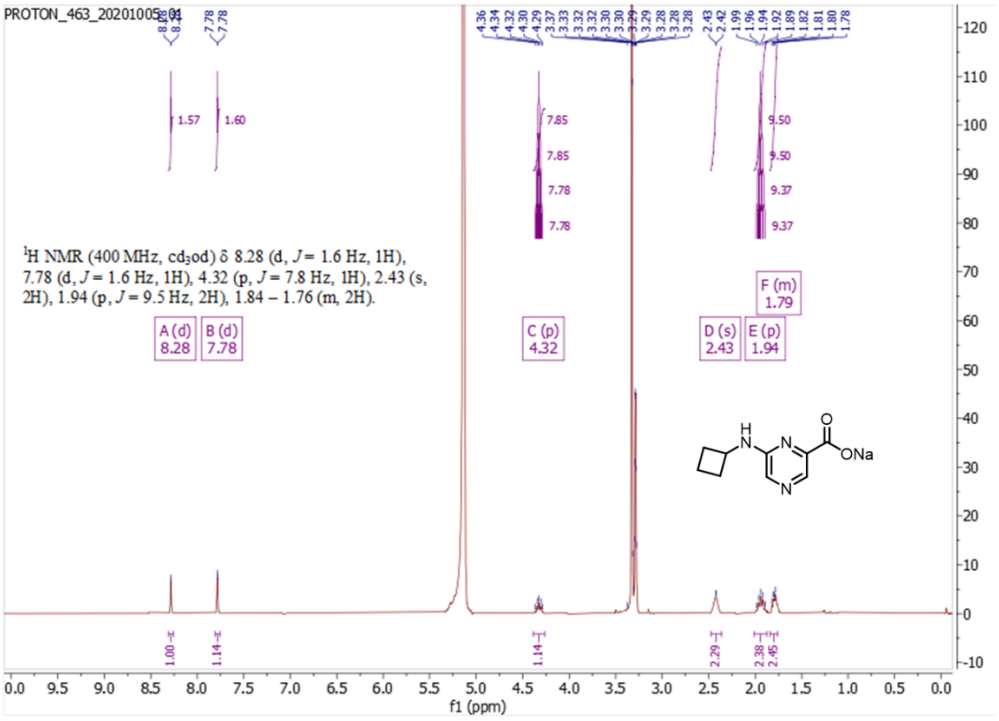

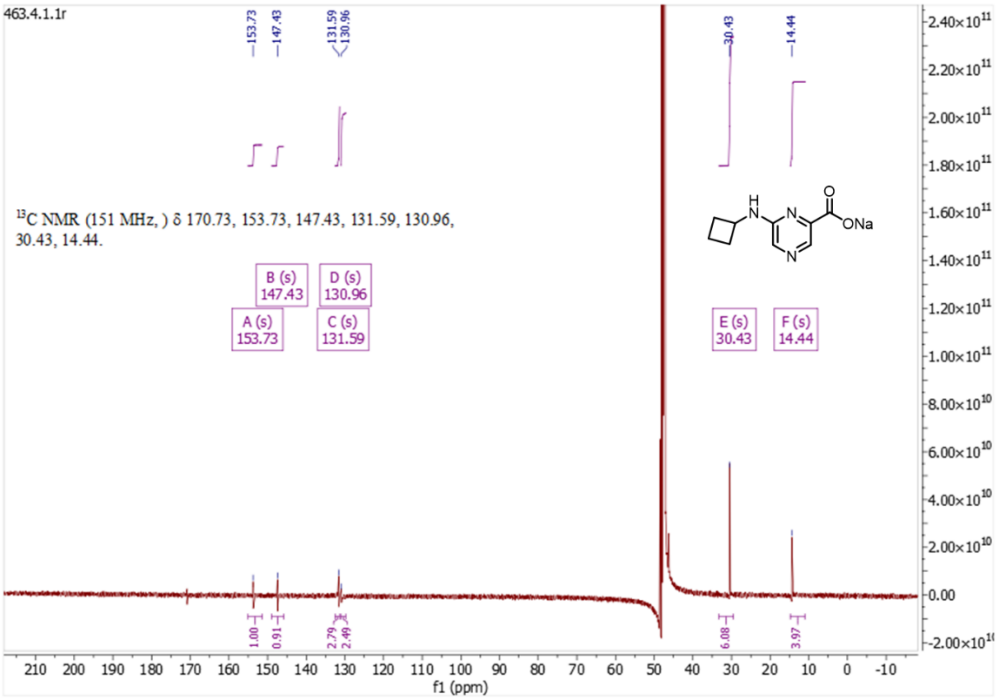

Sodium 6-ethylaminopyrazine-2-carboxylate (POA 53)

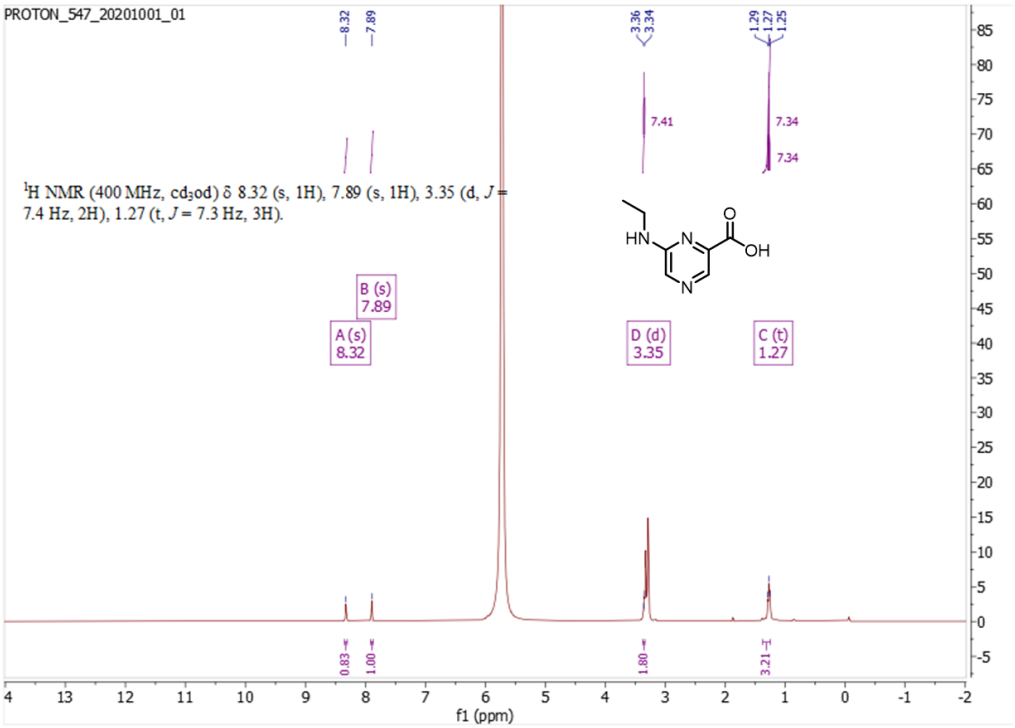

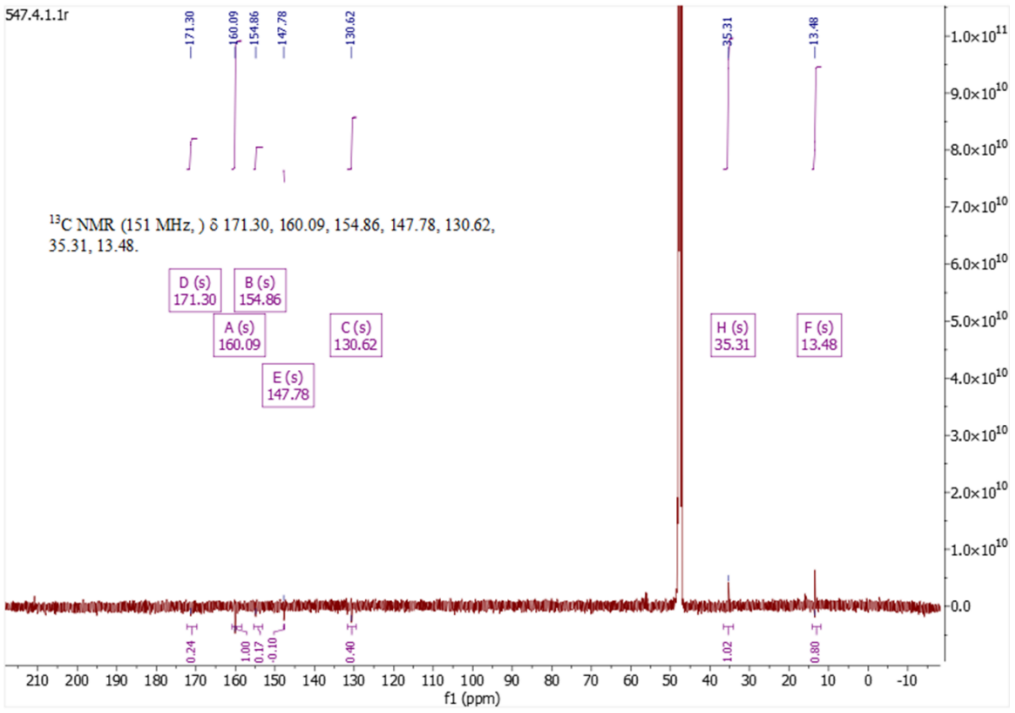

Sodium 6-Cyclopentylamino-2-pyrazinoate (POAA 054)

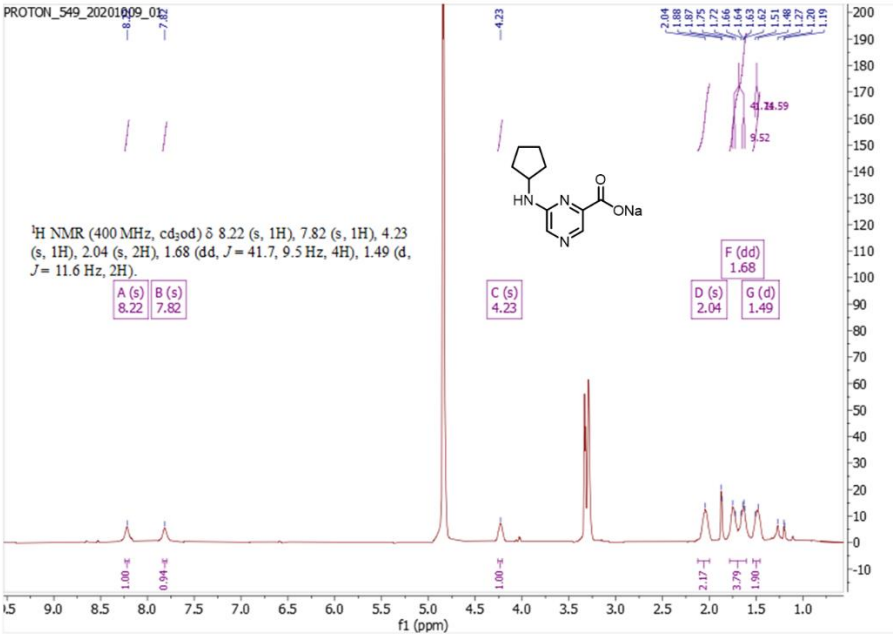

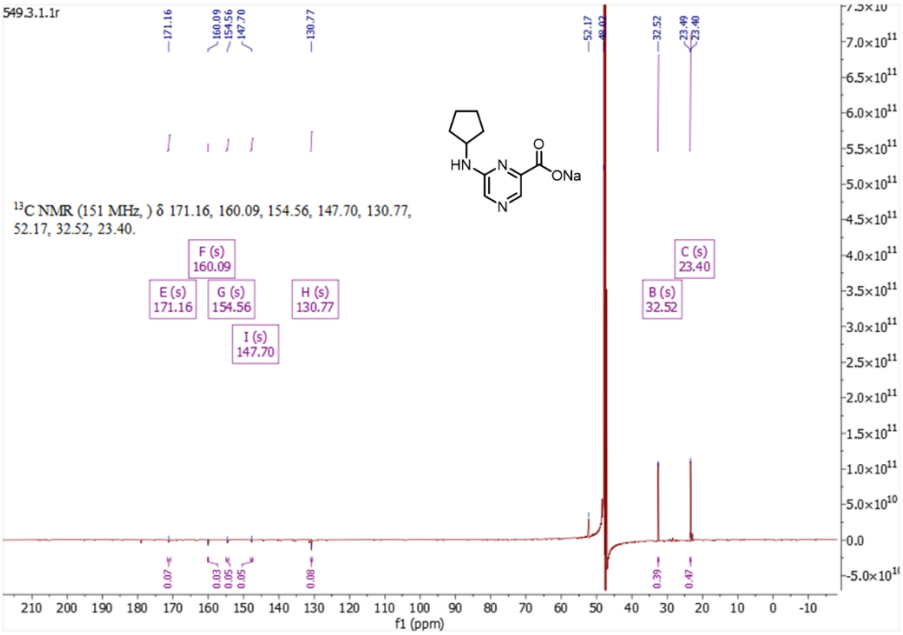

Sodium 6-isobutylaminopyrazine-2-carboxylate (POA 55)

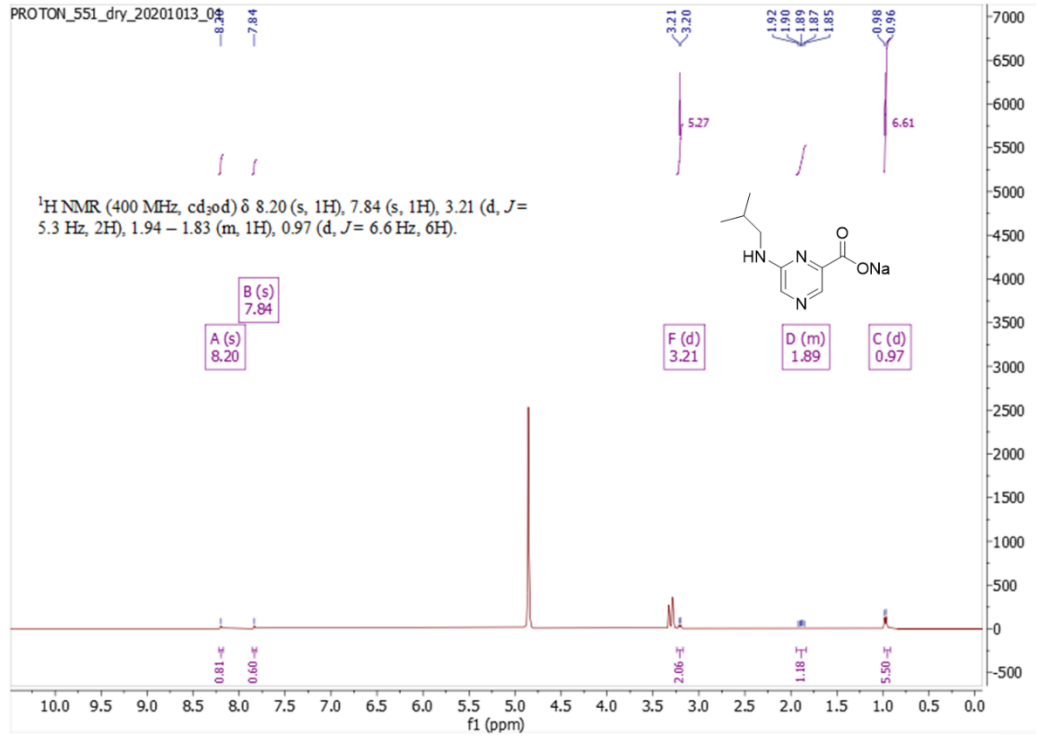

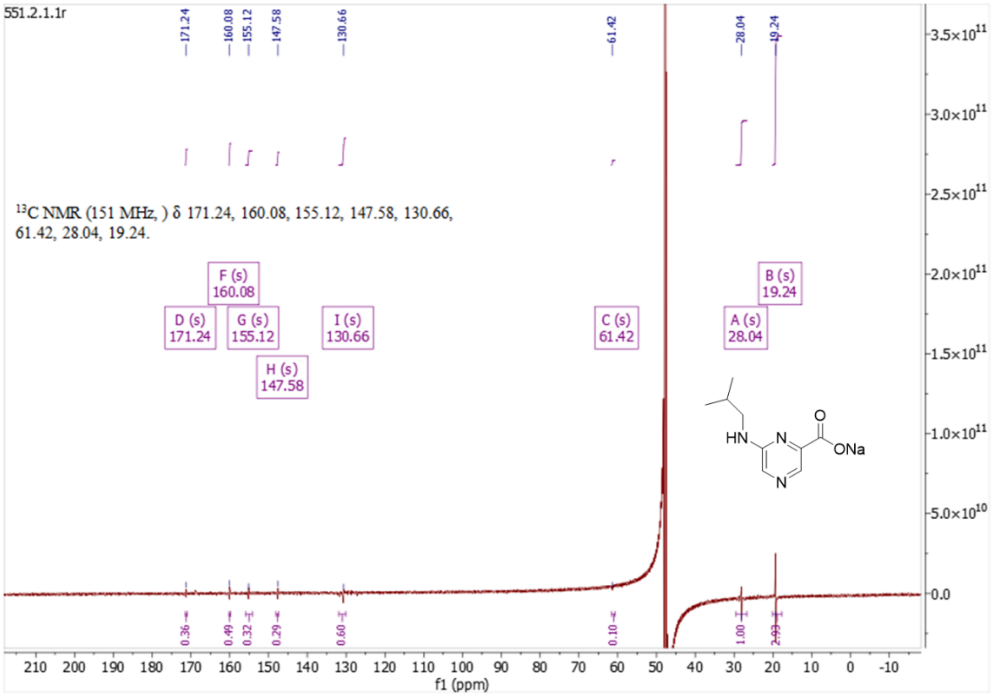

Sodium 6-phenylpyrazine-2-carboxylate (POA 56)

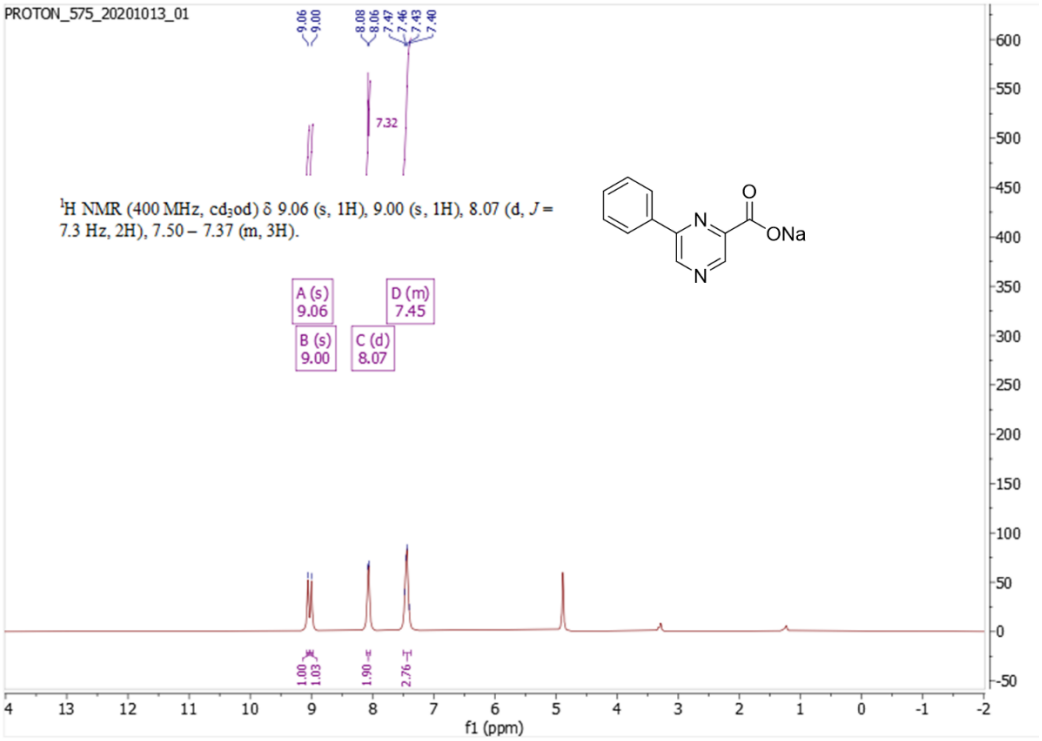

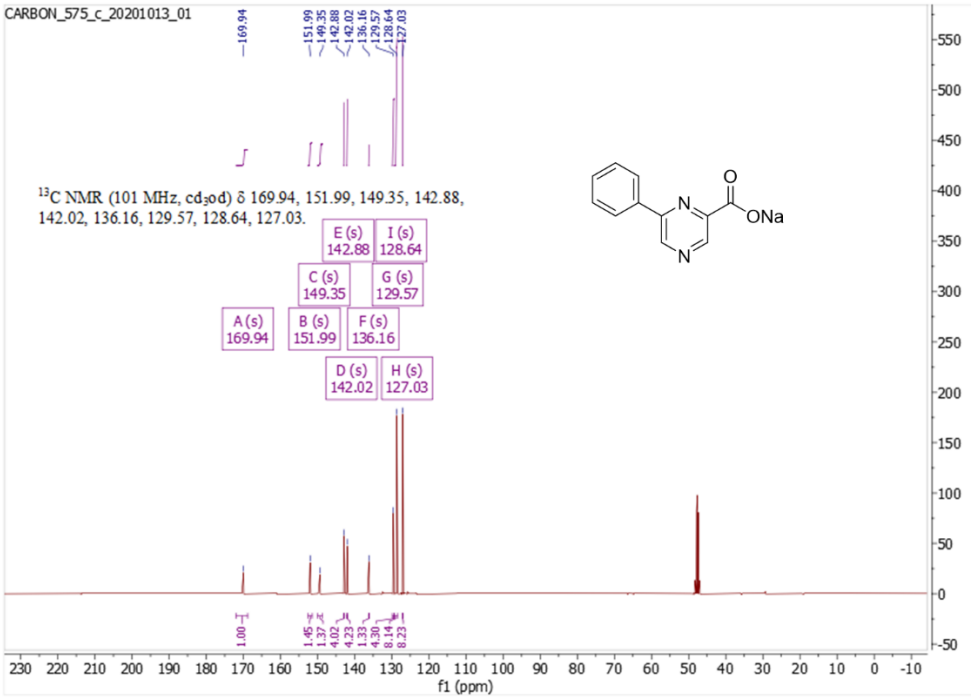

Sodium 6-(4-Fluorophenyl) pyrazine-2-carboxylic acid (POAA 057)

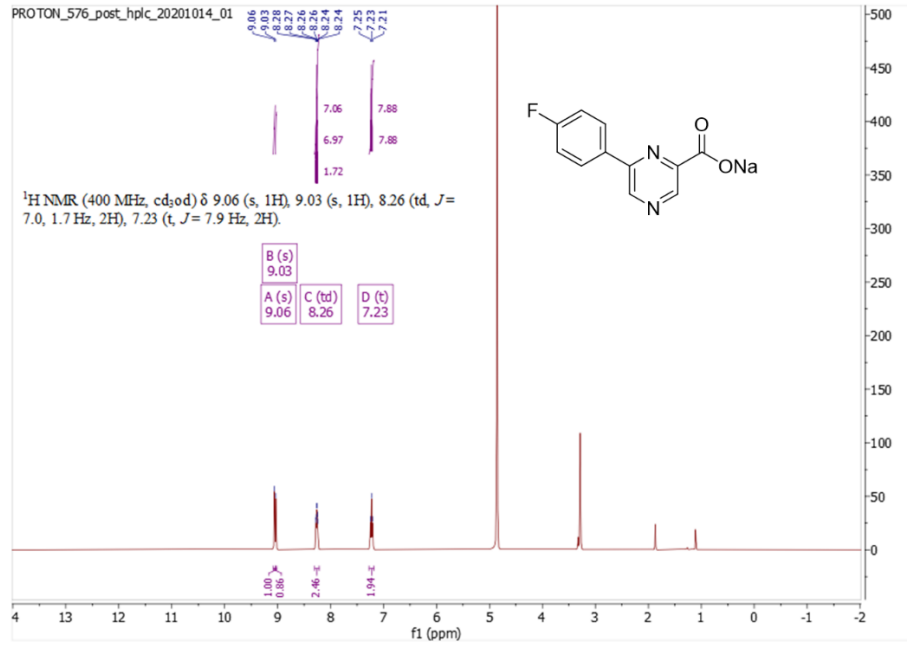

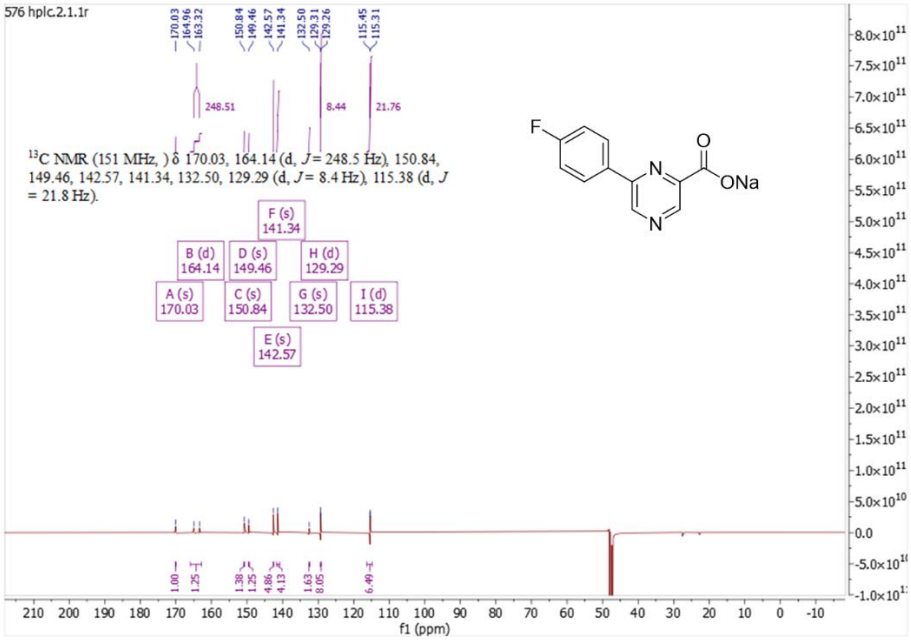

Sodium 6-(o-tolyl) pyrazine-2-carboxylic acid (POAA 058)

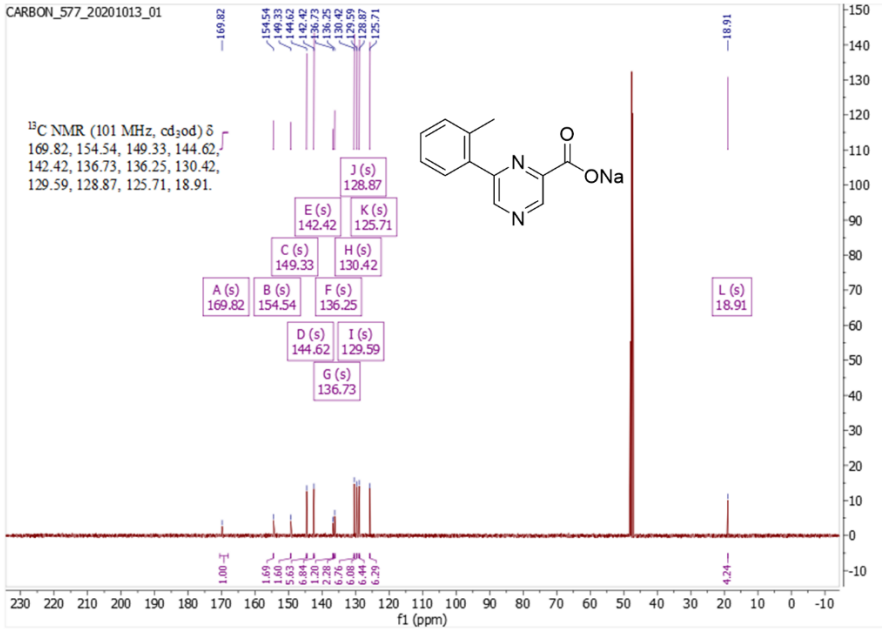

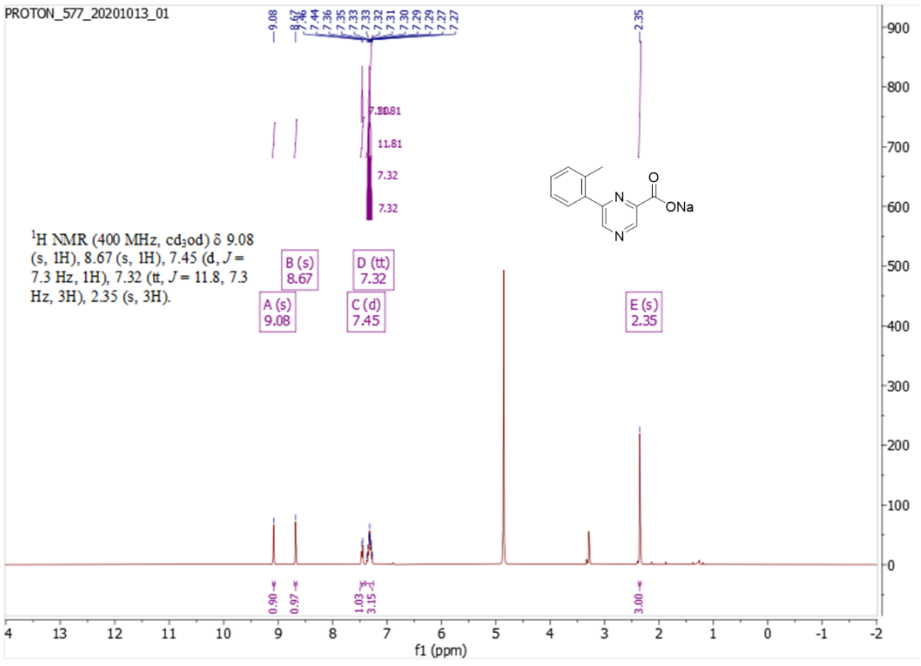

Sodium 6-(4-(methylthio) phenyl)pyrazine-2-carboxylic acid (POAA 059)

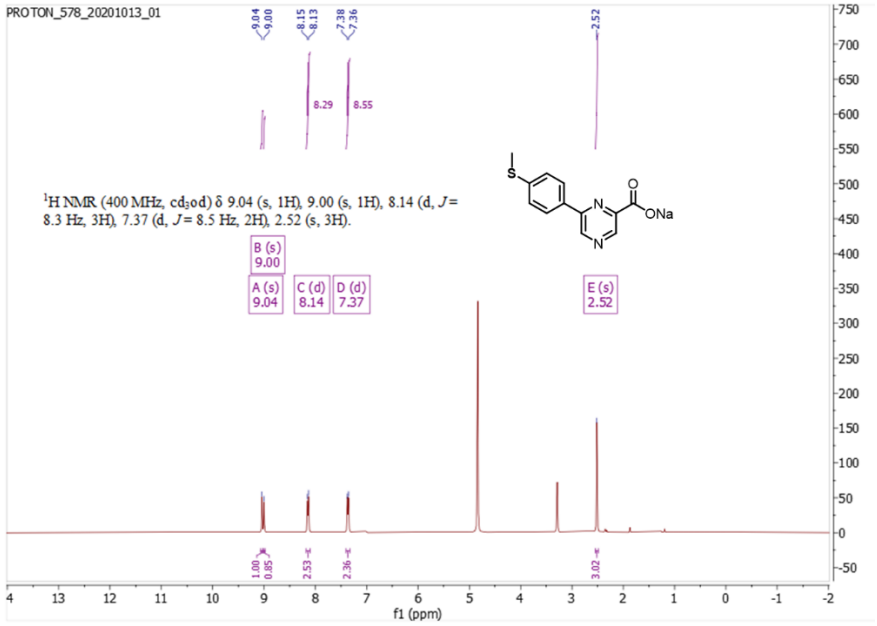

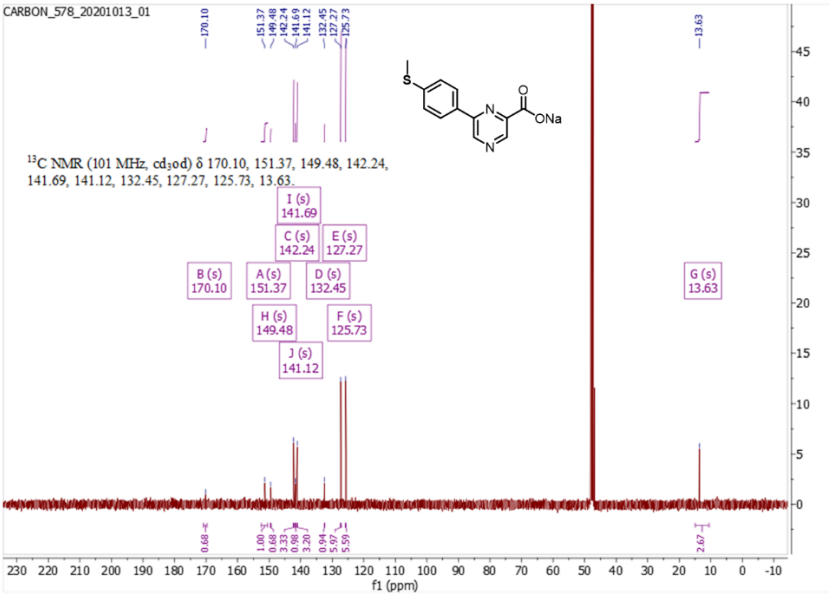

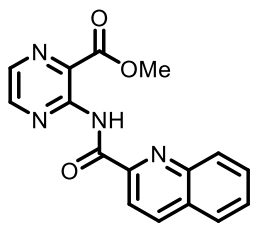
O
OMe
N
N
NH
O
N

POAA060-OMe

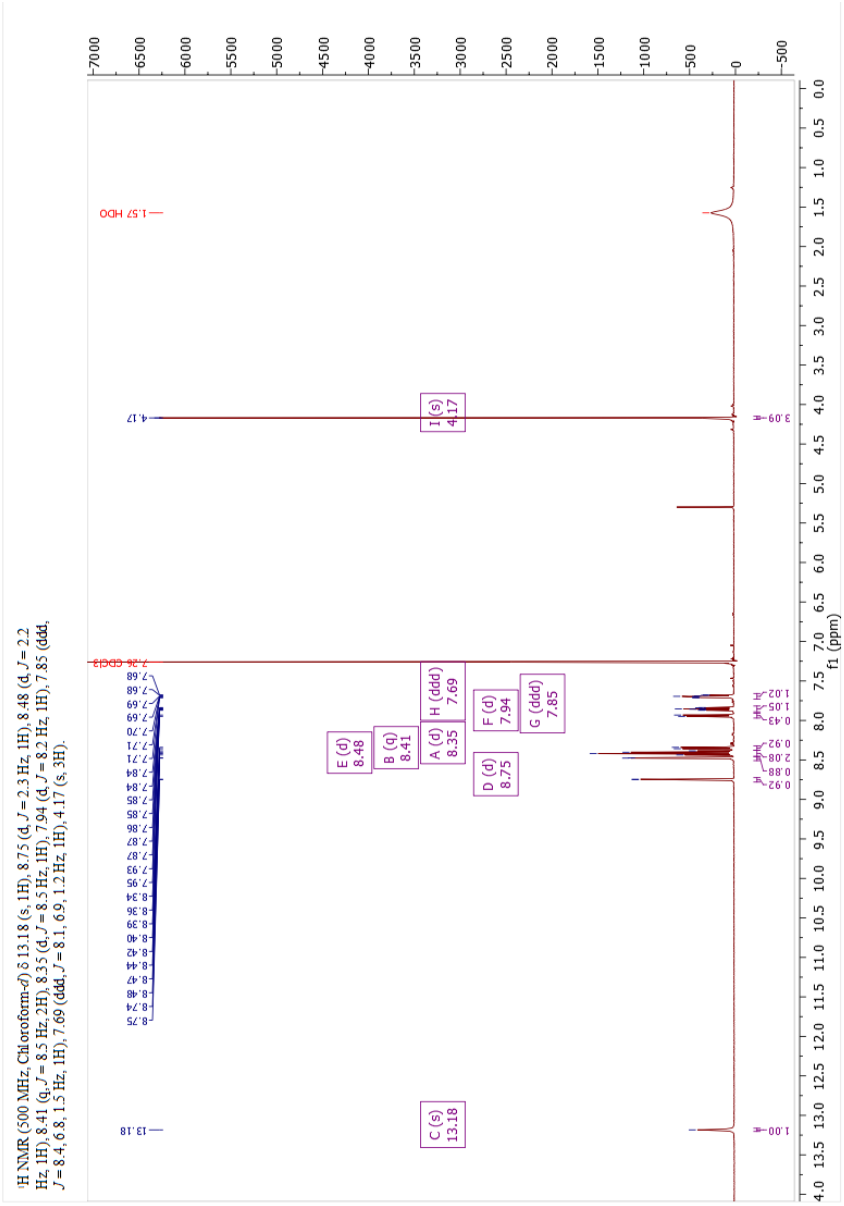
^{1}H NMR (500 MHz, Chloroform-d) δ 13.18 (s, 1H), 8.75 (d, J = 2.3 Hz, 1H), 8.48 (d, J = 2.2 Hz, 1H), 8.41 (q, J = 8.5 Hz, 2H), 8.35 (d, J = 8.5 Hz, 1H), 7.94 (d, J = 8.2 Hz, 1H), 7.85 (ddd, J = 8.4, 6.8, 1.5 Hz, 1H), 7.69 (ddd, J = 8.1, 6.9, 1.2 Hz, 1H), 4.17 (s, 3H).
I (s) 4.17
E (d) 8.48
B (q) 8.41
A (d) 8.35
H (ddd) 7.69
F (d) 7.94
G (ddd) 7.85
D (d) 8.75
C (s) 13.18
f1 (ppm)

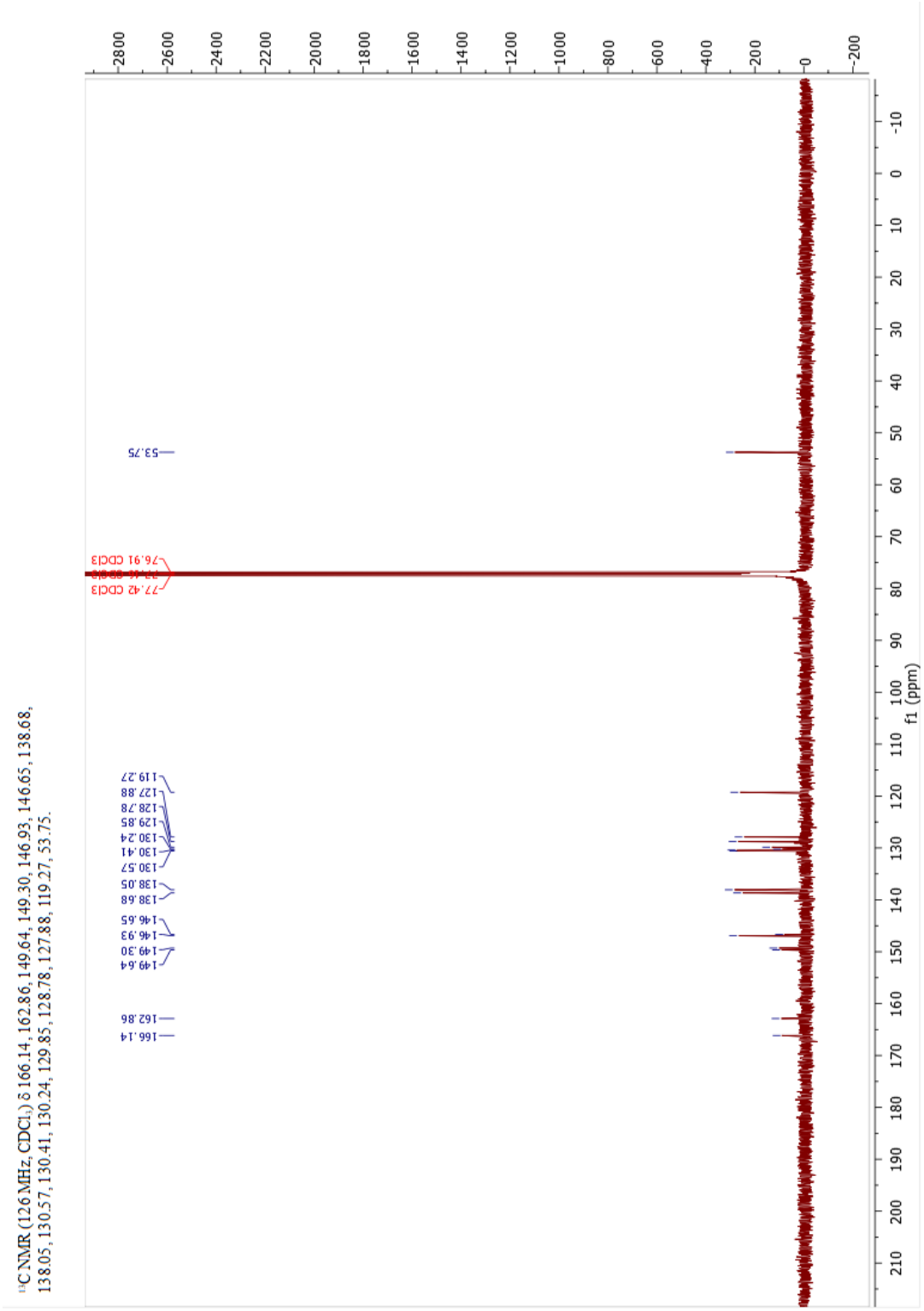

^{13}C NMR (126 MHz, $CDCl_3$) δ 166.14, 162.86, 149.64, 149.30, 146.93, 146.65, 138.68, 138.05, 130.57, 130.41, 130.24, 129.85, 128.78, 127.88, 119.27, 53.75.

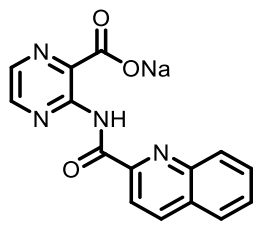
O
ONa
N
N
NH
O
N

POAA060

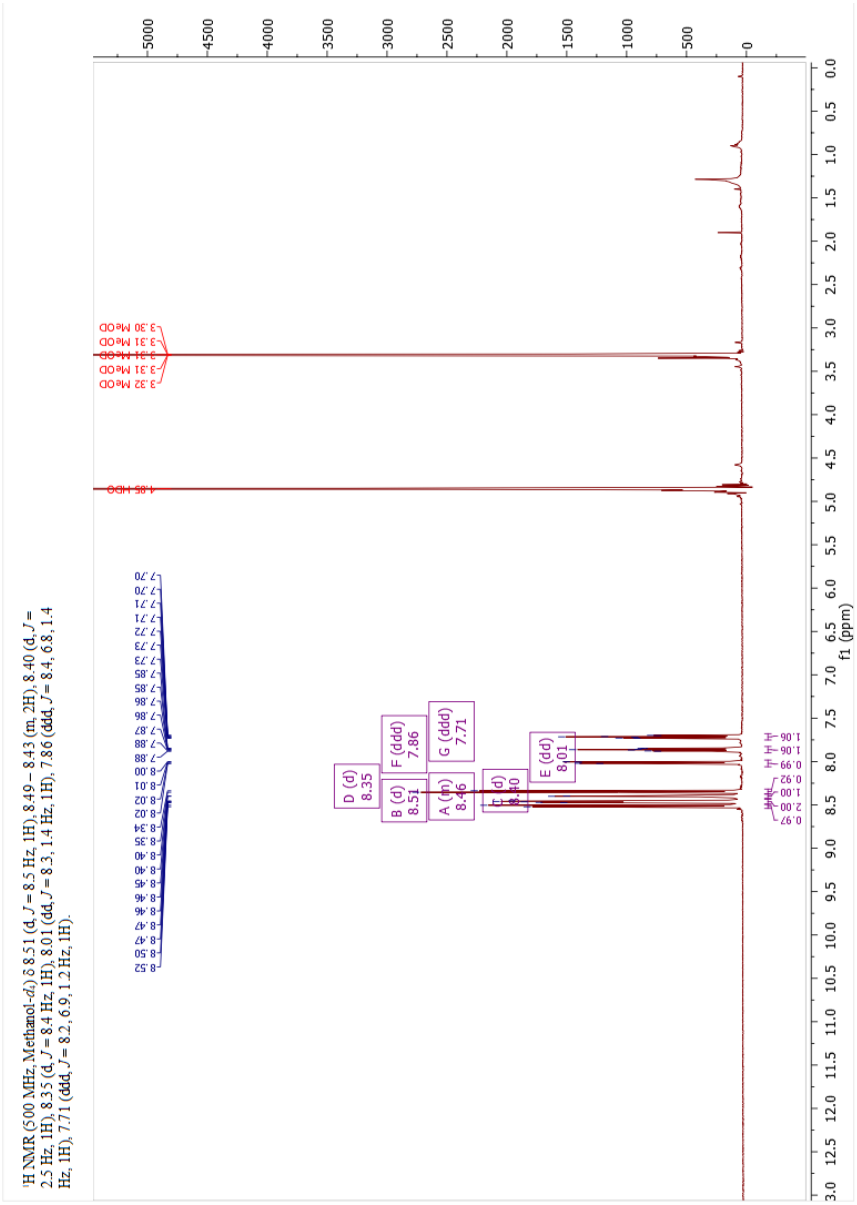
^{1}H NMR (500 MHz, Methanol-d_4) δ 8.51 (d, J = 8.5 Hz, 1H), 8.49 – 8.43 (m, 2H), 8.40 (d, J = 2.5 Hz, 1H), 8.35 (d, J = 8.4 Hz, 1H), 8.01 (dd, J = 8.3, 1.4 Hz, 1H), 7.86 (ddd, J = 8.4, 6.8, 1.4 Hz, 1H), 7.71 (ddd, J = 8.2, 6.9, 1.2 Hz, 1H).
D (d) 8.35
B (d) 8.51
F (ddd) 7.86
A (m) 8.46
G (ddd) 7.71
E (dd) 8.01
f1 (ppm)

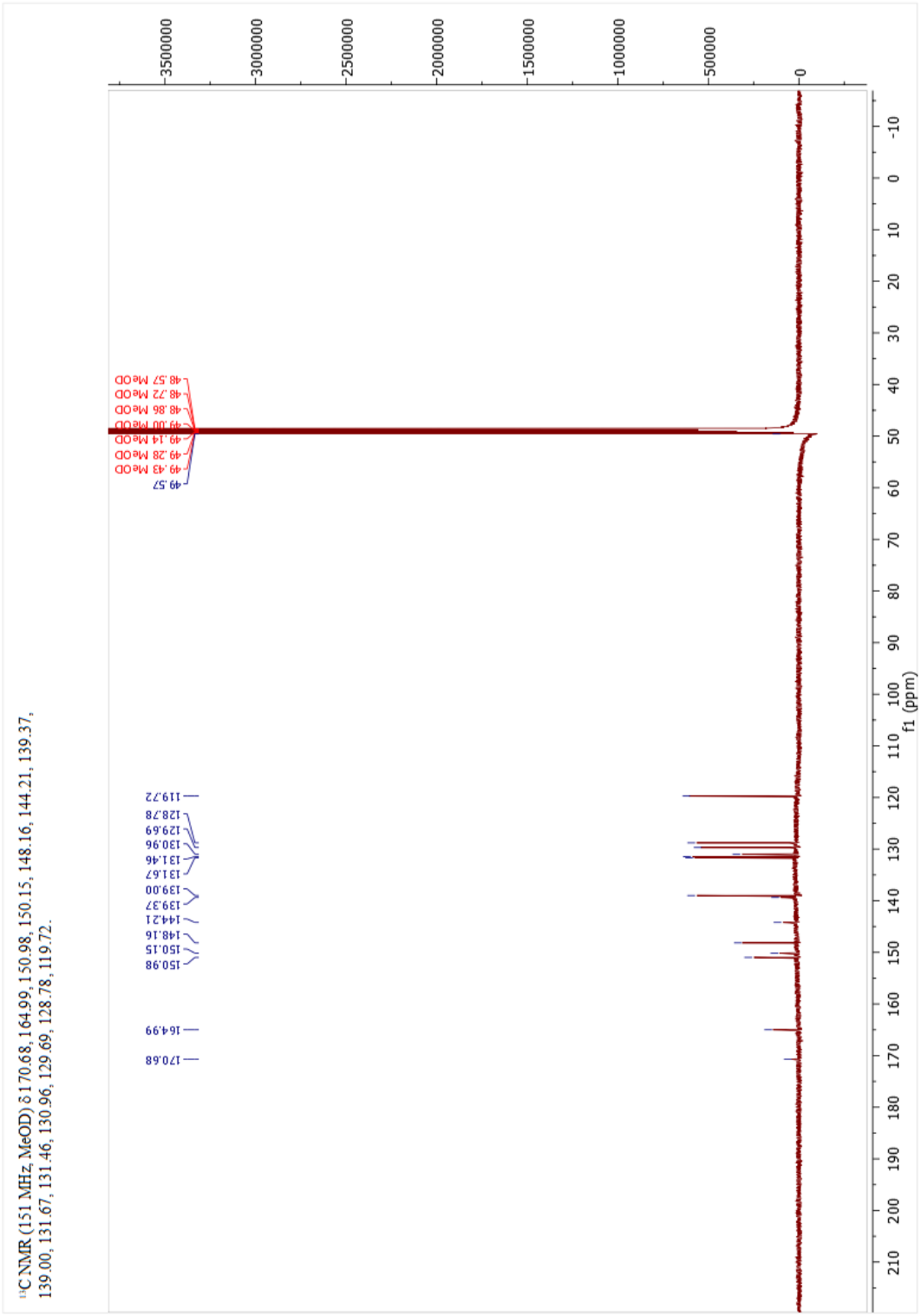
^{13}C NMR (151 MHz, MeOD) δ 170.68, 164.99, 150.98, 150.15, 148.16, 144.21, 139.37, 139.00, 131.67, 131.46, 130.96, 129.69, 128.78, 119.72.
f1 (ppm)

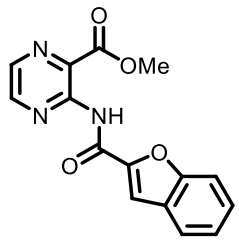

POAA061-OMe

^{1}H NMR (500 MHz, DMSO-d_6) δ 11.68 (s, 1H), 8.76 (d, J = 2.4 Hz, 1H), 8.60 (d, J = 2.4 Hz, 1H), 7.97 (d, J = 0.9 Hz, 1H), 7.86 (dd, J = 7.8, 1.1 Hz, 1H), 7.78 – 7.72 (m, 1H), 7.55 (ddd, J = 8.4, 7.2, 1.3 Hz, 1H), 7.43 – 7.35 (m, 1H), 3.83 (s, 3H).

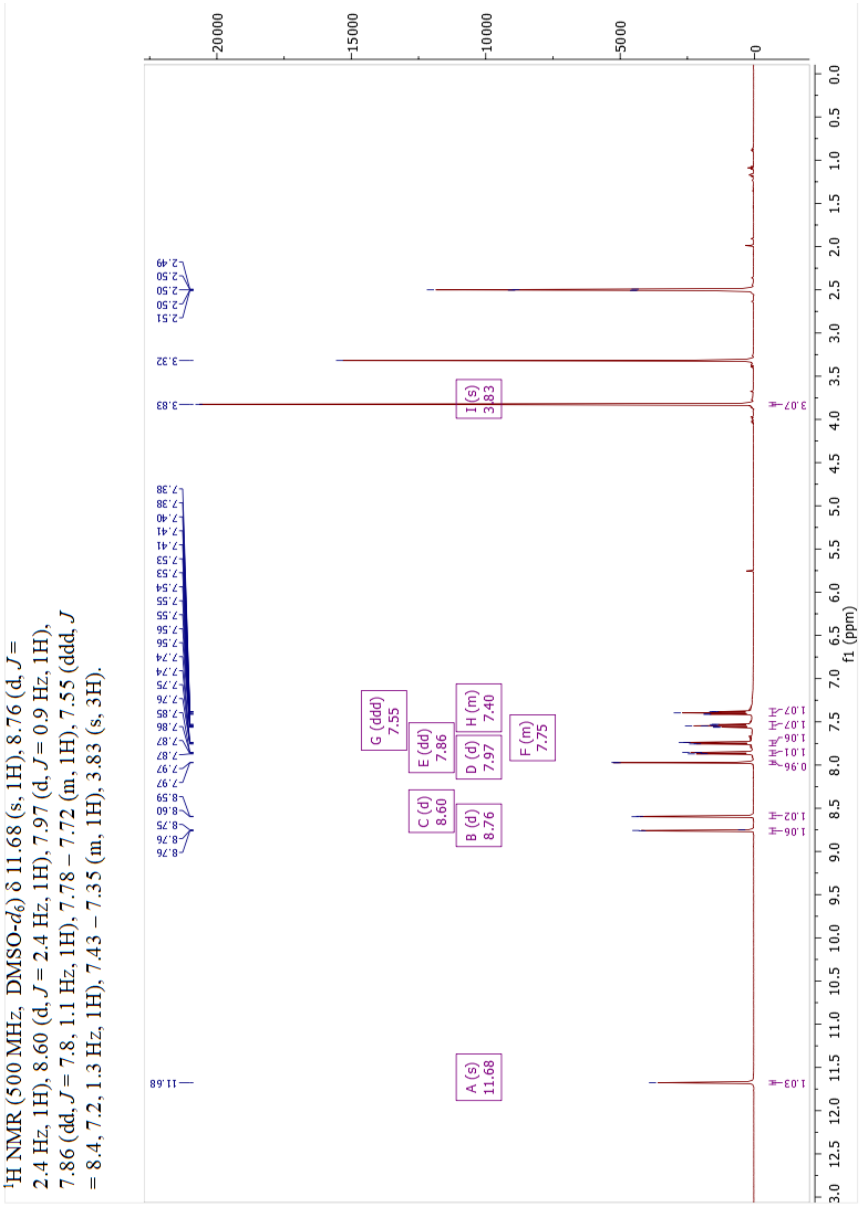

^{13}C NMR (126 MHz, DMSO) δ 164.96, 156.95, 154.69, 147.32, 145.54, 145.33, 140.16, 137.46, 127.81, 126.88, 124.07, 123.28, 112.30, 112.08, 52.57.

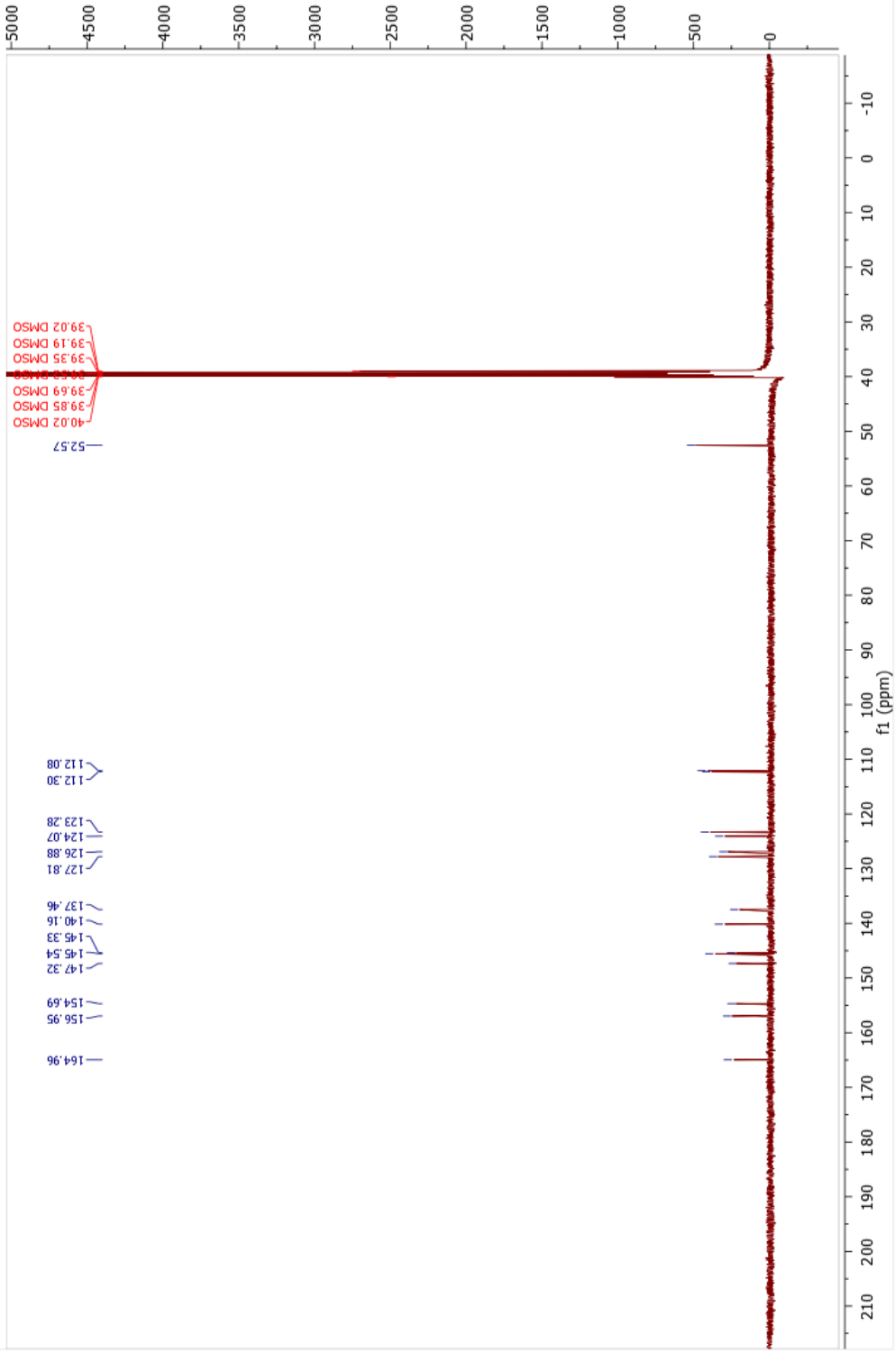

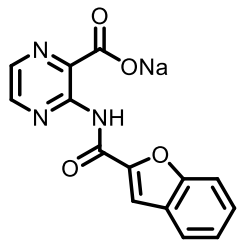
O
ONa
N
N
NH
O
O

POAA061

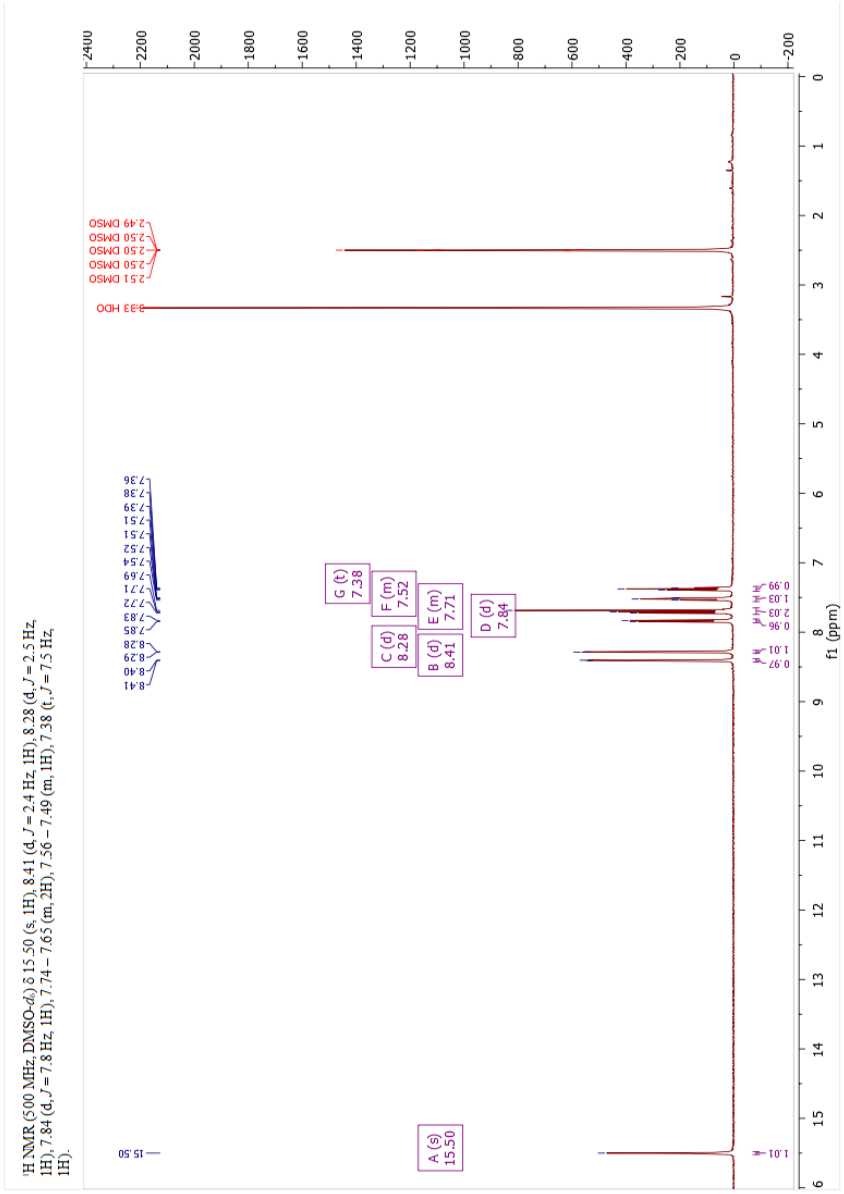
¹H NMR (500 MHz, DMSO-d6) δ 15.50 (s, 1H), 8.41 (d, J = 2.4 Hz, 1H), 8.28 (d, J = 2.5 Hz, 1H), 7.84 (d, J = 7.8 Hz, 1H), 7.74 – 7.65 (m, 2H), 7.56 – 7.49 (m, 1H), 7.38 (t, J = 7.5 Hz, 1H).
A (s) 15.50
B (d) 8.41
C (d) 8.28
D (d) 7.84
E (m) 7.71
F (m) 7.52
G (t) 7.38
f1 (ppm)

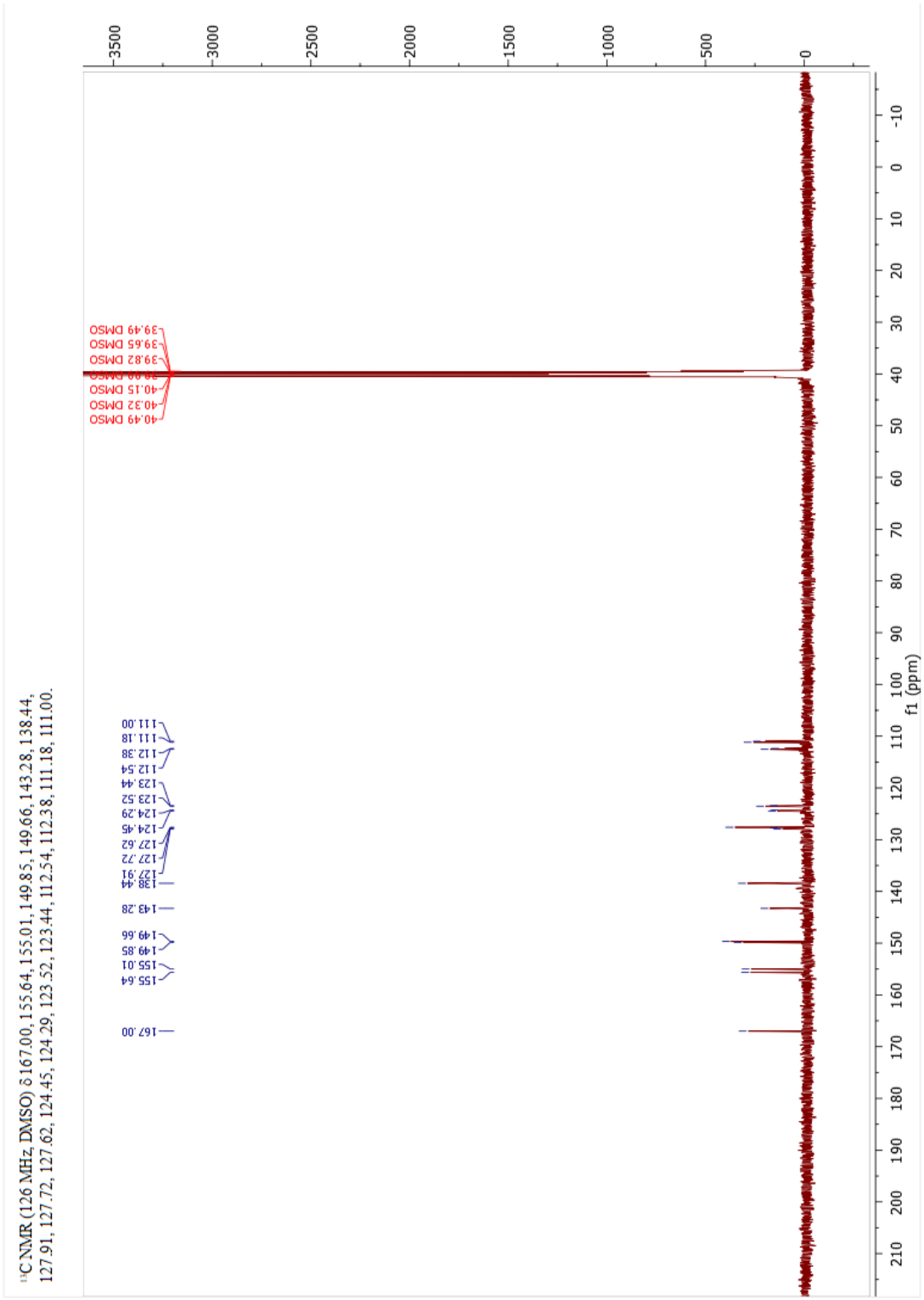
^{13}C NMR (126 MHz, DMSO) δ 167.00, 155.64, 155.01, 149.85, 149.66, 143.28, 138.44, 127.91, 127.72, 127.62, 124.45, 124.29, 123.52, 123.44, 112.54, 112.38, 111.18, 111.00.
39.49 DMSO
39.65 DMSO
39.82 DMSO
40.15 DMSO
40.32 DMSO
40.49 DMSO
111.00
111.18
112.38
112.54
123.44
123.52
124.29
124.45
127.62
127.72
127.91
138.44
143.28
149.66
149.85
155.01
155.64
167.00
f1 (ppm)